IMPACTS OF ENVIRONMENTAL VARIABILITY RELATED TO CLIMATE CHANGE ON BIOLOGICAL RESOURCES IN THE MEDITERRANEAN

EDITED BY: Bernardo Patti, Fabio Fiorentino, Tomaso Fortibuoni, Stylianos Somarakis and Jesus Garcia Lafuente

PUBLISHED IN: Frontiers in Marine Science

frontiers Research Topics

frontiers

ISSN 1664-8714
ISBN 978-2-83250-739-1
DOI 10.3389/978-2-83250-739-1

About Frontiers

Frontiers is more than just an open-access publisher of scholarly articles: it is a pioneering approach to the world of academia, radically improving the way scholarly research is managed. The grand vision of Frontiers is a world where all people have an equal opportunity to seek, share and generate knowledge. Frontiers provides immediate and permanent online open access to all its publications, but this alone is not enough to realize our grand goals.

Frontiers Journal Series

The Frontiers Journal Series is a multi-tier and interdisciplinary set of open-access, online journals, promising a paradigm shift from the current review, selection and dissemination processes in academic publishing. All Frontiers journals are driven by researchers for researchers; therefore, they constitute a service to the scholarly community. At the same time, the Frontiers Journal Series operates on a revolutionary invention, the tiered publishing system, initially addressing specific communities of scholars, and gradually climbing up to broader public understanding, thus serving the interests of the lay society, too.

Dedication to Quality

Each Frontiers article is a landmark of the highest quality, thanks to genuinely collaborative interactions between authors and review editors, who include some of the world's best academicians. Research must be certified by peers before entering a stream of knowledge that may eventually reach the public - and shape society; therefore, Frontiers only applies the most rigorous and unbiased reviews.
Frontiers revolutionizes research publishing by freely delivering the most outstanding research, evaluated with no bias from both the academic and social point of view. By applying the most advanced information technologies, Frontiers is catapulting scholarly publishing into a new generation.

What are Frontiers Research Topics?

Frontiers Research Topics are very popular trademarks of the Frontiers Journals Series: they are collections of at least ten articles, all centered on a particular subject. With their unique mix of varied contributions from Original Research to Review Articles, Frontiers Research Topics unify the most influential researchers, the latest key findings and historical advances in a hot research area! Find out more on how to host your own Frontiers Research Topic or contribute to one as an author by contacting the Frontiers Editorial Office: frontiersin.org/about/contact

IMPACTS OF ENVIRONMENTAL VARIABILITY RELATED TO CLIMATE CHANGE ON BIOLOGICAL RESOURCES IN THE MEDITERRANEAN

Topic Editors:
Bernardo Patti, Institute for the Study of Anthropogenic Impacts and Sustainability in Marine Environment, Department of Earth System Sciences and Technologies for the Environment, National Research Council (CNR), Italy
Fabio Fiorentino, Institute for Biological Resources and Marine Biotechnology, National Research Council (CNR), Italy
Tomaso Fortibuoni, Istituto Superiore per la Protezione e la Ricerca Ambientale (ISPRA), Italy
Stylianos Somarakis, Institute of Marine Biological Resources and Inland Waters, Hellenic Center for Marine Research, Greece
Jesus Garcia Lafuente, University of Malaga, Spain

Citation: Patti, B., Fiorentino, F., Fortibuoni, T., Somarakis, S., Lafuente, J. G., eds. (2022). Impacts of Environmental Variability Related to Climate Change on Biological Resources in the Mediterranean. Lausanne: Frontiers Media SA.
doi: 10.3389/978-2-83250-739-1

Table of Contents

frontiers | Frontiers in Marine Science

TYPE Editorial
PUBLISHED 25 October 2022
DOI 10.3389/fmars.2022.1059424

OPEN ACCESS

EDITED AND REVIEWED BY
Yngvar Olsen,
Norwegian University of Science and Technology, Norway

*CORRESPONDENCE
Bernardo Patti
bernardo.patti@cnr.it

SPECIALTY SECTION
This article was submitted to Marine Fisheries, Aquaculture and Living Resources, a section of the journal Frontiers in Marine Science

RECEIVED 01 October 2022
ACCEPTED 13 October 2022
PUBLISHED 25 October 2022

CITATION
Patti B, Fiorentino F, Fortibuoni T, Somarakis S and García-Lafuente J (2022) Editorial: Impacts of environmental variability related to climate change on biological resources in the Mediterranean. *Front. Mar. Sci.* 9:1059424. doi: 10.3389/fmars.2022.1059424

Editorial: Impacts of environmental variability related to climate change on biological resources in the Mediterranean

Bernardo Patti[1]*, Fabio Fiorentino[2], Tomaso Fortibuoni[3], Stylianos Somarakis[4] and Jesus García-Lafuente[5]

[1]Institute for the Study of Anthropic Impacts and Sustainability in the Marine Environment (IAS), National Research Council (CNR), Palermo, Italy, [2]Institute for Biological Resources and Marine Biotechnology (IRBIM), National Research Council (CNR), Mazara del Vallo, Italy, [3]Italian Institute for Environmental Protection and Research (ISPRA), Ozzano dell'Emilia, Italy, [4]Institute of Marine Biological Resources and Inland Waters (IMBRIW), Hellenic Centre for Marine Research (HCMR), Thalassocosmos, Gournes, Crete, Greece, [5]Instituto de Biotecnologia y Desarrollo azul (IBYDA), Physical Oceanography Group, University of Málaga, Málaga, Spain

KEYWORDS

Mediterranean sea, climate change, oceanography, biodiversity, fisheries, biomass

Editorial on the Research Topic

Impacts of environmental variability related to climate change on biological resources in the Mediterranean

Introduction

Current estimates of the increasing trend in Sea Surface Temperature (SST) from satellite-based remote sensing represent the main evidence of Mediterranean climate change (Pisano et al., 2020; Juza and Tintoré, 2021; Copernicus Marine Service Information, 2022a). The sea warming is known to affect primary production at global and regional scales by increasing stratification of the sea, reducing the input of nutrients into surface waters from mixing (Behrenfeld et al., 2006; Copernicus Marine Service Information, 2022b). The observed reduction in primary production is able to indirectly impact the biological processes governing the dynamics of fish stocks and the sustainability of fisheries, as already found in previous studies even in the Mediterranean Sea (Brander, 2007; Blanchard et al., 2012; Tzanatos et al., 2014; Corrales et al., 2018; Schickele et al., 2021). However, the observed warming trends have uneven spatial patterns, and more insights on their impacts on the primary production and on fishery resources are needed, especially in the neritic zone where most of the processes supporting fish populations take place. This Research Topic (RT) aimed to relate the available information about Mediterranean warming to a set of indicators of spatial distribution and productivity of marine populations, as well as the impacts of climate change on hydrological and biogeochemical features. Eleven manuscripts have been finally published in this RT dealing with the following main sub-topics.

Variability in hydrological and biogeochemical features

Three studies focused on oceanography in an area adjacent to the Strait of Gibraltar. A first study by Vargas-Yañez et al. (2022) searched for long-term trends of the mixed layer depth (MLD) as a potential proxy of changes in a warming scenario. Increased SST would imply greater stratification, hampering the supply of nutrients to the euphotic layer from below. The shallowing of MLD would partially compensate for this shortage, hence the interest in following changes of MLD. No noticeable changes during the observations were detected by the authors, who ascribed this fact to the effect of the accompanying salinity increase that compensates for the warming effect on water density. As a result, stratification was almost not modified, and MLD hardly changed. Authors advised some caution in their results, given that the length of the series analyzed could be insufficient to ensure the lack of trend, which could be masked by decadal variability. The second study investigated the link between large-scale variability modes of the SST and the surface chlorophyll-a (Chl-a) concentration in spring along the Alboran Sea (AS) (Western Mediterranean) (López-Parages et al.). Results indicated that El Niño Southern Oscillation (ENSO) could be used to estimate the coastal Chl-a concentration in spring in northern Alboran 4 months in advance, while the tropical North Atlantic SST allowed predicting, up to 7 months in advance, the offshore Chl-a. The third paper is an updated review of the AS oceanography based on fieldwork and numerical studies with a description of process dynamics and their role in shaping primary productivity and regional fisheries resources (Sánchez-Garrido and Nadal). Main gaps in understanding the physical drivers for transitions between the most recurrent one-gyre and two-gyre modes of circulation of the AS were identified. Research strategies based on end-to-end regional biophysical modelling were suggested to gain new insights into past and present physical control of fisheries resources and assess climate change impacts on the AS ecosystem. A fourth paper updated the knowledge on hydrological and biogeochemical patterns in the Strait of Sicily (SoS) (Central Mediterranean) in the last decade (Placenti et al.). Temperature and salinity in the intermediate waters showed a sharp annual increase at about 50% higher rates observed within the previous decade. Similar trends were also present in deep waters, although with smaller temperature and salinity variations. The time series in the intermediate waters also highlighted the presence of quasi-cyclic fluctuations that can be associated with the alternation of the circulation modes (cyclonic and anti-cyclonic) of the Northern Ionian Gyre (NIG). Moreover, an opposite trend emerged by comparing the nutrients and salinity time series in intermediate waters, while similar patterns have been evidenced between nutrients and chlorophyll-a concentration. A fifth study investigated relationships between thermohaline and biochemical patterns in the upper and intermediate water masses in the Levant Sea (Eastern Mediterranean) (Ozer et al.). Interannual fluctuations of salinity and temperature of the Levantine Intermediate Waters (LIW) were greater in the years 2008–2010, 2014–2015 and 2018–2019, coinciding with periods of anti-cyclonic circulation of the NIG. The enhanced warming in 2018–2019 has caused a decrease in density of the LIW core, bringing these nutrient-rich waters well inside the lower photic layer and supporting the observed maximum of chlorophyll recorded during 2018–2019. No significant change in the MLD but significantly higher average levels for integrated primary production, chlorophyll and bacterial abundances were observed during the anti-cyclonic period. The increase in LIW residence time and buoyancy may impact the primary producers' biomass at the photic zone and slightly counter the enhanced oligotrophication due to enhanced stratification resulting from climate change.

Hydrological pattern and species distribution

Two studies investigated the impact of hydrographical patterns on the spatial distribution of larvae of three tuna species (Atlantic bluefin tuna, bullet tuna and albacore) (Russo et al.), and on the biodiversity of ichthyoplankton assemblages (Patti et al.) in the SoS an area characterized by relatively stable mesoscale oceanographic processes, such as fronts and upwelling (Patti et al., 2010; Patti et al., 2020). The first one showed that the highest concentration of tuna larvae occurred in the easternmost part of the study area, south of Capo Passero, an area with a stable haline front and warmer, nutrient-poor water. The second study reported a decreasing trend in total larval abundance and biodiversity of ichthyoplankton assemblages, more pronounced in the shelf area and in the slope area, respectively. A third study addressed the settlement and recruitment patterns of juvenile fish in different habitats of the Adriatic Sea in relation to interannual environmental variability (Matić-Skoko et al.). Nurseries within transitional waters in the north resulted more prone to interannual water temperature changes. The associated community composition differed from that recorded in the southern Adriatic, where groups were mostly determined by water salinity and were less sensitive to interannual temperature fluctuations.

Effects of climate change and fisheries on species ecology

Two papers used Ecopath with Ecosim (EwE) and addressed the synergistic effects of climate change and fisheries exploitation in the Central and Eastern Mediterranean, contributing to the advancement of Ecosystem-Based Fishery Management approach (Heymans et al., 2016). The first study (Agnetta

et al.) presented an EwE dynamic model for the food web in the SoS, made up of 72 functional groups and including 13 fleet segments and a temporal simulation window until 2050, to evaluate the bio-economic interactive effects of the reduction of bottom trawling effort in different scenarios of fishery and climate change. A net increase in biomass of many functional groups with an immediate decline of trawlers' catches and economic incomes resulted, followed by a long-term increase mainly due to biomass rebuilding of commercial species, which lasts 5-10 years after fishing reduction. In the mid-term, the effects of trawling effort reduction are higher than those of climate change and seem to make exploitation of marine resources more sustainable over time, as well as fishery processes more efficient as a consequence of improving ecosystem health. The second study (Tsagarakis et al.) produced an EwE model for the North Aegean Sea (Eastern Mediterranean), highlighting the synergistic effect of environmental and anthropogenic processes during the three-decade hindcast period. Trends in biomasses, catches, and ecosystem indicators declined from 1993 to 2010, followed by a strong recovery thereafter. Sea warming scenarios for 2021-2050 indicated contrasting responses to increased temperature among the main commercial groups, while simulations of changes in productivity had relatively straightforward effects. Two scenarios of 10% and 25% reduction in fishing effort revealed quick increases in the biomass of most commercial species, though coupled with lower catches, except for a few groups. Adding reduction of productivity to temperature increase, the model forecasted lower biomass increases for the warm water species and even higher decreases for the cold water ones. These biomass losses were compensated by a 10% reduction in fishing effort, but this was not overall enough to counterbalance losses in catches. The last study (Scannella et al.) investigated the potential factors affecting the population dynamics of the regal cucumber (*Parastichopus regalis*), a species that is not commercialized in the SoS, to explore the impacts of fishing pressure and environmental factors on its abundance on trawlable bottoms. Long time series on species density indices (2008-2021) was modelled as a function of environmental parameters (i.e. salinity, dissolved oxygen, ammonium, pH and chlorophyll-a) and fishing effort. Results showed a big change in the species distribution over time with rarefaction of spatial distribution and a slight deepening starting from 2017 and 2011, respectively. No significant effects of fishing effort have been found. Conversely, a positive relationship with pH concentration in surface waters during the larval dispersal phase and nutrient concentration at the sea bottom has been identified, suggesting that this species is sensitive to climate change and food availability.

Conclusions

The RT evidenced contrasting regional responses to the warming of the Mediterranean Sea for the ensemble of indicators of spatial distribution and productivity of biological resources that were investigated in the contributing papers. Although the observed trends appear to be related to different sub-regional oceanographic features, similarities also emerged between the Central and Eastern Mediterranean in the ecosystem response to the alternation of the circulation modes (cyclonic and anti-cyclonic) in the Northern Ionian Gyre. In addition, it is worth noting how oceanographic processes involving the intermediate waters may impact primary production and compensate for the expected reduction in nutrient availability due to the enhanced stratification and reduced land input induced by climate change. However, this conclusion cannot be extended to all Mediterranean regions. Furhermore, the RT confirmed the complexity of interaction between climate and fisheries on biological resources dynamics. Although reduction of fishing effort was found as a main factor affecting the productivity of fisheries resources in the mid-term, the current warming phase could decrease the long term yield of fisheries in some areas of the basin. Future studies focusing on the biological response of the Mediterranean Sea to global warming have to consider these local differences to estimate trends in the biomass budget at the basin level.

Author contributions

All authors listed have made a substantial, direct, and intellectual contribution to the work and approved it for publication.

Conflict of interest

The authors declare that the research was conducted in the absence of any commercial or financial relationships that could be construed as a potential conflict of interest.

Publisher's note

References

Behrenfeld, M. J., O'Malley, R. T., Siegel, D. A., McClain, C. R., Sarmiento, J. L., Feldman, G. C., et al. (2006). Climate-driven trends in contemporary ocean productivity. *Nature* 444 (7120), 752–755. doi: 10.1038/nature05317

Blanchard, J. L., Jennings, S., Holmes, R., Harle, J., Merino, G., Allen, J. I., et al. (2012). Potential consequences of climate change for primary production and fish production in large marine ecosystems. *Philos. Trans. R. Soc Lond. B Biol. Sci.* 367, 2979–2989. doi: 10.1098/rstb.2012.0231

Brander, K. M. (2007). Climate change and food security special feature: global fish production and climate change. *Proc. Natl. Acad. Sci. U.S.A.* 104, 19 709–19 714. doi: 10.1073/pnas.0702059104

Copernicus Marine Service Information (2022a) *Mediterranean Sea Surface temperature cumulative trend map from observations reprocessing , (1993-2020)*. Available at: https://marine.copernicus.eu/access-data/ocean-monitoring-indicators/mediterranean-sea-surface-temperature-cumulative-trend-map.

Copernicus Marine Service Information (2022b) *Mediterranean Sea Chlorophyll-a trend map from observations reprocessing, (1993-2020)*. Available at: https://marine.copernicus.eu/access-data/ocean-monitoring-indicators/mediterranean-sea-chlorophyll-trend-map-observations.

Corrales, X., Coll, M., Ofir, E., Heymans, J. J., Steenbeek, J., Goren, M., et al. (2018). Future scenarios of marine resources and ecosystem conditions in the Eastern Mediterranean under the impacts of fishing, alien species and sea warming. *Sci. Rep.* 8 (1), 14284. doi: 10.1038/s41598-018-32666-x

Heymans, J. J., Coll, M., Link, J. S., Mackinson, S., Steenbeek, J., Walters, C., et al. (2016). Best practice in ecopath with ecosim food-web models for ecosystem-based management. *Ecol. Modell.* 331, 173–184. doi: 10.1016/j.ecolmodel.2015.12.007

Juza, M., and Tintoré, J. (2021). Multivariate Sub-regional ocean indicators in the Mediterranean Sea: From event detection to climate change estimations. *Front. Mar. Sci* 8:610589. doi: 10.3389/fmars.2021.610589

Patti, B., Guisande, C., Bonanno, A., Basilone, G., Cuttitta, A., and Mazzola, S. (2010). Role of physical forcings and nutrient availability on the control of satellite-based chlorophyll a concentration in the coastal upwelling area of the Sicilian channel. *Sci. Mar.* 74 (3), 577–588. doi: 10.3989/scimar.2010.74n3577

Patti, B., Torri, M., and Cuttitta, A. (2020). General surface circulation controls the interannual fluctuations of anchovy stock biomass in the central Mediterranean Sea. *Sci. Rep.* 10 (1), 1554. doi: 10.1038/s41598-020-58028-0

Pisano, A., Marullo, S., Artale, V., Falcini, F., Yang, C., Leonelli, F. E., et al. (2020). New evidence of Mediterranean climate change and variability from Sea surface temperature observations. *Remote Sens* 12 (1), 132. doi: 10.3390/rs12010132

Schickele, A., Goberville, E., Leroy, B., Beaugrand, G., Hattab, T., Francour, P., et al. (2021). European Small pelagic fish distribution under global change scenarios. *Fish Fish* 22 (1), 212–225. doi: 10.1111/faf.12515

Tzanatos, E., Raitsos, D. E., Triantafyllou, G., Somarakis, S., and Tsonis, A. A. (2014). Indications of a climate effect on Mediterranean fisheries. *Clim. Change* 122 (1-2), 41–54. doi: 10.1007/s10584-013-0972-4

frontiers in Marine Science

ORIGINAL RESEARCH
published: 18 August 2021
doi: 10.3389/fmars.2021.708775

Unveiling the Relationship Between Sea Surface Hydrographic Patterns and Tuna Larval Distribution in the Central Mediterranean Sea

Stefania Russo [1,2], Marco Torri [3]*, Bernardo Patti [4], Patricia Reglero [5], Diego Álvarez-Berastegui [5], Angela Cuttitta [2†] and Gianluca Sarà [1†]*

[1] DiSTeM-UNIPA, Department of Earth and Marine Science, University of Palermo, Palermo, Italy, [2] CNR-ISMed, National Research Council, Institute for Studies on the Mediterranean, Detached Unit of Palermo, Palermo, Italy, [3] CNR-IAS, National Research Council, Institute for the Anthropic Impacts and Sustainability in Marine Environment, Detached Unit of Capo Granitola, Trapani, Italy, [4] CNR-IAS, National Research Council, Institute for the Anthropic Impacts and Sustainability in Marine Environment, Detached Unit of Palermo, Palermo, Italy, [5] IEO-COB, Instituto Español de Oceanografía, Centro Oceanográfico de Baleares, Palma de Mallorca, Spain

Thunnus thynnus (Atlantic bluefin tuna, ABT) and other tuna species reproduce in the Mediterranean Sea during the summer period. Despite the Central Mediterranean Sea, the Strait of Sicily in particular, being a key spawning site for many tuna species, little is known on the effects of oceanographic variability on their larval distribution in this area. The abundance and presence-absence of larval specimens for three tuna species (ABT, bullet tuna and albacore) were modeled in order to examine their relationships with environmental factors, by analysing historical *in situ* information collected during seven annual surveys (2010–2016). The results revealed that most tuna larvae for the three species were found in the easternmost part of the study area, south of Capo Passero. This area is characterized by a stable saline front and warmer nutrient-poor water, and it has different environmental conditions, compared with the surrounding areas. The models used to investigate the presence-absence and abundance of the three species showed that ABT was the most abundant, followed by bullet tuna and albacore. The presence and abundance data collected are comparable with those of other spawning areas in the Mediterranean. Regarding biological and physical parameters, the results suggest that temperature, salinity, and day of the year are the key factors for understanding the ecological mechanisms and geographical distribution of these species in this area. Temperature affects the presence of ABT larvae and salinity, which, with a physical barrier effect, is a key factor for the presence-absence of bullet and albacore and for albacore abundance.

Keywords: *Thunnus thynnus, Auxis rochei*, *Thunnus alalunga*, multivariate statistical analysis, spawning, ichthyoplankton, Mediterranean Sea

OPEN ACCESS

Edited by:
Ana Rotter, National Institute of Biology (NIB), Slovenia

Reviewed by:
Benjamin Galuardi, National Oceanographic and Atmospheric Administration, Office of Habitat Conservation, Restoration Center, United States
Lorenzo Ciannelli, Oregon State University, United States
Hung-Yen Hsieh, National Dong Hwa University, Taiwan

****Correspondence:***
Marco Torri
marco.torri@ias.cnr.it
Stefania Russo
stefania.russo@ismed.cnr.it; srusso.rs@gmail.com

[†] These authors share last authorship

Specialty section:
This article was submitted to Marine Fisheries, Aquaculture and Living Resources, a section of the journal Frontiers in Marine Science

Received: *12 May 2021*
Accepted: *21 July 2021*
Published: *18 August 2021*

Citation:
Russo S, Torri M, Patti B, Reglero P, Álvarez-Berastegui D, Cuttitta A and Sarà G (2021) Unveiling the Relationship Between Sea Surface Hydrographic Patterns and Tuna Larval Distribution in the Central Mediterranean Sea. Front. Mar. Sci. 8:708775. doi: 10.3389/fmars.2021.708775

INTRODUCTION

Atlantic bluefin tuna (*Thunnus thynnus*, Linnaeus, 1758) is one of the most valuable tuna species in the world. Exploited by humans since ancient times, it has long been a valuable resource whose meat can now reach one of the highest prices in the international market (Mylonas et al., 2010; Sun et al., 2019). The International Commission for the Conservation of Atlantic Tunas (ICCAT) manages this species and considers two different stocks: the western stock whose main spawning ground is in the Gulf of Mexico (although according to new evidence spawning also occurs in the Slope Sea), and the eastern stock that spawns in the Mediterranean Sea (Muhling et al., 2017). Within the Mediterranean Sea, three main areas are well recognized, the western area located around the Balearic Islands; the central area in the Tyrrhenian Sea and around Sicily, northeast of the Gulf of Sirte, Malta, and Tunisia; and the Eastern area that comprises the Ionian Sea and the area around Cyprus (Karakulak and Yıldız, 2016; Muhling et al., 2017).

There is substantial discussion about the sub-population structure of Atlantic bluefin tuna (ABT) within the Mediterranean Sea and the occurrence of spatio-temporal mixing during spawning. The major spawning fraction is formed by large migrant adults that enter from the Atlantic Ocean following the Atlantic waters through the Strait of Gibraltar from April to May. Spawning occurs from June to July (Alemany et al., 2010; Reglero et al., 2012; Abascal et al., 2016). Some studies suggest that there is also a resident fraction of adults that remain in the Mediterranean Sea throughout the entire year or at least for a greater part of it (Cermeno et al., 2015; Livi et al., 2019). These individuals feed in different locations during the winter (Cermeno et al., 2015) depending on their ontogenetic stage (Sarà and Sarà, 2007). Although there is no conclusive scientific evidence, this resident fraction is believed to spawn in the Eastern Mediterranean and may also be in the Central Mediterranean (Cermeno et al., 2015). Migrants and residents may mix during reproductive events (Livi et al., 2019), and adult tagging data show that some individuals that remained in the Mediterranean Sea move to the Central Mediterranean during the spawning period where large migrant adults can also be found (Block et al., 2005; Fromentin, 2010). Studies to investigate the lesser-known spawning areas, such as the central Mediterranean Sea, are crucial to increase the understanding of the dynamics of the Mediterranean stock of this species. As such, questions that remain unanswered warrant attention.

The presence of larvae in the Western Mediterranean, one of the best studied spawning grounds, suggests ABT to be an environmental spawner tightly linked to the less saline Atlantic waters that enter through the Strait of Gibraltar and flow northward. There, they encounter the more saline resident water mass around the Balearic Islands, a high dynamic mesoscale area with a marked front (Alemany et al., 2010; Reglero et al., 2012; Alvarez-Berastegui et al., 2014). The Atlantic waters then enter the Strait of Sicily, flowing toward Tunisia and the South of Sicily, from west to east (García Lafuente et al., 2002; Cuttitta et al., 2004; Bonanno et al., 2014). A consecutive sampling of tuna larvae over a 3-year period has shown that the presence of tuna larvae in Tunisia is also related to this water mass (Koched et al., 2012, 2013, 2016; Zarrad et al., 2013). In contrast, little is known about the south of Sicily, an area characterized by high mesoscale variability, vortices, and meanders (García Lafuente et al., 2002) because of incoming Atlantic freshwater and warmer resident water (Robinson et al., 2001). These environmental data have not yet been analyzed with tuna larval data from oceanographic surveys in the study area.

Another common characteristic in the Balearic Islands and Tunisia is that ABT larvae are commonly found together with two other tuna species, bullet tuna (*Auxis rochei,* Risso, 1810) and albacore (*Thunnus alalunga*, Bonnaterre, 1788), suggesting that the three species have overlapping spawning grounds (Alemany et al., 2010; Koched et al., 2013). Evidence from gonad sampling suggests that the timing of spawning occurs around the same time in the Western and in the Central Mediterranean, between June and July (Heinisch et al., 2008), a pattern that is corroborated by temporal changes in the abundance of larvae (Alemany et al., 2010).

Considering these basic knowledge gaps and the apparent need for in-depth analysis, this study aims to better analyze the lesser-known central Mediterranean Sea spawning area. The objectives are to better understand the distribution and abundance of the three species and relate them to the biotic and abiotic factors of the area, thus verifying their main ecological drivers. This can enhance the knowledge of the Central Mediterranean, expanding the ecological knowledge of these species within the basin. We explored the environmental drivers affecting ABT, bullet and albacore tuna at the larval stage by analyzing presence-absence and abundance data, focusing on the early life stage.

METHODS

Field Sampling

The samples are from ichthyoplankton surveys carried out in the Strait of Sicily by the Italian National Research Council (CNR) during the summertime (June–August) from 2010 to 2016. A regular sampling grid was used ($1/10^\circ \times 1/10^\circ$ along the continental shelf, and $1/5^\circ \times 1/5^\circ$ offshore). The number of sampled sites investigated in each year, as well as the sampling period, is summarized in **Table 1**. The sites are located along transects perpendicular to the southern Sicilian coast (**Figure 1**).

Ichthyoplankton samples were collected 24 h a day, with oblique tows of a Bongo 40 net with 200 μ mesh size. It was equipped with a flow meter and towed at a ship speed of 2 knots, with a descent speed of 0.75 m/s and an ascent speed of 0.33 m/s. The net was lowered from the seabed to the surface, but sampling depths did not exceed 100 m.

The collected samples were immediately stored onboard in 70% ethanol and later processed in the land-based laboratory for identification of tuna larvae at the highest possible taxonomic level according to Rodríguez et al. (2017). Following larvae sorting, the remaining zooplankton was collected to obtain dried zooplankton weight. Water column temperature

TABLE 1 | Information on sampling strategy and statistics for the three tuna species.

Year	Sampling period	N. Sites	Species	Mean larva (m^3)	SD	Freq. of occurrence
TOT	26 June–8 August	1167	ABT	0.002	0.03	0.05
			Bullet	0.001	0.009	0.05
			Albacore	0.0004	0.003	0.02
2010	26 June–13 July	185	ABT	0.006	0.06	0.038
			Bullet	0.001	0.01	0.043
			Albacore	0	0	0
2011	9–22 July	130	ABT	0.001	0.004	0.031
			Bullet	0.004	0.021	0.1
			Albacore	0.0005	0.003	0.023
2012	5–21 July	146	ABT	0.003	0.01	0.11
			Bullet	0.003	0.01	0.11
			Albacore	0.001	0.01	0.05
2013	27 June–15 July	204	ABT	0.0009	0.005	0.039
			Bullet	0.0008	0.004	0.044
			Albacore	0.0001	0.001	0.005
2014	23 July–8 August	162	ABT	0.001	0.003	0.031
			Bullet	0.001	0.006	0.068
			Albacore	0.0004	0.003	0.031
2015	17 July–1 August	154	ABT	7.9E−05	0.001	0.006
			Bullet	1.1E−03	0.007	0.032
			Albacore	6.9E−04	0.004	0.032
2016	1–11 July	173	ABT	0.005	0.017	0.121
			Bullet	9E−05	0.001	0.006
			Albacore	0	0	0

(°C), and salinity (PSU) measurements were gathered at all sites using the multi-parameter CTD SBE 11 plus probe (underwater unit).

Data Exploration and Statistical Modeling

Mean larval densities at stations with different bottom depths were explored to identify potential spatial preferences regarding bathymetry. The distribution of observed larval presence and absence was explored using density plots. Generalized additive models (GAMs) allowed us to investigate the relationships between the spatial distribution of tuna larval specimens and environmental factors. Presence–absence data, from all the stations, and abundance data, only from positive stations, were used as dependent variables in the models. This helped determine the main covariates that control larval occurrence (calculated as the probability of presence) and the density of tuna larvae per unit area. The binomial distribution family was selected for presence–absence data and the Gamma family for abundance. To transform the catch effort for abundance, we standardized the number of larvae with the following formula:

$$CPUA = (100 * larvae/m^3) * BD$$

where CPUA is the "capture per unit area", larvae/m^3 is the number of larvae divided by the filtered water volume in m^3, and BD is the depth in meters reached by the bongo net during sampling (Alvarez-Berastegui et al., 2018). Considering the volume of filtered water and the maximum depth of the sampling gear, we were able to obtain an unbiased and normalized expression of larval density per m^2.

The first model building phase was dedicated to selecting variables that best describe the system and that were potentially useful for understanding the tuna larvae spatio-temporal distribution. This step also considered information from similar studies performed on other fish species. We started by including all the available and suitable data for the analysis, such as geographic coordinates and dissolved oxygen, but excluding stratification of the surface water, which is a typical condition characterizing the summer season in the southeastern sector of the study area, where most of the tuna larvae were found; and terrestrial runoff, because of limited drainage basin in an island such as Sicily. Finally, tidal excursion was excluded as this is very limited in the waters of the study area.

By Pearson' s correlation, the collinearity among the variables was analyzed. In case of a significant correlation between two variables, we selected the one that fitted best with the dependent variables and excluded the other. For example, longitude was positively and significantly correlated to temperature anomaly, mostly because of the upwelling in the northwestern zone (**Supplementary Material**), which, in some years, was stronger and produced lowest temperature anomaly values.

The last covariates considered in the models were: "Year" as a factor and with random effect, in order to focus the analysis on environmental relationships and not on interannual fluctuations;

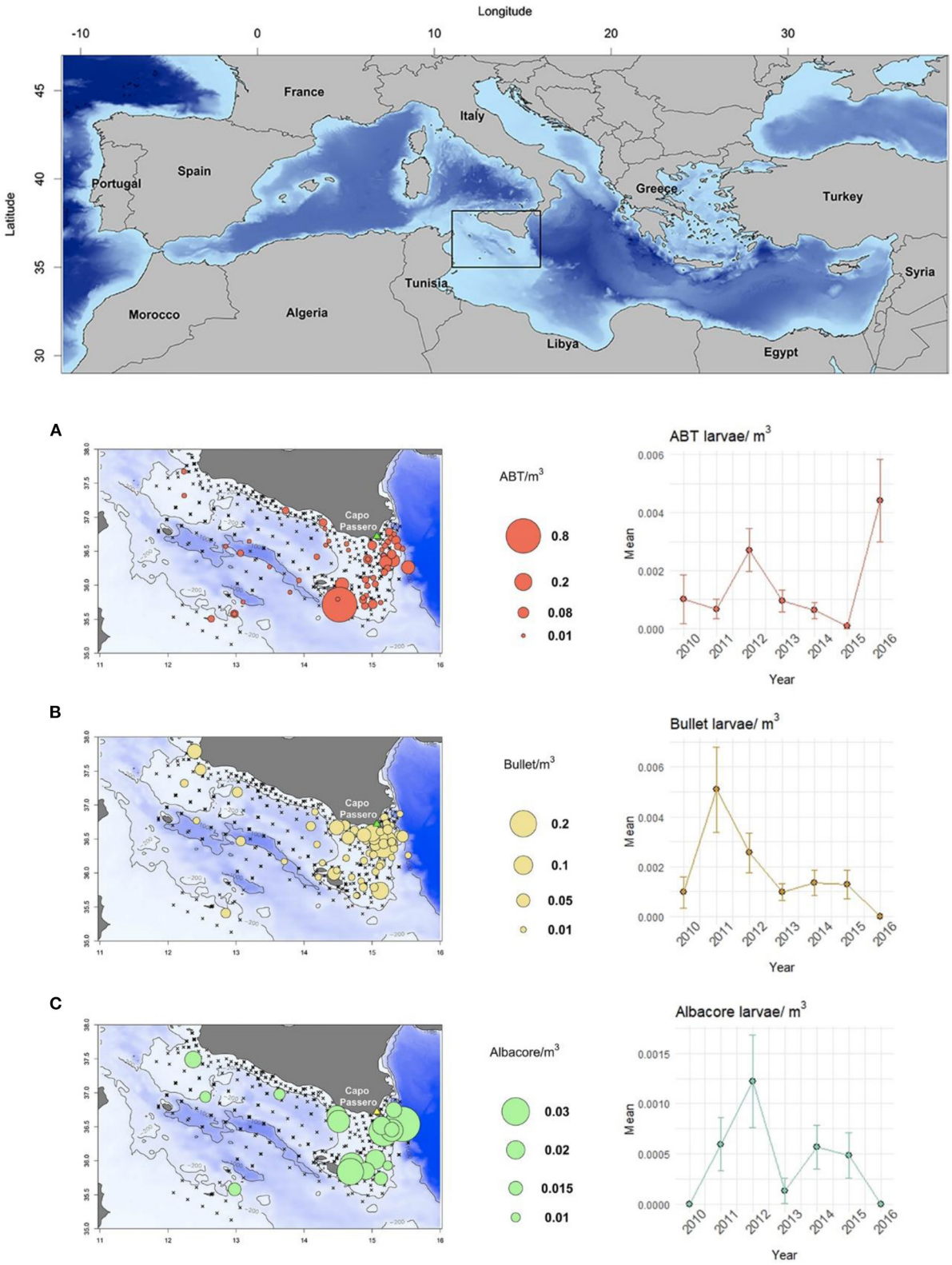

FIGURE 1 | Study area and geographical distribution of **(A)** Atlantic bluefin tuna (ABT), **(B)** bullet tuna, and **(C)** albacore tuna, and interannual changes in nominal larval densities in sites repeated annually.

surface "Salinity" (PSU) as recorded by the CTD probe at 5 m; "Day of the year," to verify the presence-absence and abundance peak, due to the temporal choice for spawning as dictated by the adults; "Zooplankton density" (standardized for the volume of filtered water, dry weight mg/Vol), to understand the role of possible food availability; "Residual of superficial temperature" (°C), calculated as the residual of a GAM, where temperature (at 5m) was fitted to the factor "Day of the year", in order to avoid the correlation between these parameters and allow for the different timing of annual surveys.

The final formulas used for the (i) presence-absence model and (ii) larval abundance model were as follows:

(*i*) $Probability\ of\ presence \sim Year + Sal. + Yearday + Zoo.\ Den. + Temp.\ residuals + Depth$

(*ii*) $CPUA \sim Year + Sal. + Yearday + Zoo.\ Den. + Temp.\ residuals + Depth$

A step-wise procedure allowed the progressive removal of non-significant covariates ($p > 0.05$), ensuring that only independent variables were used and non-significant variables were excluded. This had the effect of the most significant variables being easier to understand, removing interferences in the additive model, dictated by less significant variables.

All simulations, statistical analyses, and plotting were performed using the R statistical software (RStudio Inc, 2016). In particular, GAMs were fitted using the mgcv library (Wood, 2011).

RESULTS

Spatio-Temporal Distribution

While the three species under investigation [Atlantic bluefin tuna (ABT), bullet tuna and albacore] are commonly found in the samples (**Table 1**), other tuna and tuna-like species are sporadically found, such as *Sarda sarda*, *Euthynnus alletteratus*, and *Katsuwonus pelamis*. ABT larvae were constantly more abundant in the eastern side of the study area (between 14.5 and 15.5°E longitude) and occurred every year between Capo Passero (the southernmost tip of Sicily) and Malta Island (**Figure 1**). Similar annual abundance was found, but in 2016 there was higher average abundance (**Figure 1A**). Bullet tuna larvae had a geographical distribution similar to that of ABT annually, although they were more numerous closer to the coast and more prevalent east of longitude 15° E (**Figure 1B**). Regarding larval densities, low larval densities were found in the western part of the Strait, while higher densities were found along the eastern end of the Sicilian coast and Malta (**Figure 1B**).

Lastly, albacore, the tuna species found to have the lowest presence probabilities and abundance at positive stations, was found between 2011 and 2015 (**Figure 1C**) and in well-defined areas at the times of samplings (the shelf area between Capo Passero and Malta), with rare presence between longitudes 12 and 14° E (**Figure 1C**).

Hydrographic Conditions

Temperatures were generally warmer in the eastern zone for all the years sampled and 2010, 2013, and 2016 were the years with the coldest temperatures (**Supplementary Material**). The hottest temperature anomalies were detected in 2012, 2015, and 2016 (**Figure 2**). More marked upwellings than usual in the central-western sector were recorded in 2011, 2013, and 2014.

Salinity data showed saltier water masses in the eastern zone for all the years (**Figure 2**). A thermohaline front was found in the same area, every year, beyond 15° E of longitude.

The Zooplankton data showed oligotrophic waters every year, except for a few points with higher biomass in 2010 and general greater abundance in the western sector (**Figure 2**).

Larval Data and Environmental Factors

The mean larval density related to the bottom depth showed that the three species were distributed in areas with different bathymetric profiles (**Figure 3**). ABT was the species distributed more offshore, in areas where the bottom depth is deeper than 100 m. Bullet tuna distribution was more coastal, showing higher probabilities of presence in shallower stations (0–100 m), although individuals were found in the entire bathymetric range. Albacore was present evenly in bathymetric range deeper than 50 m. Regarding temperature, ABT larvae were present at temperatures higher than 21°C. Similarly, bullet tuna was found in waters warmer than 20.9°C, and albacore was found in waters warmer than 20°C (**Figures 4A–C**). With reference to salinity, the presence of the three species showed two peaks at around 37.5 and 38.5 (**Figures 4D–F**). The GAM analysis explored the relationship between larval distribution and putative covariate factors that may drive the presence and abundance of the three species (**Table 2**).

The presence of Atlantic bluefin tuna (ABT) was positively related to "Day of the year," "Temperature residuals," and "Year" ($p < 0.001$ for all the three variables) (**Table 2**, **Figures 5A1,A2**). The presence of ABT increased during the spawning season, reaching a maximum around day 200 (July 19th). The larvae were found in warm waters, and the probability of their presence was higher when temperatures exceeded the average temperature trends. The presence of bullet tuna was positively related to "Day of the year" ($p < 0.001$) with higher probability of finding larvae as the season advances. Regarding "Salinity" ($p < 0.05$), bullet tuna showed a flat trend of up to 38 PSU and increased from that point onward (**Figures 5B1,B2**). As seen for bullet tuna, the presence of albacore increased with the "Day of the year" ($p = 0.01$) and with "Salinity" ($p < 0.001$) (**Figures 5C1,C2**). Regarding the model used to analyze the abundance in positive stations, ABT was found to be negatively related to "Day of the year" ($p < 0.01$) (**Figure 6A**). For the bullet model, even with the stepwise procedure, none of the explanatory variables were significant. The albacore model for abundance in the positive stations showed an increasing linear trend with "Depth," a dome-shaped relation with "Salinity" with a maximum at intermediate levels; and with "Zooplankton abundance," the trend decreased until intermediate values remained constant at higher zooplankton abundances ($p < 0.05$) (**Figures 6B1–B3**). For this species, it should be considered that in the eastern sector where the larvae are more abundant, in the 2 years with greatest zooplankton abundance (2010 and 2016), we did not find

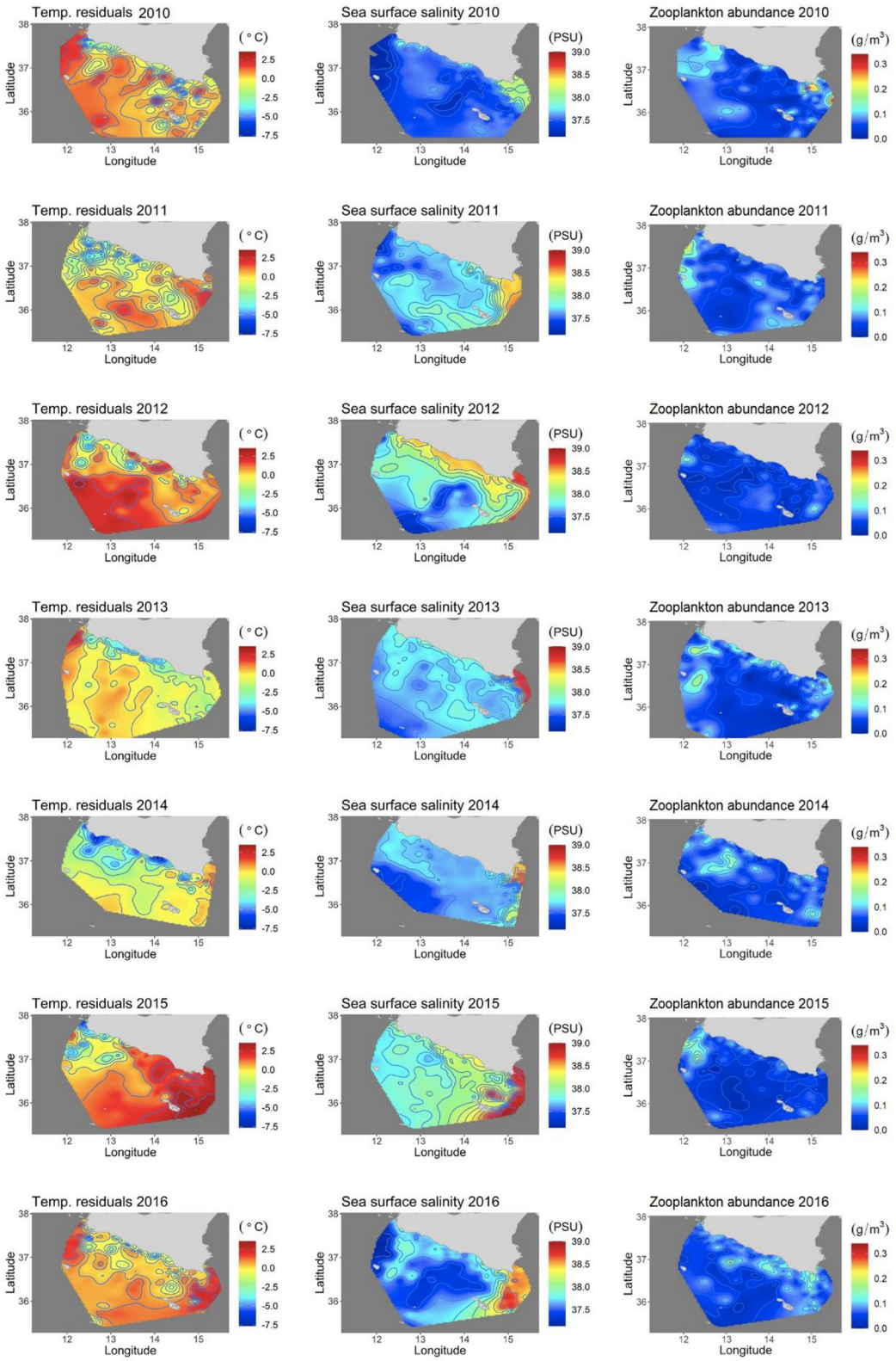

FIGURE 2 | Generalized additive model (GAM) covariates considered in the models. Temperature anomalies in the first column, salinity in the second column, and zooplankton abundance (g/m^3) in the third column.

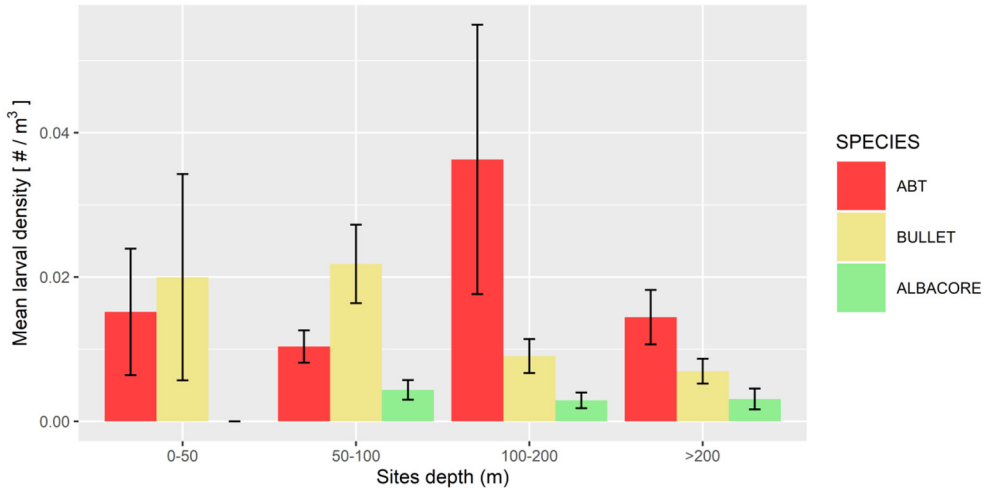

FIGURE 3 | Mean larval density (larvae/m^3) related to site depth, for the three species.

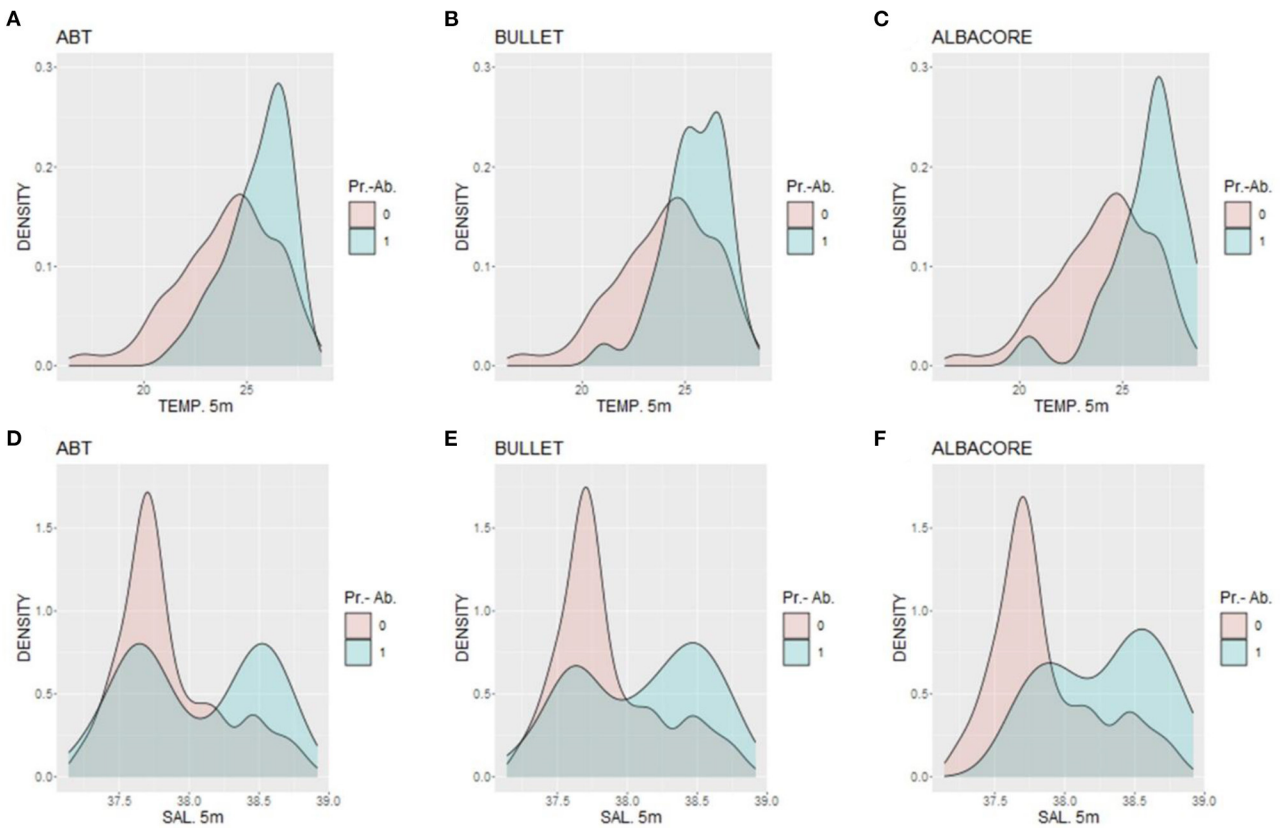

FIGURE 4 | Density of presence-absence data for the three species related to **(A–C)** temperature and **(D–F)** salinity, where 0 is absence and 1 is presence.

albacore larvae. It is also necessary to consider that there are very few events of large zooplankton abundance and that from the low to medium abundance that has been detected, the effect on albacore abundance decreases (**Figure 6B2**).

DISCUSSION

The results indicate that the central Mediterranean Sea, in particular the Strait of Sicily, is a significant larval habitat for

TABLE 2 | GAM output analysis with significance value (0 '***'; 0.001 '**'; 0.01 '*'; 0.05 '.'; > 0.05 '–').

Presence absence	Res temp.	Sal.	Zoo.	Year	Depth	Year Day	Deviance explained
ABT	***	–	–	***	–	***	19.3%
BULLET	–	*	–	***	–	***	15.7%
ALBACORE	–	***	–	–	–	*	13.9%
Larval abundance	**Res temp.**	**Sal.**	**Zoo.**	**Year**	**Depth**	**Year Day**	**Deviance explained**
ABT	–	–	–	–	–	**	14%
BULLET	–	–	–	–	–	–	–
ALBACORE	–	*	*	–	*	–	59.7%

the three tuna species considered in this study. ABT and bullet were generally more abundant than albacore, the latter having not been caught in two of the years during the sampling time series. Therefore, there is a temporal-spatial overlap during the early life stages of these species. Temperature, salinity, and day of the year emerged as key variables to better understand the spatio-temporal distribution of larval habitats of these species in the area.

Tuna larvae were found in the eastern side of the Strait, where surface water temperatures were found to be consistently warmer than those of the surrounding areas. The GAM results on the presence-absence of ABT larvae show that the day of the year is highly significant, with a dome-shaped relationship reaching a maximum at around day 200, corresponding to the beginning of the second half of July. Tuna species are found in waters above 22°C, and the timings are consistent with studies carried out in the Western Mediterranean (e.g., Alemany et al., 2010; Reglero et al., 2012) and south of the Central Mediterranean (e.g., Kached et al., 2013; Zarrad et al., 2013). The results reinforce the idea that tuna eggs and larvae are mainly found in oceanic waters and are constrained by temperatures above 20°C, at which they can develop and survive (Reglero et al., 2014). In the study area, we also found some larvae in the August period, suggesting that some adults may have spawned outside the common spawning period, when temperatures are still suitable for egg-hatching.

There was a higher probability of finding larvae at stations where the temperature was higher than the average temperature for that day. Adults can choose where to spawn and may choose to spawn when and where temperatures are favorable for the development of their larvae. ABT have very high fecundity and are multiple batch spawners (Ciannelli et al., 2015). While they are in the spawning grounds, they have a very fast ovarian development and oocyte maturation that is propelled by the presence of increasing warming water, which poses an evolutionary constraint on the spawning locations (Ciannelli et al., 2015). The results suggest that the moment in which adults choose to spawn increases up to mid-July and then decreases. Interestingly, in the study area, we also found some larvae during August. This indicates that some adults have spawned outside the common peak period. The reproductive success of these events that occur later in the year is not known. These smaller ABT that spawned later in the year might be found by larger conspecific larvae that spawned during previous spawning events. If these larger larvae have reached the piscivorous phase, they might feed on their conspecifics and carry out cannibalism (Reglero et al., 2011). As Bongo-40 nets that predominantly catch small larvae were used, statistical analyses on the difference in size distribution across the seasons and/or stations were not possible.

Regarding salinity, the minimum, maximum, and mean values recorded in the stations are typical of the study area, characterized by the confluence of Atlantic waters with Eastern Mediterranean waters in the Ionian Sea. In fact, we have detected a strong variation in salinity values, corresponding to a key oceanographic structure, the saline front in the south of Capo Passero, to the east of the study area. This structure appears to be stable during the summer period, confirming previous observations (Patti et al., 2010; Bonanno et al., 2014; Cuttitta et al., 2016). Across the front the larval occurrence is higher, and this is evident for the three species that show two presence peaks related to salinity. Larvae originating from the spawning activity in the southeastern sector of the study area accumulate with larvae advected by the Atlantic waters from the offshore western area, causing the higher concentrations observed in the retention area for the three species investigated. In the same area, this advection mechanism has also been verified for other species in previous studies (García Lafuente et al., 2002; Cuttitta et al., 2018; Patti et al., 2018). So, definitively the dynamics of this frontal area seems to play a key role for larval retention in the eastern zone. This hypothesis has been confirmed by the GAM models, as bullet and albacore tuna showed a higher probability of presence at higher salinity. This is not dictated by physiological constraints but by a purely physical factor. The different densities of the two water masses where we find higher larvae presence and the presence of the saline front every year suggest that this oceanographic structure works as a physical barrier, concentrating the tuna larvae. Geostrophy and associated surface currents play a key role in determining the fate of the early life stage, and Capo Passero assumes an important function as a retention area for eggs and larvae, not only for tuna but also for other species that gather from the northwest, resulting from along-shore advection (Torri et al., 2018; Patti et al., 2020).

Atlantic bluefin tuna (ABT) larvae were absent in the western sector. This area is characterized by coastal upwelling zones due to mistral winds that induce offshore Ekman transport of surface

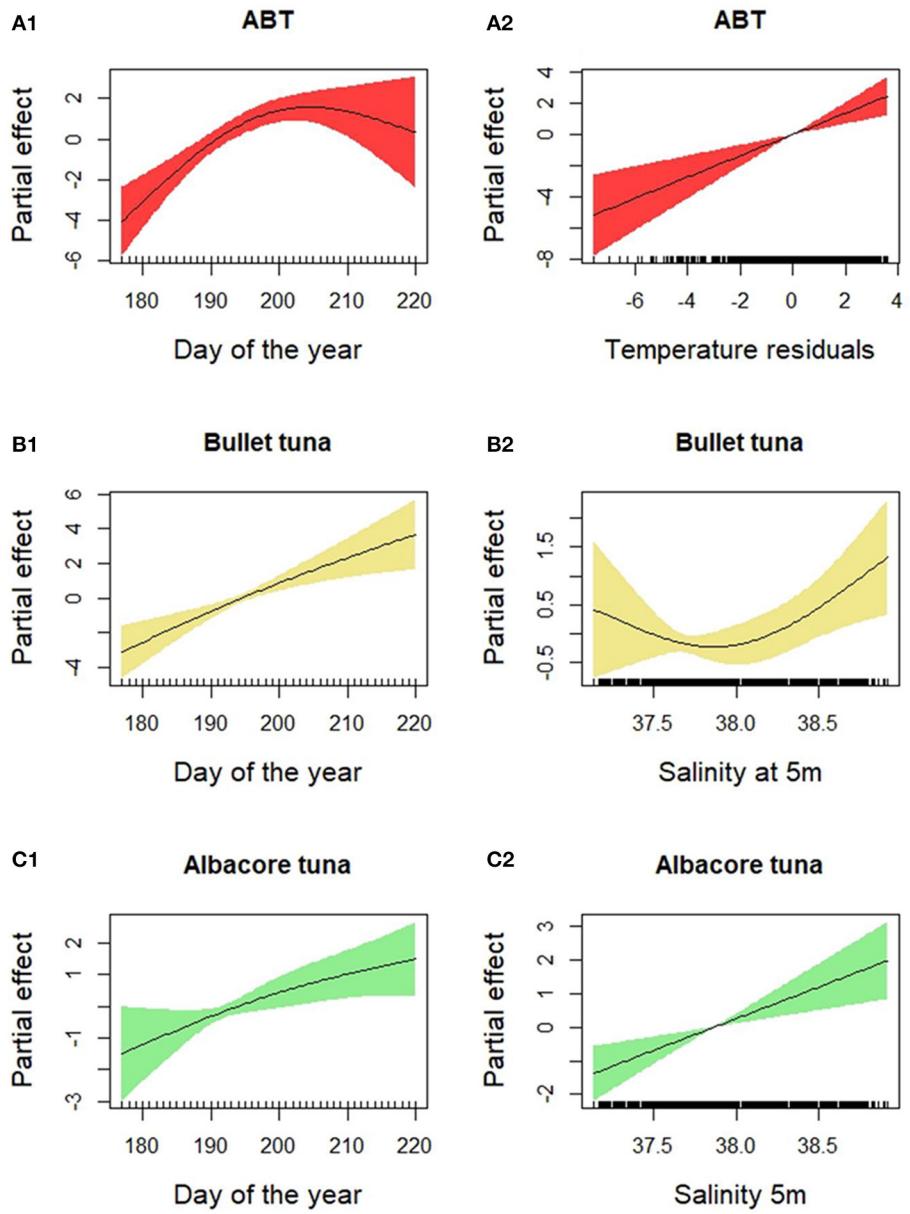

FIGURE 5 | Results of the generalized additive presence-absence models for **(A1,A2)** bluefin tuna, **(B1,B2)** bullet tuna, and **(C1,C2)** albacore tuna.

waters, causing the upwelling of cold and nutrient-rich water masses (Patti et al., 2010; Torri et al., 2018). In general, tuna larvae are found in oligotrophic areas, probably as a strategy to encounter fewer predators (Bakun, 2013). Despite the eastern area being less productive than the western area, local enrichment processes such as cold filaments from the upwelling zone together with the thermohaline front and eddies could concentrate prey, improving feeding opportunities (Cuttitta et al., 2016, 2018; Torri et al., 2018). These oceanographic processes could create patches of higher food abundance that, together with scarcity of predators, could increase the chances of larval survival.

It was not possible to depict the reproductive peak of bullet and albacore tuna in this study, since the data suggest that the spawning window of bullet is longer than the timing of the surveys (Allaya et al., 2013). This is demonstrated by the "Day of the year" results. The bullet tuna reproductive strategy is based on a protracted spawning behavior, compared with ABT. Concerning bullet tuna abundance, the lack of significant variables in the applied model highlights how the larvae of this species are heterogeneously distributed within the study area (**Figure 1B**). We chose to implement a unified model approach for the three species, both for presence-absence and

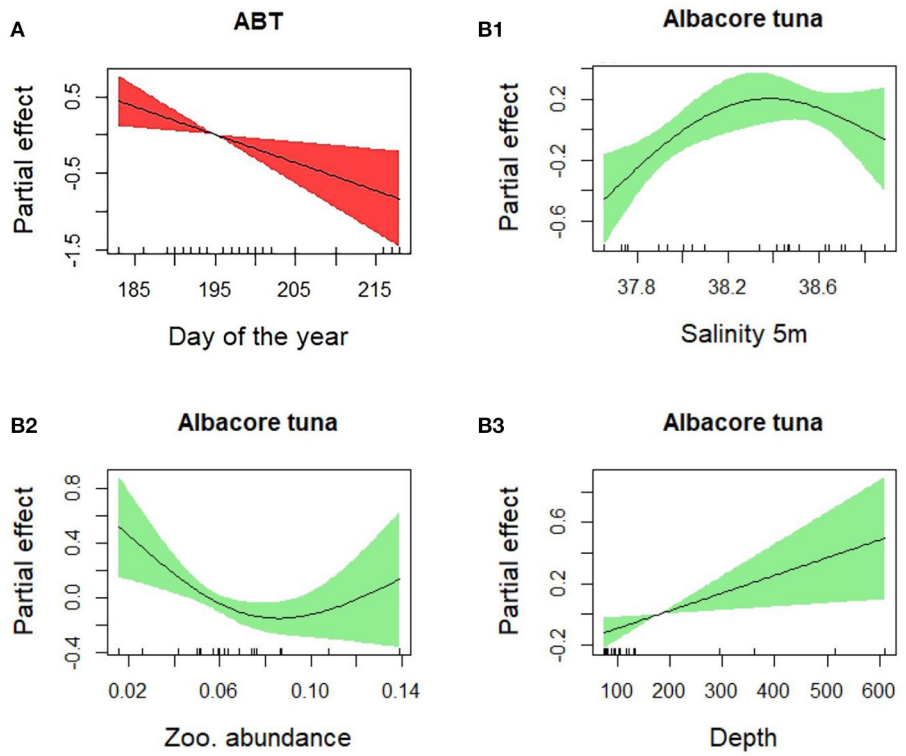

FIGURE 6 | Results of the generalized additive abundance models for **(A)** bluefin tuna and **(B1, B2, B3)** albacore tuna.

abundance, but clearly, each species has its own peculiarities, and the results suggest the need for further species-specific studies. Moreover, because of the complex nature of the ecological data, low values of explained deviance are common, also considering that other environmental variables, not available for this study, could potentially be useful to improve the knowledge of larval distribution.

CONCLUSION

The study area located in the center of the Mediterranean Sea, with direct influence of Atlantic and Levantine waters, creates unique environmental conditions selected as optimal spawning grounds by different tuna species as has been observed for other species (Falcini et al., 2020; Mangano et al., 2020; Patti et al., 2020). In this study, similarities with other well-characterized spawning grounds in the Central and Western Mediterranean were highlighted, where the three selected tuna species also coexist (Alemany et al., 2010; Koched et al., 2013). This study targets the lesser-known central Mediterranean Sea spawning area, revealing that temperature, salinity, and day of the year were the main variables driving tuna larval geographical distribution. However, the lack of a long time series in the region and the different sampling methods in the area compared with the other areas made the detection of significant temporal trends in the observed patterns difficult. As such, this study has given some interesting insights and paves the way for future studies on the impact of environmental variability on the interannual fluctuations in the abundance of these species and in their reproductive success in the Central Mediterranean Sea.

More research in the Central Mediterranean tuna spawning grounds is needed to understand its role compared with other areas in the Mediterranean Sea. It is also possible that there is a spatio-temporal mixing in spawning grounds between the two ABT Mediterranean sub-populations. The crucial issue of the ABT Mediterranean stock structure remains inconclusive. The results could indicate a reproductive event or multiple reproductive events, resulting from Atlantic or resident ABT, or both. We still need to know more about this area, as we still do not know the larval origin and if the larvae come from the resident adult fraction or not. By studying these lesser-known spawning areas, we wanted to take the first step, laying the foundations, to fill critical gaps in the understanding of the unique dynamics of the Mediterranean stock for these species that, to date, have remained unanswered.

DATA AVAILABILITY STATEMENT

The raw data supporting the conclusions of this article will be made available by the authors, without undue reservation.

AUTHOR CONTRIBUTIONS

SR, AC, and GS contributed to the conception and design of the study. MT, BP, and AC carried out the sampling. SR, AC, and PR taxonomic identification. SR, MT, and BP organized the database. SR, MT, DAB, and PR performed the statistical analysis. SR wrote the first draft of the manuscript. GS and AC secured funding. All authors contributed to manuscript revision, read, and approved the submitted version.

FUNDING

Fondo Sociale Europeo Sicilia 2020 supported SR's PhD research presented in this study. Data collection was mainly supported by the Italian National Research Council (CNR) through the USPO office, and by the FAO Regional Project MedSudMed Assessment and Monitoring of the Fishery Resources and the Ecosystems in the Straits of Sicily, funded by the Italian Ministry MIPAAF and co-funded by the Directorate-General for Maritime Affairs and Fisheries of the European Commission (DG MARE). Sampling activity was also supported by other research projects, namely, Grandi Pelagici, funded by the Sicilian Regional Government, and SSD-PESCA and the Flagship Project RITMARE—The Italian Research for the Sea—coordinated by the Italian National Research Council and funded by the Italian Ministry of Economic Development and the Italian Ministry of Education, University and Research within the National Research Program 2011–2013.

ACKNOWLEDGMENTS

We thank all the CNR and IEO-COB technicians for the support during species identification, especially Melissa Martin Quetglas and the PhD students (Catalina Mena Oliver and Daniel Ottmann Riera) for the help during preliminary data exploration, Dr. Luigi Giaramita and Carlo Patti for their support during oceanographic surveys and sampling collection. We thank Francisco J. Alemany, Walter Ingram, Lorenzo Ciannelli, and Hanane Elyaagoubi for their helpful comments on the preliminary study. We thank Mr. Emanuele Gentile, master of the R/V Urania and R/V Minerva Uno, and his crew for their work in support of plankton sampling during oceanographic cruises.

SUPPLEMENTARY MATERIAL

The Supplementary Material for this article can be found online at: https://www.frontiersin.org/articles/10.3389/fmars.2021.708775/full#supplementary-material

REFERENCES

Abascal, F. J., Medina, A., De la Serna, J. M., Godoy, D., and Aranda, G. (2016). Tracking Bluefin tuna reproductive migration into the Mediterranean Sea with electronic pop-up satellite archival tags using two tagging procedures. *Fish. Oceanogr.* 25, 54–66. doi: 10.1111/fog.12134

Alemany, F., Quintanilla, L., Velez-Belchí, P., García, A., Cortés, D., Rodríguez, J. M., et al. (2010). Characterization of the spawning habitat of Atlantic Bluefin tuna and related species in the Balearic Sea (western Mediterranean). *Prog. Oceanogr.* 86, 21–38. doi: 10.1016/j.pocean.2010.04.014

Allaya, H., Hattour, A., Hajjej, G., and Trabelsi, M. (2013). Some biological parameters of the bullet tuna *Auxis rochei* (Risso, 1810) in Tunisian waters. *Cah. Biol. Mar.* 54, 287–292. doi: 10.21411/CBM.A.8CBA0364

Alvarez-Berastegui, D., Ciannelli, L., Aparicio-Gonzalez, A., Reglero, P., Hidalgo, M., López-Jurado, J. L., et al. (2014). Spatial scale, means and gradients of hydrographic variables define pelagic seascapes of bluefin and bullet tuna spawning distribution. *PLoS ONE* 9:e109338. doi: 10.1371/journal.pone.0109338

Alvarez-Berastegui, D., Saber, S., Ingram Jr, G. W., Díaz-Barroso, L., Reglero, P., Macías, D., et al. (2018). Integrating reproductive ecology, early life dynamics and mesoscale oceanography to improve albacore tuna assessment in the Western Mediterranean. *Fish. Res.* 208, 329–338. doi: 10.1016/j.fishres.2018.08.014

Bakun, A. (2013). Ocean eddies, predator pits and bluefin tuna: implications of an inferred 'low risk–limited payoff'reproductive scheme of a (former) archetypical top predator. *Fish Fish.* 14, 424–438. doi: 10.1111/faf.12002

Block, B. A., Teo, S. L., Walli, A., Boustany, A., Stokesbury, M. J., Farwell, C. J., et al. (2005). Electronic tagging and population structure of Atlantic Bluefin tuna. *Nature* 434, 1121–1127. doi: 10.1038/nature03463

Bonanno, A., Placenti, F., Basilone, G., Mifsud, R., Genovese, S., Patti, B., et al. (2014). Variability of water mass properties in the Strait of Sicily in summer period of 1998–2013. *Ocean Sci.* 10, 759–770. doi: 10.5194/os-10-759-2014

Cermeno, P., Quilez-Badia, G., Ospina-Alvarez, A., Sainz-Trápaga, S., Boustany, A. M., Seitz, A. C., et al. (2015). Electronic tagging of Atlantic Bluefin tuna (*Thunnus thynnus* L.) reveals habitat use and behaviors in the Mediterranean Sea. *PLoS ONE* 10:e0116638. doi: 10.1371/journal.pone.0116638

Ciannelli, L., Bailey, K., and Olsen, E. M. (2015). Evolutionary and ecological constraints of fish spawning habitats. *ICES J. Mar. Sci.* 72, 285–296. doi: 10.1093/icesjms/fsu145

Cuttitta, A., Arigo, A., Basilone, G., Bonanno, A., Buscaino, G., Rollandi, L., et al. (2004). Mesopelagic fish larvae species in the Strait of Sicily and their relationships to main oceanographic events. *Hydrobiologia* 527, 177–182. doi: 10.1023/B:HYDR.0000043299.65829.2f

Cuttitta, A., Quinci, E. M., Patti, B., Bonomo, S., Bonanno, A., Musco, M., et al. (2016). Different key roles of mesoscale oceanographic structures and ocean bathymetry in shaping larval fish distribution pattern: a case study in Sicilian waters in summer 2009. *J. Sea Res.* 115, 6–17. doi: 10.1016/j.seares.2016.04.005

Cuttitta, A., Torri, M., Zarrad, R., Zgozi, S., Jarboui, O., Quinci, E. M., et al. (2018). Linking surface hydrodynamics to planktonic ecosystem: the case study of the ichthyoplanktonic assemblages in the Central Mediterranean Sea. *Hydrobiologia* 821, 191–214. doi: 10.1007/s10750-017-3483-x

Falcini, F., Corrado, R., Torri, M., Mangano, M. C., Zarrad, R., Di Cintio, A., et al. (2020). Seascape connectivity of European anchovy in the Central Mediterranean Sea revealed by weighted Lagrangian backtracking and bio-energetic modelling. *Sci. Rep.* 10, 1–13. doi: 10.1038/s41598-020-75680-8

Fromentin, J. M. (2010). Tagging Bluefin tuna in the Mediterranean Sea: challenge or mission: impossible. *Collect. Vol. Sci. Pap. ICCAT* 65, 812–821.

García Lafuente, J., García, A., Mazzola, S., Quintanilla, L., Delgado, J., Cuttitta, A., et al. (2002). Hydrographic phenomena influencing early life stages of the Sicilian Channel anchovy. *Fish. Oceanogr.* 11, 31–44. doi: 10.1046/j.1365-2419.2002.00186.x

Heinisch, G., Corriero, A., Medina, A., Abascal, F. J., De La Serna, J. M., Vassallo-Agius, R., et al. (2008). Spatial–temporal pattern of bluefin tuna (*Thunnus thynnus* L. 1758) gonad maturation across the Mediterranean Sea. *Mar. Biol.* 154(4), 623-630. doi: 10.1007/s00227-008-0955-6

Karakulak, F. S., and Yıldız, T. (2016). "Atlantic Bluefin Tuna in the Mediterranean Sea: Fisheries, Farming, Management and Conservation," in *The Turkish Part of The Mediterranean Sea Marine Biodiversity Fisheries Conservation and Governance*, eds C. Turan, B. Salihoğlu, E. O. Özbek, and B. Öztürk (Istanbul: The Turkish Marine Research Foundation (TUDAV) Press), 595, 320–332.

Koched, W., Alemany, F., Rimel, B., and Hattour, A. (2016). Characterization of the spawning area of tuna species on the northern Tunisian coasts. *Sci. Mar.* 80, 187–198. doi: 10.3989/scimar.04332.27A

Koched, W., Hattour, A., Alemany, F., Garcia, A., and Said, K. (2013). Spatial distribution of tuna larvae in the Gulf of Gabes (Eastern Mediterranean) in relation with environmental parameters. *Mediterr. Mar. Sci.* 14, 5–14. doi: 10.12681/mms.314

Koched, W., Hattour, A., Alemany, F., Zarrad, R., and García-García, A. (2012). Distribution of tuna larvae in Tunisian east coasts and its environmental scenario. *Cah. Biol. Mar.* 53, 505–515. doi: 10.21411/CBM.A.763B5CD1

Livi, S., Romeo, T., De Innocentiis, S., Greco, C., Battaglia, P., Marino, G., et al. (2019). The genetic population structure of Thunnus thynnus (Linnaeus, 1758) in the Mediterranean Sea, a controversial issue. *J. Appl. Ichthyol.* 35, 436–443. doi: 10.1111/jai.13867

Mangano, M. C., Mieszkowska, N., Helmuth, B., Domingos, T., Sousa, T., Baiamonte, G., et al. (2020). Moving toward a strategy for addressing climate displacement of marine resources: a proof-of-concept. *Front. Mar. Sci.* 7: 408. doi: 10.3389/fmars.2020.00408

Muhling, B. A., Lamkin, J. T., Alemany, F., García, A., Farley, J., Ingram, G. W., et al. (2017). Reproduction and larval biology in tunas, and the importance of restricted area spawning grounds. *Rev. Fish Biol. Fish.* 27, 697–732. doi: 10.1007/s11160-017-9471-4

Mylonas, C. C., De La Gándara, F., Corriero, A., and Ríos, A. B. (2010). Atlantic Bluefin tuna (*Thunnus thynnus*) farming and fattening in the Mediterranean Sea. *Reviews in Fisheries Science* 18, 266–280. doi: 10.1080/10641262.2010.509520

Patti, B., Guisande, C., Bonanno, A., Basilone, G., Cuttitta, A., and Mazzola, S. (2010). Role of physical forcings and nutrient availability on the control of satellite-based chlorophyll a concentration in the coastal upwelling area of the Sicilian Channel. *Sci. Mar.* 74, 577–588. doi: 10.3989/scimar.2010.74n3577

Patti, B., Torri, M., and Cuttitta, A. (2020). General surface circulation controls the interannual fluctuations of anchovy stock biomass in the Central Mediterranean Sea. *Sci. Rep.* 10:1554. doi: 10.1038/s41598-020-58028-0

Patti, B., Zarrad, R., Jarboui, O., Cuttitta, A., Basilone, G., Aronica, S., et al. (2018). Anchovy (*Engraulis encrasicolus*) early life stages in the Central Mediterranean Sea: connectivity issues emerging among adjacent sub-areas across the Strait of Sicily. *Hydrobiologia* 821, 25–40. doi: 10.1007/s10750-017-3253-9

Reglero, P., Ciannelli, L., Alvarez-Berastegui, D., Balbín, R., López-Jurado, J. L., and Alemany, F. (2012). Geographically and environmentally driven spawning distributions of tuna species in the western Mediterranean Sea. *Mar. Ecol. Prog. Ser.* 463, 273–284. doi: 10.3354/meps09800

Reglero, P., Tittensor, D. P., Álvarez-Berastegui, D., Aparicio-González, A., and Worm, B. (2014). Worldwide distributions of tuna larvae: revisiting hypotheses on environmental requirements for spawning habitats. *Mar. Ecol. Prog. Ser.* 501, 207–224.

Reglero, P., Urtizberea, A., Torres, A. P., Alemany, F., and Fiksen, Ø. (2011). Cannibalism among size classes of larvae may be a substantial mortality component in tuna. *Mar. Ecol. Prog. Ser.* 433, 205–219. doi: 10.3354/meps09187

Robinson, A. R., Leslie, W. G., Theocharis, A., and Lascaratos, A. (2001). Mediterranean Sea circulation. *Ocean Curr.* 1:19. doi: 10.1016/B978-012374473-9.00376-3

Rodríguez, J. M., Alemany, F., and Garcia, A. (2017). *A Guide to the Eggs and Larvae of 100 Common Western Mediterranean Sea Bony Fish Species*. Rome: FAO.

RStudio Inc (2016). *RStudio: Integrated Development for R*. Boston, MA. Available online at: http://www.rstudio.com/ (accessed November 12, 2018).

Sarà, G., and Sarà, R. (2007). Feeding habits and trophic levels of bluefin tuna Thunnus thynnus of different size classes in the Mediterranean Sea. *J. Appl. Ichthyol.* 23, 122–127. doi: 10.1111/j.1439-0426.2006.00829.x

Sun, C. H., Chiang, F. S., Squires, D., Rogers, A., and Jan, M. S. (2019). More landings for higher profit? Inverse demand analysis of the Bluefin tuna auction price in Japan and economic incentives in global Bluefin tuna fisheries management. *PLoS ONE* 14:e0221147. doi: 10.1371/journal.pone.0221147

Torri, M., Corrado, R., Falcini, F., Cuttitta, A., Palatella, L., Lacorata, G., et al. (2018). Planktonic stages of small pelagic fishes (*Sardinella aurita* and *Engraulis encrasicolus*) in the central Mediterranean Sea: the key role of physical forcings and implications for fisheries management. *Prog. Oceanogr.* 162, 25–39. doi: 10.1016/j.pocean.2018.02.009

Wood, S. N. (2011). Fast stable restricted maximum likelihood and marginal likelihood estimation of semiparametric generalized linear models. *J. R. Stat. Soc. Ser. B Stat. Methodol.* 73, 3–36. doi: 10.1111/j.1467-9868.2010.00749.x

Zarrad, R., Alemany, F., Rodriguez, J. M., Jarboui, O., Lopez-Jurado, J. L., and andBalbin, R. (2013). Influence of summer conditions on the larval fish assemblage in the eastern coast of Tunisia (Ionian Sea, Southern Mediterranean). *J. Sea Res.* 76, 114–125. doi: 10.1016/j.seares.2012.08.001

Conflict of Interest: The authors declare that the research was conducted in the absence of any commercial or financial relationships that could be construed as a potential conflict of interest.

Publisher's Note: All claims expressed in this article are solely those of the authors and do not necessarily represent those of their affiliated organizations, or those of the publisher, the editors and the reviewers. Any product that may be evaluated in this article, or claim that may be made by its manufacturer, is not guaranteed or endorsed by the publisher.

frontiers in Marine Science

ORIGINAL RESEARCH
published: 25 February 2022
doi: 10.3389/fmars.2022.849092

Effects of Interannual Environmental Changes on Juvenile Fish Settlement in Coastal Nurseries: The Case of the Adriatic Sea

Sanja Matić-Skoko[1], Dario Vrdoljak[1], Hana Uvanović[1], Mišo Pavičić[1], Pero Tutman[1], Dubravka Bojanić Varezić[1] and Marcelo Kovačić[2]*

[1] *Institute of Oceanography and Fisheries, Split, Croatia,* [2] *Natural History Museum Rijeka, Rijeka, Croatia*

This study tested generality in the settlement and recruitment patterns of juvenile fish in the coastal Mediterranean as driven by interannual environmental differences. A multivariate analysis of juvenile fish community data, sampled over three consecutive years, was conducted to elucidate the interannual changes of new settlers' occurrence and abundance in different nurseries along the eastern Adriatic coast. Sites were assigned to four groups of nurseries based on water type (marine or transitional) and geographical position (north or south). Statistically significant interannual differences were found in temperature but not in salinity. In general, species occurrence significantly fluctuated between years and seasons. The highest total abundance of juveniles was observed in the significantly warmer year 2018 within all study groups. Defined groups expressed significant annual differences in species richness and abundance related to variations in water temperature and salinity as environmental factors for the same consecutive years. Nurseries within transitional waters in the north are more prone to interannual water temperature changes. The associated community composition differed most from those recorded in southern marine waters, where groups were mostly defined by salinity influence and were least sensitive to interannual temperature fluctuations. The cold and rainy spring in 2019 caused late settlement and longer retention of specific economically and ecologically important fish species in the nurseries. The results suggested that settlers' delay or retention due to negative temperature deviation in the spawning period were linked to the nurseries located in the northern transitional waters that are under a stronger coastal influence. These delays can have ecological consequences on population dynamics and on inter- and intraspecific relationships within specific nursery communities.

Keywords: juvenile fish, community, settlement, nurseries, interannual changes

OPEN ACCESS

Edited by:
Stylianos Somarakis, Institute of Marine Biological Resources and Inland Waters, Hellenic Center for Marine Research, Greece

Reviewed by:
Francesco Tiralongo, University of Catania, Italy
Stefanos Kalogirou, Swedish Agency for Marine and Water Management, Sweden

****Correspondence:***
Sanja Matić-Skoko
sanja@izor.hr

Specialty section:
This article was submitted to Marine Fisheries, Aquaculture and Living Resources, a section of the journal Frontiers in Marine Science

Received: *05 January 2022*
Accepted: *27 January 2022*
Published: *25 February 2022*

Citation:
Matić-Skoko S, Vrdoljak D, Uvanović H, Pavičić M, Tutman P, Bojanić Varezić D and Kovačić M (2022) Effects of Interannual Environmental Changes on Juvenile Fish Settlement in Coastal Nurseries: The Case of the Adriatic Sea. Front. Mar. Sci. 9:849092. doi: 10.3389/fmars.2022.849092

INTRODUCTION

Coastal areas are commonly acknowledged as highly productive and valuable ecosystems that provide many favourable habitats for fish, while also supporting fundamental ecological links with other environments (Duarte, 2000; Beck et al., 2001; Hinz et al., 2019). Their role in early life stages, and also as foraging and spawning grounds for non-coastal fish species (Harmelin-Vivien, 1984;

Francour et al., 1999) is recognised throughout the Mediterranean and worldwide (Francour, 1997; Deudero et al., 2008). There is ambiguous evidence for the importance of habitat characteristics in driving patterns of population dynamics (Vasconcelos et al., 2013). Highly valuable habitats generally provide shelter and an abundance of food to juveniles that may facilitate their survival and growth processes, thus contributing to overall production and population stability (Scharf et al., 2006; Dahlgren and Eggleston, 2014; Cheminée et al., 2016). Knowing the role of habitat use is particularly valuable from a conservation and management perspective, since the vulnerability of coastal habitats to anthropogenic stressors is increasing (Sala, 2004; Halpern et al., 2008; Sala et al., 2012). Marine ecosystems have been degraded in many areas, particularly in the Mediterranean, and many critical coastal habitats are no longer available or adequate to provide nursery, feeding, or reproductive functions, with negative consequences on production and renewal of populations (Guidetti et al., 2002; Barbier et al., 2011; Matić-Skoko et al., 2020).

Population dynamics, as a complex process including reproduction, growth, survival, and demographic rates, are under environmental influences (Vasconcelos et al., 2013) and therefore they are reflected in the fisheries dynamics of exploited species (Hixon and Johnson, 2009). However, the variability of spawning success and the relationship between spawning and recruitment are among the least understood aspects of fish population dynamics. The process starts with the transition between pelagic and benthic stages (Brothers et al., 1983). Settler supply and nursery habitat availability are key factors affecting settlement and recruitment processes, determining the renewal of populations and shaping the structure of adult assemblages (Cheminee et al., 2011). In the Mediterranean, a variety of fish species inhabit coastal nurseries, some of them for life while others just for a part of life (Dulčić et al., 2007; La Mesa et al., 2011; Félix-Hackradt et al., 2014; Cheminée et al., 2017).

Settlement of juvenile fishes occurs year-round, though most species have a settlement peak between early spring and late summer (García-Rubies and Macpherson, 1995; Dulčić et al., 1997, 2007; Biagi et al., 1998). Specific settlers often have strict microhabitat requirements for potential nurseries. After settling until recruitment, their survival within a habitat largely depends on the environmental conditions encountered at the site of settlement (Beck et al., 2001). This makes temperature, salinity and bottom depth preferences even more important when choosing a nursery area. Global warming or climate change has driven significant changes in marine ecosystems in recent decades, particularly in coastal areas facing compositional and structural changes. Specifically, alterations in species distributions and ranges, composition of species assemblages, and biodiversity have all been convincingly linked to rising temperatures (Bellard et al., 2012; Doney et al., 2012) in regions where climate change has substantially altered the physical environment (see Barceló et al., 2016 and references therein). These are the main biological responses to temperature and salinity as factors of environmental modifications. Generally, changes in growth rates, shifts in the spawning season, and shifts in the spawning area (latitude) are expected after a rise in sea temperature due to global warming. Recently, shifts in the physical and biological regimes of the Adriatic Sea were connected with the climate change in the northern hemisphere (Grbec et al., 2015). Matić-Skoko et al. (2020) highlighted the importance of investigating temporal changes in littoral juvenile fish assemblages through responses to environmental factors as important causal factors of habitat modifications due to climate change. These responses represent the environmental tolerances of individual species (Martins et al., 2019). Further, the absence or occurrence of certain species may be a signal of a poleward shift in the spawning area and a temporal shift in spawning timing to avoid higher temperatures (Shoji et al., 2011).

Previous studies have generally focused on the intrinsic ecological functions of microhabitats at a local scale, e.g., for sparids along the rocky shore of Marseilles (NW Mediterranean) (Cheminee et al., 2011). The whole eastern Adriatic coast represents a mosaic of different coastal nurseries, from coastal lagoons to shallow, semi-closed coves with varying annual influence of freshwater springs, which is highest in the winter-spring period after snow melt and intensive rain (Novosel et al., 2005). These coves were previously identified as having higher fish species richness (Dulčić et al., 1997) than coastal lagoons, due to the wide connection with the sea that favours the inflow of fish eggs, larvae and young of-the-year by the tides and currents from spawning areas (Blaber et al., 1995; Potter et al., 2010; Araújo et al., 2016). However, the extent of interannual differences in settler supply along the coast and across different habitats is unknown, and little is also known about which habitats and consequently which fish species are most sensitive to such changes. Several hypotheses have thus been defined for the main aims of this study: (1) there are significant interannual variations in species presence and species abundance of settled juvenile fish along the eastern Adriatic coast, (2) different habitat types (related to water type and geographical position) respond differently to interannual changes of environmental factors, and (3) estuarine nursery areas are more susceptible to such changes than marine ones. The present study aims to further understand the relative importance of interannual changes of environmental parameters and nursery attributes at different spatial scales in settlement and post-settlement processes and how they influence recruitment level.

MATERIALS AND METHODS

Sampling Procedure

Sampling on a seasonal basis (March, June, September, and December) was conducted in three consecutive years (2017, 2018, and 2019) at 20 sites (**Table 1** and **Figure 1**) across marine and transitional waters along the eastern Adriatic coast. The specific ecological characteristics of each site are presented in **Table 1**. All sites were selected based on knowledge where juvenile fish occurrence had been previously described (Dulčić et al., 1997, 2005, 2007; Matić-Skoko et al., 2007) over a similar biotope characterised mainly by sandy (S1, S3, S5, S6, S9, S10, S12, S15, S18, and S20), rocky (S11 and S16), or mixed sandy-rocky-pebbles (S2, S4, S7, S8, S13, S14, S17, and S19) substrata covered

TABLE 1 | Summary of sampling data for juvenile fish communities along the eastern Adriatic coast within selected sites in the period 2017–2019.

No	Sites	Geographic position	Type of water	Bottom* and vegetation	Number of species			Number of individuals			Mean annual temperature (°C)			Mean annual salinity (‰)		
					2017	2018	2019	2017	2018	2019	2017	2018	2019	2017	2018	2019
S1	Prapratna	South	Marine	S/No	17	12	9	269	373	488	19.4	20.1	19.8	36.6	31.4	29.9
S2	Duba Stonska	South	Marine	R-S/Yes	13	9	16	40	94	130	18.4	19.9	18.1	37.2	34.0	36.2
S3	Mala Neretva	South	Transitional	S/Yes	30	23	19	177	241	100	20.0	21.4	20.0	28.6	24.8	22.5
S4	Drvenik	South	Marine	R-S/No	22	24	9	128	127	147	18.5	20.9	18.7	33.1	34.3	28.8
S5	Cetina ušće	South	Transitional	S/Yes	37	31	25	883	1222	452	18.4	18.7	19.1	25.3	28.7	19.6
S6	Duće	South	Transitional	S/Yes	27	21	18	370	189	424	19.1	21.4	18.5	34.1	31.6	20.9
S7	Grljevac	South	Marine	S-R/Yes	17	23	19	923	2023	540	18.3	20.0	18.4	36.0	34.2	30.9
S8	Kašjuni	South	Transitional	S-R/Yes	16	21	23	322	269	217	18.6	19.2	18.1	33.1	36.1	36.2
S9	Pantan	South	Transitional	S/Yes	21	23	22	281	578	130	19.7	22.3	18.4	34.6	26.6	28.2
S10	Stari Trogir	South	Marine	S/Yes	29	30	24	237	1008	619	19.9	20.4	17.9	37.8	35.4	37.9
S11	Primošten	North	Marine	R/Yes	22	20	16	407	627	522	19.3	20.4	19.5	38.5	38.5	38.3
S12	Žaborić	North	Marine	S/Yes	27	23	23	375	234	162	19.5	21.7	20.6	38.3	30.1	35.7
S13	Jadrija	North	Transitional	P/Yes	16	14	18	913	1125	611	17.8	17.3	19.2	18.5	14.2	19.4
S14	Sovlja	North	Marine	S-R/Yes	34	31	27	227	214	270	18.3	19.6	19.4	38.2	38.0	38.3
S15	Prosika	North	Transitional	S/Yes	29	22	22	198	268	173	18.8	19.9	19.6	34.5	28.9	33.0
S16	Sukošan	North	Marine	R/Yes	22	23	18	404	765	545	18.6	20.1	19.2	37.8	37.9	37.6
S17	Petrčani	North	Marine	S-P/Yes	22	22	21	809	348	374	18.6	19.7	18.8	38.3	35.6	38.4
S18	Nin	North	Transitional	S/No	20	15	10	262	259	185	17.6	18.8	18.4	37.4	32.1	36.8
S19	Maslenica	North	Transitional	P/Yes	17	23	10	232	184	40	16.3	17.9	16.4	17.2	17.5	19.5
S20	Karišnica	North	Transitional	S/Yes	16	17	14	353	476	263	16.2	18.5	17.0	18.7	16.6	17.2

Sites are listed as S1–S20 from south to north (border: Cape Ploča 43°29.648′N; 15°58.184′E) (Bottom: S-sandy; R-rocky, P-pebbles).*

by photophilic algae alternating with patches of *Cymodocea nodosa* seagrass beds. At each site, three replicates separated by tens of meters were performed with a specially constructed small shore seine (L = 25 m; minimum mesh size 4 mm). To ensure comparability, the same net was used during the entire study period at all sites. Hauls were also performed in the same bathymetric range, from 0 to 2.2 m depth. A total of 36 samples per site were taken over a 3-year period. Sites were divided into four groups of five locations based on water type (marine or transitional) and geographical position (north or south): transitional north (T_N), transitional south (T_S), marine north (M_N), and marine south (M_S). The border between the northern and southern sites is Cape Ploča (43°29.648′N; 15°58.184′E) as the most prominent point of land along the eastern Adriatic coast. This cape represents the geographic and climatological boundary between the northern and the southern Adriatic, and is often characterised by strong sea currents and swells as weather systems from the north and the south come in contact (Gloginja and Mitrović, 2021). Surface and bottom temperature (°C) and salinity (‰) measurements were performed using a multi-parameter probe model YSI 85. All fish individuals were identified to the species level according to Jardas (1996) and Dulčić and Kovačić (2020), measured (total length to the nearest 0.1 cm) and weighed (total body weight to the nearest 0.1 g). Sampling covered all stages of fish, but only juveniles were selected for further analysis. Further on, the species *Atherina* sp. were excluded, since they were the most dominant and most common species in all samples, and the majority of specimens were adults, while *Sardina pilchardus* and *Engraulis encrasicolus* were caught only sporadically in high abundance, thus skewing the results. The following species were excluded from further analysis as only adults, and no juvenile specimens, were caught: *Lichia amia*, *Pseudocaranx dentex*, *Sciena umbra*, *Uranoscopus scaber*, and *Zeus faber*.

Data Analysis

Total abundance (A), as the number of individuals (N) per species, and species richness (R), as the number of species (S), were counted, while the mean number of individuals and species per haul were recorded for each site and each period.

All analyses were performed using PRIMER-E software (Clarke and Gorley, 2015) with the add-on package PERMANOVA+ (Anderson, 2001; Anderson et al., 2008). Graphs were prepared using SigmaPlot (v. 13.0; Systat Software Inc., San Jose, CA, United States).

Multivariate statistical testing of abundance data for juvenile fish assemblages used a four-factor design [Year (Ye)/Season (Se)/Geographic position (Ge)/Type of water (Ty)], within one factor Period (1–12): 2017 (1–4), 2018 (5–8), and 2019 (9–12) constructed for cyclicity purposes. Factors Ye and Se were considered fixed while factors Ge and Ty were randomly nested in Se. The additional factor Period_Type of water_Geographic position was combined. Data sets for each site were imported in the PRIMER workspace and combined into a single matrix. Variability in the numbers of individual species in the samples was used to carry out dispersion weighting for each species. The dispersion-weighted data was transformed by a milder square-root transformation, as demonstrated by Clarke et al. (2014) for

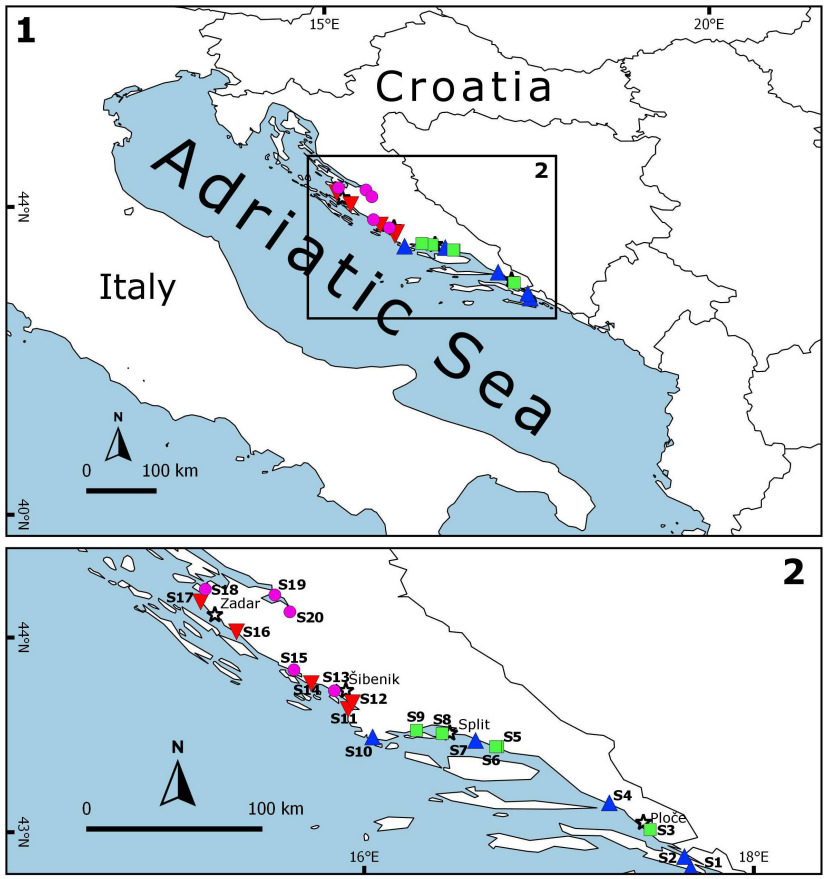

FIGURE 1 | Sampling area representing nursery areas along the eastern Adriatic coast with 20 sites across the four groups: marine_south (M_S; ▲), marine_north (M_N; ▼), transitional_south (T_S; ■) and transitional_north (T_N; ●). The map was created using QGIS Desktop 2.18.27 (version Las Palmas).

fish communities, particularly those in estuaries and nearshore coastal waters, where the prevalence of juvenile and small schooling species is high. Bray–Curtis similarity was then calculated on the dispersion weighted, transformed data.

Metric Multidimensional Scaling (mMDS) ordination used data at the same level of sample averaging for each Period, Geographical position, and Type of water combination to visualise the extents to which ichthyofaunal composition differed across Period_Type of water_Geographic position. All plots were constructed by calculating the distances between each pair of group centroids, i.e., the relevant average in the "Bray–Curtis space" of all samples (Anderson et al., 2008).

The RELATE statistic (*P*) was employed to test whether the pattern of temporal catch composition change conformed to cyclicity. If there is no tendency to cyclicity, then *P* will be close to zero (Clarke and Warwick, 2001). Separate two-way crossed analysis of similarities ANOSIM was used to interpret the relative size of the overall spatio-temporal effects on fish compositions, using the same resemblances as for the PERMANOVA tests. The species that mainly contribute to the separation between the factor Period_Type of water_Geographic position were determined by the SIMPER procedure, which shows the average contribution of each species to the dissimilarity between the groups. The results were presented for the specific season along all three consecutive years, characterised by most significant changes in communities.

To explore the data further, we used canonical variate plot (CAP) analysis. CAP is a routine for performing canonical analysis by calculating principal coordinates among groups of samples to predict group membership, positions of samples with another single continuous variable, or finding axes having maximum correlations with another set of variables (Anderson and Willis, 2003). This was initially run separately for each of the two factors: "Geographic position" and "Type of water" and then merged into a scatter plot. Particularly, CAP was used to estimate the accuracy of fish composition and environmental variables (temperature and salinity).

RESULTS

Interannual Variations of Abiotic Factors

The mean monthly variation in water temperature and salinity averaged over four groups (M_S, M_N, T_S, and T_N) are shown in **Figure 2**. The observed sea surface temperatures followed a seasonal cycle, with the highest temperatures in June-September

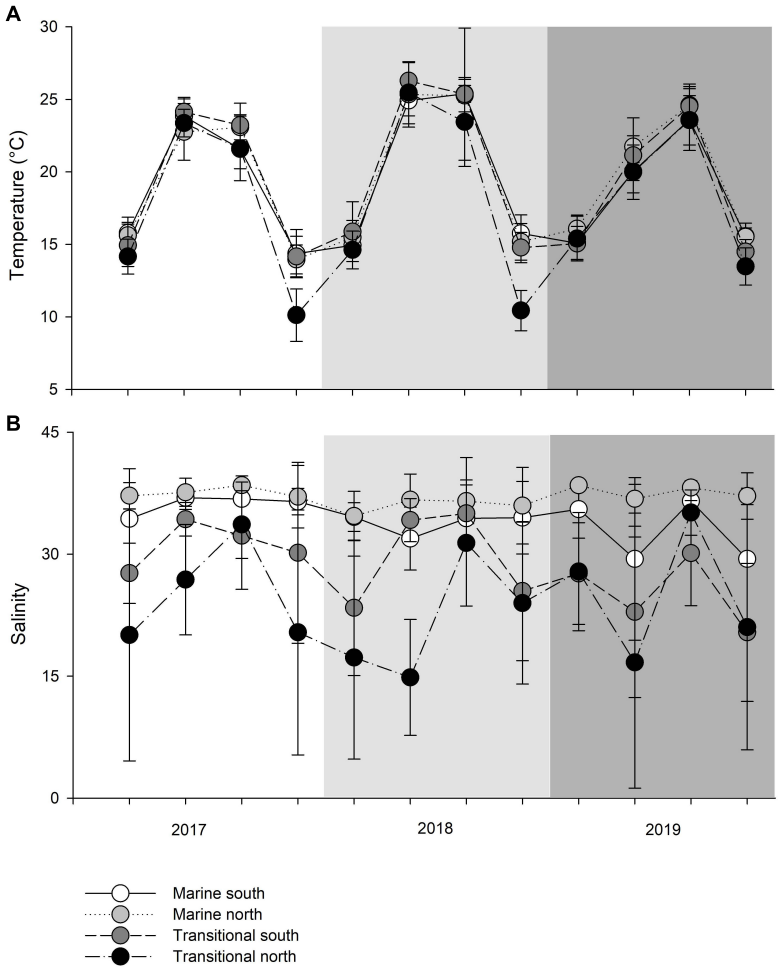

FIGURE 2 | Mean seasonal values of **(A)** temperature (°C) and **(B)** salinity (‰) among transitional and marine waters in the north and south (M_S, M_N, T_S, and T_N).

(particularly in 2018) and the lowest in December in all three years (**Figure 2A**). Observing the differences between marine and transitional waters, less variation was observed among waters in the south, regardless of the type of water (**Supplementary Table 1**). The mean seasonal temperature in T_N was always lower than in the remaining groups, though this is especially evident in December when higher and more similar results were recorded in the other three groups compared to T_N. Namely, northern transitional waters had the lowest mean values recorded in December 2017 (10.12 ± 1.81°C) and December 2018 (10.44 ± 1.39°C). It is evident that the mean temperature in December 2019 was higher for the T_N group than in the two previous years, and this was much more uniform among the groups (**Figure 2A**). Further, the mean temperature in June 2019, regardless of water type, was 2.78°C lower than in 2017 and 4.78°C lower compared to 2018. Analysis of variance revealed significant differences in temperature between years (PERMANOVA: Pseudo-F = 10.371; P = 0.0004), seasons (Pseudo-F = 50.181; P = 0.0013), interactions of years and seasons (Pseudo-F = 10.624; P = 0.0002), and among groups (M_S, M_N, T_S, and T_N) in relation to seasonal changes in temperature (Pseudo-F = 4.6813; P = 0.0008) (**Table 2**).

As expected, the measured salinity values showed greater variation between water types such that marine areas showed less seasonal fluctuations and continuous higher values (**Figure 2B** and **Supplementary Table 1**). Lower salinity values were observed for northern transitional waters (mean salinity value across the sampling period was 23.53 ± 6.23‰) than southern transitional waters. Two negative peaks of mean salinity values were observed in June and December 2019, regardless of water type. The mean salinity was always higher in 2017 and 2018 in the south, regardless of water type, while an inversion occurred in 2019 and mean salinity values were higher in the north in both types of waters. Also, every September in all three years, the mean salinity values were highest and most similar among the groups following the summer drought (**Figure 2B**). However, analysis of variance did not reveal significant differences in salinity between years, seasons, type of waters, and geographic position and their interactions, except for strong statistically significant annual variations among water type/geographic position groups (M_S,

TABLE 2 | Summary of PERMANOVA results for the multivariate analysis of the overall matrix constructed from seasonal temperature data measured in three consecutive years (2017, 2018, 2019) along the eastern Adriatic coast for 20 sites with assigned affiliation according to water type (marine or transitional) and geographic position (south or north).

	df	MS	Pseudo-F	*P*
Year (Ye)	2	1.896	10.731	**0.0004**
Season (Se)	4	49.157	50.181	**0.0013**
Geographic position (Ge)	5	0.406	0.838	0.5693
Water type (Ty)	5	0.641	1.323	0.3743
Interactions				
Ye × Se	5	1.876	10.624	**0.0002**
Ye × Ge (Se)	7	0.122	1.429	0.3213
Ye × Ty (Se)	7	0.062	0.738	0.6461
Ge (Se) × Ty (Se)	5	0.485	4.681	**0.0008**
Ye × Ge(se) × Ty (Se)	7	0.085	0.823	0.5728
Residuals	192	0.104		
Total	239			

Statistically significant values (P < 0.05) marked in bold.

TABLE 3 | Summary of PERMANOVA results for the multivariate analysis of overall matrix constructed from seasonal salinity data measured in three consecutive years (2017, 2018, 2019) along the eastern Adriatic coast for 20 sites with assigned affiliation according to water type (marine or transitional) and geographic position (south or north).

	df	MS	Pseudo-F	*P*
Year (Ye)	2	2.229	2.431	0.0776
Season (Se)	4	3.906	0.494	0.8206
Geographic position (Ge)	5	0.550	0.186	0.9520
Water type (Ty)	5	13.816	4.679	0.0669
Interactions				
Ye × Se	5	1.465	1.736	0.1713
Ye × Ge (Se)	7	0.753	1.701	0.2491
Ye × Ty (Se)	7	0.346	0.782	0.615
Ge (Se) × Ty (Se)	5	2.953	4.913	**0.0005**
Ye × Ge (Se) × Ty (Se)	7	0.443	0.737	0.646
Residuals	192	0.601		
Total	239			

Statistically significant values (P < 0.05) marked in bold.

M_N, T_S, and T_N) in relation to seasonal changes in salinity, i.e., as nested in season (Pseudo-F = 1.9354; P = 0.0001) (**Table 3**).

Interannual Variations of Juvenile Fish Composition

At all sites, a total of 720 small beach seine samples were taken across three consecutive years (**Tables 1**, **4**). A total of 24,807 fish juveniles belonging to 23 families and 92 species were included in this survey. The most abundant species were *Sarpa salpa* (2,805 individuals in total), *Pomatoschistus marmoratus* (2,028), *Pagellus acarne* (1,806), *Chelon ramada* (1712), *Diplodus annularis* (1,683), *Chelon auratus* (1,550), and *Diplodus vulgaris* (1,074), which together comprised 51.03% of the total sample. A high number of species were sporadically present throughout the 3-year study period (though with <30 individuals). Some species, such as *Symphodus roissali* and *Chelidonichthys lucerna*, were completely absent in 2019. Although the collection effort (as the total number of samples per year, month and site) was the same, the total number of species and individuals clearly fluctuated across sites (**Table 4**, **Figure 3**, and **Supplementary Table 2**) and across groups. The number of species varied among sites from 1 (at S18 and S19 in June and September 2019, respectively) to 24 species (at S16 in June 2018) and among the groups from 1 (T_N in December 2019) to 25 species (M_N in June 2018). The number of species varied less over the 3-year period at marine stations than at transitional ones, with the largest interannual changes observed in the T_N group. Moreover, PERMANOVA analysis of the number of juvenile fish species found significant differences along three consecutive years (Pseudo-F = 1.7459; P = 0.0362), across seasons among years (Pseudo-F = 1.4222; P = 0.0406) and among groups [M_S, M_N, T_S, and T_N, as Ge(Se) × Wa (Se) interactions] in relation to seasonal changes in the number of species (Pseudo-F = 2.0571; P = 0.0002) (**Table 5**).

Similar to the number of species, abundance fluctuated considerably less in marine waters and more in transitional ones, especially in the north. The abundance of individuals was the highest in 2018, and the highest in M_N group (4067 individuals). On the contrary, abundance was lowest in 2019, especially in the M_S (1,317) and T_N groups (1,407). Although some fluctuations in abundance were evident, especially the 52.5% reduction in the M_N group in 2019 (1,930), PERMANOVA analysis of juvenile fish abundance for all sites found no significant differences for the three consecutive years, seasons, type of water and geographical position together with their interactions, except among groups in relation to seasonal changes in the number of individuals (Pseudo-F = 1.9354; P = 0.0001) (**Table 6**). Regarding species, the abundance of *Boops boops*, *Pagellus acarne*, *Pagellus erythrinus*, *Symphodus tinca*, and *S. roissali* was drastically decreased in 2019 compared to previous years (**Table 4**). Additionally, *P. acarne* was only present in southern marine waters in 2017 and 2018.

On the metric MDS ordination plot, derived from the distance among centroid matrices, four groups were defined, clearly separating both geographical position and type of waters (**Table 3** and **Figure 3**) ordinating groups from transitional to marine and then from north to south (T_N, T_S, M_N, and M_S), indicating that the greatest differences were found between the groups T_N and M_S (**Figure 4**). The cyclicity of abundance data, obtained from the RELATE test, following a seasonal pattern and was less visible for T_N. It seems that there were similar patterns for marine groups, namely between M_S in 2017 (Rho = 0.621, P = 0.839) and 2018 (Rho = 0.414, P = 0.665) and M_N in 2017 (Rho = 0.828, P = 0.335) and 2018 (Rho = 0.828, P = 0.333) while in the final year of the study period, similarity dropped drastically. Interestingly, there was no similar pattern between the three consecutive years at T_S (Rho = 0.014, P = 0.365). Species composition in T_N was governed by a similar pattern in 2018 (Rho = 0.414, P = 0.679) and 2019 (Rho = 0.414, P = 0.035). Two-way crossed ANOSIM tests showed and confirmed that the fish fauna composition was significantly related to both factors, types of water (R = 0.106, P = 0.001) and geographic position (R = 0.188, P = 0.001), with the latter factor more prominent. Moreover, one-way ANOSIM for the interaction type of water_geographic

TABLE 4 | Summary of abundance data (number of individuals) for 92 juvenile fish species sampled in three consecutive years (2017–2019) along the eastern Adriatic coast with assigned affiliation to four groups according to water type (marine or transitional) and geographic position (south or north): M_S, M_N, T_S, and T_N.

		2017				2018				2019			
		M_S	M_N	T_S	T_N	M_S	M_N	T_S	T_N	M_S	M_N	T_S	T_N
Species	**Family**												
Arnoglossus laterna	Bothidae	21	26	44	2	15	22	26	2	8	11	12	3
Arnoglossus thori	Bothidae	2	0	0	0	1	0	0	0	0	0	0	0
Belone belone	Belonidae	1	8	0	1	3	2	0	4	5	42	0	0
Blennius ocellaris	Blenniidae	0	0	0	2	0	0	0	0	1	0	0	0
Boops boops	Sparidae	0	4	16	9	5	0	82	0	29	0	2	0
Bothus podas	Bothidae	38	0	17	0	56	0	20	0	25	0	0	0
Callionymus pusillus	Callionymidae	3	27	5	9	1	9	3	5	1	7	1	13
Callionymus risso	Callionymidae	3	21	36	7	10	51	8	22	0	12	6	8
Chelon labrosus	Mugilidae	43	13	0	22	3	56	1	17	2	29	6	21
Chelidonichthys lucerna	Triglidae	0	2	3	0	1	5	2	0	0	0	0	0
Chelon auratus	Mugilidae	154	188	34	350	38	80	5	558	51	79	1	12
Chelon ramada	Mugilidae	79	144	2	379	67	434	80	170	37	80	7	233
Chelon saliens	Mugilidae	5	5	3	22	15	64	2	5	14	301	0	39
Chromis chromis	Pomacentridae	0	0	0	0	1	0	10	0	0	1	0	0
Coris julis	Labridae	8	1	18	0	0	0	8	0	0	1	0	0
Deltentosteus collonianus	Gobiidae	0	0	1	0	0	0	0	0	0	0	0	0
Deltentosteus quadrimaculatus	Gobiidae	0	0	5	0	0	0	1	1	0	0	0	0
Dentex dentex	Sparidae	3	1	0	0	1	1	8	0	0	1	0	0
Dicentrarchus labrax	Moronidae	0	49	0	20	0	29	1	10	1	4	0	8
Diplodus annularis	Sparidae	32	378	85	9	59	692	80	23	63	133	124	5
Diplodus puntazzo	Sparidae	42	73	58	10	88	46	106	11	33	66	76	21
Diplodus sargus	Sparidae	0	0	1	0	0	0	10	0	0	0	0	0
Diplodus vulgaris	Sparidae	63	127	182	22	48	12	117	7	101	71	303	21
Echiichthys vipera	Trachinidae	1	8	0	3	0	1	2	1	0	1	0	2
Epinephelus costae	Serranidae	1	0	0	0	0	0	0	0	0	0	0	0
Gobius cobitis	Gobiidae	5	0	7	6	5	0	2	23	2	3	7	33
Gobius couchi	Gobiidae	3	24	33	2	10	0	126	3	1	0	33	2
Gobius cruentatus	Gobiidae	0	0	2	0	0	0	2	0	0	0	5	0
Gobius fallax	Gobiidae	0	2	11	0	0	0	43	0	0	0	19	0
Gobius geniporus	Gobiidae	3	3	0	22	1	0	1	0	0	0	1	0
Gobius niger	Gobiidae	8	136	154	104	15	326	94	182	25	124	38	160
Gobius paganellus	Gobiidae	0	0	0	0	0	2	1	0	0	0	1	0
Hippocampus hippocampus	Syngnathidae	2	0	1	1	0	0	0	0	1	0	0	0
Hippocampus ramulosus	Syngnathidae	0	0	2	0	0	0	0	0	0	0	0	0
Knipowitschia kavcasica	Gobiidae	0	0	0	0	0	0	0	2	0	0	0	0
Knipowitschia panizzae	Gobiidae	0	0	0	121	0	0	0	65	0	0	0	17
Labrus merula	Labridae	0	1	0	0	0	0	0	0	1	0	0	0
Labrus viridis	Labridae	0	0	0	1	0	0	0	0	0	0	0	0
Lichia amia	Carangidae	0	0	1	0	0	0	0	0	0	0	0	0
Lipophrys trigloides	Blenniidae	3	0	3	0	0	0	0	0	0	0	0	0
Lithognathus mormyrus	Sparidae	36	17	140	20	57	78	53	5	366	120	51	13
Monochirus hispidus	Soleidae	0	0	1	0	0	0	1	1	0	1	0	0
Microlipophrys dalmatinus	Blenniidae	1	2	0	0	0	0	0	0	0	1	0	0
Mullus barbatus	Mullidae	80	69	34	43	298	81	20	61	36	93	18	29
Mullus surmuletus	Mullidae	34	0	9	0	7	0	1	0	1	1	0	0
Nerophis maculatus	Syngnathidae	0	13	0	1	0	1	0	0	0	0	0	0
Nerophis ophidion	Syngnathidae	0	2	0	0	1	5	0	0	0	4	0	1
Oblada melanura	Sparidae	2	0	3	0	3	0	1	5	1	1	0	0
Oedalechilus labeo	Mugilidae	61	0	23	0	83	2	214	0	15	2	153	2
Pagellus acarne	Sparidae	450	8	172	74	864	90	74	0	73	0	1	0
Pagellus bogaraveo	Sparidae	0	1	0	0	0	0	0	0	0	0	0	0
Pagellus erythrinus	Sparidae	126	2	2	1	33	3	14	3	2	0	10	0
Pagrus pagrus	Sparidae	6	0	9	0	9	0	1	0	63	0	2	0
Parablennius gattorugine	Blenniidae	0	0	0	1	2	0	2	0	0	0	0	0

(Continued)

TABLE 4 | (Continued)

		2017				2018				2019			
		M_S	M_N	T_S	T_N	M_S	M_N	T_S	T_N	M_S	M_N	T_S	T_N
Parablennius sanguinolentus	Blenniidae	1	1	11	0	1	10	5	0	3	0	3	0
Parablennius tentacularis	Blenniidae	5	12	38	3	2	10	29	5	4	17	17	4
Pomatoschistus bathi	Gobiidae	0	8	15	11	0	0	26	6	1	4	7	0
Pomatoschistus canestrinii	Gobiidae	0	0	0	0	0	0	0	0	0	0	0	1
Pomatoschistus marmoratus	Gobiidae	12	172	72	430	3	218	210	339	7	133	122	310
Pomatomus saltatrix	Pomatomidae	0	0	0	0	0	0	0	0	0	0	0	1
Pseudaphya ferreri	Gobiidae	0	0	0	4	1	3	0	0	0	0	6	0
Pseudocaranx dentex	Carangidae	1	0	0	0	0	0	0	0	0	0	0	0
Salaria pavo	Blenniidae	0	18	1	12	2	68	1	82	0	27	1	8
Sarpa salpa	Sparidae	2	141	469	39	138	659	375	85	179	272	241	205
Sciaena umbra	Sciaenidae	0	0	1	0	0	0	0	0	0	1	0	0
Scorpaena notata	Scorpaenidae	0	0	0	0	0	0	0	0	0	0	0	0
Scorpaena porcus	Scorpaenidae	4	9	23	0	2	5	19	0	4	5	13	0
Serranus cabrilla	Serranidea	0	0	1	0	0	0	0	0	0	0	0	0
Serranus hepatus	Serranidea	4	1	22	0	7	0	40	1	0	0	13	2
Serranus scriba	Serranidea	5	15	6	1	4	13	16	1	2	12	14	0
Solea kleini	Soleidae	1	0	3	2	0	0	1	0	0	0	1	0
Solea solea	Soleidae	2	6	0	4	1	21	0	3	0	6	2	3
Sparus aurata	Sparidae	1	20	4	30	3	20	7	26	0	11	2	5
Sphyraena sphyraena	Sphyraenidae	1	8	1	0	1	2	1	0	0	0	2	0
Spicara flexuosa	Centracanthidae	2	0	0	0	0	0	0	1	0	0	0	0
Spicara smaris	Centracanthidae	6	1	49	2	0	393	111	13	1	3	87	0
Symphodus cinereus	Labridae	39	207	212	17	57	262	315	27	82	127	191	6
Symphodus ocellatus	Labridae	18	61	31	119	18	125	35	56	14	62	77	166
Symphodus roissali	Labridae	0	4	0	18	0	0	0	2	0	0	0	0
Symphodus rostratus	Labridae	2	3	0	0	4	7	0	0	0	5	0	0
Symphodus tinca	Labridae	2	43	20	3	3	96	24	1	3	1	15	1
Syngnathus abaster	Syngnathidae	0	0	0	1	0	0	0	0	0	1	0	9
Syngnathus acus	Syngnathidae	0	5	1	10	0	2	0	10	0	3	1	5
Syngnathus tenuirostris	Syngnathidae	1	11	8	0	3	2	14	6	0	2	5	0
Syonodus saurus	Synodontidae	0	0	0	0	1	0	0	0	1	0	0	0
Syngnathus typhle	Syngnathidae	3	14	6	8	2	27	6	2	1	11	3	4
Trachinotus ovatus	Carangidae	38	0	2	0	4	0	6	0	57	0	26	0
Trachinus draco	Trachinidae	2	2	1	1	0	0	3	0	0	0	11	1
Trachinus radiatus	Trachinidae	0	0	1	0	0	0	0	0	0	0	0	0
Trigla lyra	Triglidae	0	1	0	0	0	0	0	0	0	0	0	0
Tripterygion tripteronotum	Tripterygiidae	0	0	4	0	0	0	2	0	0	0	1	0
Zosterisessor ophiocephalus	Gobidae	0	22	1	81	0	32	0	180	0	38	0	33
Number of samples		20	20	20	20	20	20	20	20	20	20	20	20
Number of species		54	54	60	48	51	43	58	44	37	46	46	37
Number of individuals		1471	2140	2120	2060	2057	4067	2468	2032	1317	1930	1738	1407

position confirmed that the magnitude of difference was lower between groups in 2017 (R = 0.419; P = 0.001) and 2018 (R = 0.458; P = 0.001), and highest in 2019 (R = 0.899; P = 0.001).

We additionally ran a CAP analysis and related the environmental data to the community composition information. Temperature and salinity values for the four water types/geographic position groups of factors were plotted as distances among centroids based on community data (**Figure 5**), revealing that temperature had a prominent influence on community composition in T_N, less on T_S, while salinity had a positive effect on M_S and M_N. A separate CAP analysis was run for each of the two factors ("type of waters" and "geographical position"), which also gave successful discrimination. In particular, 84.03 and 78.99% of samples from marine and transitional waters, respectively, were correctly allocated based on the community composition information. Further, 72.88 and 71.67% of samples were correctly allocated to north or south, respectively. These results suggested that transitional waters are more sensitive to interannual differences, especially in the north (**Figure 6**).

The SIMPER routine revealed that 14 species (**Table 7**) in varying order of percentage contribution were responsible for the most (>50%) dissimilarities in the interactions between the composition of juvenile fish sampled in June among the three

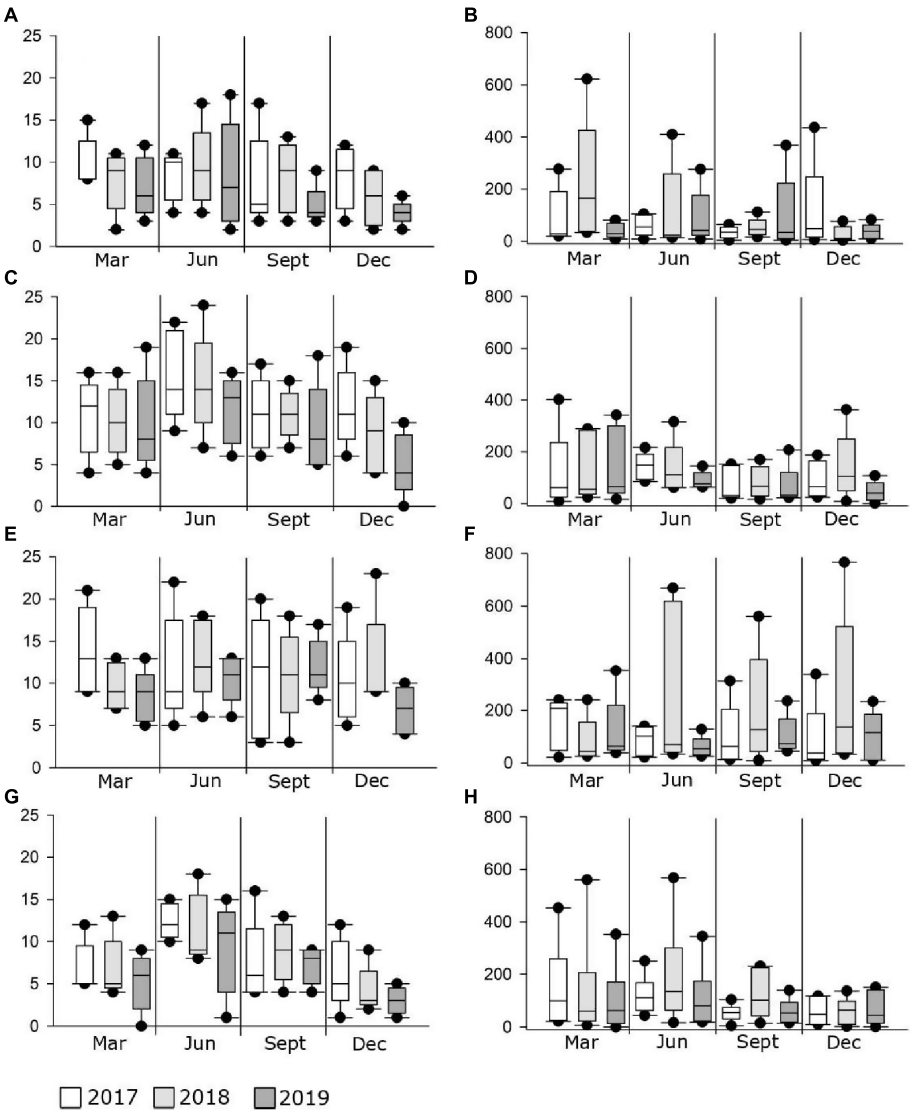

FIGURE 3 | Box plots of median values (± standard deviation) for the number of juvenile fish species and abundance across marine _south **(A,B)**, marine_north **(C,D)**, transitional_south **(E,F)**, transitional_north **(G,H)** groups during the sampling period (2017–2019) along the eastern Adriatic Sea.

consecutive years. It was evident that five species that gave a significant contribution to T_N in 2017 (e.g., *Sparus aurata*, *Diplodus vulgaris*, and *Symphodus roissali*) were not present in 2018, while other species appeared (*Sarpa salpa* and *Chelon ramada*). SIMPER revealed that the average dissimilarity was highest between M_S and T_N (90.51%) while T_S and M_N were more similar (79.41%).

DISCUSSION

The present study focussed on the patterns of use of coastal nurseries by juvenile fish species along the eastern Adriatic coast. In particular, the study sought to answer whether species occurrence and density differed between habitats and sites over three consecutive years and whether certain sites or habitats could be highlighted as important nursery areas for juveniles, and whether they are highly sensitive to environmental and other changes. Moreover, by modelling the response of juvenile occurrence and density to the environmental variables, this study identified which variables best explained the intra- and inter-coastal variability in juvenile fish distribution and abundance. Also, the strength of these parameter influences can characterise the features that define important sites for juveniles and how they varied among systems. Last but not least, more sensitive species in this context were defined.

Interannual Variations of Abiotic Factors

Generally, the determined fluctuations in sea temperature and salinity during the study period followed the well-known seasonal cycle specific to the Adriatic Sea (Grbec and Morović, 1997).

TABLE 5 | Summary of PERMANOVA results for the multivariate analysis of overall matrix constructed from juvenile fish species data sampled in three consecutive years (2017, 2018, 2019) along the eastern Adriatic coast for 20 sites with assigned affiliation according to water type (marine or transitional) and geographic position (south or north).

	df	MS	Pseudo-F	*P*
Year (Ye)	2	3944.3	1.746378	**0.0362**
Season (Se)	3	16518	1.345	0.2196
Geographic position (Ge)	4	5909.6	1.020	0.4856
Water type (Ty)	4	10682	1.844	0.1537
Interactions				
Ye × Se	6	2897.4	1.422	0.0406
Ye × Ge (Se)	8	2021.8	1.188	0.2784
Ye × Ty (Se)	8	1212.2	1.712	0.8607
Ge (Se) × Ty (Se)	4	5791.9	2.057	**0.0002**
Ye × Ge (Se) × Ty (Se)	8	1702.1	0.604	0.9973
Residuals	190	2815.6		
Total	237			

Statistically significant values (P < 0.05) marked in bold.

TABLE 6 | Summary of PERMANOVA results for the multivariate analysis of overall matrix constructed from juvenile fish abundances sampled in three consecutive years (2017, 2018, 2019) along the eastern Adriatic coast for 20 sites with assigned affiliation according to water type (marine or transitional) and geographic position (south or north).

	df	MS	Pseudo-F	*P*
Year (Ye)	2	3853.6	1.378	0.0894
Season (Se)	3	15921	1.329	0.1975
Geographic position (Ge)	4	6270.8	0.926	0.5656
Water type (Ty)	4	10800	1.595	0.1864
Interactions				
Ye × Se	6	3235.7	1.242	0.0886
Ye × Ge (Se)	8	2433.3	1.023	0.4533
Ye × Ty (Se)	8	2088.6	0.878	0.7242
Ge (Se) × Ty (Se)	4	6772.6	1.935	**0.0001**
Ye × Ge (Se) × Ty (Se)	8	2378.3	0.680	0.9995
Residuals	190	3499.3		
Total	237			

Statistically significant values (P < 0.05) marked in bold.

More pronounced interannual fluctuations in water temperature were found for transitional waters, especially those situated in the north. According to the Croatian Meteorological and Hydrological Service, mean monthly air temperatures for most of 2018 were above the average of the reference period 1961-1990, while in May 2019, temperatures were below the reference average along the entire coast. Specially in the area gravitating toward T_N, temperatures in May 2019 were nearly 5°C below average (DHMZ, 2019). Sites within this group are related to the transitional waters of the Zrmanja and Krka Rivers, whose water systems are more exposed to the mainland due to relief characteristics (heavy rains, snow melt from nearby mountains and cold north-easterly winds in spring) and the maritime influence is less pronounced. Usually, salinity fluctuations are associated with freshwater river flows, though the significantly lower temperatures of these waters, especially in the spring months are due to their origin and flow through extremely mountainous terrain. On the contrary, the transitional waters of the Neretva and Cetina Rivers have wider mouths toward the open sea, especially the Neretva Delta, and thus are more influenced by the gentle maritime environment (Krvavica and Ružić, 2020). Unlike temperature, there were no prominent interannual fluctuations in salinity. However, reduced salinity was evident in the northern transitional waters for the same reasons as mentioned above. In late spring 2019, reduced salinity was recorded along the entire coast as a consequence of an extremely rainy period. For example, the amount of precipitation in May (120 mm) and November (210 mm) 2019 in the middle of study area (S8 and S9) was twice the average cumulative amount of precipitation in the reference period 1961–1990 for those months (DHMZ, 2019). In 2017 and 2018, the average salinity in the south, regardless of water type, was always higher than in the north, confirming the unusually high rainfall in the north (DHMZ, 2019). As expected, statistically significant interannual differences in mean seasonal water temperatures also led to a change in the species occurrence among the three consecutive years. Thus, June 2019 was characterised by markedly low salinity and low temperature after a cold and rainy winter and spring, which likely caused the absence of the following species: *B. boops*, *B. podas*, *P. acarne*, *P. erythrinus*, *S. tinca*, *S. roisalli*, and *C. auratus*. All these species, except *C. auratus*, spawn in spring (Bartulović et al., 2011; Dulčić and Kovačić, 2020) and their settlers likely delayed settlement due to the prevailing conditions. Interestingly, a significantly reduced abundance of *B. boops* and *B. podas* were observed in southern transitional waters (T_S) in the same period. These species also spawn in early spring (Dulčić et al., 2004; Matić-Skoko et al., 2007; Dobroslavić et al., 2017; Zorica et al., 2020) and apparently their juveniles did not yet inhabit the nursery areas by June. Late spawning and a longer retention in the nursery area could be the reason for increased abundance of *L. mormyrus* in September 2019. Increased abundance is most often a positive response to average warmer habitat conditions (Jones et al., 2009). It seems that the longer the spawning season for a population, the higher its probability of finding suitable conditions for larval survival, resulting in a higher recruitment level (Sale, 2006). This may imply that if environmental conditions change significantly, species with a shorter spawning period may experience a more pronounced shift in spawning time and consequently in settlement onset. Interannual variability in temperature has been linked with changes in fish year-class strength for a number of species (Planque and Fox, 1998; Laurel et al., 2017; Barbeaux and Hollowed, 2018). Temperatures affect the onset of spawning and spawning period, but also the ecology of early developmental stages of fish, thus defining the moment of their migration or entry into benthic nursery areas (García-Rubies and Macpherson, 1995; Dulčić et al., 1997, 2007; Biagi et al., 1998). Also, positive relationships between temperature and impacts on settlement and recruitment are generally observed in cold-temperate regions, whilst negative relationships are observed in warm-temperate regions (Planque and Fox, 1998; Barbeaux and Hollowed, 2018; Downie et al., 2021). Environmental changes at higher latitudes that are under greater coastal influence appear

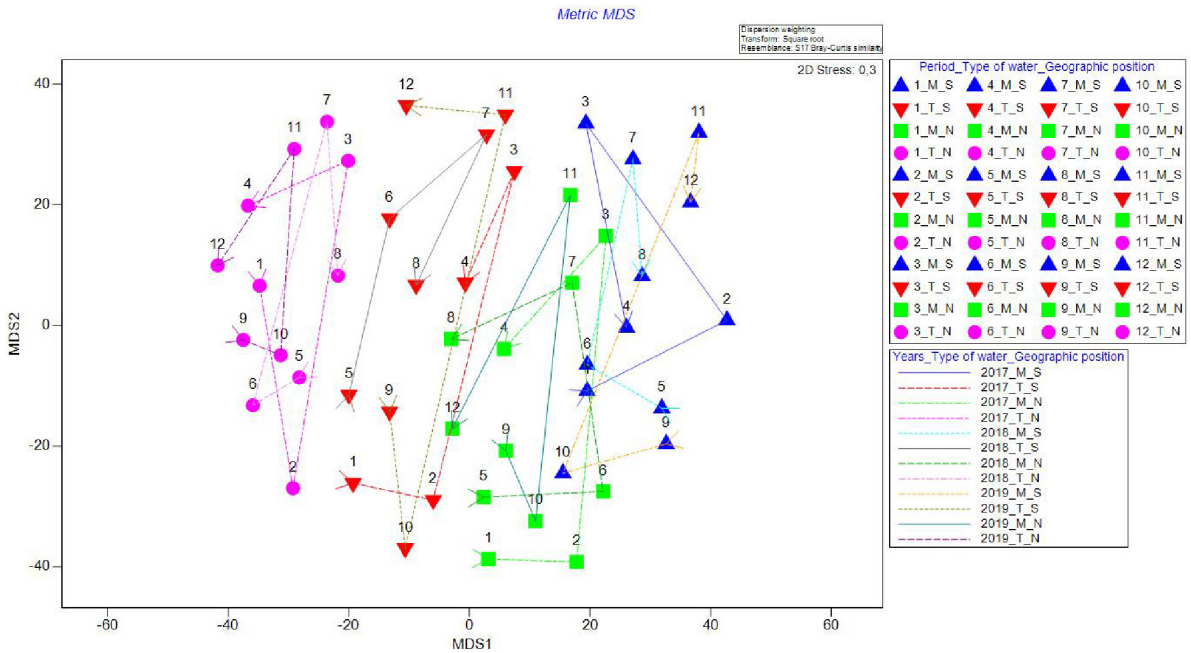

FIGURE 4 | Metric MDS for juvenile fish abundance for Period_Water type_Geographic position (periods 1–4, 5–8, and 9–12 corresponding to 2017, 2018, and 2019, water types marine and transitional and geographic positions south and north) in the four groups in the Adriatic Sea with marked cyclicity for all four groups (M_S, M_N, T_S, and T_N).

to be more drastic or more rapidly reflected in changes at the community, species or individual level.

Interannual Variations of Juvenile Fish Composition

The influence of environmental factors on species composition or occurrence is specifically evident at the fish community level for both species richness and abundance. Moreover, water temperature appears to have a greater impact on transitional waters that are often retracted deep into the mainland. This is even more relevant since more than 64% of fish juveniles representing 68 species and 28 families were recorded in estuarine nurseries, and most are species of commercial interest (Dulčić et al., 2007). On the other hand, marine waters appear to be a less volatile environment, and the establishment of the juvenile fish community was defined primarily by salinity. This is supported by the fact that the same species were recorded in marine waters in all three years. Dulčić et al. (1997) investigated several shallow marine coves on distant islands and found a similar temporal pattern and the prevalence of five dominant species, suggesting that only a low amount of variation in the juvenile fish abundance in the real marine environment can be explained by temperature and salinity. The absence of certain species (e.g., *S. roissali* and *C. lucerna*) in 2019 in both marine and transitional waters could be regulated by a factor that is more regional in nature. Similarly, Stagličić et al. (2011) reported that species abundance within littoral fish assemblages could be a consequence of factors occurring on a wider spatial scale (i.e., fisheries mismanagement, pollution, climate change). Contrary, *C. saliens* and *S. salpa* showed a higher abundance in northern marine waters (M_N) in 2019 and 2018, respectively, while *S. cinereus* was most abundant in T_S in 2018 in all four groups. However, there is the possibility that the sites where certain species were recorded are not essential or preferable nurseries for those species (i.e., poor site selection, low sample size, sampling gear selectivity). For example, *P. erythrinus* or *T. ovatus* were both lacking in southern marine areas in both 2018 and 2019. These species use other nursery areas, like marine coves on distant islands or at greater depths that are characterised by high and constant salinity (Dulčić et al., 1997; Biagi et al., 1998; La Mesa et al., 2011). In this study, *P. erythrinus* was found in 2017 exclusively at one station (S12) that is wide open toward the sea. Another typical marine species, *P. pagrus*, was also caught only at this site. The dispersal strategies of certain small migratory, shoaling species, such as *Spicara* sp. or *B. belone,* could also be the reason for their spatio-temporal absence (Hoare et al., 2000).

More Sensitive Species

If transitional waters geographically located at higher latitudes are more susceptible to interannual change, then the assumption is that more vulnerable species will select those waters for their nurseries, especially the more abundant species in the northern-central Adriatic (Dulčić et al., 2004; Matić-Skoko et al., 2007; Dulčić and Kovačić, 2020). Firstly, species of economic interest such as *D. labrax*, *S. salpa* and *S. aurata* should be highlighted here. It is also important to mention the small, resident species that also have ecological significance in the benthic communities of transitional waters, e.g., *Salaria pavo*,

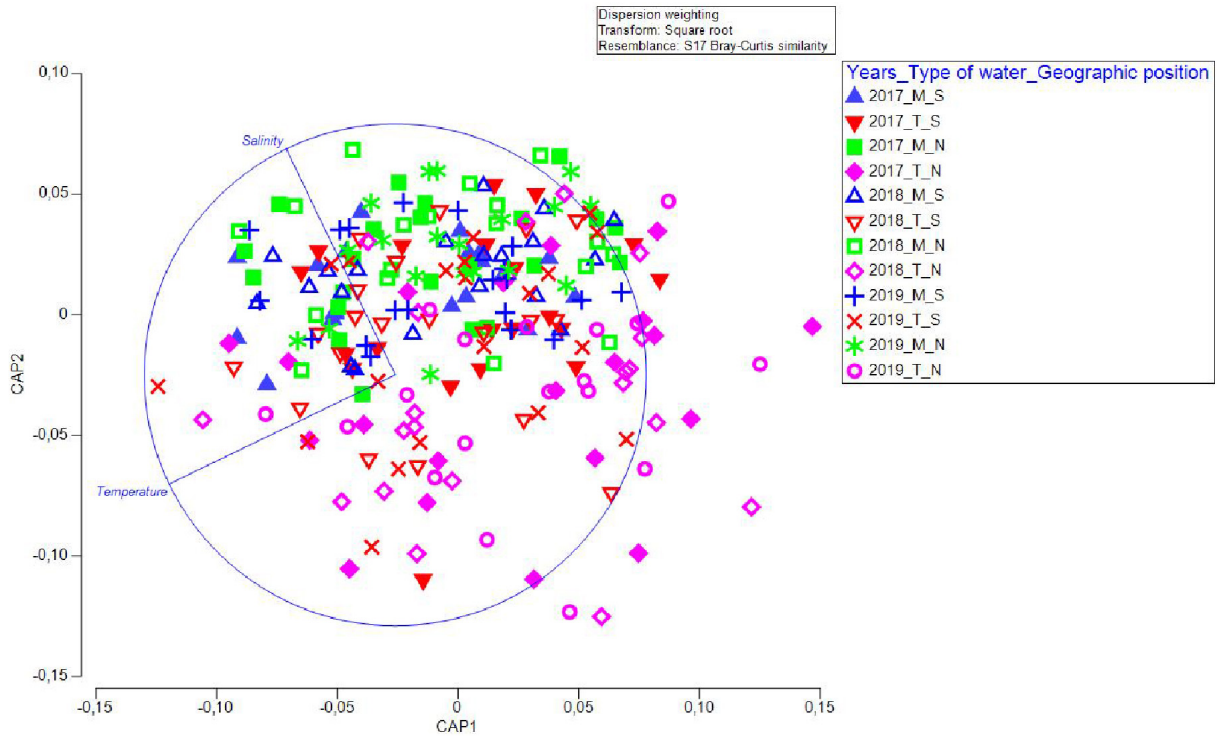

FIGURE 5 | Canonical variate plot (CAP) of juvenile fish abundance data against environmental (continuous quantitative) values of temperature and salinity showing dependence on geographical position and water type. The distance matrix based on community abundance data was related to the distance matrix based on environmental data.

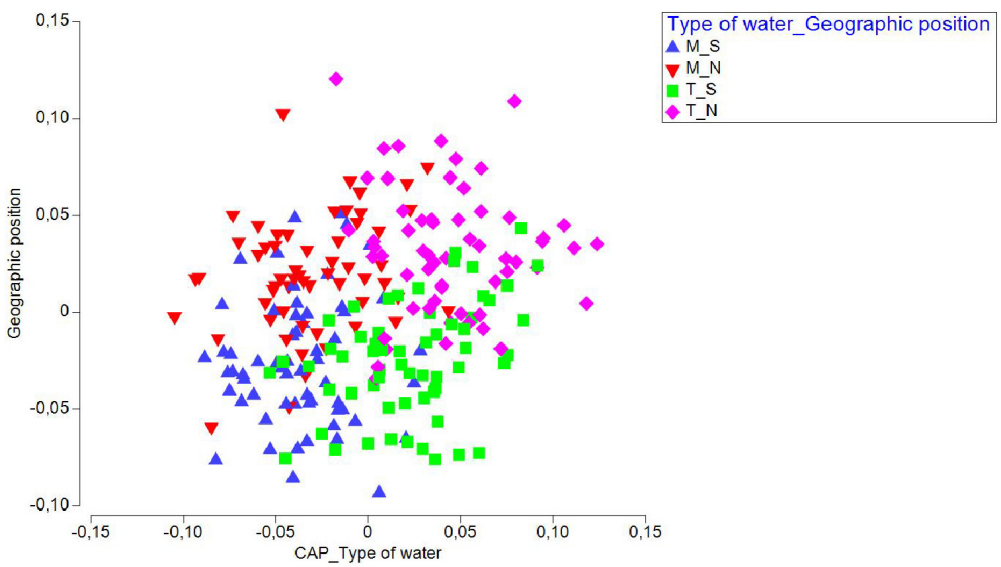

FIGURE 6 | Canonical variate plot (CAP) for juvenile fish abundances sampled in three consecutive years (2017, 2018, 2019) at 20 sites in the Adriatic Sea, grouped by "Water type" and "Geographic position."

S. ocellatus, and *Z. ophiocephalus,* as these herbivorous and omnivorous fishes seem to control both algae and invertebrates in rocky sub-littoral zones (Ruitton et al., 2000). *S. ocellatus* showed a significant association with an algal habitat, and its abundance can certainly be related to the strong seasonal differences in algal cover (Hinz et al., 2019). If species preferring transitional waters at higher latitudes also spawn in winter and/or early spring, such as *D. vulgaris*, *D. sargus*, *S. aurata* and

TABLE 7 | SIMPER: species contributing most to the dissimilarity, in terms of abundance of juvenile fish abundances among transitional waters in the north (T_N) in June 2017 (Period 2), 2018 (Period 6) and 2019 (Period 10) in the Adriatic Sea.

Species	Co (%)	Cum (%)	Av. Diss	Co (%)	Cum (%)	Av. Diss
S. ocelatus	8.79	1.00	6.92	15.25	1.00	5.77
S. aurata	16.49	0.12	6.07	22.18	0.98	5.37
G. cobitis	23.06	0.98	5.18			
K. panizzae	28.80	0.18	4.53			
G. niger	34.46	0.67	4.46	7.80	0.67	6.04
S. roissali	38.40	0.00	3.11			
D. vulgaris	42.06	0.36	2.88			
S. acus	45.62	0.31	2.80			
Z. ophiocephalus	49.14	0.29	2.78	37.69	0.29	3.44
S. pavo				28.73	0.16	5.07
C. pusillus				33.24	0.37	3.49
S. salpa				41.80	0.46	3.18
C. ramada				45.84	0.24	3.13
C. risso				49.53	0.12	2.86

Co, contribution of species; Cumm, cumulative contribution; Av. Diss., average dissimilarity. Selected species contributed up to 50% of dissimilarity.
2_T_N & 10_T_N 6_T_N & 10_T_N

D. labrax, this makes them particularly sensitive to interannual differences in environmental conditions. As mentioned earlier, they can potentially be affected by late spawning, causing delays in settlement, leaving nurseries, or even causing individuals to remain in nurseries year round. Particularly, this delay can lead to the fact that at the moment of entry there is no prey of suitable size or in sufficient quantity for all incoming settlers (Machado et al., 2017). Decreased growth can make individuals too weak to join adult populations in the open seas that season (Lanier and Scharf, 2007). Since many marine species undergo long-distance dispersal during the pelagic larval phase before settling in benthic habitats where they remain (Di Franco et al., 2012), and many species also undergo further ontogenetic changes in restricted nursery grounds, pre- and post-settlement emigration by juveniles can then have significant population-level consequences (Vasconcelos et al., 2013). Sensitivity to physical-chemical changes of the aquatic environment, lack of suitable prey, and predation are the main causes of juvenile fish mortality (Guidetti, 2001; Cuadros et al., 2018).

CONCLUSION

Durrieu de Madron et al. (2011) highlighted the need to improve our understanding of species' distributions and ecological preferences to determine marine ecosystem responses to different anthropogenic impacts in the Mediterranean that affect juvenile survival in nursery areas. Matić-Skoko et al. (2020) suggested that significantly modified juvenile fish communities in recent decades may be the result of constant human embankment and marine infrastructure construction along the coast. Such an undesirable continuous practice on a wider spatial scale could potentially lead to biological homogenisation (Cacabelos et al., 2016; Pastro et al., 2016) due to changes in sediment or bottom type. In that sense, although there is a critical need to define the value of coastal habitats as nurseries for population abundance and growth of economically important or exploited species, quantifying the value of coastal habitats at the population level is a complex task (Beck et al., 2001; Duarte et al., 2008; Fodrie et al., 2009; Vasconcelos et al., 2011). The variability or similarity of structural features among different habitats illustrates species tolerance to available nursery conditions and should provide valuable information toward future spatially explicit predictions of species' distribution responses and resilience to potential changes in coastal conditions. Furthermore, variability of spatial and environmental use patterns in coastal areas should provide knowledge on the relevance of local regulation in defining nursery function. Ultimately, determining important sites for juveniles is a fundamental step toward the accurate identification of coastal nursery areas (Beck et al., 2001) that are essential for these species' metapopulations.

DATA AVAILABILITY STATEMENT

The raw data supporting the conclusions of this article will be made available by the authors, without undue reservation.

ETHICS STATEMENT

The animal study was reviewed and approved by Ethics Committee of the Institute of Oceanography and Fisheries in Split.

AUTHOR CONTRIBUTIONS

SM-S, DV, HU and MP analysed the data end existing literature in collaboration with PT and DB. SM-S and DV wrote the draft of the manuscript. All authors conceived the research and participated in the improvement and revision of the document.

FUNDING

This study was fully supported by the Croatian Science Foundation (HRZZ) under project IP-2016-06-9884 (NurseFish).

ACKNOWLEDGMENTS

We are grateful to Marti J. Anderson (Director of PRIMER-e) for the knowledge shared with us during the PERMANOVA workshop at the University of Trieste, Italy (September 2019).

SUPPLEMENTARY MATERIAL

The Supplementary Material for this article can be found online at: https://www.frontiersin.org/articles/10.3389/fmars.2022.849092/full#supplementary-material

REFERENCES

Anderson, M. J. (2001). Permutation tests for univariate or multivariate analysis of variance and regression. *Can. J. Fish. Aquat. Sci.* 58, 626–639. doi: 10.1139/f01-004

Anderson, M. J., Gorley, R. N., and Clarke, K. R. (2008). *PERMANOVA+ for PRIMER: guide to software and statistical methods*. Plymouth: PRIMER-E, 214.

Anderson, M. J., and Willis, T. J. (2003). Canonical analysis of principal coordinates: a useful method of constrained ordination for ecology. *Ecology* 84, 511–525. doi: 10.1890/0012-9658(2003)084[0511:caopca]2.0.co;2

Araújo, F. G., Azevedo, M. C. C., and Guedes, A. P. P. (2016). Interdecadal changes in fish communities of a tropical bay in southeastern Brazil. *Reg. Stud. Mar. Sci.* 3, 107–118. doi: 10.1016/j.rsma.2015.06.001

Barbeaux, S. J., and Hollowed, A. B. (2018). Ontogeny matters: climate variability and effects on fish distribution in the eastern Bering Sea. *Fish. Ocean.* 27, 1–15. doi: 10.1111/fog.12229

Barbier, E. B., Hacker, S. D., Kennedy, C., Koch, E. W., Stier, A. C., and Silliman, B. R. (2011). The value of estuarine and coastal ecosystem services. *Ecol. Monogr.* 81, 169–193. doi: 10.1890/10-1510.1

Barceló, C., Ciannelli, L., Olsen, E. M., Johannessen, T., and Knutsen, H. (2016). Eight decades of sampling reveal a contemporary novel fish assemblage in coastal nursery habitats. *Glob. Chang. Biol.* 22, 1155–1167. doi: 10.1111/gcb.13047

Bartulović, V., Dulčić, J., Matić-Skoko, S., and Glamuzina, B. (2011). Reproductive cycles of *Mugil cephalus*, *ramada* and *Liza aurata* (Teleostei: Mugilidae). *J. Fish. Biol.* 78, 2067–2073. doi: 10.1111/j.1095-8649.2011.02953.x

Beck, M. W., Heck, K. L., Able, K. W., Childers, D. L., Eggleston, D. B., Gillanders, B. M., et al. (2001). The identification, conservation, and management of estuarine and marine nurseries for fish and invertebrates. *BioScience* 51, 633–641. doi: 10.1641/0006-3568(2001)051[0633:ticamo]2.0.co;2

Bellard, C., Bertelsmeier, C., Leadley, P., Thuiller, W., and Courchamp, F. (2012). Impacts of climate change on the future of biodiversity. *Ecol. Lett.* 15, 365–377. doi: 10.1111/j.1461-0248.2011.01736.x

Biagi, F., Gambaccini, S., and Zazzetta, M. (1998). Settlement and recruitment in fishes: the role of coastal areas. *Ital. J. Zool.* 65, 269–274. doi: 10.1080/11250009809386831

Blaber, S. J. M., Brewer, D. T., and Salini, J. P. (1995). Fish communities and the nursery role of the shallow inshore waters of a tropical bay in the gulf of Carpentaria, Australia. *Est. Coast. Shelf Sci.* 40, 177–193. doi: 10.1016/S0272-7714(05)80004-6

Brothers, E. B., Williams, D. McB, and Sales, P. F. (1983). Length of larval life in twelve families of fishes at "one tree lagoon," Great Barrier Reef, Australia. *Mar. Biol.* 76, 319–324. doi: 10.1007/bf00393035

Cacabelos, E., Martins, G. M., Thompson, R., Prestes, A. C. L., Azevedo, J. M. N., and Neto, A. I. (2016). Material type and roughness influence structure of inter−tidal communities on coastal defences. *Mar. Ecol.* 37, 801–812. doi: 10.1111/maec.12354

Cheminee, A., Francour, P., and Harmelin-Vivien, M. (2011). Assessment of *Diplodus* spp. (Sparidae) nursery grounds along the rocky shore of Marseilles (France, NW Mediterranean). *Sci. Mar.* 75, 181–188. doi: 10.3989/scimar.2011.75n1181

Cheminée, A., Merigot, B., Vanderklift, M. A., and Francour, P. (2016). Does habitat complexity influence fish recruitment? Mediterr. *Mar. Sci.* 17, 39–46. doi: 10.12681/mms.1231

Cheminée, A., Pastor, J., Bianchimani, O., Thiriet, P., Sala, E., Cottalorda, J. M., et al. (2017). Juvenile fish assemblages in temperate rocky reefs are shaped by the presence of macro-Algae canopy and its three-dimensional structure. *Sci. Rep.* 7, 1–11. doi: 10.1038/s41598-017-15291-y

Clarke, K. R., and Gorley, R. N. (2015). *PRIMER v7: User Manual/Tutorial*. Plymouth: PRIMER-E.

Clarke, K. R., Tweedley, J. R., and Valesini, F. J. (2014). Simple shade plots aid better long-term choices of data pre-treatment in multivariate assemblage studies. *J. Mar. Biol. Ass. U.K.* 94, 1–16. doi: 10.1017/S0025315413001227

Clarke, K. R., and Warwick, R. M. (2001). *Change in Marine Communities: An Approach to Statistical Analysis and Interpretation*, 2nd Edn. Plymouth, UK: Primer-E Ltd.

Cuadros, A., Basterretxea, G., Cardona, L., Cheminée, A., Hidalgo, M., and Moranta, J. (2018). Settlement and post-settlement survival rates of the white seabream (*Diplodus sargus*) in the western Mediterranean Sea. *PLoS One* 13:e0190278. doi: 10.1371/journal.pone.0190278

Dahlgren, C. P., and Eggleston, D. B. (2014). Ecological Processes Underlying Ontogenetic Habitat Shifts in a Coral Reef Fish. *Ecology* 81, 2227–2240. doi: 10.2307/177110

Deudero, S., Morey, G., Frau, A., Moranta, J., and Moreno, I. (2008). Temporal trends of littoral fishes at deep *Posidonia oceanica* seagrass meadows in a temperate coastal zone. *J. Mar. Syst.* 70, 182–195. doi: 10.1016/J.JMARSYS.2007.05.001

DHMZ (2019). *Meteorological and Hydrological Service*. Available online at: www.meteo.hr, (accessed on Dec 17, 2021)

Di Franco, A., Coppini, G., Pujolar, J. M., De Leo, G. A., Gatto, M., Lyubartsev, V., et al. (2012). Assessing Dispersal Patterns of Fish Propagules from an Effective Mediterranean Marine Protected Area. *PLoS One* 7:e52108. doi: 10.1371/journal.pone.0052108

Dobroslavić, T., Mozara, R., Glamuzina, B., and Bartulović, V. (2017). Reproductive patterns of bogue, *Boops boops* (Sparidae), in the southeastern Adriatic Sea. *Acta Adria.* 58, 117–125. doi: 10.32582/aa.58.1.9

Doney, S. C., Ruckelshaus, M., Duffy, J. E., Barry, J. P., Chan, F., English, C. A., et al. (2012). Climate change impacts on marine ecosystems. *Annu. Rev. Mar. Sci.* 4, 11–37. doi: 10.1146/annurev-marine-041911-111611

Downie, A. T., Leis, J. M., Cowman, P. F., McCormick, M. I., and Rummer, J. L. (2021). The influence of habitat association on swimming performance in marine teleost fish larvae. *Fish Fish.* 22, 1187–1212. doi: 10.1111/faf.12580

Duarte, C. M. (2000). Marine biodiversity and ecosystem services: an elusive link. *J. Exp. Mar. Biol. Ecol.* 250, 117–131. doi: 10.1016/S0022-0981(00)00194-5

Duarte, C. M., Dennison, W. C., Orth, R. J. W., and Carruthers, T. J. B. (2008). The Charisma of Coastal Ecosystems: addressing the Imbalance. *Estuar. Coast* 31, 233–238. doi: 10.1007/s12237-008-9038-7

Dulčić, J., Fencil, M., Matić-Skoko, S., Kraljević, M., and Glamuzina, B. (2004). Diel catch variations in a shallow-water fish assemblage at Duće-Glava, eastern Adriatic (Croatian coast). *J. Mar. Biol. Ass. U.K.* 84, 659–664. doi: 10.1017/S0025315404009701h

Dulčić, J., and Kovačić, M. (2020). *Ihtiofauna Jadranskog mora*. Zagreb: Golden marketing – Tehnička knjiga.

Dulčić, J., Kraljević, M., Grbec, B., and Pallaoro, A. (1997). Composition and temporal fluctuations of inshore juvenile fish populations in the Kornati Archipelago, eastern middle Adriatic. *Mar. Biol.* 129, 267–277. doi: 10.1007/s002270050167

Dulčić, J., Matić-Skoko, S., Kraljević, M., Fencil, M., and Glamuzina, B. (2005). Seasonality of a fish assemblage in shallow waters of Duće-Glava, eastern middle Adriatic. *Cybium* 29, 57–63.

Dulčić, J., Tutman, P., Matić-Skoko, S., Kraljević, M., Skaramuca, B., Glavić, N., et al. (2007). Y-O-Y fish species richness in the littoral shallows of the Neretva and Mala Neretva river estuaries (Eastern Adriatic. Croatian coast). *Acta Adriat.* 48, 89–94.

Durrieu de Madron, X., Guieu, C., Sempéré, R., Conan, P., Cossa, D., D'Ortenzio, F., et al. (2011). Marine ecosystems' responses to climatic and anthropogenic forcings in the Mediterranean. *Prog. Oceanogr.* 91, 97–166. doi: 10.1016/j.pocean.2011.02.003

Félix-Hackradt, F. C., Hackradt, C. W., Treviño-Otón, J., Pérez-Ruzafa, A., and García-Charton, J. A. (2014). Habitat use and ontogenetic shifts of fish life stages at rocky reefs in South-western Mediterranean Sea. *J. Sea Res.* 88, 67–77. doi: 10.1016/j.seares.2013.12.018

Fodrie, F. J., Levin, L. A., and Lucas, A. J. (2009). Use of population fitness to evaluate the nursery function of juvenile habitats. *Mar. Ecol. Prog. Ser.* 385, 39–49. doi: 10.3354/meps08069

Francour, P. (1997). Fish assemblages of *Posidonia oceanica* beds at Port-Cros (France. *Mar. Ecol.* 18, 157–173. doi: 10.1111/j.1439-0485.1997.tb00434.x

Francour, P., Ganteaume, A., and Poulain, M. (1999). Effects of boat anchoring in *Posidonia oceanica* seagrass beds in the Port-Cros national park (northwestern Mediterranean Sea). *Aquat. Conserv* 9, 391–400. doi: 10.1002/(SICI)1099-0755(199907/08)9:43.0.CO;2-8

García-Rubies, A., and Macpherson, E. (1995). Substrate use and temporal pattern of recruitment in juvenile fishes of the Mediterranean littoral. *Mar. Biol.* 124, 35–42. doi: 10.1007/BF00349144

Gloginja, B., and Mitrović, L. (2021). "Hydrographic and Oceanographic Characteristics of the Southern Part of the Adriatic Sea," in *The Montenegrin*

Adriatic Coast, eds A. Joksimović, M. Đurović, I. S. Zonn, A. G. Kostianoy, and A. V. Semenov (Springer: Springer Link).

Grbec, B., and Morović, M. (1997). Seasonal thermohaline fluctuations in the middle Adriatic Sea. *Il Nuovo Cimento* 20, 561–576.

Grbec, B., Morović, M., Matić, F., Ninčević, Ž, Marasović, I., Vidjak, O., et al. (2015). Climate regime shifts and multi-decadal variability of the Adriatic Sea pelagic ecosystem. *Acta Adriat.* 56, 47–66.

Guidetti, P. (2001). Population dynamics and post-settlement mortality of the ornate wrasse, *Thalassoma pavo*, in the Tyrrhenian sea (western Mediterranean). *Ital. J. Zool.* 68, 75–78. doi: 10.1080/11250000109356386

Guidetti, P., Fanelli, G., Fraschetti, S., Terlizzi, A., and Boero, F. (2002). Coastal fish indicate human-induced changes in the Mediterranean littoral. *Mar. Environ. Res.* 53, 77–94. doi: 10.1016/s0141-1136(01)00111-8

Halpern, B. S., Walbridge, S., Selkoe, K. A., Kappel, C. V., Micheli, F., D'Agrosa, C., et al. (2008). A global map of human impact on marine ecosystems. *Science* 319, 948–952. doi: 10.1126/science.1149345

Harmelin-Vivien, M. (1984). "Ichtyofaune des herbiers de posidonies du parc naturel régional de Corse," in *Internation, Workshop Posidonia oceanica Beds, Boudouresque*, eds C. F. Jeudy, A. de Grissac, and J. Olivier (Marseille: GIS Posidonie Publ.), 291–301.

Hinz, H., Reñones, O., Gouraguine, A., Johnson, A. F., and Moranta, J. (2019). Fish nursery value of algae habitats in temperate coastal reefs. *PeerJ* 7:e6797. doi: 10.7717/peerj.6797

Hixon, M. A., and Johnson, D. W. (2009). *Density dependence and independence. eLS (Encyclopedia of life sciences)*. New Jersey: John Wiley & Sons, Ltd.

Hoare, D. J., Krause, J., Peuhkuri, N., and Godin, J.-G. J. (2000). Body size and shoaling in fish. *J. Fish Biol.* 57, 1351–1366. doi: 10.1006/jfbi.2000.1446

Jardas, I. (1996). *Jadranska ihtiofauna*. Školska knjiga: Zagreb(in Croatian), 533.

Jones, G. P., Almany, G. R., Russ, G. R., Sale, P. F., Steneck, R. S., van Oppen, M. J. H., et al. (2009). Larval retention and connectivity among populations of corals and reef fishes: history, advances and challenges. *Coral Reefs* 28, 307–325. doi: 10.1007/s00338-009-0469-9

Krvavica, N., and Ružić, I. (2020). Assessment of sea-level rise impacts on salt-wedge intrusion in idealized and Neretva River Estuary. *Estua. Coast. Shelf Sci.* 234:106638. doi: 10.1016/j.ecss.2020.106638

La Mesa, G., Molinari, A., Gambaccini, S., and Tunesi, L. (2011). Spatial pattern of coastal fish assemblages in different habitats in North-western Mediterranean. *Mar. Ecol.* 32, 104–114. doi: 10.1111/j.1439-0485.2010.00404.x

Lanier, J. M., and Scharf, F. S. (2007). Experimental investigation of spatial and temporal variation in estuarine growth of age-0 juvenile red drum (*Sciaenops ocellatus*). *J. Exper. Mar. Biol. Ecol.* 349, 131–141. doi: 10.1016/j.jembe.2007.05.004

Laurel, B. J., Cote, D., Gregory, R. S., Rogers, L. A., Knutsen, H., and Olsen, E. M. (2017). Recruitment signals in juvenile cod surveys depend on thermal growth conditions. *Can. J. Fish. Aqua. Sci.* 74, 511–523. doi: 10.1139/cjfas-2016-0035

Machado, I., Calliari, D., Denicola, A., and Rodríguez-Graña, L. (2017). Coupling suitable prey field to *in situ* fish larval condition and abundance in a subtropical estuary. *Estuar. Coast. Shelf Sci.* 187, 31–42. doi: 10.1016/j.ecss.2016.12.021

Martins, G. M., Harley, C. D. G., Faria, J., Vale, M., Hawkins, S. J., Neto, A. I., et al. (2019). Direct and indirect effects of climate change squeeze the local distribution of a habitat-forming seaweed. *Mar. Ecol. Prog. Ser.* 626, 43–52. doi: 10.3354/meps13080

Matić-Skoko, S., Peharda, M., Pallaoro, A., Cukrov, M., and Baždarić, B. (2007). Infralittoral fish assemblages in the Zrmanja estuary, Adriatic Sea. *Acta Adria.* 48, 45–55.

Matić-Skoko, S., Vrdoljak, D., Uvanović, H., Pavičić, M., Tutman, P., and Bojanić Varezić, D. (2020). Early evidence of a shift in juvenile fish communities in response to conditions in nursery areas. *Sci. Rep.* 10:21078. doi: 10.1038/s41598-020-78181-wda0b5c49-0119-4a19-9b2c-81d12c0d245c

Novosel, M., Olujić, G., Cocito, S., and Požar-Domac, A. (2005). "Submarine freshwater springs in the Adriatic Sea: a unique habitat for the bryozoan *Pentapora fascialis*," in *Proceedings of the 13th International Conference of the International Bryozoology Association*, ed. G Moyano., I Hugo., J. M Cancino., P. N Wyse Jackson (London: Balkema Publishers (London)), 215–221.

Pastro, G., Dias, G. M., Pereira, G. H., and Gibran, F. Z. (2016). The consequences of small-scale variations in habitat conditions driven by a floating marina on reef fish assemblages of SE Brazil. *Ocean Coast. Manag.* 141, 98–106. doi: 10.1016/j.ocecoaman.2017.03.004

Planque, B., and Fox, C. J. (1998). Interannual variability in temperature and the recruitment of Irish Sea cod. *Mar. Ecol. Prog. Ser.* 172, 101–105. doi: 10.3354/meps172101

Potter, I. C., Chuwen, B. M., Hoeksema, S. D., and Elliott, M. (2010). The concept of an estuary: a definition that incorporates systems which can become closed to the ocean and hypersaline. *Estuar. Coast. Shelf Sci.* 87, 497–500. doi: 10.1016/j.ecss.2010.01.021

Ruitton, S., Francour, P., and Boudouresque, C. (2000). Relationships between Algae. *Estuar. Coast. Shelf Sci.* 50, 217–230. doi: 10.1006/ecss.1999.0546

Sala, E. (2004). The past and present topology and structure of the Mediterranean subtidal rocky-shore food webs. *Ecosystem* 7, 333–340. doi: 10.1007/s10021-003-0241-x

Sala, E., Ballesteros, E., Dendrinos, P., Di Franco, A., Ferretti, F., Foley, D., et al. (2012). The structure of Mediterranean rocky reef ecosystems across environmental and human gradients, and conservation implications. *PLoS ONE* 7:e32742. doi: 10.1371/journal.pone.0032742

Sale, P. F. (2006). *Coral Reef Fishes: Dynamics and Diversity in a Complex Ecosystem*. Amsterdam: Academic Press.

Scharf, F. S., Manderson, J. P., and Fabrizio, M. C. (2006). The effects of seafloor habitat complexity on survival of juvenile fishes: species-specific interactions with structural refuge. *J. Exp. Mar. Biol. Ecol.* 335, 167–176. doi: 10.1016/j.jembe.2006.03.018

Shoji, J., Toshito, S., Mizuno, K., Kamimura, Y., Hori, M., and Hirakawa, K. (2011). Possible effects of global warming on fish recruitment: shifts in spawning season and latitudinal distribution can alter growth of fish early life stages through changes in daylength. *ICES J. Mar. Sci.* 68, 1165–1169.

Stagličić, N., Matić-Skoko, S., Pallaoro, A., Grgičević, R., Kraljević, M., Tutman, P., et al. (2011). Long term trends in the structure of eastern Adriatic littoral fish assemblages: consequences for fisheries management. *Estuar. Coast. Shelf Sci.* 94, 263–271. doi: 10.1016/j.ecss.2011.07.005

Vasconcelos, R. P., Eggleston, D. B., Le Pape, O., and Tulp, I. (2013). Patterns and processes of habitat-specific demographic variability in exploited marine species. *ICES J. Mar. Sci.* 71, 638–647. doi: 10.1093/icesjms/fst136

Vasconcelos, R. P., Reis-Santos, P., Costa, M. J., and Cabral, H. N. (2011). Connectivity between estuaries and marine environment: integrating metrics to assess estuarine nursery function. *Ecol. Ind.* 11, 1123–1133. doi: 10.1016/j.ecolind.2010.12.012

Zorica, B., Čikeš Keč, V., Vrgoč, N., Isajlović, I., Piccinetti, C., Mandić, M., et al. (2020). A review of reproduction biology and spawning/nursery grounds of the most important Adriatic commercial fish species in the last two decades. *Acta Adria.* 61, 89–100. doi: 10.32582/aa.61.1.7

Conflict of Interest: The authors declare that the research was conducted in the absence of any commercial or financial relationships that could be construed as a potential conflict of interest.

frontiers | Frontiers in Marine Science

ORIGINAL RESEARCH
published: 20 May 2022
doi: 10.3389/fmars.2022.733540

Hydrological and Biogeochemical Patterns in the Sicily Channel: New Insights From the Last Decade (2010-2020)

Francesco Placenti[1], *Marco Torri*[2*], *Federica Pessini*[3], *Bernardo Patti*[4], *Vincenzo Tancredi*[1], *Angela Cuttitta*[2], *Luigi Giaramita*[1], *Giorgio Tranchida*[1] *and Roberto Sorgente*[3]

[1] National Research Council of Italy, Institute for the Study of Anthropic Impacts and Sustainability in the Marine Environment, (CNR-IAS), Campobello di Mazara, Italy, [2] National Research Council of Italy, Institute for Studies on the Mediterranean (CNR-ISMed), Palermo, Italy, [3] National Research Council of Italy, Institute for the Study of Anthropic Impacts and Sustainability in the Marine Environment (CNR-IAS), Oristano, Italy, [4] National Research Council of Italy, Institute for the Study of Anthropic Impacts and Sustainability in the Marine Environment (CNR-IAS), Palermo, Italy

OPEN ACCESS

Edited by:
Jose Luis Iriarte,
Austral University of Chile, Chile

Reviewed by:
Milena Menna,
Istituto Nazionale di Oceanografia e di Geofisica Sperimentale, Italy
Yannis Cuypers,
Sorbonne Universités, France

***Correspondence:**
Marco Torri
marco.torri@ismed.cnr.it

Specialty section:
This article was submitted to Marine Fisheries, Aquaculture and Living Resources, a section of the journal Frontiers in Marine Science

Received: 30 June 2021
Accepted: 22 April 2022
Published: 20 May 2022

Citation:
Placenti F, Torri M, Pessini F, Patti B, Tancredi V, Cuttitta A, Giaramita L, Tranchida G and Sorgente R (2022) Hydrological and Biogeochemical Patterns in the Sicily Channel: New Insights From the Last Decade (2010-2020). Front. Mar. Sci. 9:733540. doi: 10.3389/fmars.2022.733540

The hydrological and biogeochemical time series from 2010 to 2020 have highlighted specific relationships and trends in oceanographic processes and nutrient patterns in the Sicily Channel. Specifically, temperature and salinity time series in the intermediate waters showed a sharp annual increase of about 0.06°C and 0.09 within the period 2010-2020, at rates that are about 50% higher than what observed within the previous decade. Similar trends were also present in deep waters, although with lower variations of both temperature and salinity. The time series in the intermediate water, also highlighted the presence of quasi cyclic fluctuations that can be associated with the alternation of the circulation modes (cyclonic and anticyclonic) of the Northern Ionian Gyre. Moreover, an opposite trend emerged by comparing the nutrients and salinity time series in intermediate waters, while similar patterns has been evidenced between nutrients and chlorophyll-a concentration. This latter finding is not consistently present in the Mediterranean area, suggesting the need of further studies on a wider scale.

Keywords: hydrological patterns, interannual variability, biogeochemical patterns, Sicily Channel, Mediterranean Sea

INTRODUCTION

The Mediterranean Sea (MS) consists of two basins, the Western Mediterranean (WMS) and the Eastern Mediterranean (EMS), connected by the Sicily Channel (SC), and is characterized by a limited water exchange with the Atlantic Ocean. In the MS the net evaporation exceeds the precipitation, driving an anti-estuarine circulation through the Strait of Gibraltar, which has important implications on the physical and biogeochemical properties of the MS. The thermohaline circulation of the MS is described as an open basin-wide cell, which involves the gradual salinification of the fresher surface Atlantic water (AW) while propagating eastward (Gačić et al., 2013), and its transformation into intermediate water (IW), called Levantine Intermediate Water (LIW) or Cretan Intermediate Water (CIW), depending on the specific formation area (Levantine or Cretan Sea, CS). IW spreads westward

and its core is identifiable in the whole MS by a subsurface salinity maximum (S_{max}, Schroeder et al., 2017). It flows into the Ionian Sea (IS), with a significant flow northward to the Adriatic Sea (AdS), and constitutes an important preconditioning agent for the formation of both the Adriatic deep water (AdDW) and Mediterranean deep waters (eastern, EMDW and western, WMDW) (e.g. Roether et al., 1996; Gačić et al., 2013). Some authors have highlighted the presence of two main modes of circulation (cyclonic and anticyclonic) of the North Ionian Gyre (NIG), interpreted in terms of internal processes (e.g. Borzelli et al., 2009; Gačić et al., 2010; Gačić et al., 2011; Gačić et al., 2014; Theocharis et al., 2014), which, alternating on a multiannual scale, operate a different redistribution of heat and salt in the central and Levantine area of the MS. Furthermore, the quasi decadal reversal of the NIG influences the strength of the Mid-Ionian Jet (MIJ; Robinson et al., 2001) and generates cascading repercussions on the physical and chemical characteristics of the water masses in the EMS, as well as in the SC and in the WMS (Menna et al., 2019). A process to explain such reversal is a feedback mechanism, named Adriatic-Ionian Bimodal Oscillation System _BIOS_ (Civitarese et al., 2010; Gačić et al., 2010), driven by the difference in salinity between the saltier and warmer waters originating from EMS (LIW and Levantine Surface Water, _LSW_), and the less saline AW entering from the SC (Gačić et al., 2011; Gačić et al., 2014). Briefly, an anticyclonic phase (1993–1997 and 2006–2010) inhibits the AW advection (weakening the MIJ) to the southern Levantine basin and favours the production of salty and warm LIW/CIW. Conversely, a cyclonic phase (1998–2005) favoring the AW advection (strengthening the MIJ) to the southern Levantine Basin, leads to a stronger dilution in the EMS (Schroeder et al., 2017 and internal references). In particular, the anticyclonic mode represents a preconditioning mechanism for the dense-water formation processes in the Aegean Sea and eventually for Eastern Mediterranean Transient (EMT) like events (Demirov and Pinardi, 2002; Gačić et al., 2011). During these events it has been showed that, under favourable conditions, the dense water formation area can switch from the AdS to the CS, with a consequent change of the Eastern Mediterranean Deep Waters (EMDW) properties and a repercussion on the entire thermohaline cell (e.g. Gačić et al., 2013). The effects related to EMT and BIOS also show that the MS is not in a steady-state and that in the last decades it has been affected by a continuous increase in temperature and salinity (e.g. Lacombe et al., 1985; Rixen et al., 2005; Millot, 2007; Borghini et al., 2014; Schroeder et al., 2017), probably due to the effects associated with global warming. Salinity and temperature positive trends, especially in the IW, also show a specific interannual variability (e.g. Gasparini et al., 2005; Gačić et al., 2013; Bonanno et al., 2014; Schroeder et al., 2017), whose effects migrate from one to another basin and can be observed mainly in the SC with a time delay respect to the formation period of about 8 years, based on the data of the transient tracer (Roether et al., 1998), or 10-13 years on the basis of the salinity anomalies (Gačić et al., 2013). In this context, the SC can be considered as a key point for the comprehension of the phenomena underlying the thermohaline circulation at basin scale, as well as of the effects of this variability on the biogeochemical characteristics of the water masses that pass through it.

Biogeochemically, the MS is an oligotrophic basin despite being almost entirely surrounded by land with high nutrient loadings (e.g. Béthoux et al., 1998; Krom et al., 2004) derived from a large coastal population. The main source of dissolved organic phosphorus (P) and nitrogen (N) entering the WMS and EMS, primarily *via* the Straits of Gibraltar and Sicily, are mineralized to phosphate (PO_4) and nitrate (NO_3) and subsequently exported out of the basin by the prevailing anti-estuarine circulation (e.g. Powley et al., 2017). The very low productivity of the MS is therefore linked both to the anti-estuarine circulation (Krom et al., 2010) and to the chemical speciation of the dissolved P and N. They in fact reflects a switch from less bioavailable chemical forms of P and N entering the MS to more bioavailable forms leaving the MS (Powley et al., 2017). The anti-estuarine circulation also contributes to the higher primary productivity of the WMS respect to the EMS, as it acts on the lateral transport of dissolved inorganic nutrients in the deeper water, from the EMS to the WMS. It follows that deep waters (DW) of the WMS are characterized by higher NO_3 and PO_4 concentrations than those of the EMS (e.g. Ribera D'Alcalà et al., 2003) and carried up through upwelling phenomena in the photic zone. Another peculiarity of the MS is the higher molar NO_3:PO_4 DW ratios (21:1 on average in the WMS to 29:1 within the EMS, Ribera D'Alcalà et al., 2003) respect to the global ocean (N:P=16:1, Redfield et al., 1963). The debate on the anomaly of this peculiarity is still open, although recent analysis suggest that for the EMS, the high N:P ratio of the external inputs, together with very limited denitrification (Krom et al., 2010; Huertas et al., 2012; Van Cappellen et al., 2014), explains the very high NO_3:PO_4 DW ratio (Powley et al., 2017).

The aim of this study is to examine the interannual variability of thermohaline and biogeochemical properties of the water masses flowing through the SC in summer during the period since 2010 to 2020. We analyzed the potential mechanism controlling the long-term variability of the water masses properties and evaluated the impact on nutrient concentrations and on the productivity of the marine ecosystem.

DATASET AND METHODS

Oceanographic data have been acquired over 10 oceanographic surveys (named Bansic) carried out in the SC during the summer period from 2010 to 2020 (except for year 2019) aboard the Urania, Minerva Uno and Dallaporta vessels (**Figure 1** and **Table 1**). For this study, *in-situ* sampling design was focused on an inshore-offshore transect approximately perpendicular to the Sicilian coast, composed by 10 stations spaced about 12 NM, comparable to the Ross by deformation radius (Sorgente et al., 2011).

Hydrological Data

The long-term variability in the hydrological characteristics of the SC has been analyzed on the basis of vertical profiles of

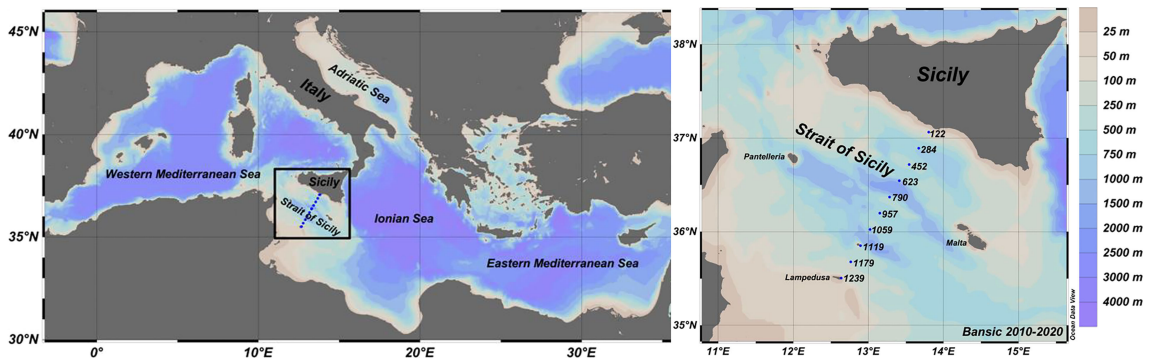

FIGURE 1 | Mediterranean Sea map (left panel); CTD and Nutrients stations in the Sicily Channel (right panel).

potential temperature (θ°C), salinity (S) and dissolved oxygen (DO mg/l) obtained from the surface to the bottom by means of a Conductivity Temperature Depth (CTD-rosette system; Tab. 1). It consists of a SBE 911 plus probe and a General Oceanic's rosette, equipped with 24 Niskin bottles. Moreover, the Chlorophyll-a concentration (Chl-a μg/l), measured from the fluorescence probe, has been examined to characterize the productivity of the upper water column. The probes were calibrated before each oceanographic survey. The collected downcast data were quality-checked and processed in agreement with the Mediterranean and ocean database instructions (Brankart, 1994), using the Seasoft-Win32 software. The overall accuracies are within 0.001°C for temperature, 0.001 sm^{-1} for conductivity, and 0.015% of full scale for pressure.

Temperature and Salinity Time Series

The interpretation of the θ, S, σ, DO profiles and of the θ_S diagram carried out in each station and in all the years has allowed us to recognize the various main water masses present in the study area, i.e. the SW (0-100 m depth, essentially consisting of AW), of the sub-superficial IW (200-500 m depth, mostly consisting of LIW) and locally also the upper part of the DW (>500 m depth) (**Figure 2A**; **Table 1**; **Supplementary 1**). Specifically, the AW and LIW were identified through the minimum and maximum of salinity that characterizes their core, respectively.

For the computation of the θ and S time series of the AW core we used, for each station and for each year, the average value of θ and S included in the layer between the minimum of salinity and 10m below it (Bonanno et al., 2014), while for the IW core we used the average value of θ and S in the layer between the maximum salinity and 100m below it (Gasparini et al., 2005). Finally, for the DW we used, for each station and for each year, the average value of θ and S included in the layer between 500m-bottom, identified by the presence of a strong vertical gradient of θ, S and DO, clearly visible during the bansic14 and bansic15 surveys (**Figure 2B**). In this context, we worked on a clear signal of water masses characteristics, minimizing as much as possible the effects related to the mixing of the various water masses.

Nutrient Data

Marine water samples were collected from the surface to the bottom by means of Niskin bottles (**Table 1**). In particular, a variable number of fixed depths has been considered (surface–25m–50m–75m–100m–150m-200m–300m–400m–500m–600m–700m–800m–900m–1000m–bottom). All materials used for water sampling were earlier conditioned with 10% HCl and rinsed 3 times with ultrapure water. Unfiltered samples were

TABLE 1 | Oceanographic surveys carried out in the sicily channel and relative sampling activities (x_CTD and o_nutrient analysis) carried out in the 2010-2020 period.

Station	Longitude [°E]	Latitude [°N]	Bottom depth [m]	Bansic10 (25 June–14 July 2010)	Bansic11 (8 July–26 July 2011)	Bansic12 (4 July–23 July 2012)	Bansic13 (26 June–16 July 2013)	Bansic14 (22 July–9 August 2014)	Bansic15 (16 July–3 August 2015)	Bansic16 (30 June–14 July 2016)	Bansic17 (13 June–29 June 2017)	Bansic18 (07-19 September 2018)	Bansic20 (16-24 September 2020)
122	13.8028	37.064	50	x	xo	xo	xo	xo	xo	xo	xo	xo	xo
284	13.67	36.892	725	x	xo	xo	xo	xo	xo	xo	xo	xo	xo
452	13.5415	36.718	350	xo	xo	xo	xo	xo	xo	xo	x	xo	xo
623	13.4108	36.545	1150	x	xo	xo	xo	xo	xo	xo	xo	xo	xo
790	13.2805	36.371	410	xo	xo	xo	xo	xo	xo	x	xo		
957	13.1512	36.199	720	x	xo	xo	xo	xo	xo	x	xo		
1059	13.0227	36.025	610	xo	xo	xo	xo	xo	xo	xo	xo		
1119	12.8937	35.851	130	x	xo	xo	xo	xo	xo	xo	xo		
1179	12.7647	35.679	280	xo	xo	xo	xo		xo	x	xo		
1239	12.636	35.506	55	x	xo	xo	xo		xo	x	xo		

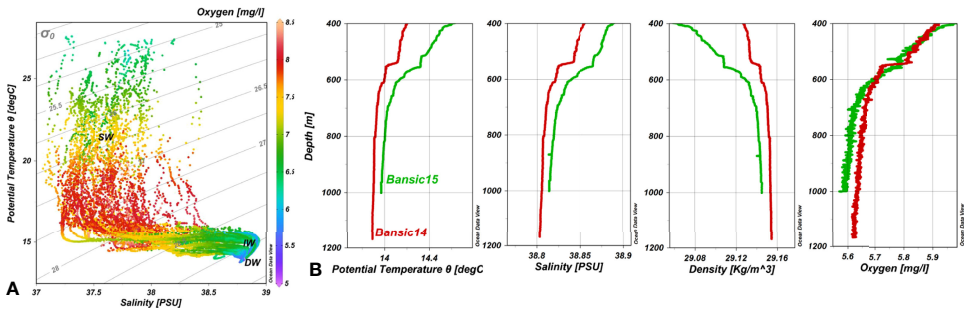

FIGURE 2 | **(A)** θ-S diagram and DO of all monitored stations. **(B)** zoom of the DW and related θ, S, σ and DO vertical profiles at the station 623 detected during Bansic 2014 (red line) and 2015 (green line) surveys.

stored at –20°C. In the laboratory, the concentration of nitrate, silicate and phosphate (μmol/l) was measured by means of a Sial Autoanalyzer ''QUAATRO'' following classical methods (Grasshoff et al., 1999), adapted to an automated system. The limit of detection for the procedure was, 0.02, 0.01 and 0.006 μmol/l for nitrates, silicates and phosphates, respectively.

Nutrient Time Series

Inorganic nutrients time series were reconstructed on the basis of the physical characterization of the water masses, through which three main layers (i.e. surface waters, SW; intermediate waters, IW; deep waters, DW) were identified with the relative depth ranges: 0-100; 200-500; 500-bottom (**Figures 2**, **5**). Specifically, each layer was associated with a load of inorganic nutrients (nitrates and silicates) calculated as the average concentration (μmol/l) detected in all the water samples contained within each layer and for each year (**Supplementary 2**).

Satellite Data

The satellite data were used in order to provide a description of the physical features occurring in the surface layers during the sampling periods. Therefore, mesoscale structures, such as currents, fronts and gyres, were observed by means of Absolute Dynamic Topography (ADT) (L4 gap-free monthly data; spatial resolution: 0.125x0.125 degree) and ADT-derived geostrophic velocity fields, produced by Copernicus Marine Environment Monitoring Service (CMEMS, http://marine.copernicus.eu/). Annual mean maps of ADT and geostrophic currents have been analysed in order to provide a description of the main surface circulation patterns occurred during the considered time series in the Central Mediterranean Sea. Furthermore, vorticity has been computed starting from the geostrophic velocities derived from satellite data for each grid point within the box [37.5°-39° N] and [17.5°-20°E], following the procedure described by Shabrang et al. (2016), more recently also applied by Notarstefano et al. (2019) and Mihanovic et al. (2021).

Statistical Analysis

The correlation between temperature and salinity patterns observed in the SC (i.e. positive/negative trends) and the circulation mode of the NIG (i.e. cyclonic/anticyclonic phase) was investigated through a cross-correlation analysis, considering a time lag ranging between 0 and 15 years and applying Cramer's V as a measure of association between the two nominal variables.

RESULTS

Temporal Trends of Hydrological Characteristics

Oceanographic surveys were carried out in different periods of the summer season (June-September, see **Table 1**). The average θ and S in the SW layer varied between 16.7°C and 19.3°C and between 37.4 and 37.6, respectively (**Figure 3**). This layer is characterized by a strong interannual and spatial variability (in terms of standard deviation), especially in 2012, and does not present a clear trend.

The IW layer is characterized by a lower spatial variability and a clear positive trend in terms of θ and S from 2010 to 2017 (dθ/dt ~0.09°C yr^{-1} and dS/dt ~0.016 yr^{-1}), while a weak decrease is registered between 2018 and 2020 (dθ/dt ~-0.04°C yr^{-1} and dS/dt ~-0.007 yr^{-1}). Our estimations are comparable with Schroeder et al. (2017), who reported a dθ/dt ~0.064°C yr^{-1} and dS/dt ~0.014 yr^{-1} in 2011-2016.

Finally, the θ and S time series recorded in the upper DW was characterized by a positive trend and by a lower variability, in which θ varied between 2010 and 2020 with an dθ/dt of 0.027°C yr^{-1}(**Figure 3**) while S varied between with an dS/dt of 0.005 yr^{-1}. The θ and S time series can be represented by two patterns, a positive one occurring from 2010 to 2016, with an dθ/dt of 0.05°C yr^{-1} and an dS/dt of 0.01 yr^{-1}, followed by a slightly negative trend where the θ dropped to 14.096°C with an dθ/dt of -0.01°C yr^{-1} while the S dropped to 38.835 with an dS/dt of -0.002 yr^{-1} (**Figure 3**).

Inorganic Nutrient Distribution Patterns

The nitrates, silicates and phosphates distribution patterns *vs* depth showed very low concentration values in SW (often below the instrumental detection limit for phosphate) most probably linked to their depletion by the phytoplankton for its

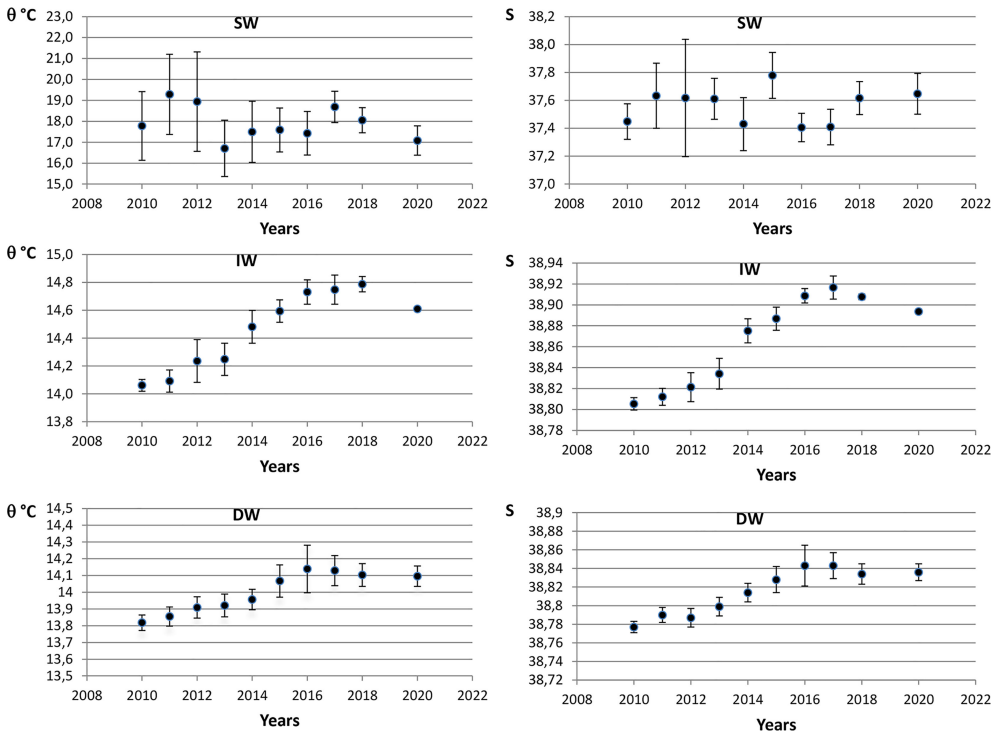

FIGURE 3 | Analysis of potential temperature (left panels) and salinity (right panels) time series computed by averaging over a water column of 10m below the S_{min} for the SW and 100m below S_{max} for the IW, which represent the core of the AW and LIW, respectively. For the DW was used the layer 500m-bottom. Bars indicate the standard deviation.

photosynthetic activity (**Figure 4**; **Table 1**; **Supplementary 2**). In the last decade the deep chlorophyll maximum (DCM) developed in the depth range 50-120 m (with peaks of maximum concentration around 70-80 m of depth), with the exception of July 2013, in which high fluorescence values (0.76 µg/l) were measured at 39 m of depth (**Figure 4**). Under the SW and the DCM, nutricline, silicocline and phosphocline developed with different slopes and depth and mirrored the decrease in dissolved oxygen. Higher oxygen concentrations were recorded close the Sicilian coast, at about 50 m depth within the nutrient depleted layer (**Figure 4**). The maximum concentrations of nitrates, silicates and phosphates of 7.66 µmol/l (St. 790 at 400m depth), 9.55 µmol/l (St. 284 at 700m depth) and 0.35 µmol/l (St. 790 at 400m depth) were detected during the 2011-2012-2017 surveys, respectively (**Figure 4**), while the average concentration of nutrients, for each water mass, are reported in **Supplementary 2**. The vertical profiles of nitrates to phosphates, in the years, show low values in the SW respect to IW and DW, with the regression line characterized by R^2>0.8 (**Figure 4**). The box plot of the N:P ratio, highlighted low values in the SW that increase to values >40 in the IW (with average value of 32), while in the DW the average value is 30 (**Figure 4**). These values are in agreement with the data reported for the SC by various authors (e.g. Ribera D'Alcalà et al., 2003; Schroeder et al., 2010; Placenti et al., 2013).

Temporal Trend of Biogeochemical Characteristics

The nitrate-silicates time series related to the SW highlighted a lower concentration values and variability over time compared to IW and DW (**Figure 5**). Nitrates showed a slightly negative trend in 2011-2016 and then it turned to be positive until 2020 (**Figure 5**). The silicates pattern was characterized by a more evident negative trend (2011-2016), in which the average concentration decreased from 0.93 to 0.38 µmol/l (-0.091 µmol/l yr^{-1}), and then increased to 0.88 µmol/l in 2020 (**Figure 5**). In the IW the nitrates and silicates highlighted similar concentration distribution patterns. Two trends can be distinguished, one negative (2011-2015) and one positive (2015-2018; **Figure 5**). In the first trend the average concentration of nitrates and silicates decreased by -0.61 and -0.54 µmol/l yr^{-1}, respectively. In the second trend, the average concentration of both nutrients increased by 0.47 µmol/l yr^{-1} (**Figure 5**). Average concentrations of nutrients dropped slightly in 2020, probably reflecting the start of a new cycle.

The DW was characterized by distribution patterns of average concentrations of nitrates and silicates similar to the IW, in which it was possible to outline two general trends: the first negative (2011-2015) and the second slightly positive (2015-2017/2018) (**Figure 5**). Finally, the average concentrations of both nutrients dropped slightly from 2017-2018 to 2020 (**Figure 5**).

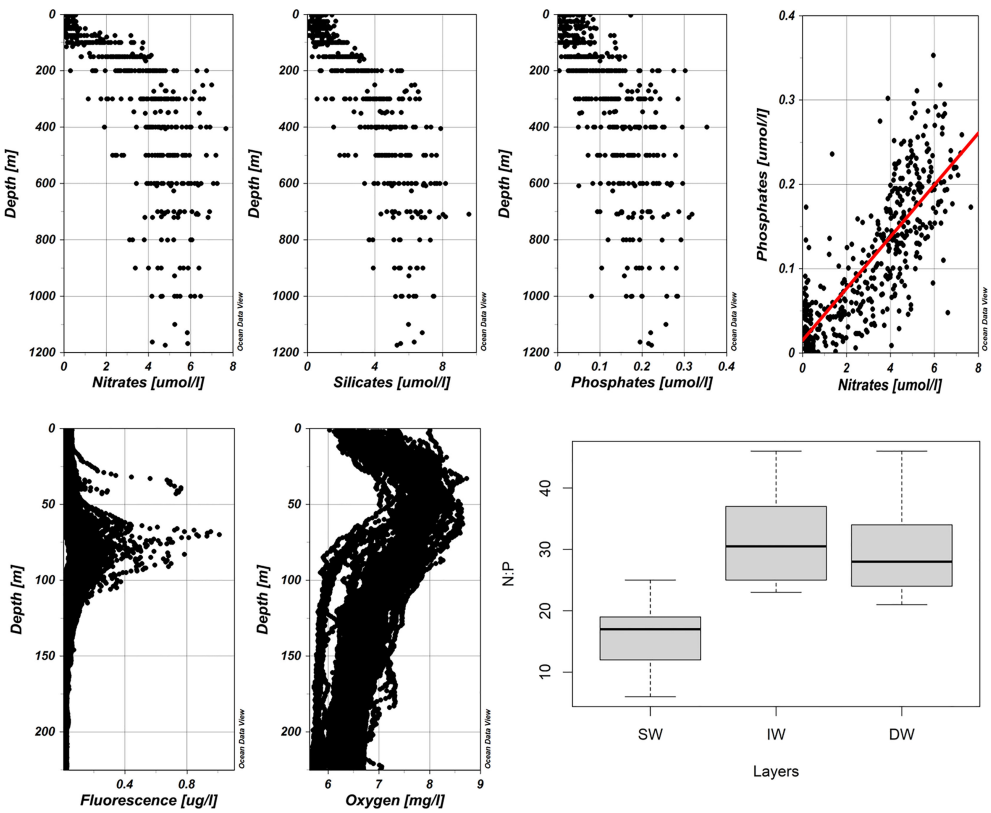

FIGURE 4 | In top panels are reported the vertical profiles of nitrates, silicates, phosphates, nitrates-phosphates diagram (in red, the regression line with the R^2>0.8). In bottom panels are reported the vertical profiles of fluorescence and dissolved oxygen of all stations, followed by the N:P ratio box plots in SW, IW and DW.

Although with higher variability, similar patterns emerged considering the chlorophyll-a concentration occurring in the surface layer (0-120m) (**Figure 5**). In particular, a significant positive Pearson correlation coefficient (r) has been computed between the sum of the scaled nutrients concentration (nitrates, silicates, phosphates) in the IW and the chlorophyll-a concentration in the upper layer (r= 0.67; p<0.05).

DISCUSSION AND CONCLUSION

While the surface temperature is able to provide the almost instantaneous signature of interactions with the atmosphere, which is by its nature subjected to great variability, the analysis of the variability of the heat and salt content in the deeper water masses provided a climate index more suitable for monitoring any changes over long periods. For this reason, we have integrated the intermediate and deep layer dataset with the previous ones carried out by Bonanno et al., 2014 and Ben Ismail et al., 2014 (**Figure 6**). Regarding the IW layer, time series presented in this study are in agreement with comparable time series collected in the SC by Gasparini et al., 2005; Gačić et al., 2013; Ben Ismail et al., 2014; Bonanno et al., 2014 and Schroeder et al., 2017. Specifically, it is thus possible to highlight a general increasing trend and the presence of "cyclic patterns" in temperature and salinity, that could be associated with the alternation of different circulation modes (cyclonic and anticyclonic) of the NIG in addition to IW formation processes. In particular, we infer an average annual increase of dT/dt ~0.047°C yr^{-1} and dS/dt ~0.01 yr^{-1} from the 1998-2007 (**Figure 6**), comparable to those estimated by Gasparini et al. (2005) and Schroeder et al. (2017). Such a trend of T and S could be related to the anticyclonic phase of the NIG estimated from 1988 to 1997 (mean ADT available from 1993 to 1997, **Figures 7A, E**), according to Bonanno et al., 2014. The anticyclonic circulation inhibits the AW advection to the southern Levantine basin, favouring the production of saltier and warmer IW, whose effects were observed in the SC with a variable time lag that deserves further studies and insights. The period 1998-2007 is followed by an abrupt reversal trend up to 2010, characterized by a dT/dt of -0.12°C yr^{-1} and dS/dt of -0.01 yr^{-1} (**Figure 6**). These trends, in agreement with Gačić et al., 2013; Ben Ismail et al., 2014; Bonanno et al., 2014; Schroeder et al., 2017, could be linked to the previous cyclonic phase of the NIG (1998-2005, **Figures 7B, E**). It favoured the strengthening of the MIJ and thus the AW advection to the southern Levantine basin, leading to an increasing of the water masses dilution in the EMS, according to Schroeder et al., 2017. Approximately, a new

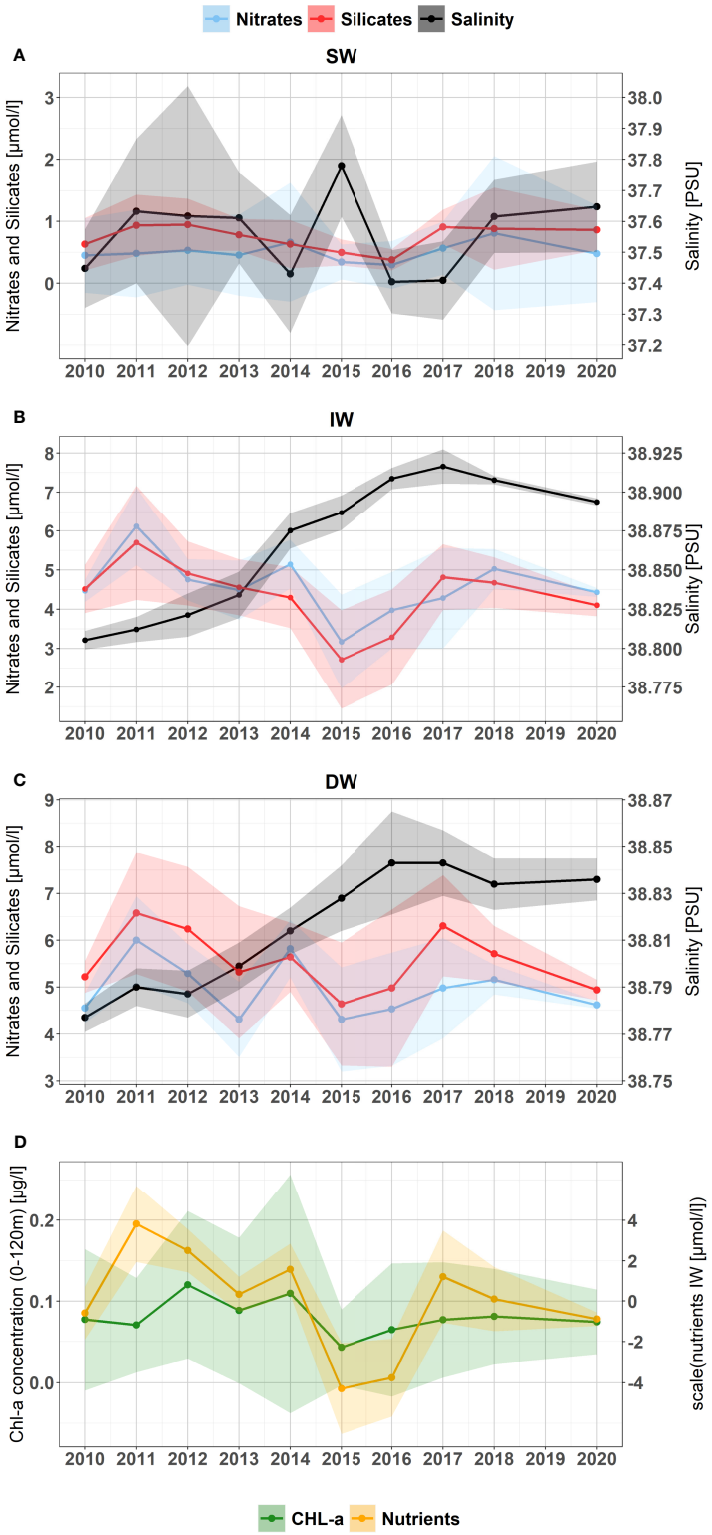

FIGURE 5 | The nitrates (blue line) and silicates (red line) time series was computed from the sum of the nitrates and silicates average concentrations within each layer **(A)** SW_0-100m, **(B)** IW_200-500m and **(C)** DW_500-bottom, for each year, in all sampling stations. In addition is reported the salinity time series (black line) described in Figure 3. **(D)** The Chl-a (green line) time series 2010-2020 was computed from the Chl-a average concentrations within each layer 0-120m depth. The related colored areas represent the standard deviations.

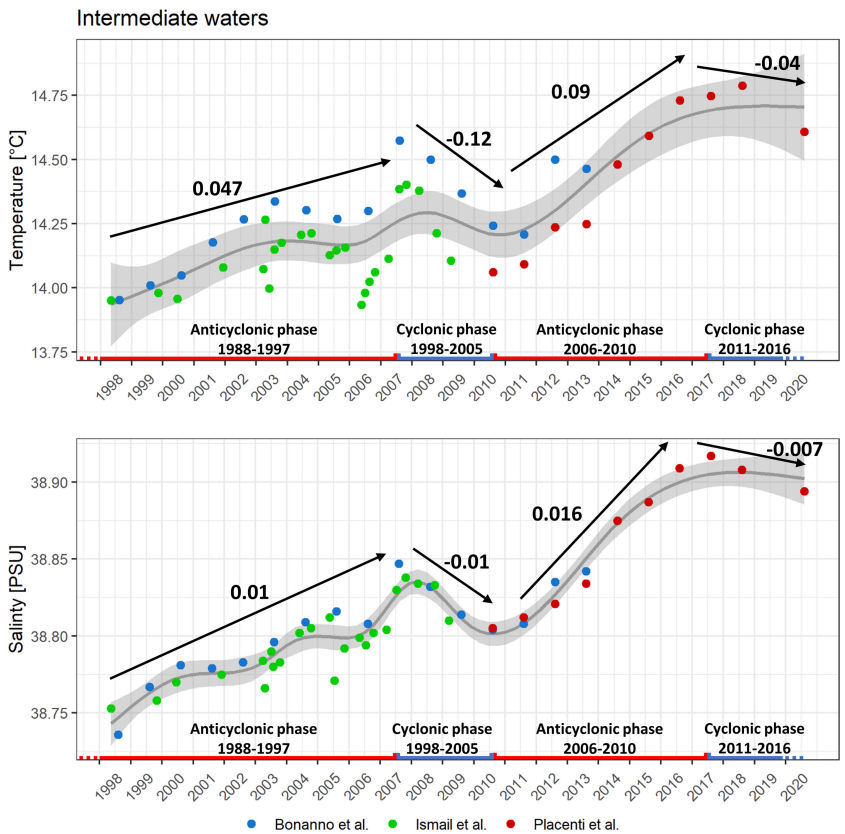

FIGURE 6 | Temperature (top panel) and salinity (bottom panel) time series of the LIW, extrapolated by Ben Ismail et. (201)4 and Bonanno et al. (2014), are indicated as green and blue dots, respectively. Potential temperature and salinity time series from this study are indicated as red dots. A cubic regression spline computed through a GAM model and the relative confidence interval has been added in gray with the aim at evidencing temporal trends. Black arrows indicate the average annual increments of hydrological parameters computed for 1998-2009 by Bonanno et al. (2014) and for 2010-2020 from data collected in this study. The position of the dots on the time axis takes into account the sampling month.

salty/warm phase occurs from 2011 until 2017 (**Figure 6**), probably associated to the previous anticyclonic phase of the NIG (2006-2010, **Figure 7C**). Compared to the first average annual increase in θ and S, attributable to the anticyclonic phase 1993-1997, this increasing trend shows considerably higher rates of dθ/dt and dS/dt, despite being related to a shorter and less defined anticyclonic circulation. Indeed, some authors identified the 1993-1997 phase as "fully anticyclonic" due to the absence or weak activity of the MIJ. Differently, during the subsequent anticyclonic phase (2006-2010), the MIJ occurs with an intense, non-negligible, zonal activity from the SC to the Levantine basin, prompting authors to distinguish this period as an "anticyclonic-zonal" phase (Bessières et al., 2013). Therefore, our considerably higher rates of increase in θ and S can be only partially associated with the anticyclonic-zonal phase of the NIG, from which a lower rate of increase would be expected. A further possible explanation could be linked to the increasing of the drying process (E-P), affecting the surface waters from which LIW and CIW originate, in agreement with Schroeder et al. (2017).

The last period of the time series (2018-2020, **Figure 6**) showed a new decreasing trend significantly lower than the previous one (i.e. 2008-2010). This last reversal trend followed the cyclonic phase occurred in 2011-2016 (**Figures 7D, E**). The comparison of the ADT averages observed during the two cyclonic phases (**Figures 7B, D**) allowed to evidence a significant difference in term of intensity and areal extension of the NIG. In the first phase the NIG extends down to 35°N while in the second phase is confined at northern latitudes, higher than 36.5°N, probably due to the presence of an anticyclonic structure in the centre of the IS (Cardin et al., 2015; Placenti et al., 2018). This structure has weakened the AW flux toward Levantine Basin (Cardin et al., 2015), limiting the influence of colder and fresher AW toward the area where the formation of the IW take place. This interpretation is supported by recent studies that found a premature inversion of the NIG from cyclonic to anticyclonic, related to the extremely strong winter 2012 in the Adriatic (Gačić et al., 2014) leading to a strong weakening of the AW flux toward Levantine Basin between mid-2012 and the first months of 2013 (Menna et al., 2019). This phenomenon probably produced, between 2012 and 2013, warmer and saltier IW in the EMS which could have modulated the decreasing rate of θ and S in the SC.

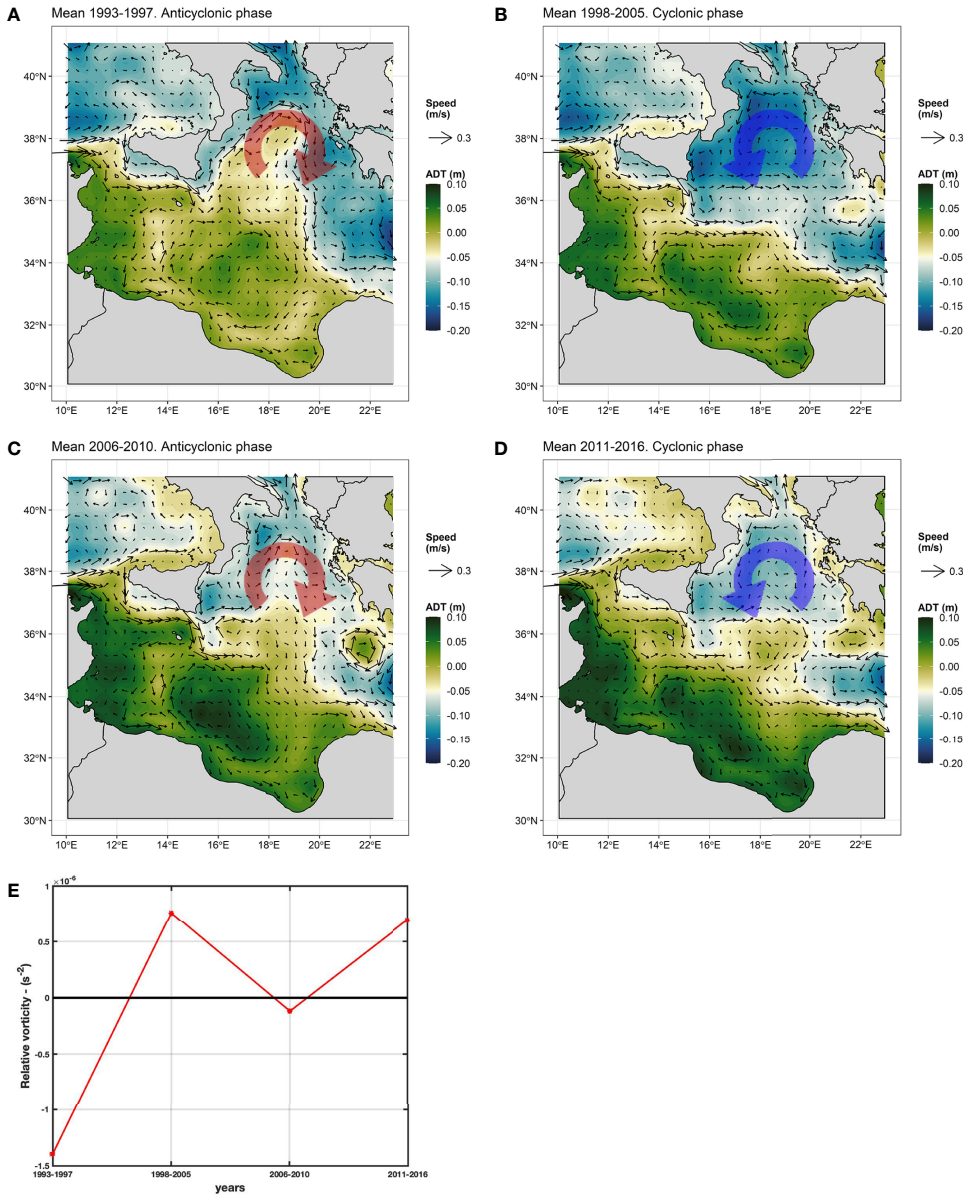

FIGURE 7 | Means map of ADT (absolute dynamic topography; colours bar) and mean geostrophic velocity field (arrows) and relative speed (m/s), in the Central Mediterranean Sea, estimated for the periods **(A)** 1993–1997, **(B)** 1998–2005, **(C)** 2006–2010 and **(D)** 2011–2016. Red and blue arrows evidence the anticyclonic and cyclonic circulation mode of the North Ionian Gyre (NIG) respectively. In the panel **(E)** the computation of the averaged relative vorticity for the four periods confirms negative values (anticyclonic circulation) from 1993 to 1997 and from 2006 to 2010, and positive values (cyclonic circulation) in the periods 1998-2005 and 2011-2016.

The correlation between the NIG circulation mode and the temperature and salinity trends observed in the SC was investigated through a cross-correlation analysis that show a significant correlation for time lag of 6 (Cramer's V = 0.456, $p < 0.05$) and 7 years (Cramer's V = 0.497, $p < 0.05$), highlighting an association between cyclonic phase-negative trends and between anticyclonic phase-positive trends. However, we recognized a temporal variability between the reversal of the circulation mode and the trend inversion that suggest the presence of unadressed additional mechanisms that tune the onset of the signals and encourage the need of further studies.

Moreover, the time series of θ and S of the DW in 2010-2020 has been investigated and showed similar trends to the IW, but characterized by lower increments (**Figure 3**). However, it is important to note that most of the data collected in this study regarding the DW are referred to the upper part of this water mass, due to the limited depths that characterize the SC. Regarding this water mass, integrating the θ and S data

discussed in Bonanno et al. (2014) and Ben Ismail et al. (2014) with our time series, it is possible to detect a general increase in the last twenty years of about 0.4°C of θ and 0.1 of S, respectively (**Figure 8**). However, the time series showed two strong break points in 2006 and 2009 characterized by an abrupt decrease of θ and S that were also discussed by Ben Ismail et al. (2014) regarding the 2006, and by Bonanno et al. (2014) regarding both years. In addition, these authors found a simultaneous increase of density (σ) in the DW, associating these findings to the presence of tEMDW in the SC. It is confirmed by our data also in 2010 (not shown), while in the following years (2011-2017) a new warm and salty phase seems to affect the deeper waters of the SC (**Figures 6** and **8**). We also hypothesize that these trends concerning the deeper layers are a direct response to the climate change, in particular in terms of net evaporation over to the eastern basin, i.e. where the deeper water is formed (Schroeder et al., 2017).

The coupling of the nitrates and silicates time series (2010-2020) with the salinity in the deeper waters of the SC showed anti-phase trends (**Figure 5**). These trends have been observed in IW both in the EMS (Ozer et al., 2017) and in the AdS (Borzelli et al., 2009; Civitarese et al., 2010). In agreement with Ozer et al. (2017), we think that a possible explanation could be related to the surface circulation dynamic of the NIG.

Specifically, during the anticyclonic phase (2006-2010, **Figure 7C**) the influx of AW, considered the main external source of P and N to the Mediterranean system (Powley et al., 2017), towards the Levantine Basin was limited, producing saltier and poorer nutrient IW. Conversely, the slight decrease in salinity and increase in nutrients observed between 2017 and 2020 (**Figure 5**) could be linked to the previous cyclonic phase of the NIG (2011-2016, **Figure 7D**).

In addition, the interannual fluctuations affecting the nutrient concentration has been compared to the variability of the Chl-a concentration, which is considered a good proxy of the phytoplankton biomass and provides useful indications on the productivity of the upper layer of the water column (e.g. Falkowski et al., 2004). Interestingly, our findings show similar trends among these time series, especially taking into account the nitrates and silicates concentration of the deeper layers. Indeed, starting from 2010, these time series were characterized by variable fluctuations and reached a simultaneous minimum peak in 2015, then followed by an increasing trend until the 2020. These observations suggest that vertical oceanographic structures, such as upwelling processes identified along the Sicilian coast (Lermusiaux and Robinson, 2001; Bignami et al., 2008; Patti et al., 2010; Torri et al., 2018), could play a significant role in the diffusion of nutrients from the lower layers, making them available for the photosynthetic activity

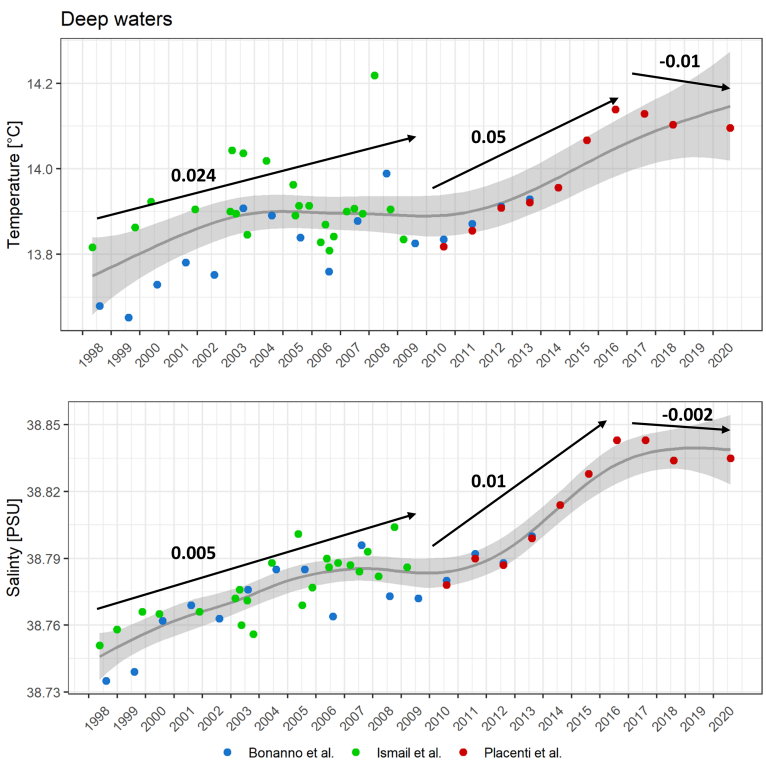

FIGURE 8 | Potential temperature (top panel) and salinity (bottom panel) time series of the DW, extrapolated by Ben Ismail et. (2014), Bonanno et al. (2014) and this study are indicated as green, blue and red dots, respectively. A cubic regression spline computed through a GAM model and the relative confidence interval has been added in gray with the aim at evidencing temporal trends. Black arrows indicate the average annual increments of hydrological parameters computed for 1998-2009 by Bonanno et al. (2014) and for 2010-2020 from data collected in this study. The position of the dots on the time axis takes depend on the sampling month.

with a cascading effect on the marine organisms that in the Central Mediterranean Sea found a suitable habitat for feeding and reproduction (e.g. Bonomo et al., 2018; Patti et al., 2020; Russo et al., 2021). Indeed, it could also be noted that the SC is a place of strong diffusion and dissipation that may favor such vertical transport (Ferron et al., 2017; Vladoiu et al., 2018). However, discordant findings regarding this relationship emerged between our study areas and the Levantine basin, in which an opposite trend has been evidenced between the nutrient concentration of the IW and the Chl-a concentration (Ozer et al., 2017), suggesting the need of further studies on a wider scale. In this context, the long-time series in the Strait of Gibraltar and Sicily, which represent key points of the entire Mediterranean thermohaline circulation, are of fundamental importance for climate studies. It is necessary to continue maintaining long-term observational points to improve our understanding of the physical mechanisms that drive climate variability and to discriminate the effects related to natural variability and the anthropogenic effect. Similarly, in these key areas, the acquisition of nutrients high-quality data on a multiannual scale are essential for understanding the relationships between oceanographic, biogeochemical and biological processes.

DATA AVAILABILITY STATEMENT

The raw data supporting the conclusions of this article will be made available by the authors, without undue reservation.

AUTHOR CONTRIBUTIONS

FPI wrote the manuscript and analyzed the dataset. MT wrote the manuscript and prepared the figures. VT, LG participated to the fieldwork and laboratory analyses. BP, AC and GT coordinated the field work and supervised the writing of the text. RS and FPe helped with some specific aspects of the manuscript and to review the manuscript. All authors contributed to the article and approved the submitted version.

FUNDING

The study was supported by the research projects SSD-PESCA, coordinated by the Ministry of the Education, University and Research (MIUR) and founded by the Ministry of Economic Development (MISE), and the Flagship Project RITMARE - The Italian Research for the Sea, coordinated by the Italian National Research Council and funded by MIUR.

ACKNOWLEDGMENTS

Masters of the Urania, Minerva Uno, Dallaporta and all their crew are thanked for their work in support to the sampling activities during the oceanographic cruises. We are grateful to Girolama Biondo, Giovanni Giacalone, Ignazio Fontana, Carmelo Buscaino and Carlo Patti for their valuable technical support and the sampling collection during the oceanographic surveys.

SUPPLEMENTARY MATERIAL

The Supplementary Material for this article can be found online at: https://www.frontiersin.org/articles/10.3389/fmars.2022.733540/full#supplementary-material

REFERENCES

Ben Ismail, S., Schroeder, K., Sammari, C., Gasparini, G. P., Borghini, M., and Aleya, L. (2014). Interannual Variability of Water Mass Properties in the Tunisia-Sicily Channel. *J. Mar. Syst.* 135, 14–28. doi: 10.1016/j.jmarsys.2013.06.010

Bessières, L., Rio, M. H., Dufau, C., Boone, C., and Pujol, M. I. (2013). Ocean State Indicators From MyOcean Altimeter Products. *Ocean Sci.* 9, 545–560. doi: 10.5194/os-9-545-2013

Béthoux, J. P., Morin, P., Chaumery, C., Connan, O., Gentili, B., and Ruiz-Pino, D. (1998). Nutrients in the Mediterranean Sea, Mass Balance and Statistical Analysis of Concentrations With Respect to Environmental Change. *Mar. Chem.* 63 (1–2), 155–169. doi: 10.1016/S0304-4203(98)00059-0

Bignami, F., Böhm, E., D'Acunzo, E., D'Archino, R., and Salusti, E. (2008). On the Dynamics of Surface Cold Filaments in the Mediterranean Sea. *J. Mar. Syst.* 74 (1-2), 429–442. doi: 10.1016/j.jmarsys.2008.03.002

Bonanno, A., Placenti, F., Basilone, G., Mifsud, R., Genovese, S., Patti, B., et al. (2014). Variability of Water Mass Properties in the Strait of Sicily in Summer Period of 1998–2013. *Ocean Sci.* 10, 759–770. doi: 10.5194/os-10-759-2014

Bonomo, S., Placenti, F., Zgozi, S., Torri, M., Quinci, E. M., Cuttitta, A., et al. (2018). Relationship Between Coccolithophores and the Physical and Chemical Oceanography of Eastern Libyan Coastal Waters. *Hydrobiologia* 821 (1), 215–234. doi: 10.1007/s10750-017-3227-y

Borghini, M., Bryden, H., Schroeder, K., Sparnocchia, S., and Vetrano, A. (2014). The Mediterranean is Becoming Saltier. *Ocean Sci.* 10, 693–700. doi: 10.5194/os-10-693-2014

Borzelli, G. L. E., Gačić, M., Cardin, V., and Civitarese, G. (2009). Eastern Mediterranean Transient and Reversal of the Ionian Sea Circulation. *Geophys. Res. Lett.* 36, L15108. doi: 10.1029/2009GL039261

Brankart, J. M. (1994). *The MODB Local Quality Control, Technical Report* Vol. p. 5 (Liege: University of Liege), 1994.

Cardin, V., Civitarese, G., Hainbucher, D., Bensi, M., and Rubino, A. (2015). Thermohaline Properties in the Eastern Mediterranean in the Last Three Decades: Is the Basin Returning to the Pre-EMT Situation? *Ocean Sci.* 11, 53–66. doi: 10.5194/os-11-53-2015

Civitarese, G., Gačić, M., Borzelli, E., and Lipizer, M. (2010). On the Impact of the Bimodal Oscillating System (BiOS) on the Biogeochemistry and Biology of the Adriatic and Ionian Seas (Eastern Mediterranean). *Biogeosciences* 7, 3987–3997. doi: 10.5194/bg-7-3987-2010

Demirov, E., and Pinardi, N. (2002). Simulation of the Mediterranean Sea Circulation From 1979 to 1993: Part I. The Interannual Variability. *J. Mar. Syst.* 33–34, 23–50. doi: 10.1016/S0924-7963(02)00051-9

Falkowski, P. G., Koblfzek, M., Gorbunov, M., and Kolber, Z. (2004). "Development and Application of Variable Chlorophyll Fluorescence Techniques in Marine Ecosystems," in *Chlorophyll a fluorescence* (Dordrecht: Springer), 757–778.

Ferron, B., Bouruet Aubertot, P., Cuypers, Y., Schroeder, K., and Borghini, M. (2017). How Important are Diapycnal Mixing and Geothermal Heating for the Deep Circulation of the Western Mediterranean? *Geophysical. Res. Lett.* 44 (15), 7845–7854. doi: 10.1002/2017GL074169

Gačić, M., Borzelli, G. L. E., Civitarese, G., Cardin, V., and Yari, S. (2010). Can Internal Processes Sustain Reversals of the Ocean Upper Circulation? The Ionian Sea Example. *Geophys. Res. Lett.* 37, L09608. doi: 10.1029/2010GL043216

Gačić, M., Civitarese, G., Borzelli, G. L. E., Kovacevic, V., Poulain, P.-M., Theocharis, A., et al. (2011). On the Relationship Between the Decadal Oscillations of the Northern Ionian Sea and the Salinity Distributions in the Eastern Mediterranean. *J. Geophys. Res.* 116, C12002. doi: 10.1029/2011JC007280

Gačić, M., Civitarese, G., Kovacevic, V., Ursella, L., Bensi, M., Menna, M., et al. (2014). Extreme Winter 2012 in the Adriatic: An Example of Climatic Effect on the BiOS Rhythm. *Ocean Sci.* 10, 513–522. doi: 10.5194/os-10-513-2014

Gačić, M., Schroeder, K., Civitarese, G., Cosoli, S., Vetrano, A., and Borzelli, G. L. E. (2013). Salinity in the Sicily Channel Corroborates the Role of the Adriatic-Ionian Bimodal Oscillating System (BiOS) in Shaping the Decadal Variability of the Mediterranean Overturning Circulation. *Ocean Sci.* 9, 83–90. doi: 10.5194/os-9-83-2013

Gasparini, G. P., Ortona, A., Budillon, G., Astraldi, M., and Sansone, E. (2005). The Effect of the Eastern Mediterranean Transient on the Hydrographic Characteristics in the Strait of Sicily and in the Tyrrhenian Sea. *Deep-Sea Res. I. Oceanogr. Res. Pap.* 52 (6), 915–935. doi: 10.1016/j.dsr.2005.01.001

Grasshoff, K., Kremling, K., and Ehrhardt, M. (1999). *Methods of Seawater Analysis* (Weinheim: Wiley-Vch Verlag).

Huertas, I. E., Rios, A. F., Garcia-Lafuente, J., Navarro, G., Makaoui, A., Sanchez-Roman, A., et al. (2012). Atlantic Forcing of the Mediterranean Oligotrophy. *Glob. Biogeochem. Cycles* 26, GB2022. doi: 10.1029/2011GB004167

Krom, M. D., Emeis, K. C., and Van Cappellen, P. (2010). Why is the Eastern Mediterranean Phosphorus Limited? *Prog. Oceanogr.* 85 (3–4), 236–244. doi: 10.1016/j.pocean.2010.03.003

Krom, M. D., Herut, B., and Mantoura, R. F. C. (2004). Nutrient Budget for the Eastern Mediterranean: Implications for Phosphorus Limitation. *Limnol. Oceanogr.* 49, 1582–1592. doi: 10.4319/lo.2004.49.5.1582

Lacombe, H., Tchernia, P., and Gamberoni, L. (1985). Variable Bottom Water in the Western Mediterranean Basin. *Prog. Oceanogr.* 14, 319–338. doi: 10.1016/0079-6611(85)90015-1

Lermusiaux, P. F. J., and Robinson, A. R. (2001). Features of Dominant Mesoscale Variability, Circulation Patterns and Dynamics in the Strait of Sicily. *Deep Sea Res. Part I.: Oceanogr. Res. Pap.* 48 (9), 1953–1997. doi: 10.1016/S0967-0637(00)00114-X

Menna, M., Reyes Suarez, N. C., Civitarese, G., Gačić, M., Rubino, A., and Poulain, P.-M. (2019). Decadal Variations of Circulation in the Central Mediterranean and its Interactions With Mesoscale Gyres. *Deep Sea Res. Part II Top. Stud. Oceanogr.* Vol. 164, 14–24. doi: 10.1016/j.dsr2.2019.02.004

Mihanović, H., Vilibić, I., Šepić, J., Matić, F., Ljubešić, Z., Mauri, E., et al. (2021). Observation, Preconditioning and Recurrence of Exceptionally High Salinities in the Adriatic Sea. *Front. Mar. Sci.* 8, 834. doi: 10.3389/fmars.2021.672210

Millot, C. (2007). Interannual Salinification of the Mediterranean Inflow. *Geophys. Res. Lett.* 34(21):L21609. doi: 10.1029/2007GL031179

Notarstefano, G., Menna, M., Legeais, J.-F., von Schuckmann, K., Le Traon, P. Y., Smith, N., et al. (2019). Reversal of the Northern Ionian Circulation in 2017. Section 4.5Copernicus Marine Service Ocean State Report, Issue 3. *J. Oper. Oceanogr.* 12 (sup1), S1–S123. doi: 10.1080/1755876X.2019.1633075

Ozer, T., Gertman, I., Kress, N., Silverman, J., and Herut, B. (2017). Interannual Thermohalin–2014) and Nutrien–2014) Dynamics in the Levantine Surface and Intermediate Water Masses, SE Mediterranean Sea. *Glob. Planet. Change* 151, 60–67. doi: 10.1016/j.gloplacha.2016.04.001

Patti, B., Guisande, C., Bonanno, A., Basilone, G., Cuttitta, A., and Mazzola, S. (2010). Role of Physical Forcings and Nutrient Availability on the Control of Satellite-Based Chlorophyll a Concentration in the Coastal Upwelling Area of the Sicilian Channel. *Sci. Mar.* 74, 577–588.

Patti, B., Torri, M., and Cuttitta, A. (2020). General Surface Circulation Controls the Interannual Fluctuations of Anchovy Stock Biomass in the Central Mediterranean Sea. *Sci. Rep.* 10 (1), 1–14. doi: 10.1038/s41598-020-58028-0

Placenti, F., Azzaro, M., Artale, V., La Ferla, R., Caruso, G., Santinelli, C., et al. (2018). Biogeochemical Patterns and Microbial Processes in the Eastern Mediterranean Deep Water of Ionian Sea. *Hydrobiologia* 815 (1), 97–112. doi: 10.1007/s10750-018-3554-7

Placenti, F., Schroeder, K., Bonanno, A., Zgozi, S., Sprovieri, M., Borghini, M., et al. (2013). Water Masses and Nutrient Distribution in the Gulf of Syrte and Between Sicily and Libya. *J. Mar. Sys.* 121–122, 36–46. doi: 10.1016/j.jmarsys.2013.03.012

Powley, H. R., Krom, M. D., and Van Cappellen, P. (2017). Understanding the Unique Biogeochemistry of the Mediterranean Sea: Insights From a Coupled Phosphorus and Nitrogen Model Global Biogeochem. *Cycles* 31, 1010–1031. doi: 10.1002/2017GB005648

Redfield, A. C., Ketchum, B. H., and Richards, F. A. (1963). "The Influence of Organisms on the Composition of Sea Water," in *The Sea, Vol. 2*. Ed. M. N. Hill (New York: Interscience), 224–228.

Ribera D'Alcalà, M., Civitarese, G., Conversano, F., and Lavezza, R. (2003). Nutrient Ratios and Fluxes Hint at Overlooked Processes in the Mediterranean Sea. *J. Geophys. Res.* 108 (C9), 8106. doi: 10.1029/2002JC0016500

Rixen, M., Beckers, J.-M., Levitus, S., Antonov, J., Boyer, T., Maillard, C., et al. (2005). The Western Mediterranean Deep Water: A Proxy for Climate Change. *Geophys. Res. Lett.* 32, L12608. doi: 10.1029/2005GL022702,2005

Robinson, A. R., Leslie, W. G., Theocharis, A., and Lascaratos, A. (2001). "Mediterranean Sea Circulation," in *Encyclopedia of Ocean Sciences* (London: Academic Press), 1689–1706.

Roether, W., Klein, B., Beitzel, V., and Manca, B. B. (1998). Property Distributions and Transient Tracer Ages in Levantine Intermediate Water in the Eastern Mediterranean. *J. Mar. Syst.* 18, 71–87. doi: 10.1016/S0924-7963(98)00006-2

Roether, W., Manca, B. B., Klein, B., Bregant, D., Georgopoulos, D., Beitzel, V., et al. (1996). Recent Changes in Eastern Mediterranean Deepwaters. *Science* 271 (5247), 333–335. doi: 10.1126/science

Russo, S., Torri, M., Patti, B., Reglero, P., Álvarez-Berastegui, D., Cuttitta, A., et al. (2021). Unveiling the Relationship Between Sea Surface Hydrographic Patterns and Tuna Larval Distribution in the Central Mediterranean Sea. *Front. Mar. Sci.* 8, 708775. doi: 10.3389/FMARS.2021.708775

Schroeder, K., Chiggiato, J., Josey, S. A., Borghini, M., Aracri, S., and Sparnocchia, S. (2017). Rapid Response to Climate Change in a Marginal Sea. *Sci. Rep.* 7, 4065. doi: 10.1038/s41598-017-04455-5

Schroeder, K., Gasparini, G. P., Borghini, M., Cerrati, G., and Delfanti, R. (2010). Biogeochemical Tracers and Fluxes in the Western Mediterranean Sea, Spring 2005. *J. Mar. Syst.* 80, 8–24. doi: 10.1016/j.jmarsys.2009.08.002

Shabrang, L., Menna, M., Pizzi, C., Lavigne, H., Civitarese, G., and Gačić, M. (2016). Long-Term Variability of the Southern Adriatic Circulation in Relation to North Atlantic Oscillation. *Ocean Sci.* 12 (1), 233–241. doi: 10.5194/os-12-233-2016

Sorgente, R., Olita, A., Oddo, P., Fazioli, L., and Ribotti, A. (2011). Numerical Simulation and Decomposition of Kinetic Energy in the Central Mediterranean: Insight on Mesoscale Circulation and Energy Conversion. *Ocean Sci.* 7, 503–519. doi: 10.5194/os-7-503-2011

Theocharis, A., Krokos, G., Velaoras, D., and Korres, G. (2014). "An Internal Mechanism Driving the Alternation of the Eastern Mediterranean Dense/Deep Water Sources," in *The Mediterranean Sea: Temporal Variability and Spatial Patterns* vol. 202. Ed. G. L. E. Borzelli, (Washington, D.C.: American Geophysical Union / Wiley), 113–137.

Torri, M., Corrado, R., Falcini, F., Cuttitta, A., Palatella, L., Lacorata, G., et al. (2018). Planktonic Stages of Small Pelagic Fishes (Sardinella Aurita and Engraulis Encrasicolus) in the Central Mediterranean Sea: The Key Role of Physical Forcings and Implications for Fisheries Management. *Prog. Oceanog.* 162, 25–39. doi: 10.1016/j.pocean.2018.02.009

Van Cappellen, P., Powley, H. R., Emeis, K.-C., and Krom, M. D. (2014). A Biogeochemical Model for Phosphorus and Nitrogen Cycling in the Eastern Mediterranean Sea (EMS). Part 1. Model Development, Initial Conditions and Sensitivity Analyses. *J. Mar. Syst.* 139, 460–471. doi: 10.1016/j.jmarsys.2014.08.016

Vladoiu, A., Bouruet-Aubertot, P., Cuypers, Y., Ferron, B., Schroeder, K., Borghini, M., et al. (2018). Turbulence in the Sicily Channel From Microstructure Measurements. *Deep Sea Res. Part I.: Oceanogr. Res. Pap.* 137, 97–112. doi: 10.1016/j.dsr.2018.05.006

Conflict of Interest: The authors declare that the research was conducted in the absence of any commercial or financial relationships that could be construed as a potential conflict of interest.

this article, or claim that may be made by its manufacturer, is not guaranteed or endorsed by the publisher.

frontiers | Frontiers in Marine Science

ORIGINAL RESEARCH
published: 10 June 2022
doi: 10.3389/fmars.2022.901893

Seasonal and Long-Term Variability of the Mixed Layer Depth and its Influence on Ocean Productivity in the Spanish Gulf of Cádiz and Mediterranean Sea

Manuel Vargas-Yáñez[1], Francina Moya[1], Rosa Balbín[2], Rocío Santiago[2], Enrique Ballesteros[1], Ricardo F. Sánchez-Leal[3], Patricia Romero[1] and Ma Carmen García-Martínez[1]*

[1] Instituto Español de Oceanografía (IEO-CSIC). Centro Oceanográfico de Málaga., Málaga, Spain, [2] Instituto Español de Oceanografía (IEO-CSIC), Centro Oceanográfico de Baleares., Palma, Spain, [3] Instituto Español de Oceanografía (IEO-CSIC), Centro Oceanográfico de Cádiz., Cádiz, Spain

OPEN ACCESS

Edited by:
Jesus Garcia Lafuente, University of Malaga, Spain

Reviewed by:
Maurizio Ribera D'Alcala', Stazione Zoologica Anton Dohrn Napoli, Italy
Iria Sala, University of Strathclyde, United Kingdom

***Correspondence:**
Manuel Vargas-Yáñez
manolo.vargas@ieo.csic.es

Specialty section:
This article was submitted to Marine Fisheries, Aquaculture and Living Resources, a section of the journal Frontiers in Marine Science

Received: *22 March 2022*
Accepted: *10 May 2022*
Published: *10 June 2022*

Citation:
Vargas-Yáñez M, Moya F, Balbín R, Santiago R, Ballesteros E, Sánchez-Leal RF, Romero P and García-Martínez MC (2022) Seasonal and Long-Term Variability of the Mixed Layer Depth and its Influence on Ocean Productivity in the Spanish Gulf of Cádiz and Mediterranean Sea. Front. Mar. Sci. 9:901893. doi: 10.3389/fmars.2022.901893

The warming of the surface ocean is expected to increase the stratification of the upper water column. This would decrease the efficiency of the wind-induced mixing, reducing the nutrient supply to the euphotic layer and the productivity of the oceans. Climatic projections show that the Mediterranean Sea will experience a strong warming and salting along the twenty first century. Nevertheless, very few works have found and quantified changes in the water column stratification of the Western Mediterranean. In this work, we obtain time series of Mixed Layer Depth (MLD) along the Spanish Mediterranean waters and the Gulf of Cádiz, using periodic CTD profiles collected under the umbrella of the Ocean Observing system of the Instituto Español de Oceanografía (IEO-CSIC). The length of the time series analyzed is variable, depending on the geographical area, but in some cases these time series extend from the beginning of the 1990s decade. Our results show that at present, no statistically significant changes can be detected. These results are confirmed by the analysis of MLD time series obtained from Argo profilers. Some of the meteorological factors that could affect the water column stratification (wind intensity and precipitation rates) did not experience significant changes for the 1990-2021 period, neither were observed long-term changes in the chlorophyll concentration. The hypothesis proposed to explain this lack of trends, is that the salinity increase of the surface waters has compensated for the warming, and consequently, the density of the upper layer of the Western Mediterranean (WMED) has remained constant. As the wind intensity has not experienced significant trends, the stratification of the Spanish Mediterranean waters and those of the Gulf of Cádiz would have not been affected. Nevertheless, we do not discard that our results are a consequence of the short length of the available time series and the large variance of the variables analyzed, evidencing the importance of the maintenance of the ocean monitoring programs.

Keywords: mixed layer depth, Western Mediterranean, climate change, ocean productivity, ocean observing system

INTRODUCTION

The oceans play a key role in the present scenario of Climate Change. They have absorbed more than 90% of the energy stored in the Earth's Climate System because of the emissions of greenhouse gasses since the end of the nineteenth century (Zanna et al., 2019). One of the possible consequences of the warming of the most superficial layers of the oceans on marine ecosystems could be the increase of the water column stratification. The enhancement of the stratification would affect to the development of the winter Mixed Layer, reducing the efficiency of the wind mixing and consequently decreasing the nutrient supply to the euphotic layer and the primary production (Bindoff et al., 2019). It would also have important effects on the light availability for phytoplanktonic cells which is linked to the intensity of turbulent mixing (Villamaña et al., 2019; Morison et al., 2020; Comesaña et al., 2021). Global coupled carbon cycle climate models predict that this trend will continue during the twenty first century on a global scale (Steinacher et al., 2010; Hammond et al., 2020), but with regional differences, with a decrease of the primary production in the mid and low latitudes, and an increase in the Southern Ocean.

At present, the estimation of primary production trends on a global scale is based on chlorophyll concentration measurements derived from satellite observations. These results coincide with model predictions, showing a decrease of chlorophyll concentration in the permanently stratified regions, such as the subtropical gyres (Polovina et al., 2008), and an increase in the Southern Ocean (Del Castillo et al., 2019; Pinkerton et al., 2021). Nevertheless, there are some discrepancies with field observations. Behrenfeld et al. (2006) pointed out that the observations did not show the increase in the primary production of the Southern Ocean predicted by the models. Boyce, D. G, and Worm, B., (2015) analyzed more than 115 chlorophyll concentration time series and found different results depending on the geographical area. These authors stressed that most of the available times series had a length shorter than 23 years and that the largest trends were associated to short time series, whereas the long-term variability was much reduced for long time series. Dutkiewicz et al. (2019) evidenced that the detection of trends in the chlorophyll concentration and primary production of the sea, required long time series, because of the large variance of these variables. These authors considered that the length of the series should be enough to accumulate an increment larger than twice the standard deviation associated to the natural variability of the variable analyzed. Hence, one of the main problems that arise when dealing with the detection of long-term changes in the productivity of the oceans is the scarcity of long time series (Boyce and Worm (2015); Del Castillo et al., 2019; Hammond et al., 2020).

The Mediterranean Sea has been considered a hotspot for Climate Change and other anthropic stressors (Cuttelod et al., 2008; Coll et al., 2011). Because of its reduced dimensions and semi-enclosed character, it could be more sensitive to Climate Change than other regions of the world oceans (Calvo et al., 2011). In the case of the Western Mediterranean, the temperature and salinity of surface waters have increased along the twentieth century and the beginning of the twenty first one (Vargas-Yáñez et al., 2021; 2017; 2010), and numerical models, based on different emission scenarios, predict that these trends will continue along the twenty first century (Adloff et al., 2015). All these changes are expected to impact the biogeochemistry of the Mediterranean Sea (Durrieu de Madron et al., 2011). One of the current hypotheses considers that the warming of the upper layer could reduce the deep convection, and weaken the thermohaline circulation of the Mediterranean Sea (Somot et al., 2006; Herrmann et al., 2008a). Macias et al. (2018) found an increase of the deep convection in the WMED until 2030, but these authors considered that the discrepancies with previous works were simply caused by the different temporal horizon of the simulations. These changes in the convection processes and the thermohaline circulation are likely to impact the nutrient supply to the euphotic layer (Pasqueron de Fommervault et al., 2015), and the ventilation of the intermediate and deep waters (Coppola et al., 2018; Ulses et al., 2020). Herrmann et al. (2014) used a coupled ocean circulation-biogeochemical model, and found that the nutrient concentrations of the upper layers would be reduced in the North Western Mediterranean along the twenty first century, but the chlorophyll concentration would increase because of the effect of the sea warming. Besides the expected changes, there are few works that have identified unambiguously current changes in the WMED marine ecosystems. Laboratory experiments (Pulina et al., 2016) have shown that the warming of the surface waters would induce an increment of the phytoplanktonic biomass, being this increment linked to small-size cells. Ribera D'alcalà et al. (2004) analyzed time series of phytoplankton in a coastal station in the Gulf of Naples from 1984 to 2000, and also found a decrease of the size of phytoplanktonic cells, but in this case the overall biomass also decreased. Mazzocchi et al. (2012) observed a negative trend for the chlorophyll concentration at the same location from 1984 to 2006. El Hourany et al. (2021) also found negative trends for the surface chlorophyll concentrations in the Mediterranean Sea, using satellite-derived time series over the period 2003-2020, but these trends were not statistically significant. Furthermore, the significance of the trends, and even their sign could strongly depend on the period of time considered. Goffart et al. (2002) found a decrease of the chlorophyll in the Villefranche B-station (Ligurian Sea) from 1979 to 1990, but this trend was not observed when the time series was extended to 2005 (Goffart et al., 2015).

The different works commented above, both for the global ocean, and for the WMED, show that the detection of changes in the productivity of the sea, requires long time series, which are scarce in the WMED. This is also true for the case for the Spanish Mediterranean waters, which cover a large area of the WMED, from the Strait of Gibraltar to the Catalan Sea, including the Balearic Islands. The oldest monitoring station in this region is the L'Estartit station, in the Catalan Sea, operating since the beginning of the 1970s decade (Salat et al., 2019), but these observations do not include biogeochemical variables. The Balearic Islands Coastal Observing System (SCIB, Tintoré

et al., 2019) includes a three-monthly multidisciplinary sampling of the Balearic Channels since 2014, but to our knowledge, no results dealing with the evolution of the chlorophyll or nutrient concentrations have been published. Bahamon et al. (2020) have analyzed physical and biological time series collected under the umbrella of the Operational Observatory of the Catalan Sea (OOCS), in a station close to the head of the Blanes submarine Canyon (Catalan Sea). Contrary to the expectations, this work found that the MLD deepened, and the chlorophyll and nutrient concentrations showed no changes during the period 2010-2017. The Blanes Bay Microbiological Observatory (BBMO) maintains a multidisciplinary monitoring station close to the coast of Blanes. The seasonal cycle of the primary production has been analyzed at this site (Gasol et al., 2016) and time series of anaerobic anoxygenic photoheterotrophic bacteria have been studied in Auladell et al. (2019), but no results are available dealing with long-term changes of the stratification and productivity of the Catalan waters.

Taking into account the projections based on different emission scenarios for the twenty first century, and the uncertainty about the present changes observed in the WMED marine ecosystems, it is of paramount importance to determine whether or not the stratification of the WMED is increasing, and if its productivity is being reduced. This possible oligotrophication of the Mediterranean Sea (Agusti et al, 2017) could be especially important in a sea that is already oligotrophic or extremely oligotrophic (Goffart et al., 2002; Siokou-Frangou et al., 2010). The Instituto Español de Oceanografía (IEO-CSIC) has developed several multidisciplinary monitoring projects in the Spanish Mediterranean and the Gulf of Cádiz since the beginning of the 1990s decade. Although these monitoring projects had different initial dates and covered different geographical areas, they were unified under the umbrella of two monitoring programs: one devoted to the Spanish Mediterranean (RADMED), and another one to the Gulf of Cádiz (STOCA). This work aims to analyze and quantify the possible changes in the MLD, using the available CTD time series from these two projects together with a MLD climatology obtained from Argo profilers. In order to check the robustness of our results, several different criteria will be used for the estimation of the MLD. We will also address the study of those factors that affect the water column stratification and the possible impact on the chlorophyll concentration of the surface waters.

DATA AND METHODS

The time series presented in this work could be classified into three categories: The first one would correspond to those data used to infer the stratification of the water column. This includes ship-borne CTD profiles from the IEO monitoring programs (red dots in **Figure 1**), and MLD values obtained from Argo profilers. The IEO monitoring of the Spanish Mediterranean and the Gulf of Cádiz started at different dates as separated projects for each geographical region (Gulf of Cádiz, Alborán Sea, Cape Palos, and Balearic Islands). All these projects were finally unified under the umbrella of two major projects contributing to the IEO-Observing System (IEOOS; Tel et al., 2016): STOCA (Time series of oceanographic data in the Gulf of Cádiz) and RADMED (Time series of oceanographic data in the Mediterranean Sea). These projects were initiated in 2009 and 2007 respectively. Nevertheless, previous monitoring programs supported by the IEO, started during the 1990s decade. Therefore, data from 1992 are available in the case of some stations (see Vargas-Yáñez et al., 2017). Three-monthly campaigns conducted in these projects include CTD profiles at all the oceanographic stations, (see Sánchez-Leal et al. (2020) and López-Jurado et al. (2015) for more details). However, it should

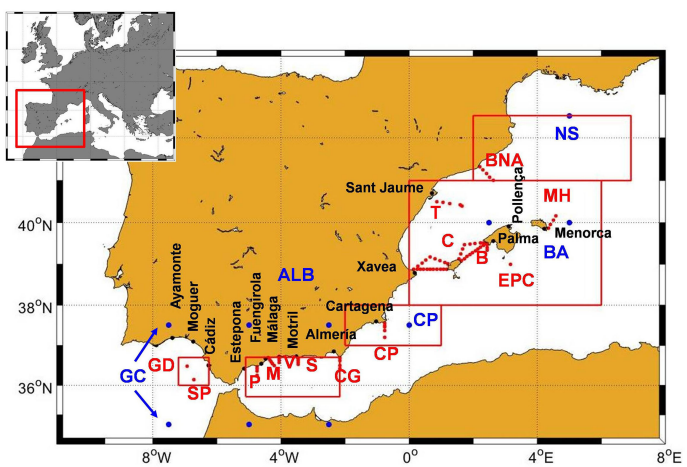

FIGURE 1 | Map of the area of study. Red dots and labels show the position of the STOCA and RADMED oceanographic stations. Black dots and labels are the position of the coastal meteorological stations from the Spanish meteorological agency (AEMET). Red rectangles are the regions where Argo MLD, Chlorophyll concentration, and SST data were averaged for obtaining monthly time series. Blue dots are the NCEP/NCAR grid points where reanalysis data were collected and averaged for obtaining monthly time series over the same regions used for MLD, Chl and SST data.

be noted that these series present some gaps due to bad weather conditions or technical problems. In this work, temperature, salinity and density profiles were used to estimate MLD time series. We have also used a climatology of MLD values downloaded from mixedlayer.ucsd.edu (Holte et al., 2017). This climatology uses temperature and salinity profiles from the international Argo program (https://argo.ucsd.edu/). We obtained all the MLD values corresponding to the following five geographical areas: Gulf of Cádiz, Alborán Sea, Cape Palos region, Balearic Islands, and a large area including the Catalan Sea and waters to the south of the Gulf of Lions that will be named hereafter as Northern Sector (see red rectangles in **Figure 1**). These data are distributed irregularly in time and space and their initial date is variable, being 2003 for the case of the Northern Sector, and 2015 for the Gulf of Cádiz.

The second category would include those variables that can have some influence on the mixing or stratification of the water column. These variables include wind intensity, air temperature, and precipitation rates, and were collected from two sources. The first one consists of several meteorological coastal stations from the Spanish meteorological service (Agencia Estatal de Meteorología, AEMET). The stations selected and their names correspond to black dots and labels in **Figure 1**. These data provide information about the meteorological conditions on a local scale. The AEMET time series are made of hourly or daily data. The wind time series extend from 1990 to 2021 in most cases, although some meteorological stations started operating more recently. Precipitation time series also extend from 1990 to 2021. In this case there are some longer time series, as Cádiz which starts in 1935, Málaga, in 1942, Menorca in 1965 and Palma, in 1978. The second data set has a broader spatial scale, and was obtained from the reanalysis of NCEP/NCAR at the NOAA (National Oceanographic and Atmospheric Agency) Physical Science Laboratory (https://psl.noaa.gov/data/gridded/index.html/, Kalnay et al., 1996). This data set consists of wind and precipitation monthly data with a 2.5° x 2.5° spatial resolution. Wind data start in 1948 and precipitation data in 1979. Blue dots and labels in **Figure 1** show the selected grid points for each of the five studied regions.

Finally, the last category is selected to analyze the possible consequences of changes in the water column stratification on ocean productivity. Surface chlorophyll concentration can be considered as a proxy for primary production (Boyce and Boris Worm (2015); Lavigne et al., 2015). Hence, monthly time series of gridded sea surface chlorophyll concentration were downloaded from the Ocean Color NASA (National Aeronautics and Space Administration) web site (https://oceancolor.gsfc.nasa.gov). We used data from the MODIS and SeaWIFS missions with a spatial resolution of 0.0833° x 0.0833°. These time series extend from 1997 to 2021. In addition, Sea Surface Temperature (SST) data were obtained from the "NOAA high-resolution blended analysis of daily SST and ice" (https://psl.noaa.gov/data/gridded/data.noaa.oisst.v2.highres.html). These data have a spatial resolution of 0.25° x 0.25° and the time series extend from 1981 to 2021. Besides the different lengths of the time series presented above, since the earliest CTD profiles obtained in the frame of the IEO monitoring programs started in 1992, the central period analyzed in this work will be 1990-2021. This is also the period analyzed for other variables. In addition, and for having a broader perspective, longer time series were collected when available. In those cases two different time series were analyzed, one corresponding to the 1990-2021 period, and a second one corresponding to the longest available period. Once again, this second long period could be different depending on the variable and the data source.

Methods

Following Vargas-Yáñez et al. (2017) all the CTD profiles from RADMED and STOCA programs were grouped and averaged by season of the year. Average or climatological profiles were calculated for winter (January, February, March), spring (April, May, June), summer (July, August, September) and autumn (October, November, December). For each climatological density profile, the square of the Brünt-Väisälä frequency was calculated in order to get some information about the degree of stratification of the water column:

$$N^2 = -\frac{g}{\rho}\frac{\partial \rho}{\partial z} \quad (1)$$

N^2 has units of s^{-2}, g is the acceleration of gravity (9.8 m s^{-2}), ρ is density expressed in kg m^{-3}, and z de vertical coordinate in meters.

For each individual CTD profile from RADMED and STOCA projects, the mixed layer depth was estimated using three different criteria. First, following de Boyer Motégut et al. (2004), we used a threshold method. In this work we have considered a temperature decrease of 0.3°C with respect to a reference value located at 10 m depth (t-threshold hereafter). This value was chosen after visual inspection of all the individual temperature profiles. A second criterion used a density threshold of 0.03 kg m^{-3} (de Boyer Motégut et al., 2004; d-threshold hereafter). Finally, the mixed layer depth was also estimated using the shallowest extreme curvature of the temperature (Lorbacher et al., 2006). In this latter case it was calculated using the matlab code provided in the supplementary information in Lorbacher et al. (2006). These time series extended from 1992 to 2021 for the case of the longest time series, and from 2009 to 2021 for the case of the shortest ones.

The MLD shows a very clear seasonal cycle worldwide (Kara et al., 2000; de Boyer Motégut et al., 2004; Lorbacher et al., 2006) and also in the case of the Western Mediterranean (Herrmann et al., 2008b; 2014; Somot et al., 2018; Testor et al., 2018; Bahamon et al., 2020). For this reason, the MLD values were grouped and averaged by season of the year. This seasonal cycle was subtracted to each individual value within the time series of MLD, and a series of anomalies or residuals was obtained. Linear trends were estimated by means of least square fits using the time series of residuals. Confidence intervals in the 95% confidence level were calculated taking into account the possible auto-correlation of the series.

According to mixedlayer.ucsd.edu/, MLD values were calculated using both temperature and density threshold

methods and those values in de Boyer Motégut et al. (2004). In this case the temperature threshold is 0.2 °C whereas the density threshold is the same used for the CTD data (0.03 kg/m^3). For each geographical area (red rectangles in **Figure 1**), and for each of the two methods used (temperature and density thresholds), the values corresponding to the same month and year were averaged for obtaining monthly time series for each region. Then, all the values corresponding to the same calendar month were grouped and averaged for obtaining a climatological seasonal cycle. This cycle was subtracted to the monthly time series to produce monthly time series of anomalies. These final times series were used for the estimation of linear trends.

Meteorological variables (zonal and meridional components of the wind, wind intensity, precipitation rates, and air temperature) from AEMET meteorological stations were also averaged to obtain monthly time series. Then, the same procedure used for MLD data was followed. An average seasonal cycle was calculated and then it was subtracted from the monthly time series for obtaining time series of residuals or anomalies. This latter time series were used for the estimation of linear trends.

In the case of NCEP/NCAR reanalysis, surface chlorophyll, and SST data sets, all the data from those grid points within each of the five geographical areas considered were averaged for obtaining monthly time series for each region. Then, average seasonal cycles and monthly time series of residuals were estimated.

RESULTS

Seasonal Water Column Stratification

The stratification of the water column in the whole area of study is characterized by both a permanent and a seasonal picnocline (thermocline and halocline). Nevertheless, there are important differences between the Gulf of Cádiz and the WMED and also within the WMED. Average temperature, salinity, density, and N^2 profiles were calculated for each oceanographic station (red dots in **Figure 1**). **Figure 2** shows those profiles for some selected

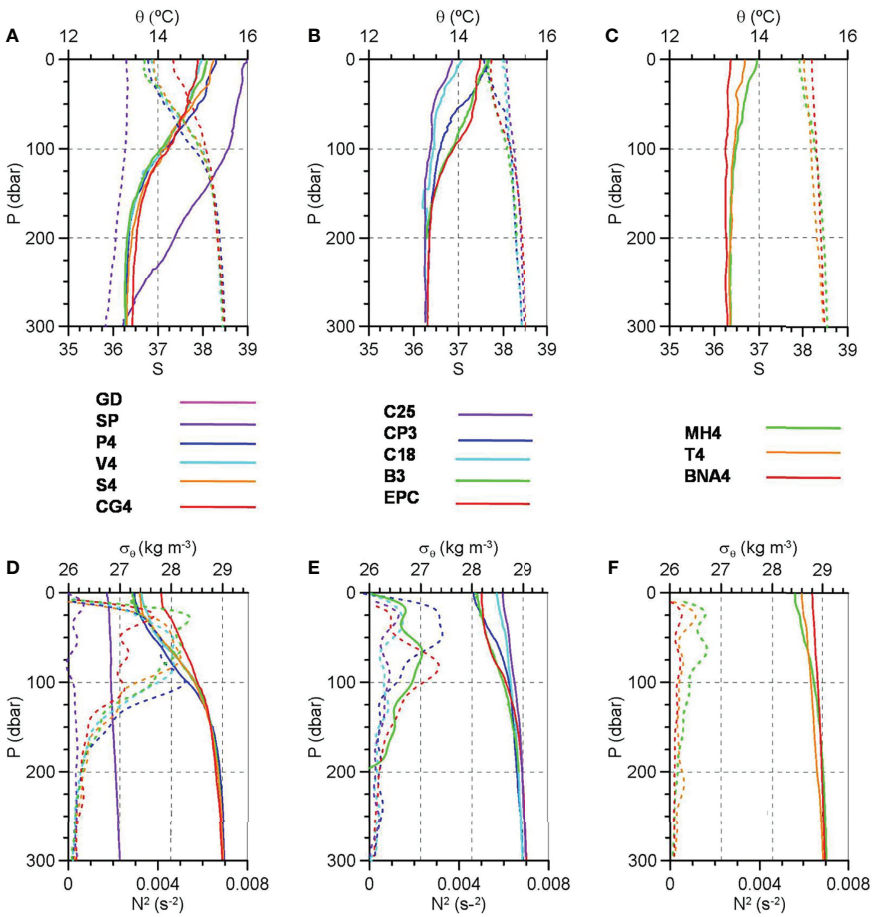

FIGURE 2 | Winter climatology computed for temperature (top panels, continuous lines), salinity (top panels, dashed lines), density (bottom panels, continuous lines), and N2 (bottom panels, dashed lines) vertical profiles at the selected oceanographic stations of the Gulf of Cádiz and the Alborán Sea **(A**, **D)**, Cape Palos and the south of the Balearic Islands **(B, E)** and those stations to the north of the Balearic Islands **(C**, **F)**. See color legend for station identification.

stations in the Gulf of Cádiz and the Alboran Sea (**Figures 2A, D**), for the Cape Palos region and the south of the Balearic Islands (**Figures 2B, E**), and for those stations to the north of the Balearic Islands (**Figures 2C, F**). These stations were selected in order to cover the southwest-northeast gradients from the Gulf of Cádiz to the northernmost stations located at the Catalan Sea. Profiles in **Figure 2** correspond to winter, when the weakest vertical gradients are observed. Similar results are presented in **Figure 3** for summer when the vertical stratification reaches its maximum value. The winter profiles show the permanent stratification. In the case of the Gulf of Cádiz, this is associated to the presence of the North Atlantic Central Water, which is characterized by a decrease of both temperature and salinity with depth. In the case of the Alboran Sea, the permanent stratification is caused by the two layer structure of the Mediterranean Sea, with the Atlantic Water laying above the Mediterranean Waters. In this case, temperature decreases with depth, while salinity increases. In the Gulf of Cádiz, only the temperature contributes to the permanent stratification, whereas in the case of the Mediterranean Sea, both temperature and salinity do. Therefore, the density difference between the sea surface and the 300 m level (the maximum one presented in **Figures 2**, **3**) is much higher in the case of the Mediterranean Sea. In summer, the seasonal thermocline develops, being the main contributor to the vertical density gradient. As a result of this, N^2 has a sharp maximum in all the geographical areas (**Figures 3D–F**) situated around 25 m depth and a much weaker secondary maximum close to 100 m, associated to the permanent picnocline. On the contrary, N^2 values do not show a clear pattern during winter, with several local maxima distributed along the upper 100 m of the water column. The winter N^2 maxima range between 0.001 s^{-2} and 0.004 s^{-2}, whereas the summer maxima are an order of magnitude higher, with values around 0.03 s^{-2}.

There are also differences within the Mediterranean Sea, with a clear southwest-northeast gradient. Winter surface temperature (salinity) decreases (increases) first, as we move eastwards in the Alboran Sea, and then to the north along the eastern coast of the Spanish Mediterranean. This thermohaline gradient produces important differences in winter surface density

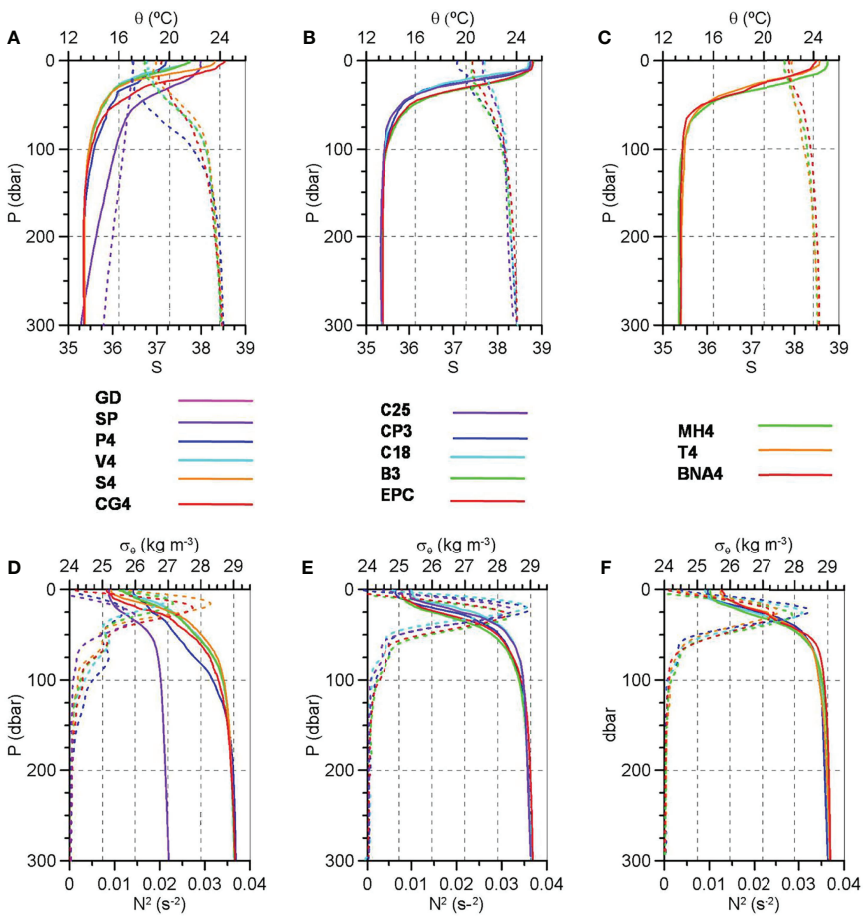

FIGURE 3 | Summer climatology computed for temperature (top panels, continuous lines), salinity (top panels, dashed lines), density (bottom panels, continuous lines), and N2 (bottom panels, dashed lines) vertical profiles at the selected oceanographic stations of the Gulf of Cádiz and the Alborán Sea **(A**, **D)**, Cape Palos and the south of the Balearic Islands **(B**, **E)** and those stations to the north of the Balearic Islands **(C**, **F)**. See color legend for station identification.

which is around 27.75 kg m^{-3} in the Alboran Sea (**Figure 2D**), 28 kg m^{-3} around Cape Palos and to the south of the Balearic Islands (**Figure 2E**), and between 28.5 and 28.75 kg m^{-3} at the northernmost stations of the sampling area (**Figure 2F**). Consequently, there is a horizontal gradient in winter stratification, with N^2 values decreasing from 0.004 s^{-2} in the Alboran Sea (**Figure 2D**), to 0.001 s^{-2} at BNA4 station, in the Catalan Sea (**Figure 2F**).

Seasonal Cycle of the MLD

Figures 4A–F show the average seasonal cycle for some selected stations in the Gulf of Cádiz and in the Alboran Sea. Continuous lines correspond to the four seasonal values obtained from the three-monthly sampling carried out in STOCA and RADMED projects. Blue lines show the results from the t-threshold method, red lines correspond to the d-threshold method (de Boyer Montégut et al., 2004) and black lines are for the temperature curvature method (Lorbacher et al., 2006). In addition, the average seasonal cycle of the MLD, obtained from Argo data (Holte et al., 2017) for the Gulf of Cádiz and for the Alboran Sea areas, are presented in **Figures 4A, C** as dashed lines, for comparison with the results obtained from ship-borne CTDs. **Figures 5A–F** show the MLD seasonal cycles for some stations in the Cape Palos area and to the south of the Balearic Islands. The Argo MLD seasonal cycle for the Cape Palos area is included in **Figure 5A**. Finally, **Figures 6A–F** show the MLD seasonal cycles for those stations situated to the north of the Balearic Islands and in the Catalan Sea. Argo MLD cycles for the Balearic Sea and for the Northern Sector are included in **Figures 6F**, **D** respectively.

In all the cases analyzed, the seasonal cycle shows maximum values in winter. MLD decreases during spring and summer when the seasonal thermocline develops, reaching minimum values in summer. It starts to increase again during autumn. The use of monthly Argo MLD, shows that the maxima are

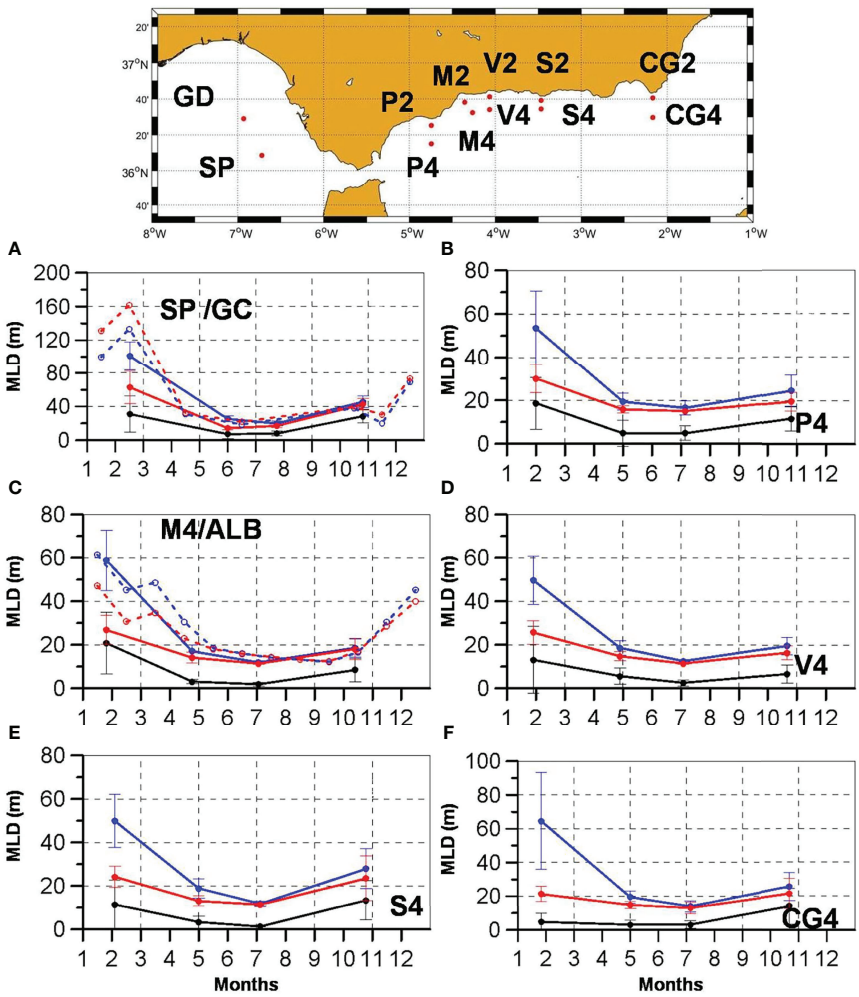

FIGURE 4 | Seasonal cycles of the MLD estimated from the three-monthly sampling of STOCA and RADMED projects (continuous lines) at some selected oceanographic stations (see labels inserted in these figures and the map for the locations), and form the Argo MLD at the regions of the Gulf of Cádiz **(A)** and the Alborán Sea **(C)** (dashed lines). Blue lines correspond to the t-threshold method, red lines to the d-threshold method, and black lines to the temperature extreme curvature method. Please, note the different ranges of the y-axis between subplots.

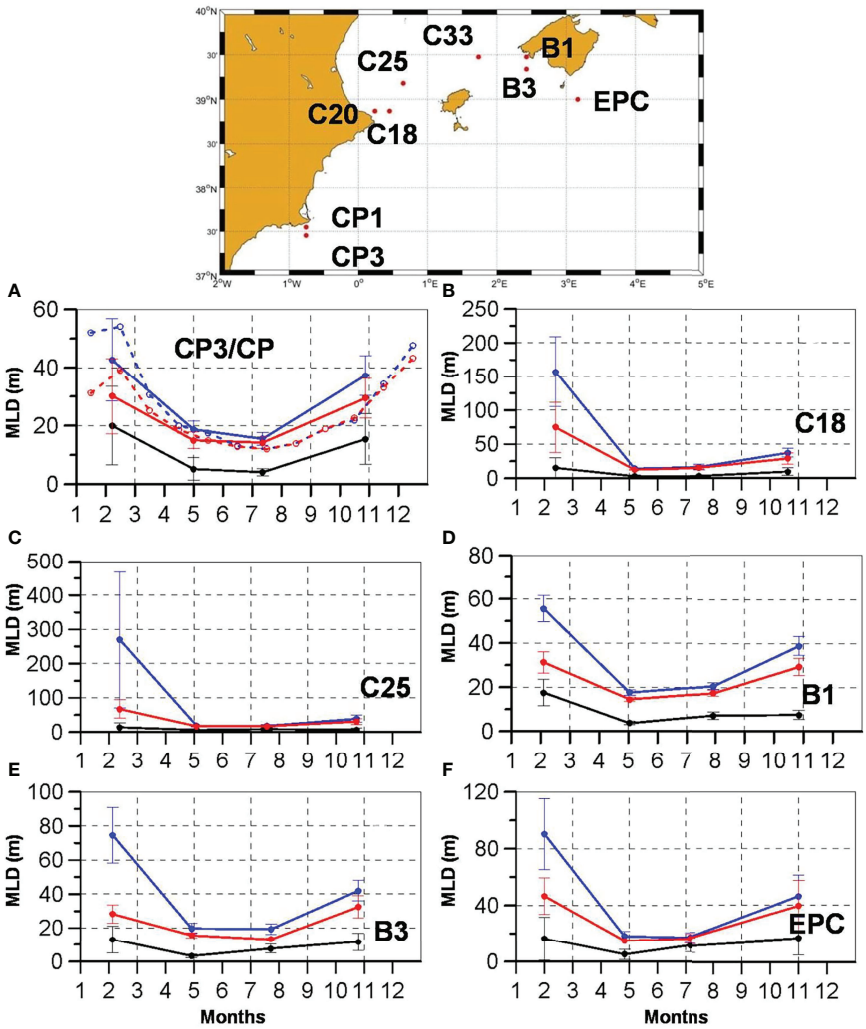

FIGURE 5 | Seasonal cycles of the MLD estimated from the three-monthly sampling of RADMED projects (continuous lines) at some selected oceanographic stations (see labels inserted in these figures and the map for the locations), and form the Argo MLD at the region of Cape Palos **(A)** (dashed lines). Blue lines correspond to the t-threshold method, red lines to the d-threshold method, and black lines to the temperature extreme curvature method. Please, note the different ranges of the y-axis between subplots.

observed in February, whereas the minima are distributed between July and September.

These results show the same southwest-northeast gradient evidenced in the vertical profiles of temperature, salinity, density, and N^2 (**Figures 2**, **3**). The winter MLD at the Alboran Sea and Cape Palos area ranges between 30 and 60 m, depending on the method used (**Figure 4**). These values increase to 75-150 m to the south of the Balearic Islands (**Figure 5**) and to 300 m in the Ibiza Channel. Finally, the deepest MLD is reached at BNA4, in the Catalan Sea (**Figure 6D**) where it ranges between 500 m and 600 m. The only exception to this spatial trend is observed in the Gulf of Cádiz, where winter MLD is deeper than in the Alboran Sea (**Figure 4**).

When using RADMED and STOCA CTD data, the MLD values calculated using the t-threshold method (blue lines in **Figures 4**–**6**) are always deeper than those obtained using a density criterion (red lines in **Figures 4**–**6**). This behavior is also observed for Argo MLD (with the only exception of the Gulf of Cádiz MLD). Nevertheless, despite the criterion and the data set used, the results are similar from a qualitative point of view. On the contrary, the extreme curvature method seems to sub-estimate the MLD in all of the cases.

MLD Linear Trends

Linear trends were estimated from the time series of anomalies of MLD for the 85 stations corresponding to STOCA and RADMED projects (red dots in **Figure 1**). For each station three different time series were available corresponding to the three methods used for determining the MLD: t-threshold, d-threshold, and extreme curvature (see methods section). In

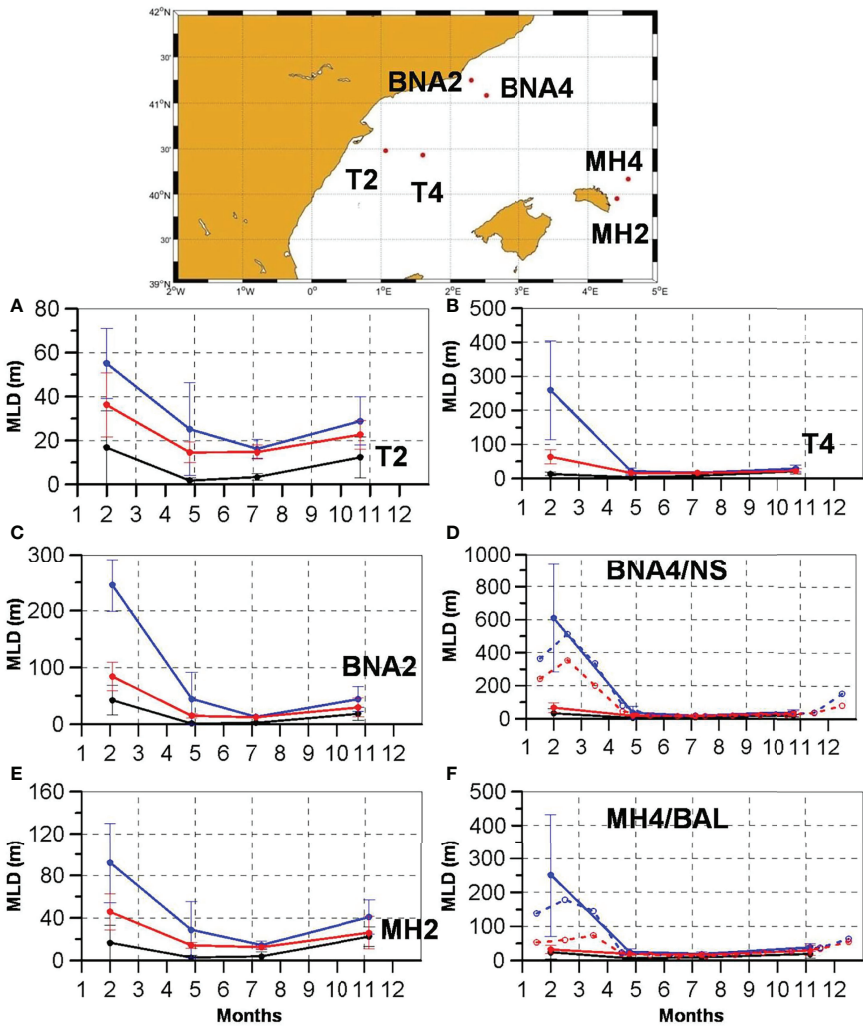

FIGURE 6 | Seasonal cycles of the MLD estimated from the three-monthly sampling of RADMED projects (continuous lines) at some selected oceanographic stations (see labels inserted in these figures and the map for the locations), and form the Argo MLD at the regions of the Northern Sector **(D)** and the Balearic Islands **(F)** (dashed lines). Blue lines correspond to the t-threshold method, red lines to the d-threshold method, and black lines to the temperature extreme curvature method. Please, note the different ranges of the y-axis between subplots.

addition to this, the MLD obtained by means of the temperature and density threshold methods were applied to smoothed temperature and density profiles. Therefore, linear trends were estimated for a total of 85 x 5 = 425 time series. In most of the cases the resulting trends were not statistically significant at the 95% confidence level, alternating positive (deepening) and negative (shallowing) trends. Table S1 in supplementary information shows such trends for a subset of the 85 oceanographic stations based on the temperature and density thresholds. In summary, trends were significant only in 1.2% of the series analyzed using the extreme curvature method, in 3.5% of the series, using the t-threshold method, and in 2.4% of the cases, using the d-threshold method. When using smoothed time series the results were very similar with 4.7% and 2.4% of significant results.

Table 1 shows the linear trends obtained for the Argo MLD time series (see these time series in **Figure S1** in **Supplementary Material**). In this case, only the results corresponding to the Balearic Sea were significant in the 95% confidence level. These trends were -4.5 ± 2.1 m yr^{-1} and -1.5 ± 1.1 m yr^{-1} for the t-threshold and d-threshold respectively.

Seasonal Cycles and Linear Trends for Wind

Figure 7 shows the average seasonal cycle and the time series of anomalies for the wind intensity and the zonal and meridional components of the wind at those meteorological stations with the longest time series (**Figures 7A–F**). Such time series extend from 1990 to 2021. The west-east component of the wind is shown in blue (left axis, positive eastwards) and the south-north

TABLE 1 | Linear trends and confidence interval at the 95% level (b ± CI 95%) for the MLD estimated from the climatology obtained from Argo profilers (mixedlayer.ucsd.edu) at the five study regions, following the temperature (t-threshold, m yr-1) and density (d-threshold, m yr-1) criteria for the longest period available.

Region	Period	t-threshold (m yr^{-1})	d-thresold (m yr^{-1})
Gulf of Cádiz	2015-2021	-0.4 ± 1.8	-0.4 ± 2.4
Alborán Sea	2006-2021	0.1 ± 0.9	0.1 ± 0.8
Cape Palos	2004-2021	0.1 ± 0.5	0.3 ± 0.5
Balearic Sea	2004-2021	**-4.5 ± 2.1**	**-1.5 ± 1.1**
Northen Sector	2003-2021	-4.8 ± 5.4	-4 ± 5

Bold numbers indicate those results that are statistically significant.

component in red (left axis, positive northwards). Black lines correspond to wind intensity (right axis). We also present the same results for the reanalysis time series corresponding to the geographical areas of the Gulf of Cádiz and the Alboran Sea (blue dots in **Figure 1**, red rectangles in **Figures 7G–J**).

There are some differences between the Gulf of Cádiz and the Alborán Sea stations, and also between those results obtained from the local meteorological stations and those from the reanalysis data. These differences indicate the influence of local factors on the seasonal evolution of the winds. Considering the reanalysis results, the Gulf of Cádiz (**Figure 7G**) shows the prevalence of winds flowing eastwards (westerlies) and southwards (northerlies) during the whole year, with a maximum intensity during the summer months. In the Alborán Sea (**Figure 7I**), the wind blows from the north all the year round. The zonal component blows from the west during most of the year, with a shift to easterly winds during summer, when the wind intensity has a minimum value. **Figure 8** shows similar results for those meteorological stations located on the eastern coast of the Spanish Mediterranean and on the Balearic Islands (**Figures 8A–F**). It also presents those results corresponding to the geographical areas named as Balearic Islands and Northern Sector (blue dots in **Figure 1** and red rectangles in **Figures 8G–J**). Once again there are important differences between the results from local meteorological stations and those from the reanalysis data. Concerning these latter results, the wind in the Balearic Islands (**Figure 8G**) follows a pattern similar to that observed in the Alboran Sea. The meridional component of the wind is negative during the whole year (northerly winds). The zonal component is directed

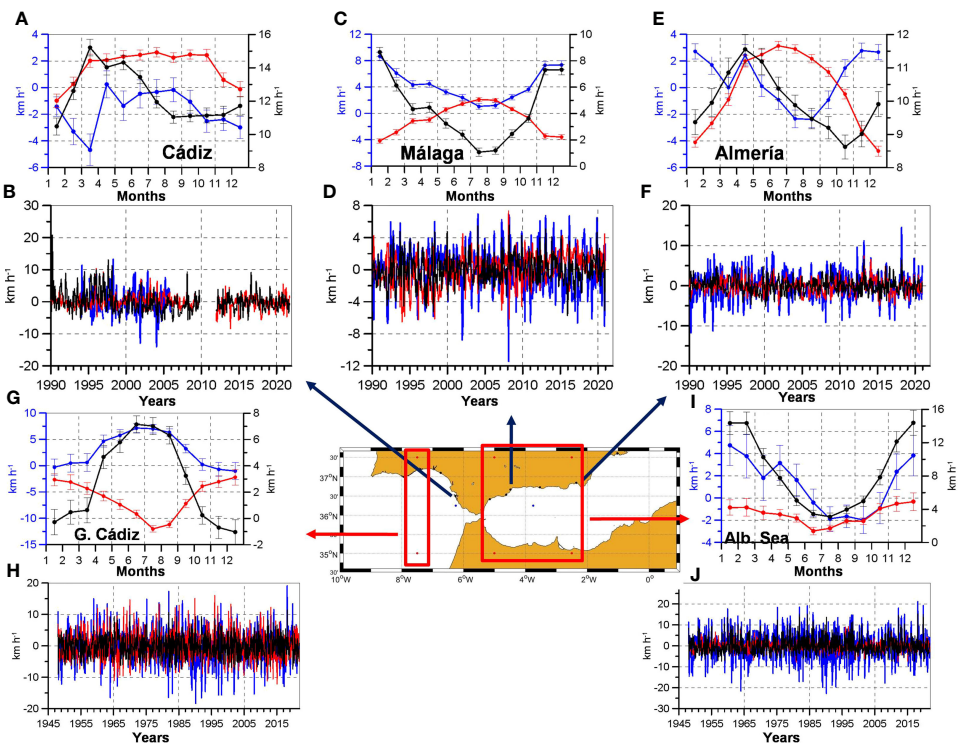

FIGURE 7 | (A, C, E) are the seasonal cycles of west-east component of the wind (blue lines and left axis), south-north component (red lines and left axis) and the wind intensity (black lines and right axis) for the meteorological stations of Cádiz, Málaga, and Almería. **(B, D, F)** are the corresponding time series of anomalies. **(G, I)** are the wind seasonal cycles for the regions of Gulf of Cádiz and the Alborán Sea, using the reanalysis data. **(H, J)** are the corresponding time series of anomalies.

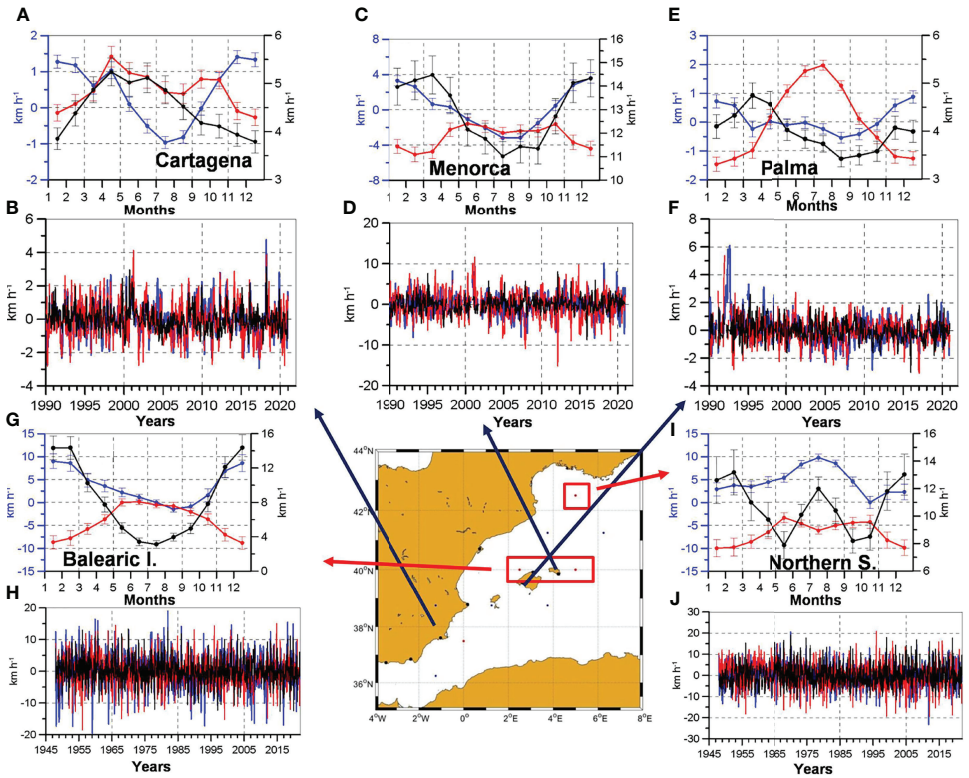

FIGURE 8 | **(A, C, E)** are the seasonal cycles of west-east component of the wind (blue lines and left axis), south-north component (red lines and left axis) and the wind intensity (black lines and right axis) for the meteorological stations of Cartagena, Menorca, and Palma. **(B, D, F)** are the corresponding time series of anomalies. **(G, I)** are the wind seasonal cycles for the regions of Balearic Islands and the Northern Sector, using the reanalysis data. **(H, J)** are the corresponding time series of anomalies.

eastwards for most of the year, with the only exception of the summer months when the prevailing direction of the wind is westwards (easterlies). The intensity of the wind also has a clear seasonal cycle with minimum values occurring in summer. The wind seasonal cycles at the Northern Sector (**Figure 8I**) exhibit some differences. On the average, the wind flows eastwards (westerlies) and southwards (northerlies), with no sign change along the year for none of both components. The maximum intensity of the wind is observed in winter, with a secondary maximum in summer.

Table 2 shows the linear trends for time series of anomalies of the wind intensity at the different local meteorological stations, and **Table 3** shows the linear trends for the wind intensity at the five regions where reanalysis data were obtained. Notice that in this latter case, data are available for a longer period of time. Therefore, trends were estimated for two different periods. First, from 1990 to 2021, for comparison with the local meteorological stations and with the MLD trends, and second, for the longest available period: 1948-2021. Trends estimated from the meteorological stations showed significant and non-significant trends (**Table 2**). Those significant trends were positive in some cases and negative in others without any clear spatial pattern. Nevertheless, many of the time series analyzed started after 1990 and had a short length. If we consider those series extending from 1990 to 2021 (Cádiz, Málaga, Almería, Cartagena and Palma, see **Figure 1** for the locations), trends were significant in all the cases, being such trends negative in four cases and positive in one case. On the contrary, reanalysis time series showed no significant trends in most of the five regions considered (**Table 3**), nor for the period 1990-2021, neither for the extended one (1948-2021). The only exceptions corresponded to the Balearic Islands during the period 1948-2021, and to the Northern Sector from 1990 to 2021.

Seasonal Cycles and Linear Trends for Precipitation Rates and Air Temperature

The seasonal cycle of precipitation rates shows the well known characteristics of the Mediterranean region. **Figure S2** in supplementary information shows these seasonal cycles and the time series of anomalies for the precipitation rates at those meteorological stations with the longest time series, and for the Gulf of Cádiz and the Alboran Sea regions (NCEP data). **Figure S3** shows similar results for the Palma and Menorca meteorological stations, and the regions Cape Palos, Balearic Islands, and Northern Sector. The average seasonal cycles are similar in all the cases, with maximum precipitations in autumn and winter, and minimum ones in summer. The only difference is the presence of a secondary maximum in spring in some locations. This secondary maximum is more pronounced in the Balearic Sea and the Northern Sector.

TABLE 2 | Linear trends and confidence interval at the 95% level (b ± CI 95%) for the wind intensity ((km h^{-1}) yr^{-1}), precipitation rate (mm yr^{-1}) and air temperature (°C yr^{-1}) at the selected coastal meteorological stations (Spanish meteorological agency, AEMET) for the longest period available.

Meteorological coastal station	Period	Wind (km h^{-1}) yr^{-1}	Precipitationmm yr^{-1}	Air temperature°C yr^{-1}
Ayamonte	1997-2003	0.07 ± 0.15	-0.6 ± 0.9	**0.073 ± 0.023**
Moguer	1997-2021	**0.048 ± 0.019**	0.3 ± 0.6	**0.067 ± 0.017**
Cádiz	1990-2021	**-0.07 ± 0.04**	0.0 ± 0.5	**0.028 ± 0.012**
	1935-2021		**-0.30 ± 0.18**	**0.019** ± 0.004
	1955-2021			
Estepona	2001-2021	**0.04 ± 0.04**	0.2 ± 1.3	0.004 ± 0.015
Fuengirola	2000-2021	**-0.05 ± 0.03**	-0.8 ± 1.0	-0.014 ± 0.017
Málaga	1990-2021	**0.022 ± 0.022**	-0.1 ± 0.6	**0.048 ± 0.009**
	1942-2021		-0.07 ± 0.15	**0.016** ± 0.003
Motril	1990-2021	0.01 ± 0.03	1.2 ± 1.3	-0.02 ± 0.04
Almería	1990-2021	-0.011 ± 0.022	0.06 ± 0.23	**0.016 ± 0.010**
	1968-2021		-0.02 ± 0.11	**0.029** ± 0.005
Cartagena	1990-2021	**-0.011 ± 0.009**	-0.0 ± 0.3	-0.005 ± 0.011
Xávea	1997-2021	**0.066 ± 0.021**	**1.1 ± 0.7**	**0.032 ± 0.017**
Sant Jaume	1997-2019	-0.02 ± 0.04	-0.67 ± 0.70	0.010 ± 0.021
Palma	1990-2021	**-0.015 ± 0.009**	0.1 ± 0.4	**0.028 ± 0.011**
	1978-2021		0.18 ± 0.22	**0.039 ± 0.007**
Pollença	1990-2021	**-0.012 ± 0.011**		
Menorca	1990-2021	0.015 ± 0.023	0.1 ± 0.4	0.007 ± 0.011
	1965-2021		-0.09 ± 0.18	**0.026 ± 0.005**

Bold numbers indicate those results that are statistically significant.

TABLE 3 | Linear trends and confidence interval at the 95% level (b ± CI 95%) for the wind intensity ((km h^{-1}) yr^{-1}), precipitation rate (mm yr^{-1}) and air temperature (°C yr^{-1}) computed from NCEP/NCAR reanalysis data sets at the five study regions.

	Wind [(km h^{-1}) yr^{-1}]		Precipitation [(mm $month^{-1}$) yr^{-1}]		Air temperature (°C yr^{-1})	
Region	1990-2021	1948-2021	1990-2021	1979-2021	1990-2021	1948-2021
G. Cádiz	0.00 ± 0.04	-0.002 ± 0.011	0.2 ± 0.5	0.0 ± 0.3	**0.022 ± 0.013**	**0.011 ± 0.004**
Alborán	-0.03 ± 0.04	0.001 ± 0.012	-0.1 ± 0.3	0.11 ± 0.20	**0.036 ± 0.014**	**0.015 ± 0.004**
C. Palos	0.02 ± 0.05	0.001 ± 0.014	0.09 ± 0.13	0.09 ± 0.13	**0.040 ± 0.011**	**0.017 ± 0.003**
Balearic Islands	0.03 ± 0.04	**-0.013 ± 0.013**	-0.08 ± 0.18	0.08 ± 0.12	**0.034 ± 0.009**	**0.014 ± 0.003**
N. Sector	**0.001 ± 0.001**	0.014 ± 0.016	-0.2 ± 0.3	-0.15 ± 0.19	**0.035 ± 0.012**	**0.019 ± 0.003**

Two different periods were analyzed: 1990-2021, and the longest available period. Bold numbers indicate those results that are statistically significant.

Linear trends for the precipitation rates at the local meteorological stations are presented in **Table 2**. For some of these locations, data were available for a longer period of time. In those cases, the trends were calculated for the period 1990-2021, and for the longest period available. Once again, trends are not significant in most of the cases, with positive and negative values alternating. When considering the reanalysis time series of precipitation rates, none of the trends were significant (**Table 3**).

Figures S4, S5 in supplementary material show the seasonal cycles of air temperature and the time series of anomalies at the same meteorological stations and geographical areas considered in **Figures S2, S3**. In the case of the meteorological stations, we include monthly values of daily minimum, maximum and mean temperatures. **Table 2**, **3** show the linear trends for the air temperature for coastal meteorological stations and reanalysis data. These results show the well known increase of the air temperatures. It is important to notice that linear trends have very large values when short periods are considered (see for instance Moguer and Ayamonte trends in **Table 2** for the period 1997-2021). The reanalysis data show lower trends, ranging between 0.01 and 0.02°C yr^{-1} for the period 1948-2021, with an intensification of these positive trends for the recent period 1990-2021.

Surface Chlorophyll Concentration and Sea Surface Temperature

Figure 9A presents the seasonal cycles of surface chlorophyll concentrations at the five geographical areas analyzed. **Figures 9B–F** are the time series of anomalies for the same regions. These figures clearly show the decrease of chlorophyll concentrations within the Mediterranean Sea. The highest chlorophyll concentrations are observed during winter in all the regions, with maximum values in March (**Figure 9A**). The only exception would be the Northern Sector where the maximum value is reached in April. These concentrations decrease from the Gulf of Cádiz to the Alboran Sea, and then along the eastern coast of the Spanish Mediterranean. The only exception corresponds to the early spring values in the Northern Sector. Notice that the variance of the time series of anomalies also decreases from the Gulf of Cádiz (**Figure 9B**) to the interior of the Mediterranean Sea (**Figures 9C–F**).

The chlorophyll concentrations did not experience any significant trend in most of the regions, with the only exception of the Cape Palos one, where it increased during the period 1997-2021 (**Table 4**).

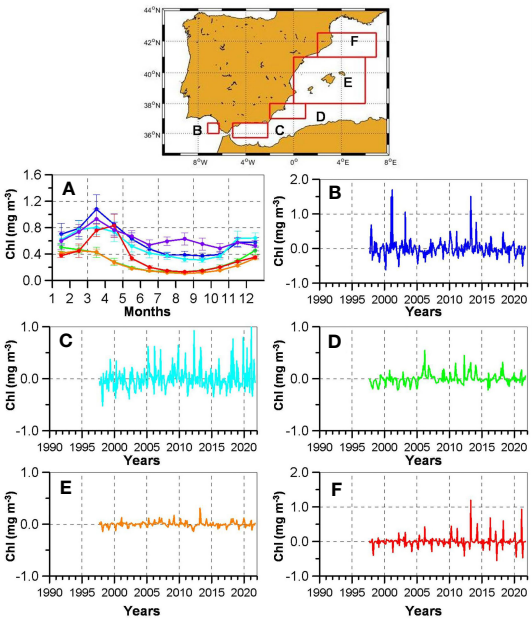

FIGURE 9 | Seasonal chlorophyll concentration **(A)** and the corresponding time series of anomalies computed for the five study regions: Gulf of Cádiz (blue line, **B**), Alborán Sea (blue light line, **C**), Cape Palos (green line, **D**),

TABLE 4 | Linear trends and confidence interval at the 95% level (b ± CI 95%) for the surface Chlorophyll concentration [(mg m^{-3}) yr^{-1}] and SST (°C yr^{-1}) computed from (add data sets information) at the five study regions for the longest period available.

	Chl [(mg m^{-3}) yr^{-1}]	SST (°C yr^{-1})
Region	1997-2021	1981-2021
G. Cádiz	-0.002 ± 0.004	**0.021 ± 0.005**
Alborán	0.003 ± 0.004	**0.024 ± 0.005**
Cape Palos	**0.003 ± 0.002**	**0.027 ± 0.005**
Balearic Islands	0.000 ± 0.001	**0.033 ± 0.005**
N. Sector	0.001 ± 0.003	**0.039 ± 0.06**

Bold numbers indicate those results that are statistically significant.

SST seasonal cycles and time series of anomalies are presented in **Figure S6**. In this case, the temperatures experienced significant and intense trends that ranged between 0.015°C yr^{-1} and 0.039°C yr^{-1} (**Table 4**).

DISCUSSION AND CONCLUSIONS

The main goal of the present work was to analyze the time evolution of the MLD along the south and east Spanish coast, from the Gulf of Cádiz to the Catalan Sea, including the de Balearic Islands. The possible existence of trends in this evolution could provide some indications about the increase of the stratification. The first step was to produce time series of MLD as long as possible for the different regions that make up our study area. There is not one single criterion to define the depth of the mixed layer (Kara et al., 2000; de Boyer Motégut et al., 2004; Lorbacher et al., 2006; Holte and Talley, 2009; Holte et al., 2017). We could not rule out *a priori* that the criterion used to define the MLD could have some impact on the trend estimation. Therefore, we followed the same approach used by Vargas-Yáñez et al. (2021; 2010; 2009) for the detection of long-term trends in the properties of the water masses in the WMED. That is, we repeated the calculations using different criteria, and then we checked if the results were sensitive to the methodology used. A similar issue could arise from the data set used. The longest available homogeneous data sets (periodic samples using the same methodology) are those from the RADMED and STOCA campaigns (three-monthly/CTD), and those temperature and salinity profiles obtained from the Argo profilers deployed within our area of interest.

Concerning the seasonal cycle of the MLD, the results obtained using the CTD time series and using both a t-threshold and a d-threshold criterion were qualitatively similar. These cycles show that the winter MLD increases from the Alboran Sea towards the Mediterranean Sea. The maximum values of MLD are observed at the northernmost stations. This southwest-northeast gradient has several causes. The Alboran Sea waters are strongly stratified because of the influence of fresher Atlantic Water flowing from the nearby Strait of Gibraltar. These waters are also warmer than the Mediterranean waters during winter. On the contrary, surface waters to the north of the Balearic Islands are highly modified after their circulation within the WMED. These geographical areas are also subject to a strong cooling during winter months that enhances the deepening of the mixed layer.

When considering the different criteria used to define the MLD, the main difference is that the t-threshold method always produced larger values than the d-threshold criterion, mainly in winter, when the MLD reaches its maximum value (see continuous blue and red lines in **Figures 4–6**). These results were also similar to those obtained using Argo data. Once again those estimations based on the temperature criterion were larger than those corresponding to the density criterion. However, in this case, one exception was observed in the winter MLD in the Gulf of Cádiz, where the MLD based on the density criterion was deeper than the one based on the temperature one (dashed lines in **Figure 4A**). This discrepancy could cast some doubts on the validity of our results. Nevertheless, they can be easily explained by the temperature and density thresholds used in each case.

Be $\frac{dT}{dz}, \frac{dS}{dz}$ the vertical gradients of temperature and salinity in the near surface waters (below the reference depth of 10 m), and $R = \frac{\alpha^{dT}/_{dz}}{\beta^{dS}/_{dz}}$ the stability ratio with α and β the thermal expansion and haline contraction coefficients. Then, if the threshold values used to determine the MLD are $|\Delta T|$ and $\Delta\rho$, then the depth where these values are reached (MLD) can be approached by the expressions:

$$\frac{-|\Delta T|}{{}^{dT}/_{dz}} \tag{2.1}$$

$$\frac{\Delta\rho}{-\rho\alpha{}^{dT}/_{dz}[1-R^{-1}]} \tag{2.2}$$

For CTD data, the 0.3 °C threshold was used. For the Argo data, it was used the same value found in de Boyer Motégut (2004) which is 0.2°C. In both cases the 0.03 kg m^{-3} value was used for the density threshold. If only the temperature effect on density was considered, the MLD based on density would always be lower than the one based on temperature, as the density change associated to 0.2°C and 0.3°C decrements are larger than 0.03 kg/m^3. When the salinity effect is taken into account, this situation holds in the case of the Mediterranean Sea, as the stability ratio *R* is negative (see expression 2.2). On the contrary, *R* is positive in the Gulf of Cádiz, and the MLD for the d-threshold is lower for a ΔT=0.3°C (CTD data) and higher for the 0.2°C threshold used by de Boyer Motégut (2004) and Holte et al. (2017).

The extreme curvature method seems to underestimate the MLD seasonal cycle. Nevertheless, if any bias existed in the MLD calculation, it would affect to the complete time series and the estimation of linear trends would not be affected. These trends were not statistically significant in most of the cases, despite the method used for the calculation of the MLD or the data set analyzed (CTD or Argo). Hence we cannot accept the existence of an increase of the stratification in the Spanish Mediterranean waters and the Gulf of Cádiz. The factors that could contribute to the increase of the stratification are the warming of the surface layer, the decrease of salinity, and the decrease of the wind intensity. According to our results, it is clear that the SST has increased from 1981 as a consequence of global warming (**Table 4**). Such warming is also evidenced by the air temperature trends observed from 1948 in the case of the reanalysis data presented in this work, and from the 1990s decade (**Tables 2**, **3**). Although we have not analyzed salinity data in this work, recent studies (Vargas-Yáñez et al., 2021; 2017) showed an increase of the surface salinity of the Mediterranean Sea as a consequence of an increase of the evaporation minus precipitation, the reduction of the rivers runoff (Skliris, 2014; Schroeder et al., 2017), or the inflow of saltier Atlantic Waters through the Strait of Gibraltar (Millot, 2007). Vargas-Yáñez et al. (2021; 2017) have shown that both temperature and salinity had increased in the different water masses of the WMED along the twentieth century and the beginning of the twenty first one, but those effects canceled each other and no significant trends were observed for the density. Other factors that could enhance the water column stratification would be the increase of precipitations and the decrease of the wind intensity. None of these variables showed significant trend (**Tables 2**, **3**).

In the case of an increase of the stratification, it would be very likely that the sea productivity would decrease as a consequence of a lower supply of nutrients to the euphotic layer, unless an increase of the nutrient concentrations had compensated for the shallowing of the MLD. However, García-Martínez et al. (2019a) have shown that no changes in the nutrient concentrations have been observed since the beginning of the 1990s decade in the Spanish Mediterranean. The surface chlorophyll concentration did not experience significant changes in most of the geographical areas analyzed. This result supports the hypothesis that the MLD has not changed in the Spanish Mediterranean since 1990. However, these results should be taken cautiously as the length of the chlorophyll time series obtained from satellite could not have the length needed to discern between decadal variability and long-term changes (Dutkiewicz et al., 2019; Hammond et al., 2020). Some works have shown that the total phytoplanktonic biomass has not changed in the Mediterranean Sea since the end of the twentieth century, or even it had increased, but its composition could have changed with a substitution of large cells, such as diatoms, by small-size phytoplankton (Marty et al., 2002; El Hourany et al., 2021). The analysis of chlorophyll concentration time series does not allow us to discern this possibility. Anyway, according to the data presented in this work, if this shift in the composition of the Mediterranean planktonic community has occurred, it could not be attributed to an increase of the stratification of the water column.

Our results support the hypothesis that in the case of the WMED, the increase of salinity has compensated for the warming of the surface waters, preventing the increase of the stratification of the upper part of the water column. According to projections for the twenty first century, both warming and salting trends will continue in the Mediterranean Sea, making it difficult to predict the evolution of the vertical density gradients. Therefore, it is of paramount importance to determine whether or not these changes are occurring in the Mediterranean waters and if such potential changes have any impact on the productivity of the sea. We have not found significant changes in the time series of MLD, neither on those variables that can have some influence on it (meteorological variables) or that can be affected by it (chlorophyll concentration). However, these results should be taken with caution and two questions should be considered: First, they are related to the winter mixing that is observed along the continental shelf and slope of a large area within the WMED, but they cannot be extrapolated to the process of deep water formation that occurs in the waters close to the Gulf of Lions under more extreme conditions and involving more complicated process. Several works have shown that deep convection processes could weaken during the twenty first century (Somot et al., 2006; Adloff et al., 2015). Second, the longest time series analyzed in the present work extend from 1992 to 2021, and in many cases they were shorter. We cannot discard the possibility that the trends observed are simply the result of decadal variability and do not represent the real long-term behavior of MLD and chlorophyll concentration in this area of the WMED. This is especially true for the case of the Gulf of Cádiz, where MLD time series only extend from 2009 to 2021 in the case of STOCA project, and from 2015 to 2021 in the case of Argo MLD. On the other hand, the larger the variance of a variable, the longer the length of the time series required to detect any trend. Hence, it cannot be discarded the possibility that the detection of trends for

variables such as MLD or chlorophyll concentration needs longer time series (Del Castillo et al., 2019; Pinkerton et al., 2021). This shortcoming is especially important when trying to detect possible changes in the specific composition of the phytoplanktonic community. Previous works analyzing RADMED time series from 1992 to 2015 did not show significant trends for the chlorophyll and nutrients concentrations along the continental shelf and slope of the Spanish Mediterranean, neither could be detected changes in the composition of the main phytoplaktonic groups (García-Martínez et al., 2019a; 2019b). These authors already pointed out that the variables analyzed had a large variance and that longer time series would be needed to detect long-term changes. To our knowledge, apart from the RADMED and STOCA projects, the only time series including phytoplanktonic sampling along the water column in the Gulf of Cádiz and the Spanish Mediterranean, are those of the Blanes Bay Microbial Observatory (BBMO, Gasol et al., 2016; Auladell et al., 2019), the Operational Observatory of the Catalan Sea (OOCS, Bahamon et al., 2020), and the Balearic Islands Coastal Observing System (SOCIB, Tintoré et al., 2019). Auladell et al. (2019) analyzed time series of anoxygenic photoheterotrophic bacteria in the BBMO, and no results are available for the phytoplankton sampling in the Balearic Channels carried out by SOCIB. Bahamon et al. (2020) found no changes in the chlorophyll and nutrient concentrations close to the Blanes Canyon (Catalan Sea), during the period 2010-2017. In summary, this work and those reviewed above, evidence the scarcity of long multidisciplinary time series, and the short length of the existent ones. Our results show that it cannot be considered that the MLD has become shallower in the Spanish Mediterranean and the Gulf of Cádiz as a result of the increase of the stratification, nor can be established a reduction in the productivity of the Mediterranean waters. Nevertheless, the length of the available time series does not allow us to discern whether this is the consequence of the compensating effects of warming and salting of the surface waters, or it is simply that the large variance of these variables requires longer time series to detect any change. In any case, these results stress the importance of completing and maintaining the existent observation systems of the Mediterranean Sea in order to answer this and other questions.

DATA AVAILABILITY STATEMENT

The datasets presented in this study can be found in online repositories. The names of the repository/repositories and accession number(s) can be found below: http://www.ba.ieo.es/ibamar.

AUTHOR CONTRIBUTIONS

MV-Y analyzed the time series and is responsible for the matlab codes for the analysis of time series. He also wrote the original manuscript. FM, EB and PR prepared the graphics, tables and participated in the review of the manuscript and redaction of the final version. They also were involved in the bibliographic review previous to the redaction of the work. RB, RS-L and RS maintained and updated the IBAMAR database and the STOCA time series, and are involved in the field works of the RADMED project. They also participated in the review and final version of the manuscript. MG-M is the responsible of the RADMED project. She took part in the redaction of the initial manuscript and its final review. All the authors took part in the discussion of the results. All authors contributed to the article and approved the submitted version.

FUNDING

This work has been carried out in the frame of the project RADMED (Series temporales de datos oceanográficos en el Mediterráneo) and STOCA (Series temporales de datos oceanográficos en el Golfo de Cádiz) founded by the Instituto Español de Oceanografía (IEO-CSIC).

SUPPLEMENTARY MATERIAL

The Supplementary Material for this article can be found online at: https://www.frontiersin.org/articles/10.3389/fmars.2022.901893/full#supplementary-material

REFERENCES

Adloff, F., Somot, S., Sevault, F., Jordà, G., Aznar, R., Déqué, M., et al. (2015). Mediterranean Sea Response to Climate Change in an Ensemble of Twenty First Century Scenarios. *Climate Dynamics* 45, 2775–2802. doi: 10.1007/s00382-015-2507-3

Agusti, S., Martinez-Ayala, J., Regaudie-de-Gioux, A., and Duarte, C. M. (2017). Oligotrophication and Metabolic Slowing-Down of a NW Mediterranean Coastal Ecosystem. *Front. Mar. Sci.* 4. doi: 10.3389/fmars.2017.00432

Auladell, A., Sánchez, P., Sánchez, O., Gasol, J. M., and Ferrera, I. (2019). Long-Term Seasonal and Interannual Variability of Marine Aerobic Anoxygenic Photoheterotrophic Bacteria. *ISME J.* 13, 1975–1987. doi: 10.1038/s41396-019-0401-4

Bahamon, N., Aguzzi, J., Ahumada-Sempoal, M. A., Bernardello, R., Reuschel, C., Company, J. B., et al. (2020). Stepped Coastal Water Warming Revealed by Multiparametric Monitoring at NW Mediterranean Fixed Stations. *Sensor* 20, 2658. doi: 10.3390/s20092658

Behrenfeld, M. J., O'Malley, R. T., Siegel, D. A., McClain, C. R., Sarmiento, J. L., Feldman, G. C., et al. (2006). Climate-Driven Trends in Contemporary Ocean Productivity. *Nature* 444, 7. doi: 10.1038/nature05317

Bindoff, N. L., Cheung, W. W. L., Kairo, J. G., Arístegui, J., Guinder, V. A., Hallberg, R., et al. (2019). "Changing Ocean, Marine Ecosystems, and Dependent Communities," in *IPCC Special Report on the Ocean and Cryosphere in a Changing Climate*. Eds. H.-O. Pörtner, D. C. Roberts, V. Masson-Delmotte, P. Zhai, M. Tignor, E. Poloczanska, K. Mintenbeck, A. Alegría, M. Nicolai, A. Okem, J. Petzold, B. Rama and N. M. Weyer (Cambridge University Press, Cambridge, UK and New York, NY, USA).

Boyce, D. G., and Worm, B. (2015). Patterns and Ecological Implications of Historical Marine Phytoplankton Change. *Mar. Ecol. Prog. Ser.* 534, 251–272. doi: 10.3354/meps11411

Calvo, E., Simó, R., Coma, R., Ribes, M., Pascual, J., Sabatés, A., et al. (2011). Effects of Climate Change on Mediterranean Marine Ecosystems: The Case of the Catalan Sea. *Climate Res.* 502011, 1–29. doi: 10.3354/cr01040

Coll, M., Piroddi, C., Albouy, C., Ben Rais Lasram, F., Cheung, W. W. L., Christensen, V., et al. (2011). The Mediterranean Sea Under Siege:Spatial Overlap Between Marine Biodiversity, Cumulative Threats and Marine Reserves. *Global Ecol. Biogeogr.* 21, 465–480. doi: 10.1111/j.1466-8238.2011.00697.x

Comesaña, A., Fernández-Castro, B., Chouciño, P., Fernández, E., Fuentes-Lema, A., Gilcoto, M., et al. (2021). Mixing and Phytoplankton Growth in an Upwelling System. *Front. Mar. Sci.* 8. doi: 10.3389/fmars.2021.712342

Coppola, L., Legendre, L., Lefevre, D., Prieura, L., Taillandiera, V., and Riquiera, E. D. (2018). Seasonal and Inter-Annual Variations of Dissolved Oxygen in the Northwestern Mediterranean Sea (DYFAMED Site). *Prog. Ocean.* 162, 187–201. doi: 10.1016/j.pocean.2018.03.001

Cuttelod, A., García, N., Abdul Malak, D., Temple, H., and Katariya, V. (2008). "The Mediterranean: A Biodiversity Hotspot Under Threat," in *The 2008 Review of The IUCN Red List of Threatened Species*. Eds. J.-C. Vié, C. Hilton-Taylor and S. N. Stuart (Switzerland: IUCN Gland).

de Boyer Motégut, C., Madec, G., Fisher, A. S., Lazar, A., and Iudicone, D. (2004). Mixed Layer Depth Over the Global Ocean: An Examination of Profile Data and a Profile-Based Climatology. *J. Geophys. Res.* 109, C12003. doi: 10.1029/2004JC002378

Del Castillo, C. E., Signorini, S. R., Karaköylü, E. M., and Rivero-Calle, S. (2019). Is the Southern Ocean Getting Greener? *Geophys. Res. Lett.* 46, 6034–6040. doi: 10.1029/2019GL083163

Durrieu deMadron, X, Guieu, C., Sempéré, R., Conan, P., Cossa, D., D'Ortenzio, F., et al. (2011). Marine Ecosystems' Responses to Climatic and Anthropogenic Forcings in the Mediterranean. *Prog. Ocean.* 91, 97–166. doi: 10.1016/j.pocean.2011.02.003

Dutkiewicz, S., Hickman, A. E., Jahn, O., Henson, S., Beaulieu, C., and Monier, E. (2019). Ocean Color Signature of Climate Change. *Nature Communications* 10, 578. doi: 10.1038/s41467-019-08457-x

El Hourany, R., Mejia, C., Faour, G., Crépon, M., and Thiria, S. (2021). Evidencing the Impact of Climate Change on the Phytoplankton Community of the Mediterranean Sea Through a Bioregionalization Approach. *J. Geophys. Research: Ocean.* 126, e2020JC016808. doi: 10.1029/2020JC016808

García-Martínez, M. C., Vargas-Yáñez, M., Moya, F., Santiago, R., Muñoz, M., Reul, A., et al. (2019a). Average Nutrient and Chlorophyll Distributions in the Western Mediterranean: RADMED Project. *Oceanologia* 61, 143—169. doi: 10.1016/j.oceano.2018.08.003

García-Martínez, M. C., Vargas-Yáñez, M., Moya, F., Santiago, R., Reul, A., Muñoz, M., et al. (2019b). Spatial and Temporal Long-Term Patterns of Phyto and Zooplankton in the W-Mediterranean: RADMED Project. *Water* 11, 534. doi: 10.3390/w11030534

Gasol, J. M., Cardelús, C., Morán, A. X. G., Balagué, V., Forn, I., Marrasé, C., et al. (2016). Seasonal Patterns in Phytoplankton Photosynthetic Parameters and Primary Production at a Coastal NW Mediterranean Site. *Sci. Mar.* 80, 63–77. doi: 10.3989/scimar.04480.06E

Goffart, A., Hecq, J.-H., and Legendre, L. (2002). Changes in the Development of the Winter-Spring Phytoplankton Bloom in the Bay of Calvi (NW Mediterranean) Over the Last Two Decades: A Response to Changing Climate? *Mar. Ecol. Prog. Ser.* 236, 45–60. doi: 10.3354/meps236045

Goffart, A., Hecq, J.-H., and Legendre, L. (2015). Drivers of the Winter-Spring Phytoplankton Bloom in a Pristine NW Mediterranean Site, the Bay of Calvi (Corsica): A Long-Term Study, (1979–2011). *Prog. Oceanogr.* 137, 121–139. doi: 10.1016/j.pocean.2015.05.027

Hammond, M. L., Beaulieu, C., Henson, S. A., and Sahu, S. K. (2020). Regional Surface Chlorophyll Trends and Uncertainties in the Global Ocean. *Sci. Rep* 10, 15273. doi: 10.1038/s41598-020-72073-9

Herrmann, M., Estournel, C., Adloff, F., and Diaz, F. (2014). Impact of Climate Change on the Northwestern Mediterranean Sea Pelagic Planktonic Ecosystem and Associated Carbon Cycle. *J. Geophys. Research Ocean.* 119, 5815–5836. doi: 10.1002/2014JC010016

Herrmann, M., Estournel, C., Déqué, M., Marsaleix, P., Sevault, F., and Somot, S. (2008a). Dense Water Formation in the Gulf of Lions Shelf: Impact of Atmospheric Interannual Variability and Climate Change. *Continent. Shelf Res.* 28, 2092–2112. doi: 10.1016/j.csr.2008.03.002

Herrmann, M., Somot, S., Sevault, F., Estournel, C., and Dé qué, M. (2008b). Modeling the Deep Convection in the Northwestern Mediterranean Sea Using an Eddy-Permitting and an Eddy-Resolving Model: Case Study of Winter 1986–1987. *J. Geophys.* 113, C04011. doi: 10.1029/2006JC003991

Holte, J., and Talley, L. D. (2009). A New Algorithm for Finding Mixed Layer Depths With Applications to Argo Data and Subantarctic Mode Water Formation. *J. Atmospher Ocean. Technol.* 26, 1920–1939. doi: 10.1175/2009JTECHO543.1

Holte, J., Talley, L. D., Gilson, J., and Roemmich, D. (2017). An Argo Mixed Layer Climatology and Database. *Geophys. Res. Lett.* 44, 5618–5626. doi: 10.1002/2017GL073426

Kalnay, E., Kanamitsu, M., Kistler, R., Collins, W., Deaven, D., Gandin, L., et al. (1996). The NCEP/NCAR 40-Year Reanalysis Project. *Bull. Am. Meteorol. Soc* 77, 437–471. doi: 10.1175/1520-04771996077<0437:TNYRP<2.0.CO;2

Kara, A. B., Rochford, P. A., and Hulburt, H. E. (2000). An Optimal Definition for Ocean Mixed Layer Depth. *J. Geophys. Res.* 105 (C7), 16803–16821. doi: 10.1029/2000JC900072

Lavigne, H., D'Ortenzio, F., D'Alcalá, M. R., Claustre, H., Sauzède, R., and Gacic, M. (2015). On the Vertical Distribution of the Chlorophyll-a Concentration in the Mediterranean Sea: A Basin-Scale and Seasonal Approach. *Biogeosciences* 12, 5021–5039. doi: 10.5194/bg-12-5021-2015

López-Jurado, J. L., Balbín, R., Alemany, F., Amengual, B., Aparicio-González, A., Fernández de Puelles, M. L., et al. (2015). The RADMED Monitoring Programme as a Tool for MSFD Implementation: Towards an Ecosystem-Based Approach. *Ocean. Sci.* 11, 897–908. doi: 10.5194/os-11-897-2015

Lorbacher, K., Demmenget, D., Niiler, P. P., and Köhl, A. (2006). Ocean Mixed Layer: A Subsurface Proxy for Ocean-Atmosphere Variability. *J. Geophys. Res. Ocean.* 111 (C7), C07010. doi: 10.1029/2003jc002157

Macias, D., Garcia-Gorriz, E., and Stips, A. (2018). Deep Winter Convection and Phytoplankton Dynamics in the NW Mediterranean Sea Under the Present Climate and Future (Horizon 2030) Scenarios. *Sci. Rep.* 8, 6626. doi: 10.1038/s41598-018-24965-0

Marty, J.-C., Chiavérini, J., Pizay, M.-D., and Avril, B. (2002). Seasonal and Interannual Dynamics of Nutrients and Phytoplankton Pigments in the Western Mediterranean Sea at the DYFAMED Time-Series Station, (1991–1999). *Deep-Sea Res. II* 49, 1965–1985. doi: 10.1016/s0967-0645(02)00022-x

Mazzocchi, M., Dubroca, L., García-Comas, C., Di Capua, I., and Ribera d'Alcalà, M. (2012). Stability and Resilience in Coastal Copepod Assemblages: The Case of the Mediterranean Long-Term Ecological Research at Station MC (LTER-Mc). *Prog. Ocean.* 97-100, 135–151. doi: 10-1016/j.pocean.2011.11.003 doi: 10.1016/j.pocean.2011.11.003

Millot, C. (2007). Interannual Salinification of the Mediterranean Inflow. *Geophys. Res. Lett.* 34, L21609. doi: 10.1029/2007GL031179

Morison, F., Franzè, G., Harvey, E., and Menden-Deuer, S. (2020). Light Fluctuations are Key in Modulating Plankton Trophic Dynamics and Their Impact on Primary Production. *Limnol. Ocean. Lett.* 5, 346–353. doi: 10.1002/lol2.10156

Pasqueron de Fommervault, O., Migon, C., D'Ortenzio, F., Ribera d'Alcalà, M., and Coppola, L. (2015). Temporal Variability of Nutrient Concentrations in the Northwestern Mediterranean Sea (DYFAMED Time-Series Station). *Deep-Sea Res. I* 100, 1–12. doi: 10.1016/j.dsr.2015.02.006

Pinkerton, M. H., Boyd, P. W., Deppeler, S., Hayward, A., Höfer, J., and Moreau, S. (2021). Evidence for the Impact of Climate Change on Primary Producers in the Southern Ocean. *Front. Ecol. Evol.* 9. doi: 10.3389/fevo.2021.592027

Polovina, J. J., Howell, E. A., and Abecassis, M. (2008). Ocean's Least Productive Waters are Expanding. *Geophys. Res. Lett.* 35, L03618. doi: 10.1029/2007GL031745

Pulina, P., Brutemark, A., Suikkanen, S., Padedda, B. M., Grubisic, L. M., Satta, C. T., et al. (2016). Effects of Warming on a Mediterranean Phytoplankton Community. *Web Ecol.* 16, 89–92. doi: 10.5194/we-16-89-2016

Ribera D'alcalà, M., Conversano, F., Corato, F., Licandro, P., Mangoni, O., Marino, D., et al. (2004). Seasonal Patterns in Plankton Communities in a Pluriannual Time Series at a Coastal Mediterranean Site (Gulf of Naples): An Attempt to Discern Recurrences and Trends. *Sci. Mar.* 68 (Suppl. 1), 65–83. doi: 10.3989/scimar.2004.68s165

Salat, J., Pascual, J., Flexas, M., Chin, T. M., and Vazquez-Cuervo, J. (2019). Fortyfive Years of Oceanographic and Meteorological Observations at a Coastal Station in Thenwmediterranean: A Ground Truth for Satellite Observations. *Ocean. Dyn.* 69, 1067–1084. doi: 10.1007/s10236-019-01285-z

Sánchez-Leal, R. F., Bellanco, M. J., Naranjo, C., García-Lafuente, J., and González-Pola, C. (2020). On the Seasonality of Waters Below the Seasonal Thermocline in the Gulf of Cádiz. *Continent. Shelf Res.* 204, 104190. doi: 10.1016/j.csr.2020.104190

Schroeder, K., Chiggiato, J., Josey, S. A., Borghini, M., Aracri, S., and Sparnocchia, S. (2017). Rapid Response to Climate Change in a Marginal Sea. *Sci. Rep.* 7, 4065. doi: 10.1038/s41598-017-04455-5

Siokou-Frangou, I., Christaki, U., Mazzocchi, M. G., Montresor, M., Ribera d'Alcalá, M., Vaqué, D., et al. (2010). Plankton in the Open Mediterranean Sea: A Review. *Biogeosciences* 7, 1543–1586. doi: 10.5194/bg-7-1543-2010

Skliris, N. (2014). "Past, Present and Future Patternsof the Thermohaline Circulation and Characteristic Water Masses of the Mediterranean Sea," in *The Mediterranean Sea: Its History and Present Challenges*. Eds. S. Goffredo and Z. Dubinsky (Springer, Dordrecht). doi: 10.1007/978-94-007-6704-1_3

Somot, S., Houpert, L., Sevault, L., Testor, P., Bosse, A., Taupier−Letage, I., et al. (2018). Characterizing, Modelling and Understanding the Climate Variability of the Deep Water Formation in the North−Western Mediterranean Sea. *Climate Dynamics* 51, 1179–1210. doi: 10.1007/s00382-016-3295-0

Somot, S., Sevault, F., and Déqué, M. (2006). Transient Climate Change Scenario Simulation of the Mediterranean Sea for the Twenty-First Century Using a High-Resolution Ocean Circulation Model. *Cliamte Dynamics* 27, 851–879. doi: 10.1007/s00382-006-0167-z

Steinacher, M., Joos, F., Frölicher, T. L., Bopp, L., Cadule, P., Cocco, V., et al. (2010). Projected 21st Century Decrease in Marine Productivity: A Multi-Model Analysis. *Biogeosciences* 7, 979–1005. doi: 10.5194/bg-7-979-2010

Tel, E., Balbín, R., Cabanas, J. M., García, M. J., García-Martínez, M. C., González-Pola, C., et al. (2016). IEOOS: The Spanish Institute of Oceanography Observing System. *Ocean. Sci. Discuss.* 12, 345–353. doi: 10.5194/os-12-345-2016

Testor, P., Testor, P., Bosse, A., Houpert, L., Margirier, F., Mortier, L., Legoff, H., et al. (2018). Multiscale Observations of Deep Convection in the Northwestern Mediterranean Sea During Winter 2012–2013 Using Multiple Platforms. *J. Geophys. Research: Ocean.* 123, 1745–1776. doi: 10.1002/2016JC012671

Tintoré, J., Pinardi, N., Álvarez-Fanjul, E., Aguiar, E., Álvarez-Berastegui, D., Bajo, M., et al. (2019). Challenges for Sustained Observing and Forecasting Systems in the Mediterranean Sea. *Front. Mar. Sci.* 6. doi: 10.3389/fmars.2019.00568

Ulses, C., Estournel, C., Fourrier, M., Coppola, L., Kessouri, F., Lefèvre, D., et al. (2020). Oxygen Budget for the North-Western Mediterranean Deep Convection Región. *Biogeosciences* 18, 937–960. doi: 10.5194/bg-18-937-2021

Vargas-Yáñez, M., García-Martíneza, M. C., Moya, F., Balbín, R., López-Jurado, J. L., Serra, M., et al. (2017). Updating Temperature and Salinity Mean Values and Trends in the Western Mediterranean: The RADMED Project. *Prog. Ocean.* 157, 27–46. doi: 10.1016/j.pocean.2017.09.004

Vargas-Yáñez, M., Juza, M., García-Martínez, M. C., Moya, F., Balbín, R., Ballesteros, E., et al. (2021). Long-Term Changes in the Water Mass Properties in the Balearic Channels Over the Period 1996–2019. *Front. Mar. Sci.* 8. doi: 10.3389/fmars.2021.640535

Vargas-Yáñez, M., Moya, F., Tel, E., García-Martínez, M. C., Guerber, E., and Bourgeon, M. (2009). Warming and Salting of the Western Mediterranean During the Second Half of the XX Century: Inconsistencies, Unknowns and the Effect of Data Processing. *Sci. Mar.* 73 (1), 7–28. doi: 10.3989/scimar.2009.73n1007

Vargas-Yáñez, M., Zunino, P., Benali, A., Delpy, M., Pastre, F., Moya, F., et al. (2010). How Much Is the Western Mediterranean Really Warming and Salting? *J. Geophys. Res.* 115, C04001. doi: 10.1029/2009JC005816

Villamaña, M., Marañón, E., Cermeño, P., Estrada, M., Fernández-Castro, B., Figueiras, F. G., et al. (2019). The Role of Mixing in Controlling Resource Availability and Phytoplankton Community Composition. *Prog. Ocean.* 178, 102181. doi: 10.1016/j.pocean.2019.102181

Zanna, L., Khatiwala, S., Gregoryc, J. M., Ison, J., and Heimbach, P. (2019). Global Reconstruction of Historical Ocean Heat Storage and Transport. *PNAS* 116 (4), 1126–1131. doi: 10.1073/pnas.1808838115

Conflict of Interest: The authors declare that the research was conducted in the absence of any commercial or financial relationships that could be construed as a potential conflict of interest.

The handling editor JL declared a past co-authorship with the author RS-L.

frontiers | Frontiers in Marine Science

ORIGINAL RESEARCH
published: 15 July 2022
doi: 10.3389/fmars.2022.919793

Drivers of the North Aegean Sea Ecosystem (Eastern Mediterranean) Through Time: Insights From Multidecadal Retrospective Analysis and Future Simulations

Konstantinos Tsagarakis[1], Simone Libralato[2], Marianna Giannoulaki[3], Konstantinos Touloumis[4], Stylianos Somarakis[3], Athanassios Machias[1], Constantin Frangoulis[5], Georgia Papantoniou[1], Stefanos Kavadas[1] and Maria Th. Stoumboudi[1]*

[1]Institute of Marine Biological Resources and Inland Waters, Hellenic Centre for Marine Research, Attica, Greece, [2]Section of Oceanography, National Institute of Oceanography and Applied Geophysics - OGS, Trieste, Italy, [3]Institute of Marine Biological Resources and Inland Waters, Hellenic Centre for Marine Research, Heraklion, Greece, [4]Fisheries Research Institute, Hellenic Agricultural Organization - DIMITRA, Kavala, Greece, [5]Institute of Oceanography, Hellenic Centre for Marine Research, Heraklion, Greece

OPEN ACCESS

Edited by:
Neil R. Loneragan, Murdoch University, Australia

Reviewed by:
Zhongxin Wu, Dalian Ocean University, China
Angela Cuttitta, Institute for Studies on the Mediterranean, National Research Council (CNR), Italy
Hector Lozano-Montes, Murdoch University, Australia

***Correspondence:**
Konstantinos Tsagarakis
kontsag@hcmr.gr

Specialty section:
This article was submitted to Marine Fisheries, Aquaculture and Living Resources, a section of the journal Frontiers in Marine Science

Received: 13 April 2022
Accepted: 13 June 2022
Published: 15 July 2022

Citation:
Tsagarakis K, Libralato S, Giannoulaki M, Touloumis K, Somarakis S, Machias A, Frangoulis C, Papantoniou G, Kavadas S and Stoumboudi MT (2022) Drivers of the North Aegean Sea Ecosystem (Eastern Mediterranean) Through Time: Insights From Multidecadal Retrospective Analysis and Future Simulations. Front. Mar. Sci. 9:919793. doi: 10.3389/fmars.2022.919793

Ecosystem models are important tools for the implementation of Ecosystem Based Fisheries Management (EBFM), especially in highly exploited ecosystems affected by climate change, such as the Mediterranean Sea. Herein, we present the development of an Ecopath ecosystem model for the North Aegean Sea (Eastern Mediterranean) in the early 1990s, as well as the parameterization of the temporal dynamic module (Ecosim) after fitting to catch and relative biomass time series for the period 1993-2020. The Ecosim model included as drivers (i) fishing, assuming a technology creep factor of 2% annual increase (0.79% for bottom trawls), (ii) Sea Surface Temperature, (iii) trophic interactions and (iv) a Primary Production (PP) Anomaly which was positively correlated with the North Atlantic Oscillation of the previous year, highlighting the synergistic effect of environmental and anthropogenic processes during the three-decades hindcast period. Trends in biomasses, catches and ecosystem indicators were characterized by a decline from 1993 to 2010 and a strong recovery thereafter. Sea warming scenarios for the period 2021-2050 indicated contrasting responses to increased temperature among the main commercial groups, while simulations of changes in productivity had relatively straightforward effects. Two scenarios of 10% and 25% reduction in fishing effort revealed quick increases in the biomass of most commercial species, though coupled with lower catches due to reduced fishing, except for few groups that their population increase was remarkably high. Although the 25% effort reduction resulted in high recoveries in the short term, it didn't necessarily lead to constantly high biomasses resulting in reduced catches towards the end of the forecast period for some groups, in contrast to the 10% reduction. When impacts of reduced productivity were added to temperature effects, the model forecasted lower biomass increases for the winners of sea warming and even higher decreases for the losers. Biomass losses were compensated by a 10% reduction in fishing effort, but this was not overall enough to counterbalance losses in catches. The

model developed here contributes to better elucidate observed changes in the past and to hind directions of change in future simulations, as well as to advance EBFM in the area.

Keywords: climate change, food web, ecosystem modelling, ecosystem approach to fisheries (EAF), trophic interactions, fisheries management, Mediterranean Sea, mixed fisheries

1 INTRODUCTION

The inclusion of ecosystem considerations in fisheries contributes to more effective management and enables accounting for trade-offs (Link, 2010a; Bundy et al., 2017). Although there is a lack of global consensus on the exact meaning of Ecosystem Based Fisheries Management (EBFM) (Trochta et al., 2018), it is often perceived as a holistic approach which integrates in its core concept the consideration of multispecies interactions, anthropogenic stresses and ecosystem processes (e.g. climate, habitats and other environmental factors), relies on good governance and scientific advice and aims in maintaining biodiversity and productivity while achieving sustainable yields (e.g. Larkin, 1996; Link, 2002; Pitcher et al., 2009; Trochta et al., 2018).

In the Mediterranean Sea, the implementation of EBFM is relatively poor (Lockerbie et al., 2020), fisheries resources are characterized by poor management effectiveness (e.g. Melnychuk et al., 2021) and governance quality (Bundy et al., 2017) and the majority of stocks are overexploited (Colloca et al., 2017; FAO, 2020). Mediterranean fisheries are mainly multi-species and multi-gear, operated by a mixture of relatively few semi-industrial and numerous artisanal vessels (FAO, 2020), resulting in a management system very different from the adjacent Northeast Atlantic (Smith and Garcia, 2014). Therefore, fisheries management in the Mediterranean is challenging and needs to be reconsidered, despite some recent signs of improvement (FAO, 2020).

In addition, the Mediterranean region is considered one of the most vulnerable areas to climate change (Giorgi and Lionello, 2008) with documented effects on specific stocks (Colloca et al., 2014), total landings (Tzanatos et al., 2014), landings' traits (Tsimara et al., 2021) and marine ecosystems (Corrales et al., 2017). Apart from the increase in sea water temperature, climate change is expected to affect precipitation and river runoffs, increase stratification in the basin and alter water circulation (e.g. Reale et al., 2020) with impacts on productivity and species composition (Hidalgo et al., 2018). In the Western Mediterranean these changes seem to lead to more oligotrophic conditions, while in the eastern basin the productivity is likely to increase and the ecosystem seems to be more impacted by species invasions and direct effects of the temperature increase (e.g. Macias et al., 2015; Hidalgo et al., 2018). However, the uncertainty related to such projections is high and there are studies which conclude that productivity is likely to decrease in the eastern basin as well (e.g. Richon et al., 2019).

Taking these into account, the implementation of EBFM is even more necessary as it can help maintain resource resilience and avoid climate-driven collapses (Holsman et al., 2020). In this framework, ecosystem models are important tools as they can simulate a large set of ecosystem processes and fishing impacts in a tailor-made approach for the ecosystem(s) under consideration (Geary et al., 2020). The Ecosim with Ecopath (EwE) modelling approach has been used in numerous applications for supporting EBFM worldwide (Colléter et al., 2015) and in the Mediterranean (Coll and Libralato, 2012). Among others, policy simulations have been applied to explore the ecological and economic effects of the Landing Obligation in the Adriatic Sea (Celić et al., 2018), environmental scenarios have been set to explore possible effects of climate change in the Eastern Mediterranean (Corrales et al., 2018) and several applications aimed at exploring the effect of fishing, including in regions of the Aegean Sea (e.g. Papapanagiotou et al., 2020; Papantoniou et al., 2021; Dimarchopoulou et al., 2022).

The Aegean Sea (Eastern Mediterranean Sea) ecosystem and fisheries have undergone considerable changes during the past decades. A peak in official landings was observed in 1994 followed by a decline which persisted for several years (ELSTAT, 2021). A climate-related regime shift in the early 1990s, reflected in the evolution of landings, has been recently reported (Damalas et al., 2021). In addition, despite the reduction of the fleet since 1990s *vs* gradual retraction of vessels with the aim to controlling fishing effort, fisheries resources have been heavily exploited (Tsikliras et al., 2013). Disentangling the effect of the factors that have contributed toward the observed directions is important not only for deciding on short-term management measures but also for the design of long-term strategies after taking into account the changing environmental conditions.

In this work we developed and applied an ecosystem model for the North Aegean Sea with the aim to (i) explain part of the changes observed during the hindcast period (1993-2020), and (ii) perform climate change simulations and fishing effort scenarios. To this end, we present the development of an Ecopath mass-balance model (Christensen and Walters, 2004) for the early 1990s (setting 1993 as the base year), based on a model previously built for a data rich period (mid-2000s; Tsagarakis et al., 2010). Furthermore, the time-dynamic module (Ecosim) was developed and calibrated after fitting to catch and relative biomass time series and by exploring Sea Surface Temperature (SST), fishing and a model-derived Primary Production (PP) Anomaly as ecosystem drivers.

2 MATERIALS AND METHODS

2.1 Updated Ecopath Model

The Ecopath with Ecosim approach (EwE) (Christensen and Walters, 2004) version 6 was used to describe the North Aegean Sea ecosystem (Eastern Mediterranean, Greece). Ecopath is a mass-balance model which provides a snapshot of an ecosystem and the initial conditions for the time dynamic simulations with Ecosim. Ecopath has been widely used to describe ecosystem structure and functioning. The energy balance within each Functional Group (FG, composed of single species, group of species sharing similar ecological features or different developmental stages of a species) is ensured through two linear equations:

$$\begin{aligned} Production &= predation\ mortality \\ &+ fishing\ mortality + other\ mortality \\ &+ biomass\ accumulation + net\ migration \end{aligned} \quad (1)$$

$$\begin{aligned} Consumption &= production + respiration \\ &+ unassimilated\ food \end{aligned} \quad (2)$$

Respiration in eq. (2) does not represent the physiological respiration but the part of the consumption that is not used for production or recycled as feces or urine (Christensen et al., 2008). For each FG, the input required is diet, exports by different fishing activities including by-catch and discards, as well as three out of the four basic parameters: biomass *(B)*, production rate *(P/B)*, consumption rate *(Q/B)*, and Ecotrophic Efficiency (*EE*; fraction of the production that is used within the system). More details on the Ecopath equations and methodology are provided in the Supplementary material Section A.

The modeled ecosystem (North Aegean Sea: Strymonikos Gulf and Thracian Sea; **Figure 1**) covers 8374 km^2 and is the major fishing ground in Greece, where ~30% of the Greek capture fisheries are produced (ELSTAT, 2021). The area boundaries include the continental shelf (>20 m) and the upper slope (<300 m) of the North Aegean Sea, limited by national borders in the east. We used an Ecopath model describing the ecosystem in the mid-2000s (i.e. 2003-2006; Tsagarakis et al., 2010; NAS2000 model hereafter) as a basis to construct a model representing the ecosystem in the early '90s (1991-1993; NAS1990 model hereafter). The mid 2000s represent a relatively data rich period as the Greek Data Collection Program (under Data Collection Regulation, DCR - Regulation (EC) 1543/2000 - and later Data Collection Framework, DCF - Regulation (EC) 199/2008) was established providing good quality information for several aspects of the fisheries sector (e.g. landings and discards quantities and composition, species composition and abundance from research surveys) in contrast to the earlier period when most surveys were sporadic, and information was relying on short-term projects. Therefore, a considerable amount of the parameters used to construct the data rich NAS2000 model were complementary used with information on species abundance and catches from earlier surveys (**Supplementary Material Table S1**) to set the basis for model development in an earlier time period. The rationale behind the construction of the NAS1990 Ecopath model was to improve the calibration of the Ecosim model (Heymans et al., 2016) by extending at maximum the hindcast period and thus exploiting the existence of survey and fisheries data since the early '90s. This permits to create a robust tool able to explore research questions especially in respect to large scale climatic patterns (see below the description of Ecosim).

Biomass flows of the N. Aegean model were expressed as t·km^{-2}·yr^{-1} and biomasses as t·km^{-2} of wet weight. For all modelled groups, *EE* was the missing parameter and was estimated by EwE solving the system of equations on the basis of known input values for *B*, *(P/B)* and *(Q/B)* as suggested by best practices on EwE model development (Christensen and Walters, 2004; Heymans et al., 2016). The NAS1990 model parameterization is shown in **Table 1**.

The NAS1990 model has 40 FGs with emphasis on commercial species (5 planktonic FGs, 9 commercial and non-commercial

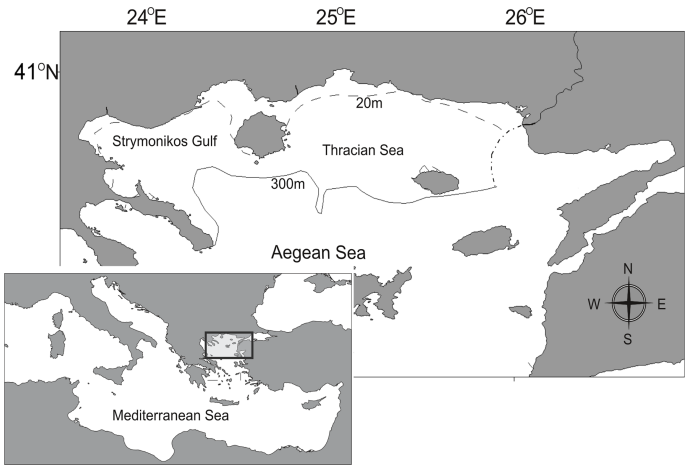

FIGURE 1 | The North Aegean Sea (Strymonikos Gulf and Thracian Sea) model area.

TABLE 1 | Functional groups and basic parameters of the Ecopath model.

	Functional Group	TL	B	P/B	Q/B	EE	U/Q	P/Q	L	D
1	Phytoplankton	1.00	4.565	117.30		0.692				
2	Microzooplankton	2.05	0.475	258.85	776.54	0.705	0.40	0.33		
3	Mesozooplankton	2.33	2.790	29.19	87.55	0.812	0.40	0.33		
4	Macrozooplankton	2.92	0.328	21.07	53.17	0.917	0.20	0.40		
5	Gelatinous plankton	3.03	2.476	4.84	12.09	0.195	0.20	0.40		
6	Small benthic crustaceans	2.21	1.109	7.32	54.40	0.981	0.30	0.13		
7	Polychaetes	2.09	5.333	1.63	12.46	0.958	0.60	0.13		
8	Shrimps	3.04	0.399	3.18	7.52	0.967	0.20	0.42	0.024	0.001
9	Crabs	2.92	0.270	2.57	4.94	0.964	0.20	0.52	0.002	0.002
10	Norway lobster	3.02	0.054	1.32	4.76	0.674	0.20	0.28	0.026	0.000
11	Bivalves & gastropods	2.05	3.782	1.15	3.27	0.984	0.43	0.35	0.001	0.000
12	Benthic invert. (no crustacea)	2.05	4.930	1.15	3.27	0.979	0.43	0.35		
13	Benthic cephalopods	3.49	0.283	2.68	5.50	0.970	0.13	0.49	0.134	0.005
14	Benthopelagic cephalopods	4.13	0.107	2.86	22.15	0.985	0.39	0.13	0.039	0.003
15	Red mullets	2.75	0.104	1.80	7.08	0.889	0.20	0.25	0.070	0.001
16	Anglerfish	4.34	0.083	0.90	4.20	0.466	0.20	0.22	0.011	0.001
17	Flatfishes	3.48	0.181	1.60	8.26	0.922	0.20	0.19	0.055	0.015
18	Blue whiting	3.77	0.150	1.10	7.41	0.994	0.20	0.15	0.021	0.006
19	Other gadiformes	3.65	0.125	1.10	7.41	0.994	0.20	0.15	0.025	0.006
20	Hake	4.27	0.287	0.75	4.13	0.989	0.20	0.18	0.083	0.005
21	DemeFish1	3.36	0.181	1.55	7.48	0.934	0.20	0.21	0.062	0.018
22	DemeFish2	4.29	0.178	1.49	5.15	0.914	0.20	0.29	0.093	0.025
23	DemeFish3	3.30	0.390	1.71	8.39	0.874	0.20	0.20	0.062	0.038
24	DemeFish4	3.10	0.182	2.22	9.00	0.874	0.20	0.25	0.055	0.018
25	Benthopelagic Fish	3.55	0.238	1.90	9.27	0.986	0.30	0.21	0.000	0.000
26	Picarels and Bogue	3.34	0.204	1.69	7.49	0.929	0.20	0.23	0.115	0.021
27	Sharks	3.57	0.101	0.58	5.16	0.628	0.20	0.11	0.007	0.006
28	Rays & skates	3.94	0.060	0.88	4.07	0.724	0.20	0.21	0.012	0.006
29	Anchovy	3.34	1.660	1.52	6.37	0.986	0.30	0.24	0.391	0.106
30	Sardine	3.31	0.908	1.28	10.42	0.993	0.30	0.12	0.396	0.128
31	Horse mackerel	3.46	0.230	1.13	7.59	0.980	0.20	0.15	0.106	0.036
32	Mackerel	3.70	0.285	1.03	5.84	0.994	0.20	0.18	0.201	0.002
33	Other small pelagic fish	3.35	0.493	0.83	6.54	0.978	0.30	0.13	0.026	0.012
34	Medium pelagic fish	4.37	0.180	0.61	3.24	0.754	0.20	0.19	0.077	0.000
35	Large pelagic fish	4.53	0.065	0.34	2.24	0.976	0.20	0.15	0.021	0.001
36	Loggerhead turtle	2.95	0.020	0.16	2.68	0.065	0.20	0.06		
37	Sea birds	3.10	0.001	4.78	111.61	0.008	0.20	0.04		
38	Dolphins	4.55	0.028	0.08	13.81	0.093	0.20	0.01		0.000
39	Detritus	1.00	31.440			0.520				
40	Discards	1.00				0.891				

P, production; B, biomass (t·km-2); Q, consumption; U, unassimilated food; EE, Ecotrophic efficiency; TL, Trophic level; L, landings (t·km^{-2}·yr^{-1}); D = Discards (t·km^{-2}·yr^{-1}).

demersal and benthic invertebrate FGs, 21 fish FGs, seabirds, dolphins, sea turtles, detritus and discards). The definition of FGs was mainly based on habitat (e.g., demersal/pelagic), taxonomic and feeding (grouping based on diet information) criteria, as described in Tsagarakis et al. (2010) and has an only slightly modified structure in comparison to the NAS2000 model. Specifically, contrary to Tsagarakis et al. (2010), the NAS1990 model (**Table 1**) (i) considered no multi-stanza groups for anchovy and sardine, (ii) described Blue whiting and Gastropods & Bivalves in dedicated groups and (iii) included cuttlefish in the Benthopelagic cephalopods group instead of the Benthic cephalopods.

The origin of information for the updated model is summarized in the **Supplementary Material Table S1**. Data from seasonal bottom trawl surveys from the period 1991-1993 (Labropoulou and Papaconstantinou, 2000; Labropoulou and Papaconstantinou, 2004), were used to estimate the biomass of demersal and benthic fish as well as that of some megafaunal benthic/demersal invertebrates using the swept-area method (i.e., estimation of biomass per area sampled by trawling), in line with Tsagarakis et al. (2010). For small pelagic fish, in the absence of surveys during the model period, average biomass estimates were extrapolated from acoustic surveys in a succeeding period (Tsagarakis et al., 2015; Leonori et al., 2021). Dolphins' biomass was updated with recent estimates from aerial surveys (Tsagarakis et al., 2021), macrozooplankton biomass was updated based on Frangoulis et al. (2017), while biomass values from the 2000s model were retained for the few remaining FGs (mainly some plankton groups, benthic invertebrate groups and Loggerhead turtle and Sea birds; **Supplementary Material Table S1**).

For each species, production (*P/B*) and consumption (*Q/B*) values were retrieved from the literature or estimated based on empirical equations (Pauly, 1980; Innes et al., 1987; Pauly et al., 1990; Trites et al., 1997; ICES, 2000) as described in detail in Tsagarakis et al. (2010), while for multispecies FGs these values were weighted with the relative biomass (or with relative

landings when biomass information was not available) of each species within the FG during the period 1991-1993. Input for diet composition was based on literature (for details, see: Tsagarakis et al., 2010) updated with more recent published information when available (e.g. for sardine and anchovy diet: Nikolioudakis et al., 2012; Nikolioudakis et al., 2014). The resulting diet matrix of the 1990s Ecopath model is shown in the **Supplementary Material Table S2**.

The model includes five commercial fishing fleets (trawls, purse seines, static nets, longlines & troll baits and pots & traps). Fisheries production in the region derived from the Hellenic Statistical Authority (ELSTAT, 2021) which reports annual catch per species or group, explicitly for bottom trawls and purse seines but aggregated for all artisanal gears. Therefore, breakdown into separate gears was done for artisanal gears using catch composition information from a later period, collected under the DCR (Kavadas et al., 2013). DCR information was also used for the estimation of discard quantities, through species- and gear-specific discard ratios from data collected onboard commercial vessels (e.g. Tsagarakis et al., 2012; Tsagarakis et al., 2017).

The pre-balance (PREBAL) diagnostics (Link, 2010b) were inspected to ensure that the Ecopath model complies with ecological rules. The FGs with the higher EE values before balancing (**Supplementary Material Table S3**) mainly included (i) FGs the biomass of which may be underestimated in bottom trawl surveys (Benthopelagic fish and Cephalopods), ii) relatively small-sized fish and commercial invertebrates (shrimps, crabs, mixed fish groups), as well as iii) FGs with poor biomass data for the specific period or area (e.g., Horse mackerels, Polychaetes). To achieve mass-balance we corrected our inputs mainly concerning (a) the diet matrix, by also taking into account expert knowledge especially for groups for which information was not originally from the modelled area, and (b) biomasses, especially for groups for which the sampling method is known to produce an underestimate. The model was considered balanced when (a) estimated EE values were realistic (<1), (b) gross food conversion efficiency was<0.5 (usually >0.1 and<0.35 with the exception of some fast-growing species or groups with higher values, and top predators with lower ones), and (c) values of Respiration/Biomass were consistent with the group's activities with high values for small organisms and top predators (Christensen et al., 2008; Link, 2010b; Heymans et al., 2016). The Pedigree routine, which allows the user to mark the data origin using pre-defined tables and can provide input for uncertainty analysis in Ecosim (Christensen and Walters, 2004), was used to categorize data quality for each parameter according to the sources of information.

2.2 Ecosim

Ecosim is the time dynamic simulation of the initial parameters of the base Ecopath model. This is achieved through a series of coupled differential equations derived from the Ecopath master equation which take the form (Christensen et al., 2008):

$$\frac{dB_i}{dt} = g_i \sum_j Q_{ji} - \sum_j Q_{ij} + I_i - \left(MO_i + q_{ik} * E_k + e_i\right) B_i \quad (3)$$

where dB_i/dt represents the growth rate during the time interval dt of group (i) in terms of its biomass B_i, g_i is the net growth efficiency (production/consumption ratio), Q is the consumption flow, MO_i the non-predation ('other') natural mortality rate, q_{ik} is the catchability term of fleet k on species i, E_k is the relative effort of fleet k, e_i is emigration rate and I_i is immigration rate. For primary producers the positive term on the right side of Eq. 3 is represented by a function of production rate (P/B), biomass of autotrophs and production anomaly over time. Usually, primary production anomaly and effort by gear over time are main forcings used in time dynamic Ecosim simulations (see Araújo et al., 2006).

The two summations estimate consumption rates, the first expressing the total consumption by group (i) on all of its preys (j), and the second the predation by all predators (j) on the same group (i). The consumption rates, Q_{ji}, are calculated based on the 'foraging arena' concept:

$$Q_{ij}(t) = \frac{a_{ij} * v_{ij} * B_i(t) * P_j(t) * T_i * T_j * M_{ij} / D_j}{v_{ij} + v_{ij} * T_i * M_{ij} + a_{ij} * M_{ij} * P_i(t) * T_j / D_j} * f\left(Env_{function}, t\right) \quad (4)$$

where prey biomasses B_i's over time (t) are divided dynamically into "vulnerable" and "invulnerable" components, and it is the transfer rate (v_{ij}; vulnerability parameter) between these two components that determines if control is top-down, bottom-up, or of an intermediate type (Christensen et al., 2008). The default vulnerability value is 2 (mixed control), while low values (close to 1) indicate bottom-up control and high values top-down effect. Regarding the remaining terms of eq. (4), a_{ij} is the effective search rate for prey (i) by predator (j), P_j is the predator abundance over time (t), T_i and T_j is the prey and predator relative feeding time, M_{ij} is mediation effects, and D_j effects of handing time as a limit to consumption rate (Christensen and Walters, 2004; Ahrens et al., 2012).

2.2.1 Model Fitting and Parameterization

The aim of the Ecosim development was twofold: first, to explore which factors have contributed to the observed changes during the hindcast period (1993-2020), and second, to apply the calibrated model for future projections under different environmental and fisheries scenarios. Therefore, climate change, environmental variations, fisheries and their synergistic effect were tested as potential drivers, together with tuned trophic interactions among FGs. The North Aegean Sea Ecosim module was parameterized after fitting the model to time series for the hindcast period. Specifically, the time series included (i) relative biomass for 17 fish, decapod and cephalopod FGs from bottom trawl (MEDITS; Spedicato et al., 2019) and acoustic (MEDIAS; Leonori et al., 2021) surveys in the area, as well as (ii) catches for 25 FGs which were estimated from landings (ELSTAT, 2021) and discard ratios from DCR/DCF (**Supplementary Material Table S4**).

The model was fitted by modifying trophic interactions which are based on the foraging arena theory (Ahrens et al., 2012): the

software's routines were used to carry out i) a sensitivity analysis to identify the most sensitive vulnerabilities by predator (i.e., one vulnerability was used for all preys of the same predator, in order to reduce the number of estimated parameters) and ii) to alter the most sensitive vulnerabilities in order to best fit the observations in terms of time series of biomasses and catches by species. Different fittings were tried considering different sets of forcings in terms of fishing effort, temperature effects and Primary Production (PP) Anomaly.

Actual estimates of fishing effort (e.g., annual days-at-sea) were not available for the whole hindcast period, therefore, three indices of fishing capacity (i.e., number of vessels, total GT and total KW per fleet) were tested as proxies of the fishing effort. A considerable reduction (by 35-40%) in the number of vessels operating in the area has been observed since 1993 for bottom trawls, static nets, longlines & troll baits, while pots & traps show a 5-fold increase and purse seines have remained relatively stable (**Supplementary Material Figure S1**). To take into account the possible improvement in the efficiency of fishing gears due to any form of technological development (known as "technology creep"), a factor of +0.79% per year was assumed for bottom trawls (as estimated by Damalas et al., 2014) and added to the proxy for effort of each year. For the remaining fishing gears for which no information on gear efficiency improvement was available in the study area, alternative levels of the technology creep factor (0%, 1% and 2% per year) were tested based on available literature for the Mediterranean fisheries (Sartor et al., 2011) and elsewhere (Cardinale et al., 2009). The fishing effort for the hindcast period under different levels of technology creep is shown in **Figure 2** as relative values (i.e., relative to the value in 1993 used as baseline year). Therefore, nine sets of fishing effort time series (3 indices of capacity X 3 technology creep factors) were applied to select the one best describing the changes within the hindcast period, in terms of components' biomasses and catches.

Sea Surface Temperature (SST) foraging responses (Bentley et al., 2017) were incorporated in Ecosim for 28 out of 38 living FGs. AquaMaps (Kaschner et al., 2021) provides model-based predictions of species distribution using large sets of occurrence data to derive estimates of environmental preferences for a series of parameters, including temperature. Although in AquaMaps each species response function has a trapezoidal shape, the effect of SST in the N. Aegean Sea model was assumed to have a Gaussian-based shape, which has been widely used to describe thermal responses (Angilletta, 2006), including in similar studies (Bentley et al., 2017; Serpetti et al., 2017). Temperature preferences and limits for each species were retrieved from AquaMaps (Kaschner et al., 2021): optimum temperatures were estimated by averaging the 10th and 90th percentiles of the observed species-specific temperature variation, while minimum and maximum temperatures were used to build the range of thermal tolerance, which was not necessarily symmetric around the optimal (**Figure 3**). To simulate the latter in Ecosim, the SD left and SD right estimates were input in the response function leading to composite Gaussian-based responses with modified ranges. For multi-species FGs, the temperature parameters were estimated after weighing with the biomasses of individual species (or landings when biomass estimates were not available), for the species with at least 98% cumulative contribution of the total FGs biomass (**Supplementary Material Table S5**).

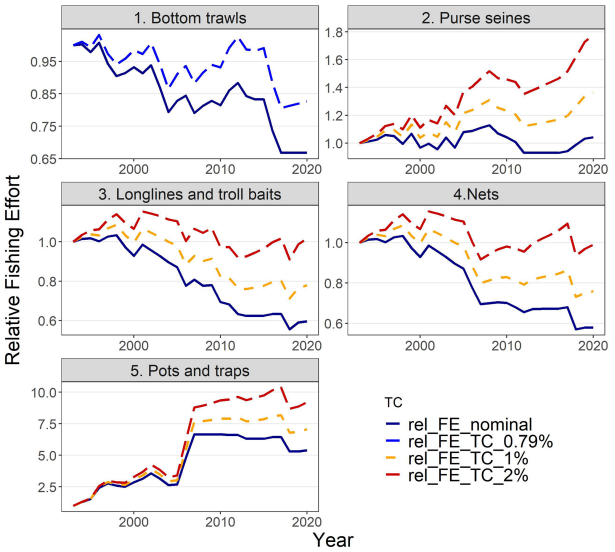

FIGURE 2 | Relative fishing effort (rel_FE; in total GT) used to drive the model under different factors of technology creep (TC): (i) no technology creep (nominal), (ii) 0.79% annually only for bottom trawls, based on Damalas et al. (2014), (iii) 1% annually and (iv) 2% annually for the remaining fishing fleets.

A PP Anomaly forcing function was applied to primary producers (i.e., Phytoplankton) and the software's routine was used to search for the shape that urged the model to best describing the observations for the whole food web components (i.e., relative biomass and catch time series).

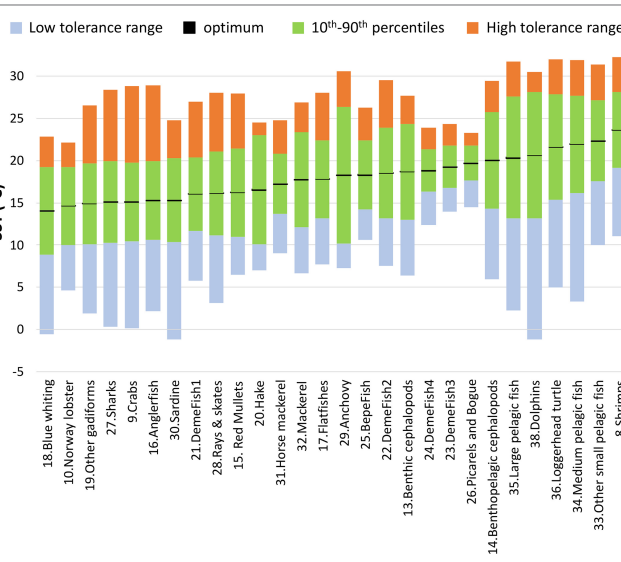

FIGURE 3 | Optimum temperatures (black lines), 10th – 90th preference range (green bars), lower tolerance range (blue bars) and higher tolerance range (orange bars) that were used to parameterize thermal responses for each FG in the Ecosim model. FGs are ranked by increasing optimal temperature.

The automated stepwise fitting procedure (Scott et al., 2016) was applied to inspect model results for every possible combination of the parameters driving and affecting the model, namely (i) SST, (ii) Fishing effort, (iii) PP Anomaly (testing for different spline points but always ≥2, Heymans et al., 2016) - and (iv) Trophic Interactions (i.e. vulnerabilities; testing for different number of predators with altered vulnerability). The number of parameters (i.e. vulnerabilities and PP anomaly spline points) to be estimated never exceeded K-1 (where K is the number of independent time series available, i.e. 42 in the N. Aegean Sea model) in order to avoid overfitting under the general assumption of autocorrelation existing within each time series (Heymans et al., 2016). The best model was selected based on the minimization of the Akaike Information Criterion corrected for small number of observations (AICc), which takes into account the Sum of Squares (SS) among observed and predicted model outputs as well as parsimony in number of estimates as a goodness of fit criteria (Heymans et al., 2016).

In order to connect the model-derived PP Anomaly with environmental processes during the hindcast period, we explored its correlation with SST and with a series of large scale climatic indices which are known to affect the Mediterranean Sea (e.g. Katara et al., 2011; Tsikliras et al., 2019; Criado-Aldeanueva and Soto-Navarro, 2020), namely the Mediterranean Oscillation Index (MOI), the North Atlantic Oscillation (NAO) (accessed through the Climatic Research Unit, University of East Anglia: https://www.uea.ac.uk/groups-and-centres/climatic-research-unit) and the Atlantic Multi-decadal Oscillation (AMO) (Trenberth et al., 2019).

2.2.2 Monte Carlo Routine

The Monte-Carlo routine was used to take into account model uncertainty by exploring the effect of alternative Ecopath input (*B, P/B, Q/B* and *Diets*) on Ecosim best fitted simulations. The Ecosampler routine (Steenbeek et al., 2018) was used to record Ecopath models having alternative balanced initial conditions, to be used on the final selected best fitted Ecosim model and subsequently estimate the range of dispersion of the simulations. In total, 100 Monte-Carlo simulations were performed. The CV allowed to vary the Ecopath input parameters for *B, P/B* and *Q/B* was obtained from the Ecopath Pedigree (**Supplementary Material Table S6**). For *Diets*, the Dirichlet distribution method was used, setting a multiplier equal to 30, which was selected after plotting the Dirichlet distributions for different values of the multiplier (between 1 and 100) (for details see Steenbeek et al., 2018).

2.2.3 Climate, Productivity and Fishing Scenarios

After fitting the model (hindcast), eight scenarios representing future conditions were applied to explore the effect of the different drivers of the Ecosim model, i.e., SST, PP Anomaly and Fishing as well as selected combinations of them (**Table 2**). In order to identify potential winners and losers of climate change and management practices in different scenarios, predicted average biomasses and catches of the FGs in the medium (year 2030) and the long term (period 2046-2050) under each scenario were compared against the baseline one (with constant conditions as in 2020 for the whole projection period). In addition, the changes in the following ecosystem indicators was explored to detect possible effects in ecosystem structure, functioning and/or services: (i) total biomass of living FGs, (ii) total catch, (iii) Fishing-in-Balance (FiB) index (Christensen, 2000), (iv) Shannon diversity index, and (v) mean Trophic level of the catch (TLc).

SST projections for the geographical boundaries of the model area were obtained from the CMIP5 (Coupled Model Intercomparison Project Phase 5) runs, accessed through the Royal Netherlands Meteorological Institute (KNMI) (KNMI Climate Explorer tool: https://climexp.knmi.nl/selectfield_cmip5.cgi?#ocean). The projections were used for the representation of temperature effects under climate change and were applied as forcing functions to SST foraging responses (Bentley et al., 2017). The MPI-ESM-LR model (Giorgetta et al., 2013) was chosen as giving a better representation of the ensemble (CERES, 2018) and as practiced in other Mediterranean studies (e.g. Chefaoui et al., 2018). Two SST scenarios (**Table 2**) were simulated based on Representative Concentration Pathways (RCP) of the Intergovernmental Panel on Climate Change (IPCC), with SST according (i) to RCP 4.5 (scenario RCP45 in **Table 2**), a moderate climate change scenario which assumes that some actions against

TABLE 2 | Scenarios applied for the future projections.

Driver(s)	Scenario name	Scenario description
No changes	Baseline	No change compared to the last year of the hindcast period (2020)
SST	RCP45	SST change according to RCP 4.5
	RCP85	SST change according to RCP 8.5
PP Anomaly	PP+5%	Progressive increase in PP Anomaly up to 5% until 2050
	PP-5%	Progressive decrease in PP Anomaly up to 5% until 2050
Fishing Effort	FE10	10% reduction in fishing effort by 2025
	FE25	25% reduction in fishing effort by 2025
Combined	ENV	Moderately negative environmental changes: SST according to RCP 4.5 and decrease in PP Anomaly up to 5% until 2050 (i.e. RCP45 and PP-5%)
	ENV FE10	Moderately negative environmental changes accompanied by 10% reduction in fishing (i.e., ENV and FE10)

climate change are taken, and (ii) to RCP 8.5 (scenario RCP85) which is the worst-case scenario as it assumes that no actions are taken. An increase in temperature has been already observed during the hindcast period and continues after 2020 in both RCP scenarios (**Figure 4**). The SST predictions between RCP 4.5 and RCP 8.5 diverge more after 2050 when the temperature increase slows down in the former contrary to the latter scenario. Nevertheless, we chose to simulate the effects up to 2050 because the uncertainty associated with temperature predictions as well as with adaptations of organisms to extreme temperatures of the RCP 8.5 scenario after 2050 may lead to unrealistic forecasts.

Contrasting patterns in trends of primary productivity under climate change have been forecasted for the Eastern Mediterranean Sea. Most studies foresee substantial increases in productivity (e.g. Lazzari et al., 2014; Adloff et al., 2015; Macias et al., 2015), while others show that the basin will become more oligotrophic (e.g. Richon et al., 2019). In all studies however, it is evident that productivity changes are less severe in the model area compared to the rest of the Aegean Sea or to the whole Eastern Mediterranean basin. Therefore, based on levels of change indicated in other simulation studies (e.g., Lazzari et al., 2014; Richon et al., 2019) we simulated moderate changes in future productivity by means of two synthetic linear trends in PP Anomaly (one increasing and one decreasing), progressively reaching ±5% by 2050 (scenarios PP+5% and PP-5%; **Table 2**).

Given that reductions of fishing effort and further retraction of vessels are probable to continue in the near future as the main management strategies aiming to improve stock status in the area, two short-term fishing effort reduction scenarios were applied (**Table 2**). The scenarios simulated decreases by 10% (FE10) and 25% (FE25) for all fleets within 5 years (from 2021 to 2025) and thereafter assume constant fishing effort at levels reached in 2025.

Finally, two scenarios based on the combination of drivers were tested (**Table 2**). The first (ENV), a moderately negative environmental scenario was developed by considering SST increase under RCP 4.5 occurring simultaneously with a 5% decrease in PP Anomaly. The second scenario (ENV_FE10), explored the above environmental conditions accompanied by a 10% reduction in fisheries, to explore if the effects of environmental conditions could be compensated by applying moderate horizontal fisheries management measures.

3 RESULTS

3.1 Ecopath

The flow diagram of the NAS1990 Ecopath model is shown in the **Supplementary Material Figure S2**. Large pelagic fish, dolphins and medium pelagic fish were the top predators of the pelagic compartment, while hake, demersal fish 2 and anglerfish had the higher Trophic Level among the demersal groups (**Table 1**). Regarding the commercial FGs, small pelagics (anchovy and sardine) were dominant in terms of biomass while shrimps, demersal fish 3 and hake were the most abundant FGs among the demersal commercial ones (**Table 1**). The PREBAL diagnostics for the Ecopath model (**Supplementary Material Figure S3**) show that biomass spectra span 5 orders of magnitude, with a slope 5.7% decline (on a log scale) with increasing trophic level; the slopes for Production/Biomass (P/B) and Consumption/Biomass (Q/B) with increasing trophic level were 8.6% and 5.1% decline respectively, i.e., within the expected range. The Gross Efficiency (P/Q) values were physiologically realistic (0.1 - 0.3 for most groups) (Christensen et al., 2008; Link, 2010b).

The pedigree index was 0.64, while the model's summary flows, common indices and statistics are provided in the **Supplementary Material Table S7**. The mean Trophic Level of the catch was 3.499, the mean Transfer Efficiency was 17.66%, the Primary Production Required to sustain the fishery (PPR, from primary producers) was 9.72%, while the probability for the ecosystem to be sustainably fished was very low, i.e., 25%. This was in line with the high fishing mortalities (F) and exploitation

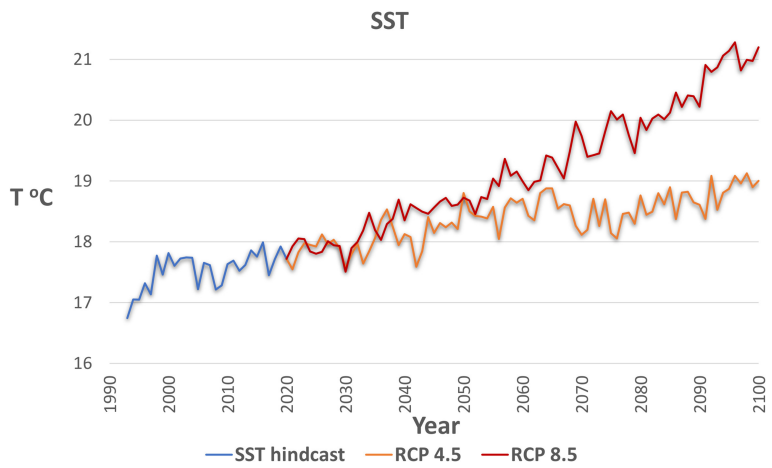

FIGURE 4 | Sea Surface Temperature (SST) of the model area during the hindcast period (1993-2020) and under the two climate scenarios considered (RCP 4.5 and RCP 8.5) for the period 2021-2100.

rates (F/Z) of some FGs, especially apex predators (e.g., hake, demersal fishes 2, large and medium pelagics), sardine and mackerels (**Supplementary Material Table S8**).

3.2 Ecosim

3.2.1 Model Parameterization and Hindcast Runs

The stepwise fitting approach indicated that the best model (with the lowest SS and AIC) was capable to reduce SS by 46.3% compared to the baseline model and included as drivers fishing, SST and PP Anomaly with calibrated trophic interactions (**Table 3**). Total GT with a technology creep factor of 2% annual increase (but 0.79% for bottom trawls) proved to be the best proxy of fishing effort as it improved the fit more than the other series of fishing effort (i.e., number of vessels or total KW and technology creep factors 0% or 1%). The optimization of the trophic interactions by estimating vulnerabilities for 34 predators greatly improved model fit (**Table 3**). Seventeen FGs had vulnerabilities equal to one (most of them low and medium trophic level organisms, e.g., micro- and macro-zooplankton, polychaetes, shrimps, benthic invertebrates, red mullets, anchovy, other small pelagic fish), indicating bottom-up effects, four FGs (small benthic crustaceans, benthopelagic fish, medium and large pelagic fish) showed very high vulnerabilities (>1000) while the remaining FGs had intermediate values (2-30.47) (**Supplementary Material Table S9**). The PP Anomaly function selected with the stepwise fitting had 6 spline points and showed a decreasing trend (with some fluctuations) from the starting period (1993) until 2010 and a relatively steep increase during the last decade of the hindcast period. The Spearman correlation of the PP Anomaly with SST and the climatic indices revealed a significant positive correlation only with NAO (r=0.45, p=0.016; **Figure 5**) and correlation increased when including a 1-year lag for NAO (r=0.56, p=0.002; **Figure 5**).

The model's fit to biomass observations was very satisfactory for some groups (e.g., shrimps, benthic cephalopods, hake, demersal fish 2, 3 and 4, picarels & bogue and sardine) and less for others (e.g., red mullets, demersal fish 1, sharks and rays & skates) (**Figure 6**). Similarly, for catches, the model's predictions reproduced relatively well the observed time series for benthic cephalopods, other gadiformes, horse mackerel and mackerel, but not very well for shrimps and rays & skates (**Figure 7**). Overall, the model slightly overestimated catches in the last 3-5 years of the time series (**Figure 7**), as it seems to be driven mainly by biomass increases observed for several FGs (e.g., cephalopods, red mullets, demersal fish 2 and 4, rays & skates) during the same period (**Figure 6**). Compared to the starting period, substantial declines in catches and biomasses at the end of the hindcast period were simulated for Norway lobster, other gadiformes, horse mackerels, mackerels and medium pelagics. On the other hand, catches of demersal fish 2 and 4, benthic and benthopelagic cephalopods as well as anchovy were increasing; however, for the three latter, the increase in catches was much higher than the increase in biomass (**Figures 6**, **7**).

Model's predictions were (with very few exceptions) within the 5%-95% percentiles of the Monte-Carlo simulations and generally close to their mean, both for biomasses and catches. In addition, the observations fall usually within the 5%-95% percentiles but not for all FGs/periods (**Figures 6**, **7**). The Monte-Carlo simulations did not identify any alternative Ecopath input that explained the Ecosim time series (i.e., in terms of SS reduction) better than the current setup.

Ecosystem indicators revealed that substantial changes have been observed during the hindcast period; the trends of total biomass, total catches and FiB index were similar, with all three metrics showing a decline from 1994 to 2010 and a strong recovery, thereafter, exceeding the levels of the baseline period (**Supplementary Material Figure S4**). The Shannon diversity

TABLE 3 | Description, Sum of Squares (SS) and Akaike Information Criterion (AIC) of selected steps of the stepwise fitting.

model	Vs	PP Anomaly spline points	Parametersestimated	SS	AIC	%SSchange
Baseline	–	–	0	1056.29	67.90	
Fishing (min)*	–	–	0	965.30	-20.92	-8.6%
Fishing (max)*	–	–	0	1064.90	75.90	0.8%
SST	–	–	0	1295.57	269.22	22.7%
PP Anomaly	–	6	6	936.20	-38.95	-11.4%
Trophic Interactions	34	–	34	1019.58	105.88	-3.5%
Fishing + SST	–	–	0	1297.25	270.50	22.8%
Fishing + PP Anomaly	–	6	6	936.89	-38.23	-11.3%
Fishing + Trophic Interactions	34	–	34	929.56	14.74	-12.0%
SST + PP Anomaly	–	6	6	1228.86	229.25	16.3%
SST + Trophic Interactions	34	–	34	689.84	-279.34	-34.7%
PP Anomaly + Trophic Interactions	34	6	40	789.15	-132.81	-25.3%
Fishing + SST + PP Anomaly	–	6	6	1251.78	247.47	18.5%
Fishing + SST + Trophic Interactions	34	–	34	665.00	-315.50	-37.0%
Fishing + PP Anomaly + Trophic Interactions	34	6	40	778.04	-146.79	-26.3%
SST + PP Anomaly + Trophic Interactions	34	6	40	605.23	-394.45	-42.7%
Fishing + SST + PP Anomaly + Trophic Interactions	**34**	**6**	**40**	**567.39**	**-458.10**	**-46.3%**

**three different proxies of fishing effort (capacity in number of vessels, Total GT, Total KW) under 3 levels of technology creep (kept constant at 0.79% for bottom trawls and varying at 0%, 1%, 2% for the other fleets) were explored, therefore only the minimum and maximum values are shown. For the remaining steps, fishing effort corresponds to Total GT with a 2% annual factor of technology creep, which is the proxy applied to the best model.*

Only steps with 6 PP anomaly spline points and/or 34 vulnerabilities (Vs) are shown, in line with the finally selected model (indicated in bold). The % change of the SS of each model compared to the baseline scenario is also shown.

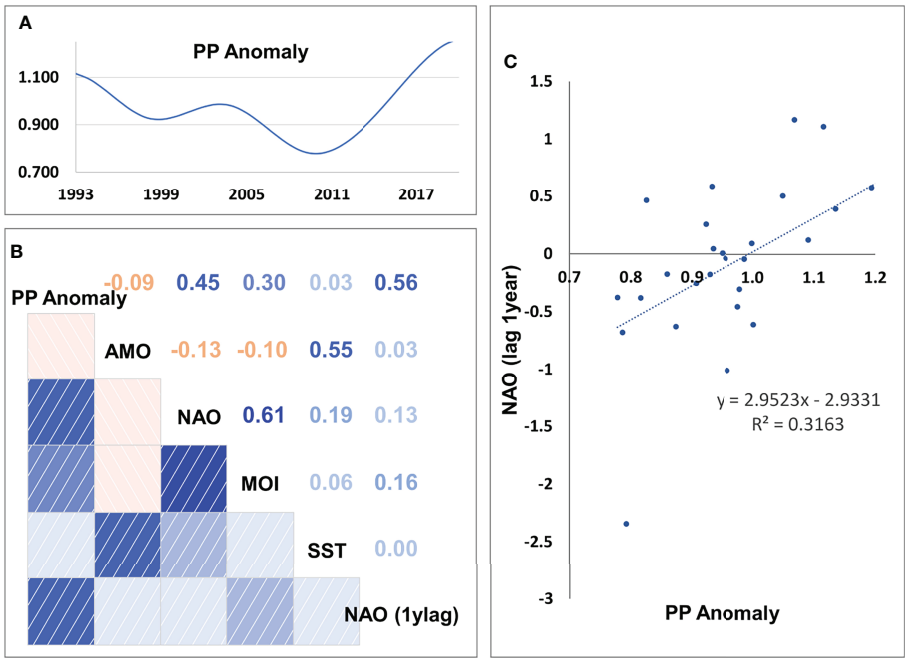

FIGURE 5 | (A) Estimated values of PP Anomaly, **(B)** correlation coefficients among PP Anomaly, Sea Surface Temperature (SST) and climatic indices (MOI, Mediterranean Oscillation Index; AMO, Atlantic Multi-decadal Oscillation; NAO, North Atlantic Oscillation; NAO (1ylag), NAO with lag of 1 year), and **(C)** scatterplot of annual mean PP Anomaly and NAO with lag of 1 year.

index had a very similar response but with some delay compared to the abovementioned metrics and with a more moderate recovery. Finally, the mean Trophic Level of the catch (TLc) increased slightly, with some fluctuations from 1994 to 2017 and returned to the early 1990s levels within just 3 years (**Supplementary Material Figure S4**).

3.2.2 Future Scenarios

The IPCC temperature scenarios indicated contrasting responses to increased temperature among FGs. Compared to the baseline scenario the highest increases in mean biomass were forecasted for the benthopelagic fish FG, and demersal fish 4 and 2 (**Figure 8**).

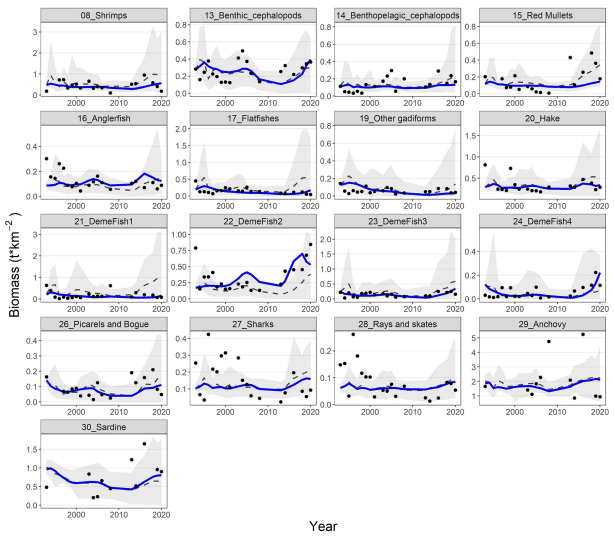

FIGURE 6 | Predicted (blue lines) and observed (dots) biomasses for 17 FGs with available biomass time series. The dashed grey lines and shaded areas are the mean and the 5%-95% percentiles of the 100 Monte-Carlo simulations respectively.

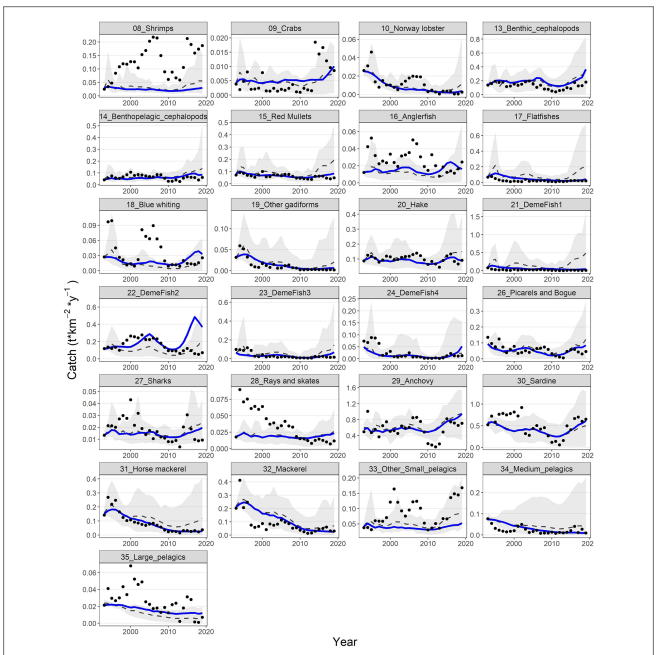

FIGURE 7 | Predicted (blue lines) and observed (dots) catches for 25 FGs with available catch time series. Dashed grey lines and shaded areas are the mean and the 5%-95% percentiles of the 100 Monte-Carlo simulations respectively.

In the medium term (year 2030; **Figure 8** and **Supplementary Table S10**), all increases were moderate, not exceeding +16%, but in the long term (average for 2046-2050) they were amplified, with the aforementioned groups exceeding +100% and the benthopelagic fish FG showing an extreme increase (**Figure 8** and **Supplementary Table S11**). Positive effects were also identified for medium and large pelagic fish, sea turtles and dolphins. For most groups, the changes were larger in the RCP85 compared to RCP45, however this was not true for all FGs, especially for the ones with moderate climate responses (e.g., the benthic cephalopods increased by +7.1% in RCP45 but only +5.3% in RCP85 in the long term; **Figure 8** and **Supplementary Table S10**). Main losers of climate change were the other gadiformes, horse mackerels and Norway lobster (**Figure 8**) for which the forecasted decline reached -89.4%, -75.6% and -74.7% respectively in RCP85 during the 2046-2050 period. The climate change effect on catches for each FG (in terms of proportional change) was identical to the effect on biomasses (**Supplementary Material Figure S5** and **Tables S11, S12**) because of linear effects as explicit in Eq. 3. Biomass and catch trends of the main commercial FGs are illustrated in the **Figures 9A**, **10A** respectively: shrimps, red mullets and sardine were negatively affected, especially after year 2035, hake and anglerfish showed clear increases, while for anchovy, practically very low positive effects were identified.

Total biomass of all living groups was forecasted to increase after 2030, either continuously under RCP85 or with some fluctuations in the RCP45, while the effect of temperature

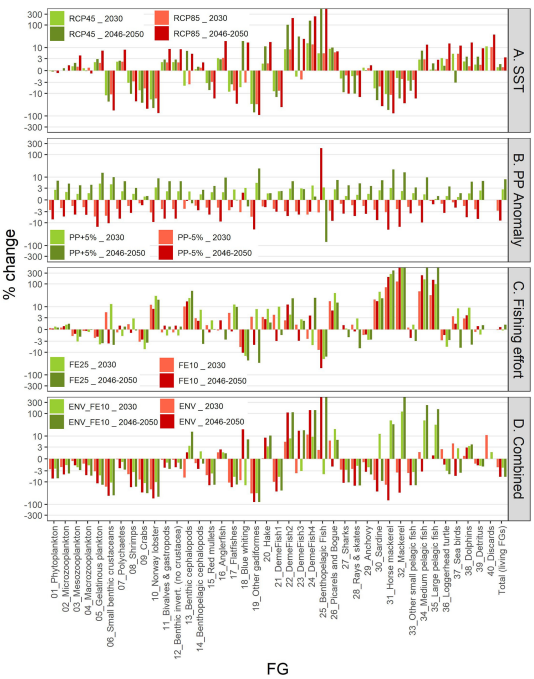

FIGURE 8 | Graphical representation of differences (%) in biomasses in 2030 and average biomasses in the period 2046-2050 for each FG under each scenario compared to the baseline scenario. Y-axis scale is pseudo-logarithmic for better representation. The description of the scenarios is provided in **Table 2**.

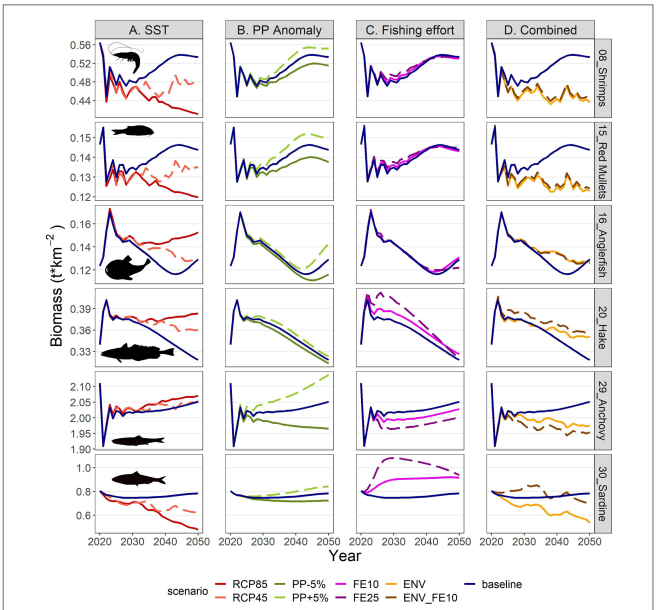

FIGURE 9 | Biomass projections for selected FGs in the period 2021-2050 under scenarios related to **(A)** SST, **(B)** PP Anomaly, **(C)** fishing effort and **(D)** combination of drivers. The description of the scenarios is provided in **Table 2**.

scenarios on total catches was very low (**Figure 11A**). Specifically, gains and losses were balanced until 2030 (**Supplementary Material Table S12**) and a 1.4-3.5% increase was shown for the long term (**Supplementary Material Table S13**). The FiB index remained relatively unchanged by increasing temperature for the first 20 years in the future but started to be lower than the baseline scenario after 2040 (**Figure 11A**). The Shannon diversity index showed high responsiveness to climate change, fluctuating in RCP45 and decreasing in RCP85, while the Trophic Level of the catch (TLc) was slightly higher in the climate scenarios compared to the baseline (**Figure 11A**).

The future scenarios with PP Anomaly had more straightforward effects on the FGs' biomasses and catches. In the medium term, almost all FGs showed limited increases in biomasses under increasing trends of PP Anomaly (PP+5%), with other gadiformes, gelatinous plankton and small benthic crustaceans increasing ~5% in the medium term (**Figure 8** and **Supplementary Material Table S10**). In the long term, as PP progressively increased, these changes were even higher (e.g., reaching 24% for other gadiformes); however, few FGs showed slight (blue whiting -1.4%, benthic cephalopods -0.7%) or substantial (benthopelagic fish -69.6%; **Figure 8**, **Supplementary Material Table S11**) decrease due to trophic interactions. Under decreasing PP Anomaly (PP-5%), the opposite patterns were evident (biomass: **Figure 8**; catches: **Supplementary Material Figure S5**). Among the main commercial FGs, anglerfish and sardine were affected the most, with changes exceeding ±7% by 2050, both in biomass and in catches (**Figures 9B**, **10B**). As expected, total biomass of living groups, total catch as well as the FiB index followed the trends of the PP Anomaly, while the

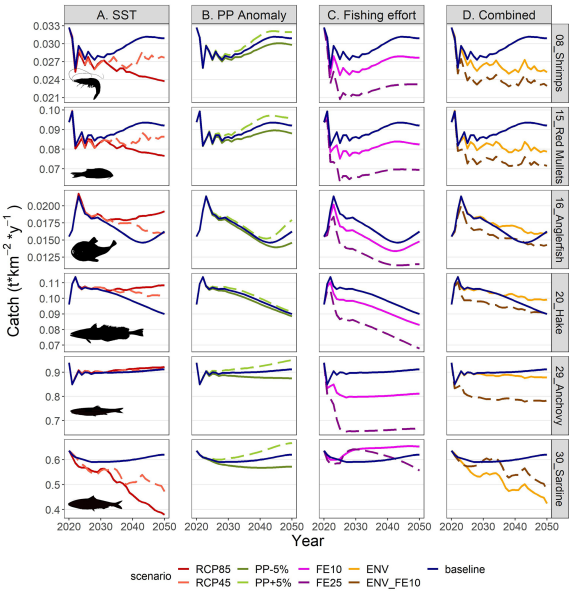

FIGURE 10 | Catch projections for selected FGs in the period 2021-2050 under scenarios related to **(A)** SST, **(B)** PP Anomaly, **(C)** fishing effort and **(D)** combination of drivers. The description of the scenarios is provided in **Table 2.**

Shannon index and TLc were negatively related to them (i.e., they increased when PP Anomaly decreased and vice versa; **Figure 11B**).

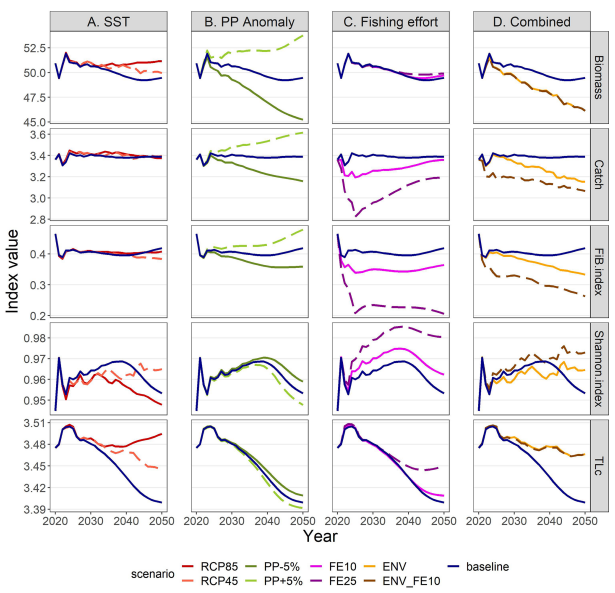

FIGURE 11 | Ecological and exploitation indices under scenarios related to **(A)** SST, **(B)** PP Anomaly, **(C)** fishing effort and **(D)** combination of drivers. The description of the scenarios is provided in **Table 2**. Biomass in t*km^{-2}; Catch in t*km^{-2}*y^{-1}

The horizontal (for all gears) reduction of fishing effort favored mainly the pelagic species, especially mackerels, horse mackerels, medium and large pelagics, sardine, and picarels & bogue. For all these FGs the biomass increase was 2.2 (sardine) to 5.3 (mackerels) times higher in the scenario of 25% effort reduction (FE25) compared to 10% reduction (FE10) in 2030 (**Figure 8**), while their catches also substantially increased despite the reduced fishing (**Supplementary Material Figure S5**). A population increase was also forecasted for 19 out of 27 fished FGs, including demersal groups, but was accompanied by a decrease in their catches (**Figure 8** and **Supplementary Material Figure S5**). A neutral or negative impact was identified for prey (e.g., anchovy, benthopelagic fish, blue whiting, mesozooplankton) or scavenging FGs (e.g., Loggerhead turtle, crabs), probably affected by discards reduction (**Figure 8**). In all cases, the FGs' response to fishing was quick after changes were applied; however, despite that the changes in fishing effort were restricted to the first five years of the simulations, changes in the FGs' biomass continued until 2050 and for some of them the biomasses in the two fishing scenarios converged (e.g., sardine) or were even reversed (e.g., anglerfish, hake) (**Figure 9C**). Therefore, large declines in fishing effort (FE25) did not lead to constantly high biomasses for all species that were initially favored, and this was reflected in their reduced catches towards the end of the forecast period when they diverged more from the baseline and the FE10 scenarios (**Figure 10C**). FE25 and FE10 led to reduction of total catches by 13.2% and 4.4% respectively in 2030 (**Supplementary Table S12**), however, in the long term (2046-2050), divergence from the baseline scenario was reduced to -5.9% and -1% respectively (**Supplementary Table S13**). Total catch, FiB and Shannon indices changed abruptly in the first five years but followed almost parallel trajectories with the baseline scenario when fishing was stabilized to new levels (i.e., in 2025; **Figure 11**). On the other hand, total biomass and TLc were close to the baseline in the early years and started to diverge after 2035. The FiB index was higher in the baseline scenario compared to less fishing, while the contrary was forecasted for Shannon diversity index and TLc which increased at relaxed fishing effort (**Figure 11**).

In the combined environmental scenario (ENV), impacts of reduced productivity were added to temperature effects, resulting in lower biomass increases for winners of sea warming (e.g., demersal fish 2, 4 and benthopelagic fish) and even higher decreases for losers (e.g., other gadiformes, horse mackerels and Norway lobster), both in medium and long term basis (**Figure 8**). Losses were high in terms of biomass (**Figure 9D**) and catches (**Figure 10D**) for shrimps, red mullets, sardine and even anchovy (which responded positively to temperature increase alone), while for anglerfish and hake, gains were only temporary and/or lower than in the RCP45 scenario. The loss in total catches reached 6.5% in the period 2046-2050 (**Supplementary Table S13**). Biomass losses were compensated when applying a 10% reduction in fishing effort (ENV_FE10 scenario) which resulted in improving the population trends for most FGs and reversing negative trends for a limited number of FGs such as sardine in the short term and mackerels, horse mackerels, picarels & bogue for the whole forecast period (**Figures 8**, **9D**). However,

compared to the baseline scenario, total catches declined even more (by 9%) than they did in the ENV scenario, since the higher catches for few pelagic groups were not enough to balance losses from the remaining groups (**Supplementary Figure S5**). At the ecosystem level, Shannon diversity index was higher in ENV_FE10 compared to the baseline and to ENV, the opposite was observed for the FiB index, while total biomass of living groups and TLc were almost identical in the two combined scenarios (**Figure 11D**).

4 DISCUSSION

4.1 Hindcast Period

A novel Ecopath model for the N. Aegean Sea considering 1993 as the starting year was developed by updating a previously published model for the mid-2000s (Tsagarakis et al., 2010). This model forms the basis for the development of the time dynamic Ecosim module that was able to describe food web changes in the N. Aegean Sea ecosystem after fitting to observed time series for the period 1993-2020. The available time series concerned mainly fish and commercial invertebrate groups and were largely missing for low trophic level groups such as plankton, benthic invertebrates and other preys (e.g., benthopelagic/mesopelagic fish); regular monitoring for such groups could help to fine-tune trophic interactions in the food web and lead to better representation of ecosystem processes and more effective models for operational use.

The hindcast period is characterized by a reduction in the fishing fleets, increase in sea water temperature (Skliris et al., 2011; Stergiou et al., 2016) as well as shifts in the biological components (Damalas et al., 2021) such as catches and biomasses, both at community and species level (e.g. Farriols et al., 2019; Tserpes et al., 2019). The Ecosim model best fitted to observations included trophic interactions (estimated vulnerabilities), which improved the model fit more than any other driver in all steps of the fitting procedure. Overall, the observed changes in the hindcast period were a result of the synergistic effect of fishing and environmental variability (SST and PP Anomaly).

The best model included dynamics of total GT assuming an annual technology creep factor of 0.79% for bottom trawls and 2% for the remaining gears, as proxy for the fishing effort. The technology creep factor reflects in practice changes in catchability due to improvement of fishing gears and other equipment. The application of this level of technology creep, which is often neglected in fisheries management (Eigaard et al., 2014), leads to lower rate of reduction of the nominal fishing capacity, or even to increases in some fleets, despite the long-lasting efforts to reduce the number of vessels in all Mediterranean waters (Eurostat, 2021). This was observed also in other systems (see Fortibuoni et al., 2017) and should be carefully taken into account for policy design and enforcement, especially in a management system based on effort control, like the Mediterranean Sea (Bellido et al., 2020).

In addition to fishing effort, the inclusion of thermal responses and SST as a driver for the period 1993-2020 improved the model fit. This result supports the findings that climate change has already affected the communities and/or composition of catches in several Mediterranean ecosystems (e.g. Corrales et al., 2017) and the Mediterranean as a whole (Tzanatos et al., 2014), as well as the composition of landings and demersal communities in the Aegean Sea (Tsikliras et al., 2015). The incorporation of FGs' responses to climate change within the N. Aegean Sea model, apart from improving its explanatory power, it also provided the possibility of using the model as a tool to explore the directions of change in climate simulations.

The inclusion of a model-derived PP Anomaly in the final selected Ecosim model confirms the importance of productivity trends in the Mediterranean ecosystems (Piroddi et al., 2017). This PP Anomaly showed positive correlation with the North Atlantic Oscillation (NAO) of the previous year (1 year lag). NAO is a large-scale climatic oscillation which can affect fisheries in the North Atlantic region and the Mediterranean Sea, with effects on abundance, recruitment, catchability and body condition (Báez et al., 2021). In the Aegean Sea, it has been shown to affect the anchovy/sardine catch ratio with one year lag (Katara et al., 2011), similarly to our findings, and which is possibly explained by a lag in recruitment or other processes (Báez et al., 2021).

Several FGs were heavily fished at the beginning of the hindcast period (see F/Z estimated ratios for NAS1990, **Table S8**). A peak in total landings has been recorded in 1994, followed by a decreasing trend for many years, not only in the study area but for the whole of Greek landings (Moutopoulos et al., 2014). Lower landings were accompanied by decreasing biomass trends for several FGs, and by decline in nominal fishing capacity which took place mostly after the late 1990s. These dynamics are coherent with an overexploitation process that was likely taking place in the Mediterranean fisheries (Vasilakopoulos et al., 2014) and/or the effect of environmental processes and climate that reduced carrying capacity. A regime shift linked to such processes, mainly climate change, has been identified in the Aegean Sea for the early 1990s (Damalas et al., 2021). Similarly, in the Adriatic Sea, multivariate analysis showed that the species composition of landings during 1994-2008 differed from the previous (1986–1993) and the following (2009-2015) periods (Fortibuoni et al., 2017). This time frame (i.e., 1994-2008) is very similar with the period of decreasing biomasses and landings in the N. Aegean Sea observed in our study (i.e., 1994-2010). Further considering the timing (i.e. early 1990s) of the shift identified by Damalas et al. (2021), it is probable that these environmental effects concern a wider scale, for at least part of the Mediterranean Sea. In the Aegean Sea, the overexploited status of fisheries resources at that period may have contributed to this shift by reducing their resilience (Damalas et al., 2021). Even though the authors consider unlikely for the ecosystem to return to its pre-1990s state (Damalas et al., 2021), our study reveals that the N. Aegean Sea showed signs of quick recovery in terms of total biomass, catches and other ecosystem indicators in the last decade (2011-2020). However, this doesn't mean that the previous state is met, since differences in the relative biomass (and catches) of FGs are evident at the end of the hindcast period in relation to the early 1990s. This partial recovery might be the result of reduction of fishing effort - which resulted in some fleets (e.g., bottom trawls) even after accounting for technology creep – and

of some technical measures that have been applied in the past decade, such as the increase in cod-end mesh size and the partial reallocation of fishing effort from shallow to deeper waters for bottom trawls (Council Regulation (EC) No 1967/2006). These measures are not considered adequate to ensure the sustainability of the stocks (Vasilakopoulos et al., 2020; Lucchetti et al., 2021), but they may have contributed to the observed improvement, at least for some species (e.g. red mullets; Tserpes et al., 2019).

4.2 Climate Simulations and Fishing Scenarios

Future scenarios incorporating IPCC temperature projections forecasted substantial changes in the North Aegean Sea communities. Positive effects were most frequent for demersal FGs, contrary to what was predicted by a Mediterranean-wide multi-species model (Moullec et al., 2019). In addition, pelagic predators such as medium and large pelagic fish, and dolphins, were favored like in other works (Libralato et al., 2015). The changes observed for each FG resulted from a combination of direct thermal responses and trophic cascading effects. Certain FGs (e.g., blue whiting, demersal fish 3, benthic cephalopods) showed less severe changes under the most extreme climate simulation (RCP85), which seems to be an outcome of complex trophic effects rather than direct impact of temperature, highlighting the importance of using multi-species models to detect possible ecosystem and resource responses.

According to the increasing SST simulations, total catches didn't seem to be substantially affected, in line with Moullec et al. (2019). However, important changes were observed at the FG level, with some of the main commercial groups (hake, benthic cephalopods) increasing and others (shrimps, red mullets) decreasing. Recently, using an hydrodynamic/biogeochemical low-trophic level model coupled with an individual-based (IBM) model, Gkanasos et al. (2021) forecasted negative climate effects on both anchovy and sardine in the North Aegean Sea due to reduced zooplankton concentrations under IPCC scenarios. Their results also showed that anchovy was impacted more than sardine because of great overlap between anchovy spawning and larval growth periods with the period of maximum yearly temperature and low prey concentration (Gkanasos et al., 2021). On the other hand, at the Mediterranean scale, positive response to climate change have been predicted for both small pelagic species (Moullec et al., 2019). Contrasting predictions on species responses is not uncommon in ecological research, not only as an outcome of the variety of methodologies applied, data used and assumptions made, but also due to different responses in each ecosystem. As an example for the latter, hake was found to be threatened by seawater warming in the Israeli Mediterranean continental shelf, contrary to the N. Aegean Sea, but SST in the southeast Mediterranean is 4-5°C warmer than in the N. Aegean and de*v*stes much more than hake's optimal temperature based on AquaMaps data (Corrales et al., 2018).

One limitation of the current modelling approach is that for multi-species FGs, the model cannot appropriately take into account contrasting specific thermal responses of species composing the FG. One approach to deal with this issue could be to define FGs according to a wider suite of ecological traits (e.g. Papapanagiotou et al., 2020) including responses to temperature, or even using them as the main criterion. Such an approach would be very useful in studies placing more focus on climate change, but it might limit the potential when other factors (e.g., fisheries, trophic relationships) need to be examined, therefore the model structure (including FG definition) should depend on the specific questions sought.

The increase in primary productivity (PP+5%), which is currently considered the most likely direction (Lazzari et al., 2014; Macias et al., 2015), will result to be beneficial to the ecosystem biomasses and fisheries production in the area. However, recent studies suggest that the productivity trend in the Eastern Mediterranean may be decreasing (Richon et al., 2019) and climate risks for marine ecosystems are globally higher than previously thought (Tittensor et al., 2021). In this direction, simulations of reduced productivity (PP-5%) showed adverse impacts on almost all groups and most ecosystem indicators resulting in declining trends, as expected. However, when the declining PP Anomaly trend was explored simultaneously with the RCP 4.5 temperature simulation (ENV scenario), biomasses, catches and ecosystem indicators showed more complex responses, more negative than the increasing temperature alone (RCP45), but less than the reduction in primary productivity alone (PP-5%). Using results from physical-biogeochemical climatic scenarios (e.g. Reale et al., 2020) might help to directly embed in ecosystem models main bottom-up effects of climatic changes in plankton community due to several factors that spam from modification of nutrient inputs, general circulation and mixing, and plankton responses to temperature changes. Thus, future efforts to produce realistic climate scenarios of bottom-up effects might account forcings obtained from coupled physical and biogeochemical models' scenarios.

Apart from temperature and productivity, climate change effects include several features that cannot be directly taken into account in our approach, such as shifts in species distributions, species invasions, changes in water circulation, increased acidification and hypoxia. Therefore, the climate simulations applied in the current study aim to explore the directions of change and their possible magnitude rather than to predict the precise levels of change. The reduction of fishing effort (ENV_FE10 scenario) reduces the climate impacts to some extend by leading to increased biodiversity (Shannon index) and by mitigating biomass decreases or even reversing the negative trends for some FGs. Although this comes with a moderate loss in total fisheries production, this may be a price worth paying in order to preserve ecosystem structure and functioning under continuous environmental changes. These results support the expectations that ecosystems in good environmental status with high diversity and which are exploited sustainably show higher resilience to climate change (Gaines et al., 2018). Thus sustainable fisheries production, even under climate change, mainly depends on the effectiveness of the fisheries management (Barange, 2019).

When explored under constant environmental conditions, the fishing simulations produced relatively similar results as in other Eastern Mediterranean ecosystems (e.g. the adjacent Thermaikos

Gulf; Dimarchopoulou et al., 2022). The reduction of fishing effort leads to quick and substantial biomass increase for most species, but also to reduced catches. However, for some of the most exploited FGs (e.g., medium pelagics, sardine) this increase was so high that was able to compensate for the lower levels of fishing and to lead to higher catches. An abrupt (25%, FE25) decrease in fishing resulted in large changes in relative biomass in the medium term, characterized by impressive recovery for most of the exploited predatory FGs and decline of their preys (fish and invertebrates), in line with other similar exercises; however, these changes did not result in a new equilibrium of high biomasses for commercial species and the medium-term increases were not fully sustained in the long term, at least not for all benefitted species. Contrary, the more moderate (10%, FE10) decrease in fishing effort resulted in fewer fluctuations throughout the forecast period, but still with important gains for commercial species in terms of biomass and very small losses in catches in the long term. In addition, since for many FGs the reduction in effort is relatively proportional to the reduction in catches, a horizontal effort reduction might not be the best strategy; instead, targeted effort reduction in gears whose target species are more exploited, might yield the best results and is worth exploring in a management strategy evaluation framework. In a further step, taking into account species traits and permitting more effort for gears that exploit species that may be favored by new environmental conditions, could be a tool to mitigate ecosystem impacts under climate risk (Papapanagiotou et al., 2020).

DATA AVAILABILITY STATEMENT

The data analyzed in this study is subject to the following licenses/restrictions: all data can be found in freely available databases, except data for scientific surveys which are subject to restrictions and a specific request should be addressed to DG MARE and/or DCF National correspondents. Requests to access these datasets should be directed to https://datacollection.jrc.ec.europa.eu/.

AUTHOR CONTRIBUTIONS

KTs, SL, AM, MG, and SS designed the study. KTo, SK, MG, GP, and CF processed and provided data and contributed to the analysis. MS acquired funding and coordinated the project. KTs performed the analysis and wrote the first draft. All authors interpreted results, contributed to writing and/or editing and approved the final draft.

FUNDING

The current work was supported by the research project "ANATHALLOI - Development of management tools for marine and freshwater ecosystems" MIS 5002500, funded by Greece and the European Regional Development Fund under the Operational Program "Competitiveness, Entrepreneurship and Innovation, NSRF 2014–2020". Earlier versions of the models were developed under the projects "PERSEUS: Policy-oriented marine Environmental Research for the Southern European Seas" (European Commission's 7th Framework Research Program (FP7); Grant Agreement No. 287600), "DISCATCH: Pilot project Catch and discard composition including solutions for limitation and possible elimination of unwanted bycatches in trawl net fisheries in the Mediterranean" (DG MARE/2012/24-Lot 2 SI2.672370) and "MINOUW: Science, Technology and Society Initiative to minimize Unwanted Catches in European Fisheries" (European Commission's Horizon 2020 Research and Innovation Program; Grant Agreement No. 634495).

ACKNOWLEDGMENTS

Part of the data used in this work, were collected under Greece's Data Collection Framework (National Program for the Collection of Fisheries Data), funded by Greece (Ministry of Rural Development and Food, Directorate General of Fisheries) and the European Union. We also thank the three reviewers for their comments and suggestions that helped improve the manuscript.

SUPPLEMENTARY MATERIAL

The Supplementary Material for this article can be found online at: https://www.frontiersin.org/articles/10.3389/fmars.2022.919793/full#supplementary-material

REFERENCES

Adloff, F., Somot, S., Sevault, F., Jordà, G., Aznar, R., Déqué, M., et al. (2015). Mediterranean Sea Response to Climate Change in an Ensemble of Twenty First Century Scenarios. *Clim. Dyn.* 45, 2775–2802. doi: 10.1007/s00382-015-2507-3

Ahrens, R. N. M., Walters, C. J. and Christensen, V. (2012). Foraging Arena Theory. *Fish. Fisheries.* 13, 41–59. doi: 10.1111/j.1467-2979.2011.00432.x

Angilletta, M. J. (2006). Estimating and Comparing Thermal Performance Curves - ScienceDirect. *J. Thermal. Biol.* 31, 541–545. doi: 10.1016/j.jtherbio.2006.06.002

Araújo, J. N., Mackinson, S., Stanford, R. J., Sims, D. W., Southward, A. J., Hawkins, S. J., et al. (2006). Modelling Food Web Interactions, Variation in Plankton Production, and Fisheries in the Western English Channel Ecosystem. *Mar. Ecol. Prog. Ser.* 309, 175–187. doi: 10.3354/meps309175

Báez, J. C., Gimeno, L. and Real, R. (2021). North Atlantic Oscillation and Fisheries Management During Global Climate Change. *Rev. Fish. Biol. Fisheries.* 31, 319–336. doi: 10.1007/s11160-021-09645-z

Barange, M. (2019). Avoiding Misinterpretation of Climate Change Projections of Fish Catches. *ICES. J. Mar. Sci.* 76, 1390–1392. doi: 10.1093/icesjms/fsz061

Bellido, J. M., Sumaila, U. R., Sánchez-Lizaso, J. L., Palomares, M. L. and Pauly, D. (2020). Input Versus Output Controls as Instruments for Fisheries Management With a Focus on Mediterranean Fisheries. *Mar. Policy* 118, 103786. doi: 10.1016/j.marpol.2019.103786

Bentley, J. W., Serpetti, N. and Heymans, J. J. (2017). Investigating the Potential Impacts of Ocean Warming on the Norwegian and Barents Seas Ecosystem Using a Time-Dynamic Food-Web Model. *Ecol. Model.* 360, 94–107. doi: 10.1016/j.ecolmodel.2017.07.002

Bundy, A., Chuenpagdee, R., Boldt, J. L., de Fatima Borges, M., Camara, M. L., Coll, M., et al. (2017). Strong Fisheries Management and Governance Positively Impact Ecosystem Status. *Fish. Fisheries.* 18, 412–439. doi: 10.1111/faf.12184

Cardinale, M., Linder, M., Bartolino, V., Maiorano, L. and Casini, M. (2009). Conservation Value of Historical Data: Reconstructing Stock Dynamics of Turbot During the Last Century in the Kattegat-Skagerrak. *Mar. Ecol. Prog. Ser.* 386, 197–206. doi: 10.3354/meps08076

Celić, I., Libralato, S., Scarcella, G., Raicevich, S., Marčeta, B., Solidoro, C., et al. (2018). Ecological and Economic Effects of the Landing Obligation Evaluated Using a Quantitative Ecosystem Approach: A Mediterranean Case Study. *ICES. J. Mar. Sci.* 75, 1992–2003. doi: 10.1093/icesjms/fsy069

CERES (2018). "Deliverable D1.3. Projections of Physical and Biogeochemical Parameters and Habitat Indicators for European Seas, Including Synthesis of Sea Level Rise and Storminess," in *EU H2020 CERES Project. "Climate Change and European Aquatic RESources"*. Available at: https://ec.europa.eu/research/participants/documents/downloadPublic?documentIds=080166e5b9fdf8fb&appId=PPGMS.

Chefaoui, R. M., Duarte, C. M. and Serrão, E. A. (2018). Dramatic Loss of Seagrass Habitat Under Projected Climate Change in the Mediterranean Sea. *Global Change Biol.* 24, 4919–4928. doi: 10.1111/gcb.14401

Christensen, V. (2000). Indicators for Marine Ecosystems Affected by Fisheries. *Mar. Freshw. Res.* 51, 447–450. doi: 10.1071/mf99085

Christensen, V. and Walters, C. J. (2004). Ecopath With Ecosim: Methods, Capabilities and Limitations. *Ecol. Model.* 172, 109–139. doi: 10.1016/j.ecolmodel.2003.09.003

Christensen, V., Walters, C. J., Pauly, D. and Forrest, R. (2008). "Ecopath With Ecosim Version 6 User Guide," in *Lenfest Ocean Futures Project*, vol. 2008. .

Colléter, M., Valls, A., Guitton, J., Gascuel, D., Pauly, D. and Christensen, V. (2015). Global Overview of the Applications of the Ecopath With Ecosim Modeling Approach Using the EcoBase Models Repository. *Ecol. Model.* 302, 42–53. doi: 10.1016/j.ecolmodel.2015.01.025

Coll, M. and Libralato, S. (2012). Contributions of Food Web Modelling to the Ecosystem Approach to Marine Resource Management in the Mediterranean Sea. *Fish. Fisheries.* 13, 60–88. doi: 10.1111/j.1467-2979.2011.00420.x

Colloca, F., Mastrantonio, G., Lasinio, G. J., Ligas, A. and Sartor, P. (2014). Parapenaeus Longirostris (Lucas 1846) an Early Warning Indicator Species of Global Warming in the Central Mediterranean Sea. *J. Mar. Syst.* 138, 29–39. doi: 10.1016/j.jmarsys.2013.10.007

Colloca, F., Scarcella, G. and Libralato, S. (2017). Recent Trends and Impacts of Fisheries Exploitation on Mediterranean Stocks and Ecosystems. *Front. Mar. Sci.* 4. doi: 10.3389/fmars.2017.00244

Corrales, X., Coll, M., Ofir, E., Heymans, J. J., Steenbeek, J., Goren, M., et al. (2018). Future Scenarios of Marine Resources and Ecosystem Conditions in the Eastern Mediterranean Under the Impacts of Fishing, Alien Species and Sea Warming. *Sci. Rep.* 8, 14284. doi: 10.1038/s41598-018-32666-x

Corrales, X., Coll, M., Ofir, E., Piroddi, C., Goren, M., Edelist, D., et al. (2017). Hindcasting the Dynamics of an Eastern Mediterranean Marine Ecosystem Under the Impacts of Multiple Stressors. *Mar. Ecol. Prog. Ser.* 580, 17–36. doi: 10.3354/meps12271

Criado-Aldeanueva, F. and Soto-Navarro, J. (2020). Climatic Indices Over the Mediterranean Sea: A Review. *Appl. Sci.* 10, 5790. doi: 10.3390/app10175790

Damalas, D., Maravelias, C. D. and Kavadas, S. (2014). Advances in Fishing Power: A Study Spanning 50 Years. *Rev. Fisheries. Sci. Aquaculture.* 22, 112–121. doi: 10.1080/10641262.2013.839620

Damalas, D., Sgardeli, V., Vasilakopoulos, P., Tserpes, G. and Maravelias, C. (2021). Evidence of Climate-Driven Regime Shifts in the Aegean Sea's Demersal Resources: A Study Spanning Six Decades. *Ecol. Evol.* 11, 16951–16971. doi: 10.1002/ece3.8330

Dimarchopoulou, D., Tsagarakis, K., Sylaios, G. and Tsikliras, A. C. (2022). Ecosystem Trophic Structure and Fishing Effort Simulations of a Major Fishing Ground in the Northeastern Mediterranean Sea (Thermaikos Gulf). *Estuarine. Coast. Shelf. Sci.* 264, 107667. doi: 10.1016/j.ecss.2021.107667

Eigaard, O. R., Marchal, P., Gislason, H. and Rijnsdorp, A. D. (2014). Technological Development and Fisheries Management. *Rev. Fisheries. Sci. Aquaculture.* 22, 156–174. doi: 10.1080/23308249.2014.899557

ELSTAT (2021) *Quantity of Fish Landed by Fishing Area and Fishing Tools*. Available at: http://www.statistics.gr.

Eurostat (2021) *Fishing Fleet by Type of Gear and Engine Power*. Available at: https://ec.europa.eu/eurostat.

FAO (2020). *The State of Mediterranean and Black Sea Fisheries 2020* (Rome, Italy: FAO). doi: 10.4060/cb2429en

Farriols, M. T., Ordines, F., Carbonara, P., Casciaro, L., Lorenzo, M. D., Esteban, A., et al. (2019). Spatio-Temporal Trends in Diversity of Demersal Fish Assemblages in the Mediterranean. *Scientia. Marina.* 83, 189–206. doi: 10.3989/scimar.04977.13A

Fortibuoni, T., Giovanardi, O., Pranovi, F., Raicevich, S., Solidoro, C. and Libralato, S. (2017). Analysis of Long-Term Changes in a Mediterranean Marine Ecosystem Based on Fishery Landings. *Front. Mar. Sci.* 4. doi: 10.3389/fmars.2017.00033

Frangoulis, C., Grigoratou, M., Zoulias, T., Hannides, C. C. S., Pantazi, M., Psarra, S., et al. (2017). Expanding Zooplankton Standing Stock Estimation From Meso- to Metazooplankton: A Case Study in the N. Aegean Sea (Mediterranean Sea). *Continental. Shelf. Res.* 149, 151–161. doi: 10.1016/j.csr.2016.10.004

Gaines, S. D., Costello, C., Owashi, B., Mangin, T., Bone, J., Molinos, J. G., et al. (2018). Improved Fisheries Management Could Offset Many Negative Effects of Climate Change. *Sci. Adv.* 4, eaao1378. doi: 10.1126/sciadv.aao1378

Geary, W. L., Bode, M., Doherty, T. S., Fulton, E. A., Nimmo, D. G., Tulloch, A. I. T., et al. (2020). A Guide to Ecosystem Models and Their Environmental Applications. *Nat. Ecol. Evol.*, 4: 1459–1471. doi: 10.1038/s41559-020-01298-8

Giorgetta, M. A., Jungclaus, J., Reick, C. H., Legutke, S., Bader, J., Böttinger, M., et al. (2013). Climate and Carbon Cycle Changes From 1850 to 2100 in MPI-ESM Simulations for the Coupled Model Intercomparison Project Phase 5. *J. Adv. Modeling. Earth Syst.* 5, 572–597. doi: 10.1002/jame.20038

Giorgi, F. and Lionello, P. (2008). Climate Change Projections for the Mediterranean Region. *Global Planetary. Change* 63, 90–104. doi: 10.1016/j.gloplacha.2007.09.005

Gkanasos, A., Schismenou, E., Tsiaras, K., Somarakis, S., Giannoulaki, M., Sofianos, S., et al. (2021). A Three Dimensional, Full Life Cycle, Anchovy and Sardine Model for the North Aegean Sea (Eastern Mediterranean): Validation, Sensitivity and Climatic Scenario Simulations. *Mediterr. Mar. Sci.* 22, 653–668. doi: 10.12681/mms.27407

Heymans, J. J., Coll, M., Link, J. S., Mackinson, S., Steenbeek, J., Walters, C., et al. (2016). Best Practice in Ecopath With Ecosim Food-Web Models for Ecosystem-Based Management. *Ecol. Model.* 331, 173–184. doi: 10.1016/j.ecolmodel.2015.12.007

Hidalgo, M., Mihneva, V., Vasconcellos, M. and Bernal, M. (2018). "Climate Change Impacts, Vulnerabilities and Adaptations: Mediterranean Sea and the Black Sea Marine Fisheries," in *Impacts of Climate Change on Fisheries and Aquaculture FAO Fisheries and Aquaculture Technical Paper (FAO)* Rome, Italy, vol. 139. (FAO).

Holsman, K. K., Haynie, A. C., Hollowed, A. B., Reum, J. C. P., Aydin, K., Hermann, A. J., et al. (2020). Ecosystem-Based Fisheries Management Forestalls Climate-Driven Collapse. *Nat. Commun.* 11, 4579. doi: 10.1038/s41467-020-18300-3

ICES (2000) *Report of the Working Group on Seabird Ecology*. Available at: http://www.ices.dk/reports/occ/2000/.

Innes, S., Lavigne, D. M., Earle, W. M. and Kovacs, K. M. (1987). Feeding Rates of Seals and Whales. *J. Anim. Ecol.* 56, 115–130. doi: 10.2307/4803

Kaschner, K., Kesner-Reyes, K., Garilao, C., Segschneider, J., Rius-Barile, J., Rees, T., et al (2021). AquaMaps: Predicted Range Maps for Aquatic Species. *Aquamaps.*

Katara, I., Pierce, G., Illian, J. and Scott, B. (2011). Environmental Drivers of the Anchovy/Sardine Complex in the Eastern Mediterranean. *Hydrobiologia* 670, 49–65. doi: 10.1007/s10750-011-0693-5

Kavadas, S., Damalas, D., Georgakarakos, C., Maravelias, C. D., Tserpes, G., Papaconstantinou, C., et al. (2013). IMAS-Fish: Integrated Management System to Support the Sustainability of Greek Fishery Resources. A Multidisciplinary Web-Based Database Management System: Implementation, Capabilities, Utilization and Future Prospects for Fisheries Stakeholders. *Mediterr. Mar. Sci.* 14, 109–118. doi: 10.12681/mms.324

Labropoulou, M. and Papaconstantinou, C. (2000). Community Structure of Deep-Sea Demersal Fish in the North Aegean Sea (Northeastern Mediterranean). *Hydrobiologia* 440, 281–296. doi: 10.1023/a:1004199917299

Labropoulou, M. and Papaconstantinou, C. (2004). Community Structure and Diversity of Demersal Fish Assemblages: The Role of Fishery. *Scientia. Marina.* 68, 215–226. doi: 10.3989/scimar.2004.68s1215

Larkin, P. A. (1996). Concepts and Issues in Marine Ecosystem Management. *Rev. Fish. Biol. Fisheries.* 6, 139–164. doi: 10.1007/BF00182341

Lazzari, P., Mattia, G., Solidoro, C., Salon, S., Crise, A., Zavatarelli, M., et al. (2014). The Impacts of Climate Change and Environmental Management Policies on the Trophic Regimes in the Mediterranean Sea: Scenario Analyses. *J. Mar. Syst.* 135, 137–149. doi: 10.1016/j.jmarsys.2013.06.005

Leonori, I., Tičina, V., Giannoulaki, M., Hattab, T., Iglesias, M., Bonanno, A., et al. (2021). The History of Hydroacoustic Surveys on Small Pelagic Fishes in the European Mediterranean Sea. *Mediterr. Mar. Sci.* 22, 751–768. doi: 10.12681/mms.26001

Libralato, S., Caccin, A. and Pranovi, F. (2015). Modelling Species Invasions Using Thermal and Trophic Niche Dynamics Under Climate Change. *Front. Mar. Sci.* 2. doi: 10.3389/fmars.2015.00029

Link, J. S. (2002). Ecological Considerations in Fisheries Management: When Does it Matter? *Fisheries* 27, 10–17. doi: 10.1577/1548-8446(2002)027<0010:ECIFM>2.0.CO;2

Link, J. (2010a). *Ecosystem-Based Fisheries Management: Confronting Tradeoffs* (Cambridge: Cambridge University Press). doi: 10.1017/CBO9780511667091

Link, J. S. (2010b). Adding Rigor to Ecological Network Models by Evaluating a Set of Pre-Balance Diagnostics: A Plea for PREBAL. *Ecol. Model.* 221, 1580–1591. doi: 10.1016/j.ecolmodel.2010.03.012

Lockerbie, E., Shannon, L., Lynam, C., Coll, M. and Jarre, A. (2020). A Comparative Framework to Support an Ecosystem Approach to Fisheries in a Global Context. *Ecol. Soc.* 25. doi: 10.5751/ES-11508-250216

Lucchetti, A., Virgili, M., Vasapollo, C., Petetta, A., Bargione, G., Veli, D. L., et al. (2021). An Overview of Bottom Trawl Selectivity in the Mediterranean Sea. *Mediterr. Mar. Sci.* 22, 566–585. doi: 10.12681/mms.26969

Macias, D. M., Garcia-Gorriz, E. and Stips, A. (2015)Productivity Changes in the Mediterranean Sea for the Twenty-First Century in Response to Changes in the Regional Atmospheric Forcing (Accessed February 12, 2022).

Melnychuk, M. C., Kurota, H., Mace, P. M., Pons, M., Minto, C., Osio, G. C., et al. (2021). Identifying Management Actions That Promote Sustainable Fisheries. *Nat. Sustainability.* 4, 440–449. doi: 10.1038/s41893-020-00668-1

Moullec, F., Barrier, N., Drira, S., Guilhaumon, F., Marsaleix, P., Somot, S., et al. (2019). An End-To-End Model Reveals Losers and Winners in a Warming Mediterranean Sea. *Front. Mar. Sci.* 6. doi: 10.3389/fmars.2019.00345

Moutopoulos, D. K., Libralato, S., Solidoro, C., Erzini, K. and Stergiou, K. (2014). Effect of Landings Data Disaggregation on Ecological Indicators. *Mar. Ecol. Prog. Ser.* 509, 27–38. doi: 10.3354/meps10856

Nikolioudakis, N., Isari, S., Pitta, P. and Somarakis, S. (2012). Diet of Sardine Sardina Pilchardus: An 'End-to-End' Field Study. *Mar. Ecol. Prog. Ser.* 453, 173–188. doi: 10.3354/meps09656

Nikolioudakis, N., Isari, S. and Somarakis, S. (2014). Trophodynamics of Anchovy in a non-Upwelling System: Direct Comparison With Sardine. *Mar. Ecol. Prog. Ser.* 500, 215–229. doi: 10.3354/meps10604

Papantoniou, G., Giannoulaki, M., Stoumboudi, M., Lefkaditou, E. and Tsagarakis, K. (2021). Food Web Interactions in a Human Dominated Mediterranean Coastal Ecosystem. *Mar. Environ. Res.* 172, 105507. doi: 10.1016/j.marenvres.2021.105507

Papapanagiotou, G., Tsagarakis, K., Koutsidi, M. and Tzanatos, E. (2020). Using Traits to Build and Explain an Ecosystem Model: Ecopath With Ecosim Modelling of the North Aegean Sea (Eastern Mediterranean). *Estuarine. Coast. Shelf. Sci.* 236, 106614. doi: 10.1016/j.ecss.2020.106614

Pauly, D. (1980). On the Interrelationships Between Natural Mortality, Growth Parameters, and Mean Environmental Temperature in 175 Fish Stocks. *J. du. Conseil. Conseil. Int. pour. l'Exploration. la. Mer.* 39, 175–192. doi: 10.1093/icesjms/39.2.175

Pauly, D., Christensen, V. and Sambilay, V. (1990). *Some Features of Fish Food Consumption Estimates Used by Ecosystem Modellers*.

Piroddi, C., Coll, M., Liquete, C., Macias, D., Greer, K., Buszowski, J., et al. (2017). Historical Changes of the Mediterranean Sea Ecosystem: Modelling the Role and Impact of Primary Productivity and Fisheries Changes Over Time. *Sci. Rep.* 7, 44491. doi: 10.1038/srep44491

Pitcher, T. J., Kalikoski, D., Short, K., Varkey, D. and Pramod, G. (2009). An Evaluation of Progress in Implementing Ecosystem-Based Management of Fisheries in 33 Countries. *Mar. Policy* 33, 223–232. doi: 10.1016/j.marpol.2008.06.002

Reale, M., Salon, S., Somot, S., Solidoro, C., Giorgi, F., Crise, A., et al. (2020). Influence of Large-Scale Atmospheric Circulation Patterns on Nutrient Dynamics in the Mediterranean Sea in the Extended Winter Season (October-March) 1961-1999. *Climate Res.* 82, 117–136. doi: 10.3354/cr01620

Richon, C., Dutay, J.-C., Bopp, L., Le Vu, B., Orr, J. C., Somot, S., et al. (2019). Biogeochemical Response of the Mediterranean Sea to the Transient SRES-A2 Climate Change Scenario. *Biogeosciences* 16, 135–165. doi: 10.5194/bg-16-135-2019

Sartor, P., Sbrana, M., Chato Osio, G., Ligas, A., Reale, B., Colloca, F., et al. (2011). *The 20th Century Evolution of Mediterranean Exploited Demersal Resources Under Increasing Fishing Disturbance and Environmental Change, EVOMED*.

Scott, E., Serpetti, N., Steenbeek, J. and Heymans, J. J. (2016). A Stepwise Fitting Procedure for Automated Fitting of Ecopath With Ecosim Models. *SoftwareX* 5, 25–30. doi: 10.1016/j.softx.2016.02.002

Serpetti, N., Baudron, A. R., Burrows, M. T., Payne, B. L., Helaouët, P., Fernandes, P. G., et al. (2017). Impact of Ocean Warming on Sustainable Fisheries Management Informs the Ecosystem Approach to Fisheries. *Sci. Rep.* 7, 13438. doi: 10.1038/s41598-017-13220-7

Skliris, N., Sofianos, S. S., Gkanasos, A., Axaopoulos, P., Mantziafou, A. and Vervatis, V. (2011). Long-Term Sea Surface Temperature Variability in the Aegean Sea. *Adv. Oceanography. Limnology.* 2, 125–139. doi: 10.1080/19475721.2011.601325

Smith, A. D. M. and Garcia, S. M. (2014). Fishery Management: Contrasts in the Mediterranean and the Atlantic. *Curr. Biol.* 24, R810–R812. doi: 10.1016/j.cub.2014.07.031

Spedicato, M. T., Massutí, E., Mérigot, B., Tserpes, G., Jadaud, A. and Relini, G. (2019). The MEDITS Trawl Survey Specifications in an Ecosystem Approach to Fishery Management. *Scientia. Marina.* 83, 9–20. doi: 10.3989/scimar.04915.11X

Steenbeek, J., Corrales, X., Platts, M. and Coll, M. (2018). Ecosampler: A New Approach to Assessing Parameter Uncertainty in Ecopath With Ecosim. *SoftwareX* 7, 198–204. doi: 10.1016/j.softx.2018.06.004

Stergiou, K. I., Somarakis, S., Triantafyllou, G., Tsiaras, K. P., Giannoulaki, M., Petihakis, G., et al. (2016). Trends in Productivity and Biomass Yields in the Mediterranean Sea Large Marine Ecosystem During Climate Change. *Environ. Dev.* 17, 57–74. doi: 10.1016/j.envdev.2015.09.001

Tittensor, D. P., Novaglio, C., Harrison, C. S., Heneghan, R. F., Barrier, N., Bianchi, D., et al. (2021). Next-Generation Ensemble Projections Reveal Higher Climate Risks for Marine Ecosystems. *Nat. Clim. Change* 11, 973–981. doi: 10.1038/s41558-021-01173-9

Trenberth, K. and Zhang, R.National Center for Atmospheric Research Staff (2019) *The Climate Data Guide: Atlantic Multi-Decadal Oscillation (AMO)*. Available at: https://climatedataguide.ucar.edu/climate-data/atlantic-multi-decadal-oscillation-amo.

Trites, A. W., Christensen, V. and Pauly, D. (1997). Competition Between Fisheries and Marine Mammals for Prey and Primary Production in the Pacific. *J. Northwest. Atlantic. Fishery. Sci.* 22, 173–187. doi: 10.2960/J.v22.a14

Trochta, J. T., Pons, M., Rudd, M. B., Krigbaum, M., Tanz, A. and Hilborn, R. (2018). Ecosystem-Based Fisheries Management: Perception on Definitions, Implementations, and Aspirations. *PLoS One* 13, e0190467. doi: 10.1371/journal.pone.0190467

Tsagarakis, K., Carbonell, A., Brčić, J., Bellido, J., Carbonara, P., Casciaro, L., et al. (2017). Old Info for a New Fisheries Policy: Discard Ratios and Lengths at Discarding in EU Mediterranean Bottom Trawl Fisheries. *Front. Mar. Sci.* 4. doi: 10.3389/fmars.2017.00099

Tsagarakis, K., Coll, M., Giannoulaki, M., Somarakis, S., Papaconstantinou, C. and Machias, A. (2010). Food-Web Traits of the North Aegean Sea Ecosystem (Eastern Mediterranean) and Comparison With Other Mediterranean Ecosystems. *Estuarine. Coast. Shelf. Sci.* 88, 233–248. doi: 10.1016/j.ecss.2010.04.007

Tsagarakis, K., Giannoulaki, M., Pyrounaki, M. M. and Machias, A. (2015). Species Identification of Small Pelagic Fish Schools by Means of Hydroacoustics in the Eastern Mediterranean Sea. *Mediterr. Mar. Sci.* 16, 151–161. doi: 10.12681/mms.799

Tsagarakis, K., Panigada, S., Machias, A., Giannoulaki, M., Foutsi, A., Pierantonio, N., et al. (2021). Trophic Interactions in the "Small Pelagic Fish - Dolphins – Fisheries" Triangle: Outputs of a Modelling Approach in the North Aegean Sea (Eastern Mediterranean, Greece). *Ocean. Coast. Manage.* 105474. doi: 10.1016/j.ocecoaman.2020.105474

Tsagarakis, K., Vassilopoulou, V., Kallianiotis, A. and Machias, A. (2012). Discards of the Purse Seine Fishery Targeting Small Pelagic Fish in the Eastern Mediterranean Sea. *Scientia. Marina.* 76, 561–572. doi: 10.3989/scimar.03452.02B

Tserpes, G., Massutí, E., Fiorentino, F., Facchini, M. T., Viva, C., Jadaud, A., et al. (2019). Distribution and Spatio-Temporal Biomass Trends of Red Mullets Across the Mediterranean. *Scientia. Marina.* 83, 43–55. doi: 10.3989/scimar.04888.21A

Tsikliras, A. C., Licandro, P., Pardalou, A., McQuinn, I. H., Gröger, J. P. and Alheit, J. (2019). Synchronization of Mediterranean Pelagic Fish Populations With the North Atlantic Climate Variability. *Deep. Sea. Res. Part II.: Topical. Stud. Oceanography.* 159, 143–151. doi: 10.1016/j.dsr2.2018.07.005

Tsikliras, A. C., Peristeraki, P., Tserpes, G. and Stergiou, K. I. (2015). Mean Temperature of the Catch (MTC) in the Greek Seas Based on Landings and Survey Data. *Front. Mar. Sci.* 2. doi: 10.3389/fmars.2015.00023

Tsikliras, A. C., Tsiros, V. Z. and Stergiou, K. I. (2013). Assessing the State of Greek Marine Fisheries Resources. *Fisheries. Manage. Ecol.* 20, 34–41. doi: 10.1111/j.1365-2400.2012.00863.x

Tsimara, E., Vasilakopoulos, P., Koutsidi, M., Raitsos, D. E., Lazaris, A. and Tzanatos, E. (2021). An Integrated Traits Resilience Assessment of Mediterranean Fisheries Landings. *J. Anim. Ecol.* 90, 2122–2134. doi: 10.1111/1365-2656.13533

Tzanatos, E., Raitsos, D., Triantafyllou, G., Somarakis, S. and Tsonis, A. (2014). Indications of a Climate Effect on Mediterranean Fisheries. *Climatic. Change* 122, 41–54. doi: 10.1007/s10584-013-0972-4

Vasilakopoulos, P., Jardim, E., Konrad, C., Rihan, D., Mannini, A., Pinto, C., et al. (2020). Selectivity Metrics for Fisheries Management and Advice. *Fish. Fisheries.* 21, 621–638. doi: 10.1111/faf.12451

Vasilakopoulos, P., Maravelias, C. D. and Tserpes, G. (2014). The Alarming Decline of Mediterranean Fish Stocks. *Curr. Biol.* 24, 1643–1648. doi: 10.1016/j.cub.2014.05.070

Conflict of Interest: The authors declare that the research was conducted in the absence of any commercial or financial relationships that could be construed as a potential conflict of interest.

Publisher's Note: All claims expressed in this article are solely those of the authors and do not necessarily represent those of their affiliated organizations, or those of the publisher, the editors and the reviewers. Any product that may be evaluated in this article, or claim that may be made by its manufacturer, is not guaranteed or endorsed by the publisher.

frontiers | Frontiers in Marine Science

TYPE Original Research
PUBLISHED 27 July 2022
DOI 10.3389/fmars.2022.958924

OPEN ACCESS

EDITED BY
Tomaso Fortibuoni,
Istituto Superiore per la Protezione e la Ricerca Ambientale (ISPRA), Italy

REVIEWED BY
Dimitris Velaoras,
Hellenic Centre for Marine Research (HCMR), Greece
Milena Menna,
Istituto Nazionale di Oceanografia e di Geofisica Sperimentale, Italy
Maurizio AZZARO di Rosamarina,
National Research Council (CNR), Italy

*CORRESPONDENCE
T. Ozer
tal@ocean.org.il
B. Herut
barak@ocean.org.il

SPECIALTY SECTION
This article was submitted to Marine Fisheries, Aquaculture and Living Resources, a section of the journal Frontiers in Marine Science

RECEIVED 01 June 2022
ACCEPTED 29 June 2022
PUBLISHED 27 July 2022

CITATION
Ozer T, Rahav E, Gertman I, Sisma-Ventura G, Silverman J and Herut B (2022) Relationship between thermohaline and biochemical patterns in the levantine upper and intermediate water masses, Southeastern Mediterranean Sea (2013–2021).
Front. Mar. Sci. 9:958924.
doi: 10.3389/fmars.2022.958924

Relationship between thermohaline and biochemical patterns in the levantine upper and intermediate water masses, Southeastern Mediterranean Sea (2013–2021)

T. Ozer*, E. Rahav, I. Gertman, G. Sisma-Ventura, J. Silverman and B. Herut*

Israel Oceanographic and Limnological Research, National Institute of Oceanography, Haifa, Israel

The relationships between the interannual variations of the Levantine intermediate water (LIW) core properties and the corresponding biochemical variations in the euphotic zone were systematically studied in the Southeastern Mediterranean during 2013–2021 and since 2002 based on a previous study. Salinity and temperature interannual fluctuations in the LIW continue to follow the Adriatic–Ionian Bimodal Oscillating System (BiOS) mechanism, with salinity and temperature peaks in the years 2008–2010, 2014–2015, and 2018–2019 coinciding with periods of anticyclonic circulation of the North Ionian Gyre (NIG). During these anticyclonic periods, the transport of Atlantic Water into the Levant is reduced together with the transport of LIW out of the basin. These interannual fluctuations are superimposed on a long-term warming trend clearly evident from previous studies, showing a maximal temperature in 2018–2019, higher than the previously mentioned temperature peaks by ~0.7°C and ~0.4°C. The enhanced warming in 2018–2019 has caused a decrease in density (sigma) values of the LIW core, which gave way to the shallowest record of this water mass (~110-m depth), bringing it well within the lower photic zone. We suggest that a higher level of nutrients became available, supporting the observed long-term rise of the intergraded chlorophyll *a* (Chl.*a*) (0.89 mg m^{-2} $year^{-1}$), with a maximum recorded during 2018–2019. The long-term record of the mixed layer depths shows no significant change; thus, the uplift of nutrients during winter mixing cannot support the trend and variations of the integrated Chl.*a*. Additional biological parameters of specific pico-phytoplankton populations and integrated bacterial production and abundance were measured in 2013–2021, but the measurements were too sparse to follow a clear interannual dynamics. Yet significantly higher average

levels for integrated primary production and bacterial abundances were observed during the anticyclonic period (as for Chl*a*). The combined impacts of the BiOS mechanism and global warming, and hence the increase in LIW residence time and buoyancy, may impact the primary producers' biomass at the photic zone. This latter feedback may slightly counter the enhanced oligotrophication due to enhanced stratification.

KEYWORDS

Mediterranean Sea, thermohaline, water masses, Levantine, biochemical, nutrients, chlorophyll, phytoplankton

Introduction

The Mediterranean Sea (MS) is dominated by an anti-estuarine thermohaline circulation driven by the salinity differences between the inflowing low-salinity Atlantic Water (AW) and mainly the outflowing highly saline Levantine intermediate water (LIW). The basin-scale circulation is broadly described in terms of a surface flow of AW from the Atlantic Ocean entering through the Strait of Gibraltar and proceeding to the eastern basin through the Strait of Sicily, and a return flow of LIW, originating in the Levantine Basin (LB), proceeding toward Strait of Gibraltar and finally exiting into the Atlantic (Tanhua et al., 2013; Malanotte-Rizzoli et al., 2014 and references therein).

Following early works on the surface circulation in the Eastern Mediterranean Sea (EMS) (Nielsen, 1912; Wust, 1961; Ovchinnikov, 1966; Bethoux, 1980), the observations achieved in the framework of the Physical oceanography of the Eastern Mediterranean (POEM) program (Malanotte-Rizzoli and Hecht, 1988) provided an important stepping stone in the understanding of the EMS circulation and yielded many studies elucidating on basin-scale circulation and sub-basin scale and mesoscale circulation patterns (Robinson et al., 1991; Ozsoy et al., 1991; POEM Group, 1992; Malanotte-Rizzoli et al., 1997). The resulting updated comprehensive description was of a set of sub-basin gyres connected by a system of jet currents (Robinson et al., 1991; Robinson and Golnaraghi, 1993). The AW coming into the EMS through the Sicily Channel follows an anticyclonic path through the southern Ionian, continuing thereon toward the Levantine to form the Mid-Mediterranean Jet, which flows from southwest to northeast in the center of the basin and joins the Asia Minor Current (Malanotte-Rizzoli et al., 1997). Later publications affirmed the previously described along-slope basin-wide circulation and gave attention to the unstable nature of the southern along-slope current developing anticyclonic eddies, which disperse part of the AW northward (Millot and Taupier-Letage, 2005; Hamad et al., 2006). In recent years, a surface circulation scheme accommodating both the along-slope cyclonic circulation (as in Millot and Taupier-Letage, 2005) and the Mid Mediterranean Jet of Robinson and Golnaraghi (1993) was demonstrated for the EMS using drifter and altimetry data (Menna et al., 2012; Menna et al., 2020). Based on a high-resolution simulation for the period of 2011 to 2020, Estournel et al. (2021) described seasonal variations of the cyclonic, along-slope current as being stronger and more stable in winter, while in summer, it tends to be interrupted, and the continuity of the circulation is maintained by a train of eddies.

LIW formation occurs mainly in the Rhodes Gyre area (Lascaratos and Nittis, 1998; Lascaratos et al., 1999), yet compelling evidence is given to additional formation sources along the Turkish and Israeli coasts (Kubin et al., 2019; Fach et al., 2021), as well as the entire basin (Lascaratos et al., 1993; Ozsoy et al., 1993). An additional established source of intermediate water in the EMS is the South Aegean Sea producing the Cretan Intermediate water (CIW) (Georgopoulos et al., 1989; Schlitzer et al., 1991; Velaoras et al., 2014; Velaoras et al., 2019). LIW generally flows westward spreading from the Levantine Basin to the Ionian Basin (IB) and then through the Sicily Channel into the Western Basin, eventually exiting the MS through the Strait of Gibraltar below the AW layer (Lascaratos et al., 1999; Tanhua et al., 2013; Malanotte-Rizzoli et al., 2014). The pathways of LIW within the EMS have high variability but can be generally described as follows. LIW flow along the coast south of Crete, with part of the LIW flowing through the straits of the eastern Cretan Arc at intermediate depths into South Aegean to exit with the CIW through the western straits. The LIW flows in the Ionian bifurcates, one track circulating in the Ionian and the other headed toward the Sicily Channel (Malanotte-Rizzoli et al., 1999; Millot and Taupier-Letage, 2005). An additional important feature of the LIW flow feeds the Southern Adriatic Sea, introducing high-salinity masses into the Adriatic, and is considered to be a preconditioning factor for the formation of Adriatic Dense Water (Gacic et al., 2010; Gacic et al., 2011;

Schroeder et al., 2012). Seasonality in the LIW flow regime was recently presented (Pinardi et al., 2019; Lyubartsev et al., 2020; Estournel et al., 2021; Menna et al., 2021) as well as their water mass properties in the East Mediterranean (Gacic and Bensi, 2020; Fedele et al., 2022 and references therein; Hayes et al., 2019). Estournel et al. (2021) outline the rim current of the Rhodes Gyre dispersing the LIW throughout the eastern Levantine in winter, while in summer, anticyclonic circulation that occupies the southeast of the basin redistributes LIW toward the south of the Levant. This LIW circulation of relatively high salinity and nutrient levels plays an important role in the deep-water formation in both the eastern and western basins (Robinson et al., 2001; Schneider et al., 2014) and the biogeochemistry of the MS (Malanotte-Rizzoli et al., 2014; Powley et al., 2014).

The LB is significantly influenced by the water exchange with the IB *via* the Cretan passage. The Adriatic–Ionian Bimodal Oscillating System (BiOS), thoroughly described in Gacic et al., 2011; Gacic et al. (2010 and experimentally by Rubino et al. (2020), controls the trajectory of the AW flow after passing through the Sicily Straits to both the Southern Adriatic (SA) and the LB, which correspond to quasi-decadal reversals in the North Ionian Gyre (NIG). The BiOS mechanism has been shown to have a significant effect on the physical and chemical dynamics in the SA (Civitarese et al., 2010; Gacic et al., 2010; Lavigne et al., 2018; Mihanovic et al., 2020; Menna et al., 2022; Placenti et al., 2022) as well as in the LB (Ozer et al., 2017). These studies proposed that the BiOS mechanism is a feedback mechanism between changes in the thermohaline structure of SA waters and the IB. In periods of cyclonic NIG, high-salinity LIW is injected into the SA, while the transport of AW is diverted to the LB. This results in buoyancy loss in the SA, which is thought to be a preconditioning factor for the formation of Adriatic Dense Water (Gacic et al., 2010; Gacic et al., 2011). During the anticyclonic NIG, AW intrusion into the Ionian and Adriatic Basins increases at the expense of the LB, and the formation of Adriatic Dense water is minimized. In accordance with these variations, Gacic et al. (2011) showed that during cyclonic NIG, surface salinity in the SA and IB increases and co-varies with nitrate levels in both the SA and IB in opposite phases (Civitarese et al., 2010). Ozer et al. (2017) described the magnitude of the long-term and superimposed thermohaline interannual variations and corresponding changes in nutrient and chlorophyll *a* (Chl.*a*) levels in the upper water masses of the LB (LSW and LIW), attributing them to the long-term climate change and the interannual BiOS mechanism, respectively.

The variability in physical and biogeochemical properties observed in the Mediterranean through the last few decades (Malanotte-Rizzoli et al., 2014; Von Schuckmann et al., 2020) calls for more systematic monitoring of this basin. Here we explore the relationships between the interannual variations of the LIW thermohaline properties and its vertical position with the corresponding biochemical variations in the euphotic zone (e.g., integrated nutrients, alkalinity, dissolved oxygen, Chl.*a*, picoplankton populations, and primary and bacterial production) at the Southeastern Mediterranean Sea. For this purpose, we make use of data collected in three deep-water stations (1,100–1,600 m) in the eastern LB, which was visited two to three times annually. The thermohaline and Chl.*a* datasets represent ~20 years (2002–2021), while the additional biological data represent the last 9 years (2013–2021). We use Mediterranean Sea Physical Reanalysis data (Escudier et al., 2020; https://doi.org/10.25423/CMCC/MEDSEA_MULTIYEAR_PHY_006_004_E3R1) to examine the relationship of our findings to variations of the mixed layer depths (MLDs) and the volume of AW in the southeastern MS. Recent results (Fedele et al., 2022; Menna et al., 2022) support the advantage of using LIW to describe the long-term warming and salinization and the interannual BiOS mechanism, which is less sensitive to the seasonal cycle but is yet shallow enough to reflect surface layer and photic zone dynamics.

Materials and methods

Sampling/cruise data

The presented data are composed mostly of new 17 Haifa Section (HaiSec) cruises extending 90 km to the northwest of the Carmel Headland, northern Israel, which were conducted during the period 2013–2021, including only deep stations H04, H05, and H06 (>1,000-m water depth) (Figure 1). Additional data from previous years (since 2002) at the same stations are included (Ozer et al., 2017), as well as 10 CTD casts at station H05. All surveys were carried out by the Israel Oceanographic and Limnological Research Institute (IOLR). The cruises were conducted aboard the *R/V Shikmona* until 2015 and since 2016 aboard the new Israeli *R/V Bat-Galim*. A Sea-Bird SBE911plus CTD system, interfaced to an SBE Carousel, was used to collect continuous profiles (24 Hz) of pressure, temperature, salinity, dissolved oxygen, and fluorescence. The manufacturer reported that the precision of the SBE911plus CTD is ±0.0025 for salinity (inferred from the ±0.0003 S/m conductivity precision) and ±0.001°C for temperature. Throughout the period covered by this dataset, the pressure, conductivity, and temperature sensors were calibrated by the manufacturer periodically every 2 years (as described in Ozer et al., 2020). CTD data were processed using the Sea-Bird data processing software following the manufacturer's recommendations. The CTD data validation procedure included lowering an additional autonomous SBE19/SBE19plus CTD (factory calibrated within the last year) parallel to the onboard SBE9plus in order to obtain duplicate casts, ensuring that any non-conformities remained within the sensors' precision. Samples of dissolved oxygen and Chl.*a* (described below) were used to calibrate the dissolved oxygen profiles from the CTD.

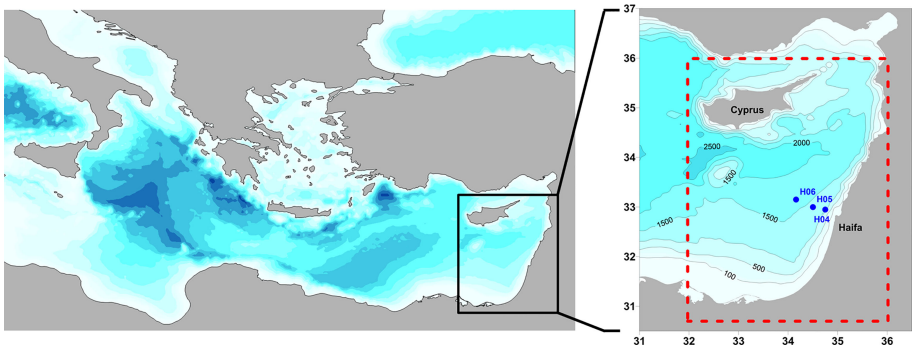

FIGURE 1
Map of hydrographic stations visited during the IOLR Haifa Section deep stations (blue dots, performed biannually). Station H05 was additionally visited in 10 cruises. Domain of CMEMS physical reanalysis used for MLD, and AW volume estimate is marked by the dotted red rectangle. IOLR, Israel Oceanographic and Limnological Research Institute; CMEMS, Copernicus Monitoring Environment Marine Service; MLD, mixed layer depth; AW, Atlantic Water.

Atlantic water volume and mixed layer depth variability

The products of monthly salinity, potential temperature, and MLD from the MS physical reanalysis provided by the E.U. Copernicus Monitoring Environment Marine Service (CMEMS) (Escudier et al., 2020) were obtained for the southeastern MS (30.7° to 36°N and 32° to 36.2°E, Figure 1) for the period of January 2002 to May 2020. The reanalysis data had a horizontal grid resolution of 1/24° (ca. 4–5 km) and 141 unequally spaced vertical levels. The MLD data were averaged over the complete domain in order to eliminate the sensitivity of the data to mesoscale activity and attain a general estimate for this part of the basin.

In order to quantify the volume of AW, we performed a volumetric statistical analysis (VSA) introduced by Cochrane (1958); Montgomery (1958), and Pollak (1958) and more recently used for the Aegean by Gertman et al. (2006). This approach is based on assigning temperature (>15°C) and salinity (<38.9) ranges, which are considered to be characteristic of AW. For each time step of the reanalysis model, the volume occupied by AW (where thermohalines values match those of AW characteristics) is summed up over the entire domain, and its percentage of the domain is calculated. In order to achieve this, we first calculated the volume (in m^3) of each data point, considering the spatial and vertical distribution of the data, as follows:

$$V_{lat,lon,z} = dlat \star dlon \star \left| Z_{(i+1)} - Z_{(i-1)} \right| \ / \ 2$$

where V is the volume of a specific grid point in m^3; *dlat* and *dlon* are the constant latitude and longitude distances of 4,620, and 4,010 m, respectively; Z is the depth level in meters. Next, a matrix of potential temperature and salinity (θ–S space) was created with the ranges of 13°C to 30°C with a 0.1°C interval for temperature and 37.8 to 39.5 with a 0.01 interval for salinity, representing the complete range of thermohaline values found in the dataset. The reanalysis data were then filtered through, and the volume of each data point was accumulated in the relevant θ–S space position, based on its rounded temperature and salinity values. For the evaluation of the total AW volume in the domain, we summed up all the matrix cells with temperatures above 15°C and salinities below 38.9, and finally, we calculated the percentage of the domain volume occupied by AW for each time step (i.e., month). The choice of these threshold values can be contested, mainly for salinity, thus changing the total volumes achieved through this method. For this reason, several iterations, with the salinity limit ranging from 38.85 to 39.95 (with 0.01 interval), were tested and gave similar trends (not presented). Thus, we considered these results to be a strong proxy for the overall volume of AW in the Levant basin, so that the variability is well presented, not the absolute volume values.

Levantine intermediate water and photic zone investigation

In order to minimize the effects of mesoscale phenomena on our analysis, we only examined the core values of LIW, which are less affected by diapycnal mixing and more controlled by isopycnal processes. The vertical position of the LIW core was identified by finding the maximal salinity value of each cast within the depth range of intermediate water (100 and 350 m; Ozer et al., 2017). Subsequently, the physical and chemical data of the LIW core depth were averaged for all the stations of each cruise, and finally, the resultant time series was smoothed, using a moving average with a time window of 1 year. Additionally, the contemporaneous biological parameters were integrated over the photic zone (0–200 m) using water column sampling and

analyses, while the Chl.*a* profiles and integrated values were obtained from the calibrated CTD fluorescence measurements.

Dissolved oxygen, alkalinity, and inorganic nutrients analysis

Water samples for dissolved oxygen and inorganic nutrients were collected at sampling depths based on the thermohaline structure of the water column, representing the different water masses. Water samples for dissolved oxygen were sampled and measured in duplicates onboard immediately after sampling following the modified Winkler method (Carpenter–Winkler titration procedure Carpenter, 1965), using an automated Metrohm Titrando 905 titration system. Duplicate samples for nutrient analysis were collected in 15-ml acid-washed plastic scintillation vials and immediately frozen.

Total alkalinity (TA) was measured by potentiometric titration with a Metrohm, 848 Titrino plus system using the Gran method to calculate it from acid volumes and corresponding pH measurements between pH 3.3 and 3.8 (Ben-Yaakov and Sass, 1977). The titration acid was 0.05 M of HCl, which was verified and adjusted using certified reference seawater supplied by the Certified Reference Materials Laboratory, Scripps Institution of Oceanography, CA (Dickson et al., 2003). Duplicate measurements were made for each sample, and the precision error was ±1 μmol kg^{-1}.

Nutrients were measured with a Seal Analytical AA-3 system (Sisma-Ventura et al., 2022). The limits of detection (LODs), estimated as three times the standard deviation of 10 measurements of the blank (low nutrient aged seawater collected from the off-shore surface at the Levantine Basin) for PO_4, $Si(OH)_4$, NO_2+NO_3 (NO_x), and NH_4, were 8, 80, 80, and 90 nM, respectively. The reproducibility of the analyses was determined using certified reference materials (CRMs): MOOS 3 (PO_4, NO_x, NH_4, and $Si(OH)_4$), VKI 4.1 (NO_x), and VKI 4.2 (PO_4 and $Si(OH)_4$). The sample analysis results were accepted when measured CRMs were within ±5% of the certified values. Quality control of the nutrient measurements over the years was performed with the use of internal and certified reference standards and by participation in international laboratory performance exercises (QUASIMEME).

Biological analyses

Seawater samples (500 ml) for chlorophyll *a* determination were filtered through GF/F filters that were then wrapped in aluminum foil and frozen (−20°C). At the lab, the chlorophyll *a* pigment was extracted from the filters using acetone (90%) overnight and determined by the non-acidification method (Welschmeyer, 1994) using a Turner Designs (Trilogy) fluorometer.

Pico-phytoplankton abundance was determined by flow cytometry. Briefly, seawater samples (1.8 ml) were fixed with glutaraldehyde (0.02% v:v, Sigma-Aldrich, St. Louis, MO, USA; G7651) at room temperature for 10 min and frozen in liquid nitrogen. The abundance of autotrophic pico-eukaryotes, *Synechococcus* and *Prochlorococcus*, was determined using an Attune® Acoustic Focusing Flow Cytometer (Applied Biosystems, Foster City, CA, USA).

Primary productivity was determined following the Steemann Nielsen (1952) protocol. Specifically, triplicate water samples from each depth (50 ml) were spiked with 5 μCi of $NaH^{14}CO_3$ (PerkinElmer, Waltham, MA, USA; specific activity 56 mCi $mmol^{-1}$) and incubated for 24 h under *in situ* natural illumination and temperature in a flow-through tank on deck. Measurements for the added activity and dark controls were also performed. The incubations were terminated by filtering the seawater through GF/F filters and acidifying them overnight in 5-ml scintillation vials containing 50 μl of 32% hydrochloric acid to remove excess ^{14}C. Lastly, 5 ml of an Ultima-Gold scintillation was added to the filters, and the radioactivity was measured using a TRI-CARB 2100 TR (Packard) liquid scintillation counter.

For measurements of bacterial abundance, heterotrophic bacteria were stained (300 μl of the initial sample) with SYBR Green Fluorescent Nucleic Acid Stain (Applied Biosystems) and enumerated by discrimination based on green fluorescence (530 nm) and side scatter (Marie et al., 1997). Bacterial production was estimated using the ^3H-leucine incorporation method. Triplicate samples (1.7 ml) were incubated with ~100 nmol hot leucine L^{-1} for 4–7 h (PerkinElmer; specific activity 100 Ci $mmol^{-1}$). 'Kill' treatments in which seawater was added with 100 μl of 100% trichloroacetic acid (TCA; 4°C) along with 3H-leucine were also carried in triplicates from representing depths (surface water was usually used). The incubations were terminated with TCA and were later processed following the micro-centrifugation technique (Smith et al., 1992) and added with 1 ml of an Ultima-Gold scintillation cocktail. The samples were counted using a TRI-CARB 2100 TR (Packard) liquid scintillation counter. A conversion factor of 1.5 kg C mol^{-1} per mol leucine incorporated was used (Simon et al., 1989).

Results and discussion

The averaged salinity and temperature time series of the LIW core present a good agreement with the presiding circulation pattern of the north Ionian, the BiOS mechanism (Civitarese et al., 2010; Gacic et al., 2010; Lavigne et al., 2018; Menna et al., 2022; Placenti et al., 2022). Periods of anticyclonic circulation (tinted in red in Figure 2) are characterized by a positive tendency in salinity and temperature, while cyclonic periods (tinted in blue) are accompanied by a decrease in the thermohaline values of LIW. In our display (Figures 2–4, Supplementary Figure S1), we extend the final cyclonic period starting in 2019 (Menna et al., 2022) through the end of the

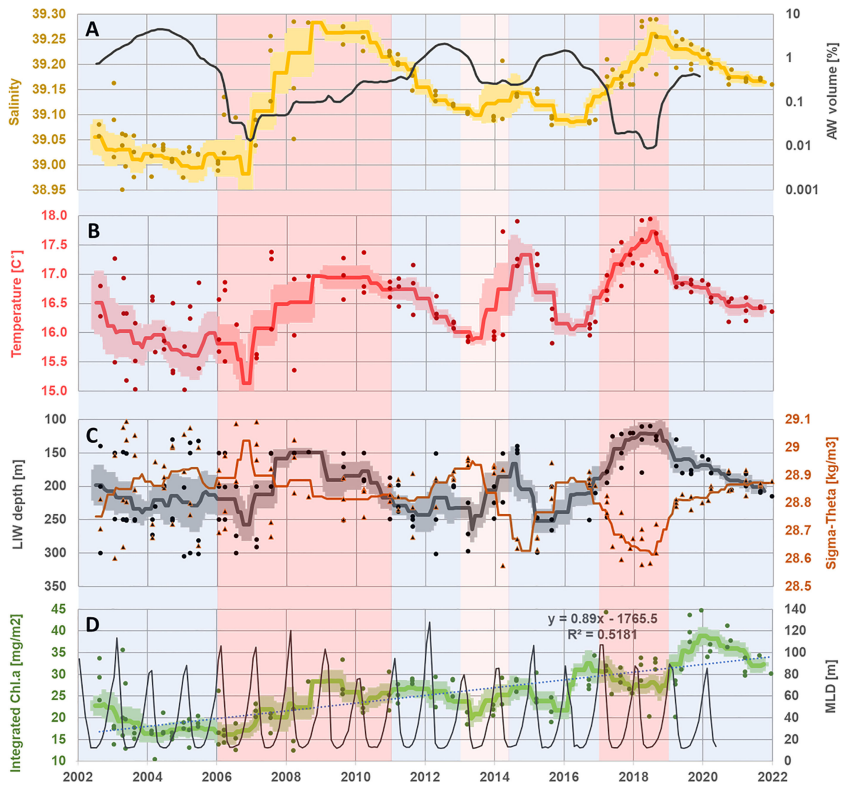

FIGURE 2
Time series of salinity (**A**; yellow), Atlantic Water volume percentage (**A**; black), temperature (**B**; red), depth (**C**; black), density (Sigma-Theta; C; orange), and mixed layer depth (MLD; D; black) performed in the core of the LIW water mass (ca. 130 m< z< 350 m) during the Haifa Section cruises (2002–2021). Time series of integrated chlorophyll *a* at the photic zone (0–200 m) (**D**; green). Station-specific values are presented in dots, the moving average is presented in a solid line, and the standard error ranges are indicated with a light-colored area. Light blue dotted line and formula show the calculated chlorophyll *a* trend. Periods of anticyclonic circulation (tinted in red in the salinity panel) and cyclonic periods (tinted in blue) (Menna et al., 2022; Placenti et al., 2022).

presented time series, as our data support it with the continuation of a negative trend in thermohaline values. The long-term warming and salinification trends are clearly evident in the presented data in agreement with previously published studies (Ozer et al., 2017; Ozer et al., 2022). The annual average LIW core depth variates from 130 to 270 m (average values) over the examined period were mostly affected by the density (Sigma-Theta) values of this water mass (Pearson's correlation value of 0.6). This relationship is most evident in 2018, where LIW core reached a record low of sigma of ~28.6 kg m^{-3}, while its average core depth decreased significantly and reached ~110 m (annual average 130 m) (Figure 2), the shallowest depth recorded here along the 20 years' time series (2002–2021). It should be noted that although the LIW reached a high-salinity content at this time (2018), which is similar to the 2008 salinity peak, it has reached a maximal temperature value of 17.7°C, attributed to the long-term warming trend, permitting a minimal density as described above.

The AW volume variability, as achieved through the VSA, closely follows the cyclonic–anticyclonic regime of the north Ionian as described thoroughly by Menna et al. (2022). In the periods of anticyclonic circulation, when the water exchange in the Levant is reduced according to the BiOS theory (Gacic et al., 2010), there is indeed a significant reduction in the volume of AW in the EMS by up to two orders of magnitude. The opposite occurs in reported periods of cyclonic circulation in the north Ionian, which are characterized by high AW volume. The AW VSA results are also in the opposite phase of the LIW salinity time series, providing important evidence of the link between the variability of the Ionian circulation to the water fluxes coming in and out of the LB and through this mechanism influencing the thermohaline and nutrient values of the LIW.

The total alkalinity concentrations (Supplementary Figure S1) are in accord with concentrations recorded in the Mediterranean Sea (~2,600 µmol kg^{-1}), showing relatively high levels (Kolker et al., 2021). We observed a peak in the total alkalinity concentration coinciding with the 2018 salinity peak (Supplementary Figure S1), yet the existing data for 2013–2021 are too small to draw a firm behavior and display concentrations, which follow the conservative behavior (linear trend) of total alkalinity with salinity (Kolker et al., 2021, and references therein).

Dissolved oxygen values correspond closely with the LIW core depth and can be related to enhanced ventilation of this water mass, as it becomes shallower and has higher oxygen demand due to organic material decomposition as it becomes deeper (Figure 3). The apparent oxygen utilization (AOU) time series behaves out of phase with the nutrient concentrations (Figure 3), reflecting the degree of organic matter degradation/oxidation. In addition, the nutrients (NO_3+NO_2 and PO_4) time series (Figures 3C) present a mirror image of the thermohaline and LIW depth data (Figures 2, 3), as they are presumably depleted from the LIW water mass when it becomes shallower and more available for primary production and is then replenished when LIW core deepens.

The integrated Chl.*a* time series also presents a general long-term positive trend. We observe a significant long-term rise in the integrated Chl.*a* of 0.89 mg m^{-2} $year^{-1}$ for the years 2002 till 2021 (Figure 2), superimposed by interannual variations. At three distinct times at the start of a shallowing period of the LIW core, at the beginning of 2007, the end of 2013, and the middle of 2016, there is a clear rise of the integrated Chl.*a* levels in the photic zone (Figures 2, 3). The Chl.*a* time series partly coincides with the periods of anticyclonic and cyclonic circulations, not always in union with the thermohaline exact peaks and lows, demanding further investigation. The maximal winter MLD values from the CMEMS physical reanalysis product do not seem to correspond with the observed integrated Chl.*a* variations or its general increasing trend (Figure 2). Therefore, the supply of nutrients from deeper water due to the annual deep winter mixing does not support the general increasing trend and interannual variability of the integrated Chl.*a*.

The rise in the buoyancy of LIW core in 2018–2019 through its reduced sigma value gave way to the shallowest record of this water mass (~110-m depth), bringing it well within the lower photic zone. The LIW core in 2018–2019 is shallower by ~50 m as compared to the 2008–2010 peak (Figure 2) and as expected shows lower AOU values at the shallower depth (Figure 3). Nevertheless, in contrast to the expected AOU behavior, both periods contain similar concentrations of NO_3, showing relatively enriched concentrations in the 2018–2019 LIW core (Figure 3). Thus, the mechanism of warming and shallowing the

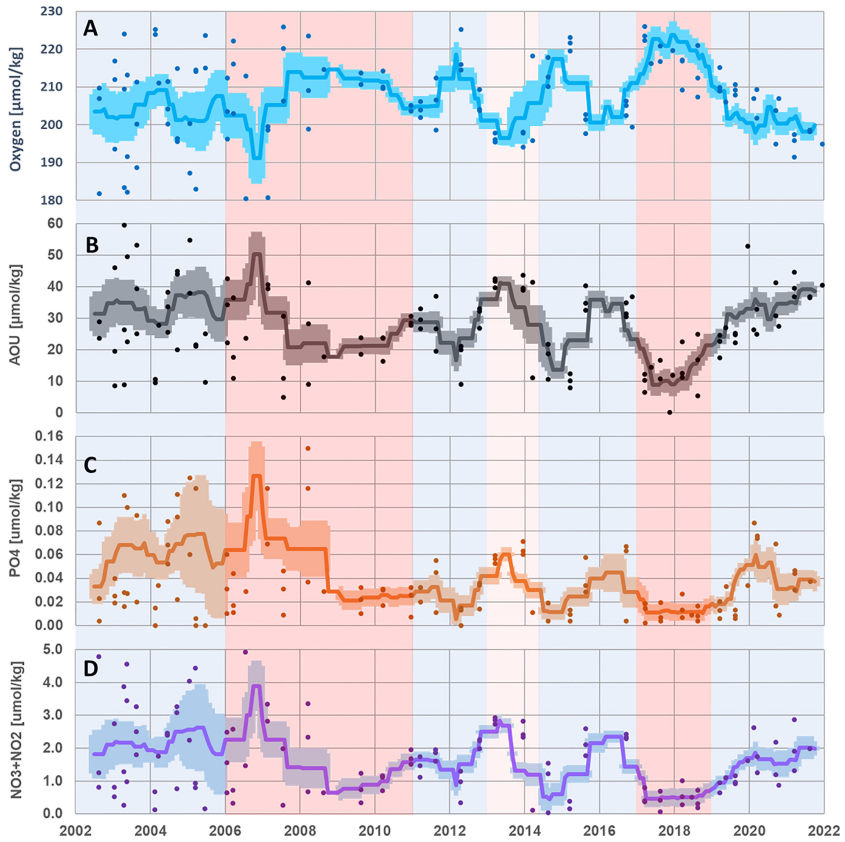

FIGURE 3
Time series of dissolved oxygen (**A**; blue), Apparent oxygen utilization (AOU; **B**; black), dissolved PO_4 concentrations (**C**; orange), and dissolved NO_3+NO_2 concentrations (**D**; purple) were performed in the core of the LIW water mass (ca. 130 m< z< 350 m) during the Haifa Section cruises (2002–2021). Station-specific values are presented in dots; the moving average is presented in a solid line, and the standard error ranges are indicated with a light-colored area. Circulation periods are presented as in Figure 2. LIW, Levantine intermediate water.

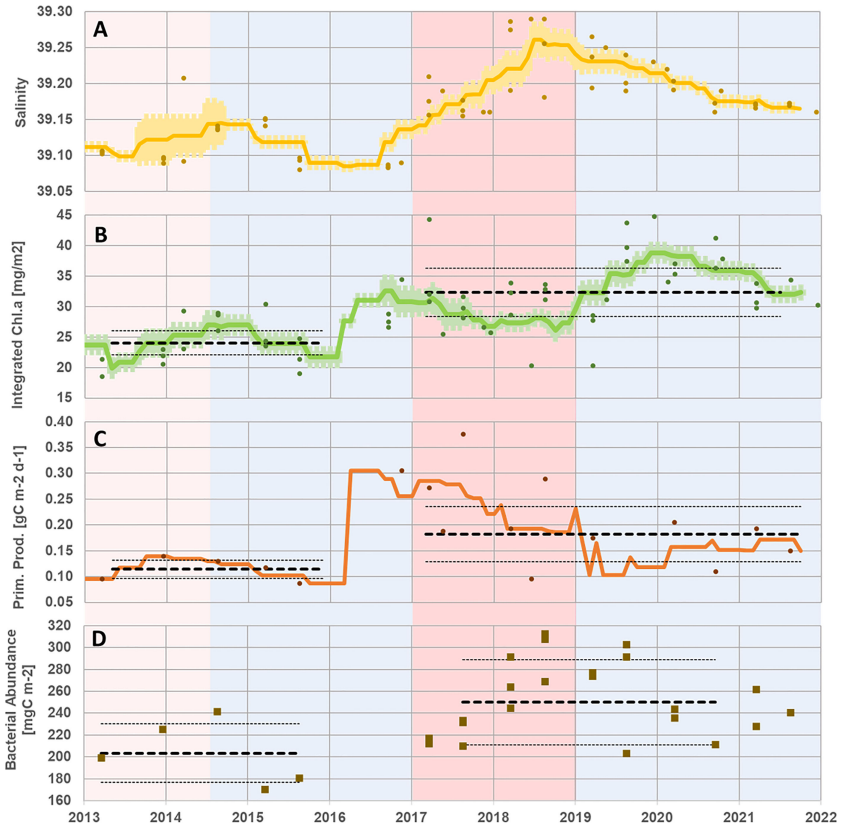

FIGURE 4
Time series of salinity (**A**; yellow) as presented in Figure 1 for the 2013–2021 time slot and time series of integrated Chl.*a* (**B**; green), integrated primary production (**C**; orange), and integrated bacterial production (**D**; brown) performed at the photic zone (0–200 m) during the Haifa Section cruises (2013–2021). Station-specific values are presented in dots, the moving average is presented in a solid line, and the standard error ranges are indicated with a light-colored area (for salinity and Chl.*a*). The bold black segmented lines and the thin dotted side lines in panels **(C)** and **(D)** represent the average and standard deviation range, respectively. Circulation periods are presented as in **Figure 2**.

LIW core due to its increased buoyancy enabled a higher level of nutrients to become available to the photic zone from below, supporting the observed rise of the intergraded Chl.*a* (or algae biomass), with a maximum recorded during 2018–2019. Accordingly, we further suggest that this mechanism of warming and shallowing the LIW core may explain the general long-term rise of the integrated Chl.*a* (Figure 2) as the LIW core becomes gradually more available for photosynthetic activity.

The 2013–2021 time series shows two distinct periods of BiOS, mainly cyclonic (2011–2016; Placenti et al., 2022) and mostly anticyclonic (2017–2019; Menna et al., 2022). It is expected that the biological response to BiOS is complex and exhibits certain delay and thus does not coincide with the detailed thermohaline interannual variations. Pearson lag correlations for the above time series presented maximal values of ~0.82 with the integrated Chl.*a* lagging ~22 months behind the thermohaline parameters, attesting to the delayed response of the biological cycle to the observed physical changes in LIW core properties. Nonetheless, considering the above two general periods, a significant ($p < 0.05$) change in the average integrated values for primary production and bacterial abundance (as for Chl.*a*) shows higher levels after 2017, during the anticyclonic period and afterward (Figure 4). Other integrated biological parameters measured during this period are too sparse to follow detailed interannual variations (Supplementary Figure S1). Specifically, data on the abundance of pico-phytoplankton populations (autotrophic pico-eukaryotes, *Synechococcus* and *Prochlorococcus*) and integrated bacterial production were too sparse, preventing any clear statistical significance (Supplementary Figure S1). Further observations are required to better assess the response of such pico-phytoplankton populations.

The changes in buoyancy, consequent of the changes in the thermohaline values, are the main mechanism controlling the

vertical position of LIW in the SE Levantine Basin. The vertical uplift of the nutrient-rich LIW water is an important and significant pathway of nutrients into the photic zone driving the primary production in this oligotrophic area, especially during anticyclonic periods, which prolong the residence time of the LIW due to its reduced outflow from the LB. Thus, global warming in combination with the BiOS mechanism, and hence LIW residence time and buoyancy, may impact the primary producers' biomass at the photic zone and hence somewhat reduce the degree of oligotrophic state. This latter feedback may slightly counter the enhanced oligotrophication due to the warming effect on enhanced stratification and mixing depths. Further observations are needed to better understand and assess these processes.

Data availability statement

The datasets presented in this study can be found in online repositories (physical updated and chemical in process). The names of the repository/repositories and accession number(s) can be found at: Israel Marine Data Center–https://isramar.ocean.org.il/isramar2009/.

Author contributions

Conceptualization: BH and TO. Data acquisition: TO, IG, ER, GS-V, BH, and JS. Formal analysis: TO, IG, ER, GS-V, JS, and BH. Project administration: BH. Writing—original draft: TO and BH with the help of IG, ER, GS-V, and JS. All authors approved the submitted version.

Funding

This study was supported by the Israel Ministries of Energy and Environmental Protection through the National Monitoring Program of Israel's Mediterranean waters.

Acknowledgments

We thank the captain and crew of the *R/V Bat-Galim* operated by the Israel Oceanographic and Limnological Research Institute (IOLR). We thank the maritime crew, electrical lab, and research assistants at the physical oceanography, marine chemistry, and biology departments at IOLR for their dedicated efforts.

Conflict of interest

The authors declare that the research was conducted in the absence of any commercial or financial relationships that could be construed as a potential conflict of interest.

Publisher's note

Supplementary material

The Supplementary Material for this article can be found online at: https://www.frontiersin.org/articles/10.3389/fmars.2022.958924/full#supplementary-material

SUPPLEMENTARY FIGURE 1
Time series of alkalinity (**A**, red), Synechococcus (**B**, blue), Prochlorococcus (**C**, orange) pico-eukaryotes (**D**, green) and integrated bacterial production (**E**, grey) performed at the photic zone (0-200m) during the Haifa Section cruises (2013–2021). Station-specific values are presented in dots and the moving average is presented in a solid line. Circulation periods are presented as in Figure 2.

References

Ben-Yaakov, S., and Sass, E. (1977). Independent estimate of the PH of dead Sea brines, limnol. *Ocean-ogr.* 22, 374–376. doi: 10.4319/lo.1977.22.2.0374

Bethoux, J. P. (1980). Mean water fluxes across sections in the Mediterranean Sea, evaluated on the basis of water and salt budgets and of observed salinities. *Oceanologica Acta* 3, 79–88.

Carpenter, J. H. (1965). The accuracy of the winkler method for dissolved oxygen analysis. *Limnology Oceanography* 10, 135–140. doi: 10.4319/lo.1965.10.1.0135

Civitarese, G., Gacic, M., Lipizer, M., and Borzelli, G. L. E. (2010). On the impact of the bimodal oscillating system (BiOS) on the biogeochemistry and biology of the Adriatic and Ionian seas (Eastern Mediterranean). *Biogeosciences* 7, 3987–3997. doi: 10.5194/bg-7-3987-2010

Cochrane, J. D. (1958). The frequency distribution of water characteristics in the pacific ocean. *Deep-Sea Res.* 5, 111–127. doi: 10.1016/0146-6313(58)90002-9

Dickson, A. G., Afghan, J. D., and Anderson, G. C. (2003). Reference materials for oceanic CO2 analysis: a method for the certification of total alkalinity. *Mar. Chem.* 80, 185–197. doi: 10.1016/S0304-4203(02)00133-0

Escudier, R., Clementi, E., Omar, M., Cipollone, A., Pistoia, J., Aydogdu, A., et al. (2020). *Mediterranean Sea Physical reanalysis (CMEMS MED-currents) (Version 1) [Data set]* (Copernicus Monitoring Environment Marine Service (CMEMS). doi: 10.25423/CMCC/MEDSEA_MULTIYEAR_PHY_006_004_E3R1

Estournel, C., Marsaleix, P., and Ulses, C. (2021). A new assessment of the circulation of Atlantic and intermediate waters in the Eastern Mediterranean. *Prog. Oceanography* 198, 102673. doi: 10.1016/j.pocean.2021.102673

Fach, B. A., Orek, H., Yilmaz, E., Tezcan, D., Salihoglu, I., Salihoglu, B., et al. (2021). Water mass variability and levantine intermediate water formation in the Eastern Mediterranean between 2015 and 2017. *J. Geophysical Research: Oceans* 126, e2020JC016472. doi: 10.1029/2020JC016472

Fedele, G., Mauri, E., Notarstefano, G., and Poulain, P.-M. (2022). Characterization of the AtlanticWater and levantine intermediate water in the Mediterranean Sea using 20 years of argo data. *Ocean Sci.* 18, 129–142. doi: 10.5194/os-18-129-2022

Gacic, M., and Bensi, M. (2020). Ocean exchange and circulation. *Water* 12 (2020), 882. doi: 10.3390/w12030882

Gacic, M., Borzelli, G. L. E., Civitarese, G., Cardin, V., and Yari, S. (2010). Can internal processes sustain reversals of the ocean upper circulation? the Ionian Sea example. *Geophys. Res. Lett.* 37, L09608. doi: 10.01029/02010GL043216

Gacic, M., Civitarese, G., Eusebi Borzelli, G. L., Kovacevic, V., Poulain, P.-M., Theocharis, A., et al. (2011). On the relationship between the decadal oscillations of the northern Ionian Sea and the salinity distributions in the Eastern Mediterranean. *J. Geophys. Res.* 116, C12002. doi: 10.1029/2011JC007280

Georgopoulos, D., Theocharis, A., and Zodiatis, G. (1989). Intermediate water formation in the Cretan Sea (South Aegean Sea). *Oceanologica Acta* 12 (4), 353–359.

Gertman, I., Pinardi, N., Popov, Y., and Hecht, A. (2006). Aegean Sea Water masses during the early stages of the Eastern Mediterranean climatic transien–90). *J. Phys. Oceanography* 36 (9), 1841–1859. doi: 10.1175/JPO2940.1

Hamad, N., Millot, C., and Taupier-Letage, I. (2006). The surface circulation in the Eastern basin of the Mediterranean Sea. *Scientia Marina* 70, 457–503. doi: 10.3989/scimar.2006.70n3457

Hayes, D., Poulain, P.-M., Testor, P., Mortier, L., Bosse, A., and Du Madron, X. (2019). Review of the circulation and characteristics of intermediate water masses of the Mediterranean–implications for cold-water coral habitats. *Coral reefs Mediterr. (CORM)* 9, ffhal–02400788. doi: 10.1007/978-3-319-91608-8_18

Kolker, D., Bookman, R., Herut, B., David, N., and Silverman, J. (2021). An initial assessment of the contribution of fresh submarine ground water discharge to the alkalinity budget of the Mediterranean Sea. *J. Geophysical Research: Oceans* 126 (8), e2020JC017085. doi: 10.1029/2020JC017085

Kubin, E., Poulain, P.-M., Mauri, E., Menna, M., and Notarstefano, G. (2019). Levantine intermediate and levantine deep water formation: An argo float study from 2001 to 2017. *Water* 11, 1781. doi: 10.3390/w11091781

Lascaratos, A., and Nittis, K. (1998). A high-resolution three-dimensional numerical study of intermediate water formation in the levantine Sea. *J. Geophys. Res.* 103 (C9), 18497–18511. doi: 10.1029/98JC01196

Lascaratos, A., Roether, W., Nittis, K., and Klein, B. (1999). Recent changes in deep water formation and spreading in the Mediterranean Sea: A review. *Prog. Oceanography* 44, 5–36. Pergamon. doi: 10.1016/S0079-6611(99)00019-1

Lascaratos, A., Williams, R. G., and Tragou, E. (1993). A mixed-layer study of the formation of levantine intermediate water. *J. Geophys. Res.* 98 (C8), 739–749. doi: 10.1029/93JC00912

Lavigne, H., Civitarese, G., Gačić, M., and D'Ortenzio, F. (2018). Impact of decadal reversals of the north Ionian circulation on phytoplankton phenology. *Biogeosciences* 15, 4431–4445. doi: 10.5194/bg-15-4431-2018

Lyubartsev, V., Borile, F., Clementi, E., Masina, S., Drudi, M., Coppini, G., et al. (2020). Interannual variability in the Eastern and Western Mediterranean overturning index. in: Copernicus marine service ocean state report, issue 4. *J. Operational Oceanography* 13:sup1, s88–s91. doi: 10.1080/1755876X.2020.1785097

Malanotte-Rizzoli, P., Manca, B.B., Ribera d'Alcala, M., Theocharis, A., Bergamasco, A., Bregant, D., et al. (1997). A synthesis of the Ionian Sea hydrography, circulation and water mass pathways during POEM-Phase I. *Prog. Oceanogr.* 39, 153–204. doi: 10.1016/S0079-6611(97)00013-X

Malanotte-Rizzoli, P., and Hecht, A. (1988). Large-Scale properties of the Eastern Mediterranean: a review. *Oceanologica Acta* 11, 4.

Malanotte-Rizzoli, P., Manca, B. B., d'Alcala, M., Theocharis, A., et al. (1997). A synthesis of the Ionian Sea hydrography, circulation and water mass pathways during POEM-phase I. *Prog. Oceanogr.* 39, 153–204. doi: 10.1016/S0079-6611(97)00013-X

Malanotte-Rizzoli, P., Manca, B. B., Ribera,, d'Alcala, M., Theocharis, A., Brenner, S., et al. (1999). The Eastern Mediterranean in the 80s and in the 90s: the big transition in the intermediate and deep circulations. *Dynamics Atmospheres Oceans* 29, 365–395. doi: 10.1016/S0377-0265(99)00011-1

Marie, D., Partensky, F., Jacquet, S., and Vaulot, D. (1997). Enumeration and cell cycle analysis of natural populations of marine picoplankton by flow cytometry using the nucleic acid stain SYBR green I. *Appl. Environ. Microbiol.* 63, 186–193. doi: 10.1128/aem.63.1.186-193.1997

Menna, M., Ga˘ci´c, M., Martellucci, R., Notarstefano, G., Fedele, G., Mauri, E., et al. (2022). Climatic, decadal, and interannual variability in the upper layer of the Mediterranean SeaUsing remotely sensed and *In-situ* data. *Remote Sens.* 14(2022), 1322. doi: 10.3390/rs14061322

Menna, M., Gerin, R., Notarstefano, G., Mauri, E., Bussani, A., Pacciaroni, M., et al. (2021). On the circulation and thermohaline properties of the Eastern Mediterranean Sea. *Front. Mar. Sci.* 8. doi: 10.3389/fmars.2021.671469

Menna, M., Notarstefano, G., Poulain, P.-M., Mauri, E., Falco, P., and Zambianchi, E. (2020). Surface picture of the levantine basin as derived by drifter and satellite data, section 3.5 of von schuckmann et al. 2020. Copernicus Mar. Service Ocean State Rep. *J. Operational Oceanography* 4, S1–S172. doi: 10.1080/1755876X.2020.1785097

Menna, M., Poulain, P.-M., Zodiatis, G., and Gertman, I. (2012). On the surface circulation of the levantine sub-basin derived from Lagrangian drifters and satellite altimetry data. *Deep-Sea Res. I* 65, 46–58. doi: 10.1016/j.dsr.2012.02.008

Mihanovic´ H, Vilibic´I., Šepic´, J., Matic´, F., Ljubešic´, Z., Mauri, E., Gerin, R., et al. (2021). Observation, preconditioning and recurrence of exceptionally high salinities in the Adriatic Sea. *Front. Mar. Sci.* 8. doi: 10.3389/fmars.2021.672210

Millot, C., and Taupier-Letage, I. (2005). "Circulation in the Mediterranean Sea," in *The handbook of environmental chemistry 5 (K)*. Ed. A. Saliot (Springer-Verlag, Heidelberg), 29–66. doi: 10.1007/b107143

Montgomery, R. B. (1958). Water characteristics of Atlantic ocean and of world ocean. *Deep-Sea Res.* 5, 134–148. doi: 10.1016/0146-6313(58)90004-2

Nielsen, J. N. (1912). Hydrography of the Mediterranean and adjacent waters. *Rep. Dan. Oceanogr. Exped.* 1908–1910, 77–192.

Ovchinnikov, M. (1966). Circulation in the surface and intermediate layers of the Mediterranean Sea. *Oceanology* 6, 48–59.

Ozer, T., Gertman, I., and Gildor, H. (2022). Thermohaline temporal variability of the SE Mediterranean coastal waters (Israel) -long-term trends, seasonality, and connectivity. *Front. Mar. Sci.* 8, 799457. doi: 10.3389/fmars.2021.799457

Ozer, T., Gertman, I., Gildor, H., Goldman, R., and Herut, B. (2020). Evidence for recent thermohaline variability and processes in the deep water of the southeastern levantine basin, Mediterranean Sea. *Deep Sea Res. Part II: Topical Stud. Oceanography*. 171, 104651.

Ozer, T., Gertman, I., Kress, N., Silverman, J., and Herut, B. (2017). Interannual thermohaline, (1979–2014) and nutrient, (2002–2014) dynamics in the levantine surface and intermediate water masses, SE Mediterranean Sea. *Global Planetary Change* 151, 60–67. doi: 10.1016/j.gloplacha.2016.04.001

Ozsoy, E., Hecht, A., Ünlüata, Ü., Brenner, S., Sur, H. I., Bishop, J., et al. (1993). A synthesis of the levantine basin circulation and hydrograph–1990. *Deep-Sea Res.* 40, 1075–1119.

Ozsoy, E., Unluata, U., Oguz, T., Latif, M. A., Hecht, A., Brenner, S., et al. (1991). A review of the levantine basin circulation and its variabilities during 1985–1988. *Dyn. Atmos. Oceans* 15, 421–456. doi: 10.1016/0377-0265(91)90027-D

Pinardi, N., Cessi, P., Borile, F., and Wolfe, C. L. P. (2019). The Mediterranean Sea overturning circulation. *J. Phys. Oceanogr.* 49, 1699–1721. doi: 10.1175/JPO-D-18-0254.1

Placenti, F., Torri, M., Pessini, F., Patti, B., Tancredi, V., Cuttitta, A., et al. (2022). Hydrological and biogeochemical patterns in the Sicily channel: New insights from the last decad-2020). *Front. Mar. Sci.* 9. doi: 10.3389/fmars.2022.733540

POEM Group (1992). General circulation of the Eastern Mediterranean. *Earth-Science Rev.* 32, 285–309. doi: 10.1016/0012-8252(92)90002-B

Pollak, M. J. (1958). Frequency distribution of potential temperature and salinities in the Indian ocean. *Deep-Sea Res.* 5, 128–133. doi: 10.1016/0146-6313(58)90003-0

Powley, H. R., Krom, M. D., Emeis, K.-C., and Van Cappellen, P. (2014). A biogeochemical model for phosphorus and nitrogen cycling in the Eastern Mediterranean Sea (EMS) part 2. response of nutrient cycles and primary production to anthropogenic forcing: 1950–2000. *J. Mar. Syst.* 139, 420–432. doi: 10.1016/j.jmarsys.2014.08.017

Robinson, A. R., and Golnaraghi, M. (1993). Circulation and dynamics of the Eastern Mediterranean sea; quasi-synoptic data-driven simulations. *Deep Sea Res.* 40 (6), 1207–1246. doi: 10.1016/0967-0645(93)90068-X

Robinson, A. R., Golnaraghi, M., Leslie, N., Artegiani, A., Hecht, A., Lazzone, E., et al. (1991). Structure and variability of the Eastern Mediterranean general circulation. *Dyn. Atmos. Oceans* 15, 215–240. doi: 10.1016/0377-0265(91)90021-7

Robinson, A. R., Leslie, W. G., Theocharis, A., and Lascaratos, A. (2001). "Mediterranean Sea Circulation," in *Encyclopedia of ocean sciences* (Academic Press), 1689–1706. doi: 10.1006/rwos.2001.0376

Rubino, A., Gacic, M., Bensi, M., Kovacevic, V., Malacic, V., Menna, M., et al. (2020). Experimental evidence of long-term oceanic circulation reversals without wind influence in the north Ionian Sea. *Sci. Rep.* 10, 1905. doi: 10.1038/s41598-020-57862-6

Schlitzer, R., Roether, W., Oster, H., Junghans, H.-G., Hausmann, M., Johannsen, H., et al. (1991). Chlorofluoromethane and oxygen in the Eastern Mediterranean. *Deep-Sea Res.* 3812, 1531–1551. doi: 10.1016/0198-0149(91)90088-W

Schneider, A., Tanhua, T., Roether, W., and Steinfeldt, R. (2014). Changes in ventilation of the Mediterranean Sea during the past 25 year. *Ocean Sci.* 10, 1–16. doi: 10.5194/os-10-1-2014

Schroeder, K., Garcia-Lafuente, J., Josey, S. A., Artale, V., Nardelli, B. B., Carrillo, A., et al. (2012). "Circulation of the Mediterranean Sea and its variability," in *The Mediterranean Climate : From past to future* (Amsterdam: Elsevier).

Simon, M., Alldredge, A., and Azam, F. (1989). Protein-content and protein-synthesis rates of planktonic marine-bacteria. *Mar. Ecol. Prog. Ser.* 51, 201–213. doi: 10.3354/meps051201

Sisma-Ventura, G., Bialik, O. M., Makovsky, Y., Rahav, E., Ozer, T., Kanari, M., et al. (2022). Cold seeps alter the near-bottom biogeochemistry in the ultraoligotrophic southeastern Mediterranean Sea. *Deep Sea Res. Part I: Oceanographic Res. Papers* 183, 103744. doi: 10.1016/j.dsr.2022.103744

Smith, D. C., Smith, D. C., Azam, F., and Azam, F. (1992). A simple, economical method for measuring bacterial protein synthesis rates in seawater using 3H-leucine. *Mar. Microbial Food Webs* 6, 107–114.

Steemann Nielsen, E. (1952). The use of radio-active carbon C14 for measuring organic production in the sea. *J. Con. Perm. Int. Explor. Mer* 18 (2), 117–140. doi: 10.1093/icesjms/18.2.117

Tanhua, T., Hainbucher, D., Schroeder, K., Cardin, V., Alvarez, M., and Civitarese, G. (2013). The Mediterranean Sea system: a review and an introduction to the special issue. *Ocean Sci.* 9, 789–803. doi: 10.5194/os-9-789-2013

Velaoras, D., Gogou, A., Zervoudaki, S., Civitarese, G., Giani, M., and Rahav, E. (2019). Revisiting the Eastern Mediterranean: Recent knowledge on the physical, biogeochemical and ecosystemic states and trends (Volume I). *Deep Sea Res. Part II* 164, 1–4, OI. doi: 10.1016/j.dsr2.2019.06.010

Velaoras, V., Krokos, G., Nittis, K., and Theocharis, A. (2014). Dense intermediate water outflow from the Cretan Sea: A salinity driven, recurrent phenomenon, connected to thermohaline circulation changes. *J. Geophys. Res. Oceans* 119, 4797–4820. doi: 10.1002/2014JC009937

Von Schuckmann, K., Le Traon, P.-Y., Smith, N., Pascual, A., Djavidnia, S., Gattuso, J.-P., et al. (2020). Copernicus Marine service ocean state report, issue 4. *J. Operational Oceanography* 13:sup1, s1–s172. doi: 10.1080/1755876X.2020.11785097

Welschmeyer, N. A. (1994). Fluorometric analysis of chlorophyll a in the presence of chlorophyll b and pheopigments. *Limnology Oceanography* 39, 1985–1992. doi: 10.4319/lo.1994.39.8.1985

Wust, G. (1961). On the vertical circulation of the Mediterranean Sea. *J. Geophys. Res.* 66, 3261–3271. doi: 10.1029/JZ066i010p03261

frontiers | Frontiers in Marine Science

TYPE Review
PUBLISHED 09 August 2022
DOI 10.3389/fmars.2022.933390

OPEN ACCESS

EDITED BY
Tomaso Fortibuoni,
Istituto Superiore per la Protezione e la Ricerca Ambientale (ISPRA), Italy

REVIEWED BY
Milena Menna,
Istituto Nazionale di Oceanografia e di Geofisica Sperimentale, Italy
Yoshikazu Sasai,
Japan Agency for Marine-Earth Science and Technology (JAMSTEC), Japan
Dagmar Hainbucher,
University of Hamburg, Germany

*CORRESPONDENCE
José C. Sánchez-Garrido
jcsanchez@uma.es

SPECIALTY SECTION
This article was submitted to Marine Fisheries, Aquaculture and Living Resources, a section of the journal Frontiers in Marine Science

RECEIVED 30 April 2022
ACCEPTED 06 July 2022
PUBLISHED 09 August 2022

CITATION
Sánchez-Garrido JC and Nadal I (2022) The Alboran Sea circulation and its biological response: A review. *Front. Mar. Sci.* 9:933390. doi: 10.3389/fmars.2022.933390

The Alboran Sea circulation and its biological response: A review

José C. Sánchez-Garrido[1,2]* and Irene Nadal[1,2]

[1]Physical Oceanography Group, Department of Applied Physics II, University of Málaga, Málaga, Spain, [2]Instituto de Biotecnología y Desarrollo Azul (IBYDA), University of Málaga, Málaga, Spain

The oceanography of the Alboran Sea (AS) has been the subject of intensive research for decades. Chief among the reasons for this interest is the variety of physical processes taking place in the basin, spanning from coastal upwelling, dynamic of density fronts, internal waves, and strong meso- and submesoscale turbulence. Historical fieldwork and an increasing number of numerical studies in recent years have led to a more complete—although more dispersed—description and knowledge of process dynamics in the AS and their role in shaping primary productivity and regional fisheries resources. In this review, we summarize and put together old and new research to get an updated picture of the AS circulation and its variability at different time scales, with an emphasis on physical–biological interactions. As part of the review, we identify gaps in our understanding regarding the physical drivers for seasonal and for rapid transitions between the most recurrent one-gyre and two-gyre modes of circulation of the AS. We also point at possible research strategies based on end-to-end regional biophysical modeling to gain new insights into past and present physical control on fisheries resources and for assessing plausible climate change impacts on the AS ecosystem.

KEYWORDS

Alboran Sea, Strait of Gibraltar, nutrient fertilization, upwelling, tidal flow, small pelagic fisheries, ocean gyres, frontal jets

1 Geographical frame, mean circulation, and water masses

The Alboran Sea (AS) is the westernmost subbasin of the Mediterranean, extending from the Strait of Gibraltar (SoG) in the west to the imagery north-to-south line joining the locations of Almeria and Oran in the east (Figure 1). On this line typically lies the so-called Almeria-Oran front, which dynamically isolates the upper AS from the rest of the Mediterranean. The AS is some 150 km wide and 370 km long, and has a maximum depth of ~2,000 m. The continental shelf is narrow, typically less than 10 km wide and 100–150 m deep. The mean upper-layer circulation is characterized by a frontal jet of Atlantic Water (Atlantic jet, hereinafter AJ) surrounding two large-scale anticyclonic gyres, the so-called Western Alboran Gyre (WAG) and the Eastern Alboran Gyre (EAG) (Figure 1). A

smaller-scale cyclonic gyre typically lies in between. The AJ has a low salinity signal of ~36.6, extends over the surface 150–200 m, and features near-surface velocities of ~1 m/s or even more (Parrilla and Kinder, 1987). The AJ is ~30 km wide and forms a sharp density front with the denser ambient Modified Atlantic Water—up to 1 unit saltier than the incoming AW through the SoG; Cheney and Doblar (1982). Underneath, saltier and colder Levantine Intermediate Water (LIW; S = 38.5, T = 13.23°C) flows toward the SoG at 200–600 m depth. The LIW is broadly distributed in the basin, although it tends to accumulate on the Spanish slope deflected north by the Coriolis acceleration. The colder and denser Western Mediterranean Deep Water (WMDW; S = 38.48, T = 12.9°C) goes predominantly south from the NW Mediterranean, possibly driven by a major trough in the center of the basin (the AS Central Trough), heading towards the SoG banked against the African slope. Other intermediate and deep waters contribute to the Mediterranean outflow, the Tyrrhenian Dense Water and Winter Intermediate Water, although they represent a minor fraction with respect to the LIW and the WMDW (Naranjo et al., 2015).

The mean circulation determines overall biochemical patterns. The WAG and the EAG are characterized by horizontally convergent upper-layer circulation, downwelling, and a depressed pycnocline (interface between the Atlantic Water and the LIW) situated at ~ 175 m depth (Viúdez and Tintoré, 1995; Vargas-Yáñez et al., 2021). Conversely, the cyclonic region between the WAG and the EAG is associated with upwelling and exhibits an uplifted pycnocline (~50 m deep). This configuration is consistent with an ageostrophic Ekman circulation in the upper layer of the gyres induced by friction with the underlying LIW. The vertical excursion of the pycnocline and the nutrient-rich LIW (~9 μM of nitrate and ~0.4 μM of phosphate; Manca et al., 2004; Ramírez et al., 2021) shapes the vertical distribution of nutrients. Depressed nutricline is found within the WAG and EAG (~70–115 m; Moran and Estrada, 2001) and, accordingly, there is generally less primary production and lower concentration of surface chlorophyll (Chl) over the gyres (Figure 2A). Phytoplankton biomass is most abundant on the north coast of the AS and along the WAG and EAG peripheries. The first pattern is partly attributable to the baking of LIW against the north continental slope and the consequent shoaling of the pycno- and nutricline on this coastal margin. Regarding primary productivity, the largest values have been measured near the frontal regions between the WAG and the AJ, with average values of ~ 632 mg C m^{-2} d^{-1}, while the minimum values correspond to the center of the WAG, with ~330 mg C m^{-2} d^{-1} (Moran and Estrada, 2001). Altogether, estimated annual primary productivity in the AS exceeds 100 g C m^{-2} yr^{-1}, making it among the highest in the Mediterranean (Uitz et al., 2012).

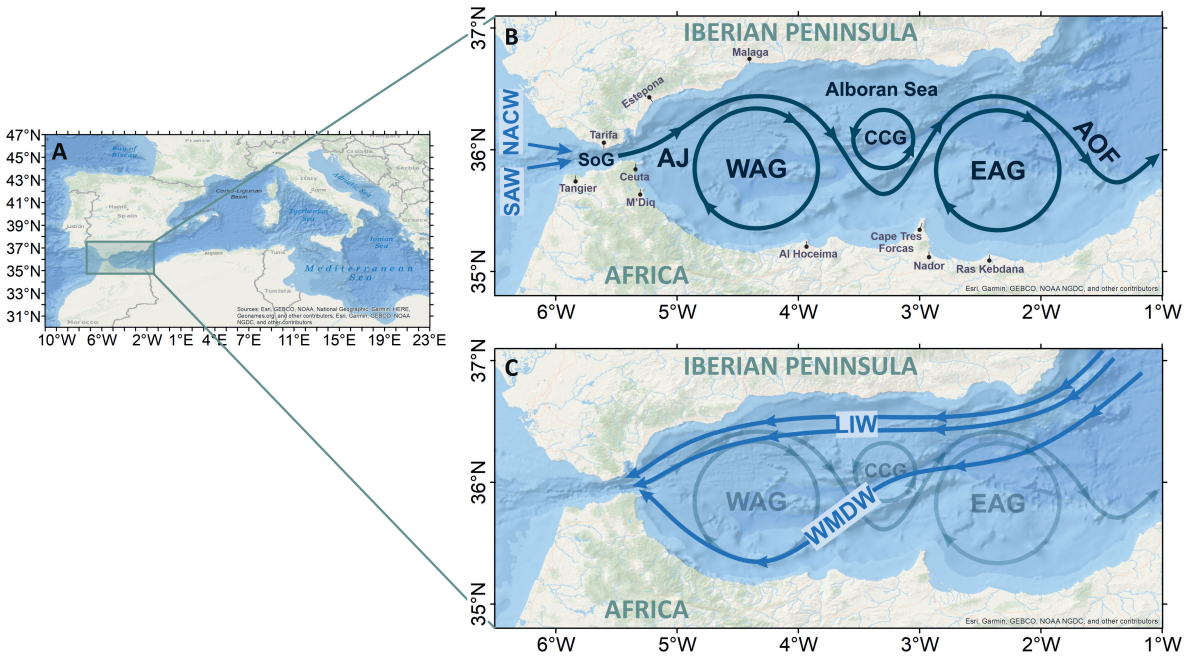

FIGURE 1
(A) Map of the Mediterranean Sea and central-eastern Atlantic Ocean showing the Alboran Sea location. **(B)** Map of Alboran Sea, tracing its general surface circulation: The Atlantic Jet (AJ), the western and eastern Alboran Gyres (WAG and EAG), the Central Cyclonic Gyre (CCG), and the Almeria-Oran front (AOF). **(C)** As panel **(B)** for the deep-pathways, sketching the mean circulation of LIW and WMDW (adapted from Kinder and Bryden, 1990).

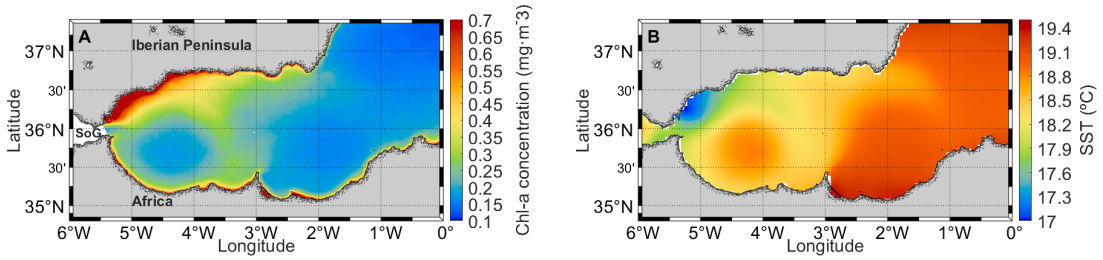

FIGURE 2
(A) Time-mean Chlorophyll-a concentration (mg/m^3) over the period 1997–2020 in the Alboran Sea, obtained from the CMEMS product OCEANCOLOUR_MED_CHL_L4_REP_OBSERVATIONS_009_078. **(B)** Time-mean Sea Surface Temperature (SST) over the period 1981–2021 in the Alboran Sea, obtained from the product SST_MED_SST_L4_REP_OBSERVATIONS_010_021.

2 Origin and maintenance of the mean circulation

Laboratory experiments and numerical simulations indicate that the WAG and EAG originate from loop currents that form off Ceuta and Cape Tres Forcas (Whitehead and Miller, 1979; Oguz et al., 2014). Such currents are fed by the AJ, which in the absence of the WAG and the associated high-pressure anomaly tends to veer south because of the Coriolis acceleration to later follow the African coast. The formation of the loop currents and the establishment of the mean circulation have been attributed to the abrupt change of orientation of the coastline at Ceuta and Cape Tres Forcas (Bormans and Garett, 1989; see locations in Figure 1). In these locations, the radius of curvature of the coastline is shorter than the inertial radius, $r = U/f$ (U is the current velocity and f the Coriolis frequency), which corresponds to the theoretical radius of curvature of the trajectory of the jet in the absence of external pressure gradients. Thus, after surpassing Ceuta and Cape Tres Forcas, the AJ separates momentarily from the coast to impinge it again at some location downstream (east). The incident angle of the jet is large enough to generate a loop coastal current (or "separation bubble") that recirculates anticyclonically. After their genesis, these small-scale currents grow fed by the AJ until reaching basin-wide dimensions, turning into the WAG and EAG themselves. The whole process lasts for 90–120 days (e.g., Oguz et al., 2014), after which both the WAG and EAG become essentially geostrophic balanced.

Once formed, a question that has attracted much attention is how the gyres maintain their heat, salt, and momentum budgets against mixing and dissipation. This question has concerned especially the WAG, probably because it is a more recurrent and long-standing feature than the EAG (Renault et al., 2012). Bryden and Stommel (1982) argued that the upward flow of WMDW over the African slope toward the SoG is a source of anticyclonic vorticity that keeps the WAG spinning against friction. The uplift of WMDW would be in turn a consequence of the outflow of LIW through the SoG, whose high velocity over the sill (~1 m/s) creates a dynamic pressure reduction that makes possible the drainage of deep waters. The term "Bernouilli aspiration" was coined to describe the process (Kinder and Bryden, 1990).

The Atlantic inflow has also been suggested to play some role in the maintenance of the WAG. Viúdez and Haney (1997) reported the existence of a permanent subsurface salinity minimum at the core of the WAG, from which it was postulated that some flow of Atlantic Water must enter the WAG ageostrophically (i.e., crossing isobars) directly from the Strait, perhaps mediated by tidal flows. The renewal of Atlantic Water in the WAG would help maintain its horizontal density gradient with ambient waters and thereby its geostrophic motion *via* thermal wind balance.

Brett et al. (2020) have recently shown from the numerical simulation of a quasi-steady WAG that its low salinity and warm temperature signals, as well as its negative vorticity budget, are not held constant but are gradually eroded by advection of ambient Modified Atlantic Water into the gyre. The salinity minimum at the center of the WAG identified by Viúdez and Haney (1997) would originate from its early formation in its loop-current stage to later decay over time. However, the dissipation of the WAG occurred so slowly that changes in the properties of the WAG were practically inappreciable over the 5-month numerical run.

3 Mesoscale and seasonal variability

The notion of a quasi-steady WAG in the previous is somewhat idealized because abrupt changes of the WAG, including its collapse (i.e., a rapid weakening) or its migration toward the eastern AS have been observed (Perkins et al., 1990; Viúdez and Haney, 1997; Flexas et al., 2006). In such situations, the AJ becomes a coastal jet that follows the African coast and the circulation in the western AS becomes predominantly cyclonic (Peliz et al., 2013). Satellite imagery shows that the AJ can maintain its coastal-jet configuration for up to two months until a perceptible WAG develops (Vargas-Yáñez et al., 2002).

Collapse and migration events of the WAG occur mainly during the fall and winter and largely determine the seasonality of the AS surface circulation (Vargas-Yáñez et al., 2002; Renault et al., 2012). Analysis of a 20-year simulation by Peliz et al. (2013) shows that the migration of the WAG and its subsequent interaction with the EAG can cause dramatic changes in the latter—e.g., one possible scenario is that both gyres merge and drift east by the Algerian Current—, suggesting that the seasonality of the EAG can be in part inherited from the WAG. This conclusion is supported by the fact that the two gyres show qualitatively similar seasonal variability, both being weaker during winter (the EAG being more elusive) and more frequent and with the largest sizes in summer (Figure 3).

The origin of the seasonal variability of the AS circulation and the drivers for the collapse and migrations of the WAG have been addressed in several investigations, most of them pointing at a possible of the inflow through the SoG (Vargas-Yáñez et al., 2002; Vélez-Belchí et al., 2005). Vargas-Yáñez et al. (2002) reported a migration episode of the WAG preceded by a significant drop of the inflow caused by meteorological forcing (storm surge flows). Meteorologically driven flows in the SoG largely account for changes in seal-level pressure over the Mediterranean (Candela et al., 1989; García-Lafuente et al., 2002), and can be large enough to halt the inflow (~0.8 Sv)—or double its magnitude—for few days (García-Lafuente and Delgado, 2004). It was speculated that the migration of the WAG was triggered by the shortening of the inertial radius of the AJ, which caused its veering toward the African coast. The stronger subinertial variability of the inflow in autumn and winter associated with the passage of synoptic atmospheric systems over the Mediterranean would be consistent with the more frequent migrations of the WAG during this time of the year. Other authors have suggested that the variability of the inflow caused by the freshwater seasonal cycle of the Mediterranean can also determine the seasonality of the WAG (Renault et al., 2012). This hypothesis seems questionable because the inflow has a minor seasonal amplitude of ~0.03–0.04 Sv (Soto-Navarro et al., 2010), one order of magnitude smaller than subinertial fluctuations. Moreover, the AJ and WAG can adjust geotropically (quasi-steadily) to the long-scale seasonal signal of the inflow.

High-resolution numerical simulations have offered insights into the circumstances preceding the migration of the WAG. Sánchez-Garrido et al. (2013) showed that the blocking of small-scale cyclonic eddies (~ 10 km) traveling around the WAG periphery, trapped between the AJ and the north coast of the AS, can trigger the south deflection of the AJ and ultimately force the WAG to migrate. These eddies originated from the separation of the northern lateral boundary layer of the SoG; eddies with anticyclonic vorticity were shed from the south boundary, leading to a Kármán vortex street. Positive and negative vorticity fluxes toward the AS, as well as the size of the generated eddies, increased with strong time dependence of the flow. The most dramatic events of eddy generation occurred when the AJ entered the AS forming a vortex dipole—mushroom-like current—after recovering from a weakening period of a few days due to adverse (westward) meteorologically-driven flows (Figure 4). This type of event is

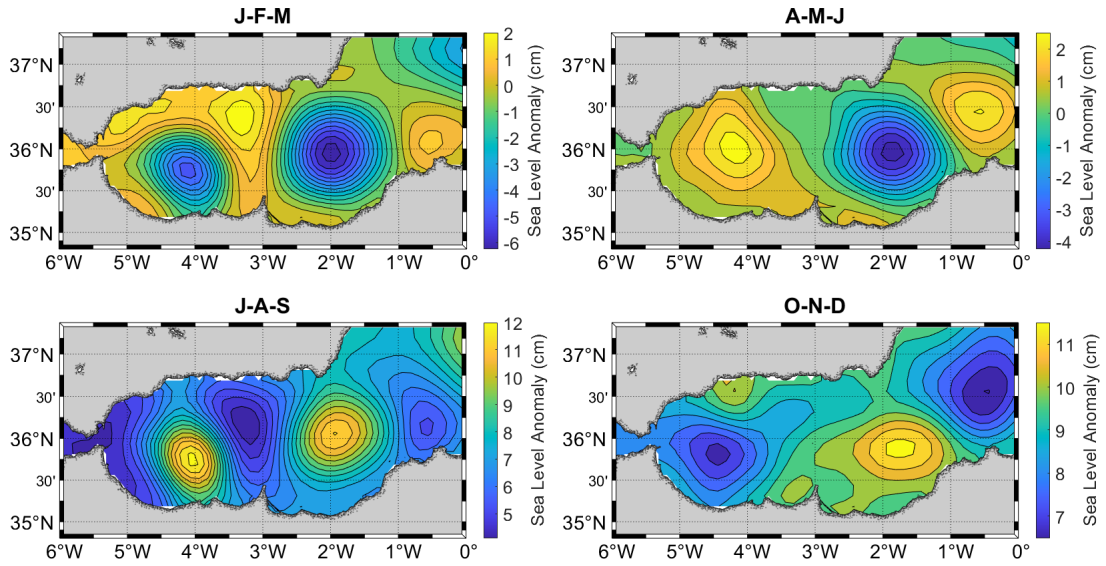

FIGURE 3
Seasonal climatology of Sea Level Anomaly (SLA) in the Alboran Sea (period 1993–2021). Isolines are shown every 0.5 cm. J-F-M: January–February–March, A-M-J: April–May–June, J-A-S: July–August–September, O-N-D: October–November–December. CMEMS product: SEALEVEL_EUR_PHY_L4_MY_008_068.

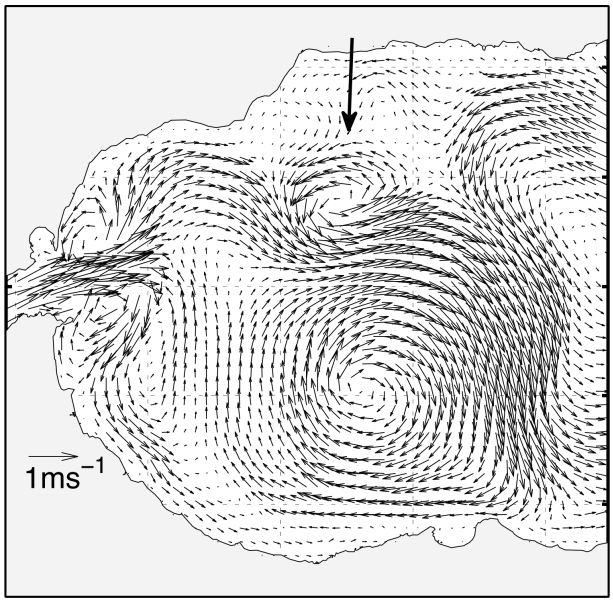

FIGURE 4
Snapshot of the surface velocity field in western Alboran from numerical simulations. The arrow indicates a cyclonic mesoscale eddy surrounding the WAG. The AJ enters the AS as a mushroom-like (ageostrophic) current. This current structure is associated to intensified inflow through the SoG by incoming meteorologically-driven flows (adapted from Sánchez Garrido et al., 2015; see this paper for other synoptic situations).

more frequent in winter, associated with the greater variability of sea-level pressure over the Mediterranean during this season.

The time variability of the flow through the SoG was unable to explain, however, most of the collapses/migrations of the WAG identified in the numerical run of Peliz et al. (2013). The most recurrent double-gyre structure (up to 48% of the time) tended to occur during periods of large internal Rossby Radius (stronger stratification) and mild winds, suggesting a possible role of eddy dynamics and intrinsic variability of the basin, rather than conditions externally forced by conditions in the SoG, in determining stability periods and alternance between one-gyre and two-gyre circulation types. Peliz et al. (2013) also found that cyclonic mesoscale eddies in the AS (of ~13 km) were most common in winter, outnumbering by far anticyclonic eddies. This links with the result of Brett et al. (2020), who noted a slow decay of the WAG by advection of cyclonic vorticity into the gyre. The decay of the WAG in winter could be hence related to the dominance of cyclonic eddies (and the consequent cyclonic vorticity anomaly) in the basin.

4 Submesoscale variability

Both meso- and submesoscale (<10 km) eddies have been observed traveling along the WAG periphery. These features were probably first reported by La Violette (1984), who noted cold-water rings around the WAG in high-resolution satellite imagery. García-Lafuente and Delgado (2004) investigated the meandering trajectory of a drifter around the WAG accidentally released at the eastern part of the SoG. The wavy path of the drifter was attributed to its trapping by a submesoscale eddy with an origin at the SoG. Both La Violette and Lacombe (1988) and García-Lafuente and Delgado (2004) point to tidal pulses of vorticity generated in the Strait, later carried by the AJ, as the likely origin of these eddies. These findings concur with the numerical results of Sánchez-Garrido et al. (2013), although the most obvious eddies found by these authors, were associated with subtidal time dependence of the flow (meteorologically-driven flows). The non-recurrent presence of these eddies in satellite images suggests that they are not necessarily tidally driven. Another possibility is that these features are too small to be detected regularly by remote sensing devices. In addition to small-scale eddies arising from the SoG, significant submesoscale activity occurs in the vicinity of the AJ associated with its nonlinear frontal dynamics (see *Frontal dynamics*).

5 Nutrient enrichment mechanisms

5.1 Mixing in the SoG

5.1.1 Mixing in the steady exchange

The Atlantic Water entering through the SoG is composed of surface Atlantic Water and colder and nutrient-richer North

Atlantic Central Water. This inflow is enriched through the Strait because of vertical mixing with the underlying Mediterranean Water. Two-layer hydraulics provides guidance as to where and how vertical mixing occurs through the Strait (Armi, 1986; Pratt and Whitehead, 2008). A useful dimensionless number is the internal composite Froude number

$$G^2 = F_1^2 + F_2^2$$

where $F_1^2 = u_1^2/g'h_1$ and $F_2^2 = u_2^2/g'h_2$; here, u_i and h_i denote velocity and thickness of the surface ($i = 1$) and bottom layers ($i = 2$), and $g' = 2g(\rho_2 - \rho_1) / (\rho_2 + \rho_1)$ is the reduced gravity. The hydraulic state of the flow is determined by the value of G^2. The flow is classified as critical, subcritical, or supercritical according to $G^2 = 1$, $G^2 < 1$, or $G^2 > 1$, respectively. The flow criticality can be interpreted in terms of the direction that information can travel through the flow by long interfacial waves. Critical flow ($G^2 = 1$) implies that one of the two interfacial waves supported by the flow is stationary (i.e., it has null phase velocity). Subcritical flow ($G^2 < 1$), typically occurring in relatively stagnant regions, implies that the two waves travel in opposite directions. Similarly, in supercritical regions ($G^2 > 1$) both waves propagate in the same direction. An important consequence is that the flow can become unstable (with respect to long waves) only in critical or subcritical regions—mathematically, the phase speed of the interfacial disturbances becomes complex conjugates. Therefore, strong mixing due to instabilities is expected to occur where the flow turns supercritical. Other recognized locations where intense mixing occurs are across hydraulic jumps, regions of the flow matching supercritical-to-subcritical conditions.

In the SoG, there is one critical section over the Camarinal Sill and a second critical section at the Tarifa Narrows (Armi and Farmer, 1988; Kinder and Bryden, 1990; García-Lafuente et al., 2000; Figure 5A), although the presence of this latter section has been suggested to be non-permanent (Garrett et al., 1990). The flow at these two sections is said to be hydraulically controlled. Immediately west and east of these two control sections are two supercritical regions, each followed by hydraulic jumps matching subcritical conditions in the connecting seas—the Gulf of Cadiz and the AS. Hence, enhanced mixing occurs immediately west of Camarinal Sill in the so-called Tangier basin, and east of Tarifa Narrows (Figure 5A). In these locations of the Strait, mixing creates an obvious intermediate mixing layer that has motivated the consideration of a three-layer model to better represent the structure of the flow (Figure 5B; Bray et al., 1995; Sannino et al., 2009). Estimates of the mixing layer thickness (ΔZ) (sketched in Figure 6A) in the hypothetical steady flow sketched in Figure 5B vary from 15 m in the Camarinal Sill to 50–80 m in the eastern part of the SoG and in the Tangier basin (Naranjo et al., 2014; Figure 6B).

5.1.2 Tidal flows and residual

The steady picture of the flow through the SoG is modified by time-dependent flows, particularly tides. Tidal flows reach peak values of up to 6 Sv, with ~3 Sv associated with the M_2 tidal constituent alone (García-Lafuente et al., 2000). The first tidal implication is the input of mechanical energy available for mixing. A second implication is the periodic reversal of both the Atlantic and the Mediterranean layers over the Camarinal Sill, so that for some time during the tidal cycle the two-way structure of the flow is temporarily lost, with both layers pointing in the same direction. This has important hydraulic consequences as well as for the dynamics of the interface mixing layer.

During the flood tide (westward tidal flow), the Mediterranean outflow current is tidally intensified, leading to faster-growing instability and enhanced mixing within the supercritical region west of Camarinal Sill. Here, Wesson and Gregg (1994) reported peak values of energy dissipation rates of up to 10^{-2} W kg^{-1} (hundreds of times larger than in the open ocean) and the presence of Kelvin–Helmholtz billows. Enhanced energy dissipation and mixing also occur across the now larger hydraulic jump west of Camarinal Sill (Sánchez-Garrido et al., 2011). As a result, an enlarged pool of mixed water is created in the Tangier basin at the end of the flood tide.

During the ebb tide (eastward tidal flow), the Mediterranean layer reverses and the Atlantic flow strengthens. The Atlantic current entrains part of the pool of mixed water that had formed in the Tangier basin during the previous few hours (Figure 5C). García-Lafuente et al. (2013) estimated that as much as 30% of the pool ultimately contributes to the inflow. One effect of the tides is therefore to add nutrient-rich mixing water into the inflow. This is reflected in the widening of the interface mixing layer at the eastern part of the SoG with respect to a non-tidal situation (Figure 6B, C).

Tides also raise the mixing layer in the eastern part of the SoG. This second effect can be understood from the upstream influence exerted by a sill-controlled flow (Pratt and Whitehead, 2008). For sill-controlled flows resembling a flow spilling down a dam, such influence is regulated by a nonlinear weir formula that links the flow rate with the height of the fluid at the dam, so that variation in one of the two magnitudes perturbs the other. In the SoG, the interface east of Camarinal Sill moves up and down in response to changes in the tidal flow rate. The net (mean) effect of the back-and-forth movement of the tides leaves the interface—taken at the mid depth of the mixing layer—shallower than in the unperturbed non-tidal flow (Figures 6D, E), further favoring primary production.

A third tidally-driven process is the radiation of large-amplitude internal waves (~100 m amplitude) from the Camarinal Sill to the AS (**Figure 5C**; Sánchez-Garrido et al., 2008; Sánchez-Garrido et al., 2011). These waves evolve from the internal hydraulic jump formed in the Camarinal Sill, which propagates eastward when hydraulic control is lost over the sill ($G^2 < 1$) as the Mediterranean current weakens. The nonlinear evolution of the hydraulic jump leads to a series of internal solitary waves. Although these waves can drive dramatic vertical oscillations of 100 m in only 20–30 min (Vlasenko et al., 2000), their role in the overall water mixing occurring in the SoG seems to be secondary. Solitary waves propagate for hundreds of kilometers with minor energy (amplitude) loss (Jackson and

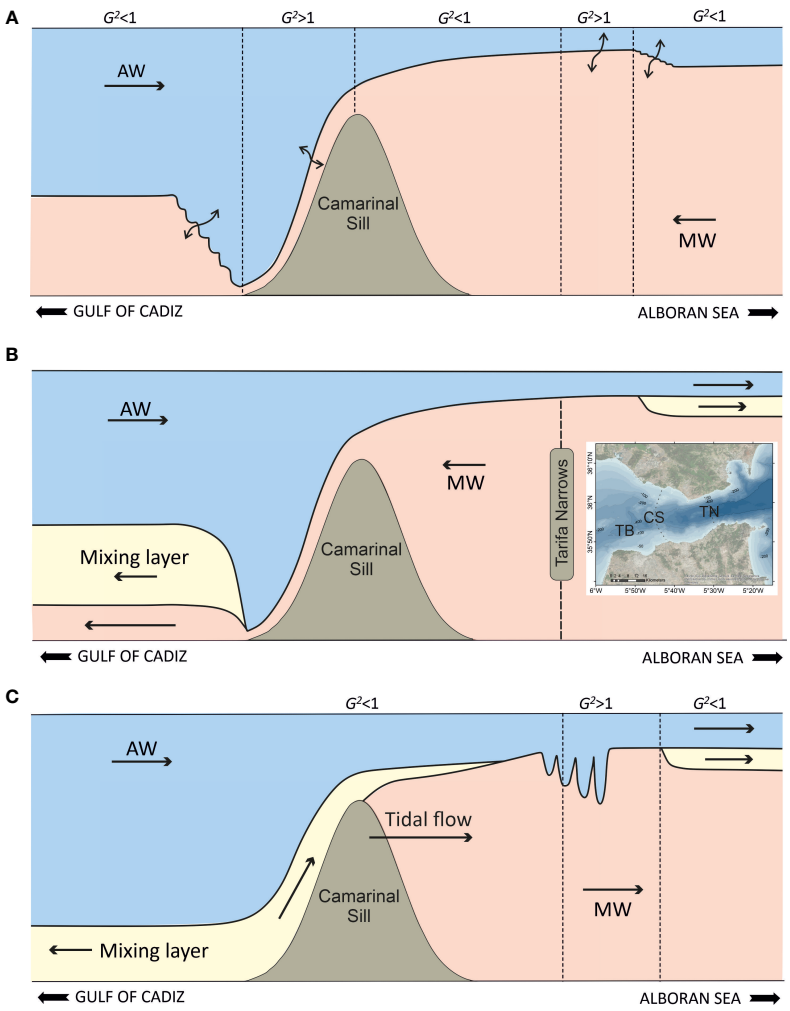

FIGURE 5
Sketches of the flow through the SoG. **(A)** The steady two-layer maximal exchange with internal hydraulic control at the Camarinal Sill and at the Tarifa Narrows. Double arrows indicate regions of enhanced mixing. The wiggling interface represents internal hydraulic jumps. **(B)** Three-layer representation of the steady flow through the SoG. Vigorous mixing has created an intermediate mixing layer that widens towards both ends of the strait (particularly west of the Camarinal Sill where mixing is strongest). The inset shows the location of the Camarinal Sill (CS) and the Tarifa Narrows (TN) within the Strait. **(C)** Snapshot of the tidally-forced three-layer exchange. Tidal flow points towards the AS; hydraulic control has been lost over the sill and the hydraulic jump can now propagate eastward, breaking up into a series of solitary waves. The Mediterranean layer over the sill has been reverted by the tidal flow, allowing for the intrusion of mixing water from the Tangier Basin (TB in the inset; west Camarinal Sill) into the AS.

Apel, 2004). The clear signature of solitary waves propagating across the AS in remote sensing images (Alpers et al., 2008) suggests that only a small fraction of their initial energy is dissipated within the SoG, probably because of partial wave breaking at the Strait's lateral boundaries (Vlasenko et al., 2009).

5.1.3 A note on the nutrient-enriched inflow and phytoplankton response

The described tidal processes lead to a nutrient-enriched inflow exposed to light at the eastern part of the SoG. Reported average nutrient concentrations of the inflow are ~3.0 μM for nitrate and ~0.25 μM for phosphate (Gómez et al., 2000; Huertas et al., 2012), much larger than typical phytoplankton semi-saturation constants (K_{NO3} = 0.5 μM, K_{PO4} = 0.05 μM; Eppley et al., 1969; Davies and Sleep, 1989). Despite the fertile inflow, phytoplankton biomass is relatively scarce within the Strait itself (Echevarría et al., 2002; Ramírez et al., 2014), a fact that can be understood from the short residence time of phytoplankton within the channel (Macías et al., 2009), estimated at ~10 h (L/U = 10 h; with L = 36 km, the distance from Tarifa to the eastern part of the Strait, and U = 1 m/s is a typical flow velocity). Considering a typical phytoplankton

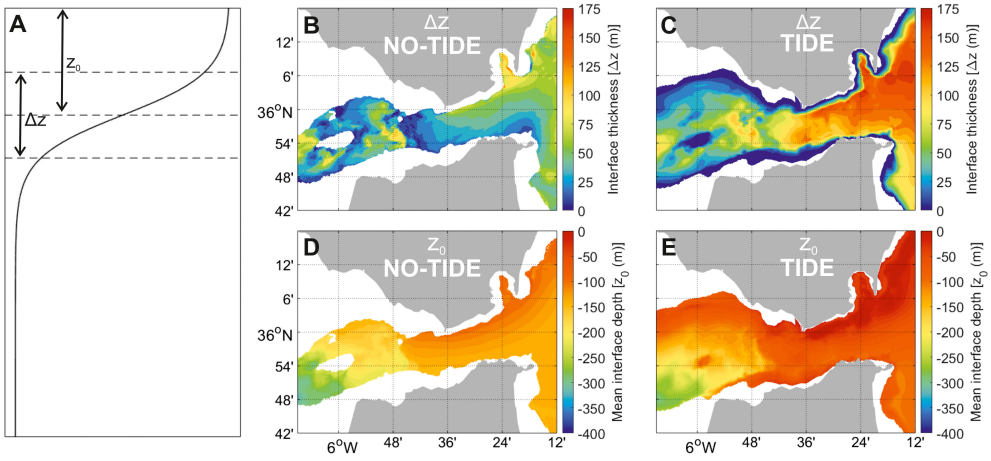

FIGURE 6
(A) Representation of the interface mixing layer thickness (Δz) and depth (z_0) for an idealized density profile. **(B, C)** Time-mean interface mixing layer thickness (Δz) in the SoG derived from a non-tidal and a tidal simulation, respectively. **(D, E)** Same as **(B, C)** for the interface mixing layer depth (z_0). Adapted from Naranjo et al., 2014).

doubling time of 1 day, a time span of 10 h is indeed too short for phytoplankton to grow significantly. The bulk of the nutrients carried by the AJ are consumed downstream in NW Alboran. Sánchez Garrido et al. (2015) estimated that the nutrient supply by tidal mixing in the SoG represents as much as ~37% of the total biomass and primary productivity in western Alboran.

5.2 Frontal dynamics

The ageostrophic frontal dynamics of the AJ is another source of fertilization of the AS surface waters. In a general context, the permanent density fronts of the AS make this sea an ideal setting for investigating the dynamics of density fronts, characterized by large vertical velocities (w) and enhanced primary productivity. Tintoré et al. (1990) and Gomis et al. (2001) estimated vertical velocities of the order of ~15 m d^{-1} in western Alboran based on the omega equation (Holton, 2004). These calculations hence rely on quasi-geostrophic theory and the assumption of slight departures from geostrophic balance, as quantified by a small Rossby number, $Ro=U/fL<<1$ (U is the downstream velocity component, L is the transversal length scale of the AJ, and f the Coriolis frequency). The pattern of vertical velocity was such that upward and downward motions occurred upstream of meander crests and troughs, respectively (Figure 7A). A similar structure has been found in the Gulf Stream and in atmospheric jet streams (Newton, 1978; McWilliams et al., 2019 and references therein). The pattern is consistent with changes in the relative vorticity of the jet $\zeta=\partial v/\partial x - \partial u/\partial y$ being controlled by curvature vorticity over crests and troughs, so that the jet is vertically stretched and squeezed over these regions to conserve potential vorticity $(\zeta+f)/h$ (here h is the vertical thickness of the jet).

The biological impact of the AJ frontal dynamics was investigated by Oguz et al. (2014) by means of process-oriented biophysical modeling. Large vertical velocities in the AJ (~30 m d^{-1}) gave rise to enhanced primary productivity and patches of phytoplankton biomass, which were then advected along the jet and stirred and dispersed within the basin by mesoscale eddies. Although the overall spatial pattern of the simulated w was consistent with previous results, finer-scale patchiness suggested an important role of submesoscale processes in driving vertical motions along the AJ. A nonlinear dynamic of the AJ beyond the formal applicability of quasi-geostrophic theory is indeed expected provided the finite Rossby number involved, $Ro\sim1$ (Sánchez-Garrido et al., 2013; Oguz et al., 2014). In such cases, vertical velocities are often due to frontogenesis; namely, rapid intensifications of cross-front density gradients that result in temporary breakdowns of geostrophic balance—frontogenesis itself can be caused by large-scale geostrophic flow tending to align lateral density gradients. Capó et al. (2021) have recently shown that frontogenesis is indeed a recurrent feature of the AS fronts. Frontogenesis prompts a cross-front vertical circulation cell with upward and downward motions at either side of the front. The origin and characteristics of this secondary ageostrophic current have been amply described in the literature of frontogenesis dynamics (Spall, 1995; McWilliams, 2021) and will now be summarized shortly. For an eastward propagating jet, the downstream acceleration of the flow in response to a rapid increase in the cross-front pressure gradient is balanced by the Coriolis acceleration. This statement follows from the quasi-

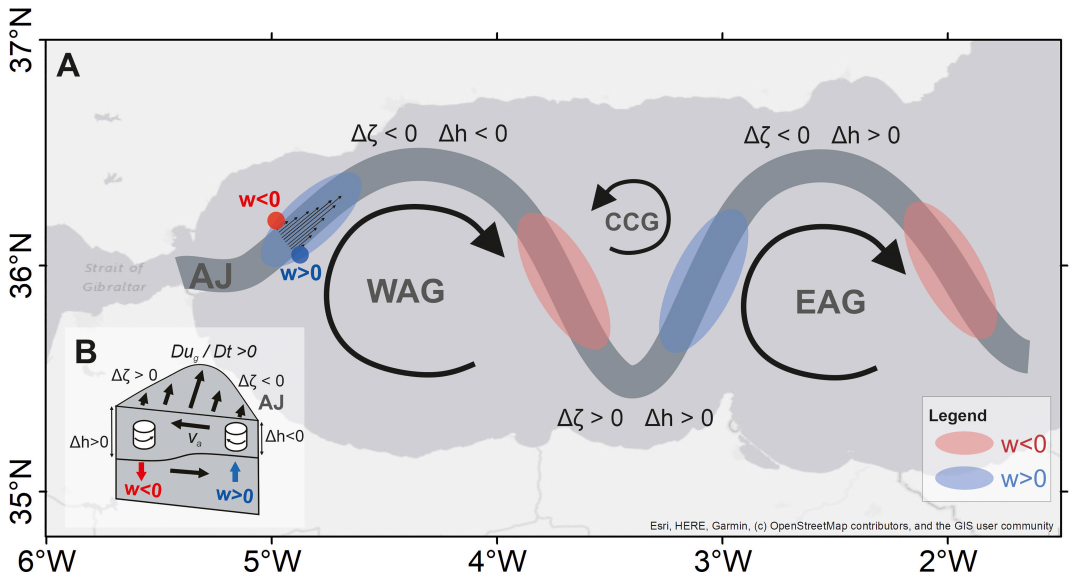

FIGURE 7
(A) Sketch of the meandering path of the AJ with vertical velocities (w) over imposed. Large patches indicate vertical velocities associated with changes of the AJ's curvature vorticity over meander crests and troughs. Small-scale patches represent (stronger) vertical velocities at both sides of the AJ in response to frontogenesis. **(B)** Sketch of the cross-front secondary circulation due to frontogenesis (see text for details; adapted from Williams and Follows, 2003).

geostrophic horizontal momentum equation, $Du_g/Dt=fv_a$ (subscripts "g" and "a" denote the geostrophic and ageostrophic contributions of the velocity field). For the prevailing eastward AJ, this balance implies a northward surface current from its anticyclonic side (south) to its cyclonic side (north) in response to frontogenesis. Stronger downstream flow also leads to enhanced anticyclonic (shear) vorticity in the anticyclonic side of the AJ and enhanced cyclonic (shear) vorticity in its cyclonic side, requiring upwelling in the first and downwelling in the latter for potential vorticity to be conserved (Figure 7B). Nondivergence of the ageostrophic circulation demands that a countercurrent flows underneath the jet. The direction of the ageostrophic circulation cell would be inverted in the case of a sudden drop in the horizontal density gradient (i.e., frontolisis).

Evidence of submesoscale frontal dynamics in the AS is scarce given the observational challenges derived from the short spatial and temporal scales involved. The most comprehensive process-oriented set of observations was probably collected by Pascual et al. (2017) and Ruiz et al. (2019) in eastern Alboran, using various instrumentation, including a set of underwater gliders and surface drifters. The footprint of submesoscale dynamics in the Almería-Oran front was revealed by the subduction of Chl up to 60 m below the deep Chl maximum. Although observational evidence is still required, submesoscale vertical velocities are expected to be stronger around the edges of the WAG, given the sharper density fronts of this region (Oguz et al., 2014; García-Jove et al., 2022). The role of submesoscale dynamics in overall phytoplankton production and export in the ocean, and in the AS in particular, is currently a subject of active research (Troupin et al., 2019; Esposito et al., 2021; Zarokanellos et al., 2022).

5.3 Coastal upwelling

Winds are mainly zonal in the AS (Figure 8). Easterlies and westerlies blow with the same strength and are similarly likely except for slight seasonal variations. The strongest winds in either direction—east or west—occur during the winter, whereas the mildest winds are found during the summer. In the summer, easterlies are also somewhat more frequent than westerlies. The overall zonal orientation of the AS shoreline makes it suitable for wind-driven coastal upwelling to occur either on the north or the south coast of the basin. Offshore Ekman transport and upwelling is driven by westerlies on the north and easterlies on the south. Despite the bimodality and symmetry of the wind regime, wind upwelling episodes turn out to be more recurrent and stronger along the Spanish coast. This north-south asymmetry is well noticed in satellite imagery of SST and ocean color, which generally shows cooler and biomass-richer waters in the north of Alboran in response to wind forcing. The shallower pycnocline and nutricline in north Alboran, resulting from the banking of LIW against the Spanish slope, are the candidate background conditions explaining the more vigorous ocean response to wind forcing in this part of the basin.

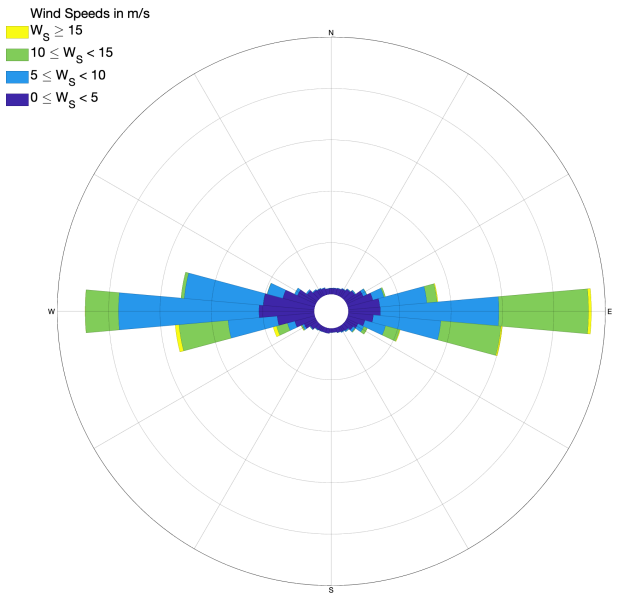

FIGURE 8
Wind rose at 10 m altitude in central Alboran, for the period 1979–2010 (from the "ERA5 hourly data on single levels from 1979 to present" dataset; Hersbach et al., 2020).

Coastal upwelling not caused by wind has also been documented in NW Alboran off Estepona. Recurrent high Chl concentration and cool SST in satellite images suggest the presence of a quasi-permanent upwelling in this region (Figure 2A, B), although part of this signal is probably accounted for advection of mixing water from the SoG. Sarhan et al. (2000) reported upwelling off Estepona associated with offshore excursions of the AJ. The AJ was observed to move offshore over a time scale of 1 week, leading to near-shore upward velocities of ~10 m d^{-1} from the mass conservation principle. Such vertical velocity implies a more moderate, but also more recurrent, upwelling than that caused by strong westerly winds. The proposed upwelling mechanism is persistent insofar as the AJ flows close to the coast, which in turn requires the presence of a well-developed WAG.

6 Physical–biological interactions during early life stages

The AS supports regionally important fisheries of anchovy and sardine (Giráldez, 2021). Nutrient enrichment and the consequent planktonic production (food supply) are the primary processes sustaining these fish populations. Enrichment is the main environmental characteristic of the triad proposed by Bakun (Bakun, 1996; Agostini and Bakun, 2002) for suitable spawning and nursery habitats; the other two propitious features are concentration and retention. Concentration, i.e., flow convergence, leads to the patchiness of aggregate plankton biomass and fish larvae, guaranteeing good feeding conditions for the latter. Retention characteristics help maintain fish early life stages—eggs and larvae—within the favorable nursery habitat.

Some coastal regions of the AS satisfy the conditions of the so-called "Bakun triad." Overall, the north coast is a more appropriate habitat than the south coast because of its higher food availability. The Estepona area and the Bay of Malaga are the main spawning and nursery grounds for anchovy and sardine. García et al. (2021) noted distinct environmental characteristics possibly limiting recruitment in the two areas. The Estepona region is abundant in food, but also openly exposed to the dispersal of early life stages by the AJ and by meso- and submesoscale eddies surrounding the WAG (Figure 4). The Bay of Malaga, relatively sheltered from the AJ because of the local shoreline and its wider continental shelf (~20 km), is less biologically productive than the Estepona region but has better retention characteristics. Leaving aside local habitat differentiations, the degree of recruitment in north Alboran as a whole depends on food supply, onshore retention of early life stages, and near-surface seawater temperature (*via* constrains of reproductive phenology and bioenergetics). These environmental conditions are largely mediated by the strength and direction of the AJ as well as by wind forcing. Inter-annual variability and trends of these conditions are assumed to play a central role in shaping ups and downs and long-term decline of anchovy and sardine recruitment (and landings) in north AS (Figure 9).

The dependence of recruitment on environmental conditions is difficult to be established because the latter also affects fish behavior. For example, the spawning strategy of sardines in north Alboran seems to depend on wind (García et al., 2021). Sardine prefers to spawn during calm wind periods

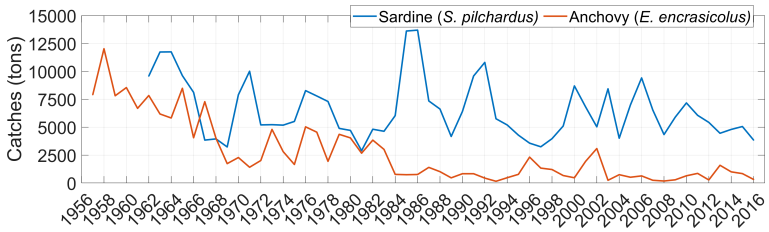

FIGURE 9
Time series of sardine (blue) and anchovy (red) landings in north Alboran. Data were obtained from the official statistics of the General Fisheries Secretariat (SGPM), Fisheries Regulatory and Market Fund (FROM), and the Spanish Institute of Oceanography (IEO).

soon after strong upwelling events by westerlies have fertilized the north coast of the AS, in an attempt to maximize both larval growth and retention (García, 2006). Overall, repeated upwelling events during the spawning season (autumn-to-winter) seem to be beneficial, provided that yearly westerly winds and Chl appear positively correlated with sardine landings in north AS (Vargas-Yáñez et al., 2020). Anchovy recruitment seems to be less dependent on the wind, perhaps because this species spawns during summer, the season of the year in which winds are mildest and do not account for much of the environmental variability. The anchovy population seems to be linked to the direction and strength of the AJ, with enhanced AJ and WAG negatively impacting the anchovy recruitment in north Alboran (Ruiz et al., 2013). The positive effect of added food supply in this region associated with a stronger AJ-WAG system (Navarro et al., 2011) would thus be overcome by exacerbated dispersion of early life stages by the same flow pattern.

Fisheries studies in south Alboran are scarcer. Annual sardine landings recently analyzed by Jghab et al. (2019) in Morocco exhibit a marked inter-annual variability as well as a decreasing trend over the last four decades. Chl statistically explained the inter-annual variability of sardine catches, whereas a long-term weakening of the Atlantic inflow through the SoG, as inferred from tidal gauges (assuming geostrophic balance), was related to the negative trend of the series. Although to the best of our knowledge such weakening needs more solid observational evidence, the interpretation of a diminished AJ impacting negatively on sardine recruitment in southern AS *via* reduced advection of nutrients and spawning material from NW Alboran entails a potential interplay between fish populations in north and south Alboran, a topic that is currently being investigated (CopeMed II, 2017; CopeMed II, 2019). The crossing of the AS implies overcoming the physical barrier that the AJ represents. Although such a crossing is not the most likely pathway, evidence of cyclonic eddies trapping relatively cold and salty water (characteristic of north Alboran) off the African coast (Viúdez and Tintoré, 1995; García-Lafuente et al., 1998) suggests that north and south AS can be indeed connected through advection. The manner in which cyclonic eddies like the one shown in Figure 4 can travel from north to south across the AJ is unknown. García-Lafuente et al. (1998, García-Lafuente et al., 2021) postulate that such eddies could have their origin in sharp meanders of the AJ pinched off near Cape Tres Forcas, where the AJ acquires maximum curvature. Similarly, the candidate location where meanders can separate from the main flow in eastern Alboran is the coastal region off Oran. Whatever the specific origin, these eddies represent intermittent north-to-south fluxes of nutrients, plankton, and fish early life stages whose role in the AS ecosystem and dynamics of fish populations is to be clarified.

7 Synthesis and future directions

The first conclusion that comes from this review is that important gaps in our understanding remain regarding what drives the variability of the basin-scale circulation of the AS, with alternance between double- and single-gyre types of circulation. These transitions have a seasonal signal, although abrupt transient events can take place year-round. Clues from observations and modeling point to the time dependence of the flow through the SoG (at atmospheric synoptic scale) as a likely driver for breaking down the most recurrent two-gyre system, although local wind stress and changes in the background stratification could also play a role (Peliz et al., 2013). A better understanding of the underlying cause (or causes) for these transitions would be needed to foresee potential changes in the AS circulation, perhaps favoring one flow type versus the other, related to climate change. The question has important biological consequences insofar as the different flow structures (one or two gyres) entail distinct pathways of the AJ, which brings nutrient-enriched water from the SoG, fertilizes the upper layer of the AS through its ageostrophic frontal dynamics, and is the primary source of meso- and submesoscale turbulence in the basin (Figure 4). Hence, the AJ has a major contribution to overall productivity (along with wind upwelling) and largely controls planktonic biomass distribution and dispersal of fish early life stages within the basin, ultimately shaping anchovy and sardine recruitment (and other's pelagic fish species) on both sides of the AS.

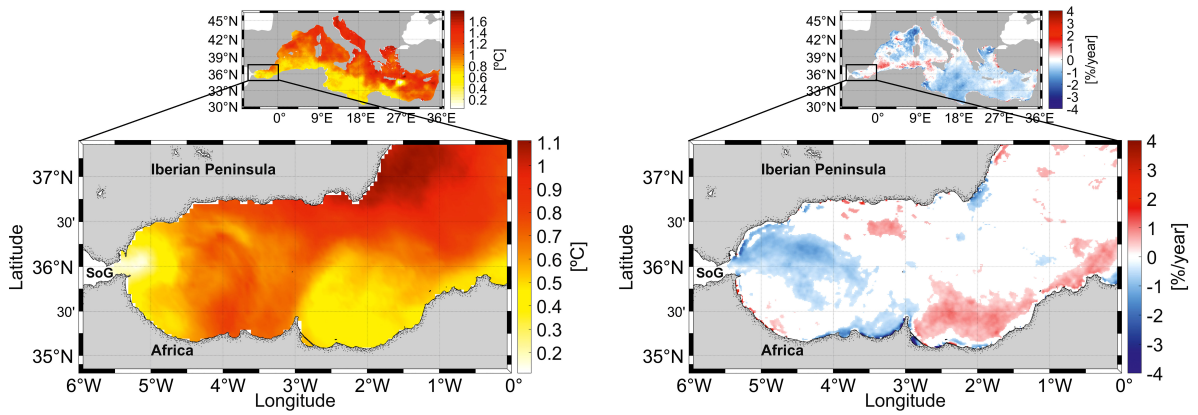

FIGURE 10
Right panels: Sea surface temperature cumulative trend over the period 1993–2020 in the Mediterranean (upper side) and in the Alboran Sea (lower side), calculated as the rate of change (°C/year) scaled by the number of time steps (28 years). CMEMS product: SST_MED_SST_L4_; REP_OBSERVATIONS_010_021. Left panels: Mediterranean Sea (top panel) and Alboran Sea (bottom panel) satellite chlorophyll trends over the period 1997–2020, expressed in % per year. CMEMS product: OCEANCOLOUR_MED_CHL_L4_REP_OBSERVATIONS_009_078.

In a general context, the AS is within the Mediterranean, which is a recognized hotspot vulnerable to climate change (Giorgi, 2006). One likely near-future scenario for mid-latitude oceans such as the Mediterranean is the decline of primary productivity due to enhanced upper ocean stratification and reduced nutrient supply into the euphotic zone (Behrenfeld et al., 2006; Steinacher et al., 2010). In view of the variety of fertilization mechanisms reviewed here, some of which appear barely affected by climate change, such as the available mechanical tidal energy for diapycnal mixing in the SoG, the AS can be less prone to oligothrophization than other regions of the Mediterranean. Although speculative, this interpretation would be supported by the fact that SST in the AS has risen by ~0.6°C since 1997, similar to other areas of the Mediterranean, whereas surface Chl has not shown a clear trend (Figure 10). This contrasts with most of the Mediterranean regions, in which Chl is in decline. The null tendency of Chl also raises the question as to whether the primary environmental driver for the long-term decline of anchovy and sardine biomass and catches in the AS during the last decades, and perhaps that to be expected during the next decades, is the gradual loss of thermal habitat rather than food limitation.

Evaluations of future climate scenarios in the Mediterranean rely on ocean models operating at ~10–20 km horizontal resolution (Ruti et al., 2016; Macias et al., 2018; Soto-Navarro et al., 2020), resolving part of the mesoscale but missing its lower range and the submesocale. The flow through the narrow SoG (14 km) is likewise poorly simulated in Mediterranean climate models. The short-scale processes impacting the circulation and primary productivity of the AS make it necessary to use dynamical downscaling solutions for (hopefully) more accurate evaluation and future projections of the regional sea climate. Another avenue for future work is the use of end-to-end (climate-to-fish) ecosystem models, which by combining ocean circulation, lower trophic (nutrients, phytoplankton, and zooplankton), and fish submodels (Fiechter et al., 2021; Sánchez-Garrido et al., 2021), can help to better understand the dynamics of anchovy and sardine populations in response to climate variability and trends, offering new insights on how environmental perturbations (e.g., changes in circulation patterns, seawater temperature, etc.) are transmitted through the food web affecting early life stage survival, reproduction, bioenergetics, and ultimately recruitment.

Author contributions

JS-G conceived the original idea. IN reviewed the literature and processed the data and figures of the manuscript. JS-G wrote the bulk of the manuscript with inputs of IN. All authors listed have made a substantial, direct, and intellectual contribution to the work and approved it for publication.

Funding

The open access publication fees of this paper were partially covered by the University of Málaga.

Acknowledgments

IN acknowledges a predoctoral fellowship from the Spanish Ministry of Science and Innovation under the project BLUEMARO (PID2020-116136RB-100). This review has been conducted using E.U. Copernicus Marine Service Information. We thank Ana Giráldez and Manuel Hidalgo for providing the

historical catches series of anchovy and sardine shown in Figure 9.

Conflict of interest

The authors declare that the research was conducted in the absence of any commercial or financial relationships that could be construed as a potential conflict of interest.

Publisher's note

References

Agostini, V., and Bakun, A. (2002). 'Ocean triads' in the Mediterranean Sea: Physical mechanisms potentially structuring reproductive habitat suitability (With example application to European anchovy, *engraulis encrasicolus*). *Fish. Oceanogr.* 11 (3), 129-42. doi: 10.1046/j.1365-2419.2002.00201.x

Alpers, W., Brandt, P., and Rubino, A. (2008). "Internal waves generated in the straits of Gibraltar and Messina: Observations from space," in *Remote sensing of the European seas*. Eds. V. Barale and M. Gade (Dordrecht: Springer). doi: 10.1007/978-1-4020-6772-3_24

Armi, L. (1986). The hydraulics of two flowing layers with different densities. *J. Fluid. Mechanic.* 163, 27–58. doi: 10.1017/S0022112086002197

Armi, L., and Farmer, D. M. (1988). The flow of Atlantic water through the strait of Gibraltar. *Prog. Oceanogr.* 21, 1–105. doi: 10.1016/0079-6611(88)90055-9

Bakun, A. (1996). Patterns in the ocean. ocean processes and marine population dynamics (California, USA: University of California Sea Grant), 323 pp. in cooperation with Centro de Investigaciones Biologicas de Noroeste, La Paz, Baja California Sur, Mexico.

Behrenfeld, M. J., O'Malley, R. T., Siegel, D. A., McClain, C., Sarmiento, J. L., Feldman, G. C., et al. (2006). Climate-driven trends in contemporary ocean productivity. *Nature* 444, 752–755. doi: 10.1038/nature05317

Bormans, M., and Garett, C. (1989). The effect of rotation on the surface inflow through the strait of Gibraltar. *Am. Meteorol. Soc.* 19 (10), 1535- 1542. doi: 10.1175/1520-0485(1989)019<1535:TEOROT>2.0.CO;2

Bray, N. A., Ochoa, J., and Kinder, T. H. (1995). The role of the interface in the exchange through the strait of Gibraltar. *J. Geophys. Res.* 100, 10755–10776. doi: 10.1029/95JC00381

Brett, G. J., Pratt, L. J., Rypina, I. I., and Sánchez-Garrido, J. C. (2020). The Western alboran gyre: An analysis of its properties and its exchange with surrounding water. *J. Phys. Oceanogr.* 50 (12), 3379–3402. doi: 10.1175/JPO-D-20-0028.1

Bryden, H. L., and Stommel, H. M. (1982). Origin of the Mediterranean outflow. *J. Mar. Res.* 40 (suppl.), 55–71.

Candela, J., Winant, C. D., and Bryden, H. L. (1989). Meteorologically forced subinertial flows through the strait of Gibraltar. *J. Geophys. Res.* 94, 12667–12679. doi: 10.1029/JC094iC09p12667

Capó, E., McWilliams, J. C., Mason, E., and Orfila, A. (2021). Intermittent frontogenesis in the Alboran Sea. *J. Phys. Oceanogr.* 51 (5), 1417–1439. doi: 10.1175/JPO-D-20-0277.1

Cheney, R. E., and Doblar, R. A. (1982). Structure and variability of the Alboran Sea frontal system. *J. Geophys. Res.* 87, 585–594. doi: 10.1029/JC087iC01p00585

CopeMed II (2017). *Report of the CopeMed II workshop on methodologies for the identification of stock units in the Alboran Sea* (Alicante, Spain), 58 pp. 3–6 April 2017. CopeMed II Technical documents N°46 (GCP/INT/028/SPA - GCP/INT/270/EC). Alicante.

CopeMed II (2019). *Report of the mid-term workshop on TRANSBORAN project, "Transboundary population structure of sardine, European hake and blackspot seabream in the Alboran Sea and adjacent waters: A multidisciplinary approach"* (Malaga, Spain), 33 pp. 22–24 July 2019. CopeMed II Technical Documents N°52 (GCP/INT/028/SPA - GCP/INT/270/EC). Málaga.

Davies, A. G., and Sleep, J. A. (1989). The photosynthetic response of nutrient-depleted dilute cultures of skeletonema costatum to pulses of ammonium and nitrate; the importance of phosphate. *J. Plankt. Res.* 11 (1), 141–164. doi: 10.1093/plankt/11.1.141

Echevarría, F., García-Lafuente, J. G., Bruno, M., Gorsky, G., Goutx, M., Gonzalez, N., et al. (2002). Physical-biological coupling in the strait of Gibraltar. *Deep-Sea. Res. II.* 49 (19), 4115–4130. doi: 10.1016/S0967-0645(02)00145-5

Eppley, R. W., Rogers, J. N., and McCarthy, J. J. (1969). Half-saturation constants for uptake of nitrate and ammonium by marine phytoplankton. *Limnol. Oceanogr.* 14, 912–920. doi: 10.4319/lo.1969.14.6.0912

Esposito, G., Berta, M., Centurioni, L., Johnston, T. M. S., Lodise, J., Özgökmen, T., et al. (2021). Submesoscale vorticity and divergence in the Alboran Sea: Scale and depth dependence. *Front. Mar. Sci.* 8. doi: 10.3389/fmars.2021.678304

Fiechter, J., Pozo Buil, M., Jacox, M. G., Alexander, M. A., and Rose, K. A. (2021). Projected shifts in 21st century sardine distribution and catch in the California current. *Front. Mar. Sci.* 8. doi: 10.3389/fmars.2021.685241

Flexas, M. M., Gomis, D., Ruiz, S., Pascual, A., and Leon, P. (2006). *In situ* and satellite observations of the Eastward migration of the Western Alboran Sea gyre. *Prog. Oceanogr.* 70, 486–509. doi: 10.1016/j.pocean.2006.03.017

García, A. (2006). Estudio sobre la variabilidad del crecimiento larvario de la sardina (Sardina pilchardus, walbaum) del mar de alborán (Spain: University of Vigo).

García-Jove, M., Mourre, B., Zarokanellos, N. D., Lermusiaux, P. F. J., Rudnick, D. L., and Tintoré, J. (2022). Frontal dynamics in the Alboran Sea: 2. processes for vertical velocities development. *J. Geophys. Res.: Ocean.* 127, e2021JC017428. doi: 10.1029/2021JC017428

García-Lafuente, J., Cano, N., Vargas, M., Rubin, J. P., and Guerra, A. (1998). Evolution of the Alboran Sea hydrographic structures during July 1993. *Deep-Sea. Res.* 45, 39–65. doi: 10.1016/S0967-0637(97)00216-1

García-Lafuente, J., Vargas, J. M., Plaza, F., Sarhan, T., Candela, J., and Bascheck, B. (2000). Tide at the Eastern section of the strait of Gibraltar. *J. Geophys. Res.: Ocean.* 105 (C6), 14197–14213. doi: 10.1029/2000JC900007

García-Lafuente, J., Alvarez, E., Vargas, J. M., and Ratsimandresy, W. (2002). Subinertial variability in the flow through the strait of Gibraltar. *J. Geophys. Res.* 107 (C10), 32.1–32.9. doi: 10.1029/2001JC0011004

García-Lafuente, J., and Delgado, J. (2004). The meandering path of a drifter around the Western alboran gyre. *J. Phys. Oceanogr.* 34 (3), 685–692. doi: 10.1175/3516.1

García-Lafuente, J., Bruque Pozas, E., Sánchez-Garrido, J. C., Sannino, G., and Sammartino, S. (2013). The interface mixing layer and the tidal dynamics at the Eastern part of the strait of Gibraltar. *J. Mar. Syst.*, 117–118. doi: 10.1016/j.jmarsys.2013.02.014

García-Lafuente, J., Sánchez-Garrido, J.C., García, A., Hidalgo, M., Sammartino, S., Laiz, R., et al (2021). Biophysical processes determining the connectivity of the Alboran Sea fish populations. In J. C. Báez, J. T. Vázquez, J. A. Caminas and M. and Malouli (editors) *Alboran Sea –Ecosystems and marine resources*. Springer Nature Switzerland AG.

García, A., Laíz-Carrión, R., Cortés, D., Quintanilla, J., Uriarte, A., Ramírez, T., et al. (2021). "Chapter 13: Evolving from fry fisheries to early life research on pelagic fish resources," in *Alboran Sea – ecosystems and marine resources*. Eds. J. C. Báez, J. T. Vázquez, J. A. Caminas and M. Malouli (Cham, Switzerland: Springer Nature Switzerland AG), ISBN: .

Garrett, C., Bormans, M., and Thomson, K. R. (1990). "Is the exchange through the strait of Gibraltar maximal or submaximal?," in *The physical oceanography of Sea straits*, vol. 318 . Ed. L. J. Pratt (Dordrecht: Springer), 271–294. (Mathematical and Physical Sciences). doi: 10.1007/978-94-009-0677-8_13

Giorgi, F. (2006). Climate change hot-spots. *Geophys. Res. Lett.* 33, 1–4. doi: 10.1029/2006GL025734

Giráldez, A. (2021). "Chapter 16: Small pelagic resources: A historic perspective and current state of the resources," in *Alboran Sea – ecosystems and marine resources*. Eds. J. C. Báez, J. T. Vázquez, J. A. Caminas and M. Malouli (Cham, Switzerland: Springer Nature Switzerland AG), ISBN: .

Gómez, F., Echevarría, F., García, C. M., Prieto, L., Ruiz, L., Reul, A., et al. (2000). Microplankton distribution in the strait of Gibraltar: Coupling between organisms and hydrodynamics structures. *J. Plankt. Res.* 22, 603–617. doi: 10.1093/plankt/22.4.603

Gomis, D., Ruiz, S., and Pedder, M. A. (2001). Diagnostic analysis of the 3D ageostrophic circulation from a multivariate spatial interpolation of CTD and ADCP data. *Deep-Sea. Res. Part I.: Oceanogr. Res. Paper.* 48 (1), 269–295. doi: 10.1016/S0967-0637(00)00060-1

Hersbach, H., Bell, B., Berrisford, P., Biavati, G., Horányi, A., Muñoz Sabater, J., et al. (2018). *The ERA5 global reanalysis. Q J R Meteorol Soc.*; 146, 1994–2049. doi: 10.24381/cds.adbb2d47

Holton, J. R. (2004). *Introduction to dynamic meteorology. 4th Edition* (Amsterdam: Elsevier), 535.

Huertas, I. E., Ríos, A. F., García-Lafuente, J., Navarro, G., Makaoui, A., Sánchez-Roman, A., et al. (2012). Atlantic Forcing of the Mediterranean oligotrophy. *Global Biogeochem. Cy.* 26, GB2022. doi: 10.1029/2011GB004167

Jackson, C. R., and Apel, J. (2004). *An atlas of internal solitary-like waves and their properties. 2nd ed* (Alexandria, Va: Global Ocean Assoc.). Available at: http://www.internalwaveatlas.com/.

Jghab, A., Vargas-Yañez, M., Reul, A., Garcia-Martínez, M. C., Hidalgo, M., Moya, F., et al. (2019). The influence of environmental factors and hydrodynamics on sardine (*Sardina pilchardus*, walbaum 1792) abundance in the southern Alboran Sea. *J. Mar. Syst.* 191, 51–63. doi: 10.1016/j.jmarsys.2018.12.002

Kinder, T. H., and Bryden, H. L. (1990). "Aspiration of deep waters through straits," in *The physical oceanography of Sea straits*. Ed. L. J. Pratt (Dordercht, The Netherlands: Kluwer Academic Publishers), 295–319, ISBN: .

La Violette, P. E (1984). The advection of cyclonic submesoscale thermal features in the Alboran Sea. *Journal of Physical Oceanography* 14 (3), 550–565. doi: 10.1175/1520-0485(1984)014<0550:TAOSTF>2.0.CO;2.

La Violette, P., and Lacombe, H. (1988). Tidal-induced pulses in the flow through the Strait of Gibraltar. *Oceanol. Acta* 13–27.

Macías, D., Navarro, G., Bartual, A., Echevarría, F., and Huertas, I. E. (2009). Primary production in the strait of Gibraltar: Carbon fixation rates in relation to hydrodynamic and phytoplankton dynamics. *Estuar. Coast. Shelf. Sci.* 83, 197–210. doi: 10.1016/j.ecss.2009.03.032

Macias, D., Stips, A., Garcia-Gorriz, E., and Dosio, A. (2018). Hydrological and biogeochemical response of the Mediterranean Sea to freshwater flow changes for the end of the 21st century. *PLoS ONE* 13,): e0192174. doi: 10.1371/journal.pone.019217

Manca, B., Burca, M., Giorgetti, A., Coatanoan, C., Garcia, M. J., and Iona, A. (2004). Physical and biochemical averaged vertical profiles in the Mediterranean regions: An important tool to trace the climatology of water masses and to validate incoming data from operational oceanography. *J. Mar. Syst.* 48, 83–116. doi: 10.1016/j.jmarsys.2003.11.025

McWilliams, J. C. (2021). Oceanic frontogenesis. *Annu. Rev. Mar. Sci.* 13, 227–253. doi: 10.1146/annurev-marine-032320-120725

McWilliams, J. C., Gula, J., and Molemaker, M. J. (2019). The gulf stream north wall: Ageostrophic circulation and frontogenesis. *J. Phys. Oceanogr.* 49 (4), 893–916. doi: 10.1175/JPO-D-18-0203.1

Moran, X. A. G., and Estrada, M. (2001). Short-term variability of photosynthetic parameters and particulate and dissolved primary production in the Alboran Sea (SW Mediterranean). *Mar. Ecol. Prog. Ser.* 212, 53–67. doi: 10.3354/meps212053

Naranjo, C., García-Lafuente, J., Sannino, G., and Sánchez-Garrido, J. C. (2014). How much do tides affect the circulation of the Mediterranean Sea? from local processes in the strait of Gibraltar to basin-scale effects. *Progress in Oceanography*. 127, 108–116. doi: 10.1016/j.pocean.2014.06.005

Naranjo, C., Sammartino, S., García-Lafuente, J., Bellanco, M., and Taupier-Letage, I. (2015). Mediterranean Waters along and acrosss the strait of Gibraltar, characterization and zonal modification. *Deep-Sea. Res. I.* 105, 41–52. doi: 10.1016/j.dsr.2015.08.003

Navarro, G., Vázquez, A., Macías, D., Bruno, M., and Ruiz, J. (2011). Understanding the patterns of biological response to physical forcing in the Alboran Sea (Western Mediterranean). *Geophys. Res. Lett.* 38, L23606. doi: 10.1029/2011GL049708

Newton, C. W. (1978). Fronts and wave distributions in gulf stream and atmospheric jet stream. *J. Geophys. Res.* 83 (9), 4697–4706. doi: 10.1029/JC083iC09p04697

Oguz, T., Macías, D., García-Lafuente, J., Pascual,, and Tintoré, J. (2014). Fueling plankton production by a meandering frontal jet: A case study for the Alboran Sea (Western Mediterranean). *PloS One* 9 (11), e111482. doi: 10.1371/journal.pone.0111482

Parrilla, G., and Kinder, T. H. (1984). The Physical Oceanography of the Alboran Sea, [Rep] 40 (1), 143–184. Oceanogr. Group Div. of Applied Sciences, Harvard Univ.

Pascual, A., Ruiz, S., Olita, A., Troupin, C., Claret, M., Casas, B., et al. (2017). A multiplatform experiment to unravel meso- and submesoscale processes in an intense front (AlborEx). *Front. Mar. Sci.* 4. doi: 10.3389/fmars.2017.00039

Peliz, A., Boutov, D., and Teles-Machado, A. (2013). The Alboran Sea mesoscale in a long-term resolution simulation: Statistical analysis. *Ocean. Model.* 72, 32–52. doi: 10.1016/j.ocemod.2013.07.002

Perkins, H., Kinder, T., and La-Violette, P. (1990). The Atlantic inflow in the Western Alboran Sea. *J. Phys. Oceanogr.* 20, 242–263. doi: 10.1175/1520-0485(1990)020<0242:TAIITW>2.0.CO;2

Pratt, L. J., and Whitehead, J. A. (2008). *Rotating hydraulics: Nonlinear topographic effects in the ocean and atmosphere* Vol. 36 (New York, NY: Springer), 589 pp. Atmos. Ocean. Sci. Libr.

Ramírez, E., Macías, D., García, C. M., and Bruno, M. (2014). Biogeochemical patterns in the Atlantic inflow through the strait. *Deep. Sea. Res.* 85, 88–100. doi: 10.1016/j.dsr.2013.12.004

Ramírez, T., Muñoz, M., Reul, A., García-Martinez, C., Moya, F., Vargas-Yáñez, M., et al. (2021). "Chapter 7: The biogeochemical context of marine planktonic ecosystems," in *Alboran Sea – ecosystems and marine resources*. Eds. J. C. Báez, J. T. Vázquez, J. A. Caminas and M. Malouli (Springer Nature Switzerland AG), ISBN: .

Renault, L., Oguz, T., Pascual, A., Vizoso, G., and Tintore, J. (2012). Surface circulation in the alborn Sea (Western Mediterranean) inferred from remotely sensed data. *J. Geophys. Res.* 117 (8), 1–11. doi: 10.1029/2011JC007659

Ruiz, S., Claret, M., Pascual, A., Olita, A., Troupin, C., Capet, A., et al. (2019). Effects of oceanic mesoscale and submesoscale frontal processes on the vertical transport of phytoplankton. *J. Geophys. Res.: Ocean.* 124 (8), 5999–6014. doi: 10.1029/2019JC015034

Ruiz, J., Macías, D., Rincón, M., Pascual, A., Catalán, I. A., and Navarro, G. (2013). Recruiting at the edge: Kinetic energy inhibits anchovy populations in the Western Mediterranean. *PloS One* 8 (2), e55523. doi: 10.1371/journal.pone.0055523

Ruti, P. M., Somot, S., Giorgi, F., Dubois, C., Flaounas, E., Obermann, A., et al. (2016). Med-CORDEX initiative for Mediterranean climate studies. *Bull. Am. Meteorol. Soc.* 97 (7), 1187–1208. doi: 10.1175/BAMS-D-14-00176.1

Sánchez-Garrido, J. C., Fiechter, J., Rose, K. A., Werner, F. E., and Curchitser, E. N. (2021). Dynamics of anchovy and sardine populations in the canary current off NW Africa: Responses to environmental and climate forcing in a climate-to-Fish ecosystem model. *Fish. Oceanogr.* 30, 232–2252. doi: 10.1111/fog.12516

Sánchez-Garrido, J. C., García-Lafuente, J., Álvarez Fanjul, E., García Sotillo, M., and de los Santos, F. J. (2013). What does cause the collapse of the Western alboran gyre? results of an operational ocean model. *Prog. Oceanogr.* 116, 142–153. doi: 10.1016/j.pocean.2013.07.002

Sánchez-Garrido, J. C., García-Lafuente, J., Criado Aldeanueva, F., Baquerizo, A., and Sannino, G. (2008). Time-spatial variability observed in velocity of propagation of the internal bore in the strait of Gibraltar. *J. Geophys. Res.* 113, C07034. doi: 10.1029/2007JC004624

Sánchez Garrido, J. C., Naranjo, C., Macías, D., García-Lafuente, J., and Oguz, T. (2015). Modeling the impact of tidal flows on the biological productivity of the Alboran Sea. *J. Geophys. Res.: Ocean.* 120 (11), 7329–7345. doi: 10.1002/2015JC010885

Sánchez-Garrido, J. C., Sannino, G., Liberti, L., García-Lafuente, J., and Pratt, L. (2011). Numerical modeling of three-dimensional stratified tidal flow over camarinal sill, strait of Gibraltar. *J. Geophys. Res.* 116, C12026. doi: 10.1029/2011JC007093

Sannino, G., Pratt, L., and Carillo, A. (2009). Hydraulic criticality of the exchange flow through the strait of Gibraltar. *J. Phys. Oceanogr.* 39, 2779–2799. doi: 10.1175/2009JPO4075.1

Sarhan, T., García-Lafuente, J., Vargas, M., Vargas, J. M., and Plaza, F. (2000). Upwelling mechanisms in the northwestern Alboran Sea. *J. Mar. Syst.* 23 (4), 317–331. doi: 10.1016/S0924-7963(99)00068-8

Soto-Navarro, J., Criado-Aldeanueva, F., García-Lafuente, J., and Sánchez-Román, A. (2010). Estimation of the Atlantic inflow through the strait of Gibraltar from climatological and *in situ* data. *J. Geophys. Res.* 115, C10023. doi: 10.1029/2010JC006302

Soto-Navarro, J., Jordá, G., Amores, A., Cabos, W., Somot, S., Sevault, F, et al. (2020). Evolution of Mediterranean Sea water properties under climate change scenarios in the med-CORDEX ensemble. *Climate Dyn* 54, 2135–2165. doi: 10.1007/s00382-019-05105-4

Spall, M. A. (1995). Frontogenesis, subduction, and cross-front exchange at upper ocean fronts. *J. Geophys. Res.* 100 (C2), 2543–2557. doi: 10.1029/94JC02860

Steinacher, M., Joos, F., Frölicher, T., Bopp, L., Cadule, P., Cocco, V., et al. (2010). Projected 21st century decrease in marine productivity: A multi-model analysis. *Biogeosciences* 7, 979–1005. doi: 10.5194/bg-7-979-2010

Tintoré, J., Wang, D., and La Violette, P. E. (1990). Eddies and thermohaline intrusions of the Shelf/Slope front off the northeast Spanish coast. *J. Geophys. Res.* 95. doi: 10.1029/JC095iC02p01627. issn: 0148-0227.

Troupin, C., Pascual, A., Ruiz, S., Olita, A., Casas, B., Margirier, F., et al. (2019). The AlborEX dataset: Sampling of Sub-mesoscale features in the Alboran Sea. *Earth Syst. Sci. Data* 11, 129–145. doi: 10.5194/essd-11-129-2019

Uitz, J., Stramski, D., Gentilli, B., D'Ortenzio, F., and Claustre, H. (2012). Estimates of phytoplankton class-specific and total primary production in the Mediterranean Sea from satellite ocean color observations. *Global Biogeochem. Cycle.* 26 (2). doi: 10.1029/2011GB004055

Vargas-Yáñez, M., García-Martinez, M., Moya, F., Balbín, R., and López-Jurado, J. (2021). "Chapter 4: The oceanographic and climatic context," in *Alboran Sea – ecosystems and marine resources*. Eds. J. C. Báez, J. T. Vázquez, J. A. Caminas and M. Malouli (Springer Nature Switzerland AG), ISBN: . doi: 10.1007/978-3-030-65516-7_4

Vargas-Yáñez, M., Giráldez, A., Torres, P., González, M., García-Martínez, MC., Moya, F., et al (2020). "Variability of oceanographic and meteorological conditions in the northern Alboran Sea at seasonal, interannual and long-term time scales and their infuence on sardine (Sardina pilchardus, Walbaum 1792) landings. *Fish. Oceanogr*. 1–14. doi: 10.1111/fog.12477

Vargas-Yáñez, M., Plaza, F., García-Lafuente, J., Sarhan, T., Vargas, J. M., and Vélez-Belchi, P. (2002). About the seasonal variability of the Alboran Sea circulation. *J. Mar. Syst.* 35 (3–4), 229–248. doi: 10.1016/S0924-7963(02)00128-8

Vélez-Belchí, P., Vargas-Yáñez, M., and Tintoré, J. (2005). Observation of a Western alboran gyre migration. *Progr. Oceanogr.* 66, 190–210. doi: 10.1016/j.pocean.2004.09.006

Viúdez, A., and Haney, R. L. (1997). On the relative vorticity of the Atlantic jet in the Alboran Sea. *J. Phys. Oceanogr.* 27, 175–185. doi: 10.1175/1520-0485(1997)027<0175:OTRVOT>2.0.CO;2

Viúdez, Á., and Tintoré, J. (1995). Time and space variability in the Eastern Alboran Sea from march to may 1990. *J. Geophys. Res.* 100 (C5), 8571–8586. doi: 10.1029/94JC03129

Vlasenko, V., Brandt, P., and Rubino, A. (2000). Structure of Large-amplitude internal solitary waves. *J. Phys. Oceanogr.* 30 (9), 2172–2185. doi: 10.1175/1520-0485(2000)030<2172:SOLAIS>2.0.CO;2

Vlasenko, V., Sánchez Garrido, J. C., Stashchuk, N., García-Lafuente, J., and Losada, M. (2009). Three-dimensional evolution of Large-amplitude internal waves in the strait of Gibraltar. *J. Phys. Oceanogr.* 39, 2230–2246. doi: 10.1175/2009JPO4007.1

Wesson, J. C., and Gregg, M. C. (1994). Mixing at camarinal sill in the strait of Gibraltar. *J. Geophys. Res. Ocean.* 99, 9847–9878. doi: 10.1029/94JC00256

Whitehead, J. A., and Miller, A. R. (1979). Laboratory simulation of the gyre in the Alboran Sea. *J. Geophys. Res.* 84. doi: 10.1029/JC084iC07p03733. issn: 0148-0227.

Williams, R. G., and Follows, M. J. (2003). Physical transport of nutrients and the maintenance of biological production. *Ocean. Biogeochem ,The Role of the Ocean Carbon Cycle in Global Change* M.J.R Fasham (Springer Nature Switzerland).

Zarokanellos, N. D., Rudnick, D. L., Garcia-Jove, M., Mourre, B., Ruiz, S., Pascual, A., et al. (2022). Frontal dynamics in the Alboran Sea: 1. coherent 3D pathways at the almeria-Oran front using underwater glider observations. *J. Geophys. Res.: Ocean.* 127, e2021JC017405. doi: 10.1029/2021JC017405

frontiers | Frontiers in Marine Science

TYPE Original Research
PUBLISHED 11 August 2022
DOI 10.3389/fmars.2022.960929

OPEN ACCESS

EDITED BY
Çetin Keskin,
Istanbul University, Turkey

REVIEWED BY
M. Pilar Olivar,
Institute of Marine Sciences, Spanish National Research Council (CSIC), Spain
Milica Mandic,
University of Montenegro, Montenegro

*CORRESPONDENCE
Marco Torri
marco.torri@cnr.it

SPECIALTY SECTION
This article was submitted to Marine Fisheries, Aquaculture and Living Resources, a section of the journal Frontiers in Marine Science

RECEIVED 03 June 2022
ACCEPTED 18 July 2022
PUBLISHED 11 August 2022

CITATION
Patti B, Torri M and Cuttitta A (2022) Interannual summer biodiversity changes in ichthyoplankton assemblages of the Strait of Sicily (Central Mediterranean) over the period 2001–2016.
Front. Mar. Sci. 9:960929.
doi: 10.3389/fmars.2022.960929

Interannual summer biodiversity changes in ichthyoplankton assemblages of the Strait of Sicily (Central Mediterranean) over the period 2001–2016

Bernardo Patti[1], Marco Torri[2]* and Angela Cuttitta[2]

[1]National Research Council of Italy, Institute for the Study of Anthropic Impacts and Sustainability in the Marine Environment, (CNR-IAS), Palermo, Italy, [2]National Research Council of Italy, Institute for Studies on the Mediterranean, (CNR-ISMed), Palermo, Italy

Interannual fluctuations in the structure and the composition of ichthyoplankton assemblages in the pelagic waters of the Strait of Sicily (SoS, Central Mediterranean) were investigated, trying to relate them to the observed variability in oceanographic conditions. Plankton data used in this study were from 16 summer surveys carried out in the SoS every year from 2001 to 2016, using oblique bongo plankton net (0–100 m) tows. Out of more than 12,000 fish larvae collected in the sampling stations included in the analysis, 9,519 of them were identified and regularly classified in 15 orders and 49 families. Ichthyoplankton assemblages, defined at the family level due to the uniform availability of this information along the time series, showed a decreasing trend over time in total larval abundance, along with taxonomic (family) richness and Shannon index (α diversity), more pronounced in the shelf area and in the slope area, respectively. Conversely, the relatively high levels of yearly compositional changes observed in the larval assemblage from both shelf and slope areas, as estimated by the Jaccard dissimilarity index (β diversity), did not show any significant linear trend. In addition, a biodiversity hotspot (both in terms of family richness and Shannon index) was evidenced in the frontal structure characterizing the southeastern part of the study area. Generalized additive models were used to evaluate the effect of oceanographic conditions on the temporal and spatial patterns of ichthyoplankton biodiversity. Results evidenced the role of salinity, surface temperature, and surface currents in modulating biodiversity indices, especially in the shelf area. Finally, the relevance of local frontal oceanographic structures in sustaining high biodiversity levels is postulated.

KEYWORDS

biodiversity, fish larvae, mesopelagic, demersal, pelagic, epipelagic, Central Mediterranean, Strait of Sicily

Introduction

Biodiversity is generally considered one of the key factors of ecosystem resilience in response to anthropogenic and natural pressures. Its positive impact on ecosystem functions and services, including fisheries production, is well established (Loreau et al., 2001; Cardinale et al., 2002; Bakun, 2006; Worm et al., 2006; Duffy, 2009; Naeem et al., 2009; Cardinale et al., 2012; Hooper et al., 2012; Tilman et al., 2012; Tilman et al., 2014), also in contrast to regime shifts (Gamfeldt et al., 2014; Ponti et al., 2014; Rocha et al., 2015).

The biodiversity in marine ecosystems is the result of the complex interconnection among all co-occurring organisms at different trophic levels, and the loss of just one ecological level may have severe effects on the functioning of the entire ecosystem community. Within this complex set of interspecific relationships, fish assemblage structure can be affected by several natural and anthropogenic processes, such as overfishing, pollution, habitat loss, and climate change (Jennings and Kaiser, 1998; Gray et al., 2005; Poulard and Blanchard, 2005; Lehodey et al., 2006; Rijnsdorp et al., 2009; Rochet et al., 2010). Therefore, a deeper understanding of the functioning of ecosystem-level processes is necessary to mitigate potential unsustainable exploitation and biodiversity losses and to support management approaches (Pikitch et al., 2004; Mittermeier et al., 2011).

In this framework, biodiversity studies based on fish early life stages can also provide information on spawning grounds and nursery areas, with implications on stock biomass fluctuations induced by recruitment variability (Houde, 2002; Ospina-Álvarez et al., 2013; Ospina-Álvarez et al., 2015; Torri et al., 2018; Patti et al., 2020). In particular, as survival and growth processes of many fish species are controlled by the impact of the marine environment on early life stages, further research on the temporal and spatial trends in the distribution and abundance of fish larvae in relation to changes in abiotic factors is highly relevant (Nonaka et al., 2000). In addition, changes in the structure and in the distribution of larval fish assemblages may be the effect of oceanographic factors, which, in turn, are also often characterized by high dynamic conditions in space and time (Moyano et al., 2009; Vilchis et al., 2009; Hernandez et al., 2010; Moyano and Hernández-León, 2011; Katsuragawa et al., 2014; Moyano et al., 2014).

In the Mediterranean Sea, previous studies on larval fish assemblages are quite limited for many taxa and are generally based on relatively short time series (Sabatés, 1990; Cuttitta et al., 2004; Isari et al., 2008; López-Sanz et al., 2009; Álvarez et al., 2012; Zarrad et al., 2013; Álvarez et al., 2015; Cuttitta et al., 2016a; Cuttitta et al., 2016b; Cuttitta et al., 2018; Malavolti et al., 2018; Zarrad et al., 2020; Zorica et al., 2020).

In particular, as far as concerns the study area of the present paper [i.e., the Strait of Sicily (SoS)], previous investigations were limited to the analysis of the structure of larval fish assemblages in relation to local physical forcings (Cuttitta et al., 2016a; Cuttitta et al., 2016b; Cuttitta et al., 2018). However, in the same area, no studies on the changes in larval biodiversity, both over time and/or among sub-regions, are still available. To our knowledge, the present study does represent the first attempt of evaluating trends in biodiversity of summer fish larval assemblages in the SoS, also using the longest reported time series (16 consecutive years) for the Mediterranean Sea.

As a model system, the SoS is a relatively small area that can be considered an optimal natural laboratory for evaluating trends in the biodiversity and structure of larval fish assemblages. This region is generally considered oligotrophic; however, the southern coast of Sicily is an upwelling area with relatively high productivity levels (Piccioni et al., 1988; Patti et al., 2010). In addition, local surface circulation and oceanographic features such as gyres and fronts (Robinson et al., 1991; Lermusiaux, 1999; Lermusiaux and Robinson, 2001; Bonanno et al., 2014; Placenti et al., 2022) were demonstrated to have an important role in concentration and retention processes for early stages of many taxa, including important pelagic fish species (García Lafuente et al., 2002; Falcini et al., 2015; Cuttitta et al., 2016a; Cuttitta et al., 2018; Torri et al., 2018; Falcini et al., 2020; Patti et al., 2020; Russo et al., 2021; Torri et al., 2021). Actually, in the SoS, the surface circulation is dominated by the motion of Atlantic waters, which is known as AIS (Atlantic Ionian Stream; Robinson et al., 1999) off the southern coast of Sicily. This along-channel meandering surface current transports fish larvae downstream (Patti et al., 2018; Falcini et al., 2020), and, in meeting the Ionian Sea water masses, originates a frontal structure where planktonic organisms are eventually concentrated and retained (García Lafuente et al., 2002). The path of AIS and its year-to-year variability may have consequences for the other predominant hydrological phenomena occurring in the region, such as the extension of upwelling, the formation of frontal features, and the strength in retention processes. In particular, the latter has been demonstrated to be the main mechanism able to modulate the interannual changes in stock biomass of local anchovy (*Engraulis encrasicolus*; Linnaeus, 1758) population (Patti et al., 2020).

In this context, although, with the aims of data analysis, the available yearly ichthyoplankton information was assembled at the family level only, the present paper intended to investigate, for the first time for the SoS, on the interannual changes in the size and the structure (α diversity) and in composition (β diversity) of larval fish assemblages, in a study area where plankton surveys were carried out during the summer season on a regular yearly basis over the period 2001–2016. In addition, the role of spatial oceanographic patterns in modulating larval biodiversity is also explored. In providing the analysis of the longest available time series of larval fish assemblages in the Central Mediterranean, this study is meant to pave the way to the evaluation of the relative importance of oceanographic

conditions on the summer biodiversity patterns of planktonic fish stages in the SoS, with special emphasis on the role that surface current strength and local mesoscale features may have in supporting biodiversity hotspots.

Material and methods

Ichthyoplankton data

The study area is located in the SoS, off the southern Sicilian coast (Figure 1), covering a surface of about 25,000 km^2.

Oceanographic data and ichthyoplanktonic samples were collected in 16 annual oceanographic surveys carried out during the summer period on board of the R/V "Urania" (2001–2014) and R/V "Minerva Uno" (2015–2016). Table 1 shows the list of surveys, including information on the survey periods and on the total number of sampled stations by year (range: 119–229). Average duration time of the surveys is about 18 days, and the central day of the surveys is 14 July.

The sampling was based on a systematic station grid of 6 × 6 nautical miles on the continental shelf (bottom depth < 200 m) and on a grid of 12 × 12 nautical miles for the offshore areas with bottom depth greater than 200 m. However, to the sake of the present study, the analyses used only data from 37 sampling sites that were sampled in each one of the annual summer surveys that were regularly carried out over the period 2001–2016, 19 of them located on the continental shelf of the study area ("shelf" sub-region) and 18 over bottom depths greater than 200 m ("slope" sub-region) (Figure 1). In total, data from n. 592 sampling hauls (i.e., 37 sites multiplied by 16 years) were used for this study (about 22% of the stations listed in Table 1). This choice was driven by the need of ensuring comparability across years, to get unbiased estimates of diversity indices, not affected by the variable sampling effort over time both in terms of number of stations and extension of covered area.

Plankton samples were collected using a bongo net (Bongo40, with 40-cm opening) towed obliquely from the surface to 100-m depth or to 5 m from the bottom in shallower stations and equipped with a 200-µm mesh size net. Stations were sampled 24 h a day, to minimize bias in the catch of fish species that, during the larval stage, typically may show relatively large diel vertical migration patterns (Olivar et al., 2001; Sabatés et al., 2008; Olivar et al., 2014). All the samples

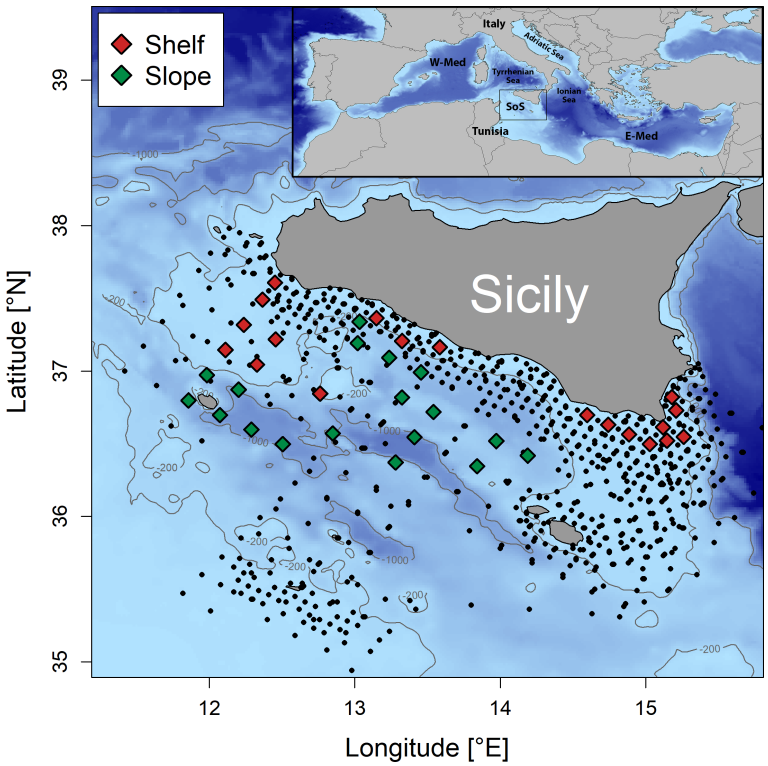

FIGURE 1
Map of locations of the sampling stations. Data collected from sites marked with squares, available for each one of 16 summer surveys carried out over the period 2001–2016, were used in the present study. Different colors refer to the bottom depth, red for stations with bottom depth ≤ 200 m ("Shelf") and green for stations with bottom depth > 200 m ("Slope"). The sites of all stations sampled in the summer surveys 2001–2016 and listed in Table 1 are also displayed with black circles for the sake of comparison (see Figures S1, S2 and related discussion).

TABLE 1 List of ichthyoplankton summer surveys carried out in the study area during the period 2001–2016.

Year	Survey	Period	Number of Stations (BONGO40 hauls)
2001	ANSIC2001	7 July to 25 July 2001	143
2002	ANSIC2002	11 July to 31 July 2002	218
2003	ANSIC2003	11 July to 2 August 2003	166
2004	ANSIC2004	18 June to 7 July 2004	180
2005	BANSIC2005	7 July to 24 July 2005	170
2006	BANSIC2006	30 July to 10 August 2006	119
2007	BANSIC2007	28 June to 17 July 2007	161
2008	BANSIC2008	25 June to 14 July 2008	182
2009	BANSIC2009	3 July to 22 July 2009	149
2010	BANSIC2010	25 June to 14 July 2010	187
2011	BANSIC2011	8 July to 26 July 2011	134
2012	BANSIC2012	4 July to 23 July 2012	154
2013	BANSIC2013	26 June to 16 July 2013	229
2014	BANSIC2014	22 July to 9 August 2014	189
2015	BANSIC2015	16 July to 3 August 2015	157
2016	BANSIC2016	30 June to 14 July 2016	170

used were from the same side and cod-end collector of the Bongo. Samples were immediately fixed after collection and preserved in a 10% buffered-formaldehyde (and/or 70% alcohol) and sea-water solution for further sorting in laboratory by stereomicroscopy.

Fish larvae were sorted from the rest of the plankton and identified, as far as possible, to the species taxonomic level. Taxonomic identification was based on Bertolini et al. (1956); Moser and Ahlstrom (1996); Costa (1999), and Tortonese (1970). However, because of heterogeneity in the capabilities of resolving the species (and/or genus) taxonomic level in sorted larvae across years (2001–2016), with the aims of the present paper, detected taxa were grouped at the family level (for a total of 49 different families identified in the selected sampling stations).

For the evaluation of rank abundance, raw counts of larval specimens were firstly standardized to numbers per square meter. Mean larval densities estimates were derived for each family and by year from the counts based on estimates of the volume of seawater filtered by mechanical flowmeters (General Oceanics Inc., FL, USA) and the tow depth for each sample.

Oceanographic data

A set of environmental parameters was selected and used for investigating on their influence on the temporal and spatial changes in biodiversity of local ichthyoplankton assemblages.

Continuous vertical profiles of temperature data were acquired in all Bongo40 plankton stations to characterize the physical properties of the water column. The collected downcast data were obtained by a multiparametric SBE 11 plus CTD probe and were quality-checked and processed according to the Mediterranean and Ocean Data Base instructions (Brankart, 1994), using the Seasoft-Win32 software. From the set of available environmental information collected in CTD casts, the parameters used in this study were bottom depth, temperature, and salinity.

As most of the larvae in the Mediterranean Sea during the summer are mainly concentrated in the mixed layer (Palomera, 1991; Mazzola et al., 2000), in this study, the 10-m depth was used as reference for temperature and salinity conditions in the selected stations. Specifically, the average values of the available measurements from the first 10 m of the water column were used, which can also be considered as representative of the surface conditions, as during the summer, the mixed layer depth (MLD; in m) is typically deeper than 10 m. The MLD (in m) itself is an additional parameter considered in the data analysis, and its value has been derived from each CTD profile using the algorithm described in Kara et al. (2000), as it is known to be an important driver for the definition of the potential spawning habitat (Planque et al., 2007).

The impact of mesoscale oceanographic features such as upwelling, cold filaments, and fronts on the ichthyoplankton spatial distribution (Torri et al., 2018; Patti et al., 2020) was also taken into account. Actually, oceanographic structures can influence the distribution of chemical and physical properties of the water column with a potential effect on larval survival and development (Cuttitta et al., 2004; Cuttitta et al., 2016a; Cuttitta et al., 2016b; Cuttitta et al., 2018). Therefore, the surface circulation features were evaluated by using data about the absolute dynamic topography (ADT; in cm) (daily data; spatial resolution: 0.125 × 0.125 degrees) and the derived u and v components of geostrophic currents, produced by Copernicus

Marine Environment Monitoring Service (CMEMS; http://marine.copernicus.eu/). ADT data are representative of important oceanographic features such as mesoscale eddies and meanders (Pujol and Larnicol, 2005), which are able to affect primary production and can act as physical barriers for the larval distribution or be responsible for their dispersal offshore. In addition, the absolute geostrophic current speed (GCS; in cm s^{-1}) was derived from the zonal (u) and meridional (v) components of surface current and used as an additional potential predictor in the subsequent modeling approach.

Finally, information about the sea surface chlorophyll-a concentration (Chl-a; in mg m^{-3}) was also applied, as Chl-a is a good proxy of primary productivity (Joint and Groom, 2000) and indirectly can be helpful in depicting the presence of favorable feeding conditions for larvae. High-resolution (1 × 1 km) satellite daily data available for download from CMEMS were used for this purpose.

For all the satellite-based information, the available data were extracted for each plankton station included in the analysis, based on the spatial and temporal position of the associated sampling hauls.

Data analysis

The analysis of temporal and spatial changes in biodiversity of larval fish assemblages can be addressed using measures of α diversity, which evaluates the change over time in the size and in the structure, and of β diversity, which aims at assessing the compositional change within the assemblage (Whittaker, 1960; Whittaker, 1972).

For measuring changes in α diversity over the 16 year long period considered in this study, we firstly applied Family richness (*Fr*), by evaluating the number of taxonomic groups at the family level by station. In addition, for each sampling station, the Shannon diversity index (*H'*, at the family level) was calculated. When needed, the two indices were averaged by year and by sub-area ("shelf" and "slope" sub-regions) and were also used to evaluate potential spatial patterns in the study area in relation to the environmental conditions. Calculations were done using the function *diversity* in the R package *vegan* (Oksanen et al., 2020; R Core Team, 2022).

Compositional shifts in the assemblages (β diversity) were evaluated by the Jaccard pair-wise dissimilarity index (Jaccard, 1908; Magurran, 2004; Magurran et al., 2019), based on presence/absence (0/1) data at station level. In particular, temporal trends were evaluated using plots in which the first year of the time series (2001) was compared with each one of the successive years (Dornelas et al., 2014). Spatial patterns were also investigated as well, calculating the index by sub-area ("shelf" and "slope").

The significance of linear trends in yearly larval standardized abundance and family richness was tested by applying a Bonferroni adjustment, to account for multiple testing and decreasing chances for a type I error (Miller, 1981).

Generalized additive models (GAMs; Hastie and Tibshirani, 1990) were used to examine the influence of environmental conditions on α and β diversity over time.

GAM is a semi-parametric extension of GLM, where the only underlying assumption made is that the functions are additive and the linear predictor is the sum of smoothing functions. This makes GAM very flexible, and they can fit very complex functions. Dependent variables were Family richness (*Fr*) and Shannon index (*H'*) for α diversity and Jaccard index for β diversity. Family richness has been modeled considering Poisson as discrete probability distribution and "log" as the link function between the stochastic and systematic parts of the model, whereas Gaussian distribution and the "identity" link have been implemented for Shannon and Jaccard indices. Explanatory variables used in GAMs were bottom depth, temperature, and salinity (at 10 m), surface Chl-a, MLD, ADT, GCS, and year. The potential non-linear relationships between covariates and the dependent variables were investigated by cubic regression splines. In addition, because one of the objectives of the analysis was to evaluate the role of the frontal feature characterizing the Eastern part of the study area as a retention mesoscale structure potentially able to favor biodiversity hotspots, latitude and longitude of sampling stations were also included among the independent variables.

Model estimations were based on a backward stepwise selection, starting from the entire set of explanatory variables that were chosen for the present study.

GAMs were implemented using the R package "mgcv" (Wood, 2011).

Results

In the selected group of 592 sampling hauls (37 sampling sites × 16 annual surveys) considered in this study, out of a total of 12,713 larvae sorted from the samples, 9,519 of these were identified (classified in 15 orders, 49 families, 64 genera, and 68 species), distributed in 6,046 larvae from stations located in the shelf area and 3,473 larvae from stations in the slope area. Four main ecological groups were singled out, i.e., meso-bathypelagic (M/B), demersal (D), pelagic/epipelagic (P/EP), and small pelagic (SP). The latter was the most abundant one, with 3,386 identified fish larvae from just two species (European anchovy, *Engraulis encrasicolus*, and Round sardinella, *Sardinella aurita*), which jointly represented more than 35% of the total number of identified larvae in the whole study area and which were mainly found in the continental shelf stations (about 75% of their total abundance was concentrated in that area for both the two species). There were also 2,916 demersal fish larvae (shelf, 2,127; slope, 789) grouped into 33 demersal families with 34 genera and 443 pelagic/epipelagic fish larvae (shelf, 304; slope,

139) grouped into five families with seven genera. Meso-bathypelagic fish larvae were 2,707 in number (shelf, 1,038; slope, 1,669) and grouped into nine families with 18 genera. They jointly represented about 29.1% of total abundance (49.0% in the slope area).

Larval density by unit surface (10 m^2) and relative abundance aggregated at the family level and distributed by sub-regions ("shelf" and "slope") are given in Table 2.

The total number of fish larvae sampled in the 37 stations included in this study across the 16 summer surveys over the period 2001–2016 fluctuated from a maximum of 860 in 2004 to a minimum of 382 in 2015, with a slight but significant ($p < 0.05$) decreasing trend that is due to the shelf sub-region, characterized by generally higher abundances compared to the slope sub-region (not shown). The same patterns are evident in Figure 2A, where yearly average larval density standardized by unit surface is shown instead. Again, the overall significant ($p < 0.05$) decreasing pattern is due to shelf stations, as larval density in slope stations does not indicate any significant trend in time.

Figure 2B shows the trend in Family richness (*Fr*) over the considered period in the 37 selected stations. The total number of families exhibits a significant decreasing trend ($p < 0.01$), from about 28 families at the early 2000 to 22 families at mid 2010. However, the overall decreasing trend is mainly due to stations located at bottom depths greater than 200 m ("slope" sub-area; $p < 0.001$). It is worth noting that, when using information from all the sampling stations listed in Table 1, family richness exhibited a very similar decreasing trend ($p < 0.05$) (Figure S1, Supplementary Material). The same applies to larval density (Figure S2, Supplementary Material). In general, the results of the comparisons show that the trends in biodiversity observed in the 37 selected stations are representative of the patterns characterizing all the sampling stations listed in Table 1.

The average number of families in the 37 selected stations over the period 2001–2016 is *Fr* = 25.1 (*Fr* = 20.6 in the 19 stations of shelf area; *Fr* = 19.1 in the 18 stations of slope area). Out of the total number of 49 identified families, just 11 taxa were always present in the time series, with 22 taxa found in at least half of the years. The taxa accumulation curve over the whole study area shows the asymptotic value (*Fr* = 49 families) after the first 10 years of the time series (Figure S3).

Temporal trends of Shannon index (*H'*) and Family richness (*Fr*) are very similar. Namely, *H'* is significantly decreasing ($p < 0.05$) over the considered periods (2001–2016), and as already observed for *Fr*, the overall pattern based on all the selected stations is mainly driven by stations in the slope area (Figure S4).

The spatial pattern of average total larval density (sum of specimens from all the identified families by unit surface) and of average *Fr* by sampling station over the entire period 2001–2016 are shown in Figure 3. Higher concentrations of larval stages are found in the southeastern part of the study area (Figure 3, left panel). The same region appears to represent a biodiversity hotspot (Figure 3, right panel).

Finally, the average yearly Jaccard dissimilarity is shown in Figure S5. The rate of compositional changes (*sensu*; Magurran et al., 2019) appears to be quite of high throughout for the whole investigated period in both shelf and slope areas, but it does not indicate any significant linear trend through time, even when information is separated by sub-area (Figure S5). However, a marked decreasing drift is apparent in the last year of the time series (2016).

Rank abundances (and proportions), reported in Figure S6, evidenced that larval densities in shelf area are about two times higher than in the slope region and are dominated by Engraulidae (one species, European anchovy), Clupeidae (one species, Round sardinella), and Gobiidae, representing more than 50% of collected larvae. Engraulidae and Clupeidae are quite abundant even in the slope area (jointly accounting for about 20% of that sub-region), where the leading families are Gonostomatidae (mostly represented by just one identified species, *Cyclothone braueri*) and Myctophidae (assembling 15 species), together accounting for more than 40% of larval abundances.

Polar rank plots of Figure S7 show for the shelf area an alternation over the length of time series in the dominance of the two most abundant species in the larval fish assemblages, i.e., European anchovy (Engraulidae) and Round sardinella (Clupeidae). Conversely, in the slope area, the abundances of the two above small pelagic species appear to be mostly synchronous and are generally lower compared to the shelf area, with greater interannual fluctuations. The most abundant family in the slope area is Gonostomatidae, followed by Myctophidae. However, the occurrence of the latter two families is quite high in the shelf area as well, although with a lower stability in rank abundance. In addition, comparing Figure 2A with Figure S7, it is worth noting how the peaks in total larval density of the slope area detected in years 2001, 2004, 2009, and 2015-2016, as well as its "lows" in 2002, 2008, 2010, and 2014, are also linked to the impact of neritic families (i.e., Clupeidae, Engraulidae, and Gobiidae).

GAM output

Results from GAM runs on the whole dataset (shelf + slope subareas) and by sub-area are presented in Figures 4, 5 for the two indices of α diversity.

Specifically, the output of GAMs for the dependent variables *Fr* (Figure 4A) and *H'* (Figure 5A) applied on all selected stations were almost coincident. The analysis of both metrics agreed in confirming the already observed general decreasing trend in biodiversity over time, at least up to 2012 (see also Figures S1, S4) and the west–east increasing diversity gradient already evidenced by Figure 3 (positive effect of greater than average values of longitude), and in showing an optimal temperature value at about 23°C–24°C and a negative effect of relatively large

10.3389/fmars.2022.960929

TABLE 2 Average density (#/m^2) and relative abundance (%, percentage) of larval fish families identified in the 37 selected stations over the summer surveys 2001–2016, by sub-areas.

Family	Ecological Group	Shelf		Slope		Total Area	
		#/10 m^2	%	#/10 m^2	%	#/10 m^2	%
Ammodytidae	D	0.32	0.12	0.55	0.35	0.43	0.20
Apogonidae	D	0.12	0.04	0.05	0.03	0.09	0.04
Blennidae	D	1.65	0.60	0.57	0.37	1.12	0.52
Bothidae	D	4.43	1.63	3.50	2.26	3.98	1.85
Callionymidae	D	3.43	1.26	0.66	0.43	2.08	0.97
Carapidae	D	0.04	0.02	0.14	0.09	0.09	0.04
Centracanthidae	D	3.90	1.43	0.76	0.49	2.37	1.10
Centriscidae	D	0.23	0.08	0.13	0.09	0.18	0.08
Cepolidae	D	0.93	0.34	0.24	0.16	0.60	0.28
Congridae	D	0.37	0.13	0.58	0.38	0.47	0.22
Cynoglossidae	D	0.00	0.00	0.04	0.03	0.02	0.01
Gadidae	D	2.36	0.87	0.84	0.54	1.62	0.75
Gobiidae	D	36.31	13.35	3.93	2.54	20.56	9.57
Labridae	D	16.13	5.93	9.49	6.14	12.90	6.00
Merlucciidae	D	0.66	0.24	0.05	0.03	0.36	0.17
Mugilidae	D	0.58	0.21	0.37	0.24	0.48	0.22
Mullidae	D	0.04	0.02	0.12	0.08	0.08	0.04
Muraenidae	D	0.08	0.03	0.09	0.06	0.08	0.04
Ophichthidae	D	0.06	0.02	0.04	0.03	0.05	0.02
Ophidiidae	D	0.36	0.13	0.15	0.09	0.26	0.12
Phycidae	D	0.04	0.01	0.00	0.00	0.02	0.01
Pleuronectidae	D	0.72	0.27	0.37	0.24	0.55	0.26
Scaridae	D	0.00	0.00	0.08	0.05	0.04	0.02
Scophthalmidae	D	0.55	0.20	0.00	0.00	0.28	0.13
Scorpaenidae	D	0.59	0.22	0.58	0.37	0.58	0.27
Serranidae	D	6.65	2.44	2.98	1.93	4.86	2.26
Soleidae	D	0.15	0.06	0.03	0.02	0.09	0.04
Sparidae	D	12.98	4.77	6.82	4.41	9.98	4.65
Syngnathidae	D	0.04	0.02	0.04	0.03	0.04	0.02
Synodontidae	D	0.10	0.04	0.11	0.07	0.11	0.05
Trachinidae	D	0.47	0.17	0.33	0.22	0.41	0.19
Trichiuridae	D	0.04	0.01	0.44	0.28	0.23	0.11
Triglidae	D	0.55	0.20	0.27	0.18	0.41	0.19
Clupeidae	SP	49.08	18.04	16.01	10.35	32.99	15.35
Engraulidae	SP	62.49	22.97	20.21	13.07	41.92	19.50
Bramidae	M/B	0.35	0.13	0.04	0.03	0.20	0.09
Caproidae	M/B	0.04	0.01	0.19	0.12	0.11	0.05
Evermannellidae	M/B	0.08	0.03	0.09	0.06	0.09	0.04
Gonostomatidae	M/B	27.31	10.04	34.71	22.44	30.91	14.38
Myctophidae	M/B	18.42	6.77	30.65	19.82	24.37	11.34
Paralepididae	M/B	1.17	0.43	3.49	2.26	2.30	1.07
Phosichthyidae	M/B	2.96	1.09	7.12	4.61	4.98	2.32
Sternoptychidae	M/B	0.60	0.22	1.35	0.88	0.97	0.45
Stomiidae	M/B	0.00	0.00	0.15	0.10	0.07	0.03
Argentinidae	P/EP	0.04	0.01	0.05	0.03	0.04	0.02
Atherinidae	P/EP	0.00	0.00	0.09	0.06	0.04	0.02

(Continued)

TABLE 2 Continued

Family	Ecological Group	Shelf		Slope		Total Area	
		#/10 m^2	%	#/10 m^2	%	#/10 m^2	%
Carangidae	P/EP	3.06	1.12	1.60	1.03	2.35	1.09
Pomacentridae	P/EP	4.64	1.70	1.82	1.17	3.26	1.52
Scombridae	P/EP	6.91	2.54	2.74	1.77	4.88	2.27
Total		272.02	100.00	154.69	100.00	214.94	100.00

Shelf: stations with bottom depth ≤ 200 m. Slope: stations with bottom depth >200 m. Ecological groups: D, demersal fish; SP, small pelagic fish; M/B, meso- bathypelagic fish; P/EP, pelagic-epipelagic fish.

Chl-a values (concentration greater than 0.1 mg m^{-3}). The only difference is the significant positive impact on family richness of "greater than average" salinity values, whereas salinity was not significant in the best model estimated for Shannon diversity index.

More detailed information was obtained by applying the same models to the shelf and slope sub-regions separately.

In the shelf area, the decreasing diversity over time and the effect of longitude are confirmed for both *Fr* (Figure 4B) and *H'* (Figure 5B), and, in addition, the positive impact on biodiversity at increasing bottom depth is evidenced. The GAM model for *Fr* also indicated a positive response at relatively lower ADT values, which locally are generally associated to coastal upwelling conditions.

In the slope area (bottom depth >200m), the decreasing diversity over time is even more pronounced and the only additional significant factor is GCS, for both *Fr* (Figure 4C) and *H'* (Figure 5C). Specifically, a negative impact on family richness for low current speed (values < 10 m s^{-1}) is evident, as well a positive effect on Shannon index for current speed higher than 14.5 m s^{-1}.

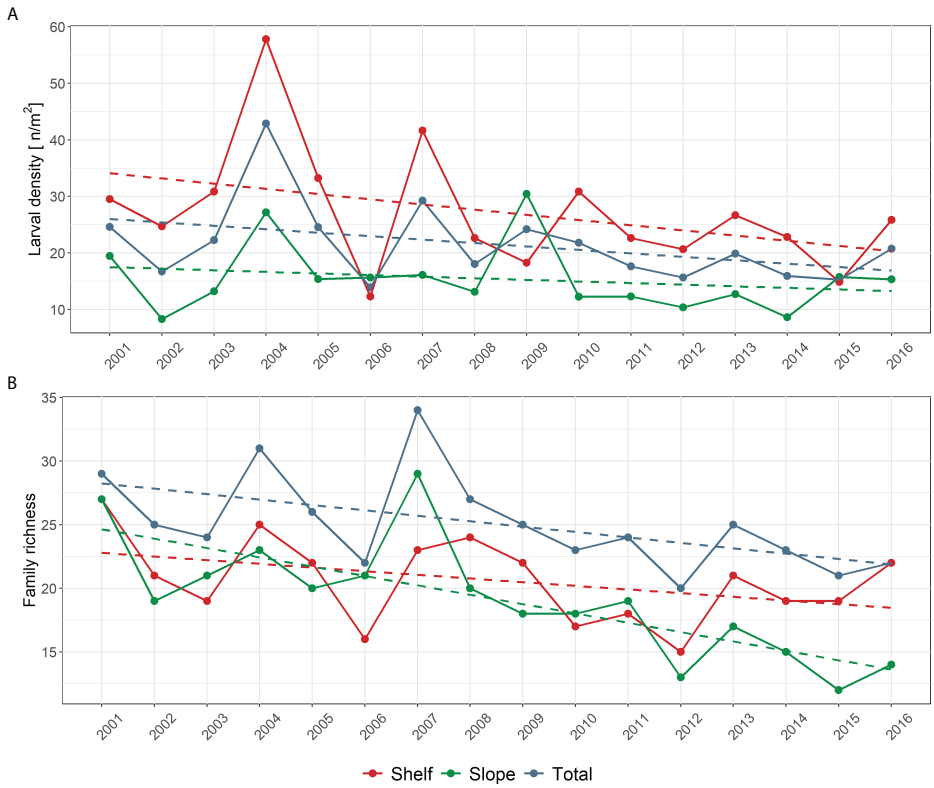

FIGURE 2
(A) Average total larval surface density (# m^{-2}) and **(B)** trends in Family richness (Fr) in summer surveys (from 2001 to 2016). The general trend in the entire study area (37 selected stations) is shown, as well the trends in the continental shelf area (19 stations) and in the slope area (18 stations) (see Figure 1).

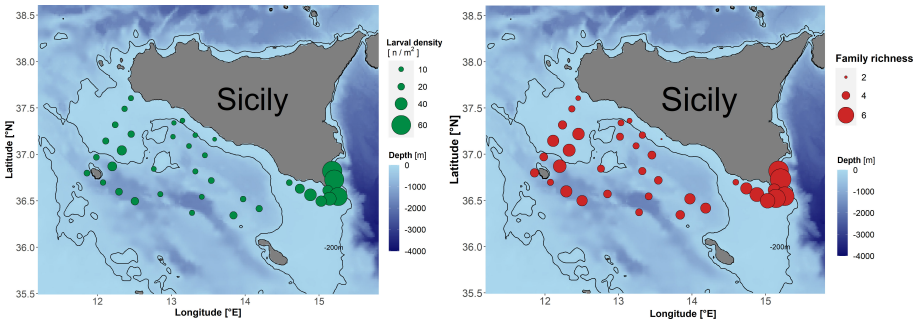

FIGURE 3
Left panel: Average larval density (# m^{-2}). Right panel: Average Family richness (*Fr*) by sampling station over the period 2001–2016.

Finally, the GAM outputs for the dependent variable "Jaccard dissimilarity" are shown in Figure 6. Specifically, plots in Figure 6A refer to all available data (shelf + slope), Figure 6B to shelf data only (bottom depth ≤ 200 m), and Figure 6C to slope data (bottom depth > 200 m).

Results suggest a general significant decreasing compositional change (lower dissimilarity values), which is related to the last years of the time series (from 2012 onward). The observed temporal response mimics the one related to the longitudinal gradient. In addition, Jaccard dissimilarity shows a decreasing trend up to the bottom depth of about 400 m, which turns to be increasing for higher values. Finally, higher compositional changes in the shelf area (Figure 6B) are positively correlated with surface current speed and with intermediate longitude values, whereas in the slope sub-region (Figure 6C), the only significant factor is bottom depth, evidencing higher compositional changes at greater depths (> 600 m).

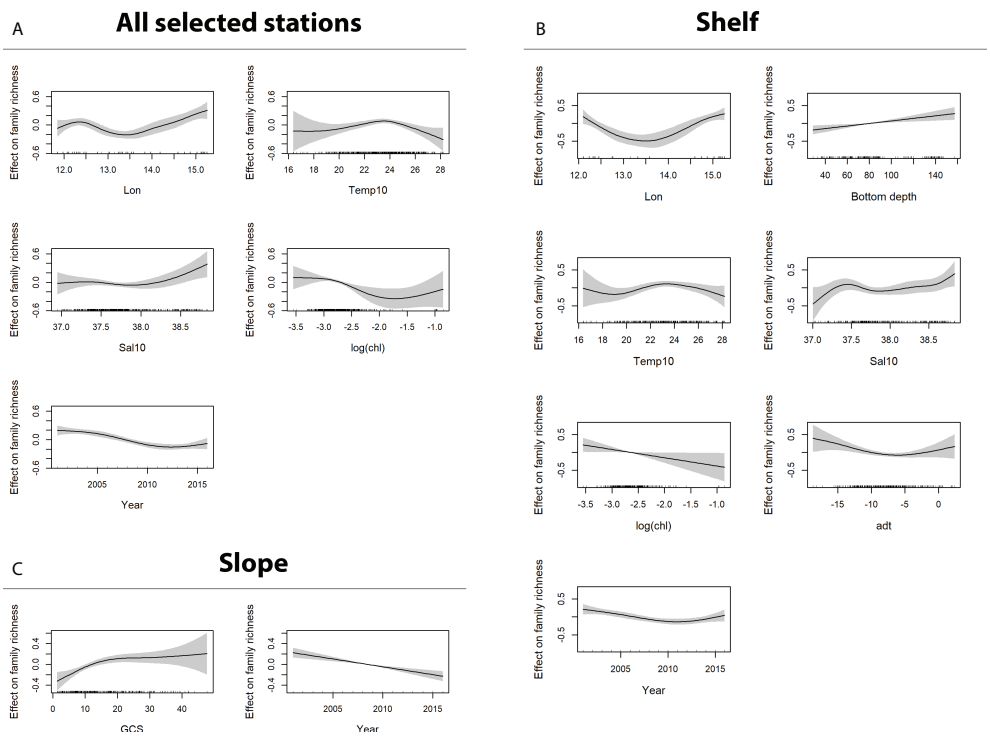

FIGURE 4
GAM output for the dependent variable *Fr* (Family richness). Sub-panels refer to model output obtained using **(A)** all data (shelf + slope), **(B)** shelf data only (bottom depth ≤ 200 m), and **(C)** slope data only (bottom depth > 200 m). Only significant factors are shown.

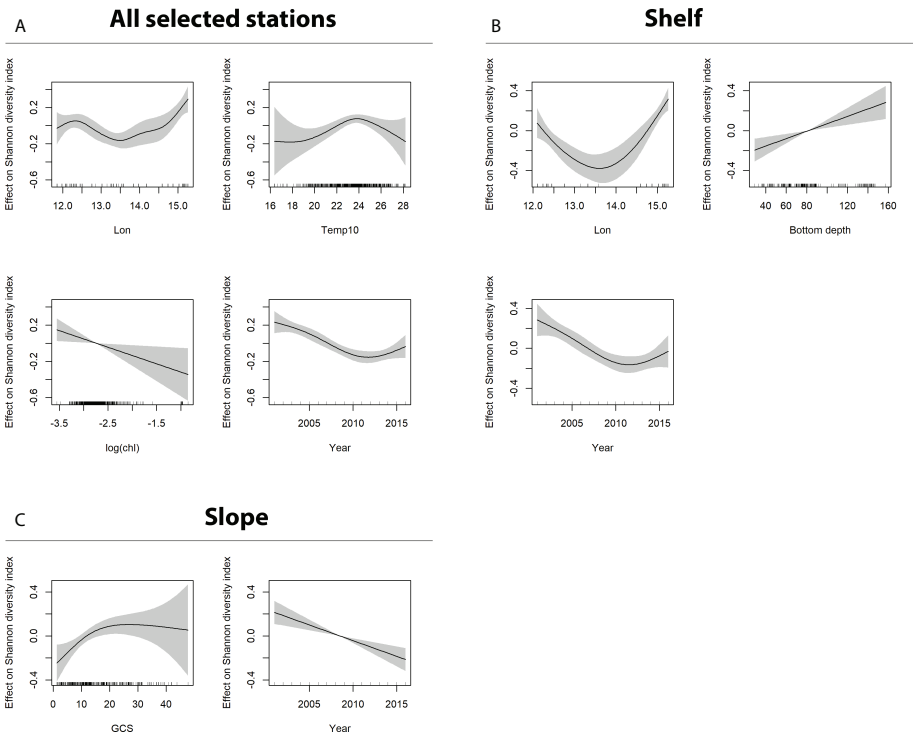

FIGURE 5
GAM output for the dependent variable *H'* (Shannon diversity index). Sub-panels refer to model output obtained using **(A)** all data (shelf + slope), **(B)** shelf data only (bottom depth ≤ 200 m), and **(C)** slope data only (bottom depth > 200 m). Only significant factors are shown.

Discussion

Larval fish assemblage refers to ichthyoplankton data collected in continental shelf and slope areas of the SoS over 16 consecutive years (summer surveys carried out from 2001 to 2016). In particular, the sampling covered the depth layer of 0–100 m of the water column, identifying demersal, pelagic/epipelagic, meso/bathypelagic, and small pelagic species from 49 different fish families. Because of the limitations in species/genus identification that were related to the variable sorting skills of dedicated personnel over the relatively long period included in the analysis, the present study was based on larval information assembled at the family level. However, the role of the single families in affecting the detected patterns in terms of biodiversity indices was specified, also investigating whenever possible on the species involved in the changes of biodiversity indices.

More than one-third of the total number of collected larvae were from two small pelagic species, anchovy (family Engraulidae) and round sardinella (family: Clupeidae), a proportion that over the continental shelf area increased up to 42.0% (Table 2). However, the presence of meso/bathypelagic taxa was important and ubiquitous as well in both the shelf and slope sub-areas. After Clupeidae and Engraulidae, the most abundant families were Myctophidae (assembling 15 species) and Gonostomatidae (mostly one single species, *Cyclothone braueri*), jointly accounting for about 25% of the total in the whole study area (41.2% in the slope sub-region) (Table 2).

In terms of larval densities (Figure S6), Engraulidae (one species, *Engraulis encrasicolus*), Clupeidae (one species, *Sardinella aurita*), and Gobiidae alone accounted for more than 50% of the total taxa in shelf sub-area, where the spawning habitats of fish species from these families are located. Here, the highest average yearly larval concentration (up to 100 m^{-2}) was found for anchovy, whose preferring spawning grounds in the study area occur at bottom depths shallower than 100 m (Quinci et al., 2022). In the slope area, the maximum average density (about 55 m^{-2}) was observed for Gonostomatidae. The prevalence of Gonostomatidae in the offshore stations is in agreement with the spawning behavior of the dominant species (*Cyclothone braueri*) belonging to this family (Yoon et al., 2007) and with the spatial distribution of its larval stages (Torri et al., 2021). However, it is worth noting how Engraulidae and Clupeidae are quite abundant even in the slope area (jointly accounting for about 20% of the total) and that even other typically coastal species belonging to Labridae, Sparidae, and Gobidae are frequently found offshore.

In general, the observed patterns in the distribution of dominant species in both shelf and slope sub-areas are

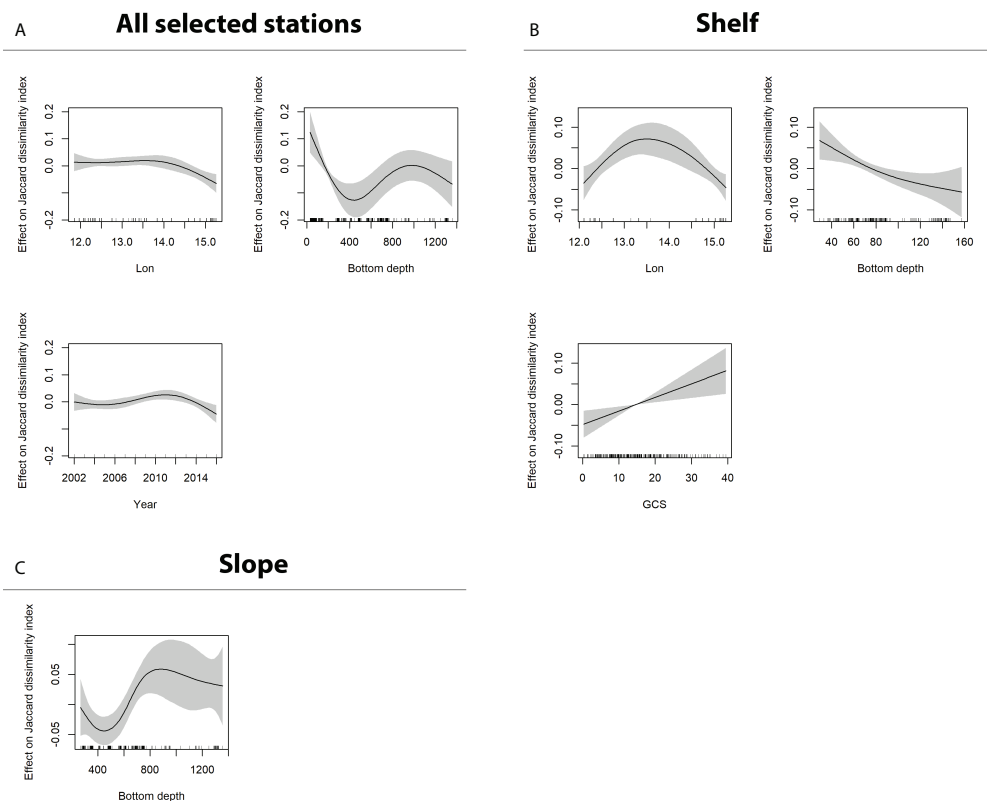

FIGURE 6
GAM output for the dependent variable Jaccard dissimilarity index. Sub-panels refer to model output obtained using **(A)** all data (shelf + slope), **(B)** shelf data (bottom depth ≤ 200 m), and **(C)** slope data (bottom depth > 200 m). Only significant factors are reported.

consistent with data reported for the Western and Central Mediterranean in previous studies (Torres et al., 2011; Cuttitta et al., 2016a; Cuttitta et al., 2016b; Cuttitta et al., 2018; Torri et al., 2018; Torri et al., 2021; Quinci et al., 2022), although further insights on the potential impact on the composition of larval assemblages by advection phenomena from/to the two sub-areas, as induced by local mesoscale oceanographic variability, are given herein. In particular, our analysis evidenced the impact of key hydrodynamic features on the ichthyoplankton biodiversity characterizing the SoS. The selection in the GAM analysis of surface current among the significant environmental factors able to affect biodiversity levels reflects this effect. However, it is interesting to note how the long-term data used in this study further support the dominance of larval stages of Clupeidae and Engraulidae in Sicilian and Tunisian waters of the SoS already found in previous investigations using much more time-limited datasets (Cuttitta et al., 2018). This is in contrast with the dominance of mesopelagic species observed in western Mediterranean (Torres et al., 2011), in the southern Tyrrhenian Sea (Cuttitta et al., 2016a), and in the Gulf of Sirte (Cuttitta et al., 2018). In addition, when considering all the stations over the period 2001–2016 listed in Table 1, the calculated yearly average taxa (family) richness (*Fr* = 33.4) is comparable with data (*Fr* = 34) reported in Cuttitta et al. (2016a), which refer to one survey carried out in the same area during the summer of 2009.

In general, the observed high abundance of myctophids and gonostomatids in the upper 100 m of the water column, even in the shelf area, confirms the epipelagic zone as an important environment for the development of larval stages of mesopelagic fishes, despite the typical depth distribution of the adult fractions of the corresponding fish populations (Watanabe et al., 2002; D'Elia et al., 2016).

The time series analysis of family richness by sub-areas evidenced greater biodiversity losses especially in the slope area during the last years of available data, from 2011 onward. This trend is probably linked the reduced advection of neritic taxa from the continental shelf and/or oceanic taxa to coastal areas. This was firstly suggested by the detected significance of surface current speed in GAMs applied to slope stations for both *Tr* and *H'*. Actually, although mesopelagic larvae dominate in the slope regions, their presence is quite common even in continental shelf probably in relation to the impact of horizontal advections linked to semi-permanent oceanographic structures that typically

characterize this region during the summer season. Specifically, in agreement to Torri et al. (2021), the meandering path of the AIS can shape the distribution of mesopelagic species, transporting planktonic stages on the Adventure Bank (northwestern shelf) and on the Sicilian-Maltese Bank (southeastern shelf). Here, the occurrence of both neritic and oceanic species typically leads to higher biodiversity levels. Conversely, the presence of larval stages of coastal species in the slope region is only due to temporary advection by local oceanographic structures affected by the atmospheric events (Bignami et al., 2008; Torri et al., 2018). As a result, a reduced advection from coastal to the offshore zone may limit the contribution of neritic species to the larval assemblage in the slope area, leading to lower overall diversity in that region.

The potential role of the reduced advection of neritic taxa on the decreasing trend in biodiversity during the last years of the time series appears to be further confirmed by the lower average current speed regime characterizing the southeastern part of the study area (Figure S8). Actually, larval data show that, over the period 2010–2016, not only the abundance of the main neritic taxa was lower in the slope area (Figure S7), but that, in addition, other less frequent coastal/neritic families such as Blennidae, Callionymidae, Centracanthidae, Pomacentridae, Scorpaenidae, and Triglidae were often not found at all in our plankton samples, so reducing the level of *Tr* and *H'* indexes (Table S1).

However, GAMs also indicated a moderate but significant decreasing temporal trend of α diversity metrics even in the shelf sub-area, where important drivers of spatial variability in biodiversity are the two factors *Temp10* and *ADT*. In particular, high *Fr* values were found at low *ADT* and intermediate water temperature (23°C–24°C). Low *ADT* values over the shelf area are locally associated to coastal upwelling conditions, which are able to pump nutrient-rich waters, so supporting higher primary productivity (Patti et al., 2010). The detected optimal temperature level suggests a detrimental effect on biodiversity induced by extremely low- or high-temperature regimes. In addition, the lower surface current speed regime that characterized even the shelf area during the last years of the time series also appears to be beneficial in reducing compositional changes in the larval assemblage, as also indicated by the significance of current speed in the GAM model applied to the Jaccard dissimilarity index. However, the most important driver of turnover in the larval assemblage appears to be the bottom depth, suggesting an enhanced stability of the community in the coastal waters of neritic zone, where more important is the contribution to biodiversity by coastal demersal species. In this framework, it is worth noting that the decreasing trend in α biodiversity in shelf area, at least up to year 2012 was found to be linked the reduced occurrence of oceanic taxa such as Ophidiidae, Sternoptychidae, and Triglidae (Table S2), supporting the role of the advection of fish larvae from meso-bathypelagic and mostly deep demersal species from the slope area toward the coastal area in modulating biodiversity levels.

The differential trends between shelf and slope sub-areas also suggested to better investigate on other more specific spatial biodiversity patterns. Actually, Figure 3B evidenced the presence of a biodiversity hotspot in the frontal area characterizing the southeastern part of the study area, off the southernmost tip of Sicily (Cape Passero), as already reported by (Cuttitta et al. 2016a, Cuttitta et al. 2018). The observed pattern is further supported by the similarity between the response plots of the two explanatory factors *Longitude* and *Salinity* in Figures 4A, B, as it known that surface salinity locally presents a west–east increasing gradient that is induced by the motion of Atlantic Modified Water toward the Eastern Mediterranean basin (Robinson et al., 1999; García Lafuente et al., 2002). Therefore, the importance of concentration and retention processes locally induced by oceanographic features is confirmed by the present study (Figure 3A), not only in support of larval growth and survival, and related enhanced probability of recruitment success for many fish species as already shown by previous studies in the SoS (Torri et al., 2018; Patti et al., 2020; Russo et al., 2021; Torri et al., 2021; Russo et al., 2022; Cuttitta et al., 2022), but also more in general for sustaining high biodiversity levels (Figure 3B). Actually, frontal structures are generally responsible for plankton aggregation, so supporting the increase in feeding opportunities for fish larvae and inducing favorable conditions for their survival, as already observed in many other marine environments including the Mediterranean Sea (Bakun, 2006; Alemany et al., 2010; Avendaño-Ibarra et al., 2013; Erisman et al., 2017; Acha et al., 2018; Sato et al., 2018; Torri et al., 2018; Patti et al., 2020; Russo et al., 2021; Torri et al., 2021). In turn, this may account for the observed increased diversity in larval fish assemblages associated to spatial and temporal patterns of mesoscale oceanographic structures (Richardson et al., 2010; Rooker et al., 2013; Meinert et al., 2020). In the study area, the surface density front South of Cape Passero is dominated by temperature and is enhanced during the summer (Lermusiaux and Robinson, 2001; García Lafuente et al., 2005). Here, we speculate about the impact on larval biodiversity of the strength of density gradient across the front, which could be modulated by the alternating cyclonic and anti-cyclonic modes charactering the North Ionian Gyre (NIG) (Borzelli et al., 2009; Gačić et al., 2010; Gačić et al., 2013), whose effects on Sicilian intermediate waters have been recently investigated by Placenti et al. (2022). In particular, what we observed with data used in this study is higher biodiversity levels (and lower compositional changes as well) in the continental shelf stations of the frontal zone when the NIG is characterized by cyclonic circulation (years 2001–2005 and 2011–2016), a mode that is associated to enhanced advection of Atlantic Water (AW) to southern Levantine basin and a reduced deflection toward the Adriatic. Actually, in the same periods, the oceanographic conditions in the frontal zone were characterized by lower surface current speed (Figure S8) and higher temperature and salinity levels, testifying of a reduced inflow of AW in this area. However, the in-depth

analysis of the relation between the quasi-decadal reversal of the NIG and larval biodiversity is out of the scope of the present paper and would deserve further insights.

Conclusion

In analyzing the temporal and spatial biodiversity patterns of larval fish assemblages in the SoS, this study may serve as a reference point for evaluating the role of changing environmental conditions on the community structure and ecosystem stability. In particular, the frontal feature characterizing during the summer the southeastern part of the study area, in favoring retention and concentration processes supporting growth and survival of early life stages, as already demonstrated in previous study on pelagic fish species, emerged as an important driver able to enhance biodiversity as well. Moreover, it has been shown that hydrological characteristics of the surface water affect ichthyoplankton biodiversity in coastal and offshore area, shading light on possible links with the quasi-decadal oceanographic variability patterns, such as the oscillation between anti-cyclonic and cyclonic phases characterizing the surface circulation of the Ionian Sea area, and encouraging further studies on possible future effects related to the climate change.

Data availability statement

The raw data supporting the conclusions of this article will be made available by the authors, without undue reservation.

Ethics statement

Ethical review and approval were not required for the animal study because this work is focused on planktonic stages in natural marine field.

Author contributions

BP analyzed the data and wrote the manuscript. MT contributed to data analyses and to the writing of the manuscript. AC contributed in sorting the plankton samples and in writing of the manuscript. All the authors contributed to develop the overall concept of the paper, interpreting the results and developing the discussion and the conclusions.

Funding

This study was mainly supported by the Italian National Research Council (CNR) through USPO office and by the FAO Regional Project MedSudMed "Assessment and Monitoring of the Fishery Resources and the Ecosystems in the Straits of Sicily", funded by the Italian Ministry MIPAAF and co-funded by the Directorate General for Maritime Affairs and Fisheries of the European Commission (DG MARE). The study was also supported by several other research projects, including the EU projects "Distribution Biology and Biomass Estimates of the Sicilian Channel Anchovy" (MED96-052) and "The Sicilian Channel Anchovy Fishery and the underlying Oceanographic and Biological Processes conditioning their Interannual Fluctuations" (MED98-070), the Proreplus-Alif Project, funded by the Regione Siciliana Government (POR 2000–2006), and the Flagship Project RITMARE—The Italian Research for the Sea—coordinated by the Italian National Research Council and funded by the Italian Ministry of Education, University and Research within the National Research Program 2011–2013. Publication fees were covered by the ERA-NET Cofund on Blue Bioeconomy - Unlocking the potential of aquatic bioresources (BlueBio) — Grant Agreement number: 817992.

Acknowledgments

Mr. Emanuele Gentile, Master of the R/V Urania, and all his crew are thanked for their work in support to the plankton sampling during the oceanographic cruises. All the participating institutes and scientists who were on-board are gratefully acknowledged for their involvement in the work carried out. Special thanks go to Gaspare Buffa, Carmelo Buscaino, Luigi Giaramita, Carlo Patti, Francesco Placenti, and all researchers–technicians and scientific collaborators (including graduate students, PhD students, and postdoctoral researchers) for their support to the oceanographic cruises, sorting of ichthyoplankton samples and data processing, and to Salvatore Mazzola†, whose scientific efforts allowed the start of the regular sampling surveys that are at the base of the our study. Last but not the least, the first author wants to send special thanks to Dino Levi†, for inspiring the study thought his research work.

Conflict of interest

The authors declare that the research was conducted in the absence of any commercial or financial relationships that could be construed as a potential conflict of interest.

Publisher's note

All claims expressed in this article are solely those of the authors and do not necessarily represent those of their affiliated

organizations, or those of the publisher, the editors and the reviewers. Any product that may be evaluated in this article, or claim that may be made by its manufacturer, is not guaranteed or endorsed by the publisher.

Supplementary material

The Supplementary Material for this article can be found online at: https://www.frontiersin.org/articles/10.3389/fmars.2022.960929/full#supplementary-material

References

Acha, E. M., Ehrlich, M. D., Muelbert, J. H., Pájaro, M., Bruno, D., Machinandiarena, L., et al (2018). "Ichthyoplankton associated to the frontal regions of the southwestern atlantic," in *Plankton ecology of the southwestern Atlantic: From the subtropical to the subantarctic realm*. Eds. M. S. Hoffmeyer, M. E. Sabatini, F. P. Brandini, D. L. Calliari and N. H. Santinelli (Berlin: Springer International Publishing), 219–246. doi: 10.1007/978-3-319-77869-3_11

Alemany, F., Quintanilla, L., Velez-Belchi, P., Garcìa, A., Cortés, D., Rodríguez, J. M., et al (2010). Characterization of the spawning habitat of Atlantic bluefin tuna and related species in the Balearic Sea (western Mediterranean). *Prog. Oceanogr.* 86, 21–38. doi: 10.1016/j.pocean.2010.04.014

Álvarez, I., Catalán, I. A., Jordi, A., Palmer, M., Sabatés, A., and Basterretxea, G. (2012). Drivers of larval fish assemblage shift during the spring-summer transition in the coastal Mediterranean. *Estuar. Coast. Shelf S.* 97, 127–135. doi: 10.1016/j.ecss.2011.11.029

Álvarez, I., Rodríguez, J. M., Catalán, I. A., Hidalgo, M., Álvarez-Berastegui, D., Balbín, R., et al (2015). Larval fish assemblage structure in the surface layer of the northwestern Mediterranean under contrasting oceanographic scenarios. *J. Plankton Res.* 37 (4), 834–850. doi: 10.1093/plankt/fbv055

Avendaño-Ibarra, R., Godínez-Domínguez, E., Aceves-Medina, G., González-Rodríguez, E., and Trasviña, A. (2013). Fish larve response to biophysical changes in the gulf of California, Mexico (Winter-summer). *J. Mar. Sci.* 2013, 1–17. doi: 10.1155/2013/176760

Bakun, A. (2006). Fronts and eddies as key structures in the habitat of marine fish larvae: Opportunity, adaptive response and competitive advantage. *Sci. Mar.* 70 (Suppl. 2), 105–122. doi: 10.3989/scimar.2006.70s2105

Bertolini, F., D'Ancona, U., Padoa Montalenti, E., Ranzi, S., Sanzo, L., Sparta, A., et al (1956). Uova, larve e stadi giovanili di teleostei. *Fauna Flora Golfo Napoli Monogr.* 38, 1–1064.

Bignami, F., Böhm, E., D'Acunzo, E., D'Archino, R., and Salusti, E. (2008). On the dynamics of surface cold filaments in the Mediterranean Sea. *J. Mar. Syst.* 74 (1-2), 429–442. doi: 10.1016/j.jmarsys.2008.03.002

Bonanno, A., Placenti, F., Basilone, G., Mifsud, R., Genovese, S., Patti, B., et al (2014). Variability of water mass properties in the strait of Sicily in summer period of 1998–2013. *Ocean Sci.* 10, 759–770. doi: 10.5194/os-10-759-2014

Borzelli, G. L. E., Gačić, M., Cardin, V., and Civitarese, G. (2009). Eastern Mediterranean Transient and reversal of the Ionian Sea circulation. *Geophys. Res. Lett.* 36, L15108. doi: 10.1029/2009GL039261

Brankart, J. M. (1994). *Technical report* (Liège: University of Liège), 5 pp.

Cardinale, B. J., Duffy, J., Gonzalez, A., Hooper, D. U., Perrings, C., Venail, P., et al (2012). Biodiversity loss and its impact on humanity. *Nature* 486, 59–67. doi: 10.1038/nature11148

Cardinale, B. J., Palmer, M. A., and Collins, S. L. (2002). Species diversity enhances ecosystem functioning through interspecific facilitation. *Nature* 415, 426–429. doi: 10.1038/415426a

Costa, F. (1999). I pesci del Mediterraneo. *Stadi larvali e giovanili*. Messina: Grafo-Editor. E. Grafo

Cuttitta, A., Arigò, A., Basilone, G., Bonanno, A., Buscaino, G., Rollandi, L., et al (2004). Mesopelagic fish larvae species in the strait of Sicily and their relationships to main oceanographic events. *Hydrobiologia* 527 (1), 177–182. doi: 10.1023/B:HYDR.0000043299.65829.2f

Cuttitta, A., Bonomo, S., Zgozi, S., Bonanno, A., Patti, B., Quinci, E. M., et al (2016b). The influence of physical and biological processes on the ichthyoplankton communities in the gulf of sirte (Southern Mediterranean Sea). *Mar. Ecol.* 37 (4), 831–844. doi: 10.1111/maec.12362

Cuttitta, A., Quinci, E. M., Patti, B., Bonomo, S., Bonanno, A., Musco, M., et al (2016a). Different key roles of mesoscale oceanographic structures and ocean bathymetry in shaping larval fish distribution pattern: A case study in Sicilian waters in summer 2009. *J. Sea Res.* 115, 6–17. doi: 10.1016/j.seares.2016.04.005

Cuttitta, A., Torri, M., Zarrad, R., Zgozi, S., Jarboui, O., Quinci, E. M., et al (2018). Linking surface hydrodynamics to planktonic ecosystem: The case study of the ichthyoplanktonic assemblages in the central Mediterranean Sea. *Hydrobiologia* 821 (1), 191–214. doi: 10.1007/s10750-017-3483-x

Cuttitta, A., Patti, B., Musco, M., Masullo, T., Placenti, F., Quinci, E. M., et al. (2022). Inferring population structure from early life stage: The case of the european anchovy in the sicilian and maltese shelves. *Water* 14, 1427. doi: 10.3390/w14091427

D'Elia, M., Warren, J. D., Rodriguez-Pinto, I., Sutton, T. T., Cook, A., and Boswell, K. M. (2016). Diel variation in the vertical distribution of deep-water scattering layers in the gulf of Mexico. *Deep Sea Res. Part I Oceanogr. Res. Pap.* 115, 91–102. doi: 10.1016/j.dsr.2016.05.014

Dornelas, M., Gotelli, N. J., McGill, B. J., Shimadzu, H., Moyes, F., Sievers, C., et al (2014). Assemblage time series reveal biodiversity change but not systematic loss. *Science* 344, 296–299. doi: 10.1126/science.1248484

Duffy, J. E. (2009). Why biodiversity is important to the functioning of real-world ecosystems. *Front. Ecol. Environ.* 7, 437–444. doi: 10.1890/070195

Erisman, B., Heyman, W., Kobara, S., Ezer, T., Pittman, S., Aburto-Oropeza, O., et al (2017). Fish spawning aggregations: where well-placed management actions can yield big benefits for fisheries and conservation. *Fish Fish.* 18, 128–144. doi: 10.1111/faf.12132

Falcini, F., Corrado, R., Torri, M., Mangano, M. C., Zarrad, R., Di Cintio, A., et al (2020). Seascape connectivity of European anchovy in the central Mediterranean Sea revealed by weighted Lagrangian backtracking and bio-energetic modelling. *Sci. Rep.* 10 (1), 1–13. doi: 10.1038/s41598-020-75680-8

Falcini, F., Palatella, L., Cuttitta, A., Buongiorno Nardelli, B., Lacorata, G., Lanotte, A. S., et al (2015). The role of hydrodynamic processes on anchovy eggs and larvae distribution in the Sicily channel (Mediterranean sea): A case study for the 2004 data set. *PLoS One* 10 (4), e0123213. doi: 10.1371/journal.pone.0123213

Gačić, M., Borzelli, G. L. E., Civitarese, G., Cardin, V., and Yari, S. (2010). Can internal processes sustain reversals of the ocean upper circulation? the Ionian Sea example. *Geophys. Res. Lett.* 37, L09608. doi: 10.1029/2010GL043216

Gačić, M., Schroeder, K., Civitarese, G., Cosoli, S., Vetrano, A., and Borzelli, G. L. E. (2013). Salinity in the Sicily channel corroborates the role of the Adriatic-Ionian bimodal oscillating system (BiOS) in shaping the decadal variability of the Mediterranean overturning circulation. *Ocean Sci.* 9, 83–90. doi: 10.5194/os-9-83-2013

Gamfeldt, L., Lefcheck, J. S., Byrnes, J. E., Cardinale, B. J., Duffy, J. E., and Griffin, J. N. (2014). Marine biodiversity and ecosystem functioning: What's known and what's next? *Oikos* 124, 252–265. doi: 10.1111/oik.01549

García Lafuente, J., García, A., Mazzola, S., Quintanilla, L., Delgado, J., Cuttitta, A., et al (2002). Hydrographic phenomena influencing early life stages of the Sicilian channel anchovy. *Fish. Oceanogr.* 11, 31–44. doi: 10.1046/j.1365-2419.2002.00186.x

García Lafuente, J., Vargas, J. M., Criado, F., García, A., Delgado, J., and Mazzola, S. (2005). Assessing the variability of hydrographic processes influencing the life cycle of the Sicilian channel anchovy, engraulis encrasicolus, by satellite imagery. *Fish. Oceanogr.* 14, 32–46. doi: 10.1111/j.1365-2419.2004.00304.x

Gray, C. A., Johnson, D. D., Broadhurst, M. K., and Young, D. J. (2005). Seasonal, spatial and gear-related influences on relationships between retained and discarded catches in a multi-species gillnet fishery. *Fish. Res.* 75, 56–72. doi: 10.1016/j.fishres.2005.04.014

Hastie, T., and Tibshirani, R. (1990). *Generalised additive models. Chapman and hall.* New York: CRC.

Hernandez, F. J.Jr., Powers, S. P., and Graham, W. M. (2010). Seasonal variability in ichthyoplankton abundance and assemblage composition in the northern gulf of Mexico off Alabama. *Fish. Bull.* 108, 193–207.

Hooper, D. U., Adair, E. C., Cardinale, B., Byrnes, J. E. K., Hungate, B. A., Matulich, K. L., et al (2012). A global synthesis reveals biodiversity loss as a major driver of ecosystem change. *Nature* 486, 105–108. doi: 10.1038/nature11118

Houde, E. (2002). "Mortality," in *Fishery science, the unique contributions of early life stages*. Eds. L. A. Fuiman and R. G. Werner (Oxford: Blackwell Science), 64–87.

Isari, S., Fragopoulu, N., and Somarakis, S. (2008). Interranual variability in horizontal patterns of larval fish assemblages in the Northeastern Aegean Sea (Eastern Mediterranean) during early summer. *Estuar. Coast. Shelf Sci.* 79 (4), 607–619. doi: 10.1016/j.ecss.2008.06.001

Jaccard, P. (1908). Nouvelles recerches sur la distribution florale. *Bull. Soc Vaud. Sci. Nat.* 44, 223–270.

Jennings, S., and Kaiser, M. J. (1998). The effects of fishing on marine ecosystems. *Adv. Mar. Biol.* 34, 201–351. doi: 10.1016/S0065-2881(08)60212-6

Joint, I., and Groom, S. (2000). Estimation of phytoplankton production from space: Current status and future potential of satellite re-mote sensing. *J. Exp. Mar. Biol. Ecol.* 250 (1-2), 233–255. doi: 10.1016/S0022-0981(00)00199-4

Kara, A. B., Rochford, P. A., and Hurlburt, H. E. (2000). An optimal definition for ocean mixed layer depth. *J. Geophys. Res.* 105 (C7), 16803–16821. doi: 10.1029/2000JC900072

Katsuragawa, M., Dias, J. F., Harari, C., Namiki, C., and Zani-Teixeira, M. L. (2014). Patterns in larval fish assemblages under the influence of the Brazil current. *Cont. Shelf Res.* 89, 103–117. doi: 10.1016/j.csr.2014.04.024

Lehodey, P., Alheit, J., Barange, M., Baumgartner, T., Beaugrand, G., Drinkwater, K., et al (2006). Climate variability, fish, and fisheries. *J. Clim.* 19, 5009–5030. doi: 10.1175/JCLI3898.1

Lermusiaux, P. F. J. (1999). Estimation and study of mesoscale variability in the strait of Sicily. *Dyn. Atm. Ocean.* 29, 255–303. doi: 10.1016/S0377-0265(99)00008-1

Lermusiaux, P. F. J., and Robinson, A. R. (2001). Features of dominant mesoscale variability, circulation patterns and dynamics in the strait of Sicily. *Deep Sea Res. I* 48, 1953–1997. doi: 10.1016/S0967-0637(00)00114-X

López-Sanz, À., Vert, N., Zabala, M., and Sabatés, A. (2009). Small-scale distribution of fish larvae around the medes islands marine protected area (NW Mediterranean). *J. Plankton Res.* 31 (7), 763–775. doi: 10.1093/plankt/fbp024

Loreau, M., Naeem, S., Inchausti, P., Bengtsson, J., Grime, J. P., and Hector, A. (2001). Biodiversity and ecosystem functioning: current knowledge and future challenges. *Science* 294, 804–808. doi: 10.1126/science.1064088

Magurran, A. E. (2004). *Measuring biological diversity* (Oxford, UK: Blackwell Science).

Magurran, A. E., Dornelas, M., Moyes, F., and Henderson, P. A. (2019). Temporal β diversity–a macroecological perspective. *Global Ecol. Biogeogr.* 28, 1949–1960. doi: 10.1111/geb.130

Malavolti, S., De Felice, A., Costantini, I., BIAGOTTI, I., Canduci, G., Grilli, F., et al (2018). Distribution of engraulis encrasicolus eggs and larvae in relation to coastal oceanographic conditions (the South-Western Adriatic Sea case study). *Mediterr. Mar. Sci.* 19 (1), 180–192. doi: 10.12681/mms.14402

Mazzola, S., Garcia, A., and Garcia Lafuente, J. (2000). "Distribution, Biology and Biomass estimates of the Sicilian Channel anchovy. DG XIV, MED 96/052, Final Report", in Many-species populations. *An introduction to Mathematical Ecology*, ed. E. C. Pielou (New York: Wiley-Interscience), 203–272.

Meinert, C. R., Clausen-Sparks, K., Cornic, M., Sutton, T. T., and Rooker, J. R. (2020). Taxonomic richness and diversity of larval fish assemblages in the oceanic gulf of Mexico: Links to oceanographic conditions. *Front. Mar. Sci.* 7. doi: 10.3389/fmars.2020.00579

Miller, R. G. (1981). *Simultaneous statistical inference. 2nd ed* (New York: Springer Verlag).

Mittermeier, R. A., Turner, W. R., Larsen, F. W., Brooks, T. M., and Gascon, C. (2011). "Global biodiversity conservation: the critical role of hotspots," in *Biodiversity hotspots*. Eds. F. Zachos and J. Habel (Berlin: Springer). doi: 10.1016/j.gecco.2014.12.008

Moser, H. G., and Ahlstrom, E. H. (1996). "Myctophidae: lanternfishes," in *The early stages on fishes in the California current region, California cooperative oceanic fisheries investigations (CalCOFI), atlas n°33.* Ed. H. G. Moser, 1505 (387–475). Lawrence, Kansas: Allen Press, Inc.

Moyano, M., and Hernández-León, S. (2011). Intra- and interannual variability in the larval fish assemblage off gran canaria (Canary islands) over 2005-2007. *Mar. Biol.* 158 (2), 257–273. doi: 10.1007/s00227-010-1556-8

Moyano, M., Rodríguez, J. M., Benítez-Barrios, V. M., and Hernández-León, S. (2014). Larval fish distribution and retention in the canary current system during the weak upwelling season. *Fish. Oceanogr.* 23 (3), 191–209. doi: 10.1111/fog.12055

Moyano, M., Rodríguez, J. M., and Hernández-León, S. (2009). Larval fish abundance and distribution during the late winter bloom off Gran Canaria Island, canary islands. *Fish. Oceanogr.* 18 (1), 51–61. doi: 10.1111/j.1365-2419.2008.00496.x

Naeem, S., Bunker, D. E., Hector, A., Loreau, M., and Perrings, C. (2009). Biodiversity, ecosystem-functioning, and human wellbeing. New York: Oxford University Press.

Nonaka, R. H., Matsuura, Y., and Suzuki, K. (2000). Seasonal variation in larval fish assemblages in relation to oceanographic conditions in the abrolhos bank region off eastern Brazil. *Fish. Bull.* 98, 767–784.

Oksanen, J., Blanchet, F. G., Friendly, M., Kindt, R., Legendre, P., McGlinn, D., et al (2020). *Vegan: Community ecology package* (R package version 2), 5–7. Available at: https://CRAN.R-project.org/package=vegan.

Olivar, M. P., Sabatés, A., Alemany, F., Balbín, R., Fernández de Puelles, M. L., and Torres, A. P. (2014). Diel-depth distributions of fish larvae off the Balearic islands (western Mediterranean) under two environmental scenarios. *J. Mar. Syst.* 138, 127–138. doi: 10.1016/j.jmarsys.2013.10.009

Olivar, M. P., Salat, J., and Palomera, I. (2001). Comparative study of spatial distribution patterns of the early stages of anchovy and pilchard in the NW Mediterranean Sea. *Mar. Ecol. Prog. Ser.* 217, 111–120. doi: 10.3354/meps217111

Ospina-Álvarez, A., Bernal, M., Catalan, A., Roos, D., Bigot, J.-L., and Palomera, I. (2013). Modeling fish egg production and spatial distribution from acoustic data: A step forward into the analysis of recruitment. *PLoS One* 8, e73687. doi: 10.1371/journal.pone.0073687

Ospina-Álvarez, A., Catalán, I. A., Bernal, M., Roos, D., and Palomera, I. (2015). From egg production to recruits: Connectivity and interannual variability in the recruitment patterns of European anchovy in the northwestern Mediterranean. *Prog. Oceanogr.* 138, 431–447. doi: 10.1016/j.pocean.2015.01.011

Palomera, I. (1991). Vertical distribution of eggs and larvae of engraulis encrasicolus in stratified waters of the Western Mediterra-nean. *Mar. Biol.* 111 (1), 37–44. doi: 10.1007/BF01986343

Patti, B., Guisande, C., Bonanno, A., Basilone, G., Cuttitta, A., and Mazzola, S. (2010). Role of physical forcings and nutrient availability on the control of satellite-based chlorophyll a concentration in the coastal upwelling area of the Sicilian channel. *Sci. Mar.* 74, 577–588. doi: 10.3989/scimar.2010.74n3577

Patti, B., Torri, M., and Cuttitta, A. (2020). General surface circulation controls the interannual fluctuations of anchovy stock biomass in the central Mediterranean Sea. *Sci. Rep.* 10, 1554. doi: 10.1038/s41598-020-58028-0

Patti, B., Zarrad, R., Jarboui, O., Cuttitta, A., Basilone, G., Aronica, S., et al (2018). Anchovy (Engraulis encrasicolus) early life stages in the central Mediterranean Sea: connectivity issues emerging among adjacent sub-areas across the strait of Sicily. *Hydrobiologia* 821 (1), 25–40. doi: 10.1007/s10750-017-3253-9

Piccioni, A., Gabrielle, M., Salusti, E., and Zambianchi, E. (1988). Wind-induced upwellings off the southern coast of Sicily. *Oceanol. Acta* 11, 309–314.

Pikitch, E. K., Santora, C., Babcock, E. A., Bakun, A., Bonfil, R., Conover, D. O., et al (2004). Ecology. ecosystem-based fishery management. *Science* 305, 346–347. doi: 10.1126/science.1098222

Placenti, F., Torri, M., Pessini, F., Patti, B., Tancredi, V., Cuttitta, A., et al (2022). Hydrological and biogeochemical patterns in the Sicily channel: New insights from the last decade (2010- 2020). *Front. Mar. Sci.* 9, 733540. doi: 10.3389/fmars.2022.733540

Planque, B., Bellier, E., and Lazure, P. (2007). Modelling potential spawning habitat of sardine (Sardina pilchardus) and anchovy (Engraulis encrasicolus) in the bay of Biscay. *Fish. Oceanogr.* 16 (1), 16–30. doi: 10.1111/j.1365-2419.2006.00411.x

Ponti, M., Perlini, R. A., Ventra, V., Grech, D., Abbiati, M., and Cerrano, C. (2014). Ecological shifts in Mediterranean coralligenous assemblages related to gorgonian forest loss. *PLoS One* 9 (7), e102782. doi: 10.1371/journal.pone.0102782

Poulard, J. C., and Blanchard, F. (2005). The impact of climate change on the fish community structure of the eastern continental shelf of the bay of Biscay. *ICES J. Mar. Sci.* 62, 1436–1443. doi: 10.1016/j.icesjms.2005.04.017

Pujol, I., and Larnicol, G. (2005). Mediterranean Sea eddy kinetic energy variability from 11 years of altimetric data. *J. Mar. Sys.* 58 (3), 121–142. doi: 10.1016/j.jmarsys.2005.07.005

Quinci, E. M., Torri, M., Cuttitta, A., and Patti, B. (2022). Predicting potential spawning habitat by ensemble species distribution models: The case study of European anchovy (Engraulis encrasicolus) in the strait of Sicily. *Water* 14, 1400. doi: 10.3390/w14091400

R Core Team (2022). *R: A language and environment for statistical computing* (Vienna, Austria: R Foundation for Statistical Computing). Available at: https://www.R-project.org/.

Rocha, J., Yletyinen, J., Biggs, R., Blenckner, T., and Peterson, G. (2015). Marine regime shifts: drivers and impacts on ecosystems services. *Philos. Trans. R. Soc. B Biol. Sci.* 370, 20130273.

Richardson, D. E., Llopiz, J. K., Guigand, C. M., and Cowen, R. K. (2010). Larval assemblages of large and medium-sized pelagic species in the straits of Florida. *Prog. Oceanogr.* 86, 8–20. doi: 10.1016/j.pocean.2010.04.005

Rijnsdorp, A. D., Peck, M. A., Engelhard, G. H., Mollmann, C., and Pinnegar, J. K. (2009). Resolving the effect of climate change on fish populations. *ICES J. Mar. Sci.* 66, 1570–1583. doi: 10.1093/icesjms/fsp056

Robinson, A. R., Golnaraghi, M., Leslie, W. G., Artegiani, A., Hetch, A., Lazzoni, E., et al (1991). The eastern Mediterranean general circulation: features structure and variability. *Dyn. Atm. Ocean.* 15, 215–240. doi: 10.1016/0377-0265(91)90021-7

Robinson, A. R., Sellschopp, J., Warn-Varnas, A., Leslie, W. G., Lozano, C. J., Haley, P. J., et al (1999). The Atlantic Ionian stream. *J. Mar. Sys.* 20, 113–128. doi: 10.1016/S0924-7963(98)00079-7

Rochet, M.-J., Trenkel, V. M., Carpentier, A., Coppin, F., Gil de Sola, L., Léauté, J.-P., et al (2010). Do changes in environmental pressures impact marine communities? an empirical assessment. *J. Appl. Ecol.* 47, 741–750. doi: 10.1111/j.1365-2664.2010.01841.x

Rooker, J. R., Kitchens, L. L., Dance, M. A., Wells, R. J., Falterman, B., and Cornic, M. (2013). Spatial, temporal, and habitat-related variation in abundance of pelagic fishes in the gulf of Mexico: Potential implications of the deepwater horizon oil spill. *PLoS One* 8, e76080. doi: 10.1371/journal.pone.0076080

Russo, S., Torri, M., Patti, B., Musco, M., Masullo, T., Di Natale, M. V., et al (2022). Environmental conditions along tuna larval dispersion: Insights on the spawning habitat and impact on their development stages. *Water* 14, 1568. doi: 10.3390/w14101568

Russo, S., Torri, M., Patti, B., Reglero, P., Álvarez-Berastegui, D., Cuttitta, A., et al (2021). Unveiling the relationship between Sea surface hydrographic patterns and tuna larval distribution in the central Mediterranean Sea. *Front. Mar. Sci.* 8. doi: 10.3389/fmars.2021.708775

Sabatés, A. (1990). Distribution pattern of larval fish populations in the northwestern Mediterranean. *Mar. Ecol. Prog. Ser.* 59 (1), 75–82. doi: 10.3354/meps059075

Sabatés, A., Zaragoza, N., Grau, C., and Salat, J. (2008). Vertical distribution of early developmental stages in two coexisting clupeoid species, sardinella aurita and engraulis encrasicolus. *Mar. Ecol. Prog. Ser.* 364, 169–180. doi: 10.3354/meps07461

Sato, M., Barth, J. A., Benoit-Bird, K. J., Pierce, S. D., Cowles, T. J., Brodeur, R. D., et al (2018). Coastal upwelling fronts as a boundary for planktivorous fish distributions. *Mar. Ecol. Prog. Ser.* 595, 171–186. doi: 10.3354/meps12553

Tilman, D., Isbell, F., and Cowles, J. M. (2014). Biodiversity and ecosystem functioning. *Annu. Rev. Ecol. Evol. Syst.* 45, 471–493. doi: 10.1146/annurev-ecolsys-120213-091917

Tilman, D., Reich, P. B., and Isbell, F. (2012). Biodiversity impacts ecosystem productivity as much as resources, disturbance, or herbivory. *Proc. Natl. Acad. Sci. U.S.A.* 109, 10394–10397. doi: 10.1073/pnas.1208240109

Torres, A. P., Reglero, P., Balbin, R., Urtizberea, A., and Alemany, F. (2011). Coexistence of larvae of tuna species and other fish in the surface mixed layer in the NWMediterranean. *J. Plankton Res.* 33, 1793–1812. doi: 10.1093/plankt/fbr078

Torri, M., Corrado, R., Falcini, F., Cuttitta, A., Palatella, L., Lacorata, G., et al (2018). Planktonic stages of small pelagic fishes (Sardinella aurita and engraulis encrasicolus) in the central Mediterranean Sea: The key role of physical forcings and implications for fisheries management. *Prog. Oceanogr.* 162, 25–39. doi: 10.1016/j.pocean.2018.02.009

Torri, M., Pappalardo, A. M., Ferrito, V., Giannì, S., Armeri, G. M., Patti, C., et al (2021). Signals from the deep-sea: Genetic structure, morphometric analysis, and ecological implications of cyclothone braueri (Pisces, gonostomatidae) early life stages in the central Mediterranean Sea. *Mar. Environ. Res.* 169, 105379. doi: 10.1016/j.marenvres.2021.105379

Tortonese, E. (1970). *Osteichthyes. pesci ossei. fauna d'Italia*. Bologna, Italia: Edizioni Caldarini.

Vilchis, L. I., Balance, L. T., and Watson, W. (2009). Temporal variability of neustonic ichthyoplankton assemblages of the eastern pacific warm pool: Can community structure be linked to climate variability? *Deep Sea Res. I* 56, 125–140. doi: 10.1016/j.dsr.2008.08.004

Watanabe, H., Kawaguchi, K., and Hayashi, A. (2002). Feeding habits of juvenile surface-migratory myctophid fishes (family myctophidae) in the kuroshio region of the Western North Pacific. *Mar. Ecol. Prog. Ser.* 236, 263–272. doi: 10.3354/meps236263

Whittaker, R. H. (1960). Vegetation of the siskiyou mountains, Oregon and California. *Ecol. Monogr.* 30, 279–338. doi: 10.2307/1943563

Whittaker, R. H. (1972). Evolution and measurement of species diversity. *Taxon* 21, 213–251. doi: 10.2307/1218190

Wood, S. N. (2011). Fast stable restricted maximum likelihood and marginal likelihood estimation of semiparametric generalized linear models. *J. R. Stat. Soc Ser. B Methodol.* 73 (1), 3–36. doi: 10.1111/j.1467-9868.2010.00749.x

Worm, B., Barbier, E. B., Beaumont, N., Duffy, J. E., Folke, C., Halpern, B. S., et al (2006). Impacts of biodiversity loss on ocean ecosystem services. *Science* 314 (5800), 787–790. doi: 10.1126/science.1132294

Yoon, W. D., Nival, P., Choe, S. M., Picheral, M., and Gorsky, G. (2007). Vertical distribution and nutritional behaviour of cyclothone braueri, nematoscelis megalops, meganyctiphanes norvegica and salpa fusiformis in the NW Mediterranean mesopelagic zone. *ICES CM* 2007/F:03, 1–28.

Zarrad, R., Alemany, F., Rodriguez, J.-M., Jarboui, O., Lopez-Jurado, J.-L., and Balbin, R. (2013). Influence of summer conditions on the larval fish assemblage in the eastern coast of Tunisia (Ionian Sea, southern Mediterranean). *J. Sea Res.* 76, 114–125. doi: 10.1016/j.seares.2012.08.001

Zarrad, R., Rodríguez, J. M., Alemany, F., Charef, A., Jarboui, O., and Missaoui, H. (2020). Larval fish community composition and distribution of the central-southern mediterranean under summer and winter conditions. *Acta Ichthyol. Piscat.* 50 (3), 313–324. doi: 10.3750/AIEP/02957

Zorica, B., Čikeš Keč, V., Vrgoč, N., Isajlović, I., Piccinetti, C., Mandić, M., et al (2020). A review of reproduction biology and spawning/nursery grounds of the most important Adriatic commercial fish species in the last two decades. *Acta Adriat.* 61 (1), 89–99. doi: 10.32582/aa.61.1.7

frontiers | Frontiers in Marine Science

TYPE Original Research
PUBLISHED 12 August 2022
DOI 10.3389/fmars.2022.909164

OPEN ACCESS

EDITED BY
Athanassios C. Tsikliras,
Aristotle University of Thessaloniki, Greece

REVIEWED BY
Peter Goethals,
Ghent University, Belgium
Sion Letizia,
University of Bari Aldo Moro, Italy

*CORRESPONDENCE
Davide Agnetta
dagnetta@ogs.it

SPECIALTY SECTION
This article was submitted to Marine Fisheries, Aquaculture and Living Resources, a section of the journal Frontiers in Marine Science

RECEIVED 31 March 2022
ACCEPTED 22 July 2022
PUBLISHED 12 August 2022

CITATION
Agnetta D, Badalamenti F, Colloca F, Cossarini G, Fiorentino F, Garofalo G, Patti B, Pipitone C, Russo T, Solidoro C and Libralato S (2022) Interactive effects of fishing effort reduction and climate change in a central Mediterranean fishing area: Insights from bio-economic indices derived from a dynamic food-web model. *Front. Mar. Sci.* 9:909164. doi: 10.3389/fmars.2022.909164

Interactive effects of fishing effort reduction and climate change in a central Mediterranean fishing area: Insights from bio-economic indices derived from a dynamic food-web model

Davide Agnetta[1*], Fabio Badalamenti[2,3,4], Francesco Colloca[4], Gianpiero Cossarini[1], Fabio Fiorentino[4,5], Germana Garofalo[5], Bernardo Patti[2], Carlo Pipitone[2], Tommaso Russo[6,7], Cosimo Solidoro[1] and Simone Libralato[1]

[1]National Institute of Oceanography and Applied Geophysics-OGS, Section of Oceanography, Trieste, Italy, [2]National Research Council, Institute of Anthropic Impacts and Sustainability in Marine Environment (CNR-IAS), Palermo, Italy, [3]School of Geosciences, University of Edinburgh, Edinburgh, United Kingdom, [4]Department of Integrative Marine Ecology, Stazione Zoologica Anton Dohrn, Rome, Italy, [5]National Research Council, Institute for Marine Biological Resources and Biotechnology (IRBIM), Mazara del Vallo, Italy, [6]Laboratory of Experimental Ecology and Aquaculture, Department of Biology, University of Rome Tor Vergata, Rome, Italy, [7]National Inter-University Consortium for Marine Sciences (CoNISMa), Rome, Italy

Disentangling the effects of mixed fisheries and climate change across entire food-webs requires a description of ecosystems using tools that can quantify interactive effects as well as bio-economic aspects. A calibrated dynamic model for the Sicily Channel food web, made up of 72 functional groups and including 13 fleet segments, was developed. A temporal simulation until 2050 was conducted to evaluate the bio-economic interactive effects of the reduction of bottom trawling fishing effort by exploring different scenarios that combine fishery and climate change. Our results indicate that direct and indirect effects produce a net increase in biomass of many functional groups with immediate decline of trawlers' catches and economic incomes, followed by a long term increase mainly due to biomass rebuilding of commercial species which lasts 5-10 years after fishing reduction. Synergistic and antagonistic effects caused by changes in the fishing effort and in climate characterize a specific functional group's response in biomass which, in turn, modulate also the catch and income of the other fleets, and especially of those sharing target resources. However, trawler's intra-fleet competition is higher than the others fleet effects. In the medium term, the effects of fishing effort reduction are higher than those of climate change and seem to make

10.3389/fmars.2022.909164

exploitation of marine resources more sustainable over time and fishery processes more efficient by improving ecosystem health.

KEYWORDS

ecosystem impact, fishery sustainability, food-webs, strait of Sicily, ecosim model

1 Introduction

Marine fisheries have a prominent role across the globe because they provide a huge diversity of seafood and economic income for millions of people (FAO, 2020). However, as the world population will grow to around ten billion people over the next three decades (UN, 2019) and the climate of our planet is changing, there is a need to understand and modulate fishing impacts on ecosystems and increase fisheries' efficiency under a sustainable framework. Basically, fisheries range between two opposite sides: industrial fishing operates mainly in the high sea while Small Scale Fisheries (SSF) are predominant nearshore, especially in the emergent countries where they provide essential animal proteins (FAO, 2020).

Industrial fisheries, mainly based on bottom trawling, tend to operate at a great cost to ecosystems because of large proportions of unwanted catches of marine organisms (i.e. bycatch and discards) (FAO, 2020) and the negative impact on habitats (De Juan et al., 2011). In addition, bottom trawling is the only activity specialized in catching highly valuable demersal species such as shrimps. However, since 2000's experimental technological advances have made progressively available potential options to reduce the impact of trawling due to unwanted catches (small-size individuals of commercial species or non-commercial species), for example by means of net modifications or benthos release panels (Soetaert et al., 2016; Vitale et al., 2018).

SSF are generally considered more sustainable because they use fishing gears that have little impact on the environment (e.g. the seabed) and incorporate traditional elements that are often in line with sustainability principles (FAO, 2019). In fact, SSF use a range of highly selective gears and are generally more flexible in terms of target species, area and season. Additionally, SSF employ 25 times more people and use three-quarters less fuel than the industrial fishery sector to catch a similar amount of edible fish (Jacquet and Pauly, 2008; Teh and Sumaila, 2013).

In the Mediterranean Sea, a wide range of fishing activities from small-scale to industrial characterizes the so-called mixed fisheries. They interact at least indirectly through the food-web (Agnetta et al., 2019) and it has also been hypothesized that they compete with each other (Raicevich et al., 2020). Nowadays, the main regulation for managing fishing in the EU waters of the Mediterranean Sea is the EU-Common Fisheries Policy (CFP), which aims at exploiting stocks at a safe level, defined according to the Maximum Sustainable Yield (MSY) paradigm. However, the resilience of a target stock relies not only on its health but also on the interactions established with other ecosystem components. Although areas with a long history of efficient and intensive stock assessments and management have shown healthy target populations (Hilborn et al., 2020), these assessments into more complex models seems to be promising for the Ecosystem Approach to Fisheries. Given that single species models tend to compress the complexity of interspecific relationships within a marine community exploited by fisheries, the adoption of multispecies and multigear models allows for a more integrated perspective of the ecosystem functioning, foresees fish and fishery patterns in mid-long temporal scales (Coll and Libralato, 2012) and helps estimate trade-offs in marine exploited ecosystems (Libralato and Agnetta, 2019).

Also, assessing ecological and economic sustainability of fisheries is urgent and awaited, particularly in places such as the Mediterranean Sea where decreased landings of shellfish and finfish observed in the last decades (Carpi et al., 2017; Colloca et al., 2017; Fiorentino and Vitale, 2021) may lead to an exacerbation of fleet competition, economically inefficient exploitation and a degradation of habitats and living resources. In addition, the fact that the Mediterranean Sea is considered a hotspot of climate change (Giorgi, 2006; Pisano et al., 2020) is leading to growing concerns for the potential negative effects on marine resources and the consequent increased critical issues for fisheries. Finally, changes in primary production driven by climate change could act in combination with fishing by varying catches and biomass of target species differently in space and time (Moullec et al., 2019) and potentially weaken the ecosystem's capacity of recovery to threats.

In the Strait of Sicily (SoS), in order to limit the negative effects of fishing on marine life and habitats, different management measures have been discussed and adopted, including the reduction of bottom trawling, the establishment of new fishery restricted areas as well as additional technological measures (Russo et al., 2019; Jarboui et al., 2022). In particular, the Italian Multiannual Management Plan has provided for a strong reduction of the fishing effort, in terms of fleet capacity

and activity, amounting to 25% from 2008 to 2013. A further reduction of fishing days by 5% in 2019 and 10% in 2020 was achieved, taking the 2018 fishing days/data as the baseline reference. Such an effort reduction is expected to determine an impressive socio-economic impact for the fishing sector, possibly affecting the medium-term survival of several enterprises. However, the effects of enforcing this measure have never been investigated in a multi-fleet context. In highly connected fishery systems such as the SoS, the intricacy of interactions among organisms, fleets and between fleets and organisms (Agnetta et al., 2019) might transfer the impact from one fleet to another and/or from one target species to another. Furthermore, given that fisheries respond to changes in bio-economic factors, it is important to take them into account in the analysis, especially in a perspective of global environmental change. It is therefore of paramount importance to evaluate the effects of the effort reduction on both the ecosystem and the fisheries performance in the short and medium term, also in relation to the future climatic scenarios for the region (Moullec et al., 2019). In this context, ecosystem food web models such as Ecopath with Ecosim represent a quantitative framework for accounting of climatic changes, fishery modifications and bioeconomy and result in an integrated modelling approach widely used (Heymans et al., 2016).

In this study, a calibrated multispecies-multifleet food web model based on Ecosim is developed and applied to quantify the ecological and bio-economic effects induced by the reduction of trawling effort under climate change scenarios. Simulations are set to disentangle potential effects of primary production changes induced by climate change, which is among the most important factor affecting ecosystem productivity over time (Moullec et al., 2019). The analysis accounts for the interaction of effects on biomass, catch and economic income in a mixed fishery Mediterranean system such as the SoS. The effort reduction is expected to produce an increase in biomass of target functional groups (fishery release) and the eventual rebuilding of stocks is quantified. Moreover, the analysis is used to test for synergism and antagonism between effort reduction and primary production levels on functional groups and the net biomass response of functional groups to changes in these two factors. Finally, the inclusion of economic aspects into the modelling allows the quantification of the extent to which group response affects catch and economic incomes of fisheries.

2 Material and methods

2.1 Modelling approach

We have used the Ecopath with Ecosim modelling approach (Christensen and Walters, 2004) by starting with a well-developed Ecopath model for the SoS (Agnetta et al., 2019). The dynamic temporal food-web model Ecosim (EwE v. 6.6.5, http://www.ecopath.org) expresses biomass dynamics based upon the initial parameters of the Ecopath master equation (Christensen and Walters, 2004) using a system of differential equations which take the form:

$$\frac{dB_i}{dt} = g_i \sum_j Q_{ji} - \sum_j Q_{ij} + I_i - (M_i + F_i + e_i)\ B_i$$

where dB_i/dt is the biomass growth rate of group (i) during the interval dt, g_i the net growth efficiency (production/consumption ratio), I_i the immigration rate, M_i and F_i the natural and fishing mortality rates of group (i), and e_i the emigration rate. The consumption rates Q_{ji} are calculated based on the "foraging arena" theory (animals balance predation risk with foraging activity) where the biomass of the preys are divided into vulnerable and invulnerable components (Christensen and Walters, 2004).

In Ecosim, the interactions between predators and prey are therefore regulated by the foraging arena theory through a set of parameters including the so called "vulnerability", which is usually considered as the tuning parameter (Christensen and Walters, 2004). The foraging arena is based on the ecological assumption that only a fraction of the biomass of prey is available to the predator, dynamically adapted through the vulnerability parameter specific for each prey-predator interaction (Walters et al., 2000). Basically, the vulnerability indicates the effect of prey and predator density on the consumption by a predator, and makes it possible to balance top-down and bottom-up processes across the trophic web (Walters and Christensen, 2007; Ahrens et al., 2012) with respect to initial conditions (Ecopath biomasses). Vulnerabilities are also tuned to fit the historical patterns of observed data under simulated dynamics forced by primary production and/or fishing effort changes (Araújo et al., 2008).

The Ecosim module was used here to integrate a massive amount of environmental, biological and fisheries information in a coherent framework and dynamically describing a series of yearly data of biomass, catch and economic income in the SoS. We started from the mass balanced Ecopath model (Agnetta et al., 2019) and, after a spin-up of 10 years (1995-2004), we fitted the dynamic food-web model for the period 2005-2017 to real data and simulated the future scenarios of climate and fisheries up to 2050. The study area, approximately 61,000 km^2 wide, coincides with the northern side of the larger SoS (Figure 1), which stretches off the southern Sicily coast and is characterized in its central portion by a narrow continental shelf that separates two wider portions of shelf (i.e. the Adventure Bank to the west and the Malta Bank to the east).

2.2 Input data

2.2.1 Biological data

The model comprises 69 living functional groups (from bacteria to large pelagic species), and 3 non-living organic

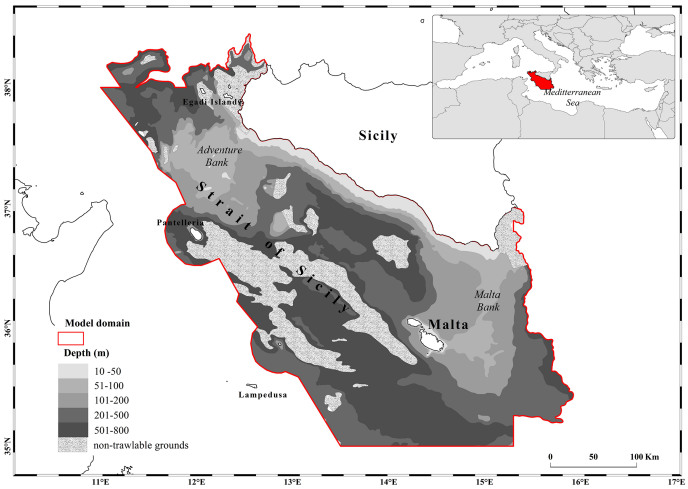

FIGURE 1
Area of the Strait of Sicily where the dynamic food web model (about 61,000 km2) is applied.

matter compartments (Table 1). Biomass of phytoplankton, zooplankton, and the concentration of suspended detritus were estimated by the Copernicus Marine Service (CMEMS) product as obtained from the 3D coupled physical and biogeochemical model for the Mediterranean Sea (Cossarini et al., 2021). Original georeferenced CMEMS data expressed as gCm^{-3} were extracted for the studied area (years 2005-2017) and integrated over depth (10-800m) in order to obtain the relative biomass as gCm^{-2}, data for plankton functional types were aggregated to represent the groups of the EwE model and then conversion factors were used in order to transform gC to wet weight (Bonanno et al., 2013; Kiørboe, 2013). Fishery-independent biomass density estimates encompassing demersal fish and shellfish were mainly obtained from bottom trawl surveys carried out in spring/summer from the mid 2000's to 2017 in the model area by the MEDITS program (Mediterranean International bottom Trawl Surveys) (Bertrand et al., 2002; Spedicato et al., 2019) and expressed as kg km^{-2} wet weight. For highly migratory species (bluefin tuna and swordfish), we used average biomass estimates provided by stock assessments in the Mediterranean Sea (ICCAT, 2010) and adapted parameters by taking into account eventual lifetime spent outside the SoS area (see more details in Agnetta et al., 2019).

2.2.2 Fishery data

Fishery landings by species and gear in the SoS during 2005-2017 were drawn from the national monitoring of commercial fleets within the European Data Collection Framework (DCF - https://datacollection.jrc.ec.europa.eu/). Data were aggregated into 13 fleet segments resulting from a combination of fishing gear (i.e. trawlers, purse-seiners, long-liners, set netters) and vessel size classes based on the length overall (LOA:<12m; 12-24m; >24m) (Table 2). Furthermore, the bottom otter trawlers were also distinguished into categories according to the main target species. Compared to 18 fleets used in the original Ecopath model (Agnetta et al., 2019), a slight reshaping of several fishing activities was necessary due to the lack of details for some fisheries.

Since the fishing activity of larger bottom trawlers (i.e. fleet 13, Table 2) targeting deep-water species (i.e. deep-water rose shrimp *Parapenaeus longirostris* and giant red shrimp *Aristaeomorpha foliacea*) spans over a larger space than the model area (Garofalo et al., 2007; Milisenda et al., 2017), about 60-70% of their important species catches was retained inside the model area (Agnetta et al., 2019). Empirical discard ratio for commercial fish and invertebrates by species and by fleet was drawn from studies carried out in the SoS or from nearby Mediterranean areas (Agnetta et al., 2019 and references therein).

2.2.3 Economic data for income per unit effort (IPUE)

Since landings (L) change dynamically in Ecosim, the revenues (R) are estimated from landings and off-vessel prices (offprice) per fleet (fl) and functional group (FG) at each time step:

$$R_{fl,FG}(t) = L_{fl,FG}(t) \;\; offprice_{fl,FG}(t)$$

The most detailed estimates of prices (per species, fleet and year) were taken into account whenever possible. The price of the main target species making up about 60% in catches of bottom trawlers such as hake (HKE), striped mullet (MUT), pandora (PAC), giant red shrimp (ARS) and deep-water rose shrimp (DPS) was updated for each year of the hindcast (2005-

TABLE 1 Summary description of 72 biological functional groups (FG).

N°	Name	FG
1	Seabirds	SB
2	Marine mammals	MM
3	Sea turtles	TUR
4	Swordfish	XIP
5	Bluefin tuna	THU
6	Large pelagic fish	LPL
7	Medium pelagic fish	MPL
8	Other small pelagic fish	SPL
9	European hake<6 cm	HKE0
10	European hake 6-12 cm	HKE1
11	European hake 12.1-22.0 cm	HKE2
12	European hake 22.1-41.0 cm	HKE3
13	European hake >41.0 cm	HKE4
14	Red mullet<8 cm	MUT0
15	Red mullet 8-12 cm	MUT1
16	Red mullet 12.1-17 cm	MUT2
17	Red mullet>17 cm	MUT3
18	Horse mackerel	TRA
19	Pandora	PAC
20	Demersal fish (slope)	DFS
21	Demersal fish crustacean feeders (shelf)	DFH
22	Demersal fish mixed food (shelf)	DSM
23	Demersal fish piscivorous (shelf)	DSP
24	Demersal fish rocky (shelf)	DSR
25	Mesopelagic fish crustacean feeders (slope)	MSC
26	Mesopelagic fish jellyfish feeders (slope)	MSG
27	Mesopelagic fish piscivorous (slope)	MSP
28	Rays and skates (shelf)	RSH
29	Rays and skates (slope)	RSS
30	Sharks (shelf)	SSH
31	Sharks (slope)	SSS
32	European anchovy	ENG
33	European pilchard	SAR
34	Epipelagic fish	EPI
35	Cephalopods benthic (shelf)	CEBH
36	Cephalopods benthic (slope)	CEBS
37	Cephalopods pelagic (shelf)	CEPH
38	Cephalopods pelagic (slope)	CEPS
39	Decapods natant (slope)	DNS
40	Decapods natant (shelf)	DNH
41	Decapods reptant (slope)	DRS
42	Decapods reptant (shelf)	DRH
43	Giant red shrimp	ARS
44	Deep water rose shrimp	DPS
45	Suprabenthos	SUP
46	Macrobenthos omnivore	O
47	Macrobenthos filter-feeder	FF
48	Macrobenthos deposit-feeder	DF
49	Macrobenthos carnivore	C
50	Macrobenthos parasite	PAR
51	Macrobenthos scavenger	SCA
52	Macrobenthos herbivore	H
53	Macrobenthos grazer	GRA
54	Macrobenthos suspension-feeder	SF
55	Macrobenthos particulate-feeder	PF
56	Meiobenthos	BO
57	Euphausiacea	EUP
58	Gelatinous zooplankton	ZG
59	Large zooplankton	ZL
60	Mesozooplankton	ZM
61	Microzooplankton	ZS
62	Pelagic bacteria	PB
63	Sediment bacteria	BB
64	Pico-phytoplankton	PS
65	Dinoflagellates	DFL
66	Diatoms	PL
67	Microphytobenthos	MB
68	Seagrass	SG
69	Macroalgae	MA
70	Detritus carrion	DC
71	Suspended particulate organic matter	SPOM
72	Benthic detritus	BD

2017) by using data collected within the DCF. In the projections (years 2018-2050) prices were kept to the last values available (2018).

These dynamically estimated revenues were standardized by using the relative effort (rel_f) of each fleet:

$$rel\_f_{fl}(t) = f_{fl}(t)/f_{fl}(t_0)$$

where f is the effort of each fleet (fl) at any time step and t_0 corresponded to the first year of the hindcast (i.e. 2005) when the model was mass balanced (ecopath model), in this way an index of income per unit effort (IPUE), was calculated as:

$$IPUE_{fl}(t) = R_{fl}(t)/\ rel\_f_{fl}(t)$$

and expressed in millions of euros (mln EUR).

2.3 Fitting procedure and basic validation of the model

A combination of trophic interaction strength (vulnerability of prey to predators), fishing effort over time and primary production changes were used for fitting the model to past biomass and catch data for the period 2005-2017 (hindcast). The hindcast EwE model was bottom-up forced using net primary

TABLE 2 List of the fleet segments considered by the combination of vessel size (i.e. length overall =LOA) and fishing gear.

N°	LOA	Metiér	fleet name
1	1	set and drifting longline	1LL
2	1	setgill and trammel net demersal fish	1GN
3	1	purse seine	1PS
4	1_2	Polyvalent license	1.2MIS
5	1_2	pots and traps demersal_small pelagic fish	1.2FPO
6	2	set and drifting longline	2LL
7	2	setgill and trammel net demersal fish	2GN
8	2_3	purse seine	2.3PS
9	2_3	mid water otter trawl mixed demersal_pelagic SP	2.3OTM
10	2	pelagic pair trawl_small pelagic fish	2PTM
11	1	bottom otter trawl	1OTB
12	2	bottom otter trawl	2OTB
13	3	bottom otter trawl (mainly deep water species)	3OTB

LOA1, vessel size<12m, LOA2, 12-24m; LOA3, >24m.

production of large (PL) and small (PS) phytoplankton. Total net primary production of the CMEMS reanalysis (Cossarini et al., 2021) was partitioned into PL and PS production anomaly by using the relative biomass of the phytoplankton functional groups included in the Biogeochemical Flux Model (BFM) (Lazzari et al., 2012; Salon et al., 2019), namely diatoms of the BFM for the PL group in EwE and the sum of picophytoplankton and nanoflagellates in BFM for PS.

In order to reconstruct fishing pressure per fleet (top-down forcing) over the years (2005-2019), we used complementary information collected under the umbrella of DCF, i.e. the vessel monitoring system (VMS) and data from the fleet register relative to the model area (https://webgate.ec.europa.eu/fleet-europa/index_en). However, VMS allows to assess the fishing activity of vessels with LOA larger than 15 m, while the fleet segment 12m< LOA< 15m is only partially covered. Hence, for this fleet segment, the observed effort in space and time was rescaled by using the official number of vessels and the footprint of VMS-equipped vessels (Russo et al., 2014; Russo et al., 2019). Moreover, fishing activity as days at sea per year was used for vessels<12 LOA.

The fitting procedure has followed an approach that foresees a series of trials for tuning the vulnerabilities (Heymans et al., 2016) and was evaluated through the sum of squared differences (SS) between the log-observed and log-predicted data (i.e. biomass or catch) (Christensen and Walters, 2004) and the Akaike's information criterion (AIC) (Alexander et al., 2015). Vulnerability by predators (i.e. common vulnerability for all preys of a given predator) were used to perform sensitivity search of the most influential vulnerabilities and nine trials for the best fit were conducted using a different number (k) of tuned vulnerabilities (Table S1), keeping remaining vulnerabilities to default values (v=2). Comparison of model outputs and data was done using annual biomass of 27 functional groups (Figure S2A) and annual catches of the most important commercial species European hake (HKE), red mullet (MUT), pandora (PAC), giant red shrimp (ARS), deep water rose shrimp (DPS), European anchovy (ENG), European pilchard (SAR), swordfish (XIP), bluefin tuna (THU) (14 FGs, Figure S2B) for a total of 41 series (S) and 511 data points (N). Assuming autocorrelation between time series and no cross-correlation, these data corresponds to S-1 = 40 degree of freedom (df).

Validation was based on a graphical evaluation of the model outputs against the observed mean yearly biomass (MEDITS) of HKE, MUT, PAC, ARS and DPS, accompanied by the calculation of the Spearman correlation coefficient. The comparison was done therefore for several commercial groups whose catches were instead used for fitting, over the hindcast period (2005-2017). Total landings and revenues relative to 6 years (2013-2018) were also compared to data collected within the DCF.

2.4 Setting of scenarios

In order to disentangle the role of fishing effort reduction and primary production driven by climate change, a set of 4 scenarios were run: they all have in common the hindcast period 2005-2017 and have specific forcing functions for the years 2018-2050, adapted and combined to address the research aims.

The scenarios implemented were i) reference scenario (REF), ii) fishing effort reduction scenario (F), iii) climate change scenario (C), and iv) combined fishing reduction and climate change (FC) (Table 3). The REF scenario was simulated with a constant effort after the year 2019 and a constant annual primary production after year 2017 (using seasonal cycles derived from climatology, years 2005-2017).

The F scenario was represented by reducing simultaneously the three fleets of bottom trawlers (1OTB, 2OTB and 3OTB respectively with LOA<12m, LOA 12-24m, LOA>24m) by 10% each year from 2022 to 2024 (each 10% yearly cut always referred to the fishing effort level in 2021, so that the total reduction over the 3-year period is 30% per fleet) and considering the climatological primary production as in the REF scenario.

The C and FC scenarios were run with the same fishing pressure of REF and F respectively, but incorporating variations in primary production induced by climate change. In these cases, a monthly primary production anomaly for phytoplankton groups (PL and PS) was estimated as done for hindcast using the results of the biogeochemical scenario simulation based on Representative Concentration Pathway (RCP) 8.5 (Reale et al., 2022). The scenario simulation features the same model configuration as in the Copernicus reanalysis: a coupling between the NEMO ocean dynamics model and the BFM biogeochemical model (Reale et al., 2022). Scenario setups (e.g., boundaries, land input) are consistent with the reanalysis (Cossarini et al., 2021) except for resolution and assimilation (Reale et al., 2022). A detrendization was also applied as in Solidoro et al. (2022), in order to remove numerical trends and eventual bias between climate scenario and reanalysis by comparing the series over the 2005-2017 period. The RCP8.5 from the IPCC is the highest greenhouse gas emissions scenario over time. It assumes a slow income growth with no important rates of technological change and energy intensity improvements (Riahi et al., 2011), a high population growth rate and a "business as usual" fisheries management (i.e., current fishing mortality). It was chosen here as the scenario was the most frequently explored in the region (Hattab et al., 2016; Corrales et al., 2018; Moullec et al., 2019), hence facilitating comparisons with other findings.

2.5 Analysis of biomass, landings and income across scenarios

Trends of biomass, landings and IPUE along temporal projection (2018-2050) and across scenarios were summarized per FG and/or per fleet. In order to assess changes between each alternative scenario (F, C, FC) and the reference one (REF), basic statistics (mean, standard deviation, minimum and maximum) were estimated after calculating ratios year by year of the projection (2018-2050) and in specific time ranges (2026-2030, 2046-2050) as: ratio (t) = scenario (t)/REF (t).

Effects of fishery and climate on FG biomass were quantified by the interaction effect index (IEI), which compares the cumulative mean size effect of two paired factors with the sum of their individual effects. IEI is given by:

$$IEI = ln\left[Abs\left(\frac{effect\ \ FC}{effect\ \ F + effect\ \ C}\right)\right]$$

where Abs = absolute value, effect FC = FC-REF, effect F = F-REF, effect C= C-REF (Allgeier et al., 2011; Villar-Argaiz et al., 2018). Values of IEI>0 allowed identifying synergistic effects (i.e. larger than purely additive), while IEI<0 enabled disentangling antagonistic effects between fisheries and climate (lower than additive effects).

The mean FG biomasses at the end of the simulation (2046-2050) were clustered by considering positive or negative FG response at each scenario with respect to REF. The FGs were also ranked for each cluster by summing mean ratio across scenarios.

3 Results

3.1 Fitting and validation of the model

The first trial was done considering the default setting for all vulnerabilities (k=0) and the fitting indices were SS= 157.96 and AIC = -559.93 (Table S1). The best fit was obtained by tuning 20 vulnerabilities despite the 40 df: SS was reduced by more than 50% with respect to the starting trial (SS= 80.12) and AIC was -905.10 (Table S1). Fitting of biomass and functional group catches was fairly successful although in several cases, such as for cephalopods (CEBH, CEPH, CEPS) and decapods (DNH, DNS), the model fails in accounting for the observed interannual fluctuations but simulates a mean value through the observed data (Figure S2A). Among catches, medium-size red mullet (MUT2) showed the worst fitting (Figure S2B).

Biomass validation of the most important commercial groups showed that the model satisfactorily fits the observed trends with the exception of juvenile red mullet (MUT1) (Figure S3).

TABLE 3 Breakdown of forcing used to the reference (REF) and the alternative projected scenarios, F=fishing effort reduction, C= climate, FC= fishing effort reduction+climate.

Scenario	Effort	Primary production
REF	kept values 2019	climatology reanalysis (mean 2005-2017)
F	30% f reduction for 3 OTB	climatology reanalysis (mean 2005-2017)
C	kept values 2019	climate incorporating RCP_8.5
FC	30% f reduction for 3 OTB	climate incorporating RCP_8.5

Landings and revenues from observations (DCF) and the model were in good accordance and showed the same order of magnitude between source of datasets throughout the years available (2013-2018) (Figures S4A, B).

3.2 Effort reduction *vs* reference scenario

Trends of the REF scenario show that keeping the fishing pressure at the current level will result in decreased biomass for most FGs, especially those targeted by bottom trawling (blue lines in Figure 2, Figures S5, S6). Large top predators such as swordfish (XIP), bluefin tuna (THU), and large pelagic fish (LPL) after an increase due to a prey release of horse mackerel (TRA), reach a plateau in 5-10 years. Benthic cephalopods (CEBH, CEBS) and crustacean decapods (DNH, DNS) were estimated to slightly increase because of a predatory relaxation resulting from depletion of carnivorous demersal (mainly hake) by fisheries (Figure 2, in blue).

When a reduction of effort was applied (scenario F, black lines in figures), valuable commercial species target of bottom trawlers such as pandora (PAC), deep-water rose shrimp (DPS), hake (HKE0-4), red mullet (MUT0-3), giant red shrimp (ARS) underwent a quick rebuilding just after 2024 (i.e. after complete effort reduction). These FGs responded with positive changes one order of magnitude higher than the rest of FGs (Figure 2). The biomass of other FGs belonging to cephalopods (CEBH, CEBS, CEPH) and rays (RSS) also resulted in an exceptional recovery. In some cases, such as for Hake, an equilibrium was reached after about 15 years, but the giant red shrimp (ARS) decreased after the year 2030. Comparing F to REF, FGs showed a mean 1.40 ± 1.10 fold increase with a minimum (0.85 ± 0.09) for horse mackerel (TRA) and a maximum (16.53 ± 21.11) for pandora (PAC) (Figure 3). Horse mackerel and large top predators (LPL and THU) assumed low values in mean increase by resulting at the bottom of the ordered group's list (Figure 3).

As concerns the impact on fleet production, in scenario F the reduction of effort in years 2022-2024 clearly caused an initial drop in bottom trawl landings (Figure 4, fleets 11-13), but from 2025, since an important rebuilding was recorded for the main target species (Figure 5), a rise of landings to or above REF can be observed (Figures 4, 6). The maximum increase was 1.28 ± 0.20 fold for 3.OTB_MDD (fleet 13, Figure 6), in spite of a mean ratio of 1.03 ± 0.09 and a minimum of 0.94 ± 0.03 fold for 2.OTM (fleet 9) with respect to the REF scenario. Effort reduction of the bottom trawlers had an indirect positive effect on landings of gillnets (2.GNS) and on small-scale longline (1.LLD) that increased by 5% and 4% respectively. On the contrary, a moderate negative effect (-4%) resulted for small purse seiners (1.PS) and mid-water trawlers (2.OTM), and a slight negative effect (-2%) was also evident on the landings of polyvalent-license vessels (1.2.MIS) (Figure 6).

The effects of the scenario on IPUE were analogous to what was observed for landings (Figure 7), but during the phase of progressive effort reduction (2022-2024) bottom trawlers did not lose IPUE. Higher positive changes resulted for bottom trawling (1.31 ± 0.18 fold) and slight to moderate negative effects (maximum IPUE loss< 10%) for small purse seiners (1.PS and 2.3PS), polyvalent-license vessels (1.2MIS) and mid-water trawlers (2.OTM) (Figure 8).

3.3 Climate (C and FC) vs reference scenario

Considering climate scenarios (C and FC vs. REF, red and green lines, respectively), most FGs showed an increase in biomass (Figures 2, S6) with a mean ratio of 1.021 ± 0.004 fold in C and 1.51 ± 2.23 fold in FC (Figure 3). Among the low trophic level FGs, small phytoplankton (PS, ~ +5%) and zooplankton small (ZS, ~ +6%) resulted in the top 15 increased FGs, whereas large phytoplankton (PL) and pelagic bacteria (PB) showed the largest biomass reduction (< -2%). As a result, total biomass of phytoplankton did not significantly change (<2%) across scenarios. Horse mackerel (TRA) and pelagic fish such as large pelagic fish (LPL) and bluefin tuna (THU) appeared high in the ordered list only in C scenario, suggesting bottom-up effects linked to prey release (Figure 3).

Climate scenarios showed an overall increase of landings per fleet (Figure 4) and per FG (Figure 5), but combined effects of effort reduction and climate change caused contrasting responses. PAC, DPS, HKE, and MUT showed the highest increase in C and FC scenarios (Figure 5) with mean ratios ranging between 1.03 (MUT3, in C) and 4.2 (DPS, in FC), though PAC in FC registered an exceptional mean increase of about 14-fold. In the FC scenario, a slight enhancement of the positive effects of trawling reduction (for example in OTBs) was also evident, as well as smoothing effect of the negative ones (for example in 1.PS) (Figure 6).

In agreement to what was observed for landings, IPUE was positively affected in the climate scenarios (Figure 7), with higher ratios in FC for bottom trawling (from 1.36 ± 0.23 to 1.52 ± 0.34 fold) than in any other fleet. Moreover, in FC a positive reinforced effect of bottom trawling reduction was evident on IPUE of small longlines (fleet 1), gillnet (fleet 7) and pair trawlers (fleet 10), while a smoothing effect resulted for all fleets affected by IPUE loss (Figure 8).

3.4 Interactive effects of effort reduction and climate on biomass

The analysis of differences in biomasses at the end of the simulation (2046-2050) for F, C and FC scenarios with respect to REF resulted in 5 clusters that are reported in Figure 9, together

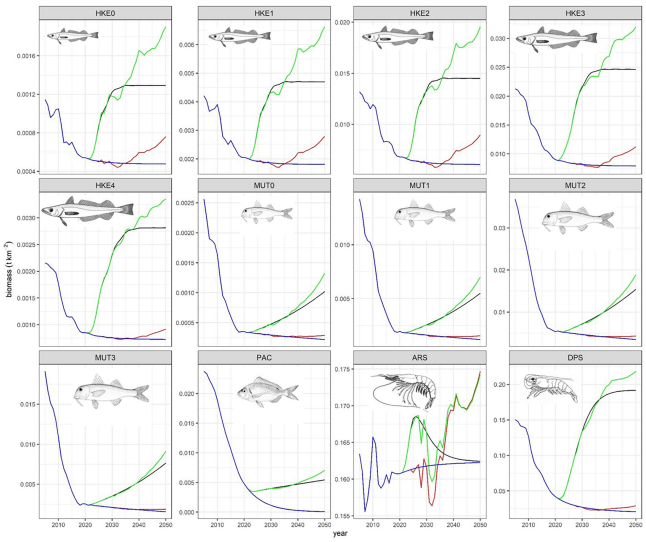

FIGURE 2
Trends of biomass along projection (2018-2050) and across scenarios, blue=REF, black= F, red= C, green= FC. The 12 groups comprise about 60% of bottom trawlers catches and 50% of total catches.

with IEI highlighting synergistic and antagonistic effects. Results show that synergistic effect of effort reduction and climate change was detected for 34 FGs, that is 47% out of total cases (72 FGs) covering the whole spectrum of trophic levels. The highest synergistic climate-fisheries effect was detected for natant decapods from the slope (DNS,IEI=0.6) and the highest antagonistic for reptant decapods from the slope (DRS) and medium pelagic fish (MPL) (IEI of -1.37 and -1.33, respectively).

The blue cluster, made up of 37 out of 72 FGs having increases in biomass in all scenarios (F, C and FC), showed that climate change and fishing effort reduction mainly had a positive synergistic effect i.e. an increase of biomass in all scenarios. The most important commercial target species of bottom trawling were at the top ten of the cluster because direct fishing release effects were predominant. This caused values of change to be orders of magnitude higher in F and FC than in C (Figure 3). The 18 FGs belonging to the yellow cluster increased in biomass in climatic scenarios (C and FC) but showed biomass reductions in F scenario. In this cluster, positive effects of climate in terms of biomass through the food web (i.e. relaxation of predation and/or release of prey) were higher than the negative ones caused by reducing fishing. The grey cluster was comprised three primary producer groups (SG, MA, MB), which benefited only from the reduction of their consumers (i.e. a mesopredator release) in scenario F. Antagonistic effects dominated yellow and grey clusters.

Eleven FGs are listed in the red cluster, which encompasses the FGs that responded positively to C scenario only, showing that the effect of reduced fishing effort embedded in the other two scenarios drives a biomass reduction. A mix of high synergistic and high antagonistic effects characterize the red cluster.

Finally, three small planktonic groups i.e. dinoflagellates (DF), phytoplankton large (PL) and pelagic bacteria (PB) (green cluster), showed a biomass decrease in all alternative scenarios indicating a negative synergistic effect of effort reduction and climate.

4 Discussion

Sustaining wild fish production, maintaining jobs and revenues of fishing enterprises while protecting biodiversity is a relevant issue to be faced by the Mediterranean fishing sector. Following the growing body of scientific evidence, the EU, national commissions and Regional Fisheries Management Organization, such as the FAO General Fisheries Commision for the Mediterranean Sea (GFCM), are supporting the development of management plans aimed at including combinations of measures to achieve sustainable fisheries. These plans are mainly based on the reduction of fishing effort and discards for trawlers and the implementation of fisheries restricted areas to protect nurseries of commercial species (see the CFP and the GFCM strategy), and should induce the reduction of fishing mortality and the rebuilding of overexploited stocks (Fiorentino and Vitale, 2021). However, recent global analyses highlighted the overfished status of resources (Froese et al., 2018) and a lack of effective rebuilding plans for the Mediterranean Sea (Melnychuk et al., 2021). This suggests the need for understanding which management measures could be considered to increase the

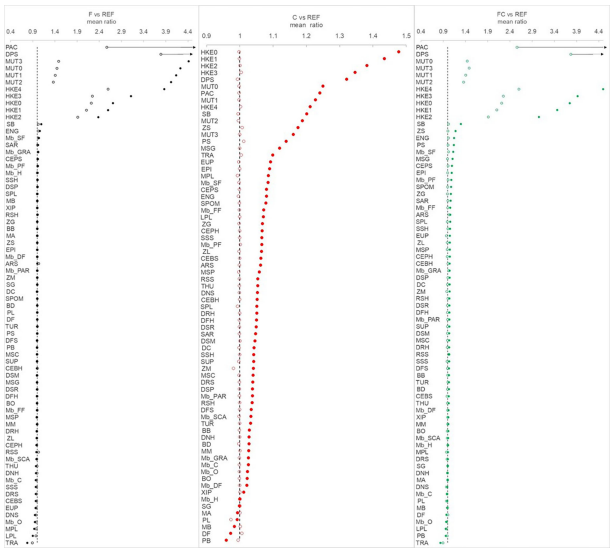

FIGURE 3
Mean ratio of biomass calculated for each functional group by comparing alternative scenarios (F, C, FC) with the reference (REF, y=1, dotted black line) across the years 2026-2030 (open circle) and 2046-2050 (solid circle). Ending values of PAC and DPS in F and FC scenario are outside of the scale (values reported in the main text).

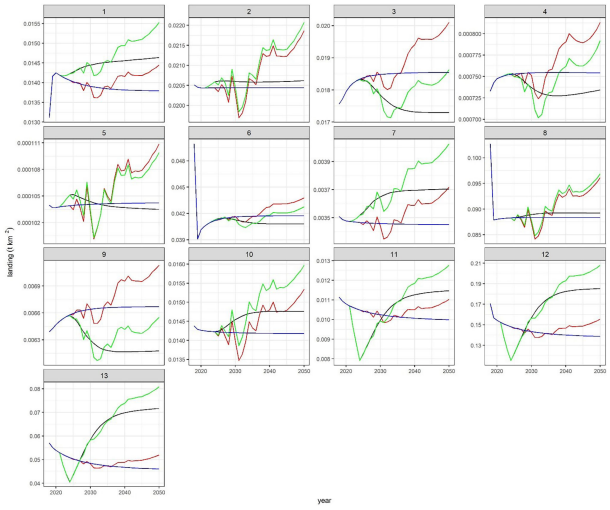

FIGURE 4
Trends of landings per fleet across reference (REF) and alternative scenarios (F,C,FC). Fleet: 1 = 1LL, 2 = 1GN, 3 = 1PS, 4 = 1.2MIS, 5 = 1.2FPO, 6 = 2LL, 7 = 2GN, 8 = 2.3PS, 9 = 2.3OTM, 10 = 2PTM, 11 = 1OTB, 12 = 2OTB, 13 = 3OTB. REF = blue, F = black, C = red, FC = green.

sustainability of fisheries, also by taking the impact of global climate change in action into account.

A dynamic food web model applied to the SoS was developed to quantify, in a multifleet-multispecies framework, the potential effects of the reduction of bottom trawling effort in combination with changes of primary production induced by climate changes.

The ongoing fisheries exploitation pattern simulated in the reference scenario showed a decreasing biomass trend for most FGs in the SoS, confirming the overexploitation status of many target species in the Mediterranean Sea as reported in several syntheses (Colloca et al., 2017; FAO, 2020). Results of the reference scenario highlight a decrease in biomass for the

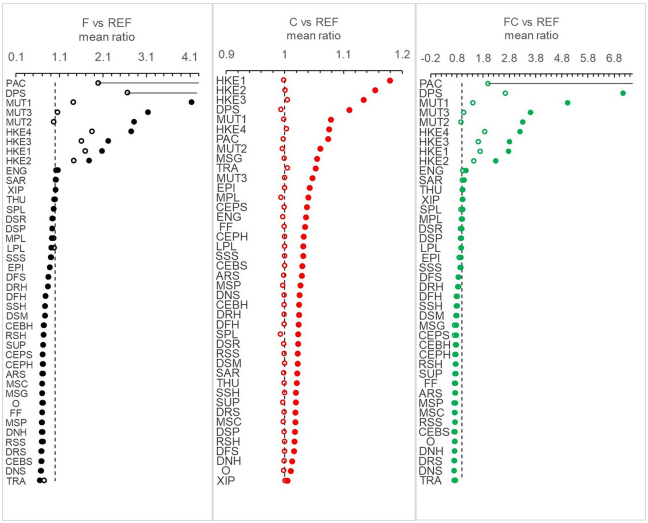

FIGURE 5
Mean ratio of landings per functional group calculated between the alternative scenarios (F, C, FC) and the reference (REF) in the years 2026-2030 and 2046-2050.

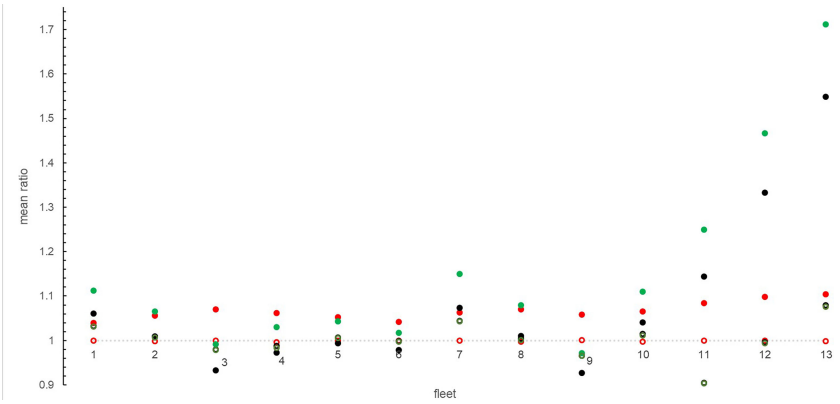

FIGURE 6
Mean ratio of fleet landings calculated between the alternative scenarios (F, C, FC) and the reference (REF) in the years 2026-2030 (open circle) and 2046-2050 (solid circle). F = black, C = red, FC = green.

main target species until 2050 under the current (2019) exploitation rate.

When a 30% reduction of bottom trawling effort (i.e. a yearly 10% decrease for 3 consecutive years) was applied, an overall increase in biomass for the main target species (hake, red mullet, deep water rose shrimp) resulted in 6-7 years. In particular, European hake reached about a 2-fold steady state biomass after 10 years since the completion of fishing effort reduction. The trend of most fished species was similar to that observed in effective marine managed areas, in coastal (Edgar et al., 2014; Dimarchopoulou et al., 2019) as well as in open sea systems (Pipitone et al., 2014). In particular, the main demersal fish species targeted by bottom trawling showed a biomass rebuilding of the same order of magnitude reported in a Sicilian trawl exclusion area (mean 8-fold increase) (Pipitone et al., 2000). In addition, a SMART model simulation considering a 15% reduction of trawl fishing effort in the SoS showed an increase of spawning biomass of red mullet and giant red shrimp after 6 years (Russo et al., 2019).

The overall fish biomass increase led to an important mid-term increase (after 2024) of landings and IPUE mainly due to direct rebuilding of target species, but also indirect food web effects deriving from the reduction of trawling. After a short time

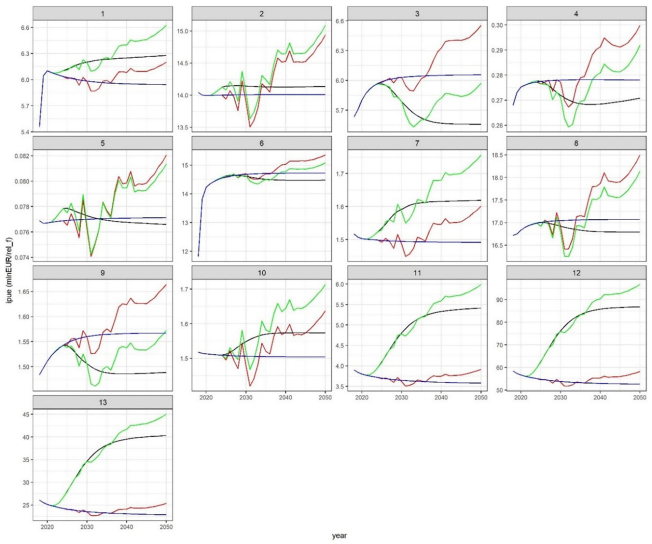

FIGURE 7
Projection (2018-2050) of income per unit of relative effort (IPUE) across scenarios for each fleet. Fleet: 1 = 1LL, 2 = 1GN, 3 = 1PS, 4 = 1.2MIS, 5 = 2FPO, 6 = 2LL, 7 = 2GN, 8 = 2.3PS, 9 = 2.3OTM, 10 = 2PTM, 11 = 1OTB, 12 = 2OTB, 13 = 3OTB.

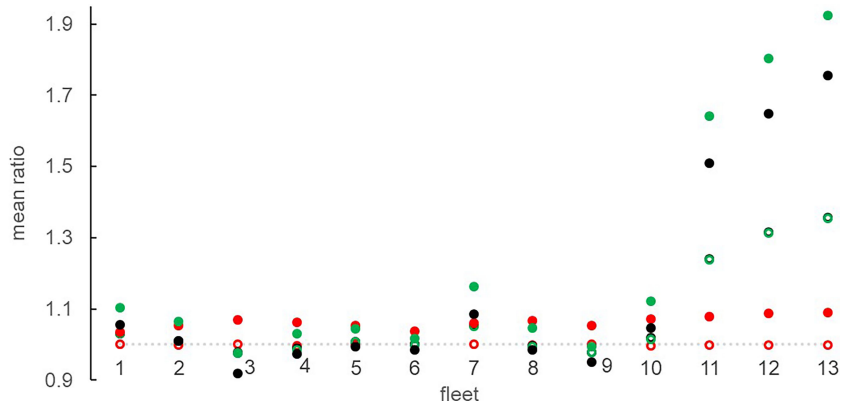

FIGURE 8
Mean IPUE ratio of 13 fleets, calculated between the alternative scenarios (F, C, FC) and the reference (REF) in the years 2026-2030 (open circle) and 2046-2050 (solid circle). F = black, C = red, CF = green.

of transition (3 years of effort reduction implementation), favorable conditions for higher catch and incomes resulted especially for bottom trawlers but also for gillnets with which they share a main target species (i.e. hake). In the scenario of fishing effort reduction for trawlers (scenario F), landings and IPUE of longlines and purse seiners would be instead negatively affected in a slight/moderate (<5%) indirect way. In fact, the trawling effort reduction caused a release of predators impacting on preys 1) directly targeted by a fleet, e.g. impairing the interactions among HKE_SAR_purse seine, and/or 2) whose target species feed on, as in the case of longline (example HKE_TRA_THU_longline). These findings suggest that bottom trawlers suffer mainly from an intra-fleet competition and secondarily a competition with the fleets sharing the main resources (GNS) or accessory catches. Results suggest that direct and indirect effects of trawl effort reduction are thus minimal on small scale fisheries (Figures 6 and 8, fleets 2, 4 and 5 in particular), although further analyses are required to explore effects of fishers adaptations (e.g., changing from trawling to SSF). However, bottom trawlers could also play a role of stabilizer on the landings of purse seiners by relaxing natural top-down effects on small pelagic fish.

10.3389/fmars.2022.909164

FG	F	C	FC	IEI
PAC	+	+	+	0.15
DPS	+	+	+	0.08
HKE4	+	+	+	0.10
HKE3	+	+	+	0.16
MUT3	+	+	+	0.10
HKE0	+	+	+	0.22
MUT0	+	+	+	0.15
MUT1	+	+	+	0.14
HKE1	+	+	+	0.19
MUT2	+	+	+	0.12
HKE2	+	+	+	0.16
SB	+	+	+	0.01
ENG	+	+	+	0.04
ZS	+	+	+	0.00
Mb_SF	+	+	+	0.02
CEPS	+	+	+	0.00
Mb_PF	+	+	+	0.01
ARS	+	+	+	-0.05
EPI	+	+	+	0.00
SAR	+	+	+	0.02
Mb_GRA	+	+	+	-0.01
SPOM	+	+	+	0.00
ZG	+	+	+	0.00
SSH	+	+	+	0.02
RSS	+	+	+	-0.06
CEBH	+	+	+	-0.04
SPL	+	+	+	0.00
DSP	+	+	+	-0.01
RSH	+	+	+	0.04
Mb_PAR	+	+	+	0.00
BB	+	+	+	0.00
TUR	+	+	+	-0.03
ZM	+	+	+	0.01
BD	+	+	+	0.00
Mb_DF	+	+	+	-0.01
XIP	+	+	+	0.01
Mb_H	+	+	+	0.06
PS	-	+	+	0.00
MSG	-	+	+	-0.01
Mb_FF	-	+	+	-0.04
DC	-	+	+	0.00
ZL	-	+	+	-0.03
SUP	-	+	+	-0.01
DSR	-	+	+	-0.03
DSM	-	+	+	-0.06
CEPH	-	+	+	-0.10
DFH	-	+	+	-0.05
MSP	-	+	+	-0.04
MSC	-	+	+	-0.02
DFS	-	+	+	-0.02
DRH	-	+	+	-0.06
EUP	-	+	+	-0.15
BO	-	+	+	-0.04
MM	-	+	+	-0.10
SSS	-	+	+	-0.12
Mb_SCA	-	+	-	-0.19
THU	-	+	-	-0.19
CEBS	-	+	-	-0.17
DNH	-	+	-	0.19
DRS	-	+	-	-1.37
Mb_C	-	+	-	0.31
MPL	-	+	-	-1.33
DNS	-	+	-	0.60
Mb_O	-	+	-	0.11
LPL	-	+	-	0.31
TRA	-	+	-	0.22
SG	+	-	+	-0.10
MA	+	-	-	-0.03
MB	+	-	-	-0.02
DF	-	-	-	0.00
PL	-	-	-	0.01
PB	-	-	-	0.00

FIGURE 9
Increase (+) or decrease (-) in mean ratio (2046-2050) of functional group (FG) biomass was evaluated as an FG response to the different scenarios and used for a qualitative clustering. In each cluster, FGs are in ascendant order by considering a cumulative response (algebraic sum of mean ratio) across scenarios. Interactive Effect Index (IEI) is given to show synergistic (blue) and antagonistic (red) effect between effort reduction and climate on FG.

Although global climate models project that net primary productivity will very likely decline by 4–11% for RCP8.5 at the end of this century (Couespel et al., 2021; Bindoff et al., 2022) with negative consequences for fish catches (Tittensor et al., 2021), the decline has expected to show regional variations due to biological and modeling factors (Bindoff et al., 2022). For the Mediterranean Sea, the specific biogeochemical model projections under high emission scenario (Solidoro et al., 2022) suggest an increment in both plankton gross productivity and system total respiration, yielding a decrement in the concentrations of total plankton biomass, chlorophyll and particulate organic carbon, among other variables. However, our results have showed that local variations of primary production related to climate change in the mid-term (2050) resulted in a small increase in total biomass (<2%) of primary producers and in a more important rearrangement of relative biomass of the lowest trophic levels. In fact, pico-nano phytoplankton (PS, +5%) and nano-micro zooplankton (ZS, +6%) increased at the expense of the larger phytoplankton (PL) and mesozooplankton (ZM) which remained quite stable or in slight decrement on average. These modifications in biomass of primary producers fuelled bottom-up energetic pathways through the food web and triggered a slight (about 1%) increase in biomass of higher trophic levels by medium-small pelagic fish groups. Similar projections have recently been obtained with the application of an end-to-end model in the Mediterranean as whole (Moullec et al., 2019) and have been suggested by other authors (Marquis et al., 2011) also in relation to past extreme global warming phases (Britten and Sibert, 2020). Keeping the fishing effort constant, the effect of climate change alone on landings and income per unit of effort was small but positive for all the fleets considered. However in this scenario, target species did not undergo any important recovery.

Notably, our results also show an interplay between fishing management and climate mediated by specific responses of food web components (i.e. FGs), so that the effects of the two drivers could act either synergistically or antagonistically.

Although uncertainty characterize projections of primary production (Kwiatkowski et al., 2020), we have showed that its changes could play a relevant role in affecting the biomass of different functional groups and their predator-prey relationships. Moreover our analysis support the conclusion that, effort reduction is the most important driver in determining the SoS ecosystem mid-term sustainable evolution. Complex and nested interactions through the SoS food web were expected (Agnetta et al., 2019), but the reliability of the results might be improved by implementing the model with processes and effects linked to spatial and habitat modifications as well as the effects of other physical factors not explicitly used here (e.g. temperature, oxygen and alkalinity changes). However, we believe this study is an important contribution towards disentangling the effects of fishery and climate change in an intricate food web such as that of the SoS.

Rebuilding exploited populations is a management objective that starts with assessing single species targets to identify specific goals, but then it has to lead to a broad ecosystem approach to fisheries management, in order to preserve the community size-structure, the ecological role of different species and the integrity of habitat functioning (Link et al., 2002; Jennings and Rice, 2011).

Here, we showed that under the current fishing regime, stock productivity and fleet profitability are generally impaired by high fishing mortality. Although climate change and fishing interact, fishing impacts are faster in producing change on marine ecosystems, therefore implementing sustainability by means of fisheries management plans is urgent. An essential aspect, however, is that of management at the transnational level (Mackelworth et al., 2019): the reduction of fishing effort in an area involving shared stocks such as the one examined in this study can be effective only if implemented to all active vessels (i.e. trawlers) in order to avoid spatial imbalances which could undermine the local management strategy measures. This aspect is even more important in areas, such as the SoS, where main stocks, such as hake, deep water rose shrimp and giant red shrimp, are shared between several coastal countries (Jarboui et al., 2022).

The reduction of the bottom trawling effort includes a short transitional period with loss in catches and incomes as reported by other authors (Russo et al., 2019) with potential short-term negative repercussions on socio-economic aspects, which should be adequately addressed by compensatory measures during the transitional period, but positive long-term effects that could outweigh the negative ones including those affecting the other fleets. Although sustainability is a trade-off process merging many aspects of our society, the reduction of the trawling effort seems a way, possibly accompanied by adaptation of fisheries and other management measures, to support the efficiency of fishery processes and the goals for sustainability. Subsidiarity, illegal fishing and slavery at sea are modern issues (Sumaila et al., 2020) not taken into account here, but we also showed that the maintenance of fixed prices during biomass rebuilding might contribute to compensate for the negative social effects produced by bottom trawl fishing reductions.

Data availability statement

The original contributions presented in the study are included in the article/Supplementary Material. Further inquiries can be directed to the corresponding author.

Author contributions

DA and SL conceptualized the work and wrote the paper. DA developed the model and analyzed the data. All the authors

contributed to the development of the model by sharing important datasets and revised the manuscript.

Funding

Catch, effort, price, and abundance at sea data were collected within the European Data Collection Framework (DCF) funded by the European Union and the Italian Ministry for Agricultural, Food and Forestry Policies.

Acknowledgments

The authors acknowledge the anonymous English reviewer provided by OGS services for its constructive comments and suggestions and others colleagues (Giovanni D'Anna and Michele Gristina from CNR) that shared some data for the previous mass balanced version of the model. A special thanks to Marco Reale (OGS) who contributed with biogeochemical model analysis for climate scenario.

Conflict of interest

The authors declare that the research was conducted in the absence of any commercial or financial relationships that could be construed as a potential conflict of interest.

Publisher's note

Supplementary material

The Supplementary Material for this article can be found online at: https://www.frontiersin.org/articles/10.3389/fmars.2022.909164/full#supplementary-material

References

Agnetta, D., Badalamenti, F., Colloca, F., D'Anna, G., Di Lorenzo, M., Fiorentino, F., et al. (2019). Benthic-pelagic coupling mediates interactions in Mediterranean mixed fisheries: An ecosystem modeling approach. *PloS One* 14, e0210659. doi: 10.1371/journal.pone.0210659

Ahrens, R. N. M., Walters, C. J., and Christensen, V. (2012). Foraging arena theory. *Fish. Fish.* 13, 41–59. doi: 10.1111/j.1467-2979.2011.00432.x

Alexander, K. A., Heymans, J. J., Magill, S., Tomczak, M. T., Holmes, S. J., and Wilding, T. A. (2015). Investigating the recent decline in gadoid stocks in the west of Scotland shelf ecosystem using a foodweb model. *ICES. J. Mar. Sci.* 72, 436–449. doi: 10.1093/icesjms/fsu149

Allgeier, J. E., Rosemond, A. D., and Layman, C. A. (2011). The frequency and magnitude of non-additive responses to multiple nutrient enrichment. *J. Appl. Ecol.* 48, 96–101. doi: 10.1111/j.1365-2664.2010.01894.x

Araújo, J. N., Mackinson, S., Stanford, R. J., and Hart, P. J. B. (2008). Exploring fisheries strategies for the western English channel using an ecosystem model. *Ecol. Modell.* 210, 465–477. doi: 10.1016/j.ecolmodel.2007.08.015

Bertrand, J. A., Gil de Sola, L., Papaconstantinou, C., Relini, G., Souplet, A., and Souplet, A. (2002). The general specifications of the MEDITS surveys. *Sci. Mar.* 66, 9. doi: 10.3989/scimar.2002.66s29

Bindoff, N. L., Cheung, W. W. L., Kairo, J. G., Arístegui, J., Guinder, V. A., Hallberg, R., et al. (2022). Changing ocean, marine ecosystems, and dependent communities In: *IPCC Special Report on the Ocean and Cryosphere in a Changing Climate*H. O. Pörtner, D. C. Roberts, V. Masson-Delmotte, P. Zhai, M. Tignor, E. Poloczanska, K Mintenbeck, et al. (eds.) (Cambridge, UK and New York, NY, USA:Cambridge University Press), pp. 447–587. doi: 10.1017/9781009157964.007

Bonanno, A., Zgozi, S., Cuttitta, A., El Turki, A., Di Nieri, A., Ghmati, H., et al. (2013). Influence of environmental variability on anchovy early life stages (Engraulis encrasicolus) in two different areas of the central Mediterranean Sea. *Hydrobiologia* 701, 273–287. doi: 10.1007/s10750-012-1285-8

Britten, G. L., and Sibert, E. C. (2020). Enhanced fish production during a period of extreme global warmth. *Nat. Commun.* 11(5636), 1–6. doi: 10.1038/s41467-020-19462-w

Carpi, P., Scarcella, G., and Cardinale, M. (2017). The saga of the management of fisheries in the adriatic sea: History, flaws, difficulties, and successes toward the application of the common fisheries policy in the mediterranean. *Front. Mar. Sci.* 4. doi: 10.3389/fmars.2017.00423

Christensen, V., and Walters, C. J. (2004). Ecopath with ecosim: Methods, capabilities and limitations. *Ecol. Modell.* 172, 109–139. doi: 10.1016/j.ecolmodel.2003.09.003

Coll, M., and Libralato, S. (2012). Contributions of food web modelling to the ecosystem approach to marine resource management in the Mediterranean Sea. *Fish. Fish.* 13, 60–88. doi: 10.1111/j.1467-2979.2011.00420.x

Colloca, F., Scarcella, G., and Libralato, S. (2017). Recent trends and impacts of fisheries exploitation on Mediterranean stocks and ecosystems. *Front. Mar. Sci.* 4. doi: 10.3389/fmars.2017.00244

Corrales, X., Coll, M., Ofir, E., Heymans, J. J., Steenbeek, J., Goren, M., et al. (2018). Future scenarios of marine resources and ecosystem conditions in the Eastern Mediterranean under the impacts of fishing, alien species and sea warming. *Sci. Rep.* 8, 14284. doi: 10.1038/s41598-018-32666-x

Cossarini, G., Feudale, L., Teruzzi, A., Bolzon, G., Coidessa, G., Solidoro, C., et al. (2021). High-resolution reanalysis of the Mediterranean Sea biogeochemistry, (1999–2019). *Front. Mar. Sci.* 8. doi: 10.3389/fmars.2021.741486

Couespel, D., Lévy, M., and Bopp, L. (2021). Oceanic primary production decline halved in eddy-resolving simulations of global warming. *Biogeosciences* 18, 4321–4349. doi: 10.5194/bg-18-4321-2021

De Juan, S., Demestre, M., and Sanchez, P. (2011). Exploring the degree of trawling disturbance by the analysis of benthic communities ranging from a heavily exploited fishing ground to an undisturbed area in the NW Mediterranean. *Sci. Mar.* 75, 507–516. doi: 10.3989/scimar.2011.75n3507

Dimarchopoulou, D., Keramidas, I., Tsagarakis, K., and Tsikliras, A. C. (2019). Ecosystem models and effort simulations of an untrawled gulf in the central Aegean Sea. *Front. Mar. Sci.* 6, 648. doi: 10.3389/fmars.2019.00648

Edgar, G. J., Stuart-Smith, R. D., Willis, T. J., Kininmonth, S., Baker, S. C., Banks, S., et al. (2014). Global conservation outcomes depend on marine protected areas with five key features. *Nature* 506, 216–220. doi: 10.1038/nature13022

FAO. (2019). *Social protection for small-scale fisheries in the Mediterranean region – a review*. (Rome:FAO). Available at: https://www.fao.org/3/ca4711en/ca4711en.pdf.

FAO. (2020). "The state of world fisheries and aquaculture 2020," in *Sustainability in action*. (Rome:FAO).

Fiorentino, F., and Vitale, S. (2021). How can we reduce the overexploitation of the Mediterranean resources? *Front. Mar. Sci.* 8. doi: 10.3389/fmars.2021.674633

Froese, R., Winker, H., Coro, G., Demirel, N., Tsikliras, A. C., Dimarchopoulou, D., et al. (2018). Status and rebuilding of European fisheries. *Mar. Policy* 93, 159–170. doi: 10.1016/j.marpol.2018.04.018

Garofalo, G., Giusti, G. B., Cusumano, S., Igrande, G., Sinacori, G., Gristina, M., et al. (2007). Catch per unit effort of red shrimp in bathyal fishing grounds fo the Eastern Mediterranean. *Biol. Mar. Mediterr.* 14, 250–251.

Giorgi, F. (2006). Climate change hot-spots. *Geophys. Res. Lett.* 33, L08707. doi: 10.1029/2006GL025734

Hattab, T., Leprieur, F., Ben Rais Lasram, F., Gravel, D., Loc'h, Le F., and Albouy, C. (2016). Forecasting fine-scale changes in the food-web structure of coastal marine communities under climate change. *Ecography (Cop.).* 39, 1227–1237. doi: 10.1111/ecog.01937

Heymans, J. J., Coll, M., Link, J. S., Mackinson, S., Steenbeek, J., Walters, C., et al. (2016). Best practice in ecopath with ecosim food-web models for ecosystem-based management. *Ecol. Modell.* 331, 173–184. doi: 10.1016/j.ecolmodel.2015.12.007

Hilborn, R., Amoroso, R. O., Anderson, C. M., Baum, J. K., Branch, T. A., Costello, C., et al. (2020). Effective fisheries management instrumental in improving fish stock status. *Proc. Natl. Acad. Sci. U. S. A.* 117, 2218–2224. doi: 10.1073/pnas.1909726116

ICCAT. (2010) *Collective volume of scientific papers - international commission for the conservation of Atlantic tunas ICCAT* (Madrid, Spain).

Jacquet, J., and Pauly, D.. (2008) Funding priorities: big barriers to small-scale fisheries. *Conserv. Policy* 22, 832–835. doi: 10.1111/j.1523-1739.2008.00978.x

Jarboui, O., Ceriola, L., and Fiorentino, F.. (2022). "Current fisheries management in the strait of Sicily and progress towords an ecosystem approach," in *Transition towards an ecosystem approach to fisheries in the Mediterranean Sea - lessons learned through selected case studies*. Eds. M. Vasconcellos and V. Ünal. (Rome:FAO), 147–162.

Jennings, S., and Rice, J. (2011). Towards an ecosystem approach to fisheries in Europe: a perspective on existing progress and future directions. *Fish. Fish.* 12, 125–137. doi: 10.1111/j.1467-2979.2011.00409.x

Kiørboe, T. (2013). Zooplankton body composition. *Limnol. Oceanogr.* 58, 1843–1850. doi: 10.4319/lo.2013.58.5.1843

Kwiatkowski, L., Torres, O., Bopp, L., Aumont, O., Chamberlain, M., Christian, J. R., et al. (2020). Twenty-first century ocean warming, acidification, deoxygenation, and upper-ocean nutrient and primary production decline from CMIP6 model projections. *Biogeosciences* 17, 3439–3470. doi: 10.5194/bg-17-3439-2020

Lazzari, P., Solidoro, C., Ibello, V., Salon, S., Teruzzi, A., Béranger, K., et al. (2012). Seasonal and inter-annual variability of plankton chlorophyll and primary production in the Mediterranean Sea: A modelling approach. *Biogeosciences* 9, 217–233. doi: 10.5194/bg-9-217-2012

Libralato, S., and Agnetta, D. (2019). From ecological trade-offs to resilience: insights from exploited marine ecosystems. *Curr. Opin. Syst. Biol.* 13, 136–141. doi: 10.1016/j.coisb.2018.12.005

Link, J. S., Brodziak, J. K., Edwards, S. F., Overholtz, W. J., Mountain, D., Jossi, J. W., et al. (2002). Marine ecosystem assessment in a fisheries management context. *Can. J. Fish. Aquat. Sci.* 59, 1429–1440. doi: 10.1139/f02-115

Mackelworth, P. C., Teff Seker, Y., Vega Fernández, T., Marques, M., Alves, F. L., D'Anna, G., et al. (2019). Geopolitics and marine conservation: Synergies and conflicts. *Front. Mar. Sci.* 6. doi: 10.3389/fmars.2019.00759

Marquis, E., Niquil, N., Vézina, A. F., Petitgas, P., and Dupuy, C. (2011). Influence of planktonic foodweb structure on a system's capacity to support pelagic production: an inverse analysis approach. *ICES. J. Mar. Sci.* 68, 803–812. doi: 10.1093/icesjms/fsr027

Melnychuk, M. C., Kurota, H., Mace, P. M., Pons, M., Minto, C., Osio, G. C., et al. (2021). Identifying management actions that promote sustainable fisheries. *Nat. Sustain.* 4, 440–449. doi: 10.1038/s41893-020-00668-1

Milisenda, G., Vitale, S., Massi, D., Enea, M., Gancitano, V., Giusto, G. B., et al. (2017). Spatio-temporal composition of discard associated with the deep water rose shrimp fisheries (Parapenaeus longirostris, Lucas 1846) in the south-central Mediterranean Sea. *Mediterr. Mar. Sci.* 18, 53–63. doi: 10.12681/mms.1787

Moullec, F., Barrier, N., Drira, S., Guilhaumon, F., Marsaleix, P., Somot, S., et al. (2019). An end-to-end model reveals losers and winners in a warming Mediterranean Sea. *Front. Mar. Sci.* 6. doi: 10.3389/fmars.2019.00345

Pipitone, C., Badalamenti, F., D'Anna, G., and Patti, B. (2000). Fish biomass increase after a four-year trawl ban in the gulf of castellammare (NW Sicily, Mediterranean Sea). *Fish. Res.* 48, 23–30. doi: 10.1016/S0165-7836(00)00114-4

Pipitone, C., Badalamenti, F., Vega Fernández, T., and D'Anna, G. (2014). "Spatial management of fisheries in the Mediterranean Sea: Problematic issues and a few success stories.,". in *Marine managed areas and fisheries*. Eds. M. L. Johnson and J. Sandell(Oxford: Academic Press), 371–402.

Pisano, A., Marullo, S., Artale, V., Falcini, F., Yang, C., Leonelli, F. E., et al. (2020). New evidence of Mediterranean climate change and variability from Sea surface temperature observations. *Remote Sens.* 12, 132. doi: 10.3390/RS12010132

Raicevich, S., Grati, F., Giovanardi, O., Sartor, P., Sbrana, M., Silvestri, R., et al. (2020). "The unexploited potential of small-scale fisheries in Italy: Analysis and perspectives on the status and resilience of a neglected fishery sector,", in *Small-scale fisheries in Europe: Status, resilience and governance*. Ed. J. Pascual-Fernández (Switzerland:Springer Nature), 191–211. doi: 10.1007/978-3-030-37371-9_10

Reale, M., Cossarini, G., Lazzari, P., Lovato, T., Bolzon, G., Masina, S., et al. (2022). Acidification , deoxygenation , nutrient and biomasses decline in a warming Mediterranean Sea. *Biogeosciences. Discuss.*, 1–44. doi: 10.5194/bg-2021-301

Riahi, K., Rao, S., Krey, V., Cho, C., Chirkov, V., Fischer, G., et al. (2011). RCP 8.5-a scenario of comparatively high greenhouse gas emissions. *Clim. Change* 109, 33–57. doi: 10.1007/s10584-011-0149-y

Russo, T., D'Andrea, L., Franceschini, S., Accadia, P., Cucco, A., Garofalo, G., et al. (2019). Simulating the effects of alternative management measures of trawl fisheries in the central Mediterranean Sea: Application of a multi-species bio-economic modeling approach. *Front. Mar. Sci.* 6. doi: 10.3389/fmars.2019.00542

Russo, T., D'Andrea, L., Parisi, A., and Cataudella, S. (2014). VMSbase: An r-package for VMS and logbook data management and analysis in fisheries ecology. *PloS One* 9, e100195. doi: 10.1371/journal.pone.0100195

Salon, S., Cossarini, G., Bolzon, G., Feudale, L., Lazzari, P., Teruzzi, A., et al. (2019). Novel metrics based on biogeochemical argo data to improve the model uncertainty evaluation of the CMEMS Mediterranean marine ecosystem forecasts. *Ocean. Sci.* 15, 997–1022. doi: 10.5194/os-15-997-2019

Soetaert, M., Lenoir, H., and Verschueren, B. (2016). Reducing bycatch in beam trawls and electrotrawls with (electrified) benthos release panels. *ICES. J. Mar. Sci.* 73, 2370–2379. doi: 10.1093/icesjms/fsw096

Solidoro, C., Cossarini, G., Lazzari, P., Galli, G., Bolzon, G., Somot, S., et al. (2022). Modeling carbon budgets and acidification in the Mediterranean Sea ecosystem under contemporary and future climate. *Front. Mar. Sci.* 8. doi: 10.3389/fmars.2021.781522

Spedicato, M. T., Massutí, E., Mérigot, B., Tserpes, G., Jadaud, A., and Relini, G. (2019). The MEDITS trawl survey specifications in an ecosystem approach to fishery management. *Sci. Mar.* 83, 9. doi: 10.3989/scimar.04915.11X

Sumaila, U. R., Zeller, D., Hood, L., Palomares, M. L. D., Li, Y., and Pauly, D. (2020). Illicit trade in marine fish catch and its effects on ecosystems and people worldwide. *Sci. Adv.* 6, eaaz3801. doi: 10.1126/sciadv.aaz3801

Teh, L. C. L., and Sumaila, U. R. (2013). Contribution of marine fisheries to worldwide employment. *Fish. Fish.* 14, 77–88. doi: 10.1111/j.1467-2979.2011.00450.x

Tittensor, D. P., Novaglio, C., Harrison, C. S., Heneghan, R. F., Barrier, N., Bianchi, D., et al. (2021). Next-generation ensemble projections reveal higher climate risks for marine ecosystems. *Nat. Clim. Change* 11, 973–981. doi: 10.1038/s41558-021-01173-9

UN (2019) *World population prospect 2019*. Available at: https://population.un.org/wpp/.

Villar-Argaiz, M., Medina-Sánchez, J. M., Biddanda, B. A., and Carrillo, P. (2018). Predominant non-additive effects of multiple stressors on autotroph C:N:P ratios propagate in freshwater and marine food webs. *Front. Microbiol.* 9. doi: 10.3389/fmicb.2018.00069

Vitale, S., Milisenda, G., Gristina, M., Baiata, P., Bonanomi, S., Colloca, F., et al. (2018). Towards more selective Mediterranean trawl fisheries: are juveniles and trash excluder devices effective tools for reducing undersized catches? *Sci. Mar.* 82, 215–223. doi: 10.3989/scimar.04751.28A

Walters, C., and Christensen, V. (2007). Adding realism to foraging arena predictions of trophic flow rates in ecosim ecosystem models: Shared foraging arenas and bout feeding. *Ecol. Modell.* 209, 342–350. doi: 10.1016/j.ecolmodel.2007.06.025

Walters, C., Pauly, D., Christensen, V., and Kitchell, J. F. (2000). Representing density dependent consequences of life history strategies in aquatic ecosystems: EcoSim II. *Ecosystems* 3, 70–83. doi: 10.1007/s100210000011

frontiers | Frontiers in Marine Science

TYPE Original Research
PUBLISHED 21 September 2022
DOI 10.3389/fmars.2022.934556

OPEN ACCESS

EDITED BY
Gualtiero Basilone,
National Research Council (CNR), Italy

REVIEWED BY
Francesco Tiralongo,
University of Catania, Italy
Eve Galimany,
Institute of Marine Sciences, (CSIC), Spain

*CORRESPONDENCE
Valentina Lauria
valentina.lauria@cnr.it

†These authors have contributed equally to this work

SPECIALTY SECTION
This article was submitted to Marine Fisheries, Aquaculture and Living Resources, a section of the journal Frontiers in Marine Science

RECEIVED 02 May 2022
ACCEPTED 22 August 2022
PUBLISHED 21 September 2022

CITATION
Scannella D, Bono G, Di Lorenzo M, Di Maio F, Falsone F, Gancitano V, Garofalo G, Geraci ML, Lauria V, Mancuso M, Quattrocchi F, Sardo G, Titone A, Vitale S, Fiorentino F and Massi D (2022) How does climate change affect a fishable resource? The case of the royal sea cucumber (*Parastichopus regalis*) in the central Mediterranean Sea. *Front. Mar. Sci.* 9:934556. doi: 10.3389/fmars.2022.934556

How does climate change affect a fishable resource? The case of the royal sea cucumber (*Parastichopus regalis*) in the central Mediterranean Sea

Danilo Scannella[1], Gioacchino Bono[1], Manfredi Di Lorenzo[1], Federico Di Maio[1,2], Fabio Falsone[1], Vita Gancitano[1], Germana Garofalo[1], Michele Luca Geraci[1,2], Valentina Lauria[1]*, Maria Mancuso[1], Federico Quattrocchi[1], Giacomo Sardo[1], Antonino Titone[1], Sergio Vitale[1], Fabio Fiorentino[1,3†] and Daniela Massi[1†]

[1]Institute for Marine Biological Resources and Biotechnology (IRBIM), National Research Council–CNR, Mazara del Vallo, Italy, [2]Department of Biological, Geological and Environmental Sciences (BiGeA) – Marine Biology and Fisheries Laboratory of Fano, University of Bologna, Fano, Italy, [3]Department of Integrative Marine Ecology, Stazione Zoologica Anton Dohrn, Rome, Italy

Holothurians or sea cucumbers are key organisms in marine ecosystems that, by ingesting large quantities of sediments, provide important ecosystem services. Among them, *Parastichopus regalis* (Cuvier, 1817) is one of the living sea cucumbers in the Mediterranean actively fished for human consumption mainly in Spain, where it is considered a gastronomic delicacy. In the Strait of Sicily (central Mediterranean Sea), this species is not exploited for commercial use even if it is used as bait by longline fishery. *P. regalis* is frequently caught by bottom trawling and discarded at sea by fishers after catch, and because of its capacity to resist air exposition (at least in cold months), it is reasonable to consider that it is not affected by fishing mortality. Having observed a significant decrease in abundance since 2018, the possible effects of some ecological factors related to current climate change (i.e., temperature and pH) were sought. Generalized additive models (GAMs) were applied to investigate the relationship among the abundance of *P. regalis* and environmental variables and fishing effort. Long time series of *P. regalis* densities (2008–2021) were extracted from the MEDITS bottom trawling survey and modeled as function of environmental parameters (i.e., salinity, dissolved oxygen, ammonium, pH, and chlorophyll α) and fishing effort (i.e., total number of fishing days per gross tonnage). Our results showed that this species prefers the soft bottoms (50–200 m) of the Adventure Bank and Malta Plateau, and its distribution changed over time with a slight deepening and a rarefaction of spatial distribution starting from 2011 and 2017, respectively. In addition, a positive relationship with pH concentration in surface waters during the larval dispersal phase (3-year lag before the survey) and nutrient concentration at sea bottom (1-year lag) has been found, suggesting that this species is sensitive to climate change

and food availability. This study adds new knowledge about the population dynamics of an unexploited stock of *P. regalis* under fishing impact and environmental under climate change in fisheries management.

KEYWORDS

sea cucumbers, unexploited resources, environmental changes, acidification, fishing impact, GAM, ecosystem services, Strait of Sicily

Introduction

The Anthropocene (*sensu* Crutzen and Stoermer, 2000) climate change has been impacting the marine environment and biodiversity since the early 20th century. Human activities mainly affect different processes such as the alteration of thermal regimes, water cycle, increase of ocean acidification and sea temperature (Huang et al., 2021), marked thermal stratification, and reduction of upwelling processes (Prakash, 2021).

The Mediterranean is a semi-enclosed sea, representing the boundary between the arid climate of North Africa and the temperate climate of Europe, and is characterized by a restricted hydrological exchange with the open ocean (Bethoux and Gentili, 1999; Diffenbaugh et al., 2007). For these reasons, it is particularly climate-vulnerable to even minor modifications, while it is warming at two to three times the rate for the global ocean (Vargas-Yáñez et al., 2010). Moreover, the Mediterranean Sea depicts a high imprint of anthropogenic CO_2, which has already affected its pH by a decrease of 0.05–0.14 pH units since pre-industrial times (Touratier and Goyet, 2011). Both the rise in CO_2 concentration and warming have directly and indirectly affected marine organisms that are vulnerable to changes in pH and temperature (González-Durán et al., 2021).

Holothurians, commonly called sea cucumbers, is an abundant and diverse group of worm-like and usually soft-bodied echinoderms. They are found almost everywhere in the marine environment ranging from the intertidal to the floor of the deepest oceans (Aydın and Erkan, 2015). Sea cucumbers are key organisms in the marine ecosystem because they provide different ecosystem services, such as recycling of nutrients and particulate organic matter, bioturbation of sediments with consequent oxygenation, bio-remediation of the bacterial component present in sediments and in the water column, and production of biomass (Ramón et al., 2010; MacTavish et al., 2012; Purcell et al., 2013; Costa et al., 2014; Purcell et al., 2016).

Similar to many other marine organisms, the holothurians are also affected by climate change (González-Durán et al., 2021). The combined effects of pH changes, water temperature, and salinity may trigger pathological responses by altering the anatomical characteristic of the sea cucumber organisms (Gullian, 2013), generating diverse biochemical and physiological adaptations (Zamora and Jeffs, 2012; Gullian, 2013; Wu et al., 2013; Gullian and Terrats, 2017), altering the concentration ratio of different inorganic carbon species CO_2, HCO_3^-, and CO_3^{-2}, and reducing the saturation state of $CaCO_3$ (Gao et al., 2019). These environmental variables can influence the population abundance of holothurians, and have been shown to negatively impact several biological aspects (e.g., the fertilization success, the larvae metamorphosis, the development time, the physiological performances, the respiratory rate as the temperature increases, and the larvae growth rate) (Asha and Muthiah, 2005; Hamel and Mercier, 2008; Pörtner, 2008; Yuan et al., 2015) and the recruitment efficiency (González-Durán et al., 2021). Furthermore, these environmental variables influence the growth and survival of juveniles and adults, although the effect exerted by the variation of pH and temperature is less than those observed in the larvae (Dong et al., 2006; Yuan et al., 2009). An indirect effect associated with sea temperature variation is related to an increase in the oxygen diffusion as well as oxygen demands to guarantee biological processes (Pörtner and Knust, 2007). To contrast hypo-metabolism, sea cucumbers most probably increase the defense mechanisms and physiological responses that generate dormancy and estivation by reducing the metabolic activity (Quiñones et al., 2002; Asha and Muthiah, 2005; Morgan, 2008; Yuan et al., 2009). Furthermore, few studies have suggested that food abundance is a key factor influencing sea cucumber larvae survival and development (Morgan, 2008; Brander, 2010).

Holothurians represent a fishery resource in many countries. Indeed, at least 66 species are fished from more than 40 countries, particularly in Asia and the Pacific regions where the catches amount to 20,000–40,000 tons/year, and most of the catches are processed locally and exported to Asian markets, where they are considered traditional medicine and gastronomic delicacy (Bruckner, 2006; Toral-Granda, 2007; Toral-Granda et al., 2008; Ramón et al., 2010; Purcell, 2010; Purcell et al., 2013; Maggi and González-Wangüemert, 2015). Sea cucumbers may be sold alive, fresh, frozen, and as "trepang" (gutted, boiled, and dried). Their edible part is usually the thick body tegument although other tissues may be consumed (Purcell et al., 2012).

The rising demand in Asian markets has resulted in the decline of many sea cucumber populations (Toral-Granda et al., 2008; Purcell et al., 2012; Eriksson and Clarke, 2015) and more than 70% of their stocks around the world were overexploited or depleted (Purcell et al., 2013). To address the problem of increasing market demands, many aquaculture practices have been developed in different parts of the world recently (Han et al., 2016; González-Wangüemert et al., 2018).

Overexploitation is considered the main risk of extinction of the most commercially valuable species, with 16 species of sea cucumbers now classified as threatened with extinction on the International Union for Conservation of Nature (IUCN) red list (Conand et al., 2014; González-Wangüemert et al., 2014). The collapse of sea cucumber stocks has prompted governments to ban or regulate fishing or exports in several sea cucumber fisheries globally (Robinson and Lovatelli, 2015). In this regard, several studies have reported that overfished populations of sea cucumber can take up to half a century of no fishing activities to rebuild (Battaglene and Bell, 1999; Skewes et al., 2000; Bruckner et al., 2003).

According to Aydın and Erkan (2015), 37 holothurian species belonging to nine families and five orders live in the Mediterranean. Historically, sea cucumber fisheries have been of scarce importance in Mediterranean countries with the exception of the Provence region (France). Nowadays, large quantities of holothurians are caught in Greece, Turkey, and Spain (Meloni and Esposito, 2018). Turkey is the main Mediterranean country involved in the catch and export of frozen, dried, and salted sea cucumbers toward Asian countries, particularly the species belonging to the genus *Holothuria* (Aydin, 2008; González-Wangüemert et al., 2014; Gonzalez-Wangüemert et al., 2015; González-Wangüemert et al., 2018). In Greece, *Holothuria (Holothuria) tubulosa* (Gmelin, 1791) has been harvested as bait in long-line fisheries for more than a century (Antoniadou and Vafidis, 2011). Conversely, in Spain, the fishery is mainly focused on royal cucumber, *Parastichopus regalis* (Cuvier, 1817). Its spatial distribution includes the Mediterranean Sea, the eastern Atlantic Ocean from the south of the Canary Islands to the north of Ireland, and the Antilles and the Gulf of Mexico in the western Atlantic (Tortonese, 1965; Míguez-Rodríguez, 2009). It is a benthic species found at a wide range of depths (5–800 m according to Tortonese, 1965), being more abundant on sandy and bioclastic bottoms between 50 and 300 m in the Mediterranean (Pawson et al., 2009; Ramón et al., 2010). The species is fished by bottom trawl and considered a gastronomic delicacy in Spain (i.e., Catalonia, Valencia and Baleares; Ramón et al., 2010; González-Wangüemert et al., 2016). This sea cucumber is the most expensive sea product in the Catalan market, where auction prices ranged between 64 and 129€/kg in 2019 (Ramón et al., 2022).

P. regalis is routinely caught by bottom trawlers operating on the outer shelf-upper slope in the Strait of Sicily (central Mediterranean Sea), and despite the long tradition of consumption of marine food by Sicilian people, it is not consumed or commercialized in Sicily and is generally discarded by fishers after catch or rarely used as bait in long-line fisheries. Conversely, holothurian shallow water species are fished in Sardinia and Apulia (Italian seas), where the amount of sea cucumbers illegally harvested and destined for the Asiatic market in 2016 and 2017 was equal to 23.9 tons, while in 2015 alone, it was about 29 tons (Meloni and Esposito, 2018). According to a precautionary approach, specimens belonging to the Holothuroidea class cannot be fished, retained on board, landed, or sold in the Italian seas since 2018 (IMAFFP, 2018).

Considering the growing interest about holothurians as a fishable resource and given its important ecological role, exploring the effect of environmental and fishing variables on their standing stock allows to make a step forward in understanding the impacts of climate change on a Mediterranean sea cucumber and to inform future fishery management plans applied to these species. In this regard, the Strait of Sicily is a suitable site to investigate population dynamics of *P. regalis* under different anthropic and natural drivers. In particular, this study aims at exploring spatial distribution and abundance over time and the potential effect of environmental factors linked to the climate change and fishing pressure.

Materials and methods

The study area

The Geographical Sub-Area 16 (GSA 16, according to the General Fisheries Commission for the Mediterranean-GFCM) is located on the northern sector of the Strait of Sicily (south-central Mediterranean Sea), sited between the landmasses of the western and southern coast of Sicily and Tunisia to the south (Figure 1). This relatively shallow borderland has a complex configuration, currently affected by active tectonics and recent volcanism and swept by bottom currents (Colantoni et al., 1992), with two platform-like areas (the Adventure Bank westward and the Malta Platform eastward), two wide northern and southern epicontinental shelves, narrow interconnected NE–SW basins, several knolls and seamounts, and volcanic edifices (Colantoni et al., 1975; Calanchi et al., 1989).

In this area, the sedimentary facies and the depositional processes are heavily influenced by the physiographic structures and coastal erosion, river runoff and/or biogenic sedimentation. The western and eastern platforms (Adventure Bank and Malta Plateau) show exposed bedrock, coarse carbonate gravels and sands, and volcano-clastic sediments. Shelf modern sediments are strongly influenced by the local production of calcareous algal and shelly materials in shallower water and by clastic supply from coastal erosion and river drainage (Reeder et al.,

2002). This seabed patchwork is highlighted by the high heterogeneity in benthic communities along the continental shelf (Di Lorenzo et al., 2018).

The currents in this region are mainly dictated by the Modified Atlantic Water (MAW) flowing eastward, and the Levantine Intermediate Water (LIW) flowing westward along the Sicilian slope in the 200–500 m depth range. Surface waters in the GSA derived from the Atlantic Ocean (Atlantic Ionian Stream, AIS) flow eastwards along the south Sicilian coast (Pinardi and Masetti, 2000; Béranger et al., 2004). The AIS shows a strong seasonal variability, being more intense during the spring–summer period in the 15–30 m depth range (Pinardi and Masetti, 2000; Sorgente et al., 2003; Sorgente et al., 2011). This surface circulation promotes the establishment of "permanent" upwellings towards the left side of the AIS in certain places, which are reinforced by westerly winds (Piccioni et al., 1988; Bonanno et al., 2014). The main source of nutrients in the area is associated with coastal upwellings and the doming of intermediate waters inside the cyclonic gyres, lying over the Adventure Bank and over the Malta shelf (Garcia Lafuente et al., 2002; Béranger et al., 2004). Primary production in the Strait of Sicily is seasonally controlled: a deep summer thermocline induces low biomass in late spring/summer; higher productivity is observed in late fall/winter, due to winter convention (D'Ortenzio and Ribera d'Alcalà, 2009; Di Donato et al., 2022).

Biological data

Spatial distribution and abundance data of *P. regalis* relative to the period 2008–2021 were collected from the bottom trawl surveys MEDITS (MEDiterranean International Bottom Trawl-Surveys) that have been carried out in the GSA16 annually in spring/summer since 1994 (Bertrand et al., 2002; Spedicato et al., 2019), except for 2013, 2014, 2017, and 2020, which were carried out in autumn due to administrative constraints. The bottom trawl surveys covered an area of about 31,400 km^2 within the 10–800 m water depth range, and a total of 1,589 hauls were sampled (2008–2021). The survey follows a stratified random sampling with the allocation of hauls proportional to strata extension (depth strata: 10–50 m, 51–100 m, 101–200 m, 201–500 m, and 501–800 m). In particular, 120 hauls were carried out each year except for 2014 (55 hauls) and 2020 (94 hauls). Hauls were carried out by a standard bottom trawl net (GOC 73) with a 20-mm opening mesh size in the cod end (Fiorentini et al., 1999). The area swept in each haul was calculated according to the formula proposed by Fiorentini et al. (1999). For each haul, *P. regalis* abundance was standardized to the haul swept area (km^2) and expressed as density index (herein DI), namely, the number of individuals per km^2 (N/km^2). The distribution curve of DI per haul as a function of depth was inspected to identify the preferred depth range of the species, which was found to be 20–200 m. The annual abundances of the species over this bathymetric range were then estimated. To account for the different numbers of hauls carried out during the time series considered in this study, DI was corrected by a common resampling without replacement procedure by reporting the number of hauls for each stratum to the minimum number observed during the time period considered (*N* of bootstrap samples = 99).

Environmental and fishery data sources

Concerning the climate-related drivers, four environmental predictors, i.e., temperature (T), salinity (S), oxygen (O_2), and pH, were considered, given that several studies have shown they

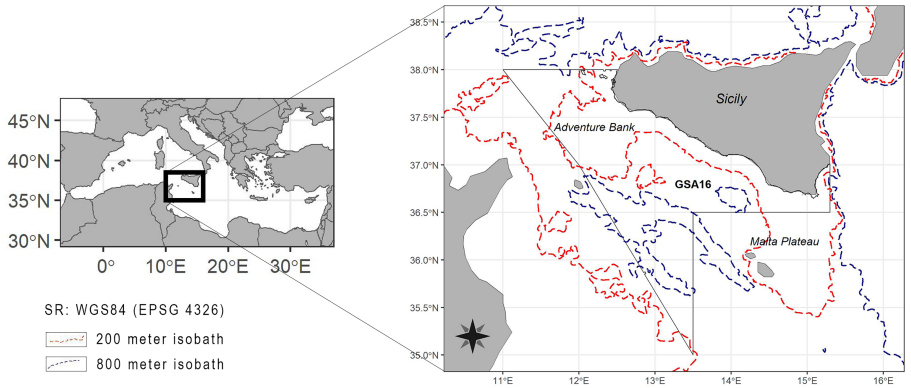

FIGURE 1
Map of the Strait of Sicily showing the location of the study area where the data of the *P. regalis* were collected: Geographical Sub-Area 16, south of Sicily. Red and blue dashed lines indicate the 200- and 800-m isobaths respectively.

can influence the population density of holothurians (Widicombe and Spicer, 2008; Brierley and Kingsford, 2009; Doney et al., 2009; González-Durán et al., 2021). Similarly, chlorophyll α (Chl) and two nutrient concentrations (i.e., ammonium, NH_4^+ and phosphate, PO_4^-) were used as a proxy for primary productivity and food availability (Huot et al., 2007).

All environmental variables used for model construction were obtained from the Copernicus marine environment monitoring service (http://marine.copernicus.eu). Specifically, for each year, mean monthly layers of all environmental predictors were extracted with a spatial resolution of 1/24° × 1/24° (about 4 × 4 km) at two different depths: surface and 100 m of depth (Escudier et al., 2020; Cossarini et al., 2021). The rationale behind the choice of using two different depths is to evaluate the possible effect of the climatic variables on the larval as well as on the juvenile–adult phase of the royal sea cucumber. The values obtained at sea surface level have been averaged over the study area (GSA16) for each year between June and September (summer season), in order to investigate the possible effect of climatic conditions during the early life larvae stages, whereas the values obtained at 100 m depth (i.e., the bathymetry where the bulk of the species inhabits, Figure 2) have firstly been spatially clipped using the extent of a polygon representing the continental shelf within the study area (GSA16) and then averaged by year.

To investigate potential time lag effects of the environmental factors on the *P. regalis* larvae, the mean values obtained at sea surface level have been lagged of 3 years prior to the year of the survey in order to consider the temporal window running from the spawning until reaching the sizes of the specimen collected in this study. This choice was supported by the most representative size class sampled by the survey (approximately 19 cm total, Supplementary Figure 1) and, in the absence of growth studies of *P. regalis*, the corresponding mean length age proposed by Glockner-Fagetti et al. (2016) and Ramírez-González et al. (2020) for the similar sea cucumber *Isostichopus fuscus* (Ludwig, 1875) in the Pacific Ocean. Instead, the time lag relationship between the abundance of *P. regalis* and the 100-m environmental variables as well as the fishing effort (Fe) were lagged 1 year prior to the year of the survey.

Since fishery pressure has been shown to have negative effects on the populations of sea cucumbers in the Mediterranean and NE Atlantic waters (i.e., decrease in abundance, reduction of genetic diversity, loss of the biggest individuals, increase of diseases, and even "local extinction" in some sites; González-Wangüemert et al., 2016), data on the Fe of bottom trawling operating in the GSA16 were used as an independent variable affecting *P. regalis* density. The trawl fleet segment mainly operating on continental shelf bottoms of the study area is composed of vessels with a length overall less of 24 m (LOA < 24) (Scannella et al., 2020; Di Maio et al., 2022). Differently, the large fishing fleet is engaged in deep-sea fishing far away from the coast on sea bottoms reaching 700–800 m (Milisenda et al., 2017; Russo et al., 2019). Annual Fe was retrieved by Fisheries Dependent Information (FDI, https://stecf.jrc.ec.europa.eu/dd/fdi) database provided by the EU Member States (DCF, Data Collection Framework context) and expressed as the total number of fishing days per gross tonnage (DayAtSea*GT) of trawl fishing vessels with LOA < 24 m operating in the GSA16.

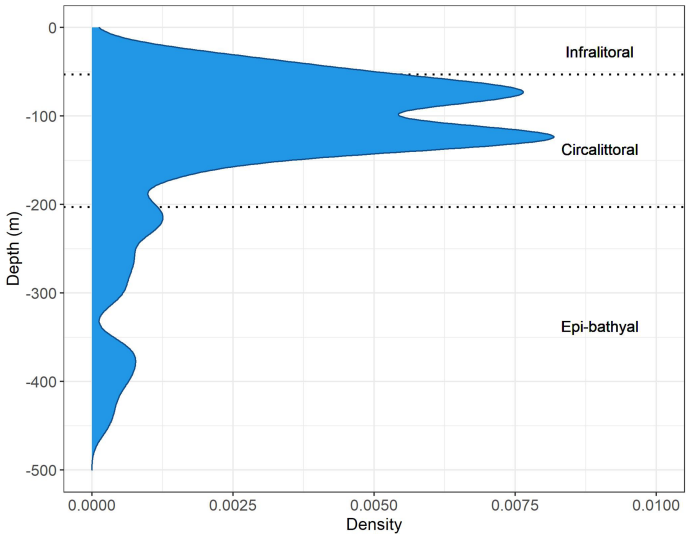

FIGURE 2
Bathymetric distribution of *P. regalis* in GSA16.

The variable acronyms, unit measurement, and some descriptive statistics are shown in Table 1.

Temporal trend and spatial analysis

Segmented regression analysis was applied to log-transformed DI to objectively define the time point in which the trend significantly changes during the time frame considered in this study, using the R "segmented" package (Muggeo, 2008).

The DI of each haul was geo-referenced to spatially identify higher-density areas (spots) of the species and qualitatively assess the variation of the spatial pattern during different time periods. The distribution maps were obtained by applying the inverse distance-weighted (IDW) interpolation algorithm on the logarithm of the DI plus 1 using Quantum GIS software (QGIS Development Team, 2020).

To evaluate the possible deepening of the royal sea cucumber distribution in the study area in response to the change in oceanographical variables, the center of gravity (CoG) of the species (Stefanescu et al., 1992; Cartes et al., 2011) was computed, for the period 2008–2021, by the formula:

$$CoG = \frac{DI1 * z1 + DI2 * z2 + \cdots}{\sum DIi}$$

where *DI*i is the standardized density of the species at depth i and zi is the mean depth of the sampling station. Correlation among CoG and years were assessed by computing the Spearman's rho (ρ) statistic and tested *via* *t*-test using a *p*-value of 0.05 to establish statistical significance.

As an exploratory analysis to evaluate the degree of association among environmental and fishery variables was conducted, the most related variables were highlighted using a matrix of Spearman's rho (ρ) rank correlation coefficients for all possible pair combinations. This was graphically displayed by means of a correlogram plot using the "corrplot" R package (Wei and Simko, 2021). Classical linear regressions were also used to analyze linear trends of explanatory variables.

Modeling

A generalized additive model (GAM) with a Gaussian distribution with the canonical (identity) link function was used to investigate the shape and the strength of the relationship of royal sea cucumber abundance with the explanatory variables considered (environmental and fishing). GAMs are flexible non-linear regression models that allow one response variable being fitted by several predictors additively (Wood, 2006; Hastie and Tibshirani, 2017). The use of smoothing functions for the regressors gives GAMs greater flexibility over linear (or other parametric) types of models (Wood, 2006). Given the sample size of the observations, to control the degree of smoothing and avoid overfitting the data, a

TABLE 1 Descriptive statistics [mean, range, and standard deviation (SD)] for selected predictor variables.

Variables	Unit of measurement	Sea surface				100 m				References
		Acronym	Mean	Range Min Max	SD	Acronym	Mean	Range Min Max	SD	
Temperature	°C	SST	24.515	23.597 25.227	0.524	100m-T	15.674	15.405 15.985	0.197	(Escudier et al., 2020)
Salinity	psu	SSS	37.705	37.413 37.990	0.139	100m-S	38.345	38.255 38.469	0.078	(Escudier et al., 2020)
Sea water pH	Reported on total scale, pH	SSpH	8.002	7.985 8.016	0.009	100m-pH	8.121	8.115 8.129	0.004	(Cossarini et al., 2021)
Dissolved oxygen	mmol/m^3	SSO_2	218.960	217.255 220.747	1.300	100m-O2	228.149	223.953 230.989	1.791	(Cossarini et al., 2021)
Ammonium	mmol/m^3	$SSNH_4$	0.121	0.093 0.134	0.011	100m-NH_4	0.311	0.272 0.339	0.021	(Cossarini et al., 2021)
Phospate	mmol/m^3	$SSPO_4$	0.010	0.008 0.012	0.001	100m-PO_4	0.091	0.084 0.103	0.006	(Cossarini et al., 2021)
Chlorophyll α	mg/m^3	SSChl	0.052	0.048 0.055	0.002					(Cossarini et al., 2021)
Fishing effort (thous.)	DayAtSea*GT					Fe	1,768.596	1,343.129 2,176.444	285.235	Fisheries Dependent Information (https://stecf.jrc.ec.europa.eu/dd/fdi)

penalty term was added in the regression, setting the gamma argument equal to 1.4 (Kim and Gu, 2004). GAMs were fitted using the R "mgcv" package (Wood, 2001).

Model construction

Because the predictor variables are measured at different scales, they were firstly re-scaled by applying the *z*-score standardization by subtracting the mean of each variable from the raw data and then dividing it by the standard deviation of the original variable. In addition, the sea royal cucumber DI were log-transformed.

All variables were tested for collinearity using the Variance Inflation Factor (VIF). Variables showing a VIF value that exceeds 5, indicating a problematic amount of collinearity (James et al., 2013), were not considered for modeling, since the information that these variables provide about the response is redundant in the presence of the other variables with lower VIF (James et al., 2013). In particular, a VIF analysis has been performed in order to assess multicollinearity among all 100 m of depth explanatory variables (T, S, pH, O_2, $NH4^+$, and PO_4^-), Fe, and all sea surface variables (SST, SSS, SSpH, SSO_2, $SSNH_4$, $SSPO_4$, and SSChl), 3 years lagged.

Model selection

Modeling selection was carried out in the framework of an information-theoretic approach (Burnham and Anderson, 2002). More specifically, starting from the full model that included all explanatory variables, the most parsimonious model has been selected based on the lowest Akaike's Information criterion (AIC) (Grueber et al., 2011; Aho et al., 2014), corrected for small sample size (AIC_c; Burnham and Anderson, 2002). Candidate models were ranked using the difference in AIC_c (ΔAIC_c) calculated as the difference in AIC between a model *i* and the first-ranked model (Buckland et al., 1997; Burnham and Anderson, 2002) and by calculating the AIC_c weights (total amount of predictive power provided by the models). Competing models of the best supported model were selected when having their AIC_c within 2 of the minimum (Burnham and Anderson, 2002). Also, the relative importance of the predictor variables was estimated by summing the AIC_c weights of each model where the variable appears (Symonds and Moussalli, 2011). The variable sum of weights (SW) varies from 0 to 1, and high values indicate strong importance for a given predictor. Model performance was measured as the proportion of variation explained by the estimated regression using adjusted R^2.

Graph plotting and statistical analysis were performed using the R v.4.1.2 software (R Core Team, 2021).

Results

P. regalis has been collected in a wide bathymetric range, from 20 to 500 m, although the largest abundances were recorded in the infralittoral and circalittoral zones, within the bathymetry of 200 m (Figure 2).

The mean DI over the shelf (10–200 m) showed a significant linear negative (r^2 = 0.31, p = 0.03) trend over time with the lowest value of 6 N/km^2 recorded in 2020 and 2021, while the highest value of 138.5 N/km^2 was recorded in 2015. The trend of the log-transformed DI is shown in Figure 3. The segmented regression analysis on log-transformed DI data estimated a break point in the year 2017, separating clearly the temporal DI trend in two parts: a steady-state phase of the species between 2008 and 2017, in which the density oscillated around a mean value of about 4.3 N/km^2 (log DI) and a decline phase reaching the lowest values of the entire time series in 2020 and 2021 (Figure 3).

Two maps of the spatial distribution of the DIs in the steady-state phase (Figure 4A) and the declining phase have been produced (Figure 4B). In particular, Figure 4A shows the DIs of the year 2015 characterized by the highest abundance in the steady-state phase (2008–2017) while Figure 4B shows those of the last year (2021) of the declining phase (2018–2021). Our results show that *P. regalis* is prevalently distributed on the

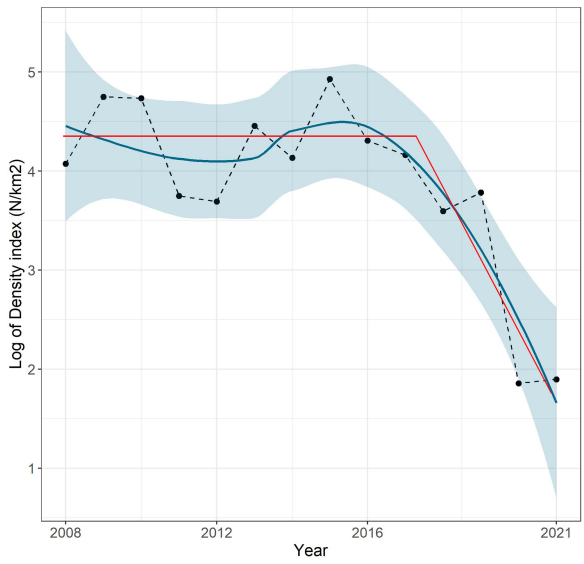

FIGURE 3
Trend of the density index logarithm (N/km^2) for *P. regalis* in the GSA16 during time series 2008–2021. The blue line represents the smooth curve obtained using the LOESS interpolation method; the blue area indicates the 95% confidence interval. The red lines visualize the segmented regression model.

continental shelf (Figures 2 and 4A, B) of the study area. The species became more abundant in the northwestern Strait of Sicily and, in particular, along the southwestern Adventure Bank, showing density indices from 900 to 3,000 N/km^2. Catches at depths over 200 m were occasional, except for two areas located in the northwestern sectors of the Adventure Bank where, however, low abundances (1–300 N/Km^2) have been recorded.

A marked difference in terms of the spatial pattern between the two phases is observed (Figures 4A, B). In particular, it is quite evident that the greatest loss of abundance occurred in correspondence of the Adventure Bank area, where the density spots are reduced substantially, and in some cases, as in the central part of the Bank, even disappear. It appears that there is also a drastic abundance reduction in the Malta Plateau area. According to the map in Figure 4B, to date, two little hot spots of the species seem to remain, one in the southernmost sector of the Adventure Bank and the other one in the eastern part of the GSA16.

During the entire time series considered (2008–2021), the shift of the CoG's royal sea cucumber towards deeper bathymetry starting from 2011 seems to occur. However, this trend was not significant according to the Spearmen correlation ($\rho = -0.41$) (Figure 5).

During the period 2008–2020, climate variables varied considerably in the GSA16 (Supplementary Figures 2, 3). The sea surface salinity (SSS) in summer increased significantly ($p = 0.03$) at a rate of 0.014 psu year^{-1}, as shown by linear regression (Supplementary Figure 2), while on the contrary, the mean sea surface pH (SSpH) decreased significantly ($p = 0.04$) at a rate of −0.0017 year^{-1}, leading to a rise in its acidity. The other six sea surface variables did not show statistically significant trends ($p > 0.05$) although $SSNH_4$, $SSPO_4$, and SST moderately increased over the years, while SSChl and SSO_2 decreased. The mean yearly temperature and salinity at 100 m depth (100m-T) in the continental shelf of the study area progressively increased in a statistically significant manner, at a rate of 0.037°C ($p = 0.012$) and 0.016 psu year^{-1} ($p < 0.001$), respectively, while 100m-pH decreased (−0.00086 units of pH year^{-1}), leading to progressive sea acidification also in deeper layers ($p < 0.001$) (Supplementary Figure 3). Conversely, 100m-NH_4, 100m-PO_4, and 100m-O_2 did not show significant trends ($p > 0.05$) although the nutrients seemed slightly to decrease while the oxygen moderately increased. Finally, the annual average of Fe showed a significant decreasing trend ($p = 0.007$) at a rate of −58,000 DayAtSea*GT year^{-1}.

The results of Spearman's correlation among *P. regalis* density index (expressed as logarithmic) and the normalized predictor variables are shown in Supplementary Figure 4. The correlogram revealed that among all environmental factors analyzed, only two variables showed a significant relationship ($p < 0.05$) to species abundance. In particular, 100m-NH_4 and SSpH seemed to act directly on the population dynamics of *P. regalis* having found a positive correlation equal to 0.76 and 0.60, respectively.

The best GAM model retained the 3-year lagged pH and NH_4^+ at 100 m as shown in Table 2, while the relative importance of predictor variables for the species is shown in Table 3. The overall model fit was good with 82.8% of the total deviance explained. In particular, the relationship with NH_4^+ at 100 m was almost linear, with a negative effect on the abundance of *P. regalis* until a value at ca. 0.315, above which the effect became positive. The effect of the 3-year lagged pH was non-linear with a local positive peak at ca 8.003, and negatively affecting the abundance of *P. regalis* at values lower than 8.00 and higher than ca. 8.012 as shown in Figure 6.

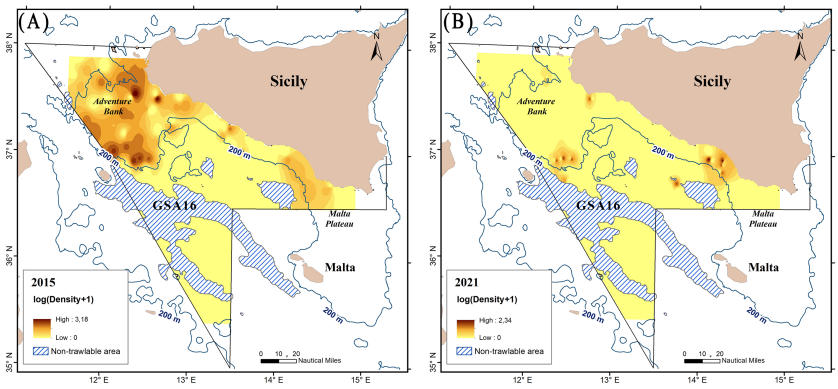

FIGURE 4
Spatial distribution, in terms of the logarithm of density index [(N+1)/km2], of P. regalis in the study area (GSA 16) **(A)** of the year (2015) with the highest density index in the steady-state phase (2008–2017) and **(B)** the last year (2021) of the declining phase (2018–2021) according to the temporal trend of the abundance of the species. The dashed areas depict water depths of more than 800 m not investigated during the MEDITS survey.

10.3389/fmars.2022.934556

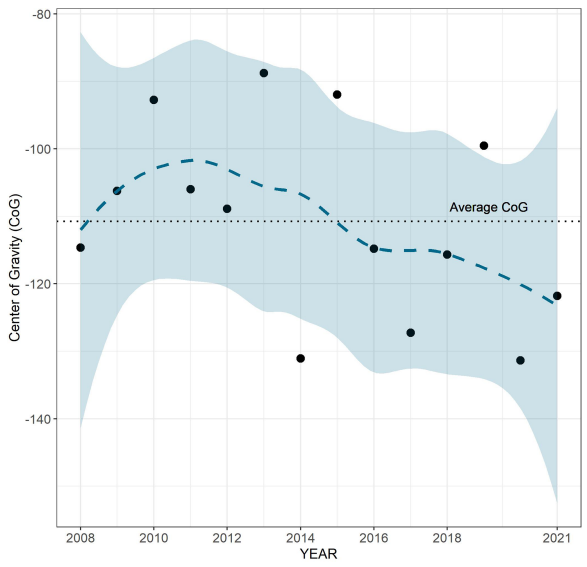

FIGURE 5
Trend of optimal average distribution (Center of Gravity, CoG) during the 2008–2021 period. The blue dotted line represents the smooth curve obtained using the LOESS interpolation method, the blue band indicates the 95% confidence interval.

Discussion

This study suggests the potential negative effect of climate change on the abundance of *P. regalis*, a species of growing interest as a fishable resource in the central Mediterranean Sea. In addition, the positive influence of nutrient availability on this species was highlighted. Despite the fact that some information on the abundance and demography of *P. regalis* in the Mediterranean is available, according to our knowledge, nothing is known on the effect of environmental factors on this species in the wild and few information exists in experimental conditions (Galimany et al., 2018). On the other hand, some data on physiological responses to environmental variability of other sea cucumber species deriving from aquaculture are available (Asha and Muthiah, 2005; Dong et al., 2006; Yuan et al., 2009). Our results showed that the species mainly inhabits the soft bottoms (25–200 m) of the Adventure Bank and Malta Plateau, while also a rarefaction of its spatial distribution and a slight shift towards deeper depths (about −20 m) have been evidenced since 2018 and 2011, respectively. Previous research has shown that this species is found on a wide range of depths (5–800 m; Tortonese, 1965) even if more abundant between 100- and 300-m depths (Massutí and Renones, 2005; Ramón et al., 2010). Ramón et al. (2010), studying the population inhabiting the continental shelf and slope of Balearic Islands, found a strongly aggregated spatial distribution of the royal cucumber population, with the abundance being the highest between 100 and 300 m. Abad et al. (2007), describing the composition and abundance of the megabenthic fauna caught by the commercial trawl fleet in the Alboran Sea, reported the high abundance (4.99 ± 1.19 kg h^{-1}) of *P. regalis* in the small seamount known as Chella Bank (310–360 m).

Concerning the role of environmental factors on the life cycle of *P. regalis*, little information is available. Galimany et al. (2018),

TABLE 2 Best supported and competing models for *P. regalis*.

	SSChl-3y	SSpH-3y	Fe	100m-NH_4	100m-O_2	100m-S	adjR^2	AICc	Δ AICc	AICc w.	Dev. exp.
Best model		+		+			0.765	32.5	0	0.557	82.8
Competing m1		+				+	0.622	36.4	3.86	0.081	70.4
Competing m2		+	+			+	0.727	36.9	4.37	0.063	80.8
Competing m3	+	+		+			0.707	37.5	4.99	0.046	79.3
Competing m4				+			0.401	37.6	5.13	0.043	46.6

Variables included in the model are indicated with the symbol +. Predictive variables included the following, chlorophyll α (SSChl-3y) and pH (SSpH-3y) at the sea surface 3 years lagged, fishing effort (Fe), ammonium (100m-NH_4), dissolved oxygen (100m-O_2), and salinity (100m-S) at 100 m depth. ΔAIC, difference in AICc between the best model and the current model; AICw, Akaike weights based on AICc; adjR^2, adjusted R^2 value; Dev.exp, percentage of deviance explained.

TABLE 3 Relative importance of predictor variables (calculated as the sum AIC weights from models that contain that variable within the 95% confidence interval) for *P. regalis*.

	SSpH	100m-NH_4	100m-S	Fe	SSChl	100m-O_2
Sum of weight (SW)	0.94	0.77	0.20	0.11	0.06	0.03
N containing models	11	8	6	3	3	2

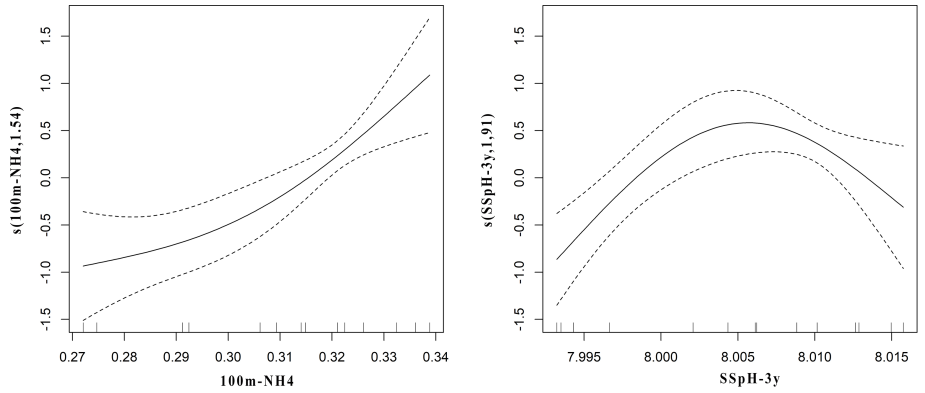

FIGURE 6
Partial GAM plots for the GAM model for *P. regalis* population in the Strait of Sicily. Each plot represents the estimated smoothing curves (solid line) obtained for 100m-NH_4 (left panel) and SSph-3y (right panel). The environmental variables are represented on the *x*-axis, and the *y*-axis shows the contribution of the smoother to the fitted values. Untransformed values are provided on the *x*-axis for easier interpretation. Dotted lines indicate the 95% confidence intervals.

comparing vital performances of specimens reared at seawater temperature higher than the preferred temperature (13°C) for aquaculture purposes, showed that 90% of the sea cucumbers exposed to 28°C died before 48 h, and at 23°C, they had 50% survivorship after 2 weeks of exposure.

Conversely, within the temperature range observed in the Strait of Sicily, namely, 15.4–25.2°C, Galimany et al. (2018) did not find significant effects on the species' density. Our results exclude a direct effect of temperature on *P. regalis* population and agreed with Galimany et al (2018) findings on adult specimens. On the other hand, considering the knowledge about life cycles of other sea cucumbers (Al Rashdi et al., 2012; Qiu et al., 2015; Rakaj et al., 2018; Neelmani and D.T. Vanghela 2018), the decreasing trend of the royal sea cucumber density in the investigated area might be influenced by the low tolerance of its larvae to the variation of sea pH during their pelagic phase.

This is in agreement with González-Durán et al. (2021), who reported that the most sensitive life stage of temperate and tropical holothurians to the adverse effects of temperature and pH was the larval dispersal and settlement phase. Conversely, Yuan et al. (2015) showed that a decrease in pH from 8.1 to 7.4 had relatively small effects on *Apostichopus japonicus* (Selenka, 1867) early life history compared to other echinoderms. On the other hand, Asha and Muthiah (2005), maintaining auricularia larvae of *Holothuria (Theelothuria) spinifera* (Théel, 1886) for 12 days at pH values ranging from 6.5 to 9.0, temperature between 28 and 32°C, and salinity at 35 psu, showed that, at pH 7.8, the larvae developed faster and grew better, showing better survival rates. All these contributions suggest that both larval development and survival rates are highly sensitive to pH than temperature and salinity. In particular, extreme alkaline values (pH 9.0) generated malformation and disintegration of individuals, while the reduction of 0.5 pH units from the optimum (pH 8.0) reduced survival rates by 49% (González-Durán et al., 2021).

Furthermore, exposing adult *A. japonicus* to different levels of pH, Yuan et al. (2016) highlighted that, the current increasing trend of acidification of the oceans may negatively influence the grazing capability and growth, thereby influencing its ecological functioning as an "ecosystem engineer" and potentially harming its culture output. More recently, Gullian and Terrats (2017) found that *Isostichopus badionotus* (Selenka, 1867) is a eurythermal organism capable of tolerating a wide range of temperatures from 16 to 34°C at pH 7.70. Environmental conditions for optimal physiological performance were found to be pH 8.17 and a temperature range of 24–28°C. The interaction between the two stressors (temperature and pH) activated antioxidant enzymes at various critical thermal limits to protect intracellular redox homeostasis.

Despite the high variability in responses observed, the effect exerted by the alteration of pH and temperature on the juveniles survival of sea cucumbers is less than those observed for the larvae. However, variations of pH and temperature from the optimal values can affect population abundance and density (Widicombe and Spicer, 2008; Brierley and Kingsford, 2009; Doney et al., 2009), impairing the success of the reproduction. Since holothurians are gonochoric and sedentary, their reproductive success depends largely on their gregarious behavior and their chemical communication, and spawning synchrony. Therefore, a reduction in density can affect fertilization, causing a further decrease in population size (Hutchings, 2014; Kuparinen and Hutchings, 2014; González-Durán et al., 2018).

However, other factors such as biotic factors could affect variation in *P. regalis* abundance. Although the available information on this species is scarce, it is well known that fishes, crustaceans, gastropods, and mainly seastars feed on holothurians, as young and adult (Francour, 1997), and they could have a relevant role as predators in regulating abundance of sea royal cucumbers. Therefore, it cannot be excluded that the effect of predation could contribute to the decreasing of the species in the Strait of Sicily.

In recent years, the harvesting of sea cucumbers in the Mediterranean Sea has been showing signs of systematic overexploitation being negative impacts observed such as decreased density, abundance, and genetic diversity; loss of larger individuals; increased incidence of some diseases; and even "local extinction" in some places (González-Wangüemert et al., 2018). Maggi and González-Wangüemert (2015), studying *P. regalis* Mediterranean populations from the Spanish coast, suggested the negative effects of overexploitation on populations living off the Catalan coast. Indeed, the population off Catalonia exhibited the highest occurrence of small individuals compared to other Spanish populations with a prevalence of mean or large-size specimens. Moreover, genetic data showed that Catalonia populations had the lowest number of haplotypes and haplotype diversity. According to the authors, the absence of shared haplotypes in Catalonia, which were present in other Spanish populations, may be due to the loss of haplotypes caused by fishing pressure.

Because of the high sensitivity to changes in environmental conditions (such as temperature and pH), the need to include the effects of pH and temperature into population models of sea cucumber has been suggested to inform the fishery management (González-Durán et al., 2021). Given the overall overexploitation of the Mediterranean resources (Colloca et al., 2017; Fiorentino and Vitale, 2021) and the growing interest of *P. regalis* as fishable species, it is necessary to improve the knowledge about its biological aspects (growth rate, longevity, reproductive aspects, thermal, and pH tolerance), abundance, and survival once hauled on deck.

In recent years, an uncontrolled fishing of sea cucumbers has been reported in Sardinia and Puglia waters (Italy) (Meloni and Esposito, 2018). Therefore, since 2018, the Italian authorities have prohibited fishing (target and/or accessory by catch), holding on board, transship, and landing of specimens belonging to the Holothuroidea class (IMAFFP, 2018).

Considering overfishing of some *P. regalis* stock in Mediterranean Sea, Ramón et al. (2022) have suggested some management measures to reach a more sustainable exploitation of the resources, namely, establishment of a fishing season and closure during spawning. Due to the high sensitivity of abundance dynamics of the species to the global change, when the impact of the fisheries seems to be weak, our results suggest that a precautionary approach in exploiting holothurians should be pursued.

The decreasing trend in abundance of *P. regalis* calls for an urgent conservation measure because its population reduction can compromise the functioning of the ecosystems with loss or reduction of the ecosystem services, such as enhanced nutrient cycling and local productivity in sediments, and trigger cascading effects on ecosystems that might diminish their ability to withstand other broad-scale stressors (Purcell et al., 2016; Ramón et al., 2019).

Data availability statement

The raw data supporting the conclusions of this article will be made available by the authors, without undue reservation.

Ethics statement

Ethical review and approval was not required for the animal study because no tests or experiments were performed on vertebrate animals.

Author contributions

DS, FFi, DM, VL, and MM: Conceptualization and design of the study. DS, VL, FQ, FFa, and GG: statistical analysis and data curation. AT, GS, VG, MLG, FD, and DM: data collection and validation. DS, FFi, and DM: writing—original draft. DS, GB, MDL, FFi, GG, MM, VL, and SV: writing—review and editing. GB and GG secured funding. All authors contributed to the article and approved the submitted version.

Funding

This work was supported by European Data Collection Framework (DCF)–Transversal Variables and MEDITS survey modules funded by the European Union and the Italian Ministry for Agricultural, Food and Forestry Policies.

Acknowledgments

This work is conducted thanks to the European Data Collection Framework (DCF)—Medits survey module—funded by the European Union and the Italian Ministry for Agricultural, Food and Forestry Policies. We are grateful to all staff of CNR-IRBIM of Mazara del Vallo, who collected and processed samples from the trawl surveys.

Conflict of interest

The authors declare that the research was conducted in the absence of any commercial or financial relationships that could be construed as a potential conflict of interest.

Publisher's note

All claims expressed in this article are solely those of the authors and do not necessarily represent those of their affiliated organizations, or those of the publisher, the editors and the reviewers. Any product that may be evaluated in this article, or claim that may be made by its manufacturer, is not guaranteed or endorsed by the publisher.

Supplementary material

The Supplementary Material for this article can be found online at: https://www.frontiersin.org/articles/10.3389/fmars.2022.934556/full#supplementary-material

References

Abad, E., Preciado, I., Serrano, A., and Baro, J. (2007). Demersal and epibenthic assemblages of trawlable grounds in the northern alboran Sea (western Mediterranean). *Sci. Mar.* 71, 513–524. doi: 10.3989/scimar.2007.71n3513

Aho, K., Derryberry, D., and Peterson, T. (2014). Model selection for ecologists: The worldviews of AIC and BIC. *Ecology* 95, 631–636. doi: 10.1890/13-1452.1

Al Rashdi, K. M., Eeckhaut, I., and Claereboudt, M. R. (2012). *A manual on hatchery of sea cucumber holothuria scabra in the sultanate of Oman* (Aquaculture Centre, Muscat: Ministry of Agriculture and Fisheries Wealth). Sultanate of Oman.

Antoniadou, C., and Vafidis, D. (2011). Population structure of the traditionally exploited holothurian *Holothuria tubulosa* in the south Aegean Sea. *Cah. Biol. Mar.* 52, 171–175.

Asha, P. S., and Muthiah, P. (2005). Effects of temperature, salinity and pH on larval growth, survival and development of the sea cucumber *Holothuria spinifera* theel. *Aquaculture* 250, 823–829. doi: 10.1016/j.aquaculture.2005.04.075

Aydin, M. (2008). The commercial sea cucumber fishery in Turkey. *SPC Beche-de-mer Infor Bull.* 28, 40–41.

Aydın, M., and Erkan, S. (2015). Identification and some biological characteristics of commercial sea cucumber in the Turkey coast waters. *Int. J. Fish Aquat.* 3, 260–265.

Battaglene, S. C., and Bell, J. D. (1999). Potential of the tropical Indo-Pacific sea cucumber, Holothuria scabra, for stock enhancement. *Proceedings First International Symposium on Stock Enhancement and Sea Ranching*, 8–11 September 1997, (Bergen, Norway: Blackwell, Oxford), 478–90.

Béranger, K., Mortier, L., Gasparini, G. P., Gervasio, L., Astraldi, M., and Crépon, M. (2004). The dynamics of the Sicily strait: a comprehensive study from observations and models. *Deep-Sea Res. II: Top. Stud. Oceanogr.* 51, 411–440. doi: 10.1016/j.dsr2.2003.08.004

Bertrand, J. A., Gil de Sola, L., Papaconstantinou, C., Relini, G., and Souplet, A. (2002). The general specifications of the MEDITS surveys. *Sci. Mar.* 66, 9–17. doi: 10.3989/scimar.2002.66s29

Bethoux, J. P., and Gentili, B. (1999). Functioning of the Mediterranean Sea: past and present changes related to freshwater input and climate changes. *J. Mar. Syst.* 20, 33–47. doi: 10.1016/S0924-7963(98)00069-4

Bonanno, A., Placenti, F., Basilone, G., Mifsud, R., Genovese, S., Patti, B., et al (2014). Variability of water mass properties in the Strait of Sicily in summer period of 1998-2013. *Ocean Sci.* 10, 759–70. doi: 10.5194/os-10-759-2014

Brander, K. (2010). Impacts of climate change on fisheries. *J. Mar. Syst.* 79, 389–402. doi: 10.1016/j.jmarsys.2008.12.015

Brierley, A. S., and Kingsford, M. J. (2009). Impacts of climate change on marine organisms and ecosystems. *Curr. Biol.* 19, R602–R614. doi: 10.1016/j.cub.2009.05.046

Bruckner, A. W. (2006). Proceedings of the CITES workshop on the conservation of sea cucumbers in the families Holothuriidae and Stichopodidae. *NOAA Technical Memorandum NMFS-OPR* (Silver Spring, MD) 34, 244.

Bruckner, A. W., Johnson, K. A., and Field, J. D. (2003). Conservation strategies for sea cucumbers. can a CITES appendix II listing promote sustainable international trade? *SPC Beche-de-mer Infor Bull.* 18, 24–33.

Buckland, S. T., Burnham, K. P., and Augustin, N. H. (1997). Model selection: An integral part of inference. *Biometrics* 53, 603–618. doi: 10.2307/2533961

Burnham, K. P., and Anderson, D. R. (2002). *Model selection and multimodel inference: A practical information-theoretic approach, 2nd edn* (NewYork: Springer).

Calanchi, N., Colantoni, P., Rossi, P. L., Saitta, M., and Serri, G. (1989). The strait of Sicily continental rift systems: physiography and petrochemistry of the submarine volcanic centres. *Mar. Geol.* 87, 55–83. doi: 10.1016/0025-3227(89)90145-X

Cartes, J. E., Maynou, F., Abelló, P., Emelianov, M., de Sola, L. G., and Solé, M. (2011). Long-term changes in the abundance and deepening of the deep-sea shrimp *Aristaeomorpha foliacea* in the Balearic basin: relationships with hydrographic changes at the levantine intermediate water. *J. Marine. Syst.* 88, 516–525. doi: 10.1016/j.jmarsys.2011.07.001

Colantoni, P., Del Monte, M., and EFK, Z. (1975). Il banco Graham: un vulcano recente del canale di sicilia. *Giornale di Geologia.* 40, 141–162. Bologna.

Colantoni, P., Gennesseaux, M., Vanney, J. R., Ulzega, A., Melegari, G., and Trombetta, A. (1992). Processi dinamici del canyon sottomarino di gioia tauro (Mare tirreno). *Giornale di Geologia.* 54, 199–213.

Colloca, F., Scarcella, G., and Libralato, S. (2017). Recent trends and impacts of fisheries exploitation on Mediterranean stocks and ecosystems. *Front. Mar. Sci.* 4. doi: 10.3389/fmars.2017.00244

Conand, C., Polidoro, B., Mercier, A., Gamboa, R., Hamel, J. F., and Purcell, S. (2014). The IUCN red list assessment of aspidochirotid sea cucumbers and its implications. *SPC Beche-de-mer Infor. Bull.* 34, 3–7.

Cossarini, G., Feudale, L., Teruzzi, A., Bolzon, G., Coidessa, G., Solidoro, C., et al. (2021). High-resolution reanalysis of the Mediterranean Sea biogeochemistry, (1999–2019). *Front. Mar. Sci.* 1537. doi: 10.3389/fmars.2021.741486

Costa, V., Mazzola, A., and Vizzini, S. (2014). *Holothuria tubulosa* gmelin 1791 (Holothuroidea, Echinodermata) enhances organic matter recycling in *Posidonia oceanica* meadows. *J. Exp. Mar. Biol. Ecol.* 461, 226–232. doi: 10.1016/j.jembe.2014.08.008

Crutzen, P. J., and Stoermer, E. F. (2000). "The 'Anthropocene'" in *The Future of Nature: Documents of Global Change*, ed. L.Robin S. and Warde SörlinP. (New Haven: Yale University Press). 2013, 479–90. doi: 10.12987/9780300188479-041

Di Donato, V., Sgarrella, F., Sprovieri, R., Di Stefano, E., Martín-Fernández, J. A., and Incarbona, A. (2022). High-frequency modification of the central Mediterranean seafloor environment over the last 74 ka. *Palaeogeogr. Palaeocl.* 593, 110924. doi: 10.1016/j.palaeo.2022.110924

Diffenbaugh, N. S., Pal, J. S., Giorgi, F., and Gao, X. (2007). Heat stress intensification in the Mediterranean climate change hotspot. *Geophys Res. Lett.* 34, L11706. doi: 10.1029/2007GL030000

Di Lorenzo, M., Sinerchia, M., and Colloca, F. (2018). The north sector of the strait of Sicily: a priority area for conservation in the Mediterranean Sea. *Hydrobiologia* 821, 235–253. doi: 10.1007/s10750-017-3389-7

Di Maio, F., Geraci, M. L., Scannella, D., Russo, T., and Fiorentino, F. (2022). Evaluation of the economic performance of coastal trawling off the southern coast of Sicily (Central Mediterranean Sea). *Sustainability* 14, 4743. doi: 10.3390/su14084743

Doney, S., Fabry, V., Feely, R., and Kleypas, J. (2009). Ocean acidification: the other CO2 problem. *Ann. Rev. Mar. Sci.* 1, 169–192. doi: 10.1146/annurev.marine.010908.163834

Dong, Y., Dong, S., Tian, X., Wang, F., and Zhang, M. (2006). Effects of diel temperature fluctuations on growth, oxygen consumption and proximate body composition in the sea cucumber *Apostichopus japonicas* selenka. *Aquaculture* 255, 514–521. doi: 10.1016/j.aquaculture.2005.12.013

D'Ortenzio, F., and Ribera d'Alcalà, M. (2009). On the trophic regimes of the Mediterranean Sea: a satellite analysis. *Biogeosciences* 6, 139–148. doi: 10.5194/bg-6-139-2009

Eriksson, H., and Clarke, S. (2015). Chinese Market responses to overexploitation of sharks and sea cucumbers. *Biol. Conserv.* 184, 163–173. doi: 10.1016/j.biocon.2015.01.018

Escudier, R., Clementi, E., Omar, M., Cipollone, A., Pistoia, J., Aydogdu, A., et al. (2020). Mediterranean Sea Physical reanalysis (CMEMS MED-currents) (version 1)[Data set]. *Copernicus Monit. Environ. Mar. Service (CMEMS)*. doi: 10.25423/CMCC/MEDSEA_MULTIYEAR_PHY_006_004_E3R1

Fiorentini, L., Dremière, P. Y., Leonori, I., Sala, A., and Palumbo, V. (1999). Efficiency of the bottom trawl used for the Mediterranean international trawl survey (MEDITS). *Aquat Living Resour.* 12, 187–205. doi: 10.1016/S0990-7440(00)88470-3

Fiorentino, F., and Vitale, S. (2021). How can we reduce the overexploitation of the Mediterranean resources? *Front. Mar. Sci* 8, 674633. doi: 10.3389/fmars.2021.674633

Francour, P. (1997). Predation on holothurians: a literature review. *Invertebr. Biol.* 116, 52–60. doi: 10.2307/3226924

Galimany, E., Baeta, M., and Ramón, M. (2018). Immune response of the sea cucumber *Parastichopus regalis* to different temperatures: Implications for aquaculture purposes. *Aquaculture* 497, 357–363. doi: 10.1016/j.aquaculture.2018.08.005

Gao, K., Beardall, J., Hä der, D. P., Hall – Spencer, J. M., Gao, G., and Hutchins, D. A. (2019). Effects of ocean acidification on marine photosynthetic organisms under the current influences of warming, UV radiationm and deoxigenation. *Front. Mar. Sci.* 6. doi: 10.3389/fmars.2019.00322

Glockner-Fagetti, A., Calderon-Aguilera, L. E., and Herrero-Pérezrul, M. D. (2016). Density decrease in an exploited population of brown sea cucumber *Isostichopus fuscus* in a biosphere reserve from the Baja California peninsula, Mexico. *Ocean Coast. Manage.* 121, 49–59. doi: 10.1016/j.ocecoaman.2015.12.009

González-Durán, E., Hernández-Flores, Á., Headley, M. D., and Canul, J. D. (2021). On the effects of temperature and pH on tropical and temperate holothurians. *Conserv. Physiol.* 9, coab092. doi: 10.1093/conphys/coab092

González-Durán, E., Hernández-Flores, A., Seijo, J. C., Cuevas-Jiménez, A., and Moreno-Enriquez, A. (2018). Bioeconomics of the allee effect in fisheries targeting sedentary resources. *ICES J. Mar. Sci.* 75, 1362–1373. doi: 10.1093/icesjms/fsy018

González-Wangüemert, M., Aydin, M., and Conand, C. (2014). Assessment of sea cucumber populations from the Aegean Sea (Turkey): First insights to sustainable management of new fisheries. *Ocean Coast. Manage.* 92, 87–94. doi: 10.1016/j.ocecoaman.2014.02.014

González-Wangüemert, M., Domínguez-Godino, J. A., and Cánovas, F. (2018). The fast development of sea cucumber fisheries in the Mediterranean and NE Atlantic waters: from a new marine resource to its over-exploitation. *Ocean Coast. Manage* 151, 165–177. doi: 10.1016/j.ocecoaman.2017.10.002

Gonzalez-Wangüemert, M., Valente, S., and Aydin, M. (2015). Effects of fishery protection on biometry and genetic structure of two target sea cucumber species from the Mediterranean Sea. *Hydrobiologia* 743, 65–74. doi: 10.1007/s10750-014-2006-2

González-Wangüemert, M., Valente, S., Henriques, F., Domínguez-Godino, J. A., and Serrão, E. A. (2016). Setting preliminary biometric baselines for new target sea cucumbers species of the NE Atlantic and Mediterranean fisheries. *Fish. Res.* 179, 57–66. doi: 10.1016/j.fishres.2016.02.008

Grueber, C. E., Nakagawa, S., Laws, R. J., and Jamieson, I. G. (2011). Multimodel inference in ecology and evolution: challenges and solutions. *J. Evol. Biol.* 24, 699–711. doi: 10.1111/j.1420-9101.2010.02210.x

Gullian, M. (2013). Physiological and immunological condition of the sea cucumber *Isostichopus badionotus* (Selenka, 1867) during dormancy. *J. Exp. Mar. Biol. Ecol.* 444, 31–37. doi: 10.1016/j.jembe.2013.03.008

Gullian, K. M., and Terrats, P. M. (2017). Effect of pH on temperature controlled degradation of reactive oxygen species, heat shock protein expression, and mucosal immunity in the sea cucumber *Isostichopus badionotus*. *PloS One* 12, e0175812. doi: 10.1371/journal.pone.0175812

James, G., Witten, D., Hastie, T., and and Tibshirani, R. (2013). *An introduction to statistical learning* (New York: Spinger). 426 p.

Hamel, J. F., and Mercier, A. (2008). "Precautionary management of cucumaria frondosa in Newfoundland and Labrador, Canada," in *Sea Cucumbers. a global review of fisheries and trade*. Eds. V. Toral-Granda, A. Lovatelli and M. Vasconcellos (Rome: FAO Fisheries and Aquaculture Technical Paper), 293–306. No. 516FAO.

Han, Q., Keesing, J. K., and Liu, D. (2016). A review of sea cucumber aquaculture, ranching, and stock enhancement in China. *Rev. Fish. Sci. Aquac.* 24, 326–341. doi: 10.1080/23308249.2016.1193472

Hastie, T. J., and Tibshirani, R. J. (2017). *Generalized additive models* (New York: Routledge). doi: 10.1201/9780203753781

Huang, B., Liu, C., Freeman, E., Graham, G., Smith, T., and Zhang, H. M. (2021). Assessment and intercomparison of NOAA daily optimum interpolation sea surface temperature (DOISST) version 2.1. *J. Climate.* 34, 7421–7441. doi: 10.1175/JCLI-D-20-0166.1

Huot, Y., Babin, M., Bruyant, F., Grob, C., Twardowski, M. S., and Claustre, H. (2007). Does chlorophyll a provide the best index of phytoplankton biomass for primary productivity studies? *Biogeosci. Discuss.* 4, 707–745.

Hutchings, J. (2014). Renaissance of a caveat: Allee effects in marine fish. contribution to the special issue: commemorating 100 years since hjort's 1914 treatise on fluctuations in the great fisheries of northern Europe. *ICES J. Mar. Sci.* 71, 2152–2157. doi: 10.1093/icesjms/fst179

IMAFFP (2018). Italian Ministry of Agricultural, Food and Forestry Policies, ministerial decree 156/2018. In: *Official Journal of the Italian Republic of February 27th, 2018*. Divieto della Pesca delle Oloturie.

James, G., Witten, D., Hastie, T., and Tibshirani, R. (2013). *An introduction to statistical learning*. (New York: Springer) 426 .

Kim, Y. J., and Gu, C. (2004). Smoothing spline Gaussian regression: more scalable computation *via* efficient approximation. *J. R. Stat. Soc Ser. B. Methodol.* 66, 337–356. doi: 10.1046/j.1369-7412.2003.05316.x

Kuparinen, A., and Hutchings, J. (2014). Increased natural mortality at low abundance can generate allee effect in a marine fish. *R. Soc Open Sci.* 1, 140075. doi: 10.1098/rsos.140075.1–5

Lafuente, J. G., Garcia, A., Mazzola, S., Quintanilla, L., Delgado, J., Cuttita, A., et al. (2002). Hydrographic phenomena influencing early life stages of the Sicilian channel anchovy. *Fish. Oceanogr.* 11, 31–44. doi: 10.1046/j.1365-2419.2002.00186.x

MacTavish, T., Stenton-Dozey, J., Vopel, K., and Savage, C. (2012). Deposit-feeding sea cucumbers enhance mineralization and nutrient cycling in organically-enriched coastal sediments. *PloSE One* 7, e50031. doi: 10.1371/journal.pone.0050031

Maggi, C., and González-Wangüemert, M. (2015). Genetic differentiation among *Parastichopus regalis* populations from Western Mediterranean Sea: potential effects of its fishery and current connectivity. *Med. Mar. Sci.* 16, 489–501. doi: 10.12681/mms.1020

Massutí, E., and Renones, O. (2005). Demersal resource assemblages in the trawl fishing grounds off the Balearic islands (western Mediterranean). *Sci. Mar.* 69, 167–181. doi: 10.3989/scimar.2005.69n1167

Meloni, D., and Esposito, G. (2018). Hygienic and commercial issues related to the illegal fishing and processing of sea cucumbers in the Mediterranean: A case study on over-exploitation in Italy between 2015 and 2017. *Reg. Stud.* 19, 43–46. doi: 10.1016/j.rsma.2018.03.009

Míguez-Rodríguez, L. J (2009). "Equinodermos (crinoideos, equinoideos y holothuroideos) litorales," in *Batiales y abisales de Galicia* (Universidade de Santiago de Compostela). dissertation thesis doctoral.

Milisenda, G., Vitale, S., Massi, D., Enea, M., Gancitano, V., Giusto, G. B., et al. (2017). Discard composition associated with the deep water rose shrimp fisheries (*Parapenaeus longirostris*, Lucas 1846) in the south-central Mediterranean Sea. *Mediterr. Mar. Sci.* 18, 53–63. doi: 10.12681/mms.1787

Morgan, A. (2008). The effect of food availability on phenotypic plasticity in larvae of the temperate sea cucumber *Australostichopus mollis*. *J. Exp. Mar. Biol. Ecol.* 363, 89–95. doi: 10.1016/j.jembe.2008.06.025

Muggeo, V. M. (2008). Segmented: an r package to fit regression models with broken-line relationships. *R News.* 8, 20–25.

Neelmani,, and Vaghela, D. T. (2018). "Reproduction and developmental biology of (Holothuria scabra) Sea cucumber," in *Research trends in agriculture sciences naresh*, Ed. R. K. Naresh (AkiNik Publications), 97–108.

Pawson, D., Vance, D. J., Messing, C., Solis-Marin, A. F., and Mah, C. L. (2009). Echinodermata of the Gulf of Mexico. In *Gulf of Mexico origin, waters, and biota*. Eds. D. L. Felder and D. K. Camp (Texas: A&M University Press), 1177–1204.

Piccioni, A., Gabriele, M., Salusti, E., and Zambianchi, E. (1988). Wind-induced upwellings off the southern coast of Sicily. *Oceanol. Acta* 11, 309–314.

Pinardi, N., and Masetti, E. (2000). Variability of the large scale general circulation of the Mediterranean Sea from observations and modelling: a review. *Palaeogeogr. Palaeocl.* 158, 153–173. doi: 10.1016/S0031-0182(00)00048-1

Pörtner, H. O. (2008). Ecosystem effects of ocean acidification in times of ocean warming: a physiologist's view. *Mar. Ecol. Prog. Ser.* 373, 203–217. doi: 10.3354/meps07768

Pörtner, H., and Knust, R. (2007). Climate change affects marine fishes through the oxygen limitation of thermal tolerance. *Science* 315, 95–97. doi: 10.1126/science.1135471

Prakash, S. (2021). Impact of climate change on aquatic ecosystem and its biodiversity: An overview. *Int. J. Biol. Innov.* 3. doi: 10.46505/IJBI.2021.3210

Purcell, S. W. (2010). Diel burying by the tropical sea cucumber *Holothuria scabra*: effects of environmental stimuli, handling and ontogeny. *Mar. Biol.* 157, 663–671. doi: 10.1007/s00227-009-1351-6

Purcell, S. W., Mercier, A., Conand, C., Hamel, J. F., Toral-Granda, M. V., Lovatelli, A., et al. (2013). Sea Cucumber fisheries: global analysis of stocks, management measures and drivers of overfishing. *Fish* 14, 34–59. doi: 10.1111/j.1467-2979.2011.00443.x

Purcell, S. W., Piddocke, T. P., Dalton, S. J., and Wang, Y. G. (2016). Movement and growth of the coral reef holothuroids *Bohadschia argus* and *Thelenota ananas*. *Mar. Ecol. Prog. Ser.* 551, 201–214. doi: 10.3354/meps11720

Purcell, S. W., Samyn, Y., and Conand, C. (2012)Commercially important sea cucumbers of the world. *FAO Species Catalogue for Fishery Purposes No. 6*.

QGIS Development Team (2020). *QGIS geographic information system* (Open Source Geospatial Foundation Project). Available at: http://qgis.osgeo.org.

Qiu, T., Zhang, T., Hamel, J. F., Mercier, A.Elsevier (2015). "Development, settlement, and post-settlement growth," in *Developments in aquaculture and fisheries science*, ed. H. Yang, J-F Hamel and A. Mercier (Developments in Aquaculture and Fisheries Science, Elsevier) 111–131.

Quiñones, J., Rosa, R., Ruiz, D., and Garcia-Arrarás, J. (2002). Extracellular matrix remodeling and metalloproteinase involvement during intestine regeneration in the sea cucumber *Holothuria glaberrima*. *Dev. Biol.* 250, 181–197. doi: 10.1006/dbio.2002.0778

Rakaj, A., Fianchini, A., Boncagni, P., Lovatelli, A., Scardi, M., and Cataudella, S. (2018). Spawning and rearing of *Holothuria tubulosa*: A new candidate for aquaculture in the Mediterranean region. *Aquac* 49, 557–568. doi: 10.1111/are.13487

Ramírez-González, J., Moity, N., Andrade-Vera, S., and Mackliff, H. R. (2020). Estimation of age and growth and mortality parameters of the sea cucumber *Isostichopus fuscus* (Ludwig 1875) and implications for the management of its fishery in the Galapagos marine reserve. *Aquac. Fish.* 5, 245–252. doi: 10.1016/j.aaf.2020.01.002

Ramón, M., Amor, M. J., and Galimany, E. (2022). Reproductive biology of the holothurian *Parastichopus regalis* in the Mediterranean Sea and its implications for fisheries management. *Fish. Res.* 247, 106191. doi: 10.1016/j.fishres.2021.106191

Ramón, M., Lleonart, J., and Massutí, E. (2010). Royal cucumber (*Stichopus regalis*) in the northwestern Mediterranean: distribution pattern and fishery. *Fish. Res.* 105, 21–27. doi: 10.1016/j.fishres.2010.02.006

Ramón, M., Simarro, G., Galimany, E., and Lleonart, J. (2019). Evaluation of sediment particle size selection during feeding by the holothurian *Parastichopus regalis* (Cuvier 1817). *Reg. Stud. Mar. Sci.* 31, 100763. doi: 10.1016/j.rsma.2019.100763

R Core Team (2021). *R: A language and environment for statistical computing* (Vienna, Austria: R Foundation for Statistical Computing). Available at: https://www.R-project.org/.

Reeder, M. S., Stow, D. A., and Rothwell, R. G. (2002). Late quaternary turbidite input into the east Mediterranean basin: new radiocarbon constraints on climate and sea-level control. *Geol. Soc Spec. Publ. London.* 191, 267–278. doi: 10.1144/GSL.SP.2002.191.01.18

Robinson, G., and Lovatelli, A. (2015). Lovatelli globalsea cucumber fisheries and aquaculture FAO's inputs over the past few years. *FAO Aquacult. Newsl.* 53, 55–57.

Russo, T., Carpentieri, P., D'Andrea, L., De Angelis, P., Fiorentino, F., Franceschini, S., et al. (2019). Trends in effort and yield of trawl fisheries: a case study from the Mediterranean Sea. *Front. Mar. Sci.* 6. doi: 10.3389/fmars.2019.00153

Scannella, D., Gancitano, V., Falsone, F., Geraci, M. L., Vitale, S., Colloca, F., et al. (2020). Stock assessment form of red mullet (M. barbatus) in GSA 16. *Zenodo*. doi: 10.5281/zenodo.4382456

Skewes, T., Dennis, D., and Burridge, C. (2000). *Survey of holothuria scabra (sandfish) on warrior reef, Torres strait* (Queensland, Australia: Report to Queensland Fisheries Management Authority).

Sorgente, R., Drago, A. F., and Ribotti, A. (2003). Seasonal variability in the central Mediterranean Sea circulation. *Ann. Geophys.* 21, 299–322. doi: 10.5194/angeo-21-299-2003

Sorgente, R., Olita, A., Oddo, P., Fazioli, L., and Ribotti, A. (2011). Numerical simulation and decomposition of kinetic energy in the central Mediterranean: insight on mesoscale circulation and energy conversion. *Ocean Sci.* 7, 503–519. doi: 10.5194/os-7-503-2011

Spedicato, M. T., Massutí, E., Mérigot, B., Tserpes, G., Jadaud, A., and Relini, G. (2019). The medits trawl survey specifications in an ecosystem approach to fishery management. *Sci. Mar.* 83, 9–20. doi: 10.3989/scimar.04915.11X

Stefanescu, C., Rucabado, J., and Lloris, D. (1992). Depth-size trends in western Mediterranean demersal deep-sea fishes. *Mar. Ecol. Prog. Ser.* 81, 205–2013. doi: 10.3354/meps081205

Symonds, M. R., and Moussalli, A. (2011). A brief guide to model selection, multimodel inference and model averaging in behavioural ecology using akaike's information criterion. *Behav. Ecol. Sociobiol.* 65, 13–21. doi: 10.1007/s00265-010-1037-6

Toral-Granda, V. (2007). Facts on sea cucumber fisheries worldwide. *SPC Bechedemer Inf. Bull.* 25, 39–41.

Toral-Granda, V., Lovatelli, A., and Vasconcellos, M. (2008). Sea Cucumbers. A global review of fisheries and trade. FAO fish. *FAO Fisheries and Aquaculture Technical Paper. No. 516.* (Rome: FAO), 317.

Tortonese, E. (1965). *Echinodermata* (Calderini. Bologna: Fauna d'Italia).

Touratier, F., and Goyet, C. (2011). Impact of the Eastern Mediterranean transient on the distribution of anthropogenic CO2 and first estimate of acidification for the Mediterranean Sea. *Deep Sea Res. Part I Oceanogr. Res. Pap.* 58, 1–15. doi: 10.1016/j.dsr.2010.10.002

Vargas-Yáñez, M., Moya, F., García-Martínez, M. D. C., Tel, E., Zunino, P., Plaza, F., et al. (2010). Climate change in the Western Mediterranean sea 1900–2008. *J. Mar. Syst.* 82, 171–176. doi: 10.1016/j.jmarsys.2010.04.013

Wei, T., and Simko, V. (2021) *R package 'corrplot': Visualization of a correlation matrix. (Version 0.92).* Available at: https://github.com/taiyun/corrplot.

Widicombe, S., and Spicer, J. I. (2008). Predicting the impact of ocean acidification on benthic biodiversity: what can animal physiology tell us? *J. Exp. Mar. Biol. Ecol.* 366, 187–197. doi: 10.1016/j.jembe.2008.07.024

Wood, S. N. (2001). Mgcv: GAMs and generalized ridge regression for r. *R news.* 1, 20–25.

Wood, S. N. (2006). *Generalized additive models: an introduction with r* (New York: chapman and hall/CRC). doi: 10.1201/9781420010404

Wu, H., Li, D., Zhu, B., Sun, J., Zheng, J., Wang, F., et al. (2013). Proteolysis of noncollagenous proteins in sea cucumber, *Stichopus japonicus*, body wall: characterization and the effects of cysteine protease inhibitors. *Food. Chem.* 141, 1287–1294. doi: 10.1016/j.foodchem.2013.03.088

Yuan, X., Shao, S., Dupont, S., Meng, L., Liu, Y., and Wang, L. (2015). Impact of CO2-driven acidification on the development of the sea cucumber *Apostichopus japonicus* (Selenka) (Echinodermata: Holothuroidea). *Mar. pollut. Bull.* 95, 195–199. doi: 10.1016/j.marpolbul.2015.04.021

Yuan, X., Yang, H., Wang, L., Zhou, Y., and Gabr, H. (2009). Bioenergetic responses of sub-adult sea cucumber *Apostichopus japonicus* (Selenka) (Echinodermata: Holothuroidea) to temperature with special discussion regarding its southernmost distribution limit in China. *J. Therm Biol.* 34, 315–319. doi: 10.1016/j.jtherbio.2009.05.001

Yuan, X., Shao, S., Yang, X., Yang, D., Xu, Q., Zong, H., et al. (2016). Bioenergetic trade-offs in the sea cucumber Apostichopus japonicus (Echinodermata: Holothuroidea) in response to CO2-driven ocean acidification. *Environ. Sci. Pollut. Res.* 23, 8453–8461. doi: 10.1007/s11356-016-6071-0

Zamora, L., and Jeffs, A. (2012). Feeding, metabolism and growth in response to temperature in juveniles of the Australasian Sea cucumber, *Australostichopus mollis*. *Aquaculture* 358, 92–97. doi: 10.1016/j.aquaculture.2012.06.024

frontiers | Frontiers in Marine Science

TYPE Original Research
PUBLISHED 03 October 2022
DOI 10.3389/fmars.2022.931832

OPEN ACCESS

EDITED BY
Jose Luis Iriarte,
Austral University of Chile, Chile

REVIEWED BY
Angela Cuttitta,
National Research Council (CNR), Italy
Wee Cheah,
University of Malaya, Malaysia

*CORRESPONDENCE
Jorge López-Parages
parages@uma.es

SPECIALTY SECTION
This article was submitted to Marine Fisheries, Aquaculture and Living Resources, a section of the journal Frontiers in Marine Science

RECEIVED 29 April 2022
ACCEPTED 30 August 2022
PUBLISHED 03 October 2022

CITATION
López-Parages J, Gómara I, Rodríguez-Fonseca B and García-Lafuente J (2022) Potential SST drivers for chlorophyll-a variability in the Alboran Sea: A source for seasonal predictability? *Front. Mar. Sci.* 9:931832. doi: 10.3389/fmars.2022.931832

Potential SST drivers for Chlorophyll-a variability in the Alboran Sea: A source for seasonal predictability?

Jorge López-Parages[1,2]*, Iñigo Gómara[3,4], Belén Rodríguez-Fonseca[3,4] and Jesús García-Lafuente[1,2]

[1]Department of Applied Physics II, Physical Oceanography Group, University of Málaga, Málaga, Spain, [2]Instituto Universitario de Biotecnología y Desarrollo Azul (IBYDA), University of Málaga, Málaga, Spain, [3]Departamento de Física de la Tierra y Astrofísica, Universidad Complutense de Madrid, Madrid, Spain, [4]Instituto de Geociencias (IGEO), Madrid, Spain

This study investigates the link between large-scale variability modes of the sea surface temperature (SST) and the surface chlorophyll-a (Chl-a) concentration in spring along the northern flank of the Alboran Sea. To this aim, surface satellite-derived products of SST and Chl-a, together with atmospheric satellite variables, are used. Our results indicate that both the tropical North Atlantic and El Niño Southern Oscillation (ENSO) could trigger the development of anomalous distribution patterns of Chl-a in spring in northern Alboran. This anomalous feature of Chl-a is, in turn, associated with the alteration of the usual upwelling taking place in northern Alboran at that time of the year. The skill of the related SST signals, over the tropical North Atlantic and the tropical Pacific, as predictors of the aforementioned Chl-a response in Alboran, has also been assessed through a statistical prediction model with leave-one-out cross-validation. Our results confirm the predictive skill of ENSO to realistically estimate the coastal Chl-a concentration in spring in northern Alboran. In particular, during the El Niño/La Niña years, this Chl-a response can be robustly predicted with 4 months in advance. On the other hand, the tropical North Atlantic SSTs allow to significantly predict, up to 7 months in advance, the Chl-a concentration in spring offshore, in particular by the north of the Western and the Eastern Alboran gyres. The results presented here could contribute to develop a future seasonal forecasting tool of upwelling variability and living marine resources in northern Alboran.

KEYWORDS

Alboran Sea, chlorophyll-a (Chl-a), SST (sea surface temperature), climate teleconnection, seasonal predictability

1 Introduction

The Alboran Sea is not only a natural barrier between the European and African continents but a region that connects Mediterranean and Atlantic water masses with very different characteristics. Due to its geographical location, the Alboran Sea also presents interesting aspects from a climatic, oceanographic, and biological point of view.

Despite the upper-level circulation of the Alboran Sea being very complex, a classical and simplified picture (see Figure 1) can be described as an incoming jet of Atlantic water (AJ) following a wavelike path around two anticyclonic gyres: the Western Alboran Gyre (WAG) and the Eastern Alboran Gyre (EAG). The northern Alboran Sea (defined as 5.3°W-2°W; 36°N-37°N; see red box in Figure 1) is also characterized by the presence of vertical transport of salty and nutrient-rich waters from below. This upwelling area can be easily observed from satellite data and contributes to enhance the biological productivity of this marine region. Indeed, the Alboran Sea is considered the most productive basin within the Mediterranean Sea (Bosc et al., 2004; Lazzari et al., 2011), particularly the Iberian coastal margin and the northern sector of the WAG (Minas et al., 1991; Reul et al., 2005).

Several mechanisms are known to foster the abovementioned upwelling along the northern Alboran Sea. According to the available literature, both the wind-driven upwelling (Mercado et al., 2012) and the meridional fluctuations of the Atlantic Jet (Sarhan et al., 2000) appear to be its main drivers. Both influence the vertical supply of nutrients to the photic zone, the generation of phytoplankton blooms, and the Chlorophyll-a spatial distribution (Sarhan et al., 2000; Ramírez, 2007). Nevertheless, it is also important to note that this upwelling is far from being spatially homogeneous. In this sense, Baldacci et al. (2001) defined two upwelling areas: the first one between the Strait of Gibraltar (~5.5°W) to the Calaburras Point (~4.5°W) and the second one (also denoted as the Atlantic-Mediterranean Transition zone; see Muñoz et al., 2017) from the Calaburras Point to Cape Gata (~2° W). Both areas present similar forcing, but they differ in their upwelling seasonality along the year. Overall, a maximum of chlorophyll-a concentration has been found in late winter and spring (Ramírez et al., 2005; Macías et al., 2007; Lazzari et al., 2011), with a progressive decline from June onward. Nevertheless, upwelling events can occur even in summer under strong favorable SW–W winds producing Ekman transport and leading to occasional blooms (Ramírez et al., 2005).

Additional to the seasonal changes, the Alboran circulation and the upwelling on its northern flank also fluctuates at shorter (~inertial) and longer (inter-annual) time scales. The former is known to be mainly associated with meso- and submeso-scale processes driven by atmospheric fluctuations (Garcıa-Lafuente et al., 1998) and smaller oceanic processes such as tidal currents. This variability has been deeply analyzed and plays a significant role in the stability of the WAG (Sánchez Garrido et al., 2008; Sánchez-Garrido et al., 2013). Contrastingly, the understanding of the physical mechanisms behind the interannual variability of the Alboran circulation still poses great challenges. Overall, the interannual variability of upwelling along the northern Alboran Sea is closely related to the prevalence of favorable SW–W winds (*Ponientes* in Spanish), which in turn must be linked to appropriate atmospheric circulation conditions (Garcia-Gorriz and Carr, 2001). Such winds are generally associated with a dipole of sea level pressure (SLP) anomalies in the North Atlantic, with relatively high (low) pressures in subpolar (subtropical) latitudes. These SLP anomalies are usually linked to the negative phase of the North Atlantic Oscillation (NAO), the dominant atmospheric variability pattern in this region (Pinto and Raible, 2012; Gómara et al., 2016). It is important to note that the year-to-year (or longer) atmospheric fluctuations can be interpreted as changes in the frequency of day-to-day meteorological fluctuations provided the hypothesis of long-term quasi-stationary climate (Cassou, 2010). In this sense, apart from NAO, other modes contributing to interannual

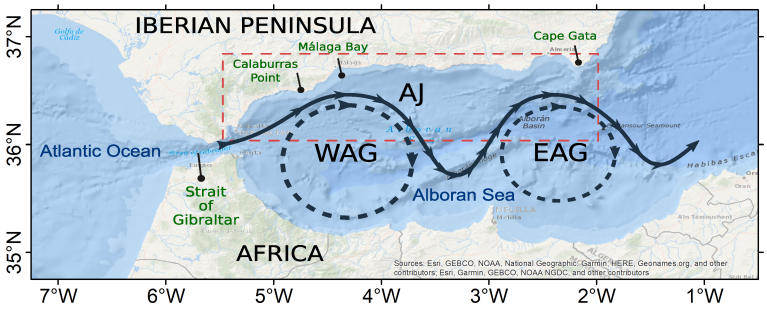

FIGURE 1
Simplified sketch of the study region and the Alboran Sea ocean dynamic. The area within the red box represents the so-called northern Alboran Sea (nAS). WAG and EAG refer to the so-called Western and Eastern Alboran Gyres, respectively, and AJ denotes the incoming jet of Atlantic water.

climate variability such as the tropical North Atlantic (Rodríguez-Fonseca et al., 2006; Losada et al., 2007) or ENSO (Brönnimann, 2007; Shaman, 2014) have been identified as drivers of wind anomalies over the western Mediterranean. ENSO and NAO have been highlighted as forcings of anomalous chlorophyll-a distributions and phytoplankton primary production in different subregions of the Mediterranean basin (Katara et al., 2008; Basterretxea et al., 2018; González-Lanchas et al., 2020). However, the specific signal of these large-scale climate modes on northern Alboran, the linking mechanisms, and the related predictive value are still questions which require further investigation. This paper investigates the interannual variability of the chlorophyll-a concentration along the northern Alboran Sea. To this aim, we analyze distribution patterns of this field and their potential links with the large-scale climate. In this context, and due to the ocean thermal inertia, it is important to mention the special relevance of those climate phenomena associated with sea surface temperature (SST) processes (Bjerknes, 1969). If we are able to find a robust cause-and-effect relationship between an SST-related variability mode and a certain distribution pattern of chlorophyll-a in the Alboran Sea, we could provide the basis for developing a novel future seasonal forecasting tool of upwelling variability in our study region. This possibility is assessed and quantified along the present study.

2 Data and methods

2.1 Reanalyzed data

This study is based on surface satellite-derived chlorophyll-a concentration data, available at 1-km lat–lon resolution from 1997 to 2021, from the Mediterranean ocean color level 4 operational multi-sensor processing dataset (Volpe et al., 2018). In particular, this satellite product has been used to analyze the spatiotemporal variability of surface chlorophyll-a concentrations (hereinafter Chl-a) along the northern flank of the Alboran Sea, which is representative of the upwelling variability in that area. The surface signature of upwelling within the Alboran Sea has been also addressed by the use of high-resolution sea surface temperature (SST) data at 0.05° × 0.05° lat–lon resolution from the CMEMS-reprocessed Mediterranean SST dataset, an optimally interpolated satellite-based estimate of the SST (Saha et al., 2018). The possible large-scale SST forcings of Chl-a variability in our study region have been assessed by the use of SST data from the NOAA AVHRR OISST V2.1 dataset (Huang et al., 2021; 0.25° × 0.25° lat-lon resolution). To characterize the atmospheric conditions associated with this variability, mean sea level pressure (SLP) and zonal and meridional surface winds with a 0.25° × 0.25° lat-lon resolution have been obtained from the fifth-generation ECMWF reanalysis ERA5 (Hersbach et al., 2018).

2.2 Assessing the Chl-a variability and the related SST drivers

To analyze the variability of the distribution patterns of Chl-a in the northern Alboran Sea (nAS, henceforth), an empirical orthogonal function (EOF) analysis (Lorenz, 1956; Preisendorfer and Mobley, 1988) of anomalous Chl-a concentration within this area has been performed. Widely used in climate and oceanography studies, the EOF tool is very successful in comprising the complex variability of an original data set into a few number of modes while retaining most of the total variance. This statistical technique is used here to determine the directions in which the maximum variability of the anomalous Chl-a field, mathematically described in a two-dimensional space-time matrix, is organized over the Alboran Sea. By diagonalizing the corresponding covariance matrix, we obtain the EOFs (eigenvectors), the percentage of variance explained by each mode (normalized eigenvalue), and the principal components (associated time evolution as a result of the projection of the original anomalous field onto the EOFs). A simple Chl-a index defined as the spatially averaged Chl-a anomalies over the nAS has been obtained to be compared with the EOF results. The possible links between the Chl-a interannual variability in the nAS and remote SST forcings has been analyzed in terms of linear regression maps. To infer the dynamical atmospheric mechanisms at interplay, regression maps of a Chl-a time series (principal component from the EOF) onto SLP and surface winds have been also obtained.

2.3 Exploring the predictive potential

The predictive skill at seasonal time scales has been assessed using cross-validated hindcasts based on the maximum covariance analysis (MCA) methodology (Bretherton et al., 1992; Suárez-Moreno and Rodríguez-Fonseca, 2015). MCA performs a singular value decomposition of the covariance matrix compounded by a predictor and a predictand field in such a way that the covariance of the associated expansion coefficients (timeseries) of the resultant modes is maximized. In the present study, the anomalous Chl-a concentration in spring (averaged in March–April) is identified as the variable to be predicted (i.e., the predictand field). On the other hand, the SST anomalies averaged over specific regions and at different monthly lags with respect to the Chl-a signal are used as the predictor fields. In particular, we retain the first three modes of variability from the MCA to predict the Chl-a response from the SST signal through a simple regression model, as follows:

$$\widehat{Z} \approx \left(\sum_{m=1}^{M=3} (Psi \cdot Y)\right) \quad (1)$$

With $\hat{Z}$ being the prediction of the anomalous Chl-a field (Z) and Y the anomalous SST field within a particular region and at a certain time lag. The coefficient *Psi* is obtained from the MCA with information provided by the resultant modes. The cross-

validation technique is applied to obtain a full record of the predicted Chl-a field. To this aim, and considering *nt* as the number of times of our fields, the MCA is repeated *nt* times by leaving out one time in the *Z* and *Y* fields each time. Thus, for each time *t*, *Psi* is calculated and $\hat{Z}$ is predicted from *Y* once the specific time *t* is omitted. The skill is quantified in terms of the anomaly correlation coefficient (ACC) in both time and space. In space, for each gridpoint, the Chl-a hindcast ($\hat{Z}$) is correlated in time with the observed Chl-a (*Z*). In time, for each time step, the simulated spatial map of Chl-a is correlated in space with the observed Chl-a. The robustness of the analysis is assessed by representing the squared covariance fraction and the expansion coefficients (time series associated with the MCA modes) obtained for each realization of the cross-validation procedure. In this way, we can analyze if the prediction is robust or, on the contrary, it is biased to a particular time.

The statistical significance of all our results have been assessed either by a bootstrap analysis with replacement or by a Student t-test that accounts for the autocorrelation of time series through the calculation of effective degrees of freedom (Bretherton et al., 1999). In all cases, the significant results are shown at a minimum of 95% confidence level (p-values less than 0.05).

3 Results

3.1 Chl-a interannual variability in the Alboran Sea

As a starting point of analysis, the seasonal cycle of Chl-a concentration (i.e., the monthly evolution along the year) has been obtained from 1998 to 2020 (not shown), finding the maximum abundance and interannual variability (in terms of the standard deviation) over the nAS in March and April. This peak in spring is consistent with previous studies within the study region (see, e.g., Ramírez et al., 2005). Then, to investigate the interannual variability of this peak of Chl-a in spring, an EOF analysis of the anomalous Chl-a concentration (averaged in March–April) within the nAS has been made. Before the EOF, all monthly anomalies are calculated by subtracting the corresponding climatology, and the effect of the long-term trends has been reduced by removing a first-order polynomial (i.e., linear trend) from all the anomalies. The resultant leading EOF explains the 63% of the total variance and is characterized by a wide area along the Spanish coast with statistically significant positive anomalies (Figure 2A). In contrast to the second and third modes, the physically meaningful identity of this leading mode is supported using the method proposed by North et al. (1982) (see Figures S1, S2 of Supplementary Material for details). Furthermore, the link between this leading mode and the Chl-a abundance along the Spanish coast is reinforced by the fact that the related time evolution (i.e., the leading principal component) also emerges by simply averaging the Chl-a anomalies within the nAS during late winter and spring months (Figure 2C). Different combinations of months (from January to April) are selected to calculate this Chl-a index, and time correlations with our Chl-a principal component of ~0.8 are found in them all.

The Chl-a pattern shown in Figure 2A has been documented in the past in relation to the upwelling of nutrient-rich waters (Baldacci et al., 2001; Basterretxea et al., 2018). It is specially marked within the Malaga Bay and largely extends offshore at approx. 3–3.5°W. As a result, two wide areas with negligible anomalies to the west and to the east are found. As can be seen in Figure 2A, the highest values of Chl-a roughly follow the spatial structure of the AJ waters (compare with Figure 1). This occurs because the water transported offshore due to the Ekman transport sinks where it meets the less dense AJ water. Another consequence of the aforementioned is that the pattern of our Chl-a mode is linked to the WAG and EAG gyres, with both structures located to the south of the AJ front and considered as convergence and oligotrophic zones associated with their anticyclonic gyres.

The link of our Chl-a variability mode with upwelling is consistent with the regression map of the associated principal component onto the sea surface temperature (SST) anomalies (Figure 2B). Thus, as expected, the upwelling zone identified within a narrow band along the coast is related not only to a significant increase in Chl-a abundance but also to a significant SST cooling associated with the rise of cold waters from below.

3.2 Link with the large-scale climate

As shown in Figure 3 (right panels), the aforementioned leading Chl-a mode begins to develop in February–March east of Cape Gata. This fact responds to the occurrence of wind-driven upwelling along this part of the Iberian Peninsula. In March–April, westerlies are anomalously strong over the nAS and, as a consequence, the upwelling signature (Chl-a and SST) emerges very clearly. This coherence between anomalous Chl-a and anomalous westerlies reinforces the link of our Chl-a mode to the wind-driven upwelling associated with the Ekman transport, which is particularly important in coastal and continental shelf waters (Sarhan et al., 2000). The proposed role of wind-driven upwelling is also consistent with the intense upwelling in spring in Alboran in coincidence with stronger westerlies (Ramírez et al., 2005). The anomalous signal of Chl-a (and SST) keeps visible in April–May and begins a progressive decline from May-June onward, in agreement with the documented evolution of Chl-a and primary production in the region (Lazzari et al., 2011). In the context of the North Atlantic atmospheric circulation (see Figure 3; left panels), the related SLP configuration over the North Atlantic changes from a negative NAO-like pattern in February–March to a wavy-like structure in April–May. Please

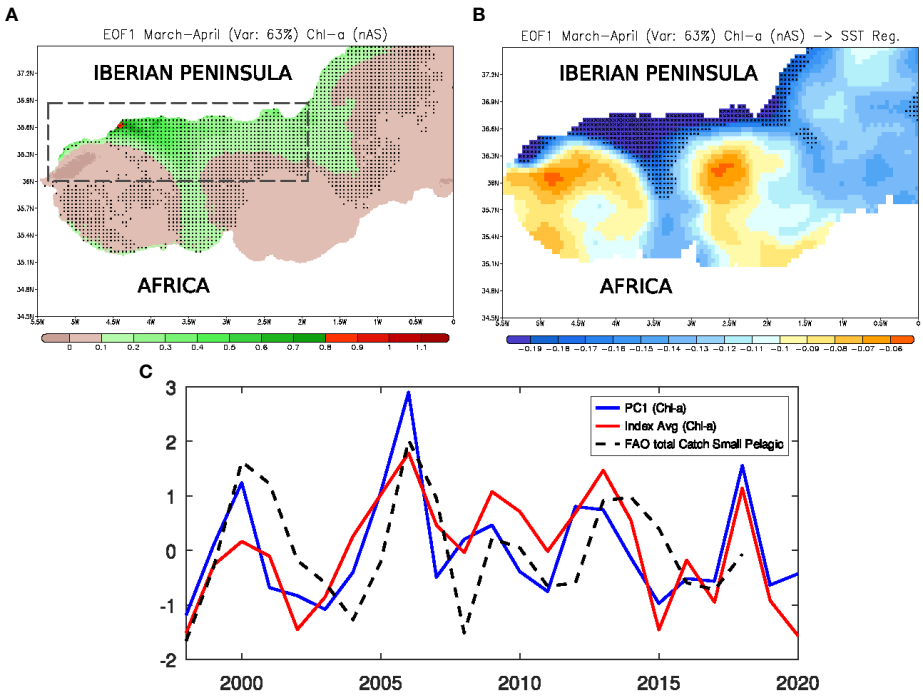

FIGURE 2
(A) Regression map of the leading empirical orthogonal function (EOF) of monthly Chl-a anomalies averaged in March–April and calculated over the nAS (see dashed box) onto the same Ch-a anomalies over the whole Alboran Sea (units in mg/m^3 per standard deviation of PC1). **(B)** Regression map of the Chl-a leading mode onto the SST anomalies averaged in March–April (units in degrees per standard deviation of PC1). **(C)** Principal component (PC1) associated with the Ch-a leading mode in March–April over the nAS (blue line), evolution of Ch-a anomalies averaged in January–April over the nAS (red line), and annually and spatially averaged catches of small pelagic species within the nAS (dashed black line). Black points indicate areas where the response is significant (p-values less than 0.02) according to a bootstrap analysis with replacement (with 500 bootstrap replications).

note how, in particular, the triggering of the upwelling favorable winds over the nAS in March–April coincides with the appearance of an anomalous low-pressure system over the British Islands and the weakening of the north–south (i.e., NAO-like) SLP structure over the North Atlantic.

To identify the potential SST drivers of these changes over the North Atlantic SLP, which in turn generate the anomalous winds behind our Chl-a response in Alboran, the regression map of the Chl-a mode (i.e., the associated principal component; see Figure 2C) onto the global SST is obtained at different monthly lags (Figure 4). In particular, we plot the statistically significant SST signals linked to our Chl-a mode from April to May of the previous year (lag -11) to March–April simultaneously with the Chl-a response (lag 0). Furthermore, the SLP (contoured in Figure 4) and the surface wind (vectored in Figure 4) are also shown to broadly address the monthly evolution of the atmospheric conditions along time.

As observed in Figure 4, two main areas with significant SST anomalies emerge: the central-western SSTs over the Tropical North Atlantic from lag -11 (April–May of year -1) to lag -6 (September–October of year -1) and the tropical Pacific SSTs from lag -4 (November–December of year -1) to lag 0 (March–April of year 0). This result suggests a link between the Tropical North Atlantic (hereinafter TNA) SSTs in spring-summer and the tropical Pacific SSTs in the following winter in such a way that warm (cold) conditions in the TNA favor the development of a La Nina (El Nino) event in the Pacific. This teleconnection has been documented during the last years (Ham et al., 2013; Wang et al., 2017) and is sustained by the excitation of an atmospheric Rossby wave from the TNA that propagates westward. In this way, when an anomalous warming occurs in the TNA, this atmospheric wave activity causes northeasterly wind anomalies over the subtropical northeastern Pacific, the development of cold SST anomalies in the subsequent seasons, and finally, the initiation of a La Nina episode in the tropical Pacific. The opposite impact (i.e., El Nino signal over the Pacific) broadly occurs when the TNA is cooler than usual in spring–summer. Please notice how the abovementioned northeasterly winds are identified in Figure 4 just before the appearance of the first significant SST anomalies in the eastern equatorial Pacific (see September–October and October–November panels in Figure 4). In parallel, a low-level anticyclone has been induced to the west, which in turn generates the development of La Nina event.

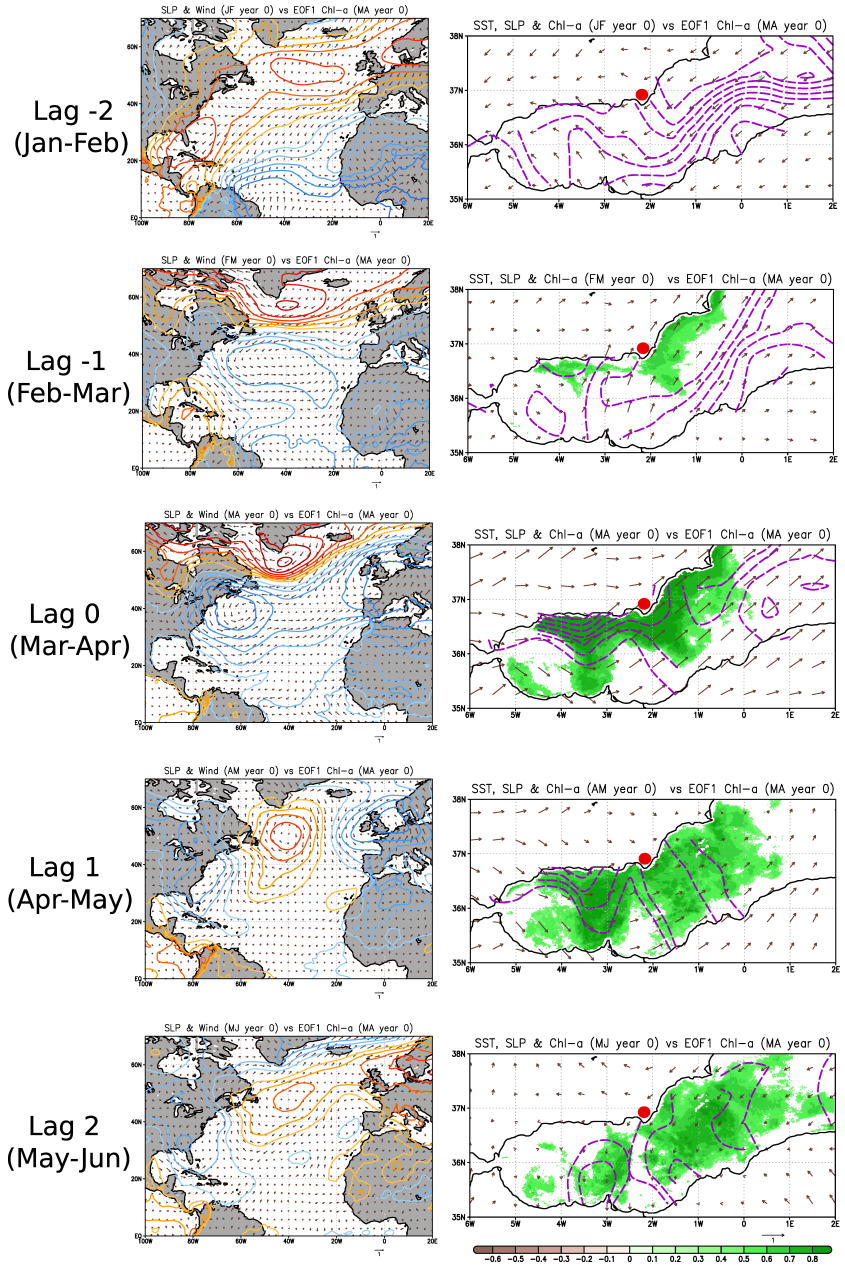

FIGURE 3
Regression maps, at different time lags, of the anomalous Chl-a variability mode calculated in March–April and within the nAS (PC1; see Figure 2C), onto 1) anomalous SLP (contoured with ci = 0.1 Pa; positive values in red colors and negative values in blue colors) and surface wind (vectors; unit in m/s) within the North Atlantic (left panels) and 2) anomalous SST (contoured; ci = 0.1 degrees), surface wind (vectors; unit in m/s), and Chl-a (shaded; units in mg/m^3) within the Alboran Sea (right panels). Only those Chl-a anomalies which are statistically significant (p-values less than 0.05) based on a Student t-test are shown. For illustrative purposes, red point highlights the location of Cape Gata.

To understand the role of these remote SST anomalies in the development of our Chl-a mode in Alboran, it is interesting to assess the evolution of the atmospheric conditions over the Atlantic sector. In particular, Figure 4 shows how the previously mentioned transition of the SLP over the North Atlantic, from a dipolar structure in winter to a wavy structure in spring (see also Figure 3), occurs in parallel to the evolution of the La Nina episode in the Pacific. Furthermore, over the equatorial Atlantic, negative SLP anomalies (i.e., a cyclone circulation) get higher as the low-level anticyclone over the equatorial Pacific increases. The teleconnection mechanisms behind these changes of the atmospheric conditions over the

10.3389/fmars.2022.931832

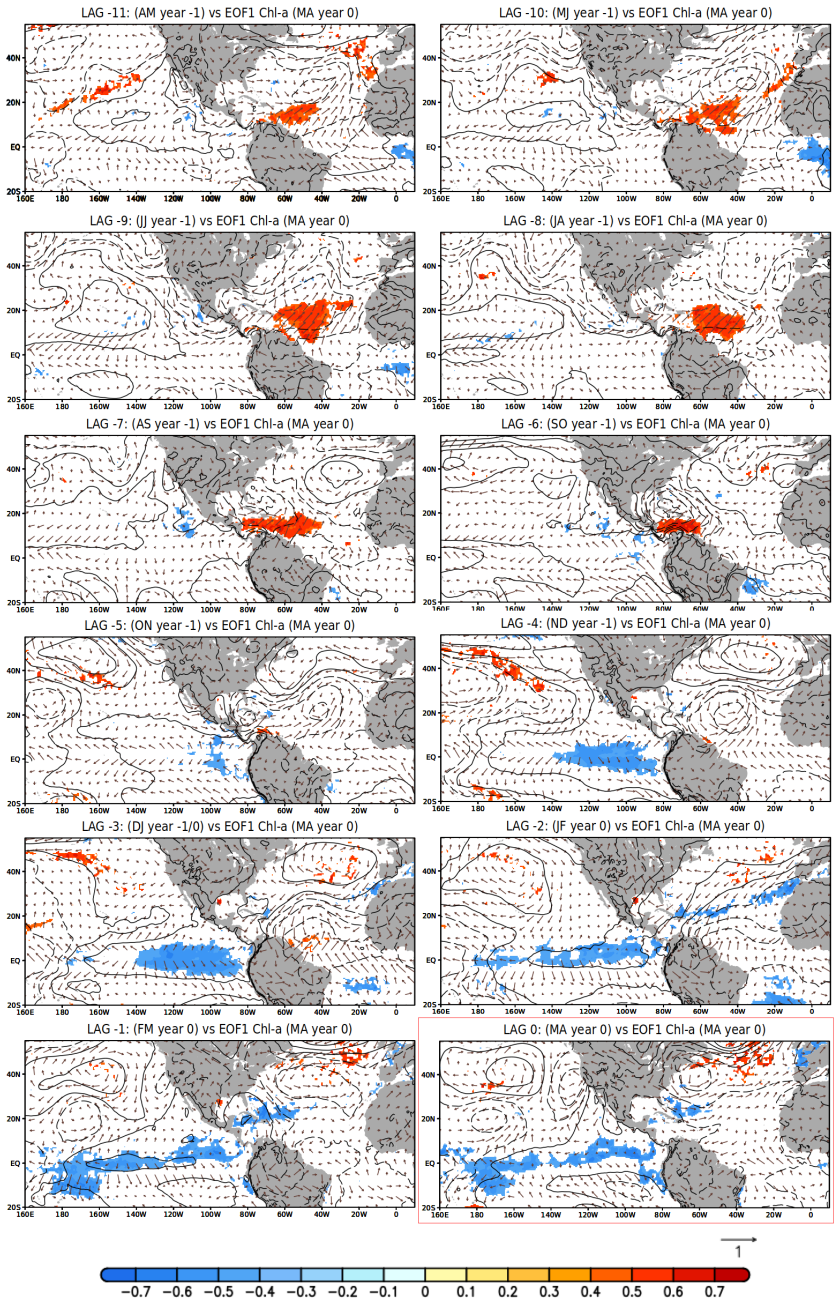

FIGURE 4
Regression maps, at different lags, of the Chl-a variability mode calculated in March–April and within the nAS (PC1; see Figure 2C), onto 1) SST anomalies (shaded; units in degrees), 2) sea level pressure anomalies (contoured with ci = 0.1 **Pa**; positive values in solid lines and negative values in dashed lines), and 3) surface wind anomalies (vectors; unit in m/s). From top-left to bottom-right panels, the responses from April to March of the previous year (lag -11) to March–April of year 0 (lag 0; highlighted in red). The corresponding lag is shown on top of each panel. Only those SST anomalies which are statistically significant (p-values less than 0.05) based on a Student t-test are shown.

Atlantic basin in parallel to the evolution of the ENSO event have been deeply analyzed in the past and are out of the scope of the present study. In particular, the wavy signature over the North Atlantic mainly responds to the triggering of atmospheric Rossby waves from the tropical Pacific to the North Atlantic sector through the troposphere (see, e.g., Jiménez-Esteve and Domeisen, 2018) and the stratosphere (see, e.g., Ayarzagüena et al., 2018), while the impact on the equatorial Atlantic is mainly linked to the alteration of the thermally driven direct circulation (i.e., the atmospheric Walker and Hadley cells) in

relation to variations in the anomalous convection (see, e.g., Chang et al., 2006). In either case, a clear consequence of the aforementioned evolution of the SLP structures over the Atlantic is that the anomalous surface winds over the Alboran region change from northeasterlies in winter to westerlies in spring (Figure 4), which ultimately seems to generate the emergence of our Chl-a variability mode (Figure 3). In the following section, the potential of this teleconnection between Chl-a and remote SSTs for long-range predictability is assessed in detail.

3.3 Assessing the potential predictability

The regression maps in Figure 4 do not represent real covariability patterns but a combination of patterns which are coupled to the Chl-a variability in the nAS. These maps allow exploring those possible regions, such as the TNA and the tropical Pacific, susceptible to act as forcings (and predictors) of the Chl-a abundance in Alboran.

In order to find real covariability patterns of SST and Chl-a and to better understand the spatiotemporal distribution of anomalous primary production in relation to a specific ocean forcing, a MCA is needed. Accordingly, two MCAs have been performed here: the first assessing the link between the TNA SSTs in August–September (lag -7) and the Chl-a concentration in the following March–April (lag 0), and the second assessing the link between the tropical Pacific SSTs in November–December (lag -4) and the Chl-a concentration in the following March–April (lag 0). The resultant modes of covariability are shown, for each case, in Figures 5, 6.

In the case of the TNA (Figure 5), the leading mode presents significant SST anomalies in the whole tropical Atlantic region in association with significant responses in Chl-a concentration along the Spanish coast. The second mode is related to an anomalous zonal SST dipole with significant anomalies in the eastern side of the TNA, together with anomalous Chl-a concentrations by the north of the WAG. This structure of anomalous Chl-a seems to be indicating an anomalous upwelling (downwelling) response due to an anomalous cyclonic (anticyclonic) gyre, both in turn linked to an anomalous warming (cooling) in the eastern TNA. These two modes, which account for almost 50% of the total covariance, reinforce the cause-and-effect relationship suggested from Figure 4: a warming (cooling) of the TNA is significantly related to more (less) Chl-a concentrations in the coastal margin of the nAS.

In the case of the tropical Pacific (Figure 6), the covariability is clearly dominated by the leading mode, which accounts by itself for more than 50% of the total covariance. As expected, a characteristic ENSO SST pattern emerges in association with this leading mode in such a way that positive (El Nino) and negative (La Nina) SST signals in the Pacific are related to a decrease and an increase in Chl-a concentration along the Spanish coast, respectively.

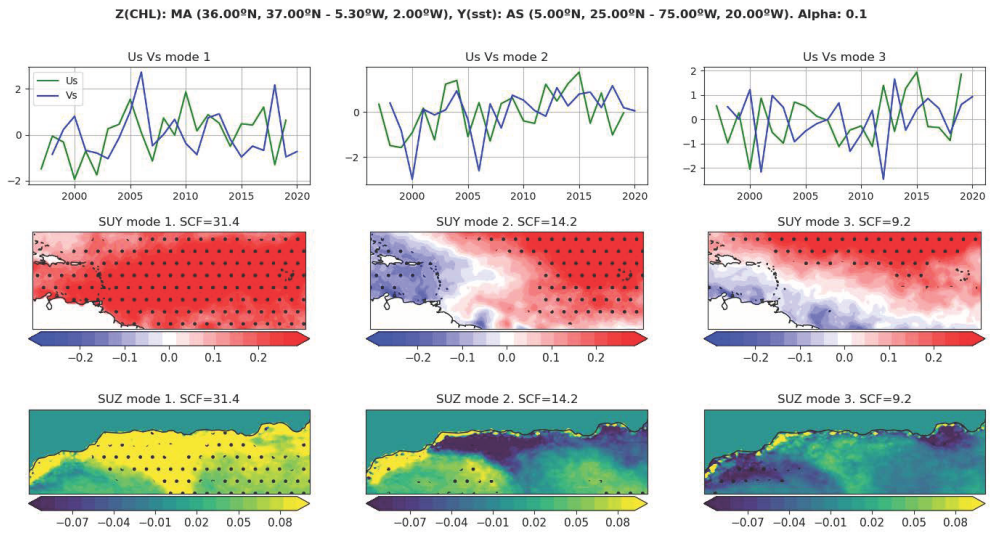

FIGURE 5
Three first covariability modes between TNA SSTs in August–September (predictor field) and Chl-a concentration in the following March–April in nAS (predictand field). From left to right, the leading, second, and third modes. From top to bottom, the associated expansion coefficients (Us for the predictor field and Vs for the predictand field), spatial pattern of the predictor field (anomalous SST; units in degrees per standard deviation in Us), and spatial pattern of the predict and field (anomalous Chl-a; units in mg/m^3 per standard deviation in Us). Black marks in maps indicate statistically significant signals (p-values less than 0.05) based on a Student t-test. Central and bottom panels show, on top, the percentage of covariation explained by each pair of spatial patterns.

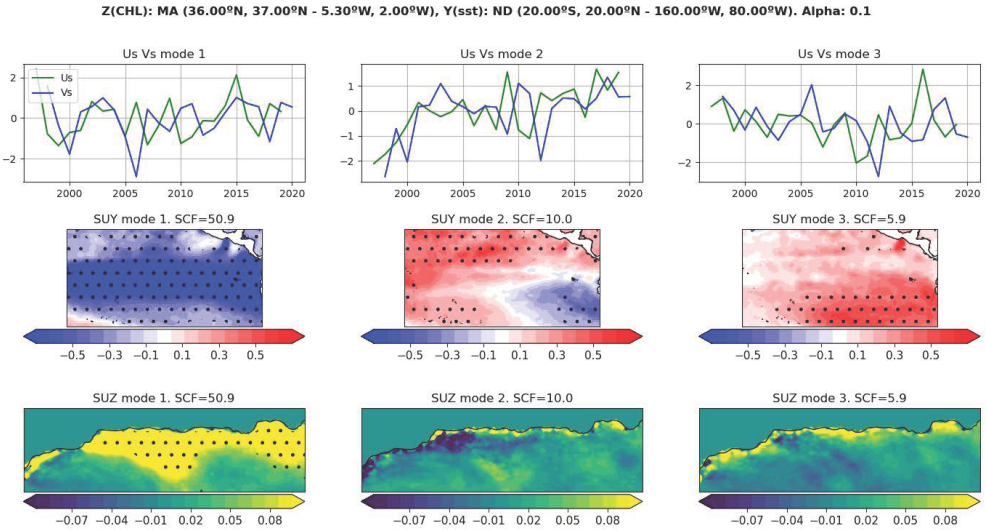

FIGURE 6
As Figure 5 but using the tropical Pacific SSTs in November–December (lag -4) as predictor.

Here, the covariability modes shown in Figures 5, 6 have been used as a basis for quantifying the skill of both TNA SSTs and Pacific SSTs to predict the Chl-a abundance in Alboran at different time lags. To this aim, a simple regression model is built and the predicted Chl-a signal is assessed through a leave-one-out cross-validation procedure (see subsection 2.3). Our results show how the ENSO-related SSTs in November–December allow to robustly predict the Chl-a concentration in March–April along the Spanish coast (Figure 7A), that is, the Chl-a signal linked to the wind-driven upwelling (see Figure 3; central panels). As expected, this skill is not stationary in time, finding years for which the spatial correlation between the predicted Chl-a pattern and the observed Chl-a pattern is higher than others (Figure 7B). The associated squared covariance fraction (Figure 7C), stable at ~0.5 along the analyzed period, reinforces the robustness of the tropical Pacific SSTs in late fall (November–December) to predict the wind-driven distribution pattern of Chl-a in nAS in spring (March–April).

On the contrary, the TNA SSTs in August–September allow to significantly predict the Chl-a concentration in March–April offshore, in particular by the north of the WAG and the EAG (Figure 7D). This skill, reasonably robust in terms of the related squared covariance fraction (Figure 7F), indicates that the Chl-a concentration in spring to the north of the WAG and the EAG might be predicted (at least for certain years; see Figure 7E) with 7 months in advance.

Continuing with the TNA, it is interesting to note that the leading and second covariability modes shown in Figure 5 indicate a similar but opposite link between TNA and coastal upwelling: warm conditions in western TNA with positive Chl-a anomalies on the one hand (left panels in Figure 5) and warm conditions in central TNA with negative Chl-a anomalies on the other hand (central panels in Figure 5). This result suggests that retaining both the leading and second covariability modes to predict the coastal Chl-a response may not be the best choice. Indeed, one can notice in Figures 5, 6 (see bottom-left panels) the remarkable similarity of Chl-a patterns identified in relation to the TNA-related (bottom-left panel in Figure 5) and ENSO-related (bottom-left panel in Figure 6) leading modes. This feature is consistent with the SST evolution shown in Figure 4 and suggests that, in the case of the TNA, the prediction based solely on the leading covariability mode (i.e., based on the western TNA SSTs) might allow to enhance the predictive power (from 4 to 7 months) in those years when warm (cold) TNA conditions in August–September trigger a La Nina (El Nino) event in the following winter. To illustrate this role of western TNA to anticipate the prediction of coastal Chl-a, please see the prediction of Chl-a concentration in 2006 made from both the TNA SSTs in August–September 2005 and the Pacific SSTs in November–December 2005 (Figure S3 of Supplementary Material).

4 Brief summary and final discussion

This study demonstrates that the Chl-a concentration in boreal spring along the northern flank of the Alboran Sea can be predicted, at least for certain years, by solely considering climate information. The explanation lies in the fact that El Niño Southern Oscillation (ENSO) can trigger the development of anomalous distribution patterns of Chl-a in Alboran. The underlying mechanisms are associated with the well-known alteration of the SLP configuration over the North Atlantic European sector in the spring following the peak of ENSO (see, e.g., Brönnimann, 2007). This remote and

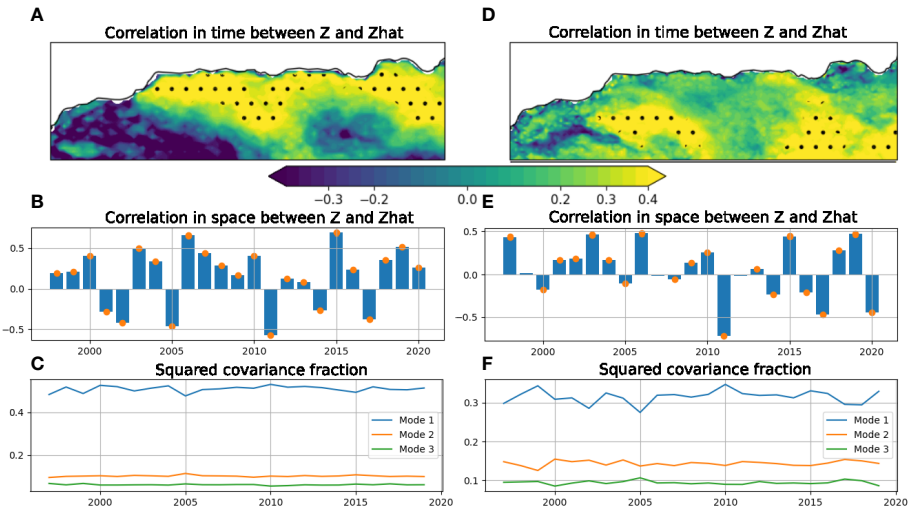

FIGURE 7
Cross-validated hindcast based on MCA (see Section 2.3). From top to bottom: for each spatial location, correlation in time between the observed and the predicted Chl-a signal **(A, D)**; for each time, correlation in space between the observed and the predicted Chl-a signal (b,e); and squared covariance fraction explained by each MCA mode **(C, F)**. Left panels show the Chl-a prediction in March–April from the Pacific SSTs in the previous November–December (lag -4); right panels show the Chl-a prediction in March-April from the TNA SSTs in August–September (lag -7). Black marks in the upper panels indicate statistically significant signals (p-values less than 0.05), based on a Student t-test.

lagged signal of ENSO impacts the western Mediterranean, modifying the winds blowing the Alboran region and the related wind-driven upwelling taking place along the southern Spanish coast in spring. As a result, the Chl-a concentration at the surface is modified. Considering the linear nature of our calculations, a high (low) Chl-a concentration in the nAS in spring is expected for La Niña (El Niño) conditions in winter over the tropical Pacific.

As mentioned, the teleconnection linking ENSO and the North Atlantic atmospheric circulation have been well evaluated in the past (García-Serrano et al., 2011; Jiménez-Esteve and Domeisen, 2018 and Hardiman et al., 2019, among others). Here, we provide a step forward in the understanding of how these large-scale climate links influence the Chl-a concentration in the coastal margin of the nAS. Furthermore, we explore the predictability of this Chl-a response from the remote SST forcings by designing a statistical regression model based on a maximum covariance analysis (MCA). This prediction, based on a 1-year *leave-out* cross-validated hindcast, has been quality-assessed and confirms that the coastal Chl-a concentration in the nAS can be reasonably well predicted, during El Nino/La Nina years, 4 months in advance. Furthermore, in those years when a significant TNA warming (cooling) precedes La Niña (El Niño) event, the aforementioned coastal Chl-a response in Alboran might be predicted over at least 7 months in advance. The role played by the amplitude of these potential SST forcings (ENSO and TNA) in modifying the time lag with respect to the related Chl-a response in Alboran has been analyzed, but no clear relationship emerges (Figure S4). The TNA SSTs in summer also allow for the prediction of another Chl-a response in Alboran in the following spring. This signal, identified offshore by the north of the WAG and the EAG (Figure 7D), does not seem to be associated with the wind-driven upwelling but with the upwelling processes associated with instabilities in the Atlantic Jet. In any case, this role of the TNA as predictor of upwelling in northern Alboran must be deeply assessed in future works.

It is important to note the fact that Chl-a concentration has been repeatedly linked in the past with upwelling (see, e.g., Ramírez et al., 2005). The limitation for directly computing physical upwelling in studies such as ours is the need of combining long (20 years or more) and high-resolution (10 km or less) datasets. However, the consistency between our Chl-mode (Figure 2A) and its related signature on the anomalous Ekman pumping (Figure S5) reinforces the link with upwelling. However, caution must be exercised when using Chl-a as a *proxy* of upwelling.

This work provides more relevant questions to be faced in future studies. For example, it is interesting to evaluate the persistence of our Chl-a response in spring. As shown in Figure 3, the statistically significant anomalies of Chl-a begin in February–March along the continental coast and persist offshore beyond the spring season. Where is this anomalous Chl-a signal supposed to go? Which other processes and related impacts are implied? These questions should be analyzed in detail in future works to better understand the role of our proposed teleconnection (ENSO influence on Chl-a in Alboran) in a wider context related to the Chl-a variability in the western Mediterranean.

Another interesting aspect to be further analyzed in the future is whether a bottom-up propagation of the climate-related signal across the marine food web subsequently takes place. To

preliminary assess this hypothesis, the annually and spatially averaged catches of small pelagic species within the Alboran Sea have been calculated (see dashed line in Figure 2C) considering Sea Around Us Project data (https://www.seaaroundus.org/). Notice that small pelagic fishes, which quickly respond to changes in the ocean conditions, are among the most economically valuable fisheries resources and represent a vital intermediate connection between plankton and large predatory species (Cury et al., 2000). In particular, the evolution of this fish group correlates with our Chl-a variability mode at lag 0 (r = 0.49; p-value less than 0.01) and at lag +1 (r = 0.72; p-value less than 0.001). The non-parametric test described by Ebisuzaki (1997), and specially designed to avoid serial correlation, is used to quantify these correlations. The marked 1-year lagged relationship is consistent to the proposed influence of Chl-a concentration in northern Alboran on the sardine abundance in the following year (Vargas-Yáñez et al., 2020). According to the latter work, food availability in autumn/winter in northern Alboran strongly influences the body condition of spawners and the annual recruitment success of the following year. Thus, those years with enhanced (reduced) Chl-a concentrations in spring would generate favorable (unfavorable) hatching periods in autumn/winter and higher (lower) recruitment success and annual landings in the following year. This mechanism would explain the marked 1-year relationship identified here between our Chl-a mode and the catches of small pelagic fishes in northern Alboran and suggests that the ENSO signature (and its related predictability) might reach the fish level. However, deeper analyses are absolutely needed to better identify and understand the processes behind and the possible related predictability (cf. Gómara et al., 2021 as example in the tropical Pacific).

Overall, we can conclude that the implications of our results is twofold. Firstly, instead of directly correlating our Chl-a-related timeseries with well-known indices such as NAO or ENSO in efforts to identified remote forcings, we address potential predictors of Chl-a in Alboran through the use of global SST regression maps at different monthly lags. This approach gives a comprehensive vision of the predictor pattern and evolution, allows finding unexpected predictors (such as the TNA here), and considers separately their associated variabilities. Secondly, this information is applied to provide a useful springboard for implementing a simple and computationally inexpensive seasonal prediction system of primary productivity in the nAS, by solely considering climate information. Nevertheless, as mentioned, many interesting aspects emerge from this study, which must be necessarily faced in future works.

Data availability statement

All data used in this study are open and available to any qualified researcher, and comply with the FAIR principle (findable, accessible, interoperable, and reusable).

Author contributions

JLP conceived the research, partially made the calculations and wrote most of the manuscript. IG significantly contributed in both the calculations and the manuscript. BRF was mainly concerned on assessing the model prediction and skill, with relevant feedbacks in the manuscript. JGL also contributed in the writing process, in particular on those aspects more related to the ocean dynamics. All authors contributed to the article and approved the submitted version.

Funding

JL-P was supported by a Postdoctoral Fellowship from the Research Own Plan of the University of Málaga ("Ayuda de Incorporación de Doctores 2020"). Thanks are also given to the projects EU-H2020 TRIATLAS (No 817578) and CARMEN (PCI2021-122061-2B), the latter funded by both the Spanish Government (MCIN/AEI/10.13039/501100011033) and the European Union (NextGenerationEU/PRTR).

Acknowledgments

The authors want to thank Pablo Durán-Rodríguez for the integration of the statistical python code in a user-friendly tool, which has let us to perform, in an efficient way, the different simulations done in this paper. Thanks are also due to Irene Nadal for her contribution in designing Figure 1 and to Simone Sammartino for useful discussions. Finally, we would like to thank the anonymous reviewers for their constructive suggestions and advice, which considerably improved the original manuscript.

Conflict of interest

The authors declare that the research was conducted in the absence of any commercial or financial relationships that could be construed as a potential conflict of interest.

Publisher's note

Supplementary material

The Supplementary Material for this article can be found online at: https://www.frontiersin.org/articles/10.3389/fmars.2022.931832/full#supplementary-material

References

Ayarzagüena, B., Ineson, S., Dunstone, N. J., Baldwin, M. P., and Scaife, A. A. (2018). Intraseasonal Effects of El niño–Southern Oscillation on North Atlantic Climate. *J. Climate* 31, 8861–8873. doi: 10.1175/JCLI-D-18-0097.1

Baldacci, A., Corsini, G., Grasso, R., Manzella, G., Allen, J., Cipollini, P., et al. (2001). A study of the Alboran sea mesoscale system by means of empirical orthogonal function decomposition of satellite data. *J. Mar. Syst.* 29, 293–311. doi: 10.1016/S0924-7963(01)00021-5

Basterretxea, G., Font-Muñoz, J. S., Salgado-Hernanz, P. M., Arrieta, J., and Hernández-Carrasco, I. (2018). Patterns of chlorophyll interannual variability in Mediterranean biogeographical regions. *Remote Sens. Environ.* 215, 7–17. doi: 10.1016/j.rse.2018.05.027

Bjerknes, J. (1969). Atmospheric teleconnections from the equatorial pacific. *Monthly weather Rev.* 97, 163–172. doi: 10.1175/1520-0493(1969)097<0163:ATFTEP>2.3.CO;2

Bosc, E., Bricaud, A., and Antoine, D. (2004). Seasonal and interannual variability in algal biomass and primary production in the Mediterranean sea, as derived from 4 years of seawifs observations. *Global Biogeochemical Cycles* 18 (1), 1–17. doi: 10.1029/2003GB002034

Bretherton, C. S., Smith, C., and Wallace, J. M. (1992). An intercomparison of methods for finding coupled patterns in climate data. *J. Climate* 5, 541–560. doi: 10.1175/1520-0442(1992)0050541:AIOMFF2.0.CO;2

Bretherton, C., Widmann, M., Dymnikov, V., Wallace, J., and Blade, I. (1999). Effective number of degrees of freedom of a spatial field. *J. Climate* 12, 1520–0442. doi: 10.1175/1520-0442(1999)012<1990:TENOSD>2.0.CO;2

Brönnimann, S. (2007). Impact of El niño-southern oscillation on European climate. *Rev. Geophysics* 45, RG3003. doi: 10.1029/2006RG000199

Cassou, C. (2010). "Euro-Atlantic regimes and their teleconnections," in *Proceedings: ECMWF seminar on predictability in the European and Atlantic regions*, 6–9. (Reading, United Kingdom:ECMWF).

Chang, P., Fang, Y., Saravanan, R., Ji, L., and Seidel, H. (2006). The cause of the fragile relationship between the pacific el niño and the atlantic niño. *Nature* 443, 324–328. doi: 10.1038/nature05053

Cury, P., Bakun, A., Crawford, R. J., Jarre, A., Quinones, R. A., Shannon, L. J., et al. (2000). Small pelagics in upwelling systems: patterns of interaction and structural changes in "wasp-waist". *ecosystems. ICES J. Mar. Sci.* 57, 603–618. doi: 10.1006/jmsc.2000.0712

Ebisuzaki, W. (1997). A method to estimate the statistical significance of a correlation when the data are serially correlated. *J. Climate* 10, 2147–2153. doi: 10.1175/1520-0442(1997)010<2147:AMTETS>2.0.CO;2

Garcia-Gorriz, E., and Carr, M.-E. (2001). Physical control of phytoplankton distributions in the Alboran sea: a numerical and satellite approach. *J. Geophysical Research: Oceans* 106, 16795–16805. doi: 10.1029/1999JC000029

García-Serrano, J., Rodríguez-Fonseca, B., Bladé, I., Zurita-Gotor, P., and de la Cámara, A. (2011). Rotational atmospheric circulation during north Atlantic-European winter: the influence of ENSO. *Climate Dynamics* 37, 1727–1743. doi: 10.1007/s00382-010-0968-y

García-Lafuente, J., Cano, N., Vargas, M., Rubın, J. P., and Hernandez-Guerra, A. (1998). Evolution of the Alboran sea hydrographic structures during july 1993. *Deep Sea Res. Part I: Oceanographic Res. Papers* 45, 39–65. doi: 10.1016/S0967-0637(97)00216-1

Gómara, I., Rodríguez-Fonseca, B., Mohino, E., Losada, T., Polo, I., and Coll, M. (2021). Skillful prediction of tropical pacific fisheries provided by atlantic niños. *Environ. Res. Lett.* 16, 054066. doi: 10.1088/1748-9326/abfa4d

Gómara, I., Rodríguez-Fonseca, B., Zurita-Gotor, P., Ulbrich, S., and Pinto, J. G. (2016). Abrupt transitions in the nao control of explosive north atlantic cyclone development. *Climate dynamics* 47, 3091–3111. doi: 10.1007/s00382-016-3015-9

González-Lanchas, A., Flores, J.-A., Sierro, F. J., Bárcena, M. Á., Rigual-Hernández, A. S., Oliveira, D., et al. (2020). A new perspective of the Alboran upwelling system reconstruction during the marine isotope stage 11: A high-resolution coccolithophore record. *Quaternary Sci. Rev.* 245, 106520. doi: 10.1016/j.quascirev.2020.106520

Ham, Y.-G., Kug, J.-S., Park, J.-Y., and Jin, F.-F. (2013). Sea Surface temperature in the north tropical atlantic as a trigger for el niño/southern oscillation events. *Nat. Geosci.* 6, 112–116. doi: 10.1038/ngeo1686

Hardiman, S. C., Dunstone, N. J., Scaife, A. A., Smith, D. M., Ineson, S., Lim, J., et al. (2019). The impact of strong el niño and la niña events on the north atlantic. *Geophysical Res. Lett.* 46, 2874–2883. doi: 10.1029/2018GL081776

Hersbach, H., Bell, B., Berrisford, P., Biavati, G., Horányi, A., Muñoz Sabater, J., et al. (2018). ERA5 hourly data on single levels from 1979 to present, copernicus climate change service (c3s) climate data store (cds). *ECMWF* 147, 5–6.

Huang, B., Liu, C., Banzon, V., Freeman, E., Graham, G., Hankins, B., et al. (2021). Improvements of the daily optimum interpolation sea surface temperature (doisst) version 2.1. *J. Climate* 34, 2923–2939. doi: 10.1175/JCLI-D-20-0166.1

Jiménez-Esteve, B., and Domeisen, D. I. (2018). The tropospheric pathway of the enso–north atlantic teleconnection. *J. Climate* 31, 4563–4584. doi: 10.1175/JCLI-D-17-0716.1

Katara, I., Illian, J., Pierce, G. J., Scott, B., and Wang, J. (2008). Atmospheric forcing on chlorophyll concentration in the Mediterranean, In V. D Valavanis (eds) *Essential fish habitat mapping in the Mediterranean. Developments in Hydrobiology,* (Dordrecht:Springer), 33–48. doi: 10.1007/978-1-4020-9141-4_4

Lazzari, P., Solidoro, C., Ibello, V., Salon, S., Teruzzi, A., Béranger, K., et al. (2011). Seasonal and inter-annual variability of plankton chlorophyll and primary production in the Mediterranean sea: a modelling approach. *Biogeosciences Discussions* 8, 5379 lazzari2011. doi: 10.5194/bgd-8-5379-2011

Lorenz, E. N. (1956). Empirical orthogonal functions and statistical weather prediction. *Technical report, Statistical Forecast Project Report 1, Dep. of Meteor.* MIT, 49.

Losada, T., Rodríguez-Fonseca, B., Mechoso, C., and Ma, H. (2007). Impacts of sst anomalies on the north atlantic atmospheric circulation: a case study for the northern winter 1995/1996. *Climate dynamics* 29, 807–819. doi: 10.1007/s00382-007-0261-x

Macías, D., Navarro, G., Echevarría, F., García, C., and Cueto, J. (2007). Phytoplankton pigment distribution in the northwestern Alboran sea and meteorological forcing: A remote sensing study. *J. Mar. Res.* 65, 523–543. doi: 10.1357/002224007782689085

Mercado, J. M., Cortés, D., Ramírez, T., and Gómez, F. (2012). Decadal weakening of the wind-induced upwelling reduces the impact of nutrient pollution in the bay of málaga (western Mediterranean sea). *Hydrobiologia* 680, 91–107. doi: 10.1007/s10750-011-0906-y

Minas, H. J., Coste, B., Le Corre, P., Minas, M., and Raimbault, P. (1991). Biological and geochemical signatures associated with the water circulation through the strait of gibraltar and in the western Alboran sea. *J. Geophysical Research: Oceans* 96, 8755–8771. doi: 10.1029/91JC00360

Muñoz, M., Reul, A., Vargas-Yáñez, M., Plaza, F., Bautista, B., García-Martínez, M., et al. (2017). Fertilization and connectivity in the garrucha canyon (se-spain) implications for marine spatial planning. *Mar. Environ. Res.* 126, 45–68. doi: 10.1016/j.marenvres.2017.02.007

North, G. R., Bell, T. L., Cahalan, R. F., and Moeng, F. J. (1982). Sampling errors in the estimation of empirical orthogonal functions. *Monthly Weather Rev.* 110, 699. doi: 10.1175/1520-0493(1982)1100699:SEITEO2.0.CO;2

Pinto, J. G., and Raible, C. C. (2012). Past and recent changes in the north atlantic oscillation. *Wiley Interdiscip. Reviews: Climate Change* 3, 79–90. doi: 10.1002/wcc.150

Preisendorfer, R. W., and Mobley, C. D. (1988). Principal component analysis in meteorology and oceanography. *Developments atmospheric Sci.* 17, 425.

Ramírez, T. (2007). *Variabilidad hidrológica y dinámica biogeoquímica en el sector noroccidental del mar de alborán.* (Universidad de Málaga:Doctoral dissertation).

Ramírez, T., Cortés, D., Mercado, J., Vargas-Yañez, M., Sebastián, M., and Liger, E. (2005). Seasonal dynamics of inorganic nutrients and phytoplankton biomass in the nw Alboran sea. *Estuarine Coast. Shelf Sci.* 65, 654–670. doi: 10.1016/j.ecss.2005.07.012

Reul, A., Rodríguez, V., Jiménez-Gómez, F., Blanco, J., Bautista, B., Sarhan, T., et al. (2005). Variability in the spatio-temporal distribution and size-structure of phytoplankton across an upwelling area in the nw-Alboran sea,(w-Mediterranean). *Continental Shelf Res.* 25, 589–608. doi: 10.1016/j.csr.2004.09.016

Rodríguez-Fonseca, B., Polo, I., Serrano, E., and Castro, M. (2006). Evaluation of the north Atlantic SST forcing on the European and northern African winter climate. *Int. J. Climatology: A J. R. Meteorological Soc.* 26, 179–191. doi: 10.1002/joc.1234

Saha, K., Zhao, X., Zhang, H., Casey, K., Zhang, D., Baker-Yeboah, S., et al. (2018). *Avhrr pathfinder version 5.3 level 3 collated (l3c) global 4km sea surface temperature for 1981-present* (Asheville, NC, USA: NOAA National Centers for Environmental Information).

Sánchez Garrido, J. C., García Lafuente, J., Criado Aldeanueva, F., Baquerizo, A., and Sannino, G. (2008). Time-spatial variability observed in velocity of propagation of the internal bore in the strait of gibraltar. *J. Geophysical Research: Oceans* 113, 1–6. doi: 10.1029/2007JC004624

Sánchez-Garrido, J. C., García Lafuente, J., Fanjul, E. Á., Sotillo, M. G., and Francisco, J. (2013). What does cause the collapse of the western Alboran gyre? results of an operational ocean model. *Prog. Oceanography* 116, 142–153. doi: 10.1016/j.pocean.2013.07.002

Sarhan, T., García Lafuente, J., Vargas, M., Vargas, J. M., and Plaza, F. (2000). Upwelling mechanisms in the northwestern Alboran sea. *J. Mar. Syst.* 23, 317–331. doi: 10.1016/S0924-7963(99)00068-8

Shaman, J. (2014). The seasonal effects of ENSO on European precipitation: Observational analysis. *J. Climate* 27, 6423–6438. doi: 10.1175/JCLI-D-14-00008.1

Suárez-Moreno, R., and Rodriguez-Fonseca, B. (2015). S4CASTv2.0: sea surface temperature based statistical seasonal forecast model. *Geoscientific Model. Dev.* 8, 3971–4018. doi: 10.5194/gmdd-8-3971-2015

Vargas-Yáñez, M., Giráldez, A., Torres, P., González, M., García-Martínez, M., d., C., et al. (2020). Variability of oceanographic and meteorological conditions in the northern Alboran sea at seasonal, inter-annual and long-term time scales and their influence on sardine (sardina pilchardus walbaum 1792) landings. *Fisheries Oceanography* 29, 367–380. doi: 10.1111/fog.12477

Volpe, G., Nardelli, B. B., Colella, S., Pisano, A., and Santoleri, R. (2018). An operational interpolated ocean colour product in the Mediterranean sea. *New Front. Operational Oceanography, (GODAE OceanView)*, 227–244. doi: 10.17125/gov2018.ch09

Wang, L., Yu, J.-Y., and Paek, H. (2017). Enhanced biennial variability in the pacific due to atlantic capacitor effect. *Nat. Commun.* 8, 1–7. doi: 10.1038/ncomms14887

Advantages of publishing in Frontiers

OPEN ACCESS
Articles are free to read for greatest visibility and readership

FAST PUBLICATION
Around 90 days from submission to decision

HIGH QUALITY PEER-REVIEW
Rigorous, collaborative, and constructive peer-review

TRANSPARENT PEER-REVIEW
Editors and reviewers acknowledged by name on published articles

Frontiers
Avenue du Tribunal-Fédéral 34
1005 Lausanne | Switzerland

Visit us: www.frontiersin.org
Contact us: frontiersin.org/about/contact

REPRODUCIBILITY OF RESEARCH
Support open data and methods to enhance research reproducibility

DIGITAL PUBLISHING
Articles designed for optimal readership across devices

FOLLOW US
@frontiersin

IMPACT METRICS
Advanced article metrics track visibility across digital media

EXTENSIVE PROMOTION
Marketing and promotion of impactful research

LOOP RESEARCH NETWORK
Our network increases your article's readership